DISSERTATION

INVESTIGATION INTO THE FUNDAMENTAL SOLID-STATE CHEMISTRY OF ACTINIDE ELEMENTS: SYNTHESIS AND CHARACTERIZATION OF TERNARY AND QUATERNARY ACTINIDE CHALCOGENIDE COMPOUNDS

Submitted by

Ryan Falcone Hess

Department of Chemistry

In partial fulfillment of the requirements

for the Degree of Doctor of Philosophy

Colorado State University

Fort Collins, Colorado

Spring 2002

COLORADO STATE UNIVERSITY

DECEMBER 6, 2001

WE HEREBY RECOMMEND THAT THE DISSERTATION PREPARED UNDER OUR SUPERVISION BY RYAN FALCONE HESS ENTITLED "INVESTIGATION INTO THE FUNDAMENTAL SOLID-STATE CHEMISTRY OF ACTINIDE ELEMENTS: SYNTHESIS AND CHARACTERIZATION OF TERNARY AND QUATERNARY ACTINIDE CHALCOGENIDE COMPOUNDS" BE ACCEPTED AS FULFILLING IN PART REQUIREMENTS FOR THE DEGREE OF DOCTOR OF PHILOSOPHY

Committee on Graduate Work

Advisor

Department Head

ABSTRACT OF DISSERTATION

Investigation Into The Fundamental Solid-State Chemistry of Actinide Elements: Synthesis and Characterization of Ternary and Quaternary Actinide Chalcogenide Compounds

The use of molten alkali metal polysulfide fluxes has had a profound impact on the synthesis of complex multinary chalcogenide compounds. This method has been used to synthesize numerous quaternary transition metal and rare-earth chalcophosphate compounds. Relatively little information is known about the solid-state chemistry of actinide elements in a chalcogen environment. The synthesis and characterization of the first quaternary thorium, uranium, and plutonium thiophosphate compounds will be discussed. Three uranium, five thorium, and five plutonium thiophosphate compounds have been characterized by single crystal X-ray diffraction, Raman spectroscopy, and diffuse reflectance UV-visible-NIR spectroscopy. These compounds exhibit structures ranging from three-dimensional extended networks found in $Cs_8U_5(P_3S_{10})_2(PS_4)_6$ to one-dimensional chains found in $K_3Pu(PS_4)_2$. A ternary plutonium selenide, KPu_3Se_8, has also been characterized using X-ray diffraction and X-ray absorption spectroscopy. The coordination environments of the actinide metals in these compounds are examined. Preferences in coordination geometry and metal oxidation state are discussed, and a consistent series of metal-chalcogen distances is developed.

Ryan Falcone Hess
Department of Chemistry
Colorado State University
Fort Collins, CO 80523
Spring 2002

Acknowledgements

The work presented in this dissertation could not have been possible without the help of many people. I would like to thank my advisor, Professor Peter Dorhout, for his invaluable instruction and guidance; I have grown both personally and professionally for having worked with you. I would also like to thank all of my friends and co-workers in Los Alamos especially, Kent Abney, Anthony Lupinetti, Warren and Susan Oldham, and Antonio Maestas. You made working in Los Alamos a great experience. Finally, I would like to thank my great friends Bridget Williams, Aaron Anderson, Britton Donharl, Kevin Frencheck, and Joe Bukowski. I have spent some of the best times of my life with you and I thank you for always being there when I needed a friend. Funding for this work was provided by the Glenn T. Seaborg Institute for Transactinium Science through David Clark at Los Alamos National Laboratory.

Dedication

To my Mom and Dad

Your love and encouragement have made this work possible. Your never-ending support and confidence in me throughout my life has meant more to me than words can say.

Thank you.

TABLE OF CONTENTS

LIST OF FIGURES

LIST OF TABLES

CHAPTER FOUR

CHAPTER FIVE

Chapter 1

Introduction to the Fundamental Solid-State Chemistry of the Actinide Elements

Actinide elements have played an important role in society since August 9, 1945; the day the first nuclear weapon was detonated. While the development of nuclear weapons and nuclear power spawned a great deal of actinide research in the second half of the 20th century, there are still large gaps in the scientific community's understanding of these interesting elements. In particular, the fundamental solid-state chemistry has been greatly overlooked. For example, as of 1997 there were only 80 plutonium compounds listed in the Inorganic Crystal Structure Database.[1] This number is very small when compared to a well-studied transition metal such as iron for example, which has 4941 crystal structures listed. Much of the early research in actinide chemistry was centered on solution chemistry (separations), metallurgy and oxide-based compounds, as this science was focused primarily on the development of weapons and reactors. Of the 80 known plutonium structures, only four contain a chalcogen element other than oxygen. The chalcogenide family is Group 16 in the periodic table and contains O, S, Se, Te, and Po. Throughout this dissertation, "Q" will be used to designate the chalcogen elements.

Fundamental Actinide Science

Unfortunately, at many universities the study of actinide elements in chemistry coursework is usually compressed into a short amount of time at the end of the semester. Furthermore, when actinide elements are discussed, they are often treated as a second rare earth series of elements that happen to be radioactive. This is a gross simplification of the chemistry and physics of both series of elements. There are numerous differences between the rare earth (4f series) and actinide elements (5f series). Evidence of these differences can be seen by looking at crystal structures of rare earth and actinide metals.[2] In their elemental, metallic form, all of the rare earth elements, except samarium, have

high symmetry, closest packed structures. The actinide elements, however, display structures ranging from face centered cubic, in the case of actinium, to seven different phases for plutonium including two monoclinic phases near room temperature. Figure 1.1 contains a plot of the connected actinide phase diagram developed by Smith and co-workers.[3] This plot shows the transition from the low symmetry structures of the early actinides to the high symmetry, rare earth like structures of the late actinides.

The properties of the valence orbitals for each series, 4f versus 5f, are also significantly different. The 5f-orbitals have a greater radial extension then the 4f-orbitals. A plot of the radial functions of Sm^{3+} ($4f^5$) and Pu^{3+} ($5f^5$) are shown in Figure 1.2[4] From these plots one can also see the greater effect of relativity on the 5f element, plutonium, compared to the isoelectronic 4f element, samarium. Another significant difference between the valence orbitals of the rare earths and actinides is the relative energies of the f-orbitals compared to the d- and s-orbitals. The 5f-orbitals are closer in energy to the 6d- and 7s-orbitals then the 4f-orbitals are to the 5d- and 6s-orbitals.[4] This is especially true for the early actinides. The result of the similarities in orbital energies can be seen by looking at the complicated outer-electron configurations of the elements in both series. A table of these configurations is shown in Table 1.1. These two characteristics of 5f orbitals pave the way for actinide elements to participate in covalent bonding in some systems.

Of all the elements in the periodic table, plutonium exhibits the most unusual behavior. While it is not uncommon for most metals to have two or even three unique

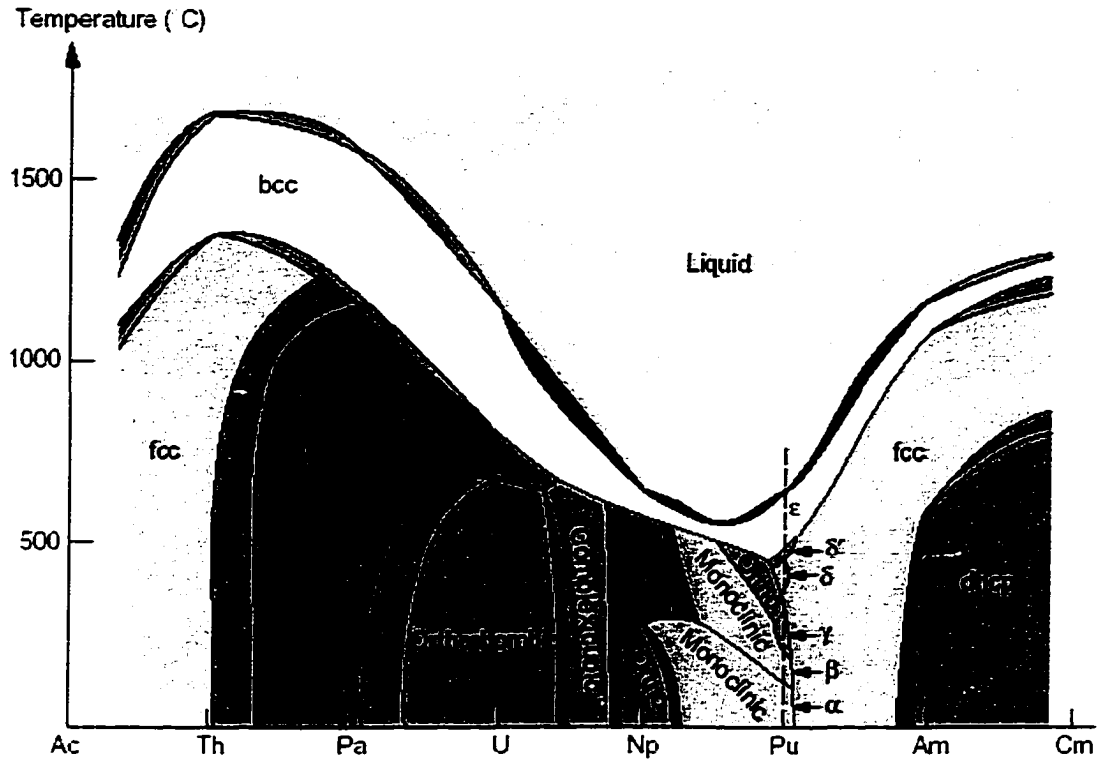

Figure 1.1. The connected actinide phase diagram developed by Smith and co-workers. This diagram shows the progression from the low-symmetry, early actinide structures to high-symmetry, late actinide structures. [3]

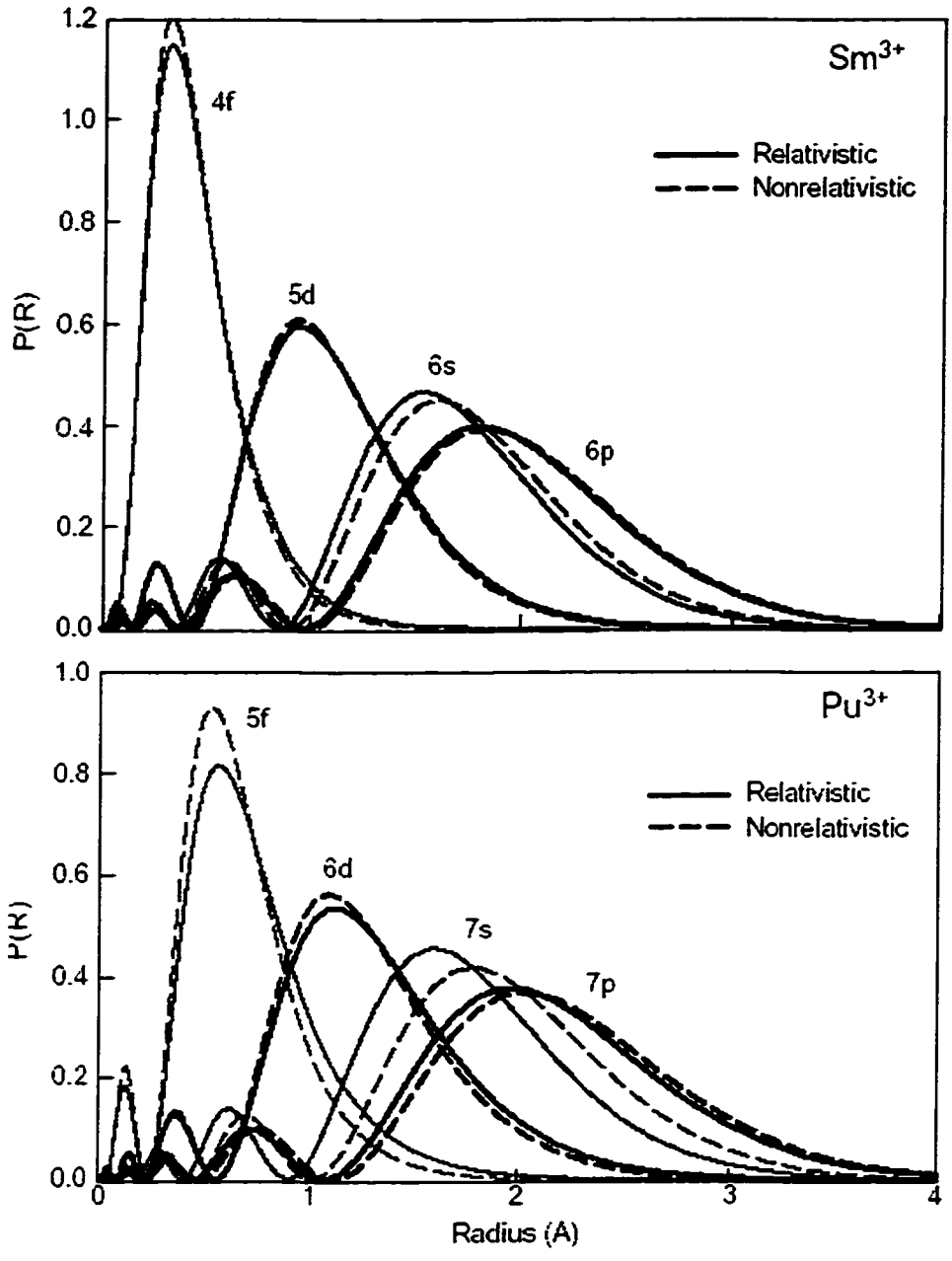

Figure 1.2. The radial distribution functions of the valence orbitals of Sm^{3+} and Pu^{3+}. From these plots one can see the greater radial extension of the 5f orbitals compared to the 4f orbitals. Also, including relativistic effects in the calculations has a much greater effect on the plutonium orbitals than it does on the corresponding samarium orbitals.[4]

Table 1.1. A list of the outer electron configurations for the lanthanide and actinide elements.[4]

Lanthanide		Configuration			Actinide		Configuration		
La	lanthanum		$5d^1$	$6s^2$	Ac	actinium		$6d^1$	$7s^2$
Ce	cerium	$4f^1$	$5d^1$	$6s^2$	Th	thorium		6d	$7s^2$
Pr	praseodymium	$4f^3$		$6s^2$	Pa	protactinium	$5f^2$	$6d^1$	$7s^2$
Nd	neodymium	$4f^4$		$6s^2$	U	uranium	$5f^3$	$6d^1$	$7s^2$
Pm	promethium	$4f^5$		$6s^2$	Np	neptunium	$5f^4$	$6d^1$	$7s^2$
Sm	samarium	$4f^6$		$6s^2$	Pu	plutonium	$5f^6$		$7s^2$
Eu	europium	$4f^7$		$6s^2$	Am	americium	$5f^7$		$7s^2$
Gd	gadolinium	$4f^7$	$5d^1$	$6s^2$	Cm	curium	$5f^7$	$6d^1$	$7s^2$
Tb	terbium	$4f^9$		$6s^2$	Bk	berkelium	$5f^9$		$7s^2$
Dy	dysprosium	$4f^{10}$		$6s^2$	Cf	californium	$5f^{10}$		$7s^2$
Ho	holmium	$4f^{11}$		$6s^2$	Es	einsteinium	$5f^{11}$		$7s^2$
Er	erbium	$4f^{12}$		$6s^2$	Fm	fermium	$5f^{12}$		$7s^2$
Tm	thulium	$4f^{13}$		$6s^2$	Md	mendelevium	$5f^{13}$		$7s^2$
Yb	ytterbium	$4f^{14}$		$6s^2$	No	nobelium	$5f^{14}$		$7s^2$
Lu	lutetium	$4f^{14}$	$5d^1$	$6s^2$	Lr	lawrencium	$5f^{14}$	$6d^1$	$7s^2$

crystal structures, plutonium metal can be found in an astounding seven different phases. Six of these phases are found at standard atmospheric pressure (α, β, γ, δ, δ', and ε) the seventh phase, ζ, is found only at higher pressures.[4,5] The alpha phase structure is unique among metals in that it has only monoclinic symmetry. The beta and gamma phases also have unusually low symmetry, body-centered monoclinic and face-centered orthorhombic, respectively. It is not until the delta phase is reached, at approximately 460 °C, that a high symmetry face centered cubic phase is obtained. Another unusual property of plutonium metal is that as the temperature is increased above 460 °C, the unit cell undergoes a contraction before finally melting at 640 °C. The final solid phase of plutonium metal has a lower density than the liquid phase. Plutonium, therefore, exhibits one of the properties that make water so unique. A plot of the percent length change of the plutonium unit cell versus temperature is shown in Figure 1.3.[2]

Chemically, plutonium is highly reactive. Plutonium metal is extremely oxophilic. In addition to being reactive with oxygen, it will form compounds or alloys with nearly all of the elements in the periodic table. This property makes handling plutonium, especially in the molten state, very difficult. Few materials are able to withstand the corrosive properties of molten plutonium. It was learned first hand during the course of this research that fused silica reaction ampoules are not one of these materials. The two most common crucibles for containing molten plutonium are tantalum metal and magnesium oxide. Plutonium can access a large number of oxidation states, from 2+ through 7+.[4] In solution, it is possible to find plutonium in four different oxidation states simultaneously, 3+, 4+, 5+, and 6+. The redox potentials of these four oxidation states

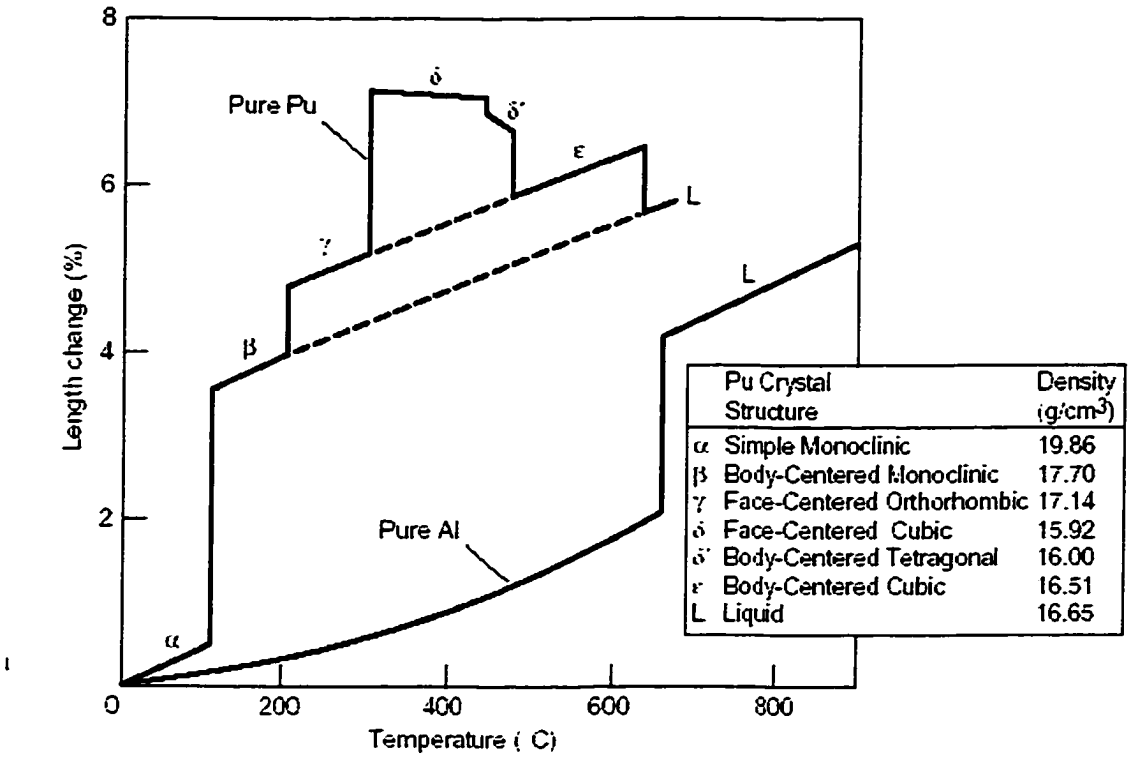

Figure 1.3. A plot of the percent length change of the plutonium metal unit cell upon increasing temperature. Before plutonium melts at 640 °C it undergoes five phase transitions. A plot of the percent length change of aluminum metal is shown for comparison.[2]

are all within approximately one volt of each other.[5] The 5+ oxidation state is relatively unstable and readily disproportionates into 4+ and 6+. Under highly basic conditions it is possible to form plutonium in the 7+ oxidation state as well.

Plutonium forms a dioxo "plutonyl" cation in the 5+ and 6+ oxidation states, PuO_2^+ and PuO_2^{2+} respectively. The formation of trans dioxo cations also occurs in uranium and neptunium chemistry. Recent research indicates that the bonding between the –yl oxygen atoms and the actinide metal is covalent. This behavior is not found in any rare earth element, though similar dioxo cations are found for numerous transition metals. However, in the case of transition metal cations, the oxygen atoms are found in a cis arrangement. Examples of transition metal cis-dioxo cations include VO_2^+, MoO_2^{2+}, and WO_2^{2+}.[6] The trans arrangement of oxygen atoms in uranium, neptunium, and plutonium is unique to the actinide series.[4]

Applications of Actinide Materials

Actinide materials have a wide variety of applications. For instance, thorium oxide has long been used in mantels for gas lanterns for its emission of intense white light when heated. Uranium oxides have been used as coloring in glazes found on dinnerware. Different concentrations yield colors such as orange, brown, and yellow. More recently, uranium has become widely known for its use in nuclear reactors and in nuclear weapons. Plutonium, of course, has become well known for the same reasons as uranium.[5]

The commercial reactors currently in operation in the United States are thermal reactors. These reactors utilize slow, thermal neutrons to form a self-sustained nuclear reaction. The fuel for these reactors starts out with uranium containing 97% ^{238}U and 3%

^{235}U.[5] It is the latter isotope that undergoes fission. When ^{235}U fissions, it releases a large amount of energy in the form of heat. This energy is used to convert water into steam, which is then used to drive turbines creating electricity. The other 97% of the fuel, ^{238}U, does not undergo fission. Instead, it absorbs excess neutrons and eventually decays forming a number of plutonium isotopes. One of the isotopes produced is ^{239}Pu, which is fissile. This isotope of plutonium is responsible for approximately 30% of a reactor's generated power.[5]

Since the 1950's, the United States has generated large amounts of plutonium both through the weapons program and through commercial reactors. The military has approximately 99 tonnes of plutonium in its stockpile. Half of that amount has been declared "excess". Since the advent of nuclear power, the commercial sector has generated over 1000 tons of plutonium. Currently, that material is destined for long-term storage. Finding safe ways to store highly radioactive materials, and ways to safely and efficiently reprocess spent fuel rods in the future, are areas of intense interest in actinide science.

In addition to nuclear power and weapons, plutonium is used in nuclear batteries. In a nuclear battery the alpha emission of plutonium is exploited. Alpha particles (^{4}He) emitted from plutonium nuclei have energies around five million electron volts. Large amounts of heat are generated during the lattice collisions of these alpha particles. This heat is converted into electricity through the use of thermoelectric materials. These power sources have the advantages of containing no movable parts that are subject to breakdown, and have a well-known lifetime. Due to the higher activity of ^{238}Pu compared to ^{239}Pu, it is the former isotope that is used in battery applications. Initially,

these nuclear batteries found applications in heart pacemakers and difficult to reach power stations on Earth. Currently, these two applications are no longer in use. However, nuclear batteries play a vital role in power sources destined for deep space. General Purpose Heat Sources (GHPS) have been used on numerous missions such as Cassini and Voyager. A single GHPS contains 150 g of $^{238}PuO_2$. When 72 GHPS are linked together the unit is capable of generating 285 watts of power. Smaller amounts of plutonium are used in Radioisotope Heater Units (RHU), only 2.7 g $^{238}PuO_2$. Radioisotope Heater Units are used to keep equipment warm in the depths of space.[7]

Finally, the most common use of an actinide material is one that few people are aware of. Americium, specifically $^{241}AmO_2$, is used as the ionizing source in household smoke detectors. Smoke detectors contain a chamber housing two electrical contacts and a small amount of AmO_2. The ionizing radiation from the americium allows current to flow through the space between contacts. When smoke particles fill the chamber they interrupt the current flow and an alarm is triggered. Though the amount of americium found in a smoke detector is extremely small it is interesting that, with the general public's fear and misunderstanding of radioactivity, it goes unnoticed.

Synthesis of Actinide Compounds

Traditionally, actinide compounds have been synthesized using classic high temperature solid-state techniques. Reactions of this type typically have used elemental starting materials that are either arc-melted together or placed in a sealed vessel and heated at temperatures greater than 1000 °C. Such high temperatures are necessary when using elemental starting materials to ensure sufficient solid-state diffusion in a timely

manner or to achieve a molten phase. These methods offer two important advantages: one is that it is sometimes possible to alter the ratio of the starting materials to achieve a high yield of a desired phase. The second advantage is that it is possible to carry out the synthesis in the absence of oxygen or under an atmosphere of a desired reactive or inert gas. Like the rare earth elements, all of the actinides are highly oxophilic. This presents a problem when trying to utilize softer chalcogenides such as sulfides and selenides.

When the target compounds are multinary and contain complex ligands, the use of high temperatures can be counter productive. In most cases, high temperature solid-state reactions yield the most thermodynamically stable phases. In the case of actinide chalcogenide systems the most likely products will be binary compounds such as An_2Q_3 and AnQ_2 (An = actinide element; Q = S, Se, Te). Also many complex ligands, such as those found in chalcophosphates, are not stable at high temperatures (greater than 1000 °C). Therefore, to synthesize quaternary actinide chalcophosphates a technique that involves oxygen-free conditions, relatively low temperatures, and can still be carried out in a reasonable timeframe is necessary. The reactive flux method is such a technique.

Reactive Flux Synthesis

The reactive flux method involves the use of fluxing agents that contain elements desired in the target compound.[8] The flux is employed both as a starting material and a solvent medium, which promotes the growth of single crystals. Fluxes consisting of an alkali metal chalcogenide salt, such as K_2S_5, and the elemental chalcogen have facilitated the synthesis of numerous quaternary chalcophosphate compounds.[8-12] Examples of these reactions include:

$$Bi + 1.5\ P_4S_{10} + 2\ K_2S + 4\ S \rightarrow KBiP_2S_7 + \text{excess flux}$$ [13]

$$La + 3\ P + 2.5\ K_2Se_4 + 3.5\ Se \rightarrow K_3La(PSe_4)_2 + \text{excess flux}$$ [14]

$$Th + 6\ P + 2\ K_2Se_3 + 8\ Se \rightarrow K_2ThP_3Se_9 + \text{excess flux}$$ [15]

The flux mixtures have much lower melting points than the actinide metals utilized as starting materials. The melting points for the fluxes used in this research are around 350 °C. When reactions are heated above this melting point, the flux becomes molten and behaves in much the same was as a conventional solvent. This molten flux is able to both oxidize reagents and increase the solubility of the actinide complex and any main group element, such as phosphorous, that react to form A-P-Q solutions.

For the chemistry in this work, complex and diverse thiophosphate ligands are formed *in situ* from a mixture of alkali metal chalcogenide salts and phosphorous. Examples of some of the thiophosphate ligands that will be discussed in this dissertation are shown in Figure 1.4.[16,17] The ligands shown in Figure 1.4 (a-c) are $(PS_4)^{3-}$, $(P_2S_7)^{4-}$, and $(P_2S_6)^{4-}$, respectively. The first two ligands contain phosphorus atoms in the 5+ oxidation state while phosphorus in $(P_2S_6)^{4-}$ is tetravalent. Chapters 3 and 4 describe the new quaternary actinide thiophosphates synthesized in this work. Reactions using alkali metal selenide fluxes were also carried out. The selenide experiments yielded a new

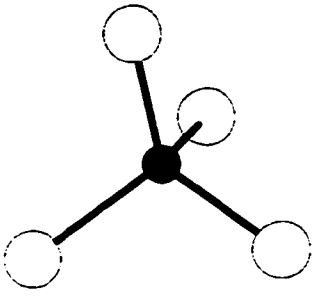

(a)

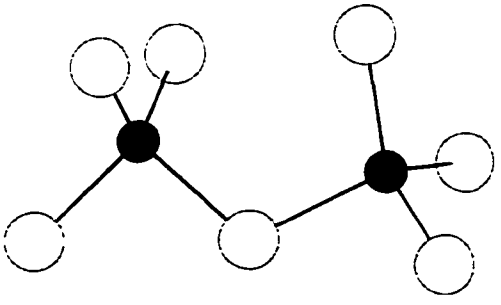

(b)

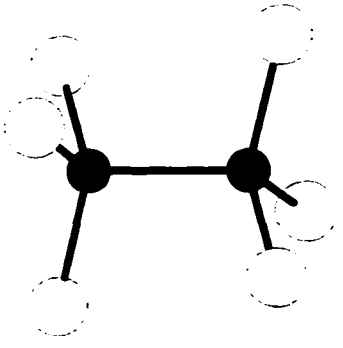

(c)

Figure 1.4. Examples of some of the thiophosphate ligands found in this dissertation. These ligands will be described in further detail in the chapters to follow. The filled circles are the phosphorous atoms and the unfilled circles are the sulfur atoms

ternary plutonium selenide compound, KPu_3Se_8. This ternary plutonium compound is discussed in Chapter 5. The relatively low temperatures utilized in flux syntheses allows for the formation of a wide variety of compounds containing complex ligands.[9,10,18,19] These compounds are often either ternary or quaternary in nature and can be far more structurally complex than the thermodynamically stable binary compounds.

The reactive flux method has been used extensively in the synthesis of quaternary lanthanide chalcophosphates. Evenson and Dorhout have characterized a number of these phases with formulas such as $K_3La(PS_4)_2$, $K_2La(P_2S_6)_{1/2}(PS_4)$, and $K_4La_{0.67}(PS_4)_2$.[16] Table 1.2 contains a list of known chalcophosphate compounds that are related to the compounds described in this dissertation. In addition, their work has shown that it was possible to synthesize complex quaternary compounds by mapping out regions of phase space that support diverse structures.[14,16] They accomplished this by plotting quasi-quaternary phase diagrams that related new compounds to the flux compositions in which they were made for a given temperature. A similar approach was used in this work as well.

There are four components in the thiophosphate system described in this dissertation: the alkali metal (A), the actinide metal (An), phosphorous (P), and sulfur (S). It is a difficult task to envision a four dimensional, or quaternary, phase diagram on a two-dimensional graph. The quaternary phase space can be plotted in a pyramid with a component on each corner. This can be seen in Figure 1.5. For simplicity, one component has been held constant, in this case sulfur the content, and a three-component phase diagram was created. This may be seen as a horizontal slice along

Table 1.2 This table contains a list of relevant lanthanide and actinide chalcogenide compounds.

Compound	Structure	Reference
$K_3La(PS_4)_2$	1D Chains	16
$K_2La(P_2S_6)_{1/2}(PS_4)$	2D Layers	16
$K_4La_{0.67}(PS_4)_2$	"Broken" 1D Chains	16
$K_{9-x}La_{1+x/3}(PS_4)_4$ (x = 0.5)	Isolated Clusters	16
$RbDy_3Se_8$	2D Layers	26
KTh_2Se_6	2D Layers	27,28
$CuTh_2Te_6$	3D Lattice	20
$SrTh_2Se_5$	3D Lattice	20
$K_2ThP_3Se_9$	2D Lattice	15
$Cs_4Th_2P_5Se_{17}$	2D Lattice	15
$K_2UP_3Se_9$	2D Layers	22
$Rb_4U_4P_4Se_{26}$	3D Lattice	23

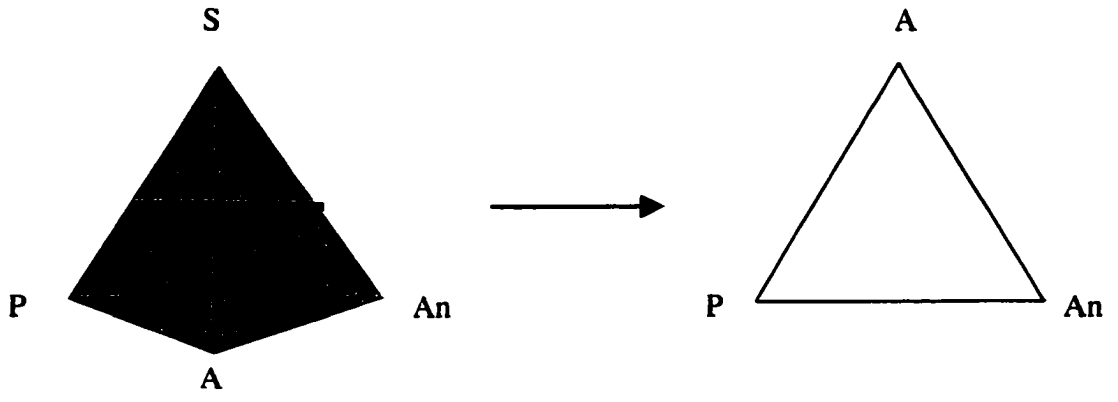

Figure 1.5 Cartoon representation of converting four dimensional phase space into a more comprehensible three-component phase diagram.

the perpendicular from one apex. Reactions are then carried out by varying the three remaining components. The starting compositions that yield single crystal structures are plotted on the diagram. In theory, when a sufficient number of points are plotted, and their structures understood, one can begin to predict which structures form depending on the flux composition.

The choice of the particular chalcogen element and its ratio to the other elements in the flux are important. It is the chalcogen component of the flux that is responsible for the oxidation of the actinide metal. Therefore, by changing the alkali metal to chalcogen ratio is it possible to change the oxidizing power of the flux.[9,10] The oxidizing power is greatly dependent on electronegativity of the chalcogen element. Because sulfur has a higher electronegativity then selenium, a thiophosphate flux will typically be more oxidizing then a selenophosphate flux. An equally important structure directing factor is the preferred bonding behavior of the chalcogen. As one moves down the chalcogenide family the elements become increasingly soft and metallic in nature. Tellurium is a much softer anion than oxygen and prefers to form linear chains and square grids containing Te-Te bonds. The lighter chalcogenides, however, tend to form isolated dianions instead.

Known Actinide Chalcogenides

The reactive flux method has also been used to synthesize multinary actinide chalcogenide compounds. Ibers and co-workers have structurally characterized a family of ternary thorium chalcogenides with the formula ATh_2Q_6 (A=K, Cs; Q=Se, Te).[20,21] These compounds exhibit a layered structure containing edge and face sharing ThQ_8 bicapped trigonal prisms. The alkali metal cations reside in-between the layers. Figure

1.6 contains a view of $CsTh_2Te_6$ down the [100] crystallographic direction. An important feature of this structure is the bonding that occurs between the tellurium atoms in the top and bottom sheet of each $[Th_2Te_6]$ layer. The tellurium atoms form one-dimensional Te-Te chains along the [010] direction. This chalcogen-chalcogen bonding does not occur in the same fashion in the analogous selenium compound. This series of ternary actinide chalcogenides is discussed in greater detail in Chapter 5.

Kanatzidis and co-workers have characterized two quaternary uranium selenophosphate compounds, $K_2UP_3Se_9$ and $Rb_4U_4P_4Se_{26}$.[22,23] Briggs-Piccoli and Dorhout have characterized thorium analogues of both structures.[24] The first compound, $K_2AnP_3Se_9$ (An = Th, U), has a two dimensional structure consisting of $[AnP_3Se_9]^{2-}$ layers. Each layer is composed of chains of $[An_2Se_{14}]$ units that are linked together in the [010] direction by $(P_3Se_6)^{4-}$ units. The actinide atoms are coordinated to nine selenium atoms in a tricapped trigonal prismatic geometry. Figure 1.7 contains a view of $K_2UP_3Se_9$ down the [100] crystallographic direction.

The second compound, $A_4An_4P_4Se_{26}$ (A = Rb, An =U; A = Cs, An = Th), has a three dimensional structure based on $[An_2Se_{13}]$ dimeric units. The dimers are linked together to form chains through edge-sharing of selenium atoms. The chains are then linked together to form a three dimensional network via $(P_2Se_9)^{6-}$ ligands. The actinide atoms are coordinated to eight selenium atoms in a bicapped trigonal prismatic geometry. Figure 1.8 contains a view of $Cs_4Th_4P_4Se_{26}$ down the [100] crystallographic direction. Of the quaternary actinide chalcophosphate compounds

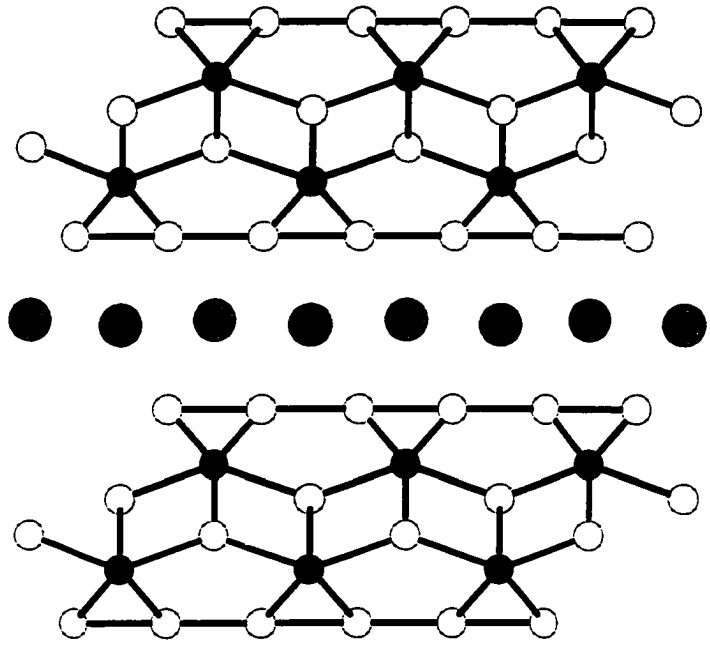

Figure 1.6. View of $CsTh_2Te_6$ down the [100] crystallographic direction. This compound has a layered structure containing $ThTe_8$ bicapped trigonal prisms. The Th atoms are the filled circles, the tellurium atoms are the unfilled circles, and the K^+ cations are the shaded circles residing between the $[Th_2Te_6]^-$ layers.

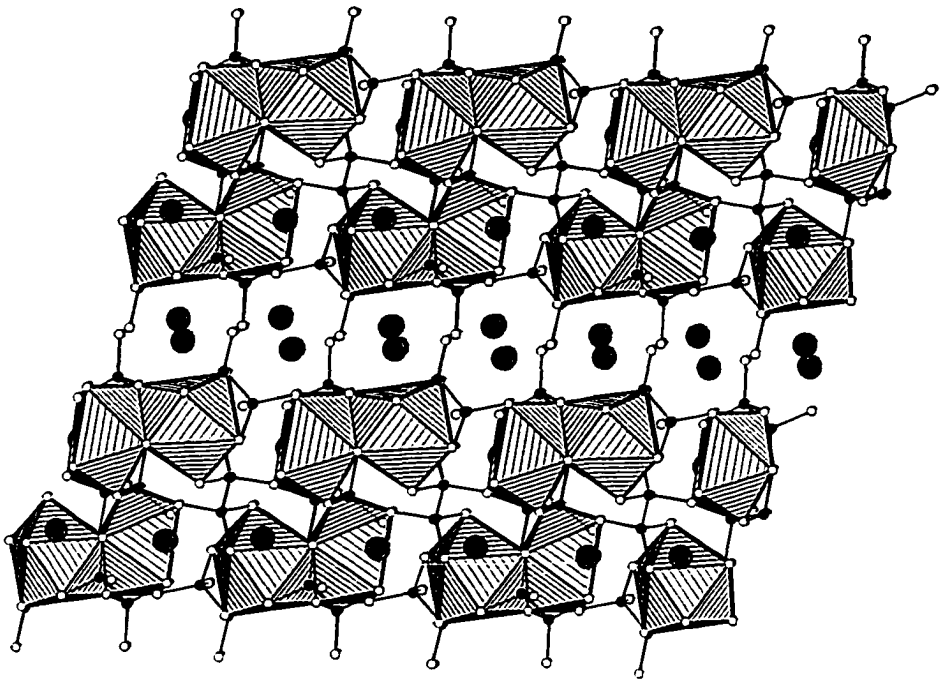

Figure 1.7. View of $K_2UP_3Se_9$ down the [100] crystallographic direction. This compound has a two-dimensional layered structure. Each layer is composed of chains of $[U_2Se_{14}]$ units that are linked together in the [010] direction by $(P_2Se_6)^{4-}$ units. The polyhedra are USe_9 tricapped trigonal prisms, the unfilled circles are selenium atoms, the filled circles are phosphorous atoms, and the shaded circles are K^+ cations.

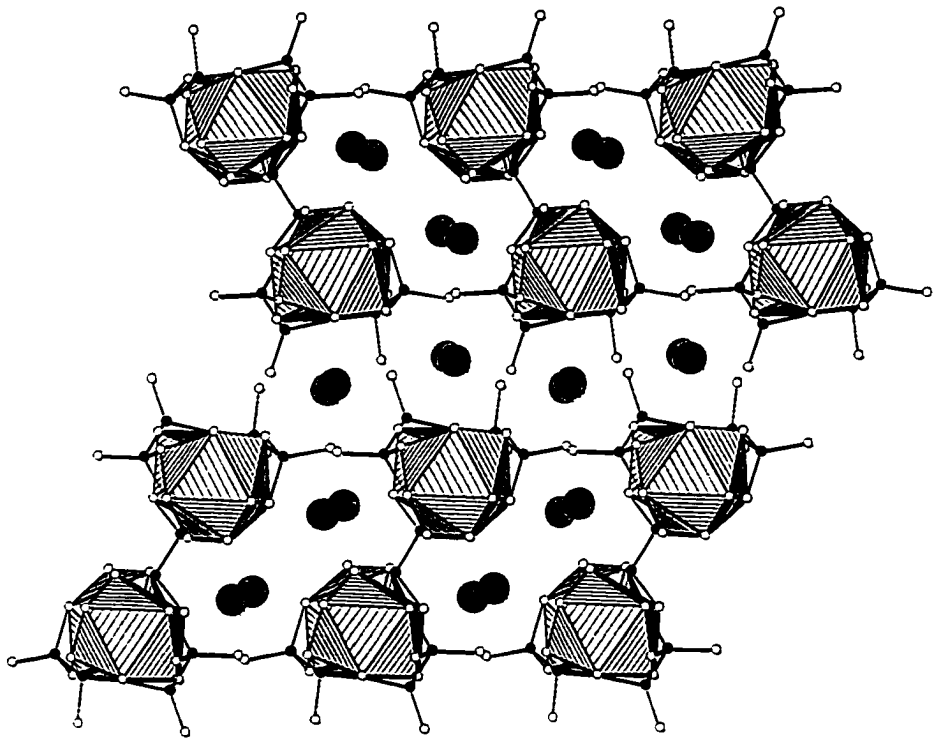

Figure 1.8. View of $Cs_4Th_4P_4Se_{26}$ down the [100] crystallographic direction. This three-dimensional structure is based on $[Th_2Se_{13}]$ dimeric units. The dimers are linked together to form chains through edge-sharing of selenium atoms. The chains are then linked together to form a three dimensional network via $(P_2Se_9)^{6-}$ ligands. The polyhedra are $ThSe_9$ bicapped trigonal prisms, the filled circles are phosphorous atoms, the unfilled circles are selenium atoms, and the shaded circles are Cs^+ cations.

that have been characterized, all have been selenophosphates, no actinide thiophosphates were known prior to this work.

This research has been an exploration into the structural chemistry of actinide thiophosphate compounds centered on three primary goals. The first goal was to examine the similarities and differences in the structural chemistry of the actinide and lanthanide elements. The second goal was to determine if there are any significant differences in structural chemistry between the actinide elements themselves by examining the trend Th→U→Pu. The third goal has been to examine the local coordination chemistry of the actinide elements in a chalcogen environment and compare these to binary sulfides. When compared to transition metals, very little is known about the coordination geometries of actinide elements.[25] This work brings to light the diverse chemistry of actinide chalcogenides and places it in context with the known chalcogenide chemistry of other elements in the periodic table.

Thus, the remainder of this dissertation is divided into five chapters. Chapter 2 contains specific information on the handling of radioactive materials both at Colorado State University and Los Alamos National Laboratory. Chapter 3 describes the new thorium and uranium thiophosphate compounds synthesized in this work and places them in context with known rare-earth chemistry. The majority of the work in Chapter 3 was completed at Colorado State University. Chapter 4 describes the synthesis and characterization new plutonium thiophosphate compounds and compares them to the early actinide element compounds and known rare-earth compounds. All of the plutonium chemistry was carried out at Los Alamos National Laboratory. Chapter 5 contains information on a ternary plutonium selenide, KPu_3Se_8, which has an interesting,

charge density wave modulated structure. Finally, Chapter 6 focuses solely on the information learned about actinide coordination chemistry during the course of this research. The coordination environments around the actinide metals in the structures described in Chapters 3-5 are summarized and compared to known literature.

Chapter 2

Working with Radioactive Elements

Radiochemistry

All of the elements in the actinide series are radioactive. The three elements studied in this work, thorium, uranium, and plutonium, all decay primarily through the emission of alpha particles. An alpha particle is a charged helium nucleus ($^{4}He^{2+}$) that is emitted from the parent atom's nucleus. This event creates both a new daughter element and a projectile in the form of the alpha particle. Equation (1) is an example of an alpha decay reaction The daughter products created during radioactive decay

$$^{A}_{Z}X \longrightarrow {}^{4}_{2}He + {}^{A-4}_{Z-2}Y \qquad (1)$$

may themselves have different decay mechanisms than the parent. Some of these daughter products decay via beta particle emission or by gamma ray emission. Equations (2) and (3) are examples of beta and gamma decay reactions, respectively

$$^{A}_{Z}X \longrightarrow {}^{0}_{-1}e + {}^{A}_{Z+1}Y + {}^{0}_{0}\bar{\nu} \qquad (2)$$

$$^{A}_{Z}X^{m} \longrightarrow \gamma + {}^{A}_{Z}X \qquad (3)$$

The isotopes used in this work are ^{232}Th (natural), ^{238}U (depleted), and ^{239}Pu (weapons grade). Weapons grade plutonium has a different isotopic ratio than reactor grade plutonium. Table 2.1 contains a list of the isotopes, and their weight percent, found in the plutonium used in this research. Table 2.2 lists the half-lives and alpha particle energies of these isotopes.[5] The decay schemes for ^{232}Th, ^{238}U, and ^{239}Pu are shown in Figures 2.1 through 2.3 respectively.[26]

Table 2.1. The approximate isotopic distribution of the plutonium used in this research.

Plutonium Isotope	Weight Percent
238	0.01
239	93.78
240	6
241	0.2
242	0.02
244	0

Table 2.2. The pertinent nuclear properties of the isotopes used in this research

Isotope	Half-life (y)	Daughter Product	Daughter Half-life	Alpha Particle Energy (MeV)
^{232}Th	$1.41x10^{10}$	^{228}Ra	5.75 y	4.016
^{238}U	$4.47x10^{9}$	^{234}Th	24.10 d	4.196
^{239}Pu	$2.41x10^{4}$	^{235}U	7.0×10^{8} y	5.155

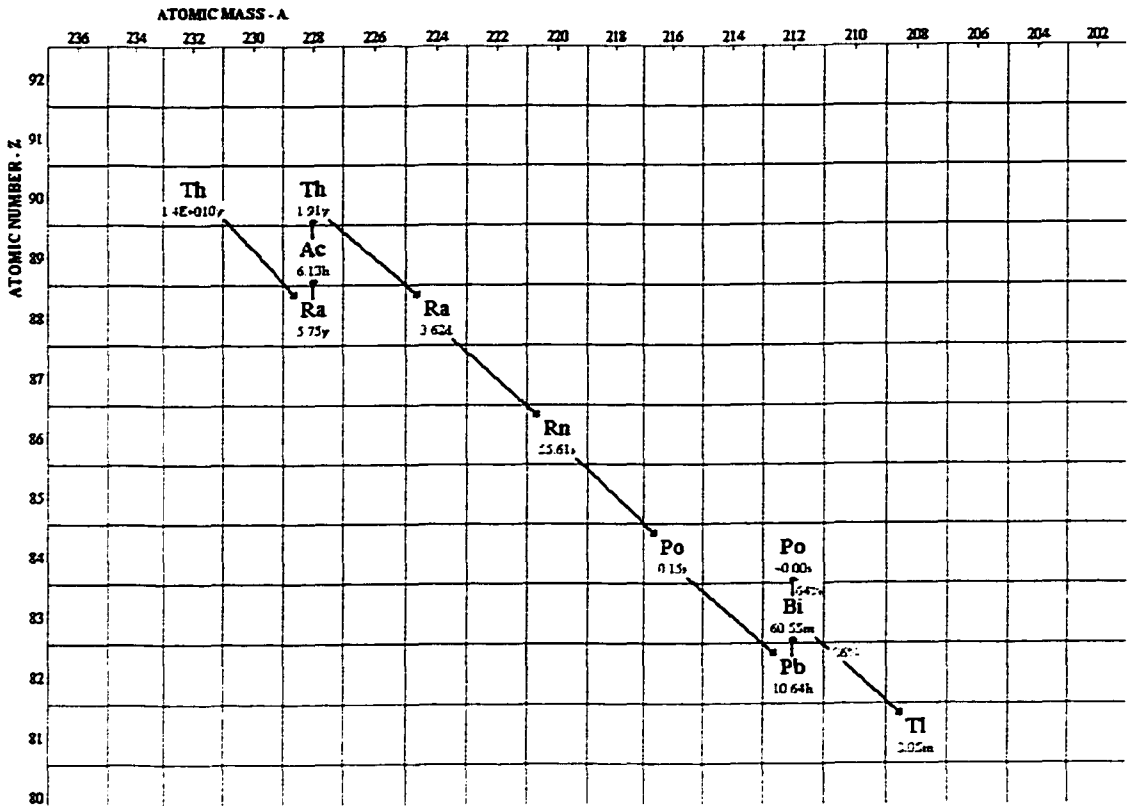

Figure 2.1. The decay scheme for ^{232}Th (ref.26).

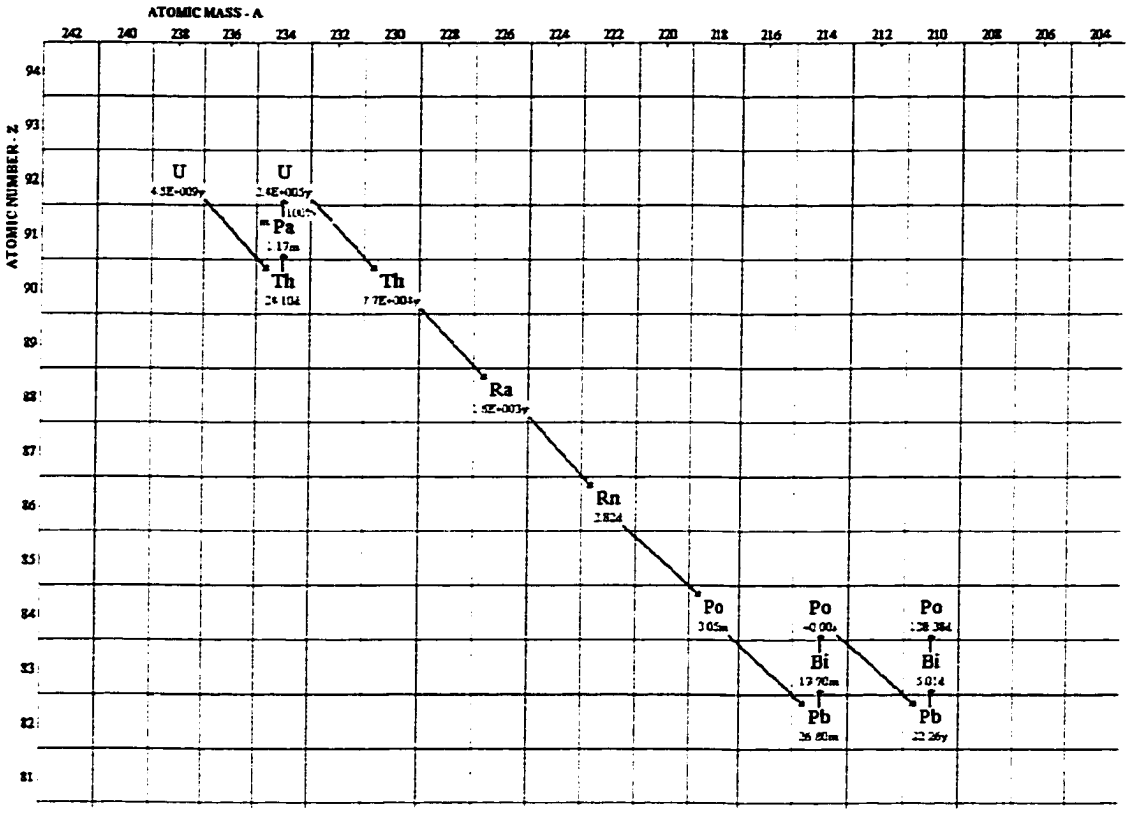

Figure 2.2. The decay scheme for ^{238}U (ref.26).

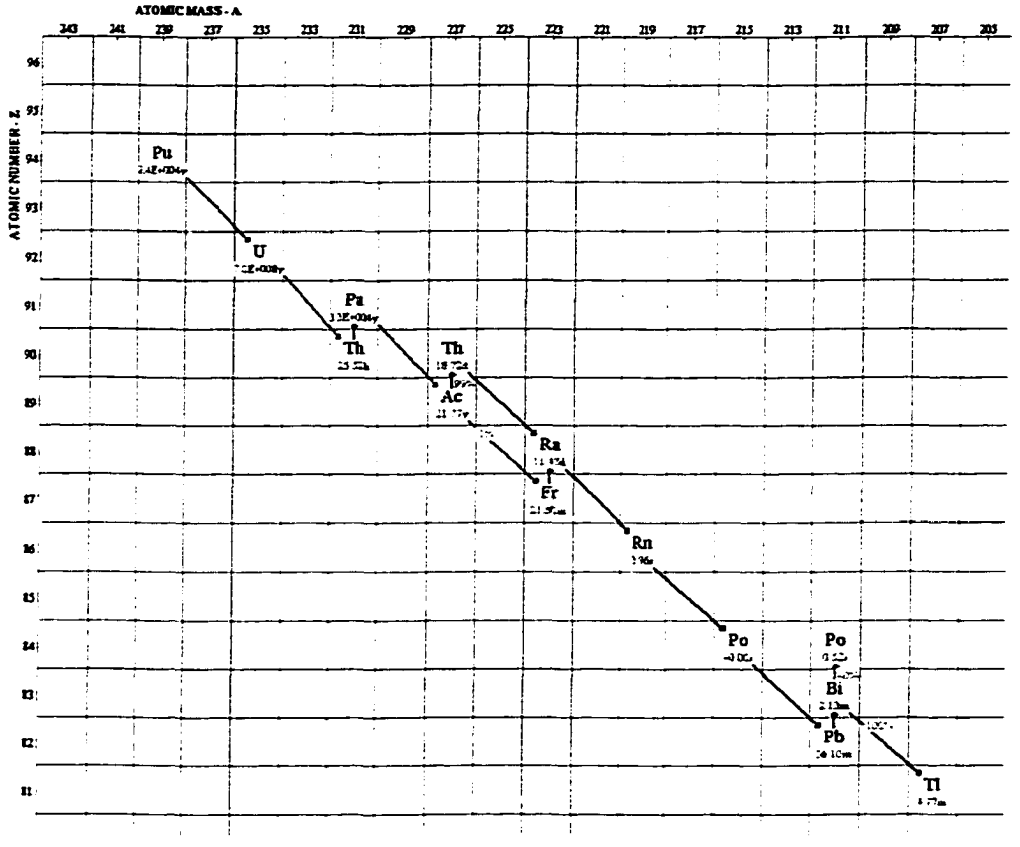

Figure 2.3. The decay scheme for ^{239}Pu (ref.26).

While alpha particles are a form of ionizing radiation they have very little penetrating power. Because alpha particles are stopped in a few microns of material, equivalent to the dead skin layer, or approximately one inch of air, shielding is not a concern when working with this material. The primary concern when dealing with alpha emitters is the inhalation of the radioactive element. Once inside the body, alpha emitters can do a tremendous amount of damage to living tissue due to the relatively high particle energies.

Preventing both the inhalation of particles, and the absorption of materials through the skin, is especially important when working with plutonium. Studies have shown that from 5 % to 25 % of the plutonium particles inhaled are retained in the body.[27] These particles can either remain in the lungs or lymph system or get absorbed by the blood and deposited in the liver or bones. Absorbing plutonium through the skin carries the highest risk of all internal contamination pathways, as nearly 100 % of the material absorbed stays in the body.[27] Ingestion of plutonium carries the least risk as only 0.001 % to 0.05 % of the material is retained in the body depending on its chemical form.[27] Fortunately, unlike plutonium, thorium and uranium pass through the body relatively quickly. In addition to being radioactive, the actinide elements have a high chemical toxicity as do most heavy metals.

A final concern that dealing specifically with plutonium is its ability to undergo a self-sustained nuclear reaction if a critical mass of material is brought together. Fortunately, due to the very small amounts of materials used in the reactions carried out in this work it would be almost impossible for a criticality accident to occur.

Source of Actinide Materials

Thorium and uranium are natural elements found in the Earth's crust. Compared to many elements, neither thorium nor uranium are exceedingly rare. Thorium has an abundance of 8.1 ppm in the Earth's crust, which is similar to boron (9 ppm). Thorium has two commercially viable mineral sources, monazite and uranothorite which is a mixed Th,U silicate. Uranium has an abundance of 2.3 ppm, which is similar to tin (2.1 ppm). Uranium also has two useful mineral sources, pitchblende (U_3O_8) and carnotite ($K_2(UO_2)_2(VO_4)_2 \cdot 3H_2O$).[5]

Plutonium, however, is not found to any reasonable extent in the Earth's crust. Due its very long half-life, 8.26×10^7 years, exceedingly small amount of ^{244}Pu may be leftover from the formation of the Earth. Also, small amounts of plutonium are formed from neutron capture of natural uranium but again it is nearly too small an amount to measure. Therefore, all of the plutonium in the world's stockpile, including the plutonium used in this research, is man-made.

Plutonium Production

The plutonium used in this research was formed in a nuclear reactor at either the Hanford or Savannah River Department of Energy sites. As described in Chapter 1, a nuclear reactor uses uranium (97% ^{238}U, 3% ^{235}U) as its fuel. When the fuel rods are bombarded with thermal neutrons the ^{235}U fissions, releasing large amounts of energy according to the chemical Equation (2).

$$^{235}U + {}^{1}n \rightarrow \text{Fission Products} + 2.5\ {}^{1}n + 200\ \text{MeV} \quad (2)$$

A portion of the ^{238}U component undergoes neutron capture and subsequent beta decay to form ^{239}Pu and other plutonium isotopes according to Equation (3). The isotopic distribution of the plutonium formed

$$^{238}U + {}^{1}n \rightarrow {}^{239}U + {}^{-1}e \rightarrow {}^{239}Np + {}^{-1}e \rightarrow {}^{239}Pu \qquad (3)$$

can be controlled by varying the neutron energies and the irradiation time. After the rods are irradiated the plutonium is separated from the leftover uranium, fission products, and heavy elements such as curium, berkelium, and californium. This separation is achieved using the Plutonium Uranium Reduction Extraction (PUREX) process. A detailed description of the PUREX process is found in Chemistry of the Actinide Elements written by Katz, Seaborg, and Morss. The end result of the PUREX process is 99.8% pure plutonium metal.

Thorium and Uranium Experiments at Colorado State University

A special laboratory was designed and setup at the Colorado State University Department of Chemistry, and approved by the university Environmental Health and Safety group, with the goal of being able to handle alpha particle emitting materials safely. A typical radioactive materials laboratory contains a number of unique pieces of equipment designed to either contain the material or to monitor the work area and personnel for potential contamination. Access to the laboratory is limited to those who have completed CSU's Radiation Safety Program. For radiation monitoring an Eberline GM-pancake probe (Model RM-20-1) was used. This probe is able to detect beta/gamma radiation only. Because thorium and uranium emit low energy alpha particles most hand-held alpha counters are not sensitive enough monitor small amounts of material. The lab

contains both a positive pressure, inert atmosphere glove box and a fume hood dedicated to radioactive materials use. A sticky "step-off" pad is located just inside the radiological controlled area. This pad helps to remove any particulate material on the booties prior to them being returned to their holding bin.

Standard procedures for working in the controlled area involve donning a lab coat, safety goggles, and protective booties. A log book is kept at the entrance and is filled out upon entering and exiting the work area. Once a day, the hand-held radiation counter is checked using ^{137}Cs source, to be sure it is in operating condition. The counter is calibrated twice a year by Radiation Safety personnel. All contaminated waste generated in the controlled area is kept separate from uncontaminated waste and is disposed of in accordance to the rules set forth by the CSU Radiation Safety committee. Any items taken from the controlled area are checked for potential contamination using the radiation counter. Upon exiting the controlled area, both hands and feet are monitored using the radiation counter. Booties are returned to their holding bin.

In addition to daily monitoring, swipes are taken of designated surfaces within the controlled area and surrounding laboratories once a month. A swipe involves taking a piece of two inch filter paper and running it along a surface of approximately 100 cm^2 in size. These swipes are then analyzed for contamination using a scintillation instrument. The analysis is carried out by CSU Radiation Safety personnel. Results from these swipes are kept in a ring binder near the entrance to the controlled area along with other pertinent records. The controlled area is also inspected twice a year by CSU Radiation Safety personnel.

Inventories are maintained of all radioactive materials used in the laboratory. Each source material is assigned an inventory number and its disposition is tracked in a log book kept with the monthly survey results. Inventories of solids in samples and in the waste are also maintained.

Plutonium Experiments At Los Alamos National Laboratory (LANL)

Thorium and uranium are handled at LANL in a similar way in which they are CSU. Many of the procedures used at CSU were derived from LANL operations. Though the fundamentals of radiation safety are the same no matter what the source, plutonium does have a much higher activity then thorium or uranium so additional precautions need to be taken. In addition, its low LD_{50} of 0.314 mg/kg for injection and 1.25 mg/kg for inhalation, also warrants specialized handling.[27]

The plutonium experiments described in this dissertation were carried out at LANL's Technical Area 48 Alpha Wing. To help prevent spread of contamination during a release, the entire laboratory room is kept under slightly negative atmospheric pressure relative to the building. The air output from the laboratory passes through HEPA filters before being reaching the outside environment.

To prevent possible inhalation of plutonium all operations using solid materials are done inside of gloveboxes. The gloveboxes used for transuranic (TRU) materials are kept under negative pressure at all times. This is to prevent the release of radioactive material into the room in the event of a punctured glove or when bringing materials in or out of the glovebox. It is important to note that finely divided plutonium metal is highly

reactive with oxygen and is kept inside vacuum desiccators to prevent oxidation of the surface. In addition to hand-held alpha, beta, and gamma counters the lab contains six continuous air monitors (CAMS) that will trigger an alarm if airborne contamination is detected. Upon exiting the lab one must pass through a hand and foot monitor. After removing laboratory protective clothing each person passes through a series of detectors that monitor the entire body for contamination. While these monitors are highly effective, they are only designed to detect external contamination. To detect internal contamination all plutonium handlers take part in a bioassay program. This program includes both *in vivo* and *in vitro* methods. Once a year an entire body scan is done using highly efficient detectors located two floors underground to prevent interference from cosmic radiation. Urine samples are also collected and analyzed for contamination on a yearly basis. The procedures and monitoring equipment described above make working in the Alpha Wing as safe as any chemistry laboratory can be.

For increased safety, when any operation is carried out where the potential for airborne plutonium contamination is high, air purifying full-face respirators are worn. Operations where this is necessary are called "hot jobs" and only essential personnel are permitted in the lab. Numerous hot jobs were carried out during the course of the research described in this dissertation. Respirators were used during the sealing of all reaction ampoules. The sealing of capillary tubes containing single crystals for diffraction experiments was also carried out using respirators until our team became well trained in the task. As a rule, anytime equipment or trash is removed from the transuranic gloveboxes respirators are necessary.

It is important to note that through routine usage, the inside surfaces of the glovebox have become highly contaminated. Swipes have indicated that contamination is present on the order of 1-2 million counts per minute (10^6 dpm). Therefore, any piece of equipment brought into to the box, even briefly, must be thoroughly decontaminated upon removal. This has lead to the development of extensive procedures needed to carry out even the simplest of techniques used in everyday solid state chemistry. Some of these procedures are listed in Appendix A.

Chapter 3

The Early Actinide Elements: Thorium and Uranium Thiophosphate Chemistry

(Sections of this work have published in the journal, Inorganic Chemistry volume 40, pages 2851-2859, 2000.)

Introduction

The application of molten polychalcogenide fluxes has proven to be very useful in the synthesis of complex, quaternary compounds. One advantage to using polychalcogenide fluxes is that it allows one to carry out reactions at much lower temperatures than would be required if relying on direct combination of the elements. Running reactions at intermediate temperatures (500 °C–750 °C) also has the advantage that it is possible to form ternary and quaternary compounds with complex ligands that would otherwise decompose at higher temperatures. In many cases, traditional solid-state reactions yield the most thermodynamically stable products. In actinide chalcogenide chemistry these stable products are most often actinide sulfide or selenide binary compounds. The goal of this work is to synthesize and structurally characterize quaternary actinide compounds. The desired compounds contain four elements: an alkali metal, actinide metal, main group metal, and a chalcogen. While numerous examples of quaternary transition metal and lanthanide chalcogenides exist, few quaternary thorium and uranium chalcogenides were known prior to this work.[14,16,23,28-33] No ternary or quaternary plutonium chalcogenides existed at all.

The new quaternary thorium and uranium thiophosphates characterized in this research will be discussed in terms of their extended structures and the local coordination environment around the actinide element. These compounds as a class will be compared with known quaternary lanthanide chalcogenides. A major goal of this work is to better understand the relationship between the lanthanide and actinide series with respect to their structural chemistry. The majority of the work discussed in this chapter has been published as a full paper in the journal, Inorganic Chemistry.[17]

Binary Thorium and Uranium Chalcogenides

While few quaternary thorium or uranium chalcogenides are known, the binary systems of these elements has been studied in detail for quite sometime. The driving force for the development of binary actinide chalcogenides has been their potential use as fuel in nuclear reactors.[25] The uranium-oxygen system is one of the most complex oxide systems of any element in the periodic table. Twenty different binary oxides are known to exist with O/U ratios from 1.0 to 3.0 for UO and UO_3 respectively.[5] The thorium-oxygen system is not nearly as complex and contains only one well-defined phase, ThO_2. Thorium dioxide is isostructural with CaF_2. A view of ThO_2 down the [111] crystallographic direction is shown in Figure 3.1.[34] The existence of ThO as an independent phase is somewhat debatable.[5] Tables 3.1 and 3.2 contain lists of the known thorium and uranium chalcogenide phases. Many of these actinide compounds have are structurally related to more widely known compounds. In the cases where this is true the structure type is listed in italics.

The thorium-sulfide system is more complex than the oxide system and contains five well-defined phases. These compounds have S/Th ratios ranging from 1.0 in the case of ThS to 2.5 in the case of Th_2S_5. Unlike in the oxide system, the monosulfide phase is stable and has a NaCl structure. The sulfur rich phase, Th_2S_5, has an interesting structure that does not resemble any known compounds[35]. This phase has three-dimensional structure that is built upon infinite chains of ThS_{10} polyhedra running along all three crystallographic directions. A view of Th_2S_5 down the [100] direction is shown in Figure 3.2. The sesquisulfide, Th_2S_3, crystallizes in the orthorhombic crystal system with the well-known Sb_2S_3 structure type.[36] A view of Th_2S_3 down the [001]

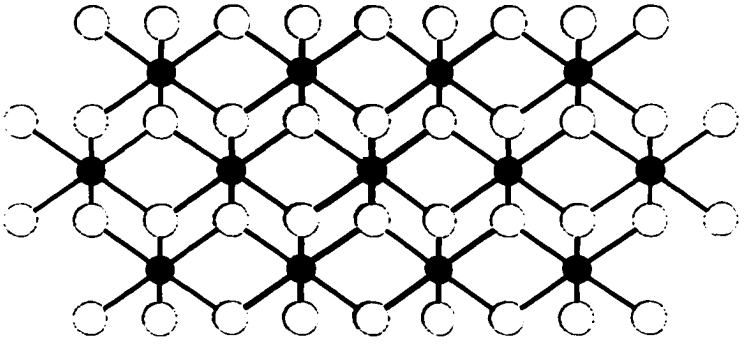

Figure 3.1. View of the ThO_2 structure down the [111] crystallographic direction. This three-dimensional structure is composed of interconnected chains of ThO_8 cubes. The filled circles are the Th atoms and the unfilled circles are the O atoms.

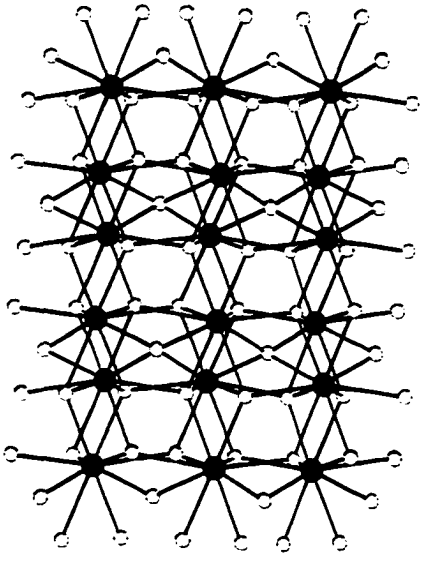

Figure 3.2. View of the Th_2S_5 structure down the [100] crystallographic direction. Like ThO_2, this three-dimensional structure is composed of interconnected chains of thorium polyhedra. The thorium atoms are coordinated to 10 sulfur atoms. The filled circles are the Th atoms and the unfilled circles are the S atoms.

Table 3.1. List of the known binary thorium chalcogenide compounds and their structure types.

Oxides	Sulfides	Selenides	Tellurides
			$ThTe_3$ *$ZrSe_3$*
	Th_2S_5 *tetragonal*	Th_2Se_5 *Th_2S_5*	
ThO_2 *CaF_2*	ThS_2 *$PbCl_2$*	$ThSe_2$ *$PbCl_2$*	$ThTe_2$ *unknown*
	Th_7S_{12} *hexagonal*	Th_7Se_{12} *hexagonal*	
	Th_2S_3 *Sb_2S_3*	Th_2Se_3 *Sb_2S_3*	Th_2Te_3 *hexagonal*
ThO (?) *unknown*	ThS *NcCl*	ThSe *NaCl*	ThTe *CsCl*

Table 3.2. List of the known binary uranium chalcogenide compounds. When characterized, their structure type is listed in italics. Though over twenty different uranium oxides are known, only the most well characterized phases are listed below.

Oxides	Sulfides	Selenides	Tellurides
			UTe_5 *unknown*
			$UTe_{3.38}$ *tetragonal*
γ-UO_3 *CaF_2*	US_3 *$ZrSe_3$*	USe_3 *$ZrSe_3$*	UTe_3 *$ZrSe_3$*
$U_{12}O_{35}$ *ortho*			
β-U_3O_9 *ortho*			
α-U_3O_8 *ortho*			
γ-U_2O_5 *mono*			
β-U_2O_5 *hexagonal*			
α-U_2O_5 *mono*			
UO_2 CaF_2	β-US_2 *$PbCl_2$*	β-USe_2 *$PbCl_2$*	
	γ-US_2 *hexagonal*	γ-USe_2 *hexagonal*	
	α-US_2 *Fe_2B*	$USe_{1.9}$ *$US_{1.9}$*	UTe_{2-x} *ortho*
			U_7Te_{12} *Th_7S_{12}*
	U_3S_5 *ortho*	U_3Se_5 *U_2S_5*	U_3Te_5 *unknown*
	U_2S_3 *Sb_2S_3*	U_2Se_3 *Sb_2S_3*	
		U_3Se_4 *Th_3P_4*	U_3Te_4 *Th_3P_4*
UO NaCl	US *NaCl*	USe *NaCl*	UTe *NaCl*

crystallographic direction is shown in Figure 3.3. Finally, the disulfide phase is isostructural with the common $PbCl_2$ structure type.[36] The thorium atoms in ThS_2 are coordinated to nine sulfur atoms in a tricapped trigonal prismatic geometry. Figure 3.4 contains a view of ThS_2 down the [001] crystallographic direction.

The thorium-selenide system is also well developed and is identical to the sulfide system. Five thorium selenides have been characterized and are reported to be isostructural with their sulfur analogs.

The thorium-telluride system, however, differs in many respects from the sulfide and selenide systems. Four phases have been identified with Te/Th ratios ranging from 1.0 in ThTe, to 3.0 in $ThTe_3$. The chalcogen rich phase, $ThTe_3$, is not found in the sulfur and selenium systems where the dichalcogenide is the highest order phase. The tritelluride has two-dimensional layered structure that is isostructural with $ZrSe_3$.[37] The zirconium triselenide structure is found in a number of lanthanide chalcogenide phases as well. The two-dimensional layers of the $ZrSe_3$ structure are composed of $ZrSe_7$ capped trigonal prisms that share triangular faces along the [010] direction. Figure 3.5 contains a view of $ZrSe_3$ down the [010] crystallographic direction. In the sulfide and selenide systems, ditelluride and sesquitelluride phases have been characterized. They are not, however, isostructural with their sulfide and selenide analogues. The ditelluride has a hexagonal structure, while the disulfide and diselenide phases have orthorhombic $PbCl_2$ structures. The sesquitelluride also has a hexagonal structure, whereas the sesquisulfide and sesquiselenide have orthorhombic Sb_2S_3 structures.[5] These two telluride phases need to be further characterized, all that is currently known about their structures is overall symmetry.

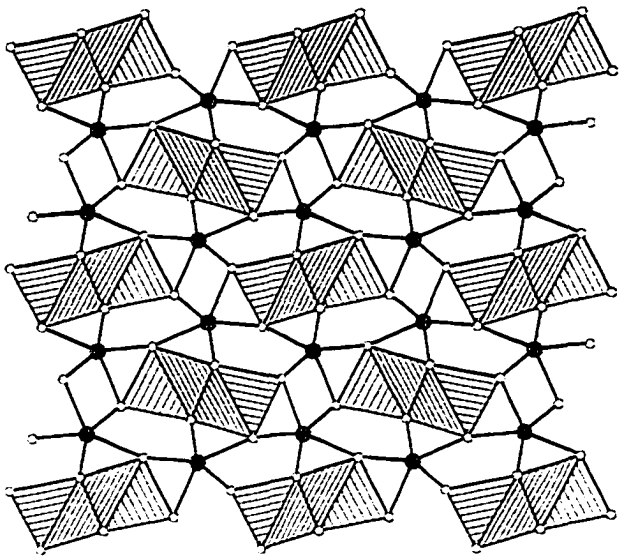

Figure 3.3. View of the sesquisulfide, Th_2S_3, down the [001] crystallographic direction. This compound is isostructural with Sb_2S_3. The structure contains slabs composed of Th(2)-Th(2) edge-sharing dimers in the *bc* plane. These slabs are then linked in the [100] direction by edge-sharing dimers composed on Th(1) polyhedra. Both thorium atoms are seven coordinate in capped trigonal prismatic geometries. The shaded circles are Th(1) atoms, the polyhedra are $Th(2)S_7$, and the unfilled circles are sulfur atoms.

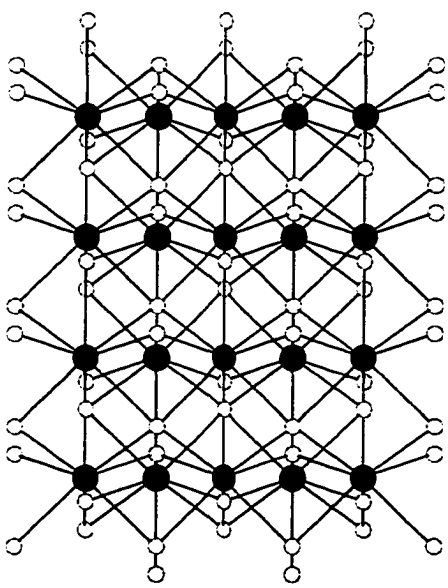

Figure 3.4. View of the ThS_2 structure down the [001] direction. ThS_2 has a three-dimensional structure that is isostructural with CaF_2. The thorium atoms are coordinated to nine sulfur atoms in a tricapped trigonal prismatic geometry. The filled circles are the thorium atoms and the unfilled circles are the sulfur atoms.

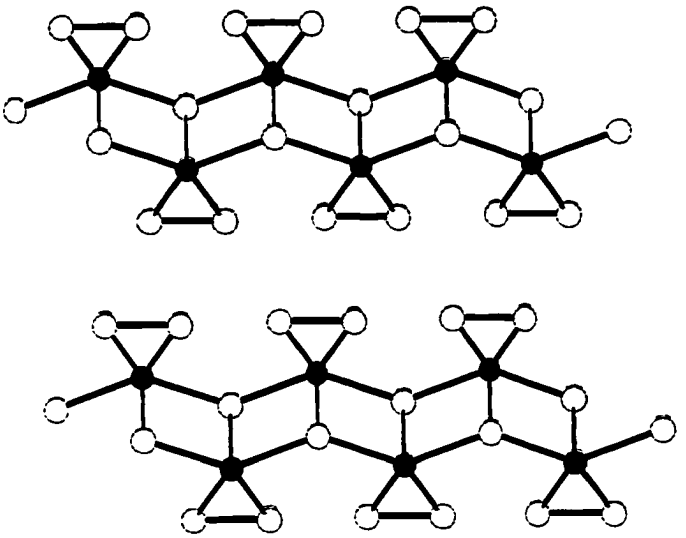

Figure 3.5. View of the two-dimensional layered compound $ZrSe_3$ down the [010] direction. The layers are composed of face and edge sharing $ZrSe_8$ bicapped trigonal prisms. Two edges of each trigonal prism are made up of $(Se_2)^{2-}$ dianions. The zirconium atoms are the filled circles and the selenium atoms are the unfilled circles.

The uranium-sulfur system is slightly more complex than the corresponding thorium system. Seven binary sulfides have been identified with S/U ratios ranging from 1.0 for US to 3.0 for US_3.[5] The trisulfide compound is isostructural with $ZrSe_3$ and $ThTe_3$. The uranium atoms in US_3 are tetravalent, not hexavalent, as one might assume if all sulfur atoms are taken to be dianions. Of the three sulfur atoms in US_3, one has a 2- charge but the other two are involved in intermediate range S-S bonding which gives them each a 1- charge. The same situation is found in $ThTe_3$, the thorium atoms are tetra- not hexavalent. One interesting phase, U_3S_5, is not found in any thorium chalcogenide system.[38] This compound has three-dimensional structure containing two crystallographically unique uranium atoms. One uranium atom is coordinated to seven sulfur atoms in a capped octahedral geometry and is tetravalent. The other uranium atom is coordinated to eight sulfur atoms in a bicapped trigonal prismatic geometry. The eight coordinate uranium atom is trivalent and occupies twice as many sites as the tetravalent seven coordinate uranium atom. All of the sulfur atoms have a 2- charge. Figure 3.6 contains a view of U_3S_5 down the [100] crystallographic direction. Another difference between the uranium-sulfur and thorium-sulfur systems in the presence of three different US_2 phases instead of just a single phase as is the case for thorium. The β-US_2 phase has a $PbCl_2$ structure like its thorium analogue. The alpha and gamma phases have a Fe_2B and a hexagonal structure, respectively.

The uranium-selenide system is nearly identical to the uranium-sulfide system. The main difference is the presence of an additional phase, U_3Se_4. This new phase has a common structure type, that of Th_3P_4.[39] A view of the Th_3P_4 structure type down the [100] crystallographic direction is shown in Figure 3.7. The uranium atoms in U_3Se_4 are

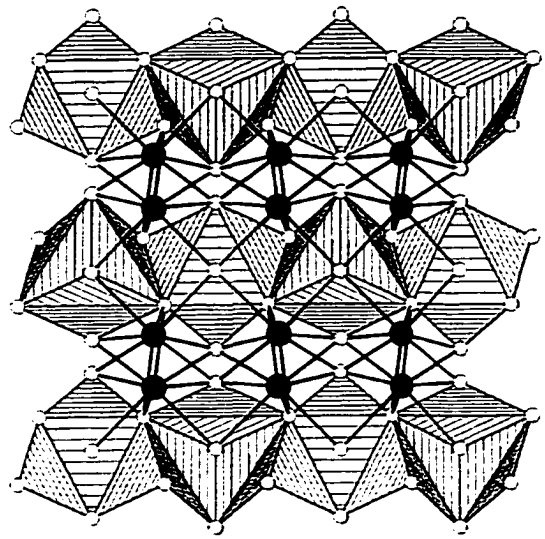

Figure 3.6. View of the three-dimensional, mixed valent U_3S_5 compound down the [100] direction. Rows of $U(2)S_7$ polyhedra lie in the *ab* plane and are linked together in the [001] direction through ribbons of $U(1)S_8$ polyhedra. The filled circles are the U(1) atoms, the polyhedra are $U(2)S_7$, and the unfilled circles are sulfur atoms.

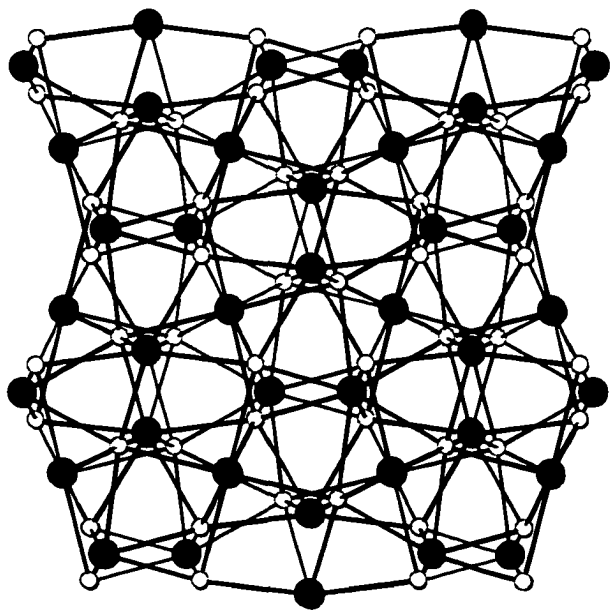

Figure 3.7. View of the Th_3P_4 structure down the [100] crystallographic direction. The filled circles are the Th atoms and the unfilled circles are the P atoms.

tetravalent. One ternary selenide compound has been characterized by Kanatzidis and co-workers and has the formula K_4USe_8.[33] This compound has a molecular structure consisting of isolated USe_8 dodecahedra. The selenium atoms in the structure are present as $(Se_2)^{2-}$ anions that bind to uranium in an η^2 fashion. Figure 3.8 contains a view of K_4USe_8.

The uranium-telluride system is more complex than the corresponding thorium system.[5] Eight binary uranium tellurides have been identified though some require further structural characterization. These phases have U:Te ratios ranging from 1.0, in UTe, to 5.0 in UTe_5. A crystal structure for the chalcogen-rich phase, UTe_5, is not currently known. The most chalcogen rich telluride that has been well characterized is UTe_3, which is isostructural with $ZrSe_3$.

Thorium and Uranium Phosphates

Recently, a great deal of interest has been expressed in the chemistry of actinide phosphates as potential storage forms for radioactive waste. The reason for this is that many thorium and uranium phosphates occur in nature and all are highly stable, robust materials.

Monazite sands are currently the source of most of the world's thorium.[25] Monazite is a rare earth phosphate mineral with the formula $RE(PO_4)$ where RE = Ce, La, or Nd. Thorium is capable of substituting for one or more of the rare-earth atoms. Because thorium is tetravalent and is substituted for a trivalent cation, a charge imbalance occurs. This can be rectified in many cases by the substitution of $(PO_4)^{3-}$ anions for

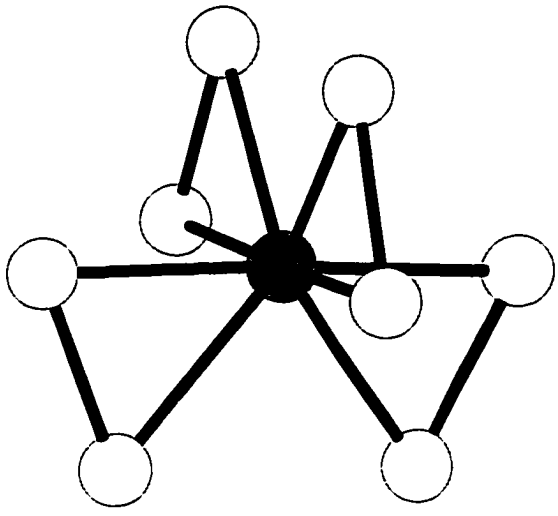

Figure 3.8. View of the molecular K_4USe_8 compound. The U atom is coordinated by eight selenium atoms in a dodecahedral geometry. The filled circle is the U atom and the unfilled circles are Se atoms. The K atoms are removed for clarity.

$(SiO_4)^{4-}$ anions. A theoretical formula for such a mineral could be $CeTh(PO_4)(SiO_4)$. Figure 3.9 contains a view of the monazite structure.[40]

For uranium, the most commercially viable minerals are uranium oxides, though some uranium phosphates are found in nature.[25] Autunite is one such mineral and has the chemical formula, $Ca(UO_2)_2(PO_4)_2$. A view of the autunite structure is shown in Figure 3.10.[41] Torbernite is another uranium phosphate mineral and has the formula, $Cu(UO_2)_2(PO_4)_2$.

All of the above minerals contain only $(PO_4)^{3-}$ ligands. Researchers in the area of actinide phosphates have synthesized numerous thorium and uranium phosphates with more complex structures. These compounds contain ligands such as $(P_2O_7)^{4-}$, $(P_3O_{10})^{5-}$, and other large polymeric anions based on corner-sharing phosphate tetrahedra. The compound $KThP_3O_{10}$ has a three-dimensional structure consisting of ThO_8 square anti-prisms linked together solely through $(P_3O_{10})^{5-}$ ligands.[42] A view of $KThP_3O_{10}$ is shown in Figure 3.11. Another interesting compound, $(UO_2)_2(P_6O_{17})$, has a two-dimensional layered structure contain uranium atoms coordinated to seven oxygen atoms in a pentagonal bipyramidal geometry.[43] The uranium polyhedra are linked into layers through a network of interconnected PO_4 tetrahedra. The tetrahedra form the network in the *ac* plane by corner-sharing with one another. Figure 3.12 contains a view of $(UO_2)_2(P_6O_{17})$ down the [100] crystallographic direction.

Known Quaternary Thorium and Uranium Chalcophosphates

Five quaternary actinide chalcophosphates were characterized prior to this research and are listed in Table 3.3. All of them are selenophosphates. The three

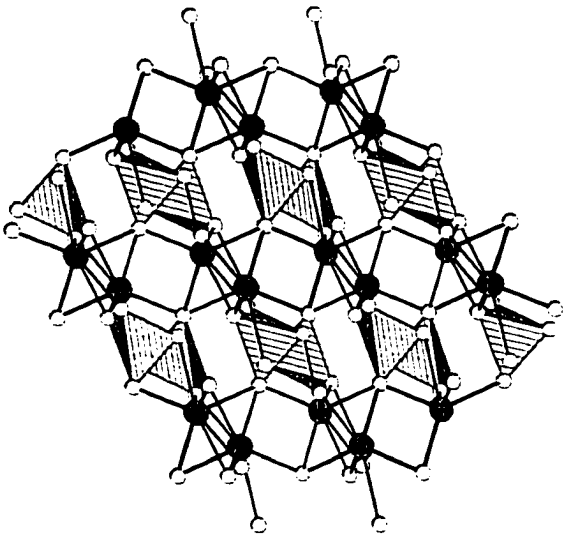

Figure 3.9. View of the monazite, $CePO_4$, structure down the [010] direction. Monazite has a three-dimensional structure consisting of rows of CeO_8 dodecaheda that are linked together through $(PO_4)^{3-}$ ligands. The polyhedra are $(PO_4)^{3-}$ ligands, the filled circles are Ce atoms, and the unfilled circles are O atoms.

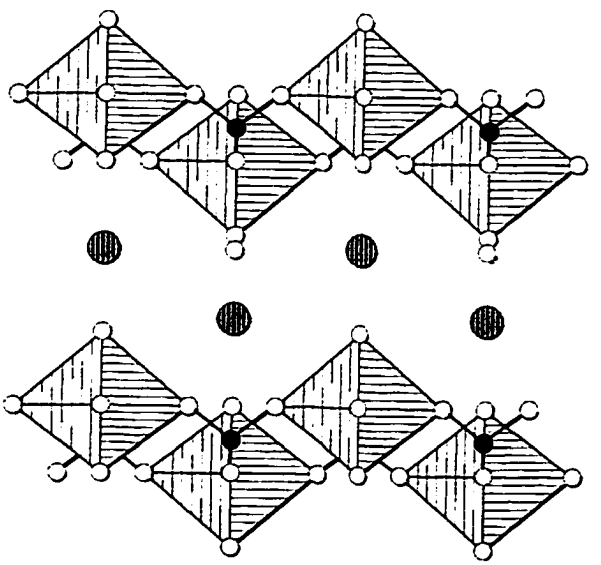

Figure 3.10. View of the autunite, $Ca(UO_2)_2(PO_4)_2$, structure down the [100] direction. This two-dimensional compound is composed of UO_6 octahedra linked together through $(PO_4)^{3-}$ ligands to form layers in the *ab* plane. The Ca^{2+} cations lie in the inter-layer space. The polyhedra are UO_6, the filled circles are P atoms, the Ca^{2+} ions are the shaded circles, and the unfilled circles are O atoms.

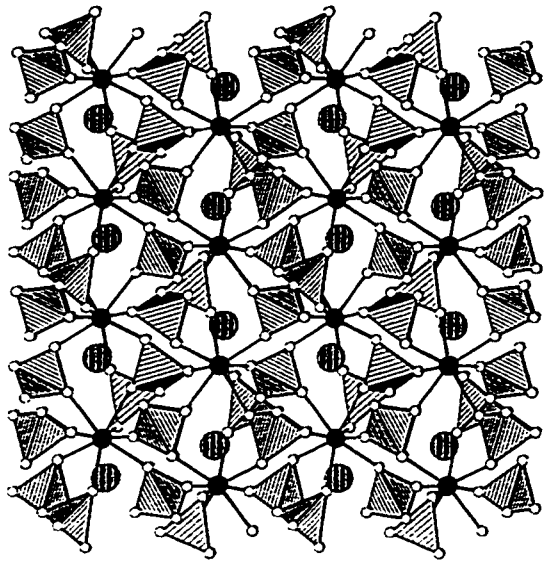

Figure 3.11. View of the $KThP_3O_{10}$ structure down the [100] crystallographic direction. In this view one can see the chains of $(P_3O_{10})^{5-}$ ligands running along the [001] direction. The filled circles are the Th atoms, the unfilled circles are the O atoms, and the polyhedra are the $(P_3O_{10})^{5-}$ ligands.

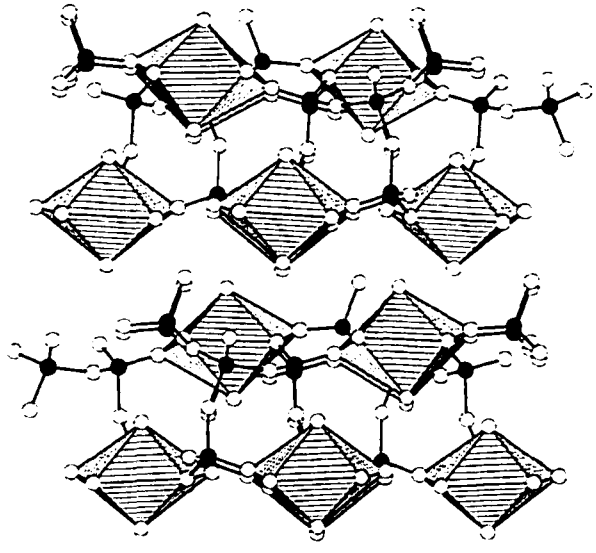

Figure 3.12. View of the $(UO_2)_2(P_6O_{17})$ structure down the [100] direction. The polymeric phosphate ligands link UO_7 polyhedra in the *ac* plane forming a layered structure. The polyhedra are UO_7, the filled circles are the P atoms, and the unfilled circles are the O atoms.

Table 3.3. List of known quaternary actinide chalcophosphates and their structures.

Compound	Structure
$K_2UP_3Se_9$	Two-dimensional layers
$A_2ThP_3Se_9$ (A = K, Rb)	Two-dimensional layers
$Cs_4Th_2P_5Se_{17}$	One-dimensional ribbons
$Rb_4U_4P_4Se_{26}$	Three-dimensional network
$Cs_4Th_4P_4Se_{26}$	Three-dimensional network

compounds, $K_2UP_3Se_9$, $K_2ThP_3Se_9$, and $Rb_2ThP_3Se_9$ are isostructural.[15,32] The uranium compound was characterized by Kanatzidis and co-workers while the thorium compounds were characterized by Briggs-Piccoli, Dorhout and co-workers. Because they are isostructural, only $K_2ThP_3Se_9$ will be described. This compound has a two-dimensional layered structure containing two crystallographically unique thorium atoms.[15] Both thorium atoms are coordinated to nine selenium atoms in a tricapped trigonal prismatic geometry. A view of $K_2ThP_3Se_9$ is shown in Figure 3.13. The two $ThSe_9$ polyhedra face-share with each other forming $[Th_2Se_{14}]$ dimers. The dimers then corner-share with neighboring dimers to form chains along the [001] direction. These chains are then linked into layers via ethane-like $(P_2Se_6)^{4-}$ ligands.

The thorium compound, $Cs_4Th_2P_5Se_{17}$, has a one-dimensional structure containing two crystallographically unique thorium atoms.[15] One thorium atom is coordinated to eight sulfur atoms in a bicapped trigonal prismatic geometry. The other thorium atom is coordinated to nine sulfur atoms but is still arranged in a bicapped trigonal prism as two of the selenium atoms form a $(Se_2)^{2-}$ ligand and only occupy one coordination site. Figure 3.14 contains a view of $Cs_4Th_2P_5Se_{17}$ down the [100] crystallographic direction. As in the $K_2ThP_3Se_9$ structure, the two thorium atoms face-share with one another forming dimers. These dimers then corner-share with neighboring dimers, and with the assistance of $(P_2Se_6)^{4-}$ ligands, form chains along the [100] direction. In this compound there is no cross-linking of the chains to form layers.

The remaining quaternary actinide chalcophosphates are $Rb_4U_4P_4Se_{26}$ and $Cs_4Th_4P_4Se_{26}$.[24,44] These two compounds are isostructural but have been described differently in the literature. The overall structure will be described in terms of the

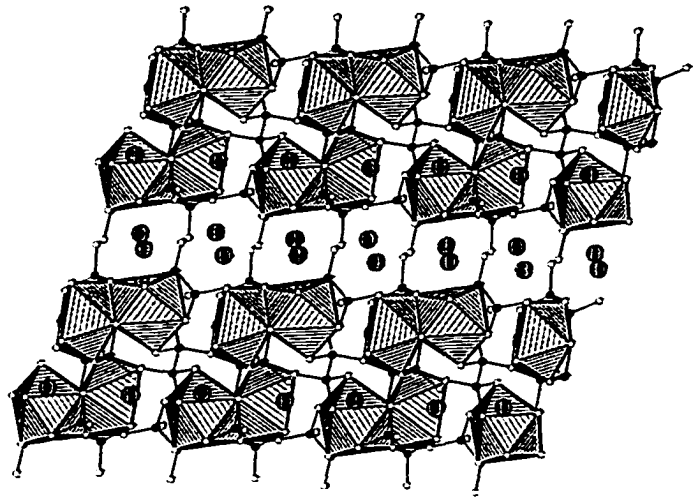

Figure 3.13. View of the $K_2ThP_3Se_9$ structure down the [100] direction. This compound has a two-dimensional structure consisting of layers of $ThSe_9$ tricapped trigonal prisms. The chains of thorium dimers can be seen running along the [100] direction. The chains are linked together to form layers via $(P_2Se_6)^{4-}$ ligands. The polyhedra are $ThSe_9$, the filled circles are P atoms, the unfilled circles are Se atoms, and the shaded circles are K^+ atoms.

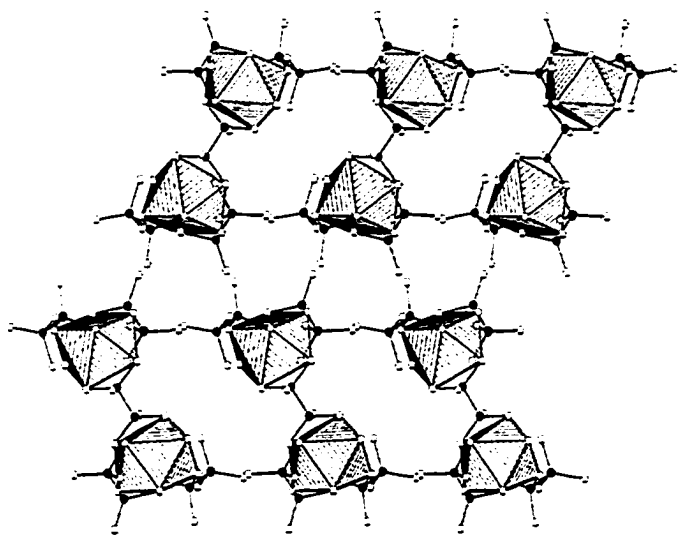

Figure 3.14. View of the $Cs_4Th_2P_5Se_{17}$ structure down the [100] crystallographic direction. This compound has a one-dimensional structure composed of dumbbell-like ribbons. Unlike $K_2ThP_3Se_9$ this ribbons in this structure are not linked together to form layers. The polyhedra of $ThSe_9$, the filled circles are P atoms, and the unfilled circles are Se atoms. The Cs^+ cations have been removed for clarity.

thorium phase. Figure 3.15 contains a view of $Cs_4Th_4P_4Se_{26}$.[24] This compound has a three-dimensional structure containing two crystallographically unique thorium atoms. Both thorium atoms are coordinated to nine selenium atoms in a tricapped trigonal prismatic geometry. The thorium polyhedra form dimers via face-sharing with one another and through $(Se_2)^{2-}$ ligands. The dimers edge-share with neighboring dimers forming chains along the [010] direction. These chains are then linked together in all three directions via $[P_2Se_9]^{6-}$ ligands. The $[P_2Se_9]^{6-}$ ligand consists of two PSe_4 tetrahedra that are linked together through an additional Se atom forming a Se_3 chain between the two phosphorous atoms. The Se-Se bond distances in this chain are relatively long but are still much shorter than the van der Waals contact for selenium (2.64 Å versus 3.80 Å). The angle along this Se chain is nearly linear at 171°. This implies the presence of three lone pairs on the central Se atom. Another way to write the formula for the thorium compound would be $[Cs_4Th_2(P_2Se_9)(Se_2)_2]_2$. Charge balancing this formula using $(P_2Se_9)^{6-}$ and $(Se_2)^{2-}$ places thorium in the 4+ oxidation state. This is by far the most reasonable oxidation state for thorium.

It is in the description of the selenophosphate ligand that the description of the two compounds differs. In the uranium phase the authors described the selenophosphate ligand as two separate $(PSe_4)^{3-}$ ligands and an isolated Se^{2-}.[45] Based on this description, and on magnetic and spectroscopic data, they stated uranium was in the 5+ oxidation state. As stated above, the Se-Se distance between the atoms in the selenium chain are too close together for the central selenium atom to be a truly isolated dianions. Also, magnetic data of actinide compounds is very difficult to interpret unambiguously. While pentavalent uranium complexes are known, they are exceedingly rare. Based on the

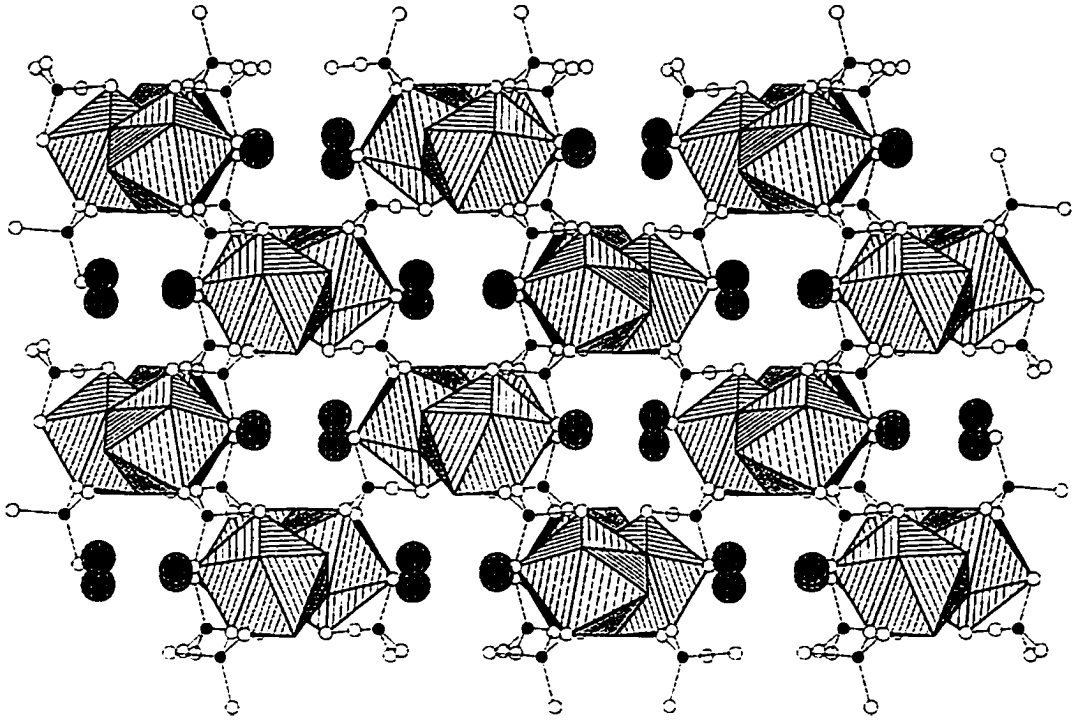

Figure 3.15. View of the $Cs_4Th_4P_4Se_{26}$ structure down the [010] direction. This compound has a three-dimensional structure that consists of chains of $ThSe_9$ polyhedra running along the [010] direction. These chains are linked together in three directions through $(P_2Se_9)^{6-}$ ligands. The polyhedra are $ThSe_9$ tricapped trigonal prisms, the filled circles are P atoms, the unfilled circles are Se atoms, and the shaded circles are Cs^+ cations.

characterization of the isostructural thorium compound, and given that Th^{5+} would be nearly impossible to form, it is more likely that the uranium atoms in $Rb_4U_4P_4Se_{26}$ are pentavalent.

Experimental

General Synthesis. Red phosphorous powder (99.9%) was obtained from Cerac. Selenium shot (99.999%) was purchased from Johnson Matthey. ^{232}Th ribbon was obtained from Los Alamos National Laboratory. ^{238}U turnings (99.7%) were obtained from Cerac. A_2S_2 and A_2S_5 (A = K, Rb, Cs) were prepared from a stoichiometric ratio of the elements in liquid ammonia as described elsewhere.[46] *N,N* – dimethylformamide (DMF) was obtained from Aldrich and used without further purification. Ampoules for the reactions were all fused-silica tubes with 4 mm inner diameter and a 6 mm outer diameter. All reagents were stored and manipulated in a helium filled glovebox. *Warning: ^{232}Th and ^{238}U are radioactive elements with half-lives of 1.41 x 10^{10} years and 4.47 x 10^9 years respectively. Although their own activity is low, the inevitable daughter products of decay can render samples highly radioactive over time (gamma).*

Synthesis of $Cs_8U_5(P_3S_{10})_2(PS_4)_6$, I: $Cs_8U_5(P_3S_{10})_2(PS_4)_6$ was synthesized from a mixture of 0.0248 (0.34 mmol) U, 0.0129g (1.15 mmol) P, 0.0251g (3.27 mmol) S, 0.0666g (0.710 mmol) Cs_2S_5. The mixture was loaded into a fused silica ampoule and sealed under vacuum. The ampoule was then heated to 750 °C over 16 hours and held there for 100 hours. The ampoule was cooled to ambient temperature at a rate of 4 °C per hour. Excess flux was removed by washing with DMF. Amber rods were then isolated by filtration and selected crystals were hand-picked for analysis.

Synthesis of $K_{10}Th_3(P_2S_7)_4(PS_4)_2$, II: $K_{10}Th_3(P_2S_7)_4(PS_4)_2$ was synthesized from a mixture of 0.084g (0.36 mmol) Th, 0.0379g (1.22 mmol) P, 0.0447g (1.39 mmol) S, 0.1805g (0.760 mmol) K_2S_5. The mixture was loaded into a fused silica ampoule and sealed under vacuum. The ampoule was then heated to 500 °C over 16 h and held there for 288 h. The ampoule was cooled to ambient temperature at a rate of 3 °C/h. Excess flux was removed by washing with DMF. Colorless rods were then isolated by filtration and selected crystals were hand-picked for analysis.

Synthesis of $K_5U(PS_4)_3$, III: $K_5U(PS_4)_3$ was synthesized from a mixture of 0.1041 (0.34 mmol) U, 0.0305g (1.15 mmol) P, 0.1713g (3.27 mmol) S, 0.0994g (0.710 mmol) K_2S_2. The mixture was loaded into a fused silica ampoule and sealed under vacuum. The ampoule was then heated to 500 °C over 16 hours and held there for 288 hours. The ampoule was cooled to ambient temperature at a rate of 3 °C per hour. Excess flux was removed by washing with DMF. Amber plates were then isolated by filtration and selected crystals were hand-picked for analysis.

Synthesis of $K_5Th(PS_4)_3$, IV: $K_5Th(PS_4)_3$ was synthesized from a mixture of 0.0626 (0.27 mmol) Th, 0.0252g (0.81 mmol) P, 0.0846g (2.64 mmol) S, 0.0812g (0.57 mmol) K_2S_2. The mixture was loaded into a fused silica ampoule and sealed under vacuum. The ampoule was then heated to 500 °C over 16 h and held there for 288 h. The ampoule was cooled to ambient temperature at a rate of 3 °C/h. Excess flux was removed by washing with DMF. Colorless irregular-shaped crystals were then isolated by filtration and selected crystals were hand-picked for analysis.

Synthesis of $Rb_5Th(PS_4)_3$, V: $Rb_5Th(PS_4)_3$ was synthesized from a mixture of 0.0779 (0.34 mmol) Th, 0.0356g (1.15 mmol) P, 0.1047g (3.27 mmol) S, 0.1665g (0.710

mmol) Rb_2S_2. The mixture was loaded into a fused silica ampoule and sealed under vacuum. The ampoule was then heated to 500 °C over 16 h and held there for 288 h. The ampoule was cooled to ambient temperature at a rate of 3 °C/h. Excess flux was removed by washing with DMF. Colorless rods were then isolated by filtration and selected crystals were hand-picked for analysis.

Synthesis of $Cs_5Th(PS_4)_3$, VI: $Cs_5Th(PS_4)_3$ was synthesized from a mixture of 0.0619g (0.34 mmol) Th, 0.0299g (1.15 mmol) P, 0.0320g (3.27 mmol) S, 0.2320g (0.710 mmol) Cs_2S_5. The mixture was loaded into a fused silica ampoule and sealed under vacuum. The ampoule was then heated to 500 °C over 16 hours and held there for 288 hours. The ampoule was cooled to ambient temperature at a rate of 3 °C per hour. Excess flux was removed by washing with DMF. Translucent, slightly green-tinted polyhedral cyrstals were then isolated by filtration and selected crystals were hand-picked for analysis.

Synthesis of $Cs_4Th_2(P_2S_6)_3$, VII: $Cs_4Th_2(P_2S_6)_3$ was synthesized from a mixture of 0.0590g (0.254 mmol) Th, 0.0473g (1.52 mmol) P, 0.0571g (1.77 mmol) S, 0.217g (0.500 mmol) Cs_2S_5. The mixture was loaded into a fused silica ampoule and sealed under vacuum. The ampoule was then heated to 500 °C over 16 hours and held there for 288 hours. The ampoule was cooled to ambient temperature at a rate of 3 °C per hour. Excess flux was removed by washing with DMF. Colorless chunks were then isolated by hand.

Synthesis of $U(P_2S_6)_2$, VIII: $U(P_2S_6)_2$ was synthesized from a mixture of 0.0632g (0.266 mmol) U, 0.0411g (1.36 mmol) P, 0.0937g (2.93 mmol) S. The mixture was loaded into a fused silica ampoule and sealed under vacuum. The ampoule was then

heated to 500 °C over 16 hours and held there for 200 hours. The ampoule was cooled to ambient temperature at a rate of 3 °C per hour. Colorless chunks were then isolated by hand.

Physical Characterization. Single-crystal X-ray diffraction was performed on a modified Siemens P4 four-circle diffractometer equipped with a SMART CCD system detector or a Siemens SMART CCD system using graphite-monochromated Mo Kα radiation. Elemental analysis confirming the stoichiometries of the compounds was obtained from Energy Dispersive Spectroscopy on a Philips 505 scanning electron microscope system equipped with a Kevex Analyst 8000 microanalyzer. UV-visible-NIR spectra were recorded as diffuse reflectance spectra using a Cary 500 spectrometer equipped with praying-mantis reflectance focusing optics. The data were evaluated using the Kubelka-Munk relationship for diffuse reflectance data.[47] Only the data for the uranium compounds are shown. Raman spectra were recorded on a home-built optical bench using an Acton Research Spectra Pro-275 LN_2-cooled CCD detector (256 x 1024) using a controller model ST130 and a 50 mW HeNe laser line at 632.8 nm.

Structure Determination. Crystals were selected from the reaction mixtures and mounted in grease and placed directly into the cold stream of the diffractometer on a glass fiber with the long axis of the crystals oriented roughly parallel to the length of the fiber. Cell constants for all structures were initially calculated from reflections taken from approximately 30 frames of reflections. Final cell constants were calculated from all reflections observed in the actual data collection. Table 3.4 summarizes the crystal structure parameters for compounds **I-VIII**. For each structure, the data were processed and corrected for absorption using SADABS.[48] The structures were solved by direct

Table 3.4. Crystallographic Data for Compounds **I** through **VIII.**

	I	II	III	IV
Empirical Formula	$Cs_4U_{2.5}P_6S_{22}$	$K_5Th_{1.5}P_5S_{18}$	$K_5UP_3S_{12}$	$K_5ThP_3S_{12}$
fw	2017.85	1275.49	911.16	905.17
a, Å	33.2897(1)	32.8085(6)	14.6132(1)	9.7436(1)
b, Å	14.9295(1)	9.0482(2)	17.0884(2)	11.3894(2)
c, Å	17.3528(2)	27.2972(3)	9.7082(1)	20.0163(3)
β, deg	115.478(1)	125.720(1)	108.63(1)	90.041(1)
V, Å^3	7785.6(1)	6579.0(2)	2297.31(4)	2221.28(6)
Z	8	8	4	4
λ(Mo Kα),Å	0.71073	0.71073	0.71073	0.71073
space group	$P2_1/c$ (14)	C2/c (15)	$P2_1/c$ (14)	$P2_1/n$ (14)
temp., K	163(2)	163(2)	163(2)	163(2)
$\rho_{calc.}$, g/cm^3	3.443	2.575	2.634	2.707
μ, mm^{-1}	15.50	8.80	9.26	8.98
R1 % [a]	0.0590	0.0346	0.0376	0.0363
wR2 % [a]	0.1156	0.0714	0.0744	0.0780

	V	VI	VII	VIII
Empirical Formula	$Rb_5ThP_3S_{12}$	$Cs_5ThP_3S_{12}$	$Cs_4Th_2P_6S_{18}$	UP_4S_{12}
fw	1137.02	1374.22	879.31	746.63
a, Å	13.197(4)	13.5624(1)	12.303(4)	12.840(4)
b, Å	9.997(4)	10.3007(1)	12.471(4)	12.840(4)
c, Å	18.189(7)	18.6738(1)	12.541(4)	9.779(4)
α, deg	90	90	114.607(8)	90
β, deg	100.77(1)	100.670(1)	102.547(6)	90
γ ,deg	90	90	99.889(7)	90
V, Å^3	2357(2)	2563.66(3)	1631.5(9)	1615.5(10)
Z	4	4	1	4
λ(Mo Kα),Å	0.71073	0.71073	0.71073	0.71073
space group	$P2_1/c$ (14)	$P2_1/c$ (14)	P –1 (No. 2)	$I4/_1a$ (No.88)
temp., K	163(2)	163(2)	163(2)	163(2)
$\rho_{calc.}$, g/cm^3	3.204	3.560	3.580	3.070
μ, mm^{-1}	17.84	13.97	14.95	11.96
R1 % [a]	0.0501	0.0452	0.0421	0.0966
wR2 % [a]	0.1111	0.1182	0.0952	0.1929

methods allowing the unambiguous space group assignments, and refined in full-matrix least-squares using the program SHELXTL[49] under the XSHELL package of programs.[50] For nearly every case, the final cycle of refinement included all anisotropic displacement parameters. Secondary extinction coefficients were applied to the final refinements. Additional experimental details are given in the supporting information found in Appendix D. Specific refinement issues related to each structure are explained in the Results and Discussion section.

The Structure of $Cs_8U_5(P_3S_{10})_2(PS_4)_6$

The compound was isolated from the flux of the reaction by dissolution of the flux in DMF. Amber rod-like crystals were isolated by filtration and by hand sorting from undissolved flux. Table 3.4 lists specifics about the data collection and refinement. For the 19,869 reflections collected, the space group $P2_1/c$ was selected (R_{int} = 0.097) based on systematic absences. Refinement of the model's 313 parameters to the data (9153 reflections) provided an excellent goodness-of-fit resulting in a relatively flat electron density difference map (max. = 2.728 $e^-/Å^3$, min. = -1.960 $e^-/Å^3$). Table 3.5 lists the atomic coordinates and Table 3.6 lists relevant bond distances.

Figure 3.16 shows a polyhedral view of the structure down the [-10-1] axis. This compound has a three dimensional network structure built up of US_8 polyhedra and two different types of thiophosphate ligands, $[PS_4]^{3-}$ and the previously unknown $[P_3S_{10}]^{5-}$, a unit comprising three corner-sharing PS_4-tetrahedra. Three crystallographically distinct uranium atoms are found in the structure as US_8 bi-capped trigonal prisms with an average U–S bond distance of 2.85(1) Å, distances comparable to uranium sulfide binary compounds. From Figure 3.16, one can see that the structure comprises layers bridged by

Table 3.5. Fractional Atomic Coordinates and Equivalent Isotropic Displacement Parameters ($Å^2$ x 10^3)[a] for $Cs_8U_5(P_3S_{10})_2(PS_4)_6$, **I.**

	x	y	z	U(eq)
U(1)	0.0000	0.4182(1)	0.2500	12(1)
U(2)	0.0647(1)	0.1648(1)	0.3708(1)	11(1)
U(3)	-0.1585(1)	-0.2452(1)	0.1448(1)	12(1)
P(1)	0.1097(1)	-0.0399(3)	0.3649(3)	12(1)
P(2)	-0.0840(1)	-0.4267(3)	0.1907(2)	14(1)
P(3)	0.0459(1)	0.2487(3)	0.1568(2)	12(1)
P(4)	0.2494(1)	0.2396(3	0.3284(3)	17(1)
P(5)	0.1369(1)	0.2172(3)	0.5834(2)	12(1)
P(6)	-0.2330(1)	-0.2944(3)	-0.1169(2)	13(1)
S(1)	0.0777(1)	0.3107(3	0.2744(2)	13(1)
S(2)	0.0390(1)	0.5424(3)	0.1869(2)	18(1)
S(3)	0.0723(1)	0.4886(3)	0.3891(2)	18(1)
S(4)	0.0160(1)	0.3111(3)	0.4026(2)	13(1)
S(5)	0.0944(1)	0.1103(3)	0.5404(2)	15(1)
S(6)	0.0297(1)	0.1229(3)	0.1854(2)	15(1)
S(7)	0.1269(1)	0.2925(3)	0.4795(2)	16(1)
S(8)	0.1391(1)	0.0840(3)	0.3756(2)	16(1)
S(9)	0.0478(1)	-0.0183(3)	0.3597(3)	16(1)
S(10)	-0.1291(1)	-0.2912(3)	0.3261(2)	15(1)
S(11)	-0.2425(1)	-0.3245(3)	0.1034(3)	18(1)
S(12)	-0.0743(1)	-0.2966(3)	0.1668(3)	17(1)
S(13)	-0.1467(2)	-0.1206(3)	0.0353(2)	19(1)
S(14)	-0.1058(1)	-0.1015(3)	0.2429(2)	13(1)
S(15)	-0.1786(1)	-0.3390(3)	-0.0164(2)	19(1)
S(16)	-0.2159(1)	-0.1179(3)	0.1580(3)	17(1)
S(17)	-0.1475(1)	-0.4350(3)	0.1762(3)	17(1)
S(18)	0.0800(1)	-0.2491(3)	0.5887(2)	18(1)
S(19)	0.2002(1	-0.1562(3)	0.1281(3)	16(1)
S(20)	0.2719(2)	0.1201(3)	0.3225(3)	22(1)
S(21)	0.2049(1)	0.2909(3)	0.2059(2)	16(1)
S(22)	0.2901(2)	-0.2449(3)	0.1152(3)	23(1)
Cs(1)	-0.0126(1)	-0.2209(1)	0.3882(1)	23(1)
Cs(2)	0.1574(1)	0.0680(1)	0.1819(1)	23(1)
Cs(3)	0.3743(1)	0.0193(1)	-0.1161(1)	26(1)
Cs(4)	0.2574(1)	-0.0446(1)	0.0054(1)	25(1)

[a] U(eq) is defined as one third of the trace of the orthogonalized U_{ij} tensor.

Table 3.6. Selected Bond Distances (Å) for $Cs_8U_5(P_3S_{10})_2(PS_4)_6$, **I.**

U(1)-S(2)	2.747(4)	P(1)-S(13)	2.032(6)
U(1)-S(3)	2.780(4)	P(1)-S(14)	2.038(6)
U(1)-S(1)	2.915(4)	P(1)-S(9)	2.048(6)
U(1)-S(4)	2.939(4)	P(1)-S(8)	2.063(6)
U(2)-S(8)	2.725(4)	P(2)-S(3)	2.033(6)
U(2)-S(9)	2.781(4)	P(2)-S(2)	2.058(6)
U(2)-S(5)	2.792(4)	P(2)-S(17)	2.022(6)
U(2)-S(7)	2.849(4)	P(2)-S(12)	2.041(6)
U(2)-S(1)	2.891(4)	P(3)-S(18)	1.961(6)
U(2)-S(4)	2.910(4)	P(3)-S(4)	2.084(6)
U(2)-S(6)	2.928(4)	P(3)-S(1)	2.069(6)
U(2)-S(6)	2.980(4)	P(3)-S(6)	2.073(6)
U(3)-S(12)	2.772(4)	P(4)-S(20)	1.954(6)
U(3)-S(16)	2.773(4)	P(4)-S(22)	1.961(6)
U(3)-S(13)	2.804(4)	P(4)-S(21)	2.142(6)
U(3)-S(11)	2.829(4)	P(4)-S(19)	2.171(6)
U(3)-S(14)	2.831(4)		
U(3)-S(17)	2.880(4)		
U(3)-S(15)	2.937(4)		
U(3)-S(10)	2.946(4)		

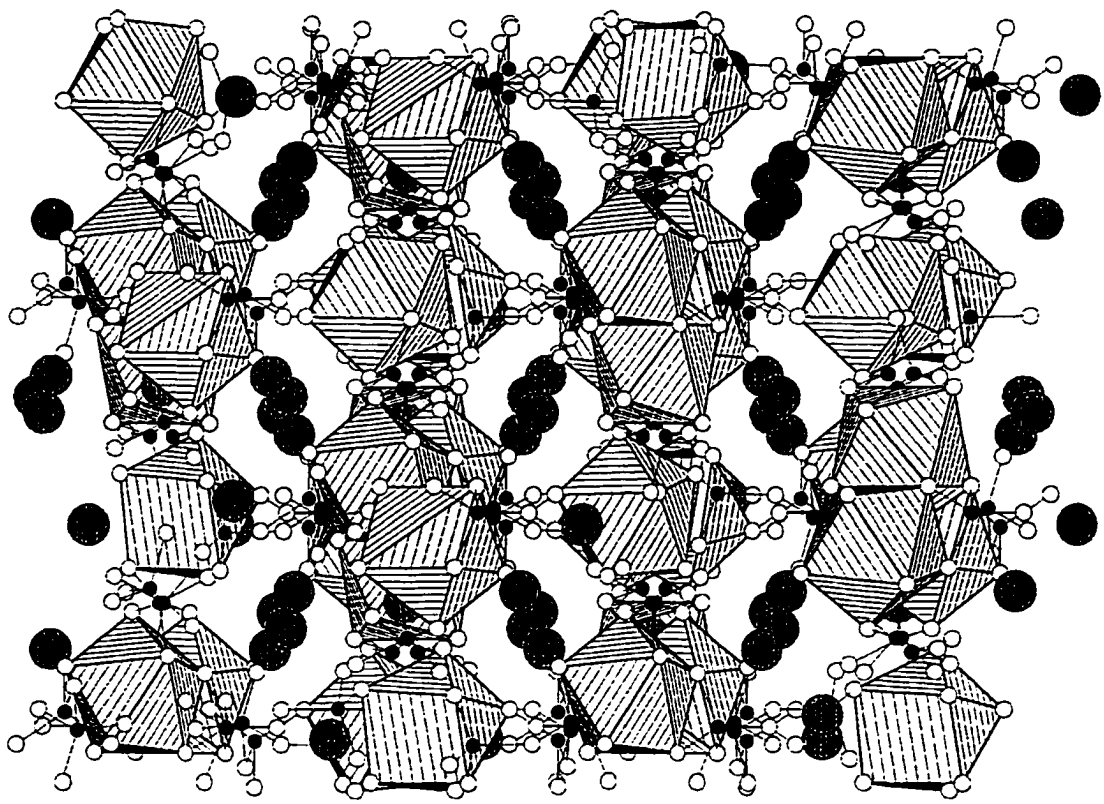

Figure 3.16. $Cs_8U_5(P_3S_{10})_2(PS_4)_6$, **I**, as viewed down [-10-1]. Polyhedra are US_8, cesium atoms are shaded, phosphorous are filled, and sulfur are open circles.

thiophosphate groups. A view of one such layer is seen in Figure 3.17. In this view, one can easily distinguish the two types of thiophosphate polyhedra, $[PS_4]$ and $[P_3S_{10}]$. It is also possible to recognize that the uranium atoms form trimeric units (U1 and two U2) and isolated atoms (U3). Figure 3.18 shows a thermal ellipsoid plot of the trimeric unit. In this trimer of U(1) and two U(2) atoms, one finds four sulfur atoms on each metal that are shared with the neighboring U atom. This edge sharing among the U(1) and U(2) polyhedra forms a trimer unit where two $[PS_4]^{3-}$ tetrahedra cap the top and bottom of the trimer. The fourth S atom of the $[PS_4]^{3-}$ tetrahedron is a terminal atom, coordinating only with Cs^+ counter cations. The cavity formed inside the trimer has the approximate dimensions: 4.85 Å x 4.83 Å x 5.32 Å and the closest U· · · U contact is 4.41(6) Å.

This trimer is the fundamental building block in this structure. Each individual trimer is linked to six U(3) polyhedra, two to U(1) and two to each U(2) polyhedra. It is through these U(3) polyhedra that the trimers are linked together to form a layer in the *ab* plane. The U(3) polyhedra are connected to the U(1) and U(2) polyhedra through two different thiophosphate tetrahedra, $[P(1)S_4]^{3-}$ and $[P(2)S_4]^{3-}$, seen in Figure 3.19. The U(3) polyhedra are also linked to each other via one end of the previously unknown $[P_3S_{10}]^{5-}$ ligand, as seen in the thermal ellipsoid plot, Figure 3.20. The $[P_3S_{10}]^{5-}$ unit effectively "chelates" one face of a U(3) atom while bridging U(2) and U(3) atoms and establishing connectivity along the *a* direction. There is sufficient twisting in the $[P_3S_{10}]^{5-}$ that it no longer resembles 3/4 of the $[P_4S_{12}]^{4-}$ ring that has been observed previously[51] or the $[P_4S_{10}]^{4-}$ cyclohexane-type thiophosphate.[52] The P(1) and P(2) tetrahedra both link to two U(3) polyhedra by sharing two of the thiophosphate-group

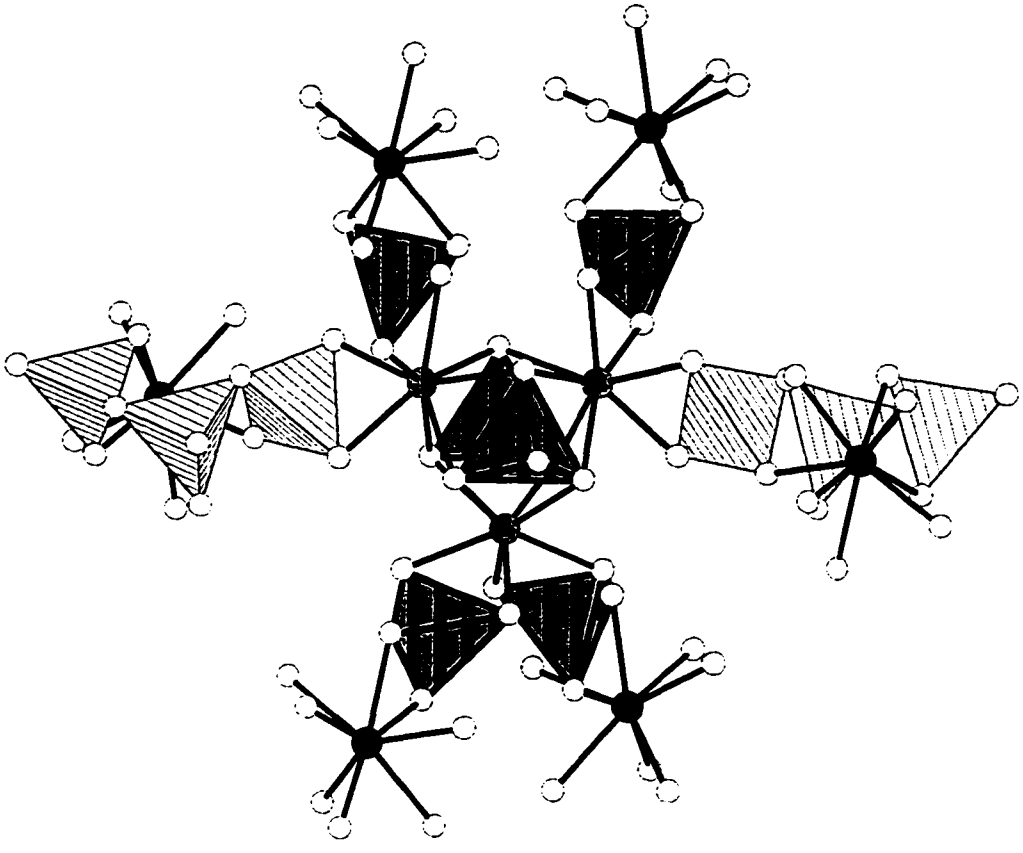

Figure 3.17. View of one layer in $Cs_8U_5(P_3S_{10})_2(PS_4)_6$, **I**, along [10-1] showing a U(1) and U(2) trimer (half-filled atoms) linked to six filled U(3) atoms by the $P_3S_{10}^{5-}$ units (thin striped tetrahedra). The PS_4^{3-} tetrahedra are the thick striped tetrahedra.

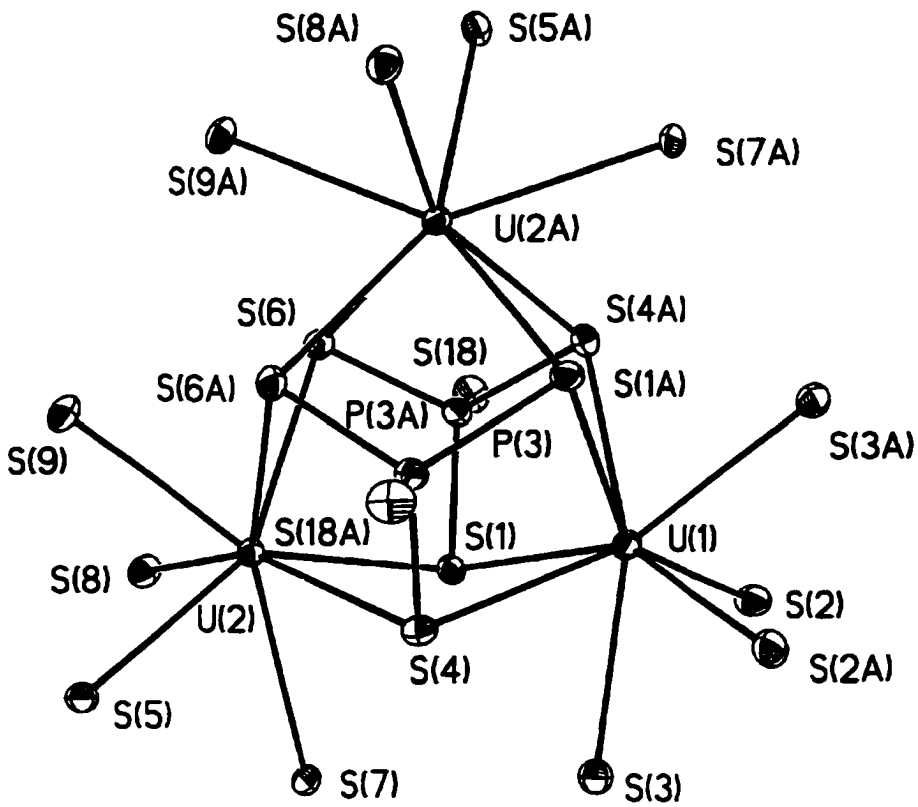

Figure 3.18. Thermal ellipsoid plot (50%) of the uranium trimer in $Cs_8U_5(P_3S_{10})_2(PS_4)_6$, I.

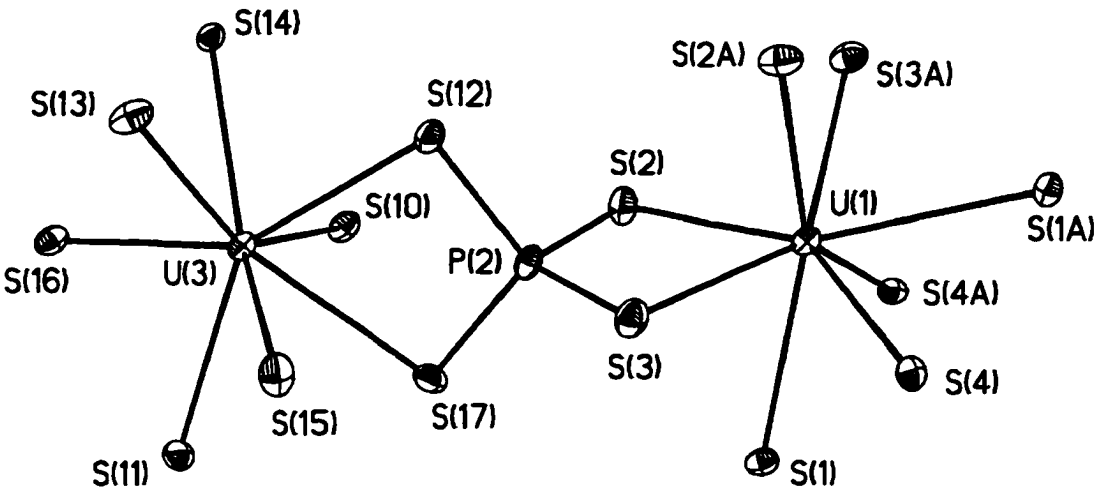

Figure 3.19. Thermal ellipsoid plot (50%) of the U(1)U(3) unit in $Cs_8U_5(P_3S_{10})_2(PS_4)_6$, **I**, showing the PS_4 link.

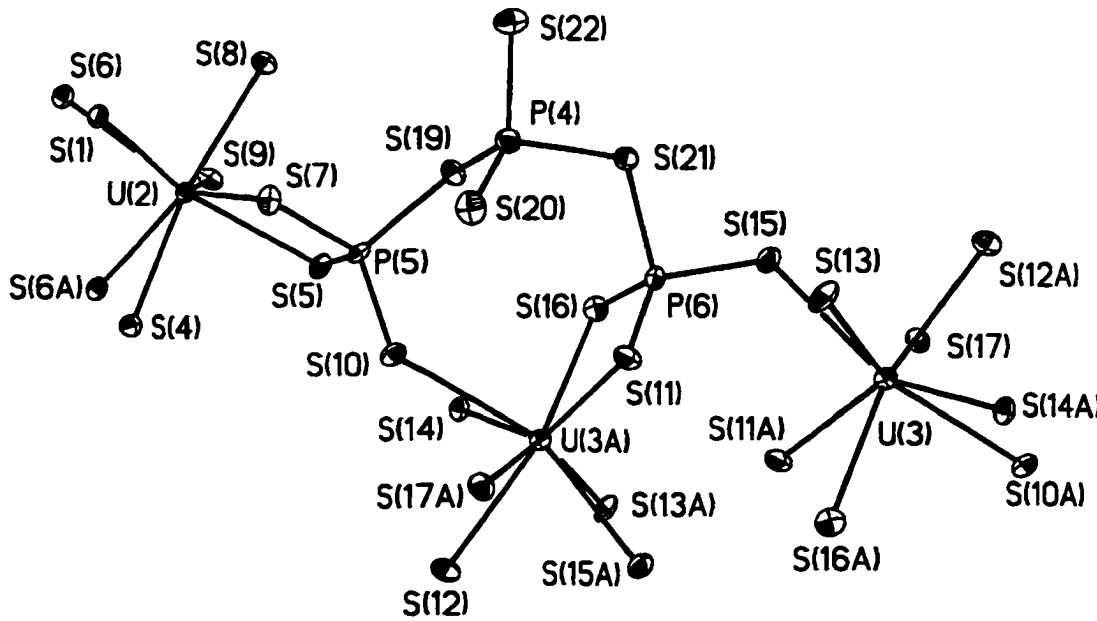

Figure 3.20. Thermal ellipsoid plot (50%) of the linkage to the new $[P_3S_{10}]^{5-}$ by three uranium atoms in $Cs_8U_5(P_3S_{10})_2(PS_4)_6$, **I**.

edges. The individual layers are connected together along the *c* direction through $[P_3S_{10}]^{5-}$ ligands.

This connectivity creates tunnels that propagate through the structure. Tunnels exist along three different unit cell directions. One tunnel can be seen when the structure is viewed down the [101] direction and has the dimensions 5.9 Å × 18.8 Å. Two other tunnels can be seen when the structure is viewed down the [001] and [100] directions. Their respective dimensions are 8.7 Å × 8.9 Å and 6.7 Å × 11.5 Å. Four distinct Cs^+ cations exist in the structure and reside inside the tunnels. The Cs^+ cations are all coordinated by sulfur atoms only. Cs(1), Cs(2), and Cs(4) are all nine coordinate, Cs(3) is eight coordinate. All the elements in this structure are found in oxidation states consistent with their known chalcogenide chemistry: Cs^+, U^{4+}, P^{5+}, and S^{2-}.

The Structure of $K_{10}Th_3(P_2S_7)_4(PS_4)_2$, II.

This compound crystallized as colorless rods in the centered monoclinic space group *C2/c* (R_{int} = 0.044) based on systematic absences in the data; crystallographic details can be found in Table 3.4. Tables 3.7 and 3.8 list the atomic coordinates and the relevant bond distances. The structure was solved without complications, except for the need for a secondary extinction coefficient (5.5×10^{-5}), leaving peaks in the difference map of 1.7 e/Å^3 (max) and -1.837 e$^-$/Å^3 (min).

This compound displays a two-dimensional layered structure containing two crystallographically distinct Th atoms. Th(1) and Th(2) are both coordinated to eight sulfur atoms in a distorted dodecahedral geometry. Figure 3.21 is a polyhedral view of the structure down the [010] direction, showing the layers in the (011) planes that comprise two corrugated, interpenetrating layers of thorium thiophosphates. Figure 3.22

Table 3.7. Fractional Atomic Coordinates and Equivalent Isotropic Displacement Parameters ($Å^2$ x 10^3)[a] for $K_{10}Th_3(P_2S_7)_4(PS_4)_2$, II.

	x	y	z	U(eq)
Th(1)	0.0000	0.09651(1)	0.2500	13(1)
Th(2)	0.1366(1)	0.06960(1)	0.5557(1)	13(1)
K(1)	0.1836(1)	0.0460(2)	0.4264(1)	27(1)
K(2)	0.0718(1)	0.2228(2)	0.6005(1)	64(1)
K(3)	0.0281(1)	1.3851(2)	0.3734(1)	34(1)
K(4)	0.2733(1)	0.4315(2)	0.7363(1)	28(1)
K(5)	0.1478(1)	0.5546(2)	0.3369(1)	44(1)
P(1)	0.0717(1)	0.8057(2)	0.3999(1)	15(1)
P(2)	0.0977(1)	0.6242(2)	0.6522(1)	16(1)
P(3)	0.1838(1)	0.0637(2)	0.6089(1)	15(1)
P(4)	0.1825(1)	0.3743(2)	0.5294(1)	18(1)
P(5)	0.1009(1)	0.1405(2)	0.2533(1)	16(1)
S(1)	0.0410(1)	0.6939(2)	0.3201(1)	21(1)
S(2)	0.0495(1)	1.2435(2)	0.2608(1)	19(1)
S(3)	0.0598(1)	1.0252(2)	0.3776(1)	20(1)
S(4)	0.0909(1)	0.9172(2)	0.2559(1)	25(1)
S(5)	0.0399(1)	0.7345(2)	0.4413(1)	19(1)
S(6)	0.1465(1)	0.7591(2)	0.4586(1)	18(1)
S(7)	0.2260(1)	0.5350(2)	0.5918(1)	19(1)
S(8)	0.1138(1)	0.3927(2)	0.5132(1)	22(1)
S(9)	0.2276(1)	0.8777(2)	0.6370(1)	19(1)
S(10)	0.1696(1)	0.6377(2)	0.6782(1)	21(1)
S(11)	0.0526(1)	0.6136(2)	0.5603(1)	21(1)
S(12)	0.1113(1)	1.0003(2)	0.5463(1)	20(1)
S(13)	0.0759(1)	0.8403(2)	0.6619(1)	21(1)
S(14)	0.0838(1)	0.0690(2)	0.6918(1)	24(1)
S(15)	0.1876(1)	0.3800(2)	0.4602(1)	40(1)
S(16)	0.2129(1)	0.1602(2)	0.5638(1)	18(1)
S(17)	0.1899(1)	0.1946(2)	0.6714(1)	22(1)
S(18)	0.1696(1)	0.2172(2)	0.3116(1)	24(1)

[a] U(eq) is defined as one third of the trace of the orthogonalized U_{ij} tensor.

Table 3.8. Selected Bond Distances (Å) for $K_{10}Th_3(P_2S_7)_4(PS_4)_2$, **II.**

Th(1)-S(3)	2.879(1)	P(1)-S(5)	2.039(2)
Th(1)-S(1)	2.912(2)	P(1)-S(6)	2.044(2)
Th(1)-S(3)	2.879(1)	P(2)-S(10)	2.032(2)
Th(1)-S(1)	2.913(2)	P(2)-S(11)	2.039(2)
Th(1)-S(2)	2.918(2)	P(2)-S(13)	2.150(2)
Th(1)-S(2)	2.918(2)	P(2)-S(14)	1.982(2)
Th(1)-S(4)	2.924(2)	P(3)-S(9)	2.049(2)
Th(1)-S(4)	2.924(2)	P(3)-S(12)	2.040(2)
Th(2)-S(12)	2.844(2)	P(3)-S(16)	2.136(2)
Th(2)-S(7)	2.886(1)	P(3)-S(17)	1.988(2)
Th(2)-S(5)	2.893(1)	P(4)-S(7)	2.053(2)
Th(2)-S(10)	2.898(1)	P(4)-S(8)	2.033(2)
Th(2)-S(8)	2.903(2)	P(4)-S(15)	1.992(2)
Th(2)-S(6)	2.911(1)	P(4)-S(16)	2.129(2)
Th(2)-S(11)	2.926(1)	P(5)-S(13)	2.131(2)
Th(2)-S(9)	2.968(1)	P(5)-S(18)	1.977(2)
P(1)-S(1)	2.055(2)	P(5)-S(2)	2.037(2)
P(1)-S(3)	2.047(2)	P(5)-S(4)	2.055(2)

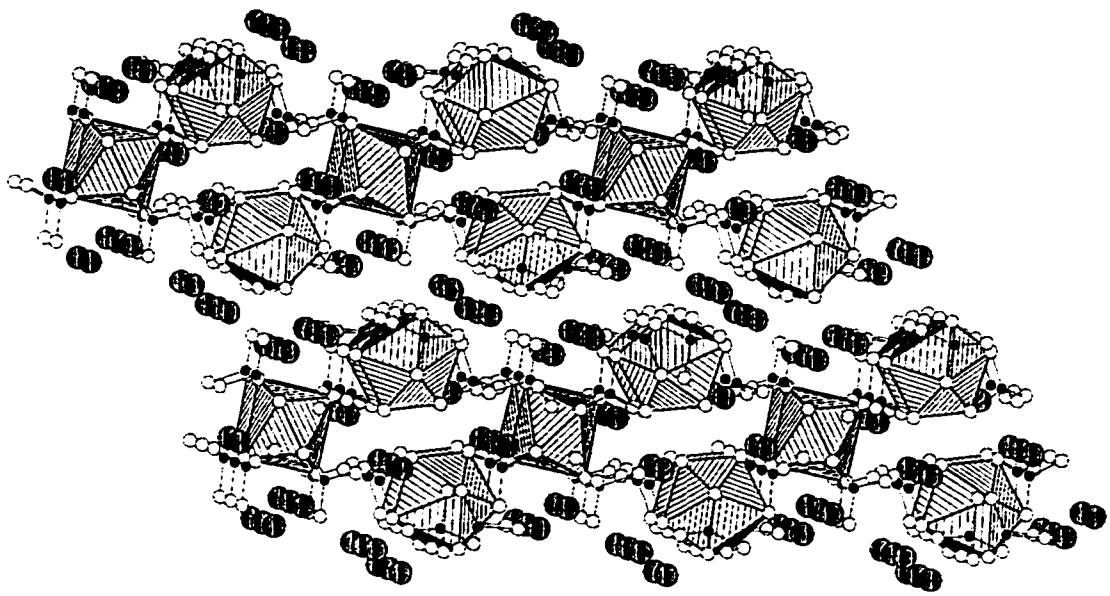

Figure 3.21. A polyhedral view of $K_{10}Th_3(P_2S_7)_4(PS_4)_2$, **II**, down [010]. Polyhedra are ThS_8, potassium atoms are shaded spheres, phosphorous are filled circles, and sulfur are open circles.

shows thermal ellipsoid plots of the coordination around each thorium atom and the $[PS_4]^{3-}$ and $[P_2S_7]^{4-}$ units. The Th–S bond distances range from 2.844(2) Å to 2.924(2) Å with an average distance of 2.905(6) Å. These ThS_8 dodecahedra are linked together to form layers via the two distinct thiophosphate ligands. All of the sulfur atoms coordinated to Th(1) and Th(2) are sulfide, S^{2-}, and are linked to phosphorous in the thiophosphate ligands. Th(1) is coordinated by one $[PS_4]^{3-}$ and two $[P_2S_7]^{4-}$ ligands while Th(2) is coordinated by one $[PS_4]^{3-}$ and three $[P_2S_7]^{4-}$ ligands (for clarity, all the thiophosphates are not included in the thermal ellipsoid plot). The unique $[PS_4]^{3-}$ ligand consists of a phosphorous atom, P(1), surrounded by four sulfur atoms in a distorted tetrahedral geometry. The P(1)–S bond distances range from 2.044(2) Å to 2.055(2) Å with an average distance of 2.046(4) Å, consistent with typical thiophosphate bond distances. This thiophosphate ligand links the Th(1) and Th(2) polyhedra along *c* crystallographic direction by sharing one edge (S(3) and S(1)) with Th(1) and another edge (S(5) and S(6)) with Th(2), as shown in Figure 3.22. Two distinct $[P_2S_7]^{4-}$ units exist in this structure. Both ligands are composed of two PS_4 tetrahedra that corner-share one sulfur atom, S(16) or S(13) in Figure 3.22. One $[P_2S_7]^{4-}$ ligand contains P(2) and P(5) with S(13) as the bridging atom. This ligand edge-shares to both Th(1) and Th(2) polyhedra thus connecting them along the *c* crystallographic direction. Two of the sulfur atoms in this ligand, S(14) and S(18), are not coordinated to thorium but are free terminal atoms that point into the interlayer space, interacting with potassium cations through long ionic interactions (3.1(2) Å – 3.9(2) Å). The other $[P_2S_7]^{4-}$ ligand contains P(3) and P(4) with S(16) as the bridging atom. This ligand links two different Th(2) polyhedra together along the *b* direction. Both S(15) and S(17) are terminal atoms that coordinate to

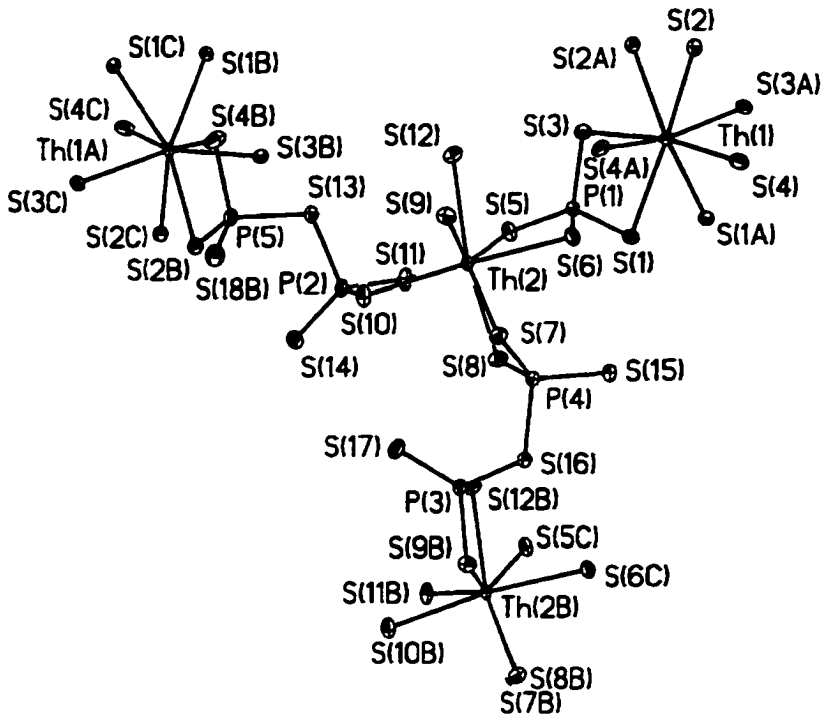

Figure 3.22. Thermal ellipsoid plot (50%) of the thorium thiophosphate network in $K_{10}Th_3(P_2S_7)_4(PS_4)_2$, **II**.

interlayer potassium atoms. In the case of the two $[P_2S_7]^{4-}$ ligands, the phosphorous-to-corner-shared sulfur atom distances are typically 0.1Å longer than the average P–S distance. The phosphorous-to-terminal sulfur atom distances are significantly shorter (0.04Å) than the average distance and are approximately equidistant between a phosphorous single and a double bond. The S–P–S bond angles are within the range expected for a PS_4 tetrahedron.

Each individual layer in this structure can be described as containing two rows of Th(2) polyhedra separated by one row of Th(1) polyhedra, where the rows run along the *b* direction in the layers, as shown in Figure 3.23. The Th(2) polyhedra are linked together along the c direction through Th(1) polyhedra. These polyhedra are linked via both $[PS_4]^{3-}$ and $[P_2S_7]^{4-}$ ligands. When a single layer is viewed down [101], as in Figure 3.23, it becomes apparent that the layer is built up of two intertwined chains with the composition Th(2) – $[P_2S_7]^{4-}$ – Th(1) – $[PS_4]^{3-}$ – Th(2). Connectivity between Th(1) and Th(2) along the *b* direction is established though $[P_2S_7]^{4-}$ only. These intertwined chains create channels that run along the *b* direction within each layer. These channels have dimensions 13.667 Å × 4.358 Å. The closest Th•••Th distance within the layers is 7.210Å.

Five distinct K^+ cations exist in this structure, all of which are coordinated to S atoms. K(1) and K(4) are coordinated by seven S atoms, K(2) is coordinated by five S atoms, K(3) is coordinated by eight S atoms, and K(5) is coordinated by six S atoms. The average K–S distance is 3.371(5) Å. The potassium atoms K(1), K(4), and K(5) all lie between the layers, though not symmetrically situated with respect to the centers of the channels. The potassium atoms K(2) and K(3) both lie within the channels contained in

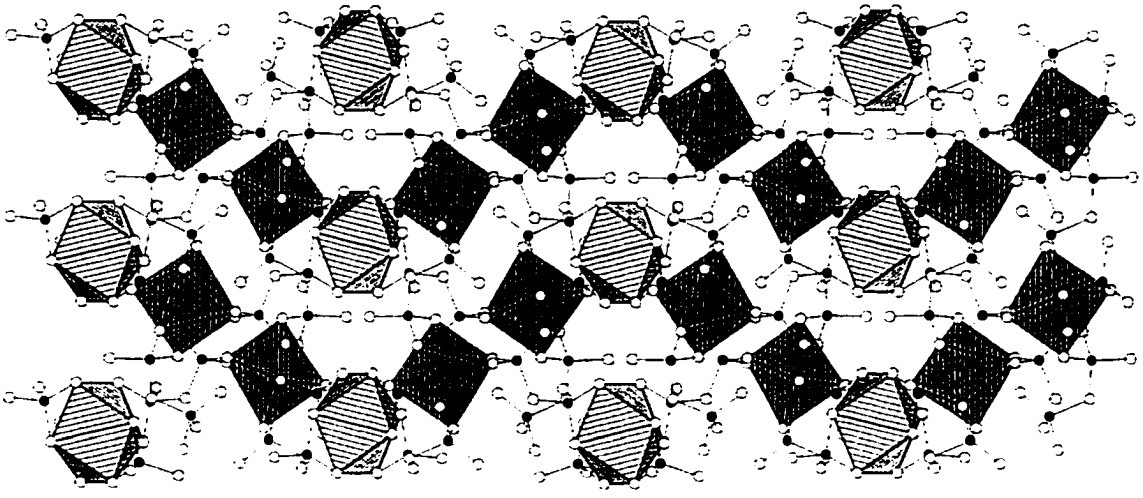

Figure 3.23. View down [101] of one layer of $K_{10}Th_3(P_2S_7)_4(PS_4)_2$, **II**. Th(1) are hatched polyhedra, Th(2) are shaded polyhedra. Potassium atoms have been removed for clarity.

the *bc* plane, described above. As there are no S–S bonds present in this structure, the oxidation states of the elements can be assigned as follows: K^{+}, Th^{4+}, P^{5+}, and S^{2-}. Thorium in the 4+ oxidation state is consistent with its known chalcophsophate chemistry.[15,53]

Differential thermal analysis data indicate that, while the $K_{10}Th_3(P_2S_7)_4(PS_4)_2$ was prepared by heating to 500 °C in a flux, it decomposes at 391 °C under nitrogen. A large exothermic peak is found just before the decomposition peak that may indicate a phase change that is not reversible.

Structures of $K_5U(PS_4)_3$ (III), $K_5Th(PS_4)_3$ (IV), $Rb_5Th(PS_4)_3$ (V), and $Cs_5Th(PS_4)_3$ (VI).

Compounds **III** - **VI** are nearly isostructural, consisting of dimers of actinide atoms linked through thiophosphate bridges with significant differences in the packing arrangements of these dimers and the coordination of the thiophosphates within each dimer. Each compound (**III** - **VI**) crystallizes in a primitive monoclinic space group, as listed in Table 3.4. The atomic coordinates for **III**, **IV**, and **V** and relevant bond distances are listed in Tables 3.9 – 3.14, respectively.

$K_5U(PS_4)_3$ (III). This structure consists of discrete dimers of uranium polyhedra packed in the unit cell with potassium cations filling the voids between the dimers, as shown in the polyhedral representation in Figure 3.24. Packing problems associated with the larger $[U_2(PS_4)_6]^{10-}$ dimeric unit and relatively small potassium cations caused a disorder problem in the solution of the structure - K(1) and K(1A) are each modeled as 50% occupied and could not be modeled well with anisotropic thermal ellipsoids. The

Table 3.9. Fractional Atomic Coordinates and Equivalent Isotropic Displacement Parameters ($Å^2 \times 10^3$)[a] for $K_5U(PS_4)_3$, **III.**

	x	y	z	U(eq)[a]	Frac. Occup.
U(1)	0.3337(1)	0.5008(1)	0.8902(1)	12(1)	
K(1)	0.2083(3)	0.8052(2)	0.6065(4)	37(1)	0.5
K(1A)	0.2306(2)	0.8070(2)	0.6748(4)	26(1)	0.5
K(2)	0.0143(1)	0.4704(1)	0.2153(2)	26(1)	
K(3)	-0.0765(1)	0.7037(1)	0.3429(2)	32(1)	
K(4)	0.3140(1)	0.4948(1)	0.4432(2)	33(1)	
K(5)	0.5530(1)	0.7008(1)	0.7185(2)	47(1)	
S(1)	0.4058(1)	0.6461(1)	0.0349(2)	18(1)	
S(2)	0.4783(1)	0.4759(1)	0.1717(2)	20(1)	
S(3)	0.3738(1)	0.3792(1)	0.7182(2)	28(1)	
S(4)	0.2790(1)	0.3512(1)	0.9537(2)	18(1)	
S(5)	0.2137(1)	0.5131(1)	0.0655(2)	17(1)	
S(6)	0.1585(1)	0.4860(1)	0.6577(2)	17(1)	
S(7)	0.3089(1)	0.6273(1)	0.6982(2)	21(1)	
S(8)	0.0820(1)	0.6721(1)	0.6840(2)	28(1)	
S(9)	0.1303(1)	0.6160(1)	0.3853(2)	28(1)	
S(10)	0.4361(2)	0.6275(1)	0.3892(2)	46(1)	
S(11)	0.2288(1)	0.3488(1)	0.2697(2)	27(1)	
S(12)	0.0509(1)	0.3663(1)	0.9574(2)	21(1)	
P(1)	0.1628(1)	0.6029(1)	0.6009(2)	15(1)	
P(2)	0.4835(1)	0.5943(1)	0.2274(2)	18(1)	
P(3)	0.1900(1)	0.3921(1)	0.0660(2)	16(1)	

[a] U(eq) is defined as one third of the trace of the orthogonalized U_{ij} tensor.

Table 3.10. Selected Bond Distances (Å) for $K_5U(PS_4)_3$, **III.**

U(1)-S(7)	2.802(2)	P(1)-S(6)	2.078(2)
U(1)-S(4)	2.805(1)	P(1)-S(7)	2.083(2)
U(1)-S(5)	2.814(2)	P(2)-S(10)	1.991(3)
U(1)-S(6)	2.832(1)	P(2)-S(10A)	2.032(2)
U(1)-S(3)	2.842(2)	P(2)-S(2)	2.052(2)
U(1)-S(2)	2.881(1)	P(2)-S(1)	2.089(2)
U(1)-S(1)	2.903(1)	P(3)-S(11)	2.015(2)
U(1)-S(2A)	3.021(2)	P(3)-S(12)	2.017(2)
P(1)-S(9)	2.005(2)	P(3)-S(4)	2.068(2)
P(1)-S(8)	2.012(2)	P(3)-S(5)	2.098(2)

Table 3.11. Fractional Atomic Coordinates and Equivalent Isotropic Displacement Parameters ($Å^2$ x 10^3)[a] for $K_5Th(PS_4)_3$, **IV.**

	x	y	z	U(eq)[a]
Th(1)	0.1070(1)	0.6489(1)	0.0806(1)	10(1)
K(1)	0.1131(4)	0.6558(1)	-0.2574(1)	20(1)
K(2)	0.1814(2)	0.9057(2)	-0.0974(1)	29(1)
K(3)	-0.3595(2)	0.5902(2)	0.0834(1)	39(1)
K(4)	0.6706(3)	0.6062(2)	-0.2498(1)	32(1)
K(5)	0.3802(2)	0.1412(1)	0.0795(1)	20(1)
P(1)	0.3810(2)	0.8118(2)	0.0793(1)	13(1)
P(2)	-0.0930(3)	0.6718(1)	-0.0812(1)	12(1)
P(3)	0.4023(3)	0.8312(2)	-0.2623(1)	13(1)
S(1)	0.2638(2)	0.4343(2)	0.0801(2)	19(1)
S(2)	-0.0772(2)	0.4367(2)	0.0692(1)	14(1)
S(3)	0.0949(4)	0.7732(2)	0.0026(1)	34(1)
S(4)	0.0737(2)	0.5672(2)	0.2197(1)	16(1)
S(5)	-0.0954(4)	0.7784(2)	0.1554(1)	27(1)
S(6)	0.2017(2)	0.9064(2)	0.0784(2)	24(1)
S(7)	0.3589(2)	0.7025(2)	0.1603(1)	19(1)
S(9)	0.0582(2)	0.6000(2)	-0.4194(2)	18(1)
S(10)	-0.0942(3)	0.7732(2)	-0.1621(1)	19(1)
S(11)	0.2742(3)	0.4256(2)	-0.2383(1)	21(1)
S(12)	0.4167(3)	0.7358(2)	-0.1778(1)	19(1)

[a] U(eq) is defined as one third of the trace of the orthogonalized U_{ij} tensor.

Table 3.12. Selected Bond Distances for $K_5Th(PS_4)_3$, **IV.**

Th(1)-S(1)	2.882(2)	P(1)-S(8)	2.056(3)
Th(1)-S(5)	2.882(2)	P(1)-S(7)	2.058(3)
Th(1)-S(3)	2.883(3)	P(2)-S(10)	1.989(3)
Th(1)-S(4)	2.954(2)	P(2)-S(3)	2.036(3)
Th(1)-S(8)	2.980(2)	P(2)-S(1)	2.057(3)
Th(1)-S(2)	3.020(2)	P(2)-S(2)	2.082(3)
Th(1)-S(7)	3.021(2)	P(3)-S(12)	2.016(3)
Th(1)-S(6)	3.074(2)	P(3)-S(11)	2.027(4)
Th(1)-S(2A)	3.168(2)	P(3)-S(4)	2.063(4)
P(1)-S(9)	1.998(2)	P(3)-S(5)	2.068(3)
P(1)-S(6)	2.052(3)		

Table 3.13. Fractional Atomic Coordinates and Equivalent Isotropic Displacement Parameters ($Å^2$ x 10^3)[a] for $Rb_5Th(PS_4)_3$, **V.**

	x	y	z	U(eq)
Th(1)	0.1853(1)	0.1010(1)	0.0351(1)	8(1)
P(1)	0.2871(2)	0.3717(3)	-0.0193(2)	10(1)
P(2)	0.0326(2)	0.9086(3)	-0.1346(2)	10(1)
P(3)	0.6428(2)	0.1040(3)	-0.1800(2)	11(1)
S(1)	0.0422(2)	0.2557(3)	0.1020(2)	13(1)
S(2)	0.0289(2)	-0.0732(3)	0.0893(2)	14(1)
S(3)	0.1840(2)	-0.0956(3)	-0.0823(2)	18(1)
S(4)	0.2758(2)	0.0680(3)	0.1952(2)	14(1)
S(5)	0.3436(2)	-0.1036(3)	0.0645(2)	19(1)
S(6)	0.3573(2)	0.1989(3)	-0.0449(2)	15(1)
S(7)	0.1351(2)	0.3395(3)	-0.0666(2)	14(1)
S(8)	0.2933(2)	0.3541(3)	0.0943(1)	13(1)
S(9)	0.6574(2)	0.4525(3)	0.0475(2)	14(1)
S(10)	0.0238(2)	0.9044(3)	-0.2453(2)	17(1)
S(11)	0.7072(2)	0.2720(3)	-0.2128(2)	15(1)
S(12)	0.4932(2)	0.0927(3)	-0.2299(2)	16(1)
Rb(1)	0.5151(1)	0.3877(1)	-0.1281(1)	16(1)
Rb(2)	0.1527(1)	0.6118(1)	-0.1910(1)	16(1)
Rb(3)	0.2044(1)	0.1570(1)	-0.2221(1)	31(1)
Rb(4)	0.5296(1)	0.1768(1)	0.1240(1)	25(1)
Rb(5)	0.1407(1)	-0.3608(1)	0.0526(1)	23(1)

[a] U(eq) is defined as one third of the trace of the orthogonalized U_{ij} tensor.

Table 3.14. Selected Bond Distances (Å) for $Rb_5Th(PS_4)_3$, **V.**

Th(1)-S(1)	2.881(3)
Th(1)-S(3)	2.899(3)
Th(1)-S(5)	2.901(3)
Th(1)-S(4)	2.953(3)
Th(1)-S(8)	3.003(3)
Th(1)-S(2)	3.004(3)
Th(1)-S(7)	3.015(3)
Th(1)-S(6)	3.076(3)
Th(1)-S(2A)	3.285(3)
P(1)-S(9)	2.008(4)
P(1)-S(6)	2.055(4)
P(1)-S(7)	2.055(4)
P(1)-S(8)	2.060(4)
P(2)-S(10)	1.995(4)
P(2)-S(3)	2.047(4)
P(2)-S(1)	2.061(4)
P(2)-S(2)	2.073(4)
P(3)-S(12)	2.017(4)
P(3)-S(11)	2.022(4)
P(3)-S(4)	2.073(4)
P(3)-S(5)	2.076(4)

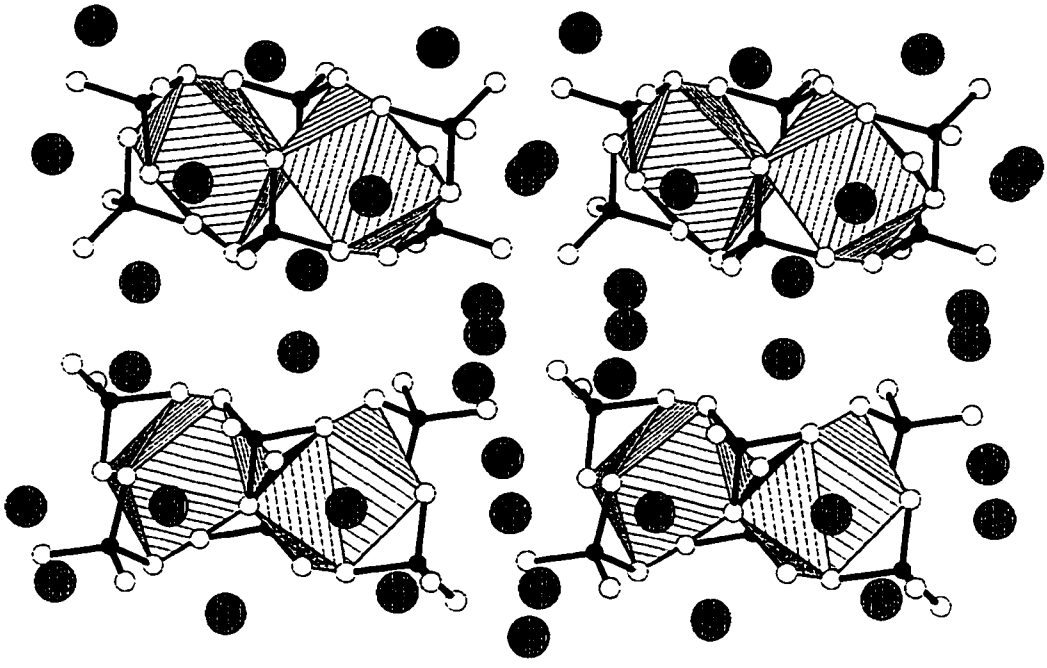

Figure 3.24. Polyhedral view of $K_5U(PS_4)_3$, **III**, down [00-1]. Potassium atoms are shaded circles, phosphorous atoms are filled circles, and sulfur atoms are open circles.

dimers are composed of two crystallographically identical uranium atoms that are linked together through sharing of two $[PS_4]^{3-}$ ligands across an inversion center. A thermal ellipsoid plot of the local coordination may be seen in Figure 3.25. The uranium atom is coordinated to eight sulfur atoms in distorted square anti-prismatic geometry. All eight sulfur atoms belong to face-capping or edge-bridging distinct $[PS_4]^{3-}$ ligands, each of which has a slightly distorted tetrahedral geometry. The tetrahedron centered on P(1) has two sulfur atoms (S(6) and S(7)) that are bound to one uranium atom in an edge-sharing arrangement with the two sulfur atoms (S(8) and S(9)) coordinated only to potassium cations. The P(2) tetrahedron and the U(1) polyhedron share a common edge of atoms S(2) and S(3) and the P(2) tetrahedron and the U(1A) polyhedron share a common edge of atoms S(1) and S(2). The fourth sulfur atom on P(2), S(10), is terminal, being coordinated only to potassium cations. Finally, the P(3) tetrahedron and the U(1) polyhedron also share a common edge of two sulfur atoms (S(4) and S(5)). The other two sulfur atoms on P(3), S(11) and S(12), are terminal. The bridging nature of the thiophosphates is not enough to bring the electron-poor uranium atoms within bonding distance, the closest U–U contact is 4.643(2) Å.

What will become significant later in the discussion of compounds **III** - **VI** are the bond distances across the dimer from An(1)–S(2A) and from S(2A)–An(1A), as well as the S(9)–P(1)–An(1) tilt angle of the $P(1)S_4$ tetrahedron. In **III**, the key U–S(2A) and S(2A)–U(1A) distances are 2.903(2) and 3.021(2) Å, respectively. The angle of tilt in the $P(1)S_4$ tetrahedron, S(9)–P(1)–U(1), is 139°, indicating that the triangular face comprising S(6), S(7), and S(8) is tilted away from the uranium polyhedron and S(8) is not within bonding distance to U(1); the U(1)–S(8) contact distance is 4.625(2) Å. Table

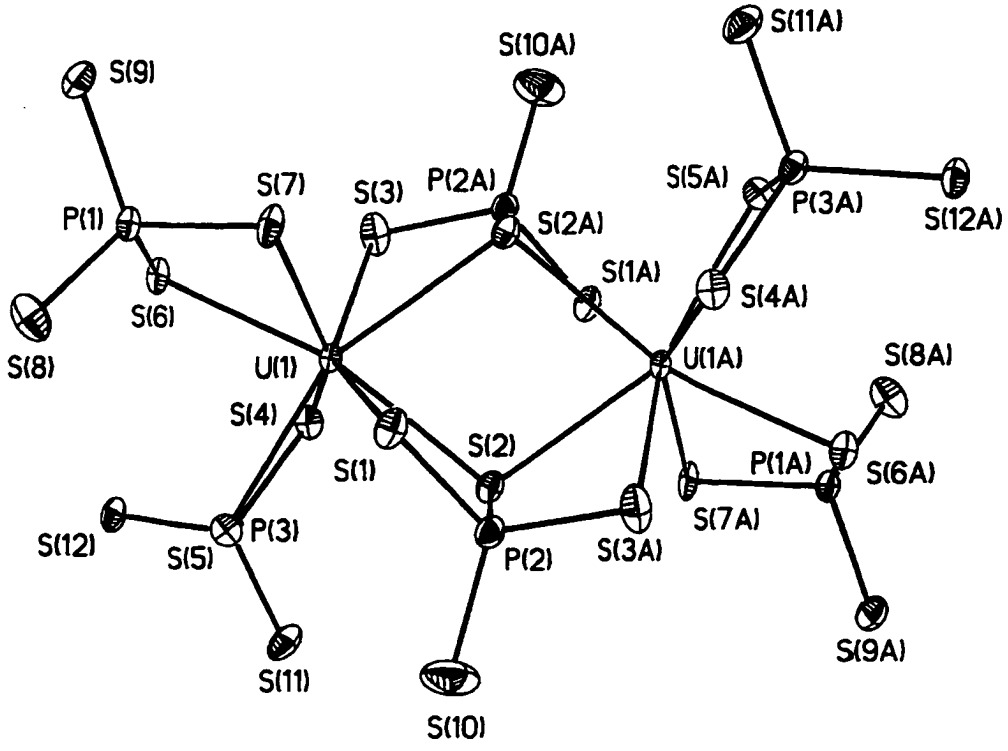

Figure 3.25. Thermal ellipsoid plot (50%) of the $[U_2(PS_4)_6]^{10-}$ dimer in $K_5U(PS_4)_3$, **III**.

3.15 summarizes the pertinent structural data that describing the differences between the $A_5An(PS_4)_3$ compounds.

Finally, all five K^+ cations are coordinated only to S atoms. K(1), K(2), and K(4) are eight coordinate while K(3) and K(5) are both nine coordinate. The K–S bond distances range from 3.170(4) Å to 3.960(4) Å with an average distance of 3.52(1) Å.

$K_5Th(PS_4)_3$, IV. The structure of **IV** is related to **III** in that it also consists of two actinide atoms, coordinated by thiophosphate ions, to form dimeric units in the monoclinic lattice. It was necessary to solve the structure of **IV** as a pseudo-merohedrally-twinned monoclinic unit cell, with the final twin component of the modeled lattice refining to a BASF value of 0.553(1).[54] Note the relationship of the 9.7 Å *c*-axis in **III** to the 9.7 Å *a*-axis in **IV**.

Figure 3.26 shows the thermal ellipsoid plot of the thorium dimer, **IV**. The most striking contrasts between **III** and **IV** can be found in the P(1) thiophosphate ligands. In **IV**, thiophosphate $P(1)S_4$ caps a triangular face of the 9-coordinate thorium atoms; whereas in **III**, the same phosphate group is only edge-bridging. Now S(8) is located 3.074(2) Å from Th(1). The angle formed by S(9)–P(1)–Th(1) is 175° - a nearly linear arrangement, indicating that the triangular face formed by S(6), S(7), and S(8) is nearly perpendicular to the S(9)–Th(1) vector.

As in **III**, the dimer is bridged by two edges on the $P(2)S_4$ sharing across the gap, having S(2) on phosphate P(2) bridging to both Th(1) and Th(1A) through bonds 3.167(2) and 3.020(2) Å, thereby causing the two P(2) phosphates, related by the center of inversion, to act as η^2-type ligands on each thorium atom as we saw in **III**. It should be noted that the long Th-S(2) bond distance of 3.167(2) is significantly longer than

Table 3.15. Summary of essential structural data describing the differences between $A_5An(PS_4)_3$ compounds.

	$K_5U(PS_4)_3$	$K_5Th(PS_4)_3$	$Rb_5Th(PS_4)_3$	$Cs_5Th(PS_4)_3$
Metal Coordination	US_8	ThS_9	ThS_8	ThS_8
An(1)-S(2A), Å	2.903(2)	3.167(2)	3.285(3)	2.990(3)
S(2A)-An(1), Å	3.021(2)	3.020(2)	3.004(2)	3.429(3)
$P(1)S_4$ tilt angle S(9)-P(1)-An(1), °	139	175	174	175
$P(1)S_4$ coordination mode to An(1)	edge-sharing	face-sharing	face-sharing	face-sharing
dimer packing style	parallel layers	herring-bone layers	herring-bone layers	herring-bone layers

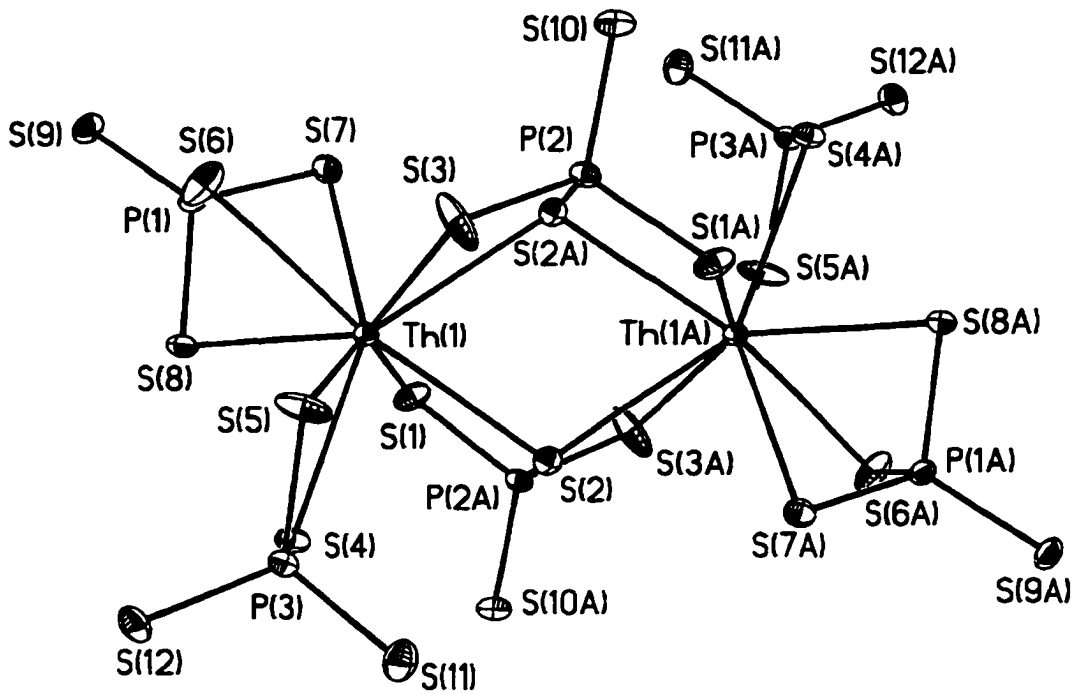

Figure 3.26. Thermal ellipsoid plot (50%) of the $[Th_2(PS_4)_6]^{10-}$ dimer in $K_5Th(PS_4)_3$, **IV**.

3.021(2) Å seen in **III** for U-S(2). The result is that the two Th(IV) centers are 5.125(2) Å apart, a much longer An–An interaction than in **III**.

Finally, all five K^+ cations in **IV**, are coordinated only to S atoms. K(1), K(2), and K(4) are eight coordinate. K(3) and K(5) are both nine coordinate. The K–S bond distances range from 3.170 Å to 3.96 Å with an average distance of 3.52(1) Å.

The structural differences between **III** and **IV** may arise from arrangements in packing. Viewed along the common *a*-axis dimension, the two structures display significant differences. Both pack the dimers in layers, with interleaving potassium cations, but the packing arrangements are significantly different. In **III**, the dimers pack in parallel, tilted within one layer, with the alternating layer packing in the opposite direction. In **IV**, the packing resembles a herringbone arrangement within and between layers.

$Rb_5Th(PS_4)_3$ and **$Cs_5Th(PS_4)_3$, V** and **VI.** These two compounds are isostructural to each other and are related to the monoclinic cells of compounds **III** and **IV** by the unique axis of the monoclinic cells of **V** and **VI** being the 9.9 - 10 Å axis (the *c*-axis in **III** and the *a*-axis in **IV**). Only **V** will be shown for brevity; a thermal ellipsoid plot of **VI** is available in the Supporting Information. A thermal ellipsoid plot of **V** is shown in Figure 3.27. As found in **III** and **IV**, the compound consists of isolated dimers of actinides linked through thiophosphate ligands. In **V**, the $P(2)S_4$ unit bridges Th(1) and Th(1A) through sharing the S(2)S(1) edge with Th(1) but bonding to Th(1A) through only S(3A). The distance between S(2) and Th(1A) is a long 3.285(3) Å, as indicated by a dotted line in the figure. By contrast, the S(2)–Th(1) distance is 3.004(2) Å. The S(9)–P(1)–Th(1) tilt angle of the PS_4 tetrahedron is again nearly linear in **V**, at 174°, compared

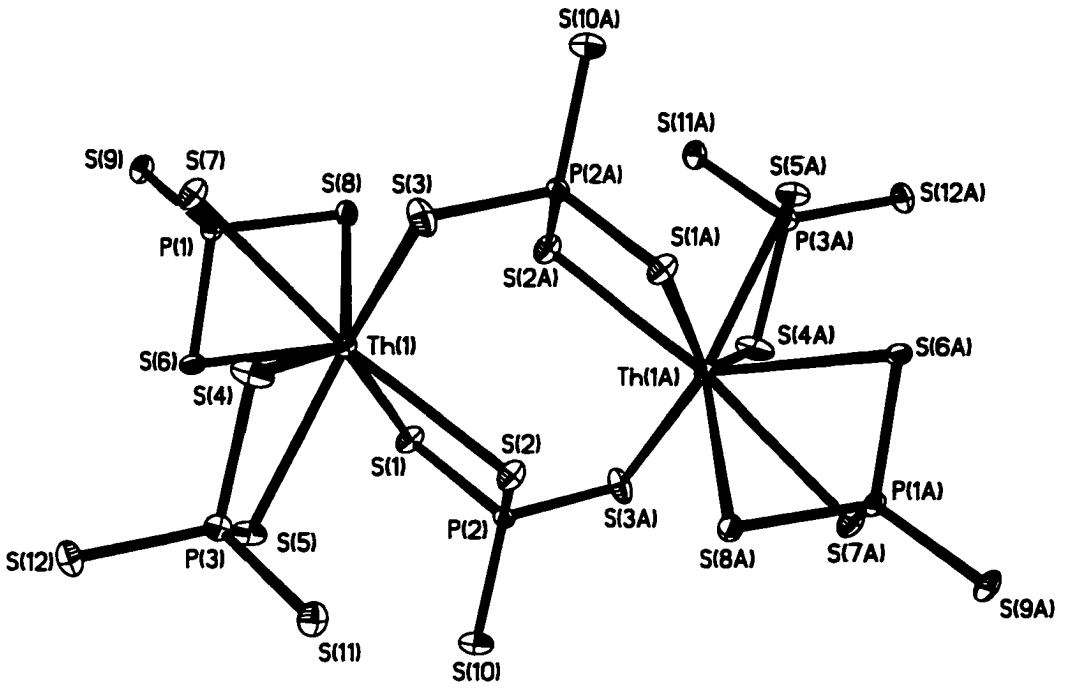

Figure 3.27. Thermal ellipsoid plot (50%) of the $[Th_2(PS_4)_6]^{10-}$ dimer in $Rb_5Th(PS_4)_3$, **V**. Note that the thorium polyhedra are no longer edge-sharing with one another.

to the same angle in **IV** (175°). The dimer in **VI** has even more contrasting features with the Th(1)–S(2) and Th(1)–S(2A) distances being 2.990(3) and 3.429(3) Å, respectively. However, the tilt angle of the PS_4 tetrahedron, S(9)–P(1)–Th(1) is quite comparable at 175°. Packing of the dimers in **V** and **VI** are quite similar to the packing found in compound **IV**, with a herring bone-style packing arrangements in the layers. It is likely that the increased lengthening of the S(2)–Th(1) interactions is due to packing interactions related to the different alkali metal cations within the lattice. The tilting of the $P(1)S_4$ tetrahedra on the dimers may also be due to packing forces. For a direct comparison, however, it would be necessary to compare the alkali metal series A = K, Rb, Cs directly between the different actinide elements. However, to date, we have been unable to isolate $A_5U(PS_4)_3$, where A = Rb, Cs. Instead, either only compound **I** is found in the reactions or new phases, yet to be identified, were isolated.

$Cs_4Th_2(P_2S_6)_3$, VII. The compound crystallizes as colorless blocks in the triclinic space group P-1 (r_{int}=0.0363) based on the systematic absences observed in the data. Refinement of the model's 272 parameters to the data (7605 reflections) provided an excellent goodness-of-fit (GOF = 0.871) resulting in a relatively flat electron density difference map (max. = 5.200 $e^-/Å^3$, min. = -3.500 $e^-/Å^3$). Table 3.4 contains the specific data collection and refinement information. Tables 3.16 and 3.17 contain the atomic coordinates and relevant bond distances respectively.

This compound is composed of two-dimensional $[Th_2(P_2S_6)_3]^{4-}$ layers. The Cs^+ cations reside in-between the layers and inside holes within each layer. The layered nature of this structure is seen in Figure 3.28. There are two crystallographically independent Th atoms in this structure. Th(1) is coordinated to 10 sulfur atoms in a

Table 3.16. Fractional Atomic Coordinates and Equivalent Isotropic Displacement Parameters ($Å^2$ x 10^3)[a] for $Cs_4Th_2(P_2S_6)_2$, **VII.**

	x	y	z	U(eq)
Th(1)	0.6466(1)	0.6783(1)	-0.0041(1)	8(1)
Th(2)	1.3900(1)	0.7148(1)	-0.3203(1)	8(1)
Cs(1)	0.9004(1)	0.4317(1)	-0.2606(1)	15(1)
Cs(2)	1.1242(1)	0.8535(1)	-0.1024(1)	17(1)
Cs(3)	1.1692(1)	0.2283(1)	-0.4459(1)	22(1)
Cs(4)	1.6495(1)	1.0745(1)	-0.2719(1)	21(1)
P(1)	0.7844(3)	0.4532(3)	0.0119(3)	10(1)
P(2)	1.3167(3)	0.5831(3)	-0.1261(3)	10(1)
P(3)	1.2352(3)	1.2007(3)	0.1883(3)	10(1)
P(4)	1.3552(3)	0.3649(3)	-0.6412(3)	8(1)
P(5)	1.3007(3)	1.0301(3)	-0.2537(3)	10(1)
P(6)	0.7749(3)	0.1302(3)	-0.5556(3)	10(1)
S(1)	0.6630(3)	0.4282(3)	-0.1398(3)	11(1)
S(2)	0.8442(3)	0.7261(3)	-0.0876(3)	12(1)
S(3)	0.5999(3)	0.8180(3)	0.2452(3)	14(1)
S(4)	0.8544(3)	0.6391(3)	0.1254(3)	11(1)
S(5)	0.5357(2)	0.5587(3)	-0.2886(3)	10(1)
S(6)	0.4261(3)	0.7567(3)	-0.0510(3)	11(1)
S(7)	0.6438(3)	0.8651(3)	-0.1110(3)	11(1)
S(8)	0.8261(3)	0.9182(3)	0.1854(3)	13(1)
S(9)	0.5816(3)	0.5312(3)	0.1366(3)	11(1)
S(10)	1.1532(3)	0.7317(3)	-0.4099(3)	12(1)
S(11)	1.2639(3)	0.4695(3)	-0.5540(3)	12(1)
S(12)	1.3989(3)	0.9598(3)	-0.1593(3)	14(1)
S(13)	1.2052(3)	0.5530(3)	-0.2873(3)	12(1)
S(14)	1.5553(3)	0.7108(3)	-0.4492(3)	12(1)
S(15)	1.3698(3)	0.8295(3)	-0.4835(3)	14(1)
S(16)	0.8780(3)	0.0980(3)	-0.4360(3)	16(1)
S(17)	1.1342(3)	1.0857(3)	0.2221(3)	16(1)
S(18)	1.1117(3)	0.6518(3)	0.0210(3)	13(1)

[a] U(eq) is defined as one third of the trace of the orthogonalized U_{ij} tensor.

Table 3.17 Bond Distances (Å) for $Cs_4Th_2(P_2S_6)_3$

Th(1)-S(2)	2.914(3)	P(3)-S(17)	1.975(4)
Th(1)-S(1)	2.934(3)	P(3)-S(2)	2.029(4)
Th(1)-S(4)	2.949(3)	P(3)-S(7)	2.053(4)
Th(1)-S(8)	3.001(3)	P(4)-S(11)	2.002(4)
Th(1)-S(9)	3.051(3)	P(4)-S(14)	2.024(4)
Th(1)-S(6)	3.059(3)	P(4)-S(5)	2.063(4)
Th(1)-S(5)	3.094(3)	P(5)-S(8)	2.012(4)
Th(1)-S(3)	3.119(3)	P(5)-S(3)	2.019(4)
Th(1)-S(7)	3.136(3)	P(6)-S(16)	1.967(4)
Th(1)-S(9A)	3.150(3)	P(6)-S(15)	2.035(4)
Th(2)-S(12)	2.842(3)	P(6)-S(10)	2.049(4)
Th(2)-S(14)	2.854(3)	P(1)-P(2)	2.219(4)
Th(2)-S(15)	2.939(3)	P(3)-P(4)	2.211(4)
Th(2)-S(5A)	2.949(3)	P(5)-P(6)	2.235(4)
Th(2)-S(10)	2.964(3)		
Th(2)-S(13)	2.991(3)		
Th(2)-S(11)	3.047(3)		
Th(2)-S(6A)	3.110(3)		
Th(2)-S(7A)	3.238(3)		
P(1)-S(18)	1.967(4)		
P(1)-S(1)	2.016(4)		
P(1)-S(4)	2.044(4)		
P(2)-S(13)	2.024(4)		
P(2)-S(6)	2.034(4)		
P(2)-S(9)	2.035(4)		

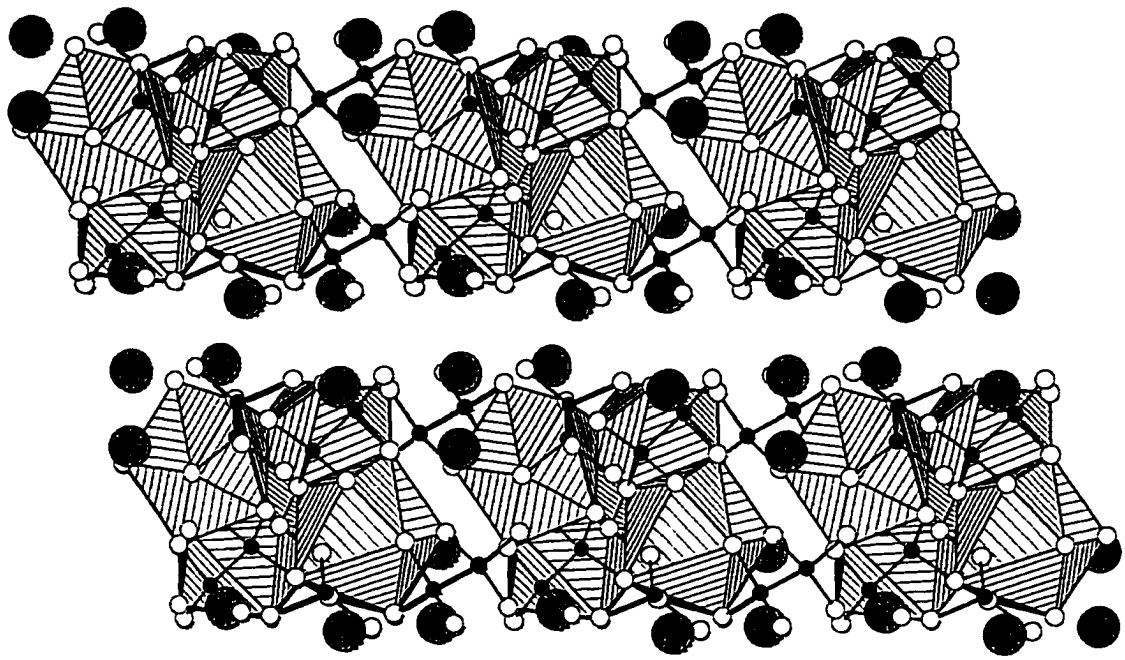

Figure 3.28. Edge on view of two $[Th_2(P_2S_6)_3]^{4-}$ layers. The polyhedra are ThS_9 and ThS_{10}, the filled circles are phosphorous, the unfilled circles are sulfur, and the shaded circles are Cs^+ cations.

sphenocoronal geometry. Th(2) is coordinated to nine sulfur atoms in a distorted tricapped trigonal prismatic geometry. The Th(1)-S bond distances range from 2.914(3) Å to 3.150(3) Å with an average distance of 3.04(8) Å. The Th(2)-S bond distances range from 2.842(3) Å to 3.238(3) Å with an average distance of 2.99(1) Å. These bond distances are expected for thorium in the 4+ oxidation state. Figures 3.29 and 3.30 contain thermal ellipsoid plots for the coordination environments of Th(1) and Th(2) respectively. The thorium polyhedra are linked into layers through the presence of three distinct $(P_2S_6)^{4-}$ ligands. The $(P_2S_6)^{4-}$ ligand has an ethane-like structure containing a P-P bond. The phosphorous atoms in the $(P_2S_6)^{4-}$ ligands are tetravalent. The bonding modes of the three $(P_2S_6)^{4-}$ ligands are shown in Figure 3.31. Each ligand coordinates five of its six sulfur atoms to one or more thorium atoms. The sixth sulfur atom is terminal and is bonded only to phosphorous and Cs^+ cations. All of the sulfur atoms coordinated to Th(1) and Th(2) belong to thiophosphate ligands, there are no terminal sulfur atoms bound to thorium.

The fundamental unit that comprises each layer is a tetramer of thorium polyhedra. This tetramer is linked to neighboring tetramers in the *bc* plane through two $(P_2S_6)^{4-}$ ligands (the P(3)P(4) and P(5)P(6) ligands). Figure 3.32 contains a view of a single $[Th_2(P_2S_6)_3]^{4-}$ layer while Figure 3.33 contains a view of the fundamental tetramer unit. Each tetramer contains two Th(1) and two Th(2) polyhedra linked together in a chain-like arrangement. The two Th(1) polyhedra form the interior portion of the chain and are linked together in an edge-sharing configuration through S(9) and S(9A). The two Th(2) polyhedra reside at the ends of the chain are linked to Th(1) by sharing one triangular face through S(5), S(6), and S(7). The tetramers are linked together to form

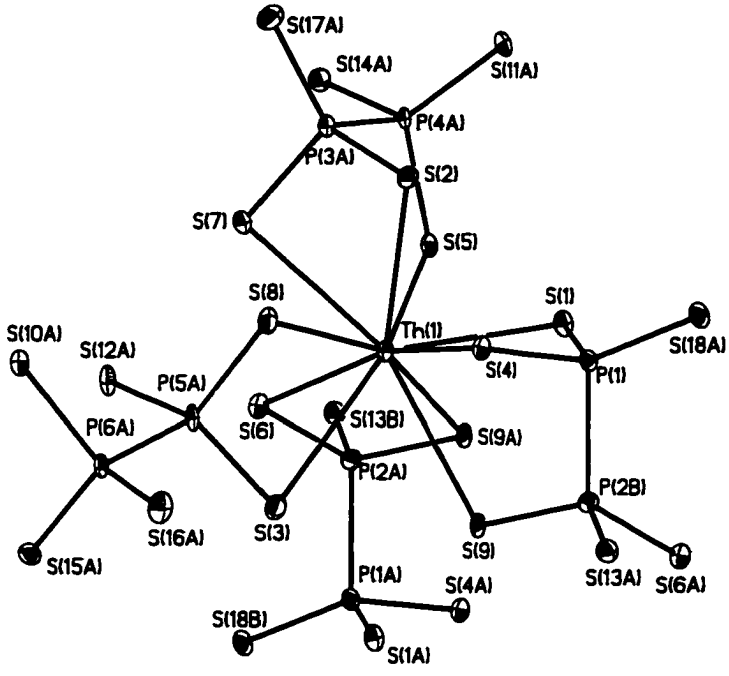

Figure 3.29. Coordination environment of Th(1) in $Cs_4Th_2(P_2S_6)_3$. Th(1) is coordinated to ten sulfur atoms that are distorted from any idealized ten-coordinate geometry

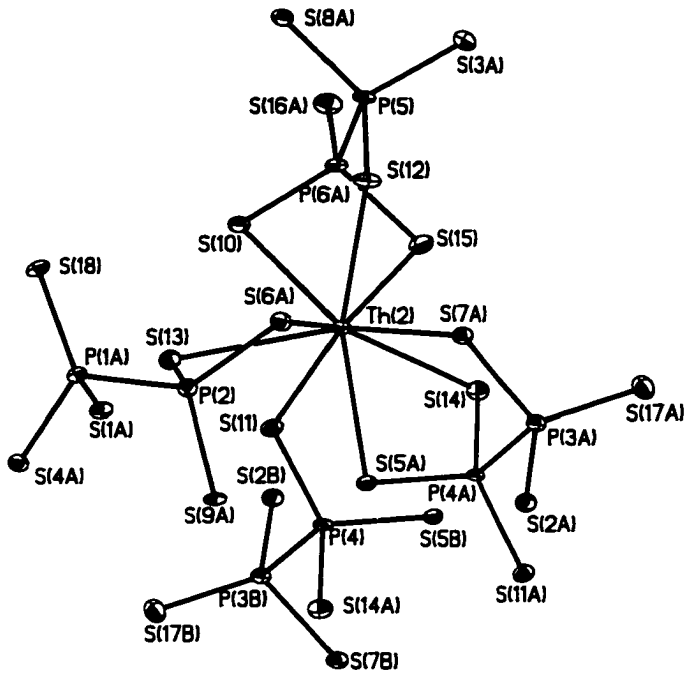

Figure 3.30. Coordination environment of Th(2) in $Cs_4Th_2(P_2S_6)_3$. Th(2) is coordinated to nine sulfur atoms in a distorted tricapped trigonal prismatic geometry.

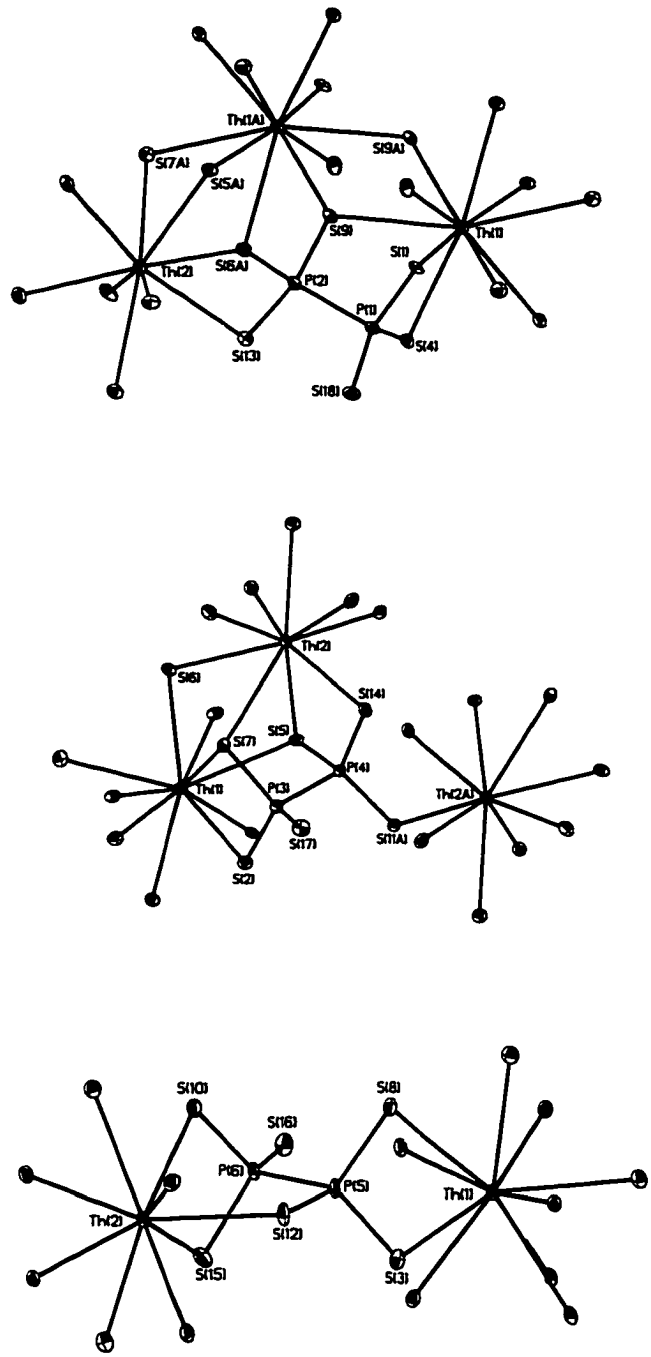

Figure 3.31. The three binding modes of the $(P_2S_6)^{4-}$ ligands found in $Cs_4Th_2(P_2S_6)_3$.

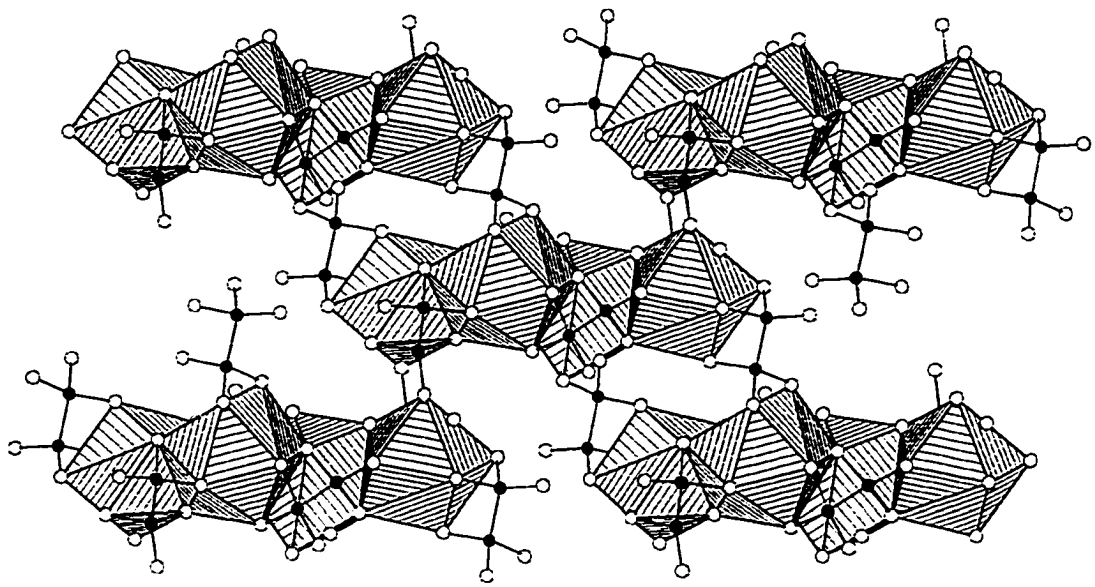

Figure 3.32. Polyhedral representation of a single $[Th_2(P_2S_6)_3]^{4-}$ layer. The polyhedra are ThS_9 and ThS_{10}, the filled circles are phosphorous, and the unfilled circles are sulfur. The Cs^+ cations are removed for clarity.

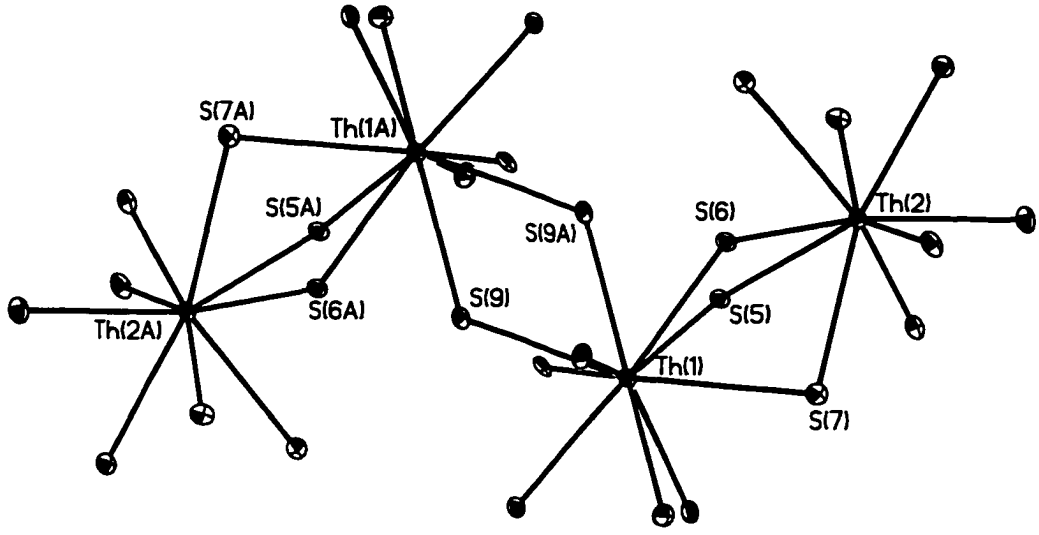

Figure 3.33. Thermal ellipsoid plot of the fundamental tetramer unit. The $Th(1)S_{10}$ and $Th(2)S_9$ polyhedra face-share to form dimers. The Th(1) atoms also edge-share with each other resulting in the formation of tetramers.

layers through the $(P_2S_6)^{4-}$ ligands containing P(1)P(2) and P(3)P(4). The $P_2S_6^{4-}$ ligand containing P(1)P(2) does not bond between tetramers.

There are four unique Cs^+ cations in this structure. Cs(1) and Cs(4) are coordinated 10 sulfur atoms while Cs(2) and Cs(3) are coordinated to 9 sulfur atoms. The Cs-S bond distances range from 3.423 Å to 3.972 Å.

$U(P_2S_6)_2$, VIII. The compound crystallizes as orange colored rectangular blocks in the tetragonal space group I $4_1/a$ (r_{int}=0.1417) based on the systematic absences observed in the data. Refinement of the model's 39 parameters to the data (525 reflections) provided a reasonable goodness-of-fit (GOF = 1.498) resulting in a relatively flat electron density difference map (max. = 1.151$e^-/Å^3$, min. = -1.173 $e^-/Å^3$). Table 3.4 contains the specific data collection and refinement information. Tables 3.18 and 3.19 contain the atomic coordinates and relevant bond distances respectively. This compound is structurally related to UP_2S_6, a compound reported by Do and co-workers in 1983.[55] While both compounds have 3D lattices the ligand geometry in each compound is significantly different. During the preparation of this dissertation Tremel and co-workers published the $U(P_2S_6)_2$ structure.[56] The structural details **VIII** will be described below and then related to Do's UP_2S_6 compound.[55]

VIII exhibits a three-dimensional structure containing one crystallographically unique uranium atom, which is coordinated to eight sulfur atoms in a square antiprismatic geometry. Figure 3.34 contains a view of the structure down the [001] crystallographic direction while Figure 3.35 contains a view of the coordination environment around U(1). Each US_8 polyhedron is linked to four neighboring polyhedra through $(P_2S_6)^{2-}$ ligands. There is no sulfur atom sharing between US_8 polyhedra. The P_2S_6 ligands in this structure

Table 3.18. Fractional atomic coordinates and equivalent isotropic displacement parameters ($Å^2 x\ 10^3$)[a] for $U(P_2S_6)_2$.

	x	y	z	U(eq)
U(1)	5000	7500	1250	13(1)
P(1)	6832(5)	7431(5)	-1318(6)	19(2)
S(1)	5822(5)	6304(5)	-966(6)	26(2)
S(2)	8322(5)	6848(5)	-1771(6)	22(2)
S(3)	3187(5)	6557(5)	240(6)	21(2)

* U(eq) is defined as one third of the trace of the orthogonalized U^{ij} tensor.

Table 3.19. Selected Bond lengths [Å] for $U(P_2S_6)_2$

U(1)-S(1)	2.861(6)	P(1)-S(1)	1.973(8)
U(1)-S(1A)	2.861(6)	P(1)-S(3)	2.005(9)
U(1)-S(1B)	2.861(6)	P(1)-S(2)	2.099(8)
U(1)-S(1C)	2.861(6)	P(1)-S(2A)	2.102(9)
U(1)-S(3)	2.804(6)		
U(1)-S(3A)	2.804(6)		
U(1)-S(3B)	2.804(6)		
U(1)-S(3C)	2.804(6)		

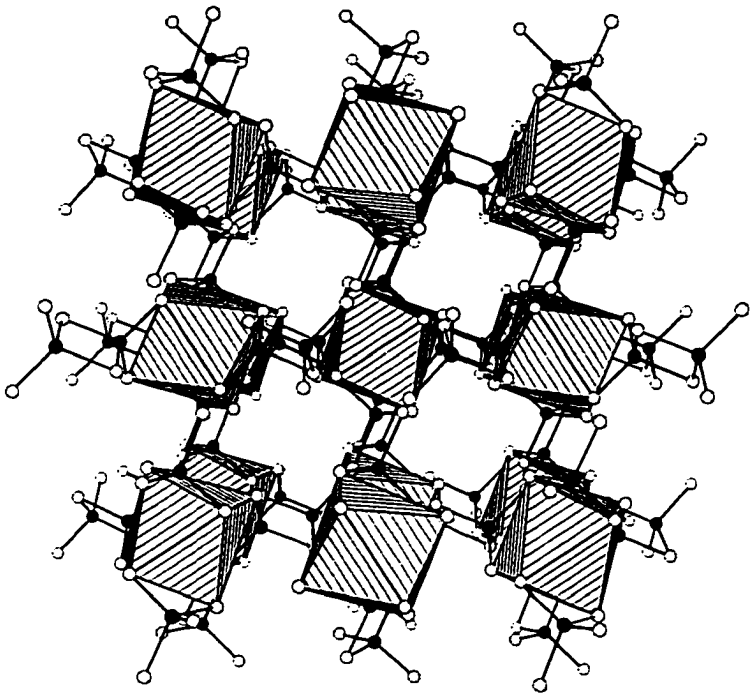

Figure 3.34. View of the $U(P_2S_6)_2$ structure down the [001] crystallographic direction. The polyhedra are US_8, the P atoms are filled circles, and the S atoms are the unfilled circles. It is important to note that the US_8 polyhedra are linked together solely through $(P_2S_6)^{2-}$ ligands. The polyhedra do not share any S atoms.

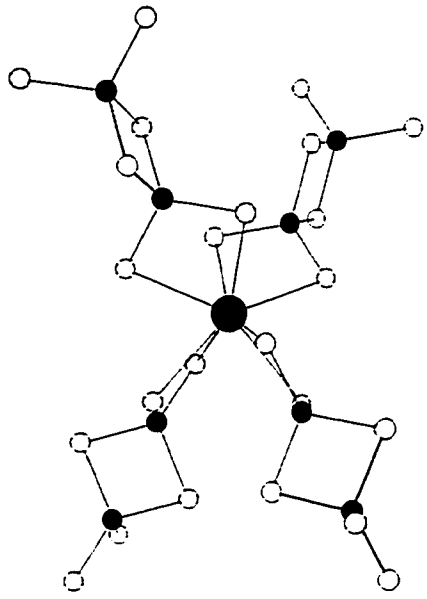

Figure 3.35. View of the coordination environment around U(1). U(1) is coordinated to eight S atoms in a distorted square anti-prismatic geometry. The S atoms belong to four $(P_2S_6)^{2-}$ ligands each of which share one of its edges. The U atom is the large filled circle, the P atoms are the small filled circles, and the S atoms are the unfilled circles.

adopt a diborane-like geometry that consists of two edge-sharing PS_4 units. As seen in Figure 3.35, no P-P bond is present, therefore P is in the 5+ oxidation state and the ligand has an overall 2- charge. Four of these ligands are bound to each uranium atom. All of the sulfur atoms coordinated to uranium belong to P_2S_6 ligands, there are no terminal sulfur atoms present. The US_8 polyhedra are arranged in such a way that there are channels, with dimensions 3.92 Å x 5.20 Å, running throughout the structure.

UP_2S_6

This compound has a three-dimensional lattice that is composed of US_8 dodecahedra linked together by $(P_2S_6)^{4-}$ ligands. Figure 3.36 contains two views of the UP_2S_6 structure. Figure 3.36(a) contains a view of UP_2S_6 down the [001] crystallographic direction while Figure 3.36(b) contains a view of a single layer of the structure in the *bc* plane. The key difference between the UP_2S_6 and $U(P_2S_6)_2$ is the geometry of the thiophosphate ligand. The $(P_2S_6)^{4-}$ ligand in UP_2S_6 has an ethane-like geometry and contains a P-P bond. In this ligand, phosphorus is tetravalent. Identical ligands are found in $Cs_4Th_2(P_2S_6)_3$. As described above, the $(P_2S_6)^{2-}$ ligands found in $U(P_2S_6)_2$ have a diborane-like geometry and do not contain a P-P bond. Therefore the phosphorous atoms present in $U(P_2S_6)_2$ are in the 4+ oxidation state. Another significant difference between the two structures is in the interconnectivity of the US_8 polyhedra. In UP_2S_6, each US_8 polyhedron shares two edges with neighboring polyhedra to form chains along the [001] direction. These chains are linked together to form a three-dimensional lattice through the coordination of $(P_2S_6)^{4-}$ ligands. This structure contains channels as well, with dimensions 3.54 Å x 5.83 Å.

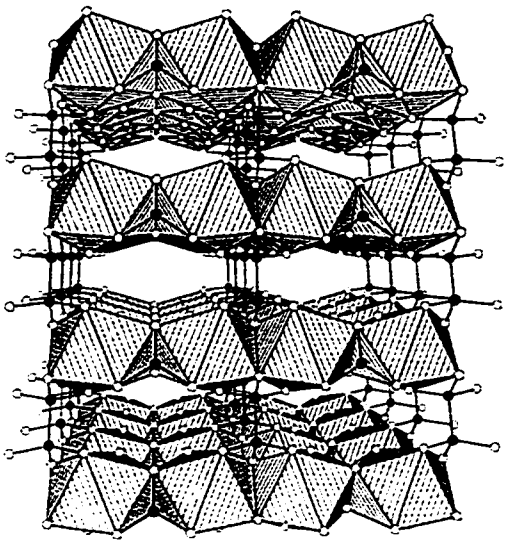

(a)

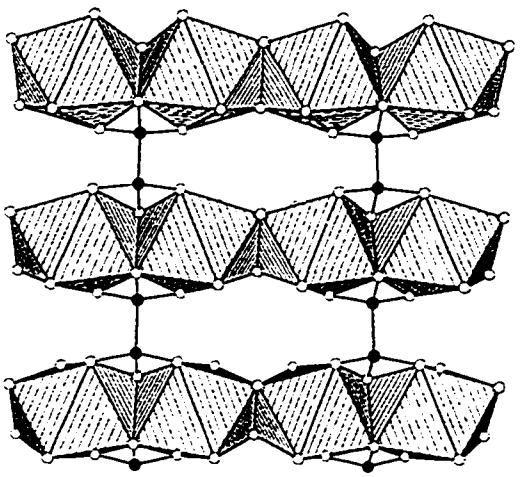

(b)

Figure 3.36. (a) View of the UP_2S_6 structure down the [001] crystallographic direction. (b) view of the *bc* plane in the UP_2S_6 structure. In both figures note the edge-sharing between US_8 polyhedra. The US_8 polyhedra in $U(P_2S_6)_2$ are linked only through $(P_2S_6)^{2-}$ ligands. Also note the presence of the P-P bond in each $(P_2S_6)^{4-}$ ligand. The polyhedra are US_8, the P atoms are the filled circles, and the S atoms are the unfilled circles.

Electronic Spectroscopy

Diffuse reflectance spectroscopy was used to analyze the electronic structure of the materials. The spectra for the two uranium compounds, **I** and **III**, are shown in Figure 3.37 while the spectra for the three thorium compounds, **II**, **IV**, and **VII**, are shown in Figure 3.38. Band gap analysis using UV-vis-NIR diffuse reflectance spectroscopy indicates that $K_{10}Th_3(P_2S_7)_4(PS_4)_2$, **II**, has a band gap energy of 3.3 eV, $K_5Th(PS_4)_3$, **IV**, has a band gap energy of 3.0 eV, and $Cs_4Th_2(P_2S_6)_3$, **VII**, has a band gap energy of 2.7 eV. These values are expected for colorless compounds. Based on the analysis of compounds **I** and **III**, the materials have a complex electronic structure dominated by the U(IV) electronic manifold. The classical ligand-to-metal charge transfer peak seen in electronic spectra of aqueous U(IV) ions near 660 nm is observed in our compounds at around 730 nm (~1.7 eV).[5] Indeed, some fine structure is observed in the spectrum of **III**. The shift to lower energy is likely because the energy levels of the thiophosphate ligand are closer to the empty f-orbitals on uranium, indicating a more *covalent* bonding relationship with the thiophosphate than is observed in the ionic or dipolar relationships found in solution. Another general feature of the spectra is that they both show a broad rise in relative absorption beginning near 1.9 eV, consistent with the color of the materials and indicating some level of band structure to the electronic structure of the materials.

Raman Spectroscopy

Raman spectra were collected on hand-picked crystals of the compounds and are shown in Figures 3.39 and 3.40. The general features of the spectra in Figure 3.39 comprise low-energy peaks indicative of the PS_4 tetrahedral units, spectra dominated by

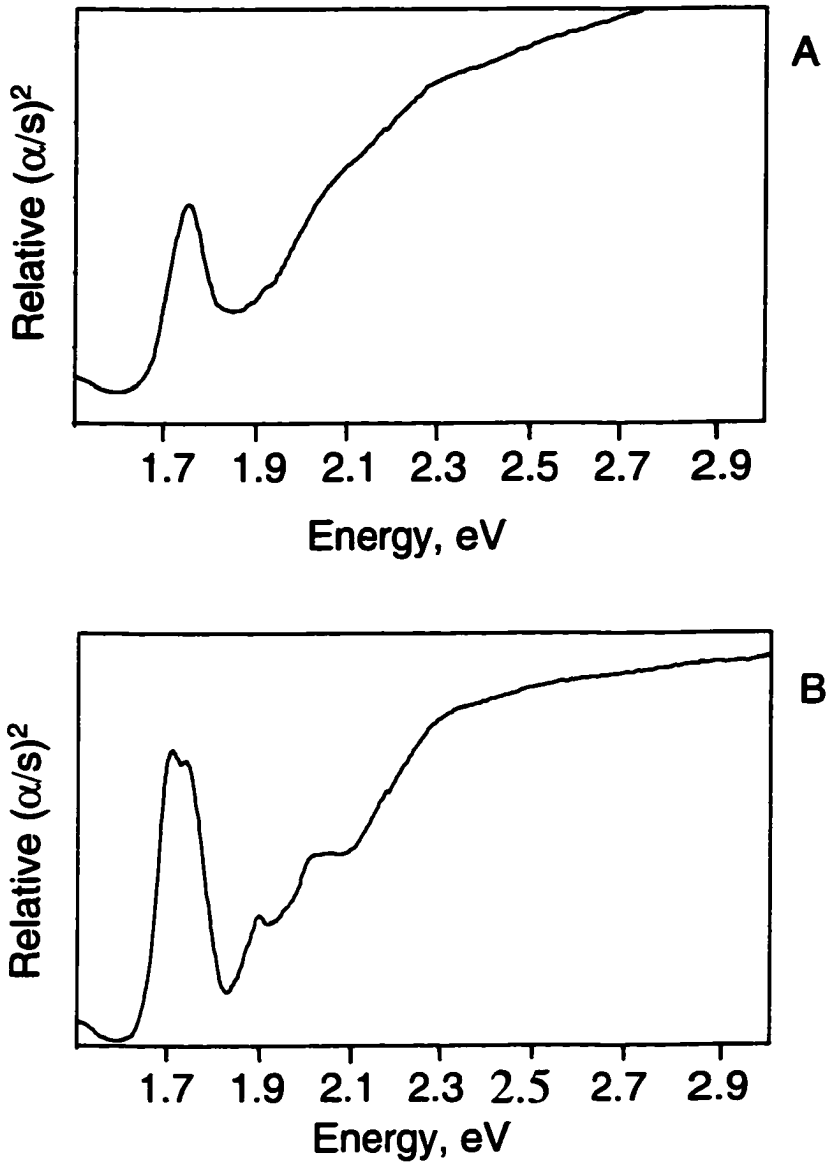

Figure 3.37. Diffuse reflectance spectra of A. $Cs_8U_5(P_3S_{10})_2(PS_4)_6$, **I**, B. $K_5U(PS_4)_3$, **III**. α is defined as the absorption coefficient and s is defined as the scattering coefficient.

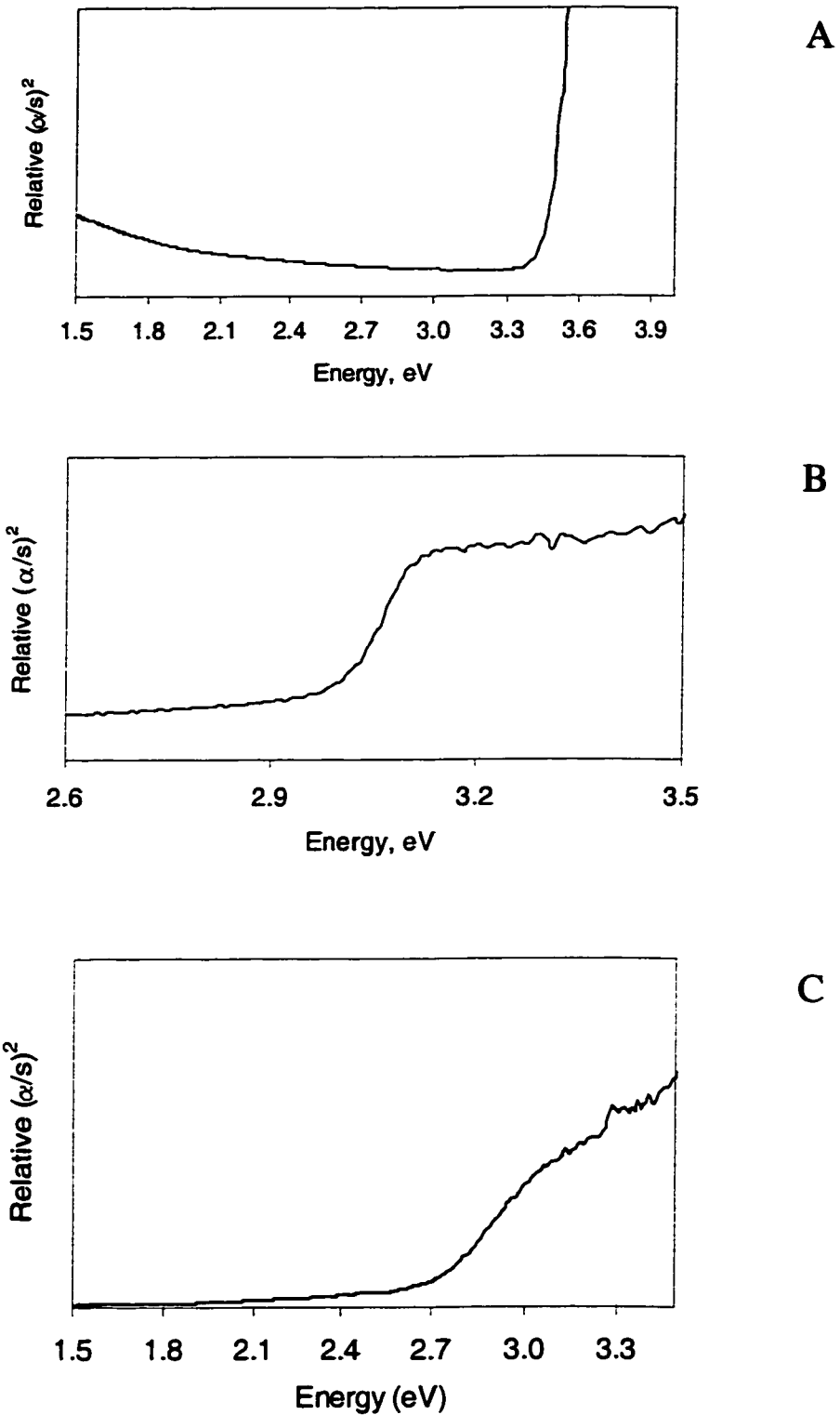

Figure 3.38. Diffuse reflectance spectra of A. $K_{10}Th_3(P_2S_7)_4(PS_4)_2$, **II**, B. $K_5Th(PS_4)_3$, **IV**, C. $Cs_4Th_2(P_2S_6)_3$, **VII**. α is defined as the absorption coefficient and s is defined as the scattering coefficient.

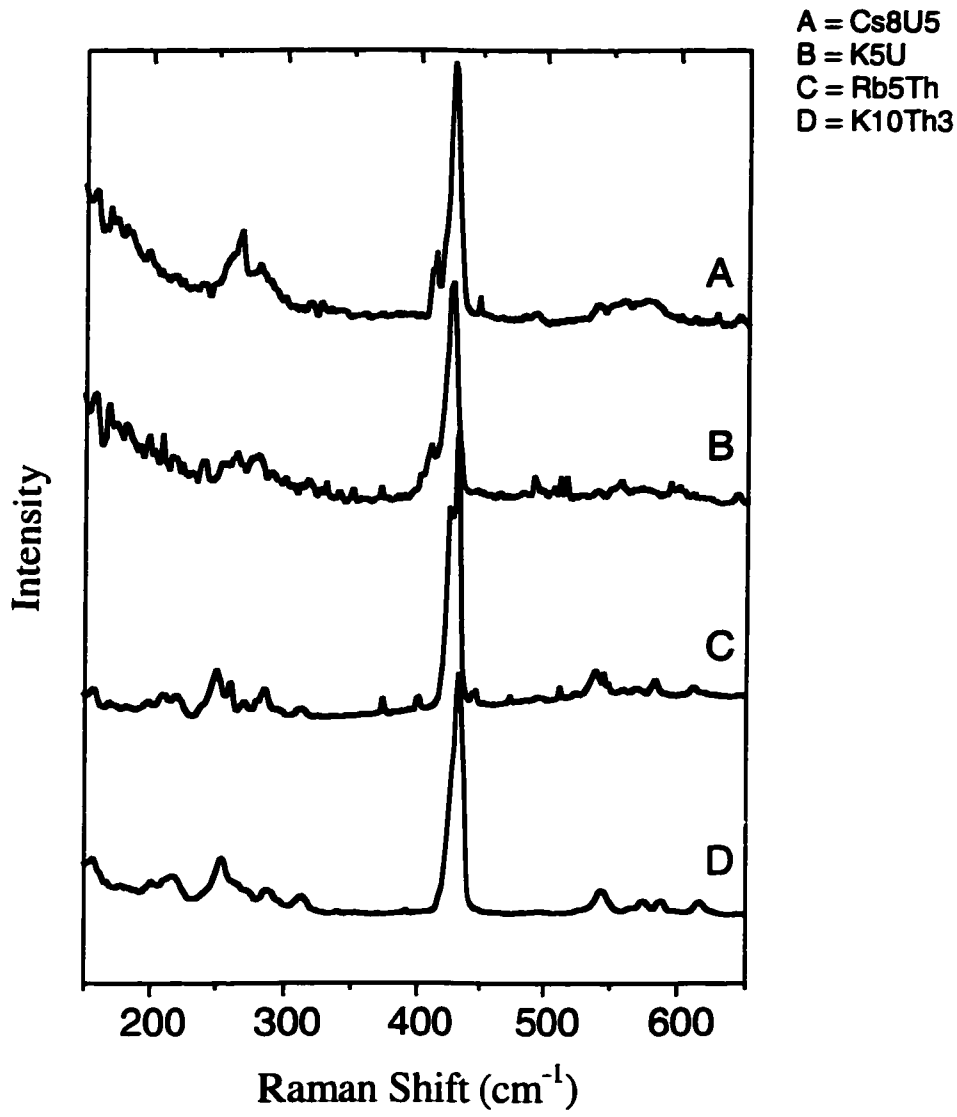

Figure 3.39. Raman spectra of A. $Cs_8U_5(P_3S_{10})_2(PS_4)_6$, **I**, B. $K_5U(PS_4)_3$, **III**, C. $Rb_5Th(PS_4)_3$, **V**, D. $K_{10}Th_3(P_2S_7)_4(PS_4)_2$, **II**.

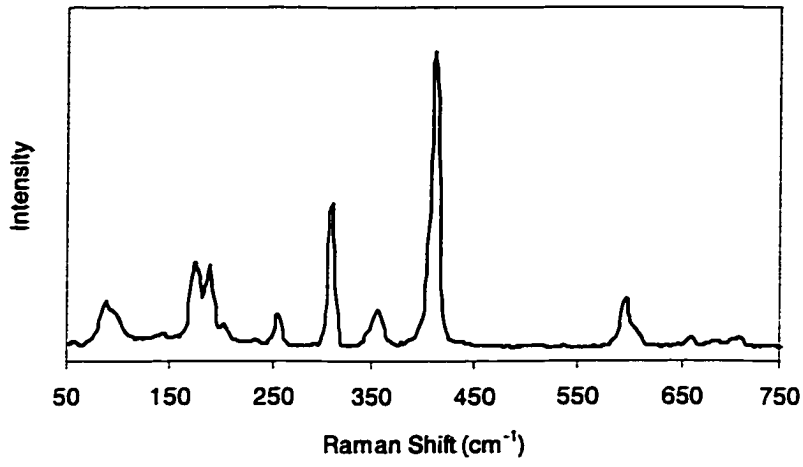

Figure 3.40. Raman spectrum of $Cs_4Th_2(P_2S_6)_3$.

the symmetric stretch near 430 cm^{-1}. Specifically, peaks are recorded in Table 3.20 and assigned based on the pseudo-tetrahedral symmetry of the PS_4 units in all compounds and the P_2S_7 or P_3S_{10} units in compounds **I** and **II**.[57-58] The general features of the spectrum in Figure 3.40 of $Cs_4Th_2(P_2S_6)_3$ are indicative of the $(P_2S_6)^{4-}$ ethane-like unit. The peaks are recorded in Table 3.21 and are assigned based on the pseudo-D_{3d} symmetry of the $(P_2S_6)^{4-}$ unit. These spectra are in relatively good agreement with the literature except for the shift to higher energy of the totally symmetric, high-intensity peak in all the spectra that can come about due to the relative binding of the thiophosphate to the actinide metal atoms. The main symmetric stretching mode of the PS_4 units is observed in each sample. Several other low energy peaks related to the tetrahedral stretching modes (four total) or pseudo-C_{2v} symmetry of the P_2S_7 unit found in $Ag_4P_2S_7$.[59]

Comparison with Known Chalcophosphate Chemistry

The eight compounds described above are all new thiophosphate structure types. No isostructural rare earth analogs are known. In addition, $Cs_8U_5(P_3S_{10})_2(PS_4)_6$, contains the $(P_3S_{10})^{5-}$ ligand which is not found in any other thiophosphate compound. A key difference between the actinide and lanthanide chemistry is the availability of multiple oxidation states. For nearly all rare-earth elements 3+ is the most common oxidation state. The actinide elements, however, can obtain oxidation states ranging from 2+ to 7+ depending on their position in the series. With only one exception, all of the known thorium compounds contain thorium in the 4+ oxidation state. The organometallic compound, $[(\eta^5\text{-Cp''})_3Th]$, contains thorium(III).[60] While uranium chemistry is more diverse, 3+, 4+, and 6+ are common, nearly all known uranium chalcogenide compounds contain tetravalent uranium. Kanatzidis and co-workers published the structure of

Table 3.20. Raman Spectral Data of Selected Compounds*. Assignments are From References [59,61].

$Cs_8U_5P_{12}S_{44}$	$K_{10}Th_3P_{10}S_{36}$	$K_5UP_3S_{12}$	$Rb_5ThP_3S_{12}$	$CuHgPS_4$ Ref. 59	Assign. PS_4 in T_d	$Ag_4P_2S_7$ Ref. 61.	Assign. P_2S_7 in C_{2v}
	215 m		210 w			203 m	ν_{20} (B_2)
265 m	254 m	260 w	254 m	236 m	ν_2 (E)	247 m	ν_9 (A_2)
300 w	289 m, 315 m	279 w	287 m	298 s	ν_4 (T_2)	300 m	ν_{13} (B_2)
425 vs	431 vs	424 s	430 vs	402 vs	ν_1 (A_1)	400 vs	ν_3 (A_1)
480 w						477 m	ν_{17} (B_2)
		500 w	490 vw	509 w	ν_3 (T_2)		
						516 m	ν_2 (A_1)
540 w	540 m	550 w	540 m	540 m	ν_3 (T_2)	555 m	ν_2 (A_1)
570 w	570 w	575 w	579 w	570 m	ν_3 (T_2)		
	590 w					590 w	ν_1 (A_1)
	615 w					602 w	ν_{12} (B_1)

* Vibrational frequencies, cm^{-1} and relative intensities

Table 3.21. Raman Spectral Data of Selected Compounds*

$Cs_4Th_2(P_2S_6)_3$	$KLaP_2S_6$	$K_2FeP_2S_6$	Assign P_2S_6 ref 62
89	90		
97	111		
	153		
174			
188		183	ν_3 (A_{1g})
204	204		
	217		
		228	ν_8 (E_g)
255		245	ν_{11} (E_u)
	259		
	275		
	288	280	ν_8 (E_g)
310			
358			
		378	
412	387	391	ν_2 (A_{1g})
	561	565	ν_4 (A_{1g})
596	589	585	ν_7 (E_g)

* Vibrational frequencies, cm^{-1} and relative intensities.

$Rb_4U_4P_4Se_{26}$ and claimed that U is in the 5+ oxidation state.[23] The merits of their assignment and how it relates to $Cs_4Th_4P_4Se_{26}$ was discussed in the Introduction section of this chapter. It is important to note that the structures of **I-VIII** are also unique with respect to known actinide selenophosphates. This is not true in the case of some rare earth chalcophosphate compounds where isostructural sulfur and selenium phases are known.

Of the known rare-earth thiophosphate compounds only two are structurally related to the actinide thiophosphates described above. $KLaP_2S_6$, shown in Figure 3.41, has a 2D layered structure that is similar to the $Cs_4Th_2(P_2S_6)_3$ structure.[62] In both compounds the only thiophosphate ligand present is $(P_2S_6)^{4-}$. The coordination environment around La(1) and Th(2) are very similar. Both metals are coordinated to nine sulfurs belonging to four ligands. Two $(P_2S_6)^{4-}$ ligands are coordinated to the metal atom in a face-sharing arrangement, one ligand is edge-sharing and one is corner-sharing. The key difference in the structures is the way in which the polyhedra link together to form layers. In the thorium compound the polyhedra edge and face share with each other to form tetramers. These tetramers are then linked together to form layers through $(P_2S_6)^{4-}$ ligands. The lanthanum structure however does not rely solely on its ligands to provide 2D connectivity. In this compound the would-be tetramers undergo an additional edge-sharing interaction and form a more densely packed layer. The $(P_2S_6)^{4-}$ ligands simply provide additional cross-linking of LaS_9 polyhedra.

The second related rare earth structure is $K_4La_{0.67}(PS_4)_2$ which shares many interesting structural features with $K_5U(PS_4)_3$.[62] The lanthanum compound forms quasi-infinite 1D chains consisting of LaS_8 polyhedra that are linked together through edge-

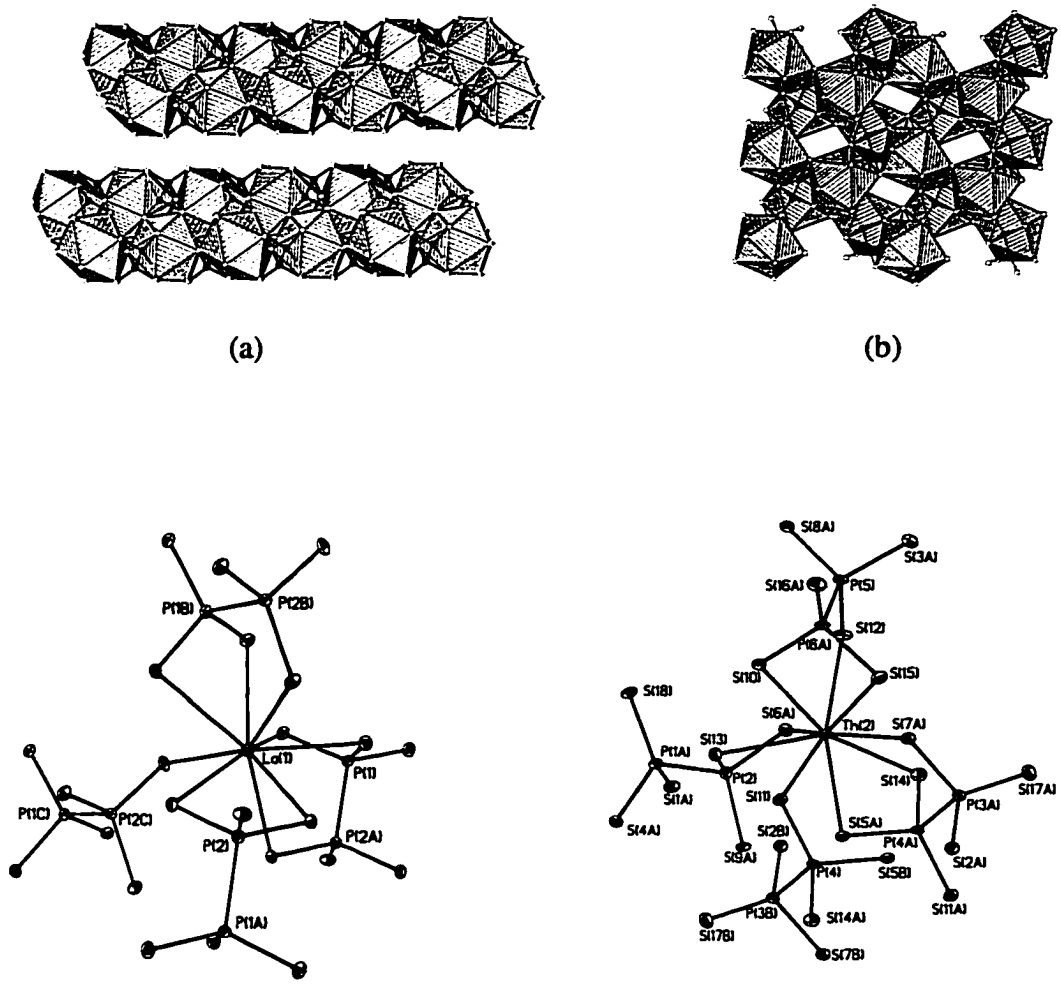

Figure 3.41. Two views of the $KLaP_2S_6$ structure (a) and (b); (c) shows the coordination environment around the La atom in $KLaP_2S_6$; (d) shows the coordination environment around Th(2) in $Cs_4Th_2(P_2S_6)_3$ for comparison.

sharing with neighboring polyhedra and $(PS_4)^{3-}$ ligands. A view of this structure is found in Figure 3.42(a). The La(1) position is only 2/3 occupied, however, which in effect causes the random formation of dimers instead of a truly infinite chain. These "dimers" are remarkably similar in structure to the $K_5U(PS_4)_3$ compound described earlier in this chapter. This similarity can be clearly seen in Figure 3.42(b). In both structures, the metal polyhedra are linked together through two distorted $(PS_4)^{4-}$ ligands. This can be seen by looking at P(1C) and P(1A) in Figure 3.42(a), and P(2) and P(2A) in Figure 3.42(b). In each PS_4 ligand one of the sulfur atoms bridges two metals together forming an edge-sharing interaction. Interestingly, the bridge is asymmetric with one metal sulfur bond longer than the other. The four "terminal" PS_4 ligands in both structures are bound to the metals via the same edge-sharing interactions.

Conclusions

We have synthesized six new thiophosphate actinide materials using the thiophosphate intermediate-temperature flux reaction on actinide metals. The use of a reactive flux has allowed us to form complex structures at relatively low temperatures. These compounds range in structural diversity from three-dimensional solids interconnected through the new $(P_3S_{10})^{3-}$ ligand to a series of related dimers bridged by the $(PS_4)^{3-}$ ligand and affected by packing forces. The new compounds have been studied by electronic spectroscopy (diffuse reflectance) and by Raman vibrational analysis. These methods confirm the electronic and structural diversity that comprise these new compounds. Magnetic measurements, which were not performed on these compounds, are being considered. These thorium and uranium studies have demonstrated the unique differences between lanthanide and actinide chemistry. While

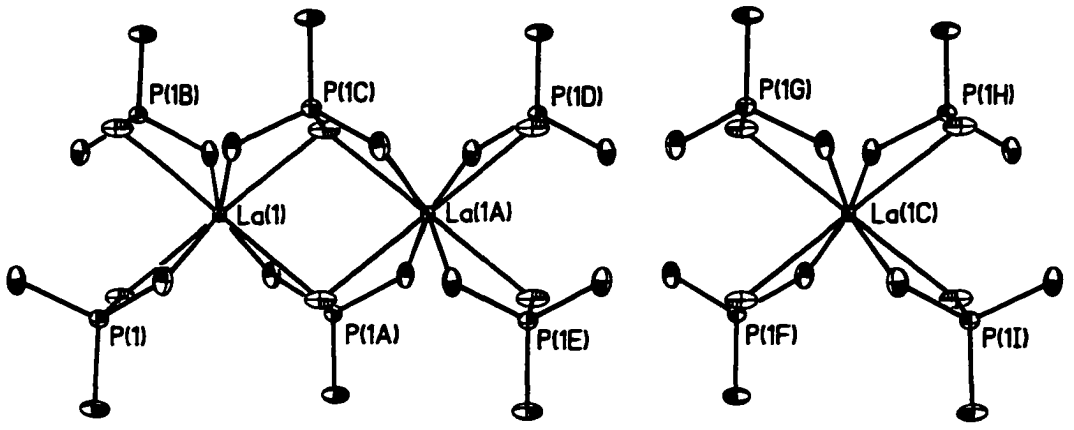

(a)

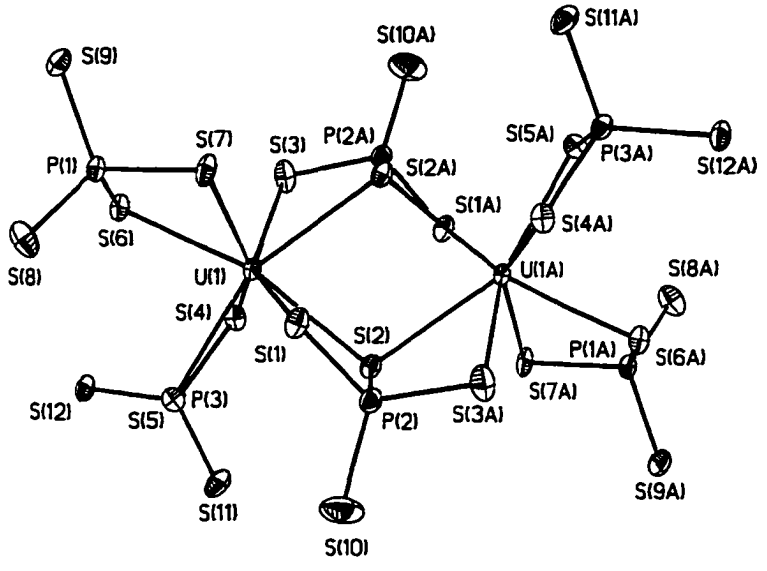

(b)

Figure 3.42.(a) View of the $K_4La_{0.67}(PS_4)_2$ along the chain axis. Note that the effect of La partial occupancy is the random formation of dimers. Figure 3.42(b) contains a view of a dimer in $K_5U(PS_4)_3$.

some similarities between **I-VIII** and rare earth thiophosphates exist, the overall structures are entirely unique.

Chapter 4

Plutonium Thiophosphate Chemistry

(Sections of this work have published in the Journal of the American Chemical Society, in press, 2001.)

Introduction

The fundamental chemistry of plutonium has been summarized in several sources.[63-65] Aside from the extensive work in metal oxide chemistry and metallurgy, many of the fundamental bonding characteristics, coordination geometries, and solid state chemical properties of other compositions of this rare metal have been overlooked due to the hazards associated with its inherent radioactivity. Nevertheless, the extreme stability to high temperatures (mp = 2350 °C) and its relative inert behavior toward steam at 250 °C makes PuS an attractive candidate for fast reactor nuclear fuel, possessing chemical stability that exceeds that of nitrides and phosphides.[66] Because of the importance of stockpiles of plutonium to the world energy stores, there still remains a need for the study of fundamental solid-state chemistry of more complex plutonium sulfides.

Two members of the Dorhout group, Drs. John Chen and Carl Evenson, carried out extensive explorations into the quaternary phase space of rare-earth metal chalcophosphate systems and investigated many of the bonding characteristics and coordination geometries of the 4f-elements, with the softer members of the chalcogen family.[16-17] The goal of the research described in this chapter was to better understand the fundamental solid state chemistry of plutonium in chalcogen rich environments. At the time this work was carried out, only 80 plutonium crystal structures were listed in the Inorganic Crystal Structure Data Base (ICSD). By far, the vast majority of known plutonium structures were intermetallic or oxide based compounds. Of these 80 structures, only four contained sulfur and all of them were binary compounds. No plutonium selenide or telluride compounds were listed. The known binary plutonium

chalcogenide phases and their structures are discussed in a separate section later in this chapter.

The new plutonium structures described in this chapter will be compared to not only lanthanide based compounds but also the quaternary chalcogenide compounds containing the early actinide elements thorium and uranium. It is interesting to note the differences in the structural chemistry of the actinide elements as one progresses from the early to mid sections of the 5f-series.

The use of moderate-temperature (300-800 °C) reactive molten salts is the key to the synthetic paradox that has limited plutonium solid-state chemistry. The low melting point of plutonium (640°C) and the vigorous reactivity of the liquid with most conventional reaction vessels prevent a safe exploration of any moderate-to-high temperature synthetic chemistry.[64,65] As has been shown for transition metal and lanthanide metal chemistry, the thiophosphate flux can facilitate the low-to-moderate temperature reactions of metals with the flux components while promoting the nucleation and growth of single-crystalline products.

The synthesis and characterization of the first plutonium thiophosphate compounds $K_3Pu(PS_4)_2$ (**I**), $APuP_2S_7$ (**II**, **III**, **IV**), where A = K, Rb, Cs, and $Rb_4Pu_2(P_2S_6)(PS_4)_2$ (**V**) is described below. Compound **I** is isostructural with $K_3Ce(PS_4)_2$ synthesized by Brec and co-workers and our $K_3La(PS_4)_2$ and has an isolated, infinite chain structure.[14,67] Compounds **II-IV** are isostructural with $KSmP_2S_7$ and are comprised of layers of plutonium atoms linked by $(P_2S_7)^{4-}$ ligands, a structural building unit that has not been seen in any of the corresponding actinide work. Compound **V** is isostructural with $K_4La_2(P_2S_6)(PS_4)_2$ and is comprised of layers of plutonium atoms linked by $(P_2S_6)^{4-}$

and $(PS_4)^{3-}$ ligands. Compound **V** is the first actinide thiophosphate compound to contain the ethane-like $(P_2S_6)^{4-}$.

This chapter will reveal a series of consistent bond distances and coordination geometries for an environment of sulfur around plutonium (III) and we will develop some guidelines for the description of soft donor ligands around a relatively soft actinide cation.[68] Finally, since compounds **II** - **IV** are isostructural, only the detailed description of **II** will be given here. Pertinent bond distances and angles for **III** and **IV** will be included in the discussion of the structures for the sake of comparison.

Binary Plutonium Chalcogenides

While numerous binary plutonium chalcogenides have been synthesized, structural information on these compounds is widely scattered. A detailed search of the literature identifies a number of oxide, sulfide, selenide, and telluride compounds. Table 4.1 contains a list of known binary plutonium chalcogenides and their related structure types. What is known about the structures of these phases comes primarily from powder X-ray diffraction experiments. The majority of these compounds were identified by comparison of their powder diffraction patterns with those of rare earth chalcogenides and well-known structure types. No single crystal X-ray diffraction studies on binary plutonium chalcogenides have been carried out to date.

The plutonium-oxygen system is the most thoroughly characterized plutonium chalcogenide system. This is due to the fact that understanding the oxidation of plutonium metal is critical to a number of applications ranging weapons and reactor fuel materials, to waste storage forms. Six plutonium oxides have been characterized with O/Pu ratios from 1.0 (PuO) to 2.0 (PuO_2). Plutonium dioxide has the highest chalcogen

Table 4.1. List of known binary plutonium chalcogenide compounds and their structure types.

Oxides		Sulfides		Selenides		Tellurides	
						$PuTe_3$	$NdTe_3$
PuO_2	CaF_2	PuS_2	$CeSe_2$			$PuTe_{2.02}$	$CeSe_2$
		$PuS_{1.9}$	Fe_2As	$PuSe_{1.9}$	Fe_2As	$PuTe_{2-x}$	Fe_2As
				$PuSe_{1.8}$	Fe_2As	$PuTe_{1.81}$	Fe_2As
α-Pu_2O_3	Mn_2O_3	α-Pu_2S_3	Ce_2S_3	γ-Pu_2Se_3	Th_3P_4	γ-Pu_2Te_3	Th_3P_4
				η-Pu_2Se_3	U_2S_3	η-Pu_2Te_3	Nd_2Te_3
α'-Pu_2O_3	Mn_2O_3	β-Pu_2S_{3-x}	Ce_5S_7				
β-Pu_2O_3	La_2O_3	γ-Pu_2S_{3-x}	Th_3P_4	γ-Pu_2Se_{3-x}	Th_3P_4		
		Pu_3S_4	Th_3P_4				
PuO	NaCl	PuS	NaCl	PuSe	NaCl	PuTe	NaCl

content of the known plutonium oxide phases. Like thorium dioxide, PuO_2 has a CaF_2 structure. Figure 3.1 contains an example of the CaF_2 structure type viewed down the [111] crystallographic direction. The plutonium atoms are coordinated to eight oxygen atoms in a cubic geometry. The PuO_8 polyhedra share edges and faces with neighboring polyhedra to form a three-dimensional network. Three plutonium sesquioxides have been characterized. The alpha and alpha prime phases have Mn_2O_3 structures, while the beta phase crystallizes with the La_2O_3 structure. A monoxide phase, PuO, has also been observed and, like the uranium system, has a sodium chloride structure.[5]

The plutonium-sulfur system is more complex than the oxide system and contains seven phases.[5] Interestingly, none of the sulfides are isostructural with the oxides except for PuS, which has the NaCl structure. The seven sulfide phases have S/Pu ratios from 1.0 (PuS) to 2.0 (PuS_2). Plutonium disulfide has a much more complex structure compared to PuO_2. Plutonium disulfide crystallizes in the tetragonal crystal system and is isostructural with $CeSe_2$. A view of $CeSe_2$ down the [010] crystallographic direction is shown in Figure 4.1. Cerium disulfide has a three-dimensional structure containing one unique cerium atom coordinated to nine Se atoms in a capped square anti-prismatic geometry. The plutonium-sulfur bond distances found in PuS_2 are 2.89 Å and 2.92 Å. A defect disulfide phase has been characterized and has the formula $PuS_{1.9}$. This compound crystallizes with the Fe_2As structure and is not isostructural with PuS_2. A view of the Fe_2As structure down the [100] crystallographic direction is shown in Figure 4.2. Iron arsenide has a three-dimensional structure that is similar to $CeSe_2$.

Three plutonium sesquisulfide phases have been characterized. The alpha and beta phases are isostructural with the cerium sulfides, Ce_2S_3 and Ce_5S_7 respectively. The

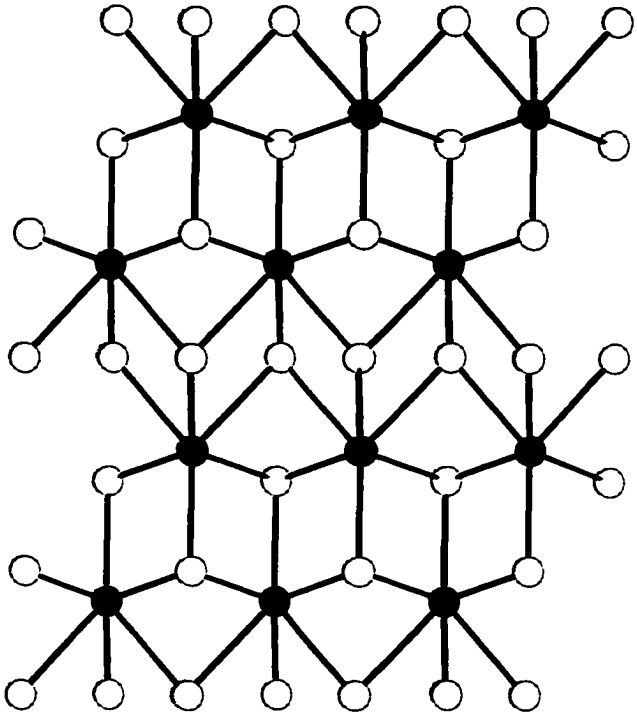

Figure 4.1. View of the $CeSe_2$ structure down the [010] crystallographic direction. Plutonium disulfide is isostructural with $CeSe_2$. The filled circles are the Ce atoms and the unfilled circles are the Se atoms.

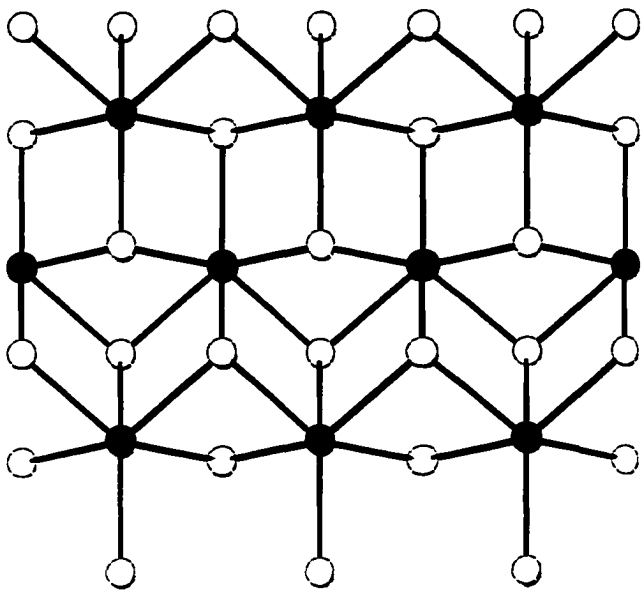

Figure 4.2. View of the Fe_2As structure down the [100] crystallographic direction. The filled circles are the As atoms and the unfilled circles are the Fe atoms.

gamma phase crystallizes in the Th_3P_4 structure type. A view of Th_3P_4 is shown in Figure 3.7. The alpha phase contains one crystallographically unique plutonium atom coordinated to eight sulfur atoms in a dodecahedral. The PuS_8 dodecahedra share edges and faces with neighboring polyhedra to form a complex three-dimensional network. Zacharisen and co-workers reported Pu-S distances of 2.93 Å in the alpha phase structure.[36] The remaining plutonium sulfide phase, Pu_3S_4, has a Th_3P_4 structure similar to γ-Pu_2S_3.[5]

The plutonium-selenium system contains six known phases, all of which are structurally similar to the corresponding plutonium sulfides.[5] The two compounds with the highest Se/Pu ratio are $PuSe_{1.9}$ and $PuSe_{1.8}$. Both of these compounds have Fe_2As structures. No $PuSe_2$ phases have been reported. Three sesquiselenide phases have been characterized. The γ-Pu_2Se_3 and γ-Pu_2Se_{3-x} phases have Th_3P_4 structures while η-Pu_2Se_3 phase is isostructural with U_2S_3 and Sb_2S_3. A view of the antimony sulfide structure type is shown in Figure 3.3. A monoselenide phase has been characterized and crystallizes in the NaCl structure.

The plutonium-tellurium system contains seven known phases with Te/Pu ratios from 1.0 (PuTe) to 3.0 ($PuTe_3$). While in the uranium chalcogenide systems trisulfide, triselenide, and tritelluride phases have all been observed, only the tritelluride has been characterized for plutonium. Plutonium tritelluride is isostructural with the rare earth chalcogenide, $NdTe_3$. No plutonium ditelluride phase exists with an exact Pu:Te ratio of 1:2 but, three defect phases have been characterized with the formulas: $PuTe_{2.02}$, $PuTe_{2-x}$, and $PuTe_{1.81}$. The first compound, $PuTe_{2.02}$ is isostructural with $CeSe_2$, while the other two are isostructural with Fe_2As. Two sesquitellurides have been characterized, γ-Pu_2Te_3

and η-Pu_2Te_3. These compounds are isostructural with Th_3P_4 and Nd_2Te_3 respectively. As was the case for the plutonium sulfur and selenium systems, a monotelluride has been characterized and is isostructural with NaCl.

Experimental

General Synthesis. Red phosphorous powder (99.9%) was obtained from Cerac. Sulfur powder (99.999%) was purchased from Johnson Matthey. ^{239}Pu shot was obtained from Los Alamos National Laboratory purified from the metal halide by electrorefining. K_2S_3, Rb_2S_5, and Cs_2S_2 were prepared from the reaction of stoichiometric amounts of the elements in liquid ammonia as described elsewhere.[46,69] Ampoules for the reactions were fused-silica tubes with 4 mm inner diameter and a 6 mm outer diameter. All reagents were stored and manipulated in an argon-filled negative pressure specialty glovebox. *Warning: ^{239}Pu is a radioactive element with a half-life of $2.41x10^4$ years – extreme caution must be used to prevent inhalation or ingestion.*

Synthesis of $K_3Pu(PS_4)_2$: $K_3Pu(PS_4)_2$ was synthesized from a mixture of 0.1150g (0.481 mmol) Pu, 0.0298g (0.962 mmol) P, 0.1619g (5.05 mmol) S, 0.1259g (0.723 mmol) K_2S_3. The mixture was loaded into a fused silica ampoule and sealed under vacuum. The ampoule was then heated to 500 °C over 16 hours and held there for 200 hours. The ampoule was cooled to ambient temperature at a rate of 3 °C per hour. The ampoules were opened in an inert atmosphere glove box and the products were removed from the container. Excess flux was removed by washing with DMF. Emerald green plates (quantitative in Pu) were then isolated by filtration and selected crystals were handpicked for analysis. No unreacted Pu metal was evident.

Synthesis of $APuP_2S_7$ (II - IV): $KPuP_2S_7$ (II) was synthesized from a mixture of 0.0930g (0.389 mmol) Pu, 0.0723g (2.34 mmol) P, 0.1497g (4.67 mmol) S, 0.0831g (0.584 mmol) K_2S_3. For $RbPuP_2S_7$ (III), a mixture of 0.0550g (0.230 mmol) Pu, 0.0279g (0.921 mmol) P, 0.0554g (1.727 mmol) S, 0.1140g (0.345 mmol) Rb_2S_5. For $CsPuP_2S_7$ (IV), a mixture of 0.0660g (0.276 mmol) Pu, 0.0341g (1.10 mmol) P, 0.1062g (3.31 mmol) S, 0.1367g (0.414 mmol) Cs_2S_2 was used. The mixtures were loaded into fused silica ampoules and sealed under vacuum. The ampoules were then heated to 500 °C over 16 hours and held there for 200 hours. The ampoules were cooled to ambient temperature at a rate of 3 °C per hour. The ampoules were opened in an inert atmosphere glovebox and the products were removed from the container. Excess flux was removed by washing with DMF. Emerald green needles (quantitative in Pu) were then isolated by filtration and selected crystals were handpicked for analysis. No unreacted Pu metal was evident.

Synthesis of $Rb_2Pu(P_2S_6)_{1/2}(PS_4)$ (V): $Rb_2Pu(P_2S_6)_{1/2}(PS_4)$ was synthesized from a mixture of 0.0980g (0.410 mmol) Pu, 0.0761g (2.51 mmol) P, 0.0986g (3.07 mmol) S, 0.2037g (0.615 mmol) Rb_2S_5. The mixture was loaded into a fused silica ampoule and sealed under vacuum. The ampoule was then heated to 500 °C over 16 hours and held there for 200 hours. The ampoule was cooled to ambient temperature at a rate of 3 °C per hour. The ampoules were opened in an inert atmosphere glove box and the products were removed from the container. Excess flux was removed by washing with DMF. Emerald green plates (quantitative in Pu) were then isolated by filtration and selected crystals were handpicked for analysis. No unreacted Pu metal was evident.

Structure Determination. Single-crystal X-ray diffraction was performed on a modified Siemens P4 four-circle diffractometer equipped with a SMART CCD system using graphite-monochromated MoKα radiation.[54] Crystals were selected from the reaction mixtures and placed in a pool of epoxy. The crystals were then removed from the epoxy and placed inside a 0.5 mm capillary tubes. The capillary tubes were then removed from the glovebox, trimmed to the appropriate length and the ends sealed with epoxy. A coating of acrylic was applied to the surface of capillary tubes to provide the third and final layer of containment. The capillary tubes were then placed in the cold stream of the diffractometer. Data collection parameters are found on page 62. Supplementary information is given in Appendix E. as CIF files.

Physical Characterization. UV-visible-NIR spectra were recorded as diffuse reflectance spectra using a Perkin Elmer Lambda 9 UV-visible-NIR spectrometer equipped with a 60 mm integrating sphere. The samples were prepared as a dispersion of single crystals mounted on a Teflon disk that was covered by a cylindrical glass cap sealed with epoxy. Raman vibrational spectra were obtained by exciting from an Ar^+ laser (Spectra Physics, Model 2025) using 514.5 m line. The laser power at the sample was 10mW or less. The scattered light was dispersed and analyzed on a SPEX Model 1403 scanning double monochrometer equipped with an 1800 groove/mm grating and a single-photon-counting detection system. The spectra width was maintained at 5 cm^{-1} resolution. Scan parameters were 1 cm^{-1} increments between points, integration for 2-3 s at each point, and at least 75-90 scans averaged for the final spectrum. Samples were contained within a 9 mm fused silica tube fitted with a Teflon spacer.

Table 4.2. Crystallographic Data for **I – V**

	I	**II**	**III**	**IV**	**V**
Empirical Formula	$K_3PuP_2S_8$	$KPuP_2S_8$	$RbPuP_2S_7$	$CsPuP_2S_7$	$Rb_2PuP_2S_7$
fw	677.72	567.46	613.83	661.27	1398.60
a, Å	9.157(1)	9.641(1)	9.8011(6)	10.1034(7)	22.943(1)
b, Å	16.866(2)	12.255(1)	12.3977(7)	12.5412(9)	6.819(3)
c, Å	9.538(1)	9.0152(8)	9.0263(5)	9.0306(6)	18.826(1)
β, deg	90.610(3)	90.218(2)	90.564(1)	91.007(1)	122.005(1)
V, $Å^3$	1473.0(3)	1065.1(2)	1096.7(1)	1144.1(1)	2498.0(2)
Z	4	4	4	4	4
λ(Mo Kα), Å	0.71073	0.71073	0.71073	0.71073	0.71073
space group	$P2_1/c$ (No.14)	$P2_1/c$ (No.14)	$P2_1/c$ (No.14)	$P2_1/c$ (No.14)	C2/c (No. 15)
temp., K	163(2)	163(2)	163(2)	163(2)	163(2)
$\rho_{calc.}$, g/cm^3	3.056	3.539	3.718	3.839	3.719
R1 % [a]	0.0371	0.0324	0.0510	0.0486	0.0453
wR2 % [a]	0.0918	0.0689	0.1455	0.1221	0.1198

The Structure of $K_3Pu(PS_4)_2$

The compound crystallized as emerald green plates in the monoclinic space group $P2_1/c$ (r_{int}=0.0182) based on the systematic absences observed in the data. Refinement of the model's 127 parameters to the data (1726 reflections) provided an excellent goodness-of-fit (GOF = 1.065) resulting in a relatively flat electron density difference map (max. = 1.916 e^-, min. = -1.744 e^-). Table 4.2 contains the specific data collection and refinement information. Tables 4.3 and 4.4 contain the atomic coordinates and relevant bond distances respectively.

This compound comprises isolated linear chains of PuS_8 bicapped trigonal prisms linked together through both edge-sharing with neighboring PuS_8 polyhedra and $(PS_4)^{3-}$ thiophosphate anions. Figure 4.3 shows a polyhedral packing view of the chains of plutonium (III) thiophosphate and Figure 4.4 shows the coordination environment around the Pu atoms in chains running down [100]. All eight sulfur atoms bound to Pu are part of the thiophosphate anions. The Pu–S bond distances range from 2.846(3) Å to 3.210(3) Å with an average distance of 2.979(8) Å. The two longest bonds in the Pu–S coordination sphere belong to the capping sulfur atoms, S(3) and S(6) with distances of 3.210(3) Å and 3.120(3) Å respectively. In this phase, plutonium should be in the 3+ oxidation state based on charge balance and the relative Pu–S bond distances that are close to those reported for the sesquisulfide and Pu_2O_2S. The green color of the material cannot be the only indicator of plutonium oxidation state – while Pu(III) perchlorate solutions show a strong absorption between 550 and 610 nm (ε = 40 $cm^{-1}M^{-1}$), Pu(IV) solutions will possess an equally strong absorption at 650 nm, along with an absorption at 470 nm.[65] The relative redox potentials of Pu(III) and Pu(IV) in solutions also suggest

Table 4.3. Fractional Atomic Coordinates and Equivalent Isotropic Displacement Parameters ($Å^2 \times 10^3$)[a] for $K_3Pu(PS_4)_2$

	x	y	z	U(eq)
Pu(1)	0.7286(1)	-0.0142(1)	0.5243(1)	21(1)
P(1)	0.0250(3)	0.0979(2)	0.7208(2)	22(1)
P(2)	0.4956(3)	-0.0999(2)	0.7447(3)	22(1)
K(1)	0.7686(3)	0.4679(2)	0.4861(2)	38(1)
K(2)	0.3787(4)	0.2936(2)	0.3745(3)	54(1)
K(3)	0.8841(5)	0.2125(2)	0.3665(3)	68(1)
S(1)	0.8366(4)	-0.1580(2)	0.4085(3)	30(1)
S(2)	0.8137(4)	0.1274(2)	0.6718(3)	31(1)
S(3)	0.0418(4)	-0.0220(2)	0.6781(3)	27(1)
S(4)	0.4648(3)	-0.1207(2)	0.5335(3)	26(1)
S(5)	0.7153(3)	-0.1123(2)	0.7743(3)	31(1)
S(6)	0.4422(4)	0.0174(2)	0.7604(3)	33(1)
S(7)	0.3827(4)	-0.1770(2	0.8604(3)	35(1)
S(8)	0.0671(4)	0.1255(2)	0.9215(3)	31(1)

[a] U(eq) is defined as one third of the trace of the orthogonalized U_{ij} tensor.

Table 4.4. Bond Distances (Å) for $K_3Pu(PS_4)_2$.

Pu(1)-S(1)	2.846(3)	P(1)-S(8)	2.003(3)
Pu(1)-S(2)	2.875(3)	P(1)-S(1)	2.046(3)
Pu(1)-S(5)	2.905(3)	P(1)-S(2)	2.047(3)
Pu(1)-S(4A)	2.933(3)	P(1)-S(3)	2.068(3)
Pu(1)-S(3A)	2.934(3)	P(2)-S(7)	2.000(4)
Pu(1)-S(4)	3.012(3)	P(2)-S(5)	2.039(4)
Pu(1)-S(6)	3.120(3)	P(2)-S(6)	2.043(4)
Pu(1)-S(3)	3.210(3)	P(2)-S(4)	2.061(3)

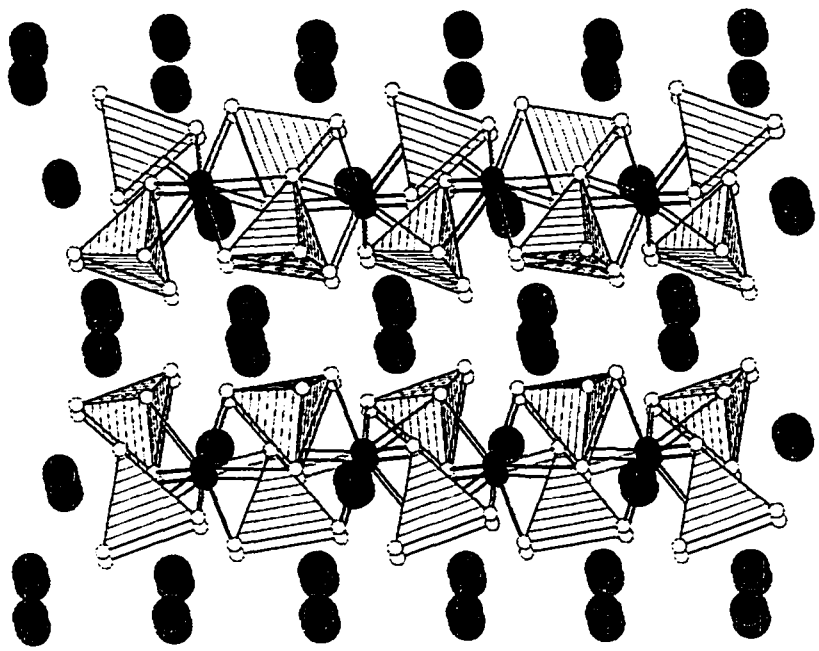

Figure 4.3. Chains of $[Pu(PS_4)_2]^{3-}$ running along [100] as viewed down [001] in $K_3Pu(PS_4)_2$. Dark filled circles are Pu, open circles are S, polyhedra are PS_4 units, and gray circles are K.

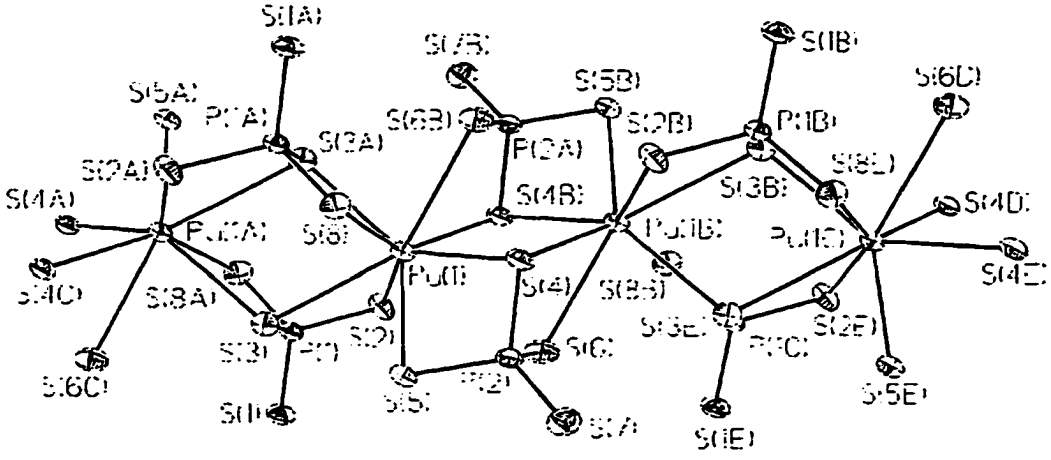

Figure 4.4. Thermal ellipsoid plot (50%) for $K_3Pu(PS_4)_2$ of the environment around the chain of Pu atoms showing the coordination of the $(PS_4)^{3-}$ anions.

that the trivalent state will be the most stable under our reaction conditions.[71] Diffuse reflectance UV-vis-NIR spectroscopy was utilized to empirically determine the oxidation state of plutonium.[26] The results of these experiments are discussed below in the section on electronic spectroscopy .

Each PuS_8 polyhedron shares two of its edges (through S(3) and S(4)) with two other polyhedra to form quasi-infinite chains of $^{1}_{\infty}[Pu(PS_4)_2]^{3-}$. The two shared edges are on opposite sides of the polyhedron and are perpendicular to each other. This bonding arrangement causes the chains to have a kinked morphology as seen in the polyhedral rendering in Figure 4.5. Two distinct $(PS_4)^{3-}$ anions are present in this structure. Both anions share three of their sulfur atoms with Pu atoms. The fourth sulfur atom in both anions (S(1) and S(7)) points away from the plutonium atoms and is bound only to K^+ cations through ionic interactions. In the P(1) thiophosphate anion, S(2) and S(8) are bound to two different plutonium atoms while S(3) bridges the same two atoms. The P(2) thiophosphate anion also has one sulfur atom, S(4), that bridges two plutonium atoms and two sulfur atoms, S(5) and S(6), that are only bound to only one plutonium atom. A significant difference in the two $(PS_4)^{3-}$ anions is their orientation with respect to the chain axis. The triangular face shared by $P(1)S_4$ lies almost parallel to the chain axis and between two plutonium atoms, thus sharing two of its tetrahedral edges with the plutonium polyhedron. The bridging sulfur atom, S(3), has a perfect tetrahedral angle, Pu(1)-S(3)-Pu(1), of 109.50°. The tetrahedron designated as $P(2)S_4$ shares two edges with the plutonium polyhedra, with the bridging sulfur atom, S(4), forming a Pu(1)-S(4)-Pu(1) angle of 90.85°. The differences in the bridging angles of S(3) and S(4) and in the thiophosphate coordination lead to two different Pu•••Pu distances. In the case where two

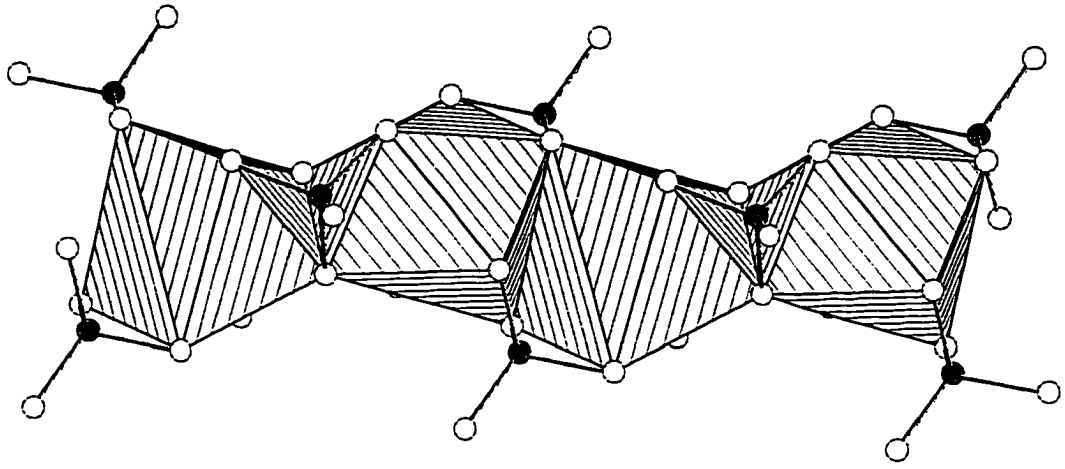

Figure 4.5. Polyhedral view of one chain in $K_3Pu(PS_4)_2$ showing the edge-sharing of plutonium polyhedra. Gray circles are P, open circles are S. Potassium atoms have been removed for clarity.

plutonium atoms are bridged by S(3) (Pu(1) and Pu(1A) in Figure 4.3), the Pu•••Pu distance is 5.02 Å; whereas the two plutonium atoms bridged by S(4) display a Pu···Pu distance of 4.24 Å – both cases are outside the van der Waals radius of plutonium (III).

The charge-compensating K^+ cations fill the void between the plutonium thiophosphate chains, as seen in Figure 4.3. K(1) and K(2) are both coordinated to eight sulfur atoms while K(3) is coordinated to seven sulfur atoms. The K–S bond distances range from 3.174(4) Å to 3.709(4) Å with an average distance of 3.38(1) Å.

The Structure of $KPuP_2S_7$

This compound crystallized as emerald green needles in the monoclinic space group $P2_1/c$ (r_{int} = 0.0423) based on the systematic absences in the data. Refinement of the model's 100 parameters to the data (1376 reflections) provided an excellent goodness-of-fit (GOF = 1.061) resulting in a relatively flat electron density difference map (max. = 2.248 e^-, min. = -0.987 e^-). Table 4.2 contains the specific data collection and refinement information. Tables 4.5 and 4.6 contain the atomic coordinates and relevant bond distances respectively. The main structural features of $KPuP_2S_7$ are the charged corrugated layers of $^2_\infty[PuP_2S_7]^-$ containing one crystallographically distinct Pu atom. The corrugated nature of the layers in this structure is seen in the polyhedral representation shown in Figure 4.6. Each Pu atom is coordinated to eight sulfur atoms in a distorted square antiprismatic geometry. Figure 4.7 shows the coordination environment around the Pu atom, including the $(P_2S_7)^{4-}$ ligands. The Pu–S bond distances range from 2.861(3) Å to 3.056(3) Å with an average distance of 2.938(8) Å. These distances are all consistent with those reported for the sesquisulfide and the

Table 4.5. Fractional Atomic Coordinates and Equivalent Isotropic Displacement Parameters ($Å^2 \times 10^3$)[a] for $KPuP_2S_7$

	x	y	z	U(eq)
Pu(1)	0.8563(1)	0.6429(1)	0.1082(1)	11(1)
K(1)	0.3929(3)	0.6936(2)	-0.1314(3)	25(1)
S(1)	0.0163(3)	0.4404(2)	0.1804(3)	14(1)
S(2)	0.6621(3)	0.5244(2)	-0.0704(3)	16(1)
S(3)	0.1492(3)	0.6949(2)	0.1452(3)	14(1)
S(4)	0.6270(3)	0.5550(2)	0.2898(3)	17(1)
S(5)	0.9095(3)	0.8331(2)	-0.0725(3)	14(1)
S(6)	0.6254(3)	0.7938(2)	0.1119(3)	16(1)
S(7)	0.7502(3)	0.0555(2)	0.0785(3)	14(1)
P(1)	0.1867(3)	0.5371(2)	0.1981(3)	12(1)
P(2)	0.7226(3)	0.8999(2)	-0.0226(3)	11(1)

[a] U(eq) is defined as one third of the trace of the orthogonalized U_{ij} tensor.

Table 4.6. Bond Distances (Å) for $KPuP_2S_7$.

Pu(1)-S(2)	2.861(3)	P(1)-S(2)	2.007(4)
Pu(1)-S(5)	2.890(3)	P(1)-S(3)	2.024(4)
Pu(1)-S(6)	2.894(3)	P(1)-S(1)	2.032(4)
Pu(1)-S(3)	2.912(3)	P(1)-S(7)	2.115(4)
Pu(1)-S(5A)	2.937(3)	P(2)-S(4)	2.001(4)
Pu(1)-S(4)	2.960(3)	P(2)-S(6)	2.011(4)
Pu(1)-S(1)	2.993(3)	P(2)-S(5)	2.031(4)
Pu(1)-S(1A)	3.056(3)	P(2)-S(7)	2.130(4)

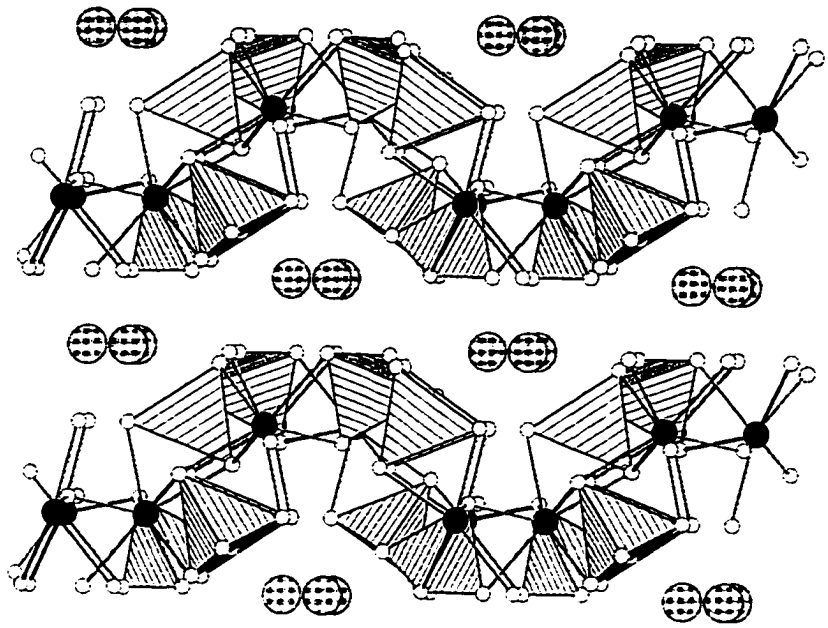

Figure 4.6. Corrugated layers of $[PuP_2S_7]^-$ in $KPuP_2S_7$ viewed down [001]. Dark filled circles are Pu, open circles are S, polyhedra are PS_4 units, and gray circles are K.

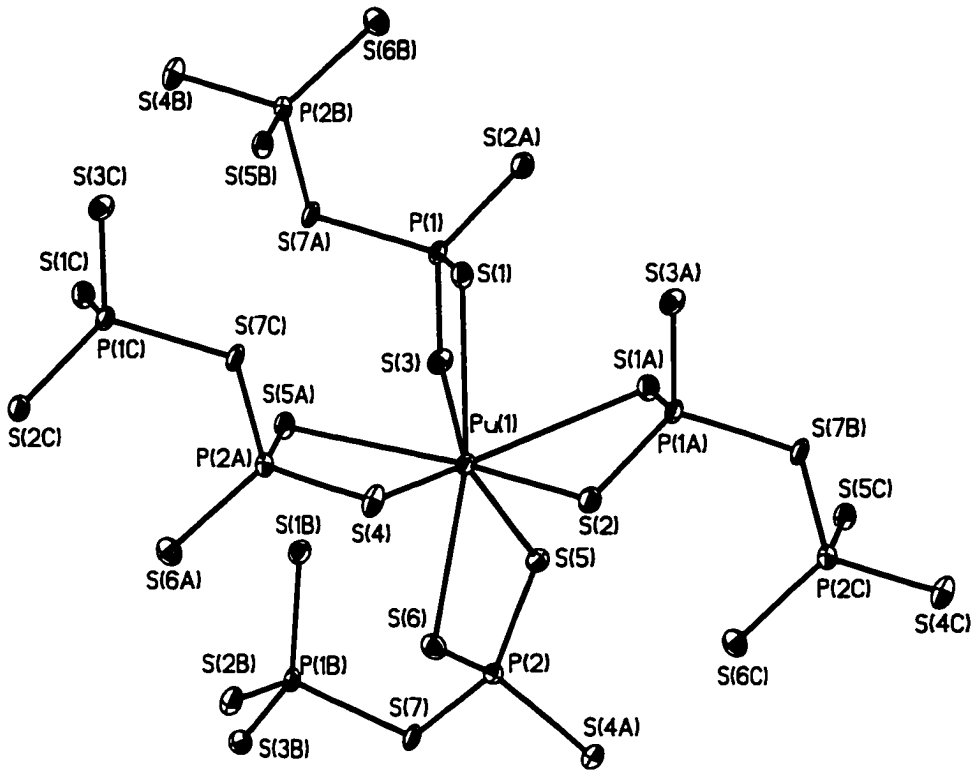

Figure 4.7. Thermal ellipsoid plot (50%) for $KPuP_2S_7$ of the environment around one Pu atom showing the coordination of the $(P_2S_7)^{4-}$ anions.

oxysulfide, Pu_2O_2S. All eight of the coordinated sulfur atoms belong to the $(P_2S_7)^{4-}$ thiophosphate ligand.

Unlike in the chain compound, **I**, the PuS_8 polyhedron shares only one edge with a neighboring PuS_8 polyhedron to form a dimer. Each Pu atom in the dimer corner shares one of its sulfur atoms with another PuS_8 polyhedron. Figure 4.8A illustrates this 2-dimensional network of plutonium sulfide. In addition to the Pu-S-Pu bonding, the $(P_2S_7)^{4-}$ ligands further link the plutonium polyhedra together in a chelate fashion. The $(P_2S_7)^{4-}$ ligand comprises two PS_4 tetrahedral units that corner share one sulfur atom and has been observed in such compounds as $RbV(P_2S_7)$.[72] In compouds **II** - **IV**, the $(P_2S_7)^{4-}$ ligand chelates two plutonium atoms in a tetradentate fashion, shown in Figure 4.8B, where the $(PS_4)^{3-}$ polyhedra have been added to Figure 4.8A. This arrangement of both edge and corner sharing among PuS_8 polyhedra and the tetradentate $(P_2S_7)^{4-}$ ligands leads a corrugated layered structure that contains channels running perpendicular to the layers. The channels, clearly seen in Figure 4.8A, have the dimensions 4.29 Å x 4.24 Å. The layers are not offset from one another allowing the channels to run through the entire structure. The nine-coordinate K^+ cations lie in the interlayer spacing within the channels with interaction distances ranging from 3.232(4) to 3.887(4)Å. The closest Pu•••Pu interaction in this structure is 4.877 Å, and the interlayer spacing is 3.430 Å.

An alternate way of describing the structure in one layer is that the PuS_8 polyhedra corner share through S(5) to form chains running along the [001] direction. The polyhedra also edge share (through S(1) and S(1A)) with neighboring PuS_8 polyhedra along the [010] direction to form layers in the *bc* plane. Based on these corner and edge sharing interactions one can see in Figure. 4.8A that the layers contain 12-

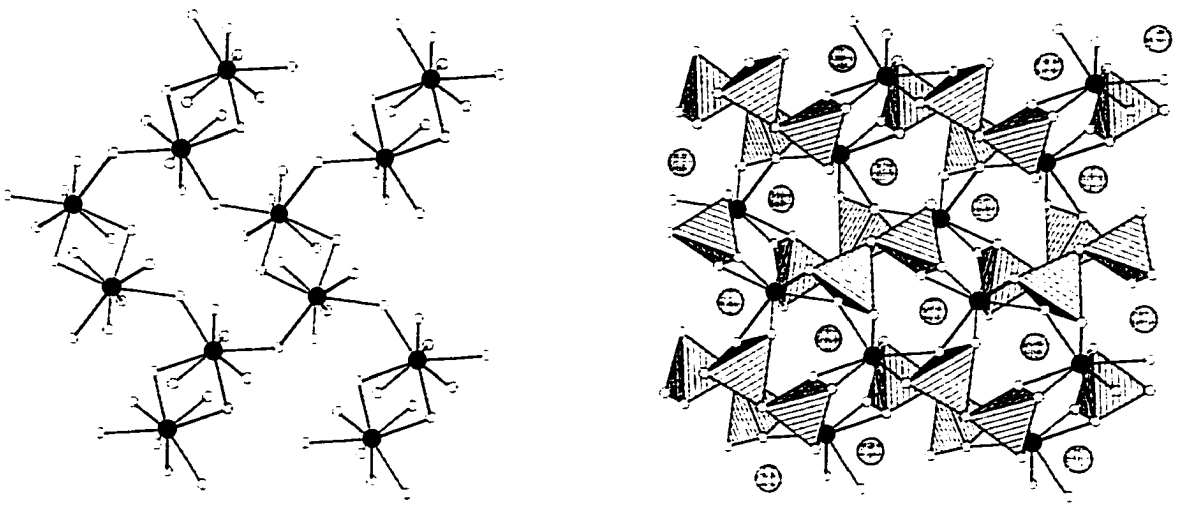

A B

Figure 4.8 A. A view of one layer of $KPuP_2S_7$ in the bc plane with phosphorus and potassium atoms removed for clarity. Zig zag chains of corner sharing PuS_8 run along [001] linked through edge sharing PuS_8 along [010]. **B.** The same layer shown with PS_4 polyhedra and potassium atoms added. The plutonium atoms are the filled circles, the sulfur atoms are the unfilled circles, and the potassium atoms are the shaded circles.

membered rings made built up of two Pu dimeric units linked together through two corner sharing Pu polyhedra creating a 12^3-type net.[73]

The complete bond distance tables for $RbPuP_2S_7$ (**III**), and $CsPuP_2S_7$, (**IV**), can be found in the supporting information; however, for the sake of comparison, the Pu–S bond distances within these structures are all identical to **II**, within the standard deviations of the positional parameters. The layers in **III** and **IV** are propped apart slightly from **II**, a result of the longer Rb–S and Cs–S interactions (3.318(3) – 3.917(4)Å, and 3.454(4) – 3.965(4)Å, respectively).

The Structure of $Rb_2Pu(P_2S_6)_{1/2}(PS_4)$

The compound crystallized as emerald green plates in the monoclinic space group C2/c (r_{int}=0.0254) based on the systematic absences observed in the data. Refinement of the model's 110 parameters to the data (2567 reflections) provided an excellent goodness-of-fit (GOF = 1.146) resulting in a relatively flat electron density difference map (max. = 7.068 e^-, min. = -4.757e^-). Table 4.2 contains the specific data collection and refinement information. Tables 4.7 and 4.8 contain the atomic coordinates and relevant bond distances respectively.

Compound **V** has a two-dimensional layered structure containing PuS_8 square antiprisms and two thiophosphate ligands $[PS_4]^{3-}$ and $[P_2S_6]^{4-}$. The Pu-S bond distances range from 2.865(3) Å to 3.240(3) Å with an average distance of 2.966(4) Å .The Rb^+ cations lie in the van der Waals gap in-between layers. These layers reside in the *ab* plane. Figure 4.9 contains a view highlighting the layered nature of the compound. Figures 4.10 contains a polyhedral view of a single $[Pu(P_2S_6)_{1/2}(PS_4)]^{2-}$ layer. Each layer

Table 4.7. Fractional Atomic Coordinates and Equivalent Isotropic Displacement Parameters ($Å^2 \times 10^3$)[a] for $Rb_2Pu(P_2S_6)_{1/2}(PS_4)$.

	x	y	z	U(eq)
Pu(1)	0.1511(1)	0.5308(1)	0.2313(1)	11(1)
Rb(1)	0.1976(1)	0.4971(2)	0.0275(1)	24(1)
Rb(2)	-0.0158(1)	1.0141(2)	0.1132(1)	21(1)
P(1)	0.1659(1)	-0.0092(3)	0.1366(1)	11(1)
P(2)	0.0474(1)	0.4828(3)	-0.1878(2)	12(1)
S(1)	0.2209(1)	0.9352(4)	0.2630(1)	15(1)
S(2)	0.1004(1)	0.7607(4)	0.3157(1)	16(1)
S(3)	0.2651(1)	0.5039(4)	0.4008(2)	17(1)
S(4)	0.1007(1)	0.2779(4)	0.3137(1)	15(1)
S(5)	0.1013(1)	0.7597(4)	0.0817(1)	15(1)
S(6)	0.1081(1)	0.2378(4)	0.1020(1)	16(1)
S(7)	-0.0146(1)	0.5176(4)	0.1082(2)	16(1)

Table 4.8. Bond Distances (Å) for $Rb_2Pu(P_2S_6)_{1/2}(PS_4)$.

Pu(1)-S(3)	2.865(3)	P(1)-S(5)	2.031(3)
Pu(1)-S(5)	2.875(2)	P(1)-S(3)	2.048(3)
Pu(1)-S(2)	2.881(2)	P(1)-S(1)	2.053(3)
Pu(1)-S(6)	2.889(2)	P(2)-S(7)	2.002(3)
Pu(1)-S(4)	2.936(2)	P(2)-S(4)	2.031(3)
Pu(1)-S(1)	2.955(2)	P(2)-S(2)	2.038(3)
Pu(1)-S(1A)	3.085(2)	S(6)-P(1)	2.026(3)
Pu(1)-S(7)	3.240(3)	P(2)-P(2)	2.194(5)

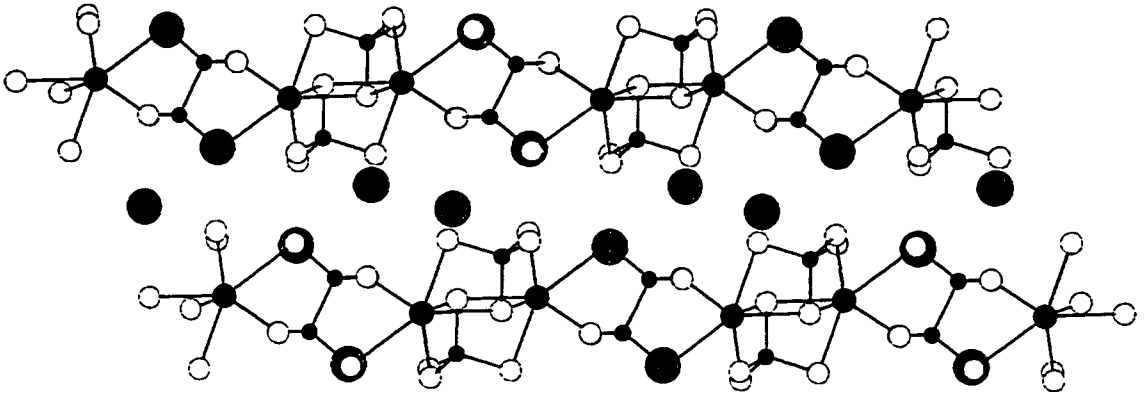

Figure 4.9. A ball and stick representation of two $[Pu(P_2S_6)_{1/2}(PS_4)]^{2-}$ layers with Rb^+ cations both in-between layers and in the spaces in-between $[Pu(PS_4)]$ chains.

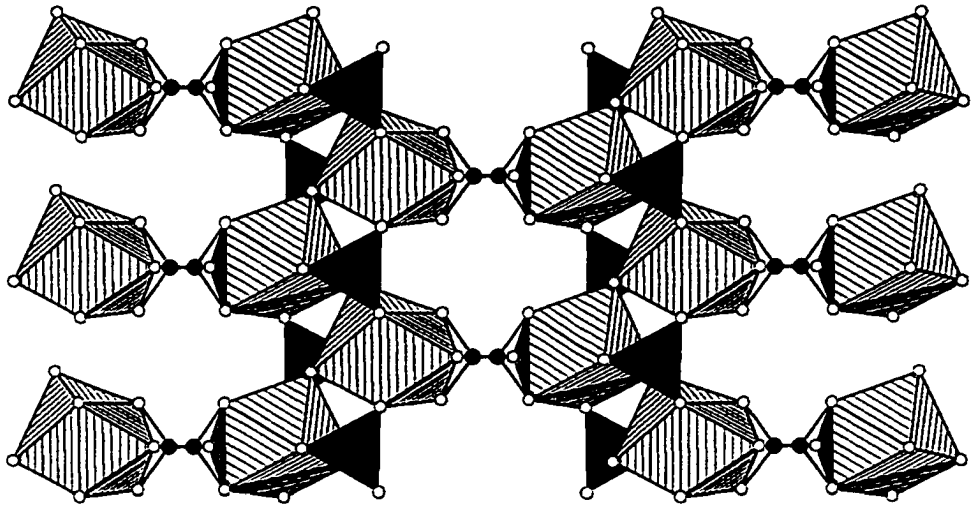

Figure 4.10. Polyhedral representation of a single $[Pu(P_2S_6)_{1/2}(PS_4)]^{2-}$ layer in the *bc* plane. The PuS_8 polyhedra are striped, the $[PS_4]^{3-}$ ligands are black polyhedra, the black circles are P(2) atoms belonging to $[P_2S_6]^{4-}$, and the unfilled circles are sulfur.

consists of chains of PuS_8 polyhedra linked together through corner sharing S(1) atoms with two neighboring PuS_8 polyhedra. These chains run along the [010] crystallographic direction. In addition to corner sharing, the PuS_8 polyhedra are also linked together through the presence of $[PS_4]^{3-}$ ligands. Each $[PS_4]^{3-}$ ligand is coordinated to three PuS_8 polyhedra through both edge and corner sharing sulfur atoms. All of the sulfur atoms present in $[PS_4]^{3-}$ are coordinated to Pu(1). The $[Pu(PS_4)]$ chains are linked together to for 2D layers through $[P_2S_6]^{4-}$ ligands. This ligand has a staggered ethane-like geometry with all six sulfur atoms being coordinate to Pu(1). Each $[P_2S_6]^{4-}$ ligand bridges two PuS_8 polyhedra with three sulfur atoms coordinated to each plutonium atom. Figure 4.11 contains a view of the coordination environment around Pu(1). Figures 4.12 and 4.13 contain views of the $[PS_4]^{3-}$ and $[P_2S_6]^{4-}$ ligands respectively.

There are two unique Rb^+ cations present in this structure. Rb(1) is coordinated to nine sulfur atoms while Rb(2) is coordinated to ten sulfur atoms. The Rb-S bond distances range from 3.329(2) Å to 3.842(3) Å with an average distance of 3.541(5) Å.

Electronic Spectroscopy

Diffuse reflectance UV-vis-NIR spectroscopy was used to determine the oxidation state of plutonium in compounds **I**, **II**, and **V**. These spectra are shown in Figure 4.14. All three are nearly identical and have eight absorption bands all of which are found in the spectrum of Pu^{3+} in HCl. These bands are found at 502, 586, 622, 681, 926, 1052, 1129, and 1165 nanometers. Most of these bands originate from f-f transitions. Because the f-orbitals are not as involved in bonding as the d-orbitals the bands found in these actinide spectra are far sharper than what would be found in

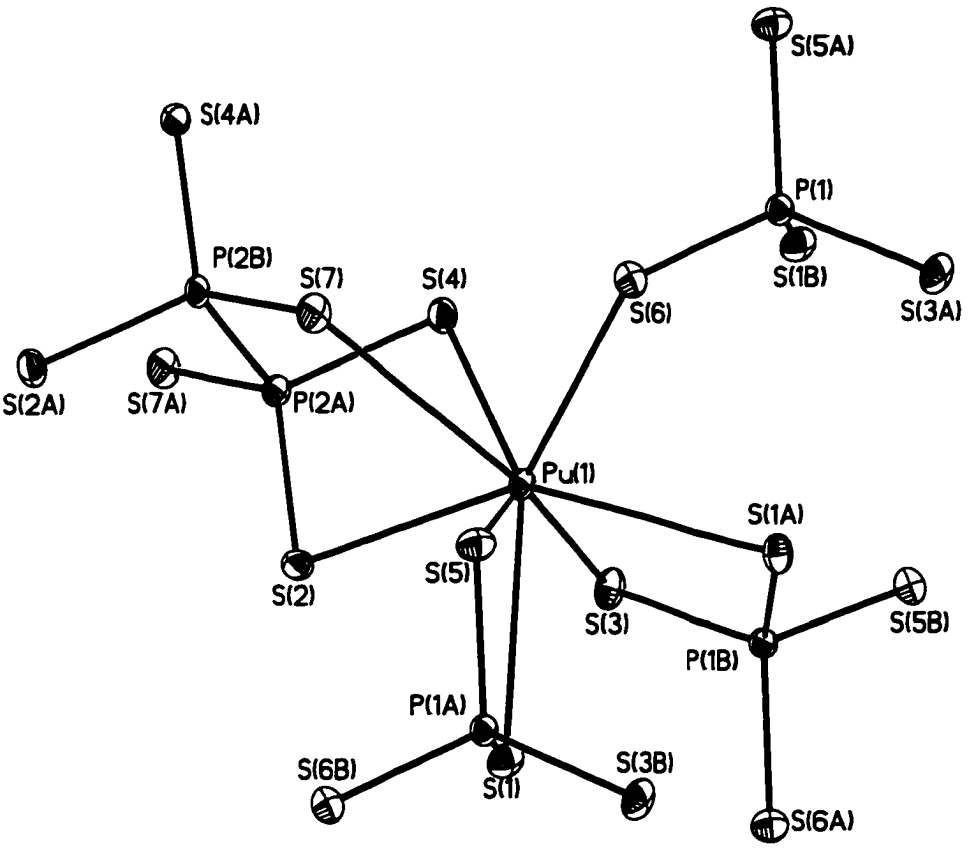

Figure 4.11. Thermal ellipsoid plot of the Pu(1) coordination environment. Pu(1) is coordinated to eight sulfur atoms in a distorted square antiprismatic geometry.

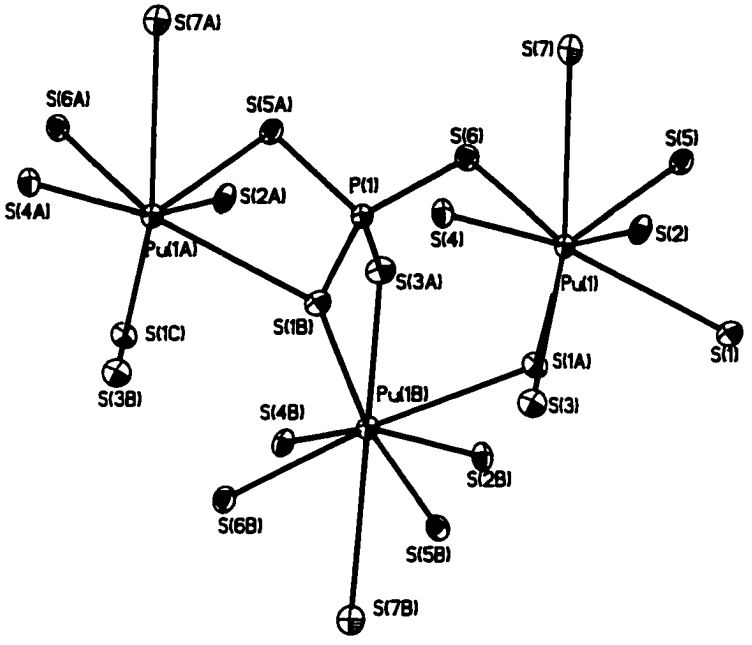

Figure 4.12. Thermal ellipsoid plot of the $[PS_4]^{3-}$ bonding mode. Each $[PS_4]^{3-}$ ligand links three PuS_8 polyhedra together.

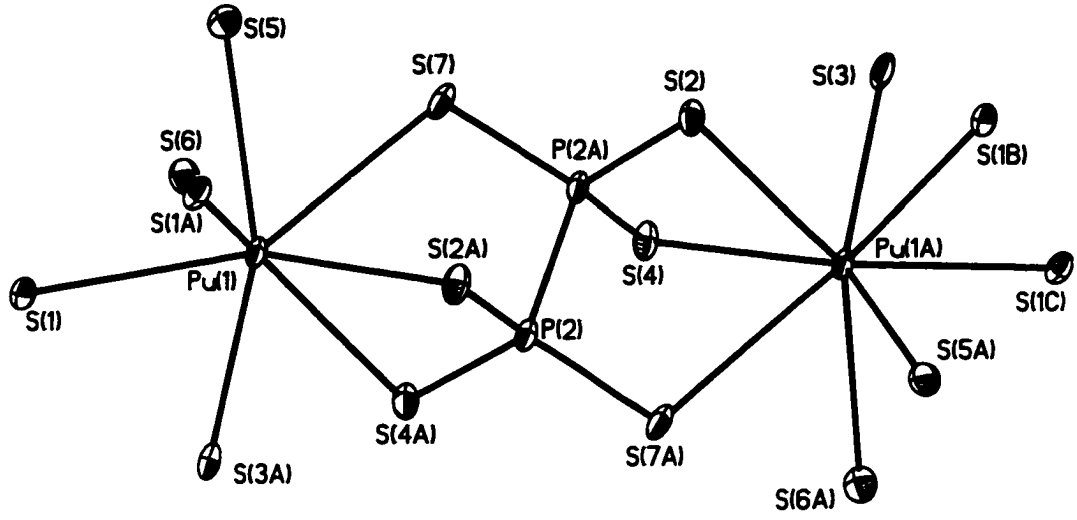

Figure 4.13. Thermal ellipsoid plot of the $[P_2S_6]^{4-}$ bonding mode. Each $[P_2S_6]^{4-}$ ligand links two PuS_8 polyhedra together. This ligand is responsible for linking the one-dimensional $[Pu(PS_4)]$ chains into layers.

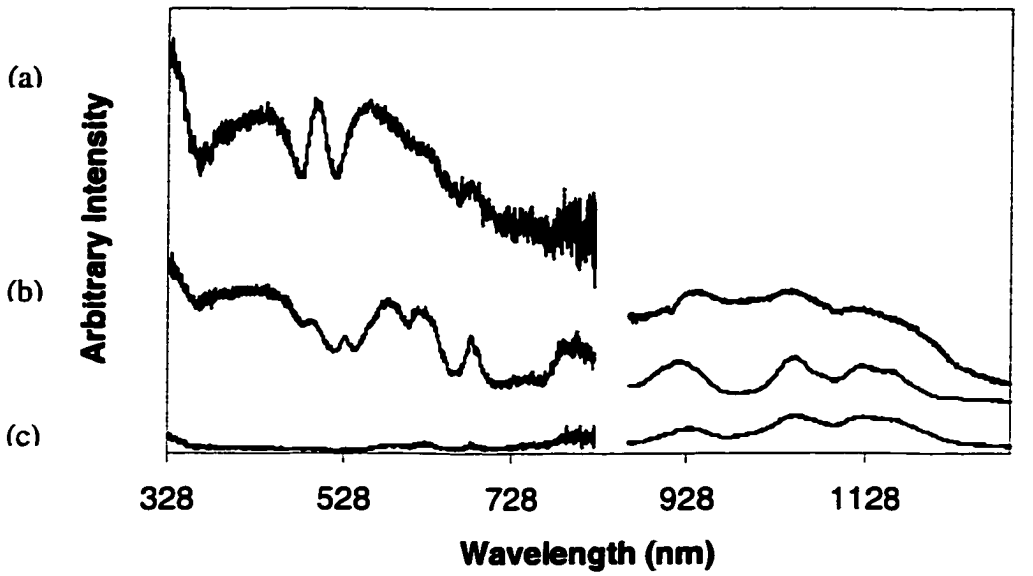

Figure 4.14. Diffuse reflectance UV-vis-NIR spectra of (a) $Rb_2Pu(P_2S_6)_{1/2}(PS_4)$, (b) $RbPuP_2S_7$, (c) $K_3Pu(PS_4)_2$. All of the bands in these spectra are indicative of plutonium in the 3+ oxidation state.

analogous transition metal compounds. From these spectra it is clear that plutonium in all three compounds is present in the 3+ oxidation state.

Raman Spectroscopy

Raman spectra were collected on compounds I, III, and V and are shown in Figure 4.15. The peaks are recorded in Table 4.9. The general features of the spectra comprise low-energy peaks of the PS_4 fundamental units and the P-P stretch of the P_2S_6 unit. The PS_4 symmetric stretches for $K_3Pu(PS_4)_2$, $RbPuP_2S_7$, and $Rb_4Pu_2(P_2S_6)(PS_4)_2$ are found at 411 cm^{-1}, 472 cm^{-1}, and 428 cm^{-1} respectively. The spectrum of $Rb_4Pu_2(P_2S_6)(PS_4)_2$ contains an intense peak at 390 cm^{-1}, which is assigned to the symmetric stretch of the P-P bonded P_2S_6 unit.

Comparison with Known Chalcophosphate Chemistry

All of the plutonium compounds described above are structurally unique with respect to the thorium and uranium chalcogenide chemistry described in Chapter 3. That is, no isostructural Th, U, and Pu compounds exist. However, compounds **I-V** all have isostructural rare earth analogues. That the above plutonium thiophosphates have rare-earth counterparts is not unexpected. In general, as one proceeds across the actinide series from thorium to lawrencium, a significant change in properties occurs. The early actinides, from thorium to plutonium, typically exhibit transition metal like behavior. They can readily access multiple oxidation states and their 5f electrons are generally itinerant in nature. The elements from americium to lawrencium exhibit behavior that resembles rare-earth elements. The trivalent state becomes increasingly stable and the 5f

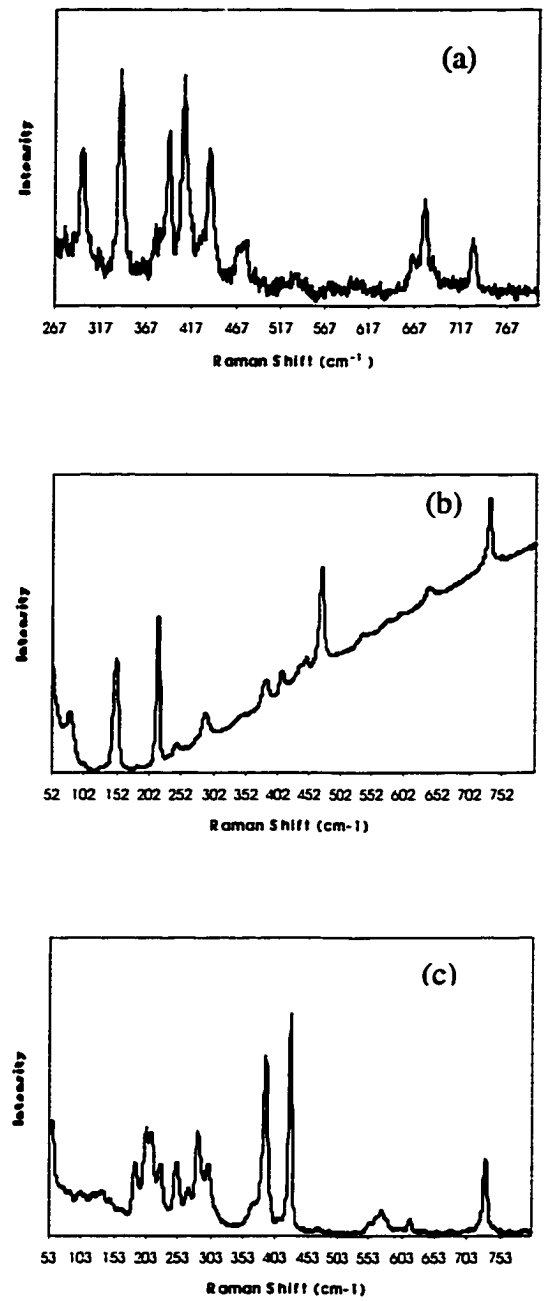

Figure 4.15. Raman spectra of (a) $K_3Pu(PS_4)_2$, (b) $RbPuP_2S_7$, and (c) $Rb_2Pu(P_2S_6)_{1/2}(PS_4)$.

Table 4.9. Raman Spectral Data of Selected Compounds*

$K_3Pu(PS_4)_2$	$RbPuP_2S_7$	$Rb_2Pu(P_2S_6)_{1/2}(PS_4)$
63	82	60
133	153	188
184	219 (s)	205
213	247	213
229	410	228
299	447	252
342 (s)	472 (s)	286
395	641	302
411 (s)		390 (vs)
440 (m)		428 (vs)
475		555
532		574
666		617
680		

* Vibrational Frequencies, cm^{-1}, and Relative Intensities

electrons are more localized than those found in the early actinide elements. Plutonium sits precisely at the center of this transition. In the case of its chalcogenide chemistry, plutonium behaves much like a rare earth element.

The infinite chain compound, $K_3Pu(PS_4)_2$, has two rare-earth analogues, a lanthanum phase and a cerium phase.[16,67] This series of compounds is particularly interesting in that the plutonium and rare earth thiophosphate phases both contain alternating metal-metal distances. These compounds exhibit two different ligand orientations that result in a slightly kinked chain arrangement as described earlier in this chapter. The origin of the chain distortion is not clear. It resembles the Peierls distortions seen in other 1D chain structures such as VO and NbI_2. Peierls distortions occur mainly in 1D structures and can form when partially filled bands are present.[74,75] The cerium thiophosphate compound exhibits the same distortion.[67]

The series of compounds with the formula $APuP_2S_7$ (A = K, Rb, Cs) has a samarium analog recently characterized by Goh and co-workers.[76] It is interesting that in this compound samarium is found in the 3+ oxidation state. Samarium is one of the few rare earth elements that can easily access the 2+ oxidation state. $Rb_4Pu_2(P_2S_6)(PS_4)_2$ is isostructural with a lanthanum phase characterized by Evenson and Dorhout.[14]

K-Pu-P-S Phase Diagram

One of the frontiers of solid-state chemistry is the rational synthesis of complex ternary or quaternary compounds. Traditional solid-state synthesis, from elemental starting materials, has often been referred to as "heat and beat" chemistry. The reactive flux method, however, offers the possibility of systematically varying the flux

composition to synthesize a compound with a specific structure. The formation of a detailed phase diagram is a necessary step towards achieving that goal. As discussed in Chapter 1, there are four components in this reaction system (A-An-P-S) if one holds temperature and time constant. A ternary phase diagram was constructed, and is shown in Figure 4.16 by holding the S content of each reaction listed on the diagram constant. Each point on the phase diagram represents a flux composition that yielded the compounds listed in Table 4.10. From this diagram one can see that $K_3Pu(PS_4)_2$ formed under three different flux compositions. One disadvantage of this flux system is that growth of single crystals is necessary for characterization and subsequent addition to the phase diagram. Though numerous reactions were carried out only a few yielded X-ray quality single crystals. It is also important to note that the alkali metal plays an important role in the flux and in structure formation. Ionic radii, electronegativity, and Lewis basicity are three of the properties that change depending on whether K, Rb, or Cs is present in the flux. Therefore, three different phase diagrams would need to be made, one for each alkali metal. To date, the K phase diagram is the most well developed and has been shown here to note that with future reactions it may be possible to form at phase diagram that makes the rational synthesis of plutonium compounds feasible.

Conclusions

We have extended the study of solid-state actinide chemistry using molten alkali metal thiophosphate melts to include plutonium. With the isolation of **I-V**, which are isostructural with the earlier 4f-congeners, and the fact that in compounds **I–V** plutonium could be found in the 3+ oxidation state, we can conclude that the thiophosphate

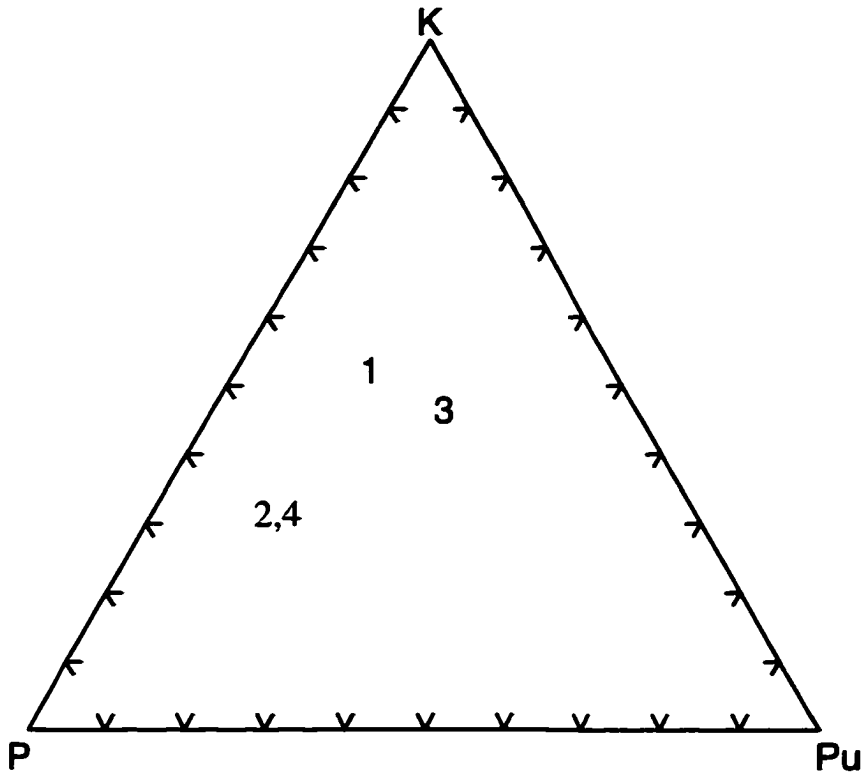

Figure 4.16. Phase diagram of the K-Pu-P-S system. The sulfur content is held fixed at 15 equivalents. The compound that corresponds with each point is listed below in Table 4.9

Table 4.10 Structurally characterized compounds of the K-Pu-P-S system and their flux compositions* for each point on the phase diagram shown in Figure 4.16.

Data Point	Compound	K / sum	Pu / sum	P / sum
1.	$K_3Pu(PS_4)_2$	0.50	0.16	0.30
2.	$K_3Pu(PS_4)_2$	0.30	0.60	0.10
3.	$K_3Pu(PS_4)_2$	0.46	0.23	0.30
4.	$KPuP_2S_7$	0.30	0.60	0.10

* K / sum , Pu / sum, and P / sum are the mole fractions of the respective components in a given flux.

chemistry of plutonium is more rare-earth like than that of the earlier actinide elements thorium and uranium.

In our thiophosphate studies carried out using Th and U, we have yet to characterize compounds that are isostructural with any rare-earth chalcophosphates. This may be due to the difference in preferred oxidation states of the earlier 5f metals.

For both Th and U, the 4+ oxidation state is by far the most common in chalcogenide chemistry and likely the most stable oxidation state, according to their redox potentials in solution.[71] Moving towards the heavier actinides, the 3+ oxidation state becomes increasingly more common and stable. In the plutonium compounds characterized thus far, we can argue that Pu (III) is likely the oxidation state based on charge balancing arguments, although a compound with Pu(IV) would not be unreasonable.[21,77] It is more likely that neptunium compounds could be isolated in higher oxidation states due to the relative redox potentials of the Np(III), Np(IV) and Np(V) series.[71] Finally, we have established coordination geometry preferences (bicapped trigonal prismatic or distorted square antiprimsatic) for the PuS_8 polyhedra as well as bond distance parameters that are consistent with the few other known Pu(III) sulfides and oxysulfides: 2.850(3)–3.050(3) Å for a typical Pu–S bond, while longer bonding interactions were also found up to 3.210 Å, generally in the face-capping atoms of a bicapped trigonal prism of sulfurs around plutonium (III). These bond distances are also consistent with the An–S distances found in our previously reported Th(IV) and U(IV) thiophosphates.[17] Our ongoing studies in complex plutonium chalcogen materials will continue to elucidate some of the mysteries that surround this rare element.

Chapter 5

A New Ternary Plutonium Selenide: KPu_3Se_8

Introduction

The number of known ternary and even binary plutonium chalcogenides is small compared to transition metal and rare earth compounds. As discussed in Chapter 1, there are only four known plutonium sulfides listed in the Inorganic Crystal Structure Database, and all of them are binary compounds. The binary plutonium-chalcogenide systems were discussed in the Introduction section of Chapter 4. The information presented there covers much of what is known about the chalcogenide chemistry of plutonium. The thorium chalcogenide system is somewhat more developed, in that many ternary thorium chalcogenides have been characterized. Ibers and co-workers at Northwestern University have been responsible for the synthesis and characterization of many of these compounds including the ones listed in Table 5.1.

Of the eight known ternary thorium chalcogenides, five of them contain alkali or alkaline earth elements. The remaining two contain transition metals. The first two compounds listed in Table 5.1, $MnThTe_3$ and $MgThTe_3$, are isostructural with one another.[21] They have a three-dimensional structure consisting of alternating slabs of MTe_6 (M = Mn, Te) octahedra and $ThTe_8$ bicapped trigonal prisms. The MTe_6 octahedra form layers through edge-sharing with neighboring octahedral in the *ac* plane. These layers are linked to adjacent MTe_6 layers through edge-sharing with $ThTe_8$ bicapped trigonal prisms. Because this structure contains neither short nor intermediate range Te-Te interactions, each Te atom can be assigned a 2- charge. The Mn and Mg atoms both have 2+ charges leaving Th in the tetravalent state.

The other known ternary thorium chalcogenide that contains a transition metal is $CuTh_2Te_6$.[78] The compound has a three-dimensional structure composed of $[Th_2Te_6]^{2-}$

Table 5.1. List of ternary thorium chalcogenide compounds.

Compound	Structure
$MgThTe_3$	Three-dimensional network[21]
$MnThTe_3$	Three-dimensional network[21]
$CuTh_2Te_6$	Three-dimensional network[20]
$SrTh_2Se_5$	Three-dimensional network[20]
KTh_2Se_6	Two-dimensional layers[78,79]
$CsTh_2Se_6$	Two-dimensional layers[78]
KTh_2Te_6	Two-dimensional layers

layers. Figure 5.1 contains a view of $CuTh_2Te_6$ down the [100] crystallographic direction. The compound contains one crystallographically unique thorium atom that is coordinated to eight tellurium atoms in a bicapped trigonal prismatic geometry. The $ThTe_8$ polyhedra are linked in one direction through the sharing of triangular faces with neighboring polyhedra and in the second direction through the sharing of capping atoms with neighboring polyhedra. The $[Th_2Te_6]^{2-}$ layers are linked together in the [001] direction by $CuTe_4$ tetrahedra. Three unique Te atoms are found in the structure. One Te atom is coordinated to five thorium atoms and resides inside the $[Th_2Te_6]^{2-}$ layers. The other two Te atoms compose the top and bottom tellurium sheets of each $[Th_2Te_6]^{2-}$ layer and form infinite, linear Te-Te chains. The distance between the Te atoms in these chains in intermediate between that of a normal single Te-Te bond and the van der Waals contact distance, 2.76 Å and 4.10 Å respectively. If the chains were composed of normal single Te-Te bonds, each Te atom would have a 1- charge instead of the 2- charge associated with isolated Te anions. The intermediate Te-Te distances found in this structure make the assignment of the Th oxidation state difficult as the Te atoms in the chains have a fractional oxidation state between –1 and -2.

The strontium compound, $SrTh_2Se_5$, has a much more complex structure compared to $CuTh_2Te_6$.[20] It has a three-dimensional structure that is isostructural with the U_3Q_5 family of compounds. Figure 5.2 contains a view of $SrTh_2Se_5$ down the [100] crystallographic direction. The compound contains two unique thorium atoms, Th(1) is coordinated to eight Se atoms in a bicapped trigonal prismatic geometry while Th(2) is coordinated to seven Se atoms in a capped octahedral geometry. The Th(1) polyhedra share Se atoms with one another to form layers in the *bc* plane. These layers have

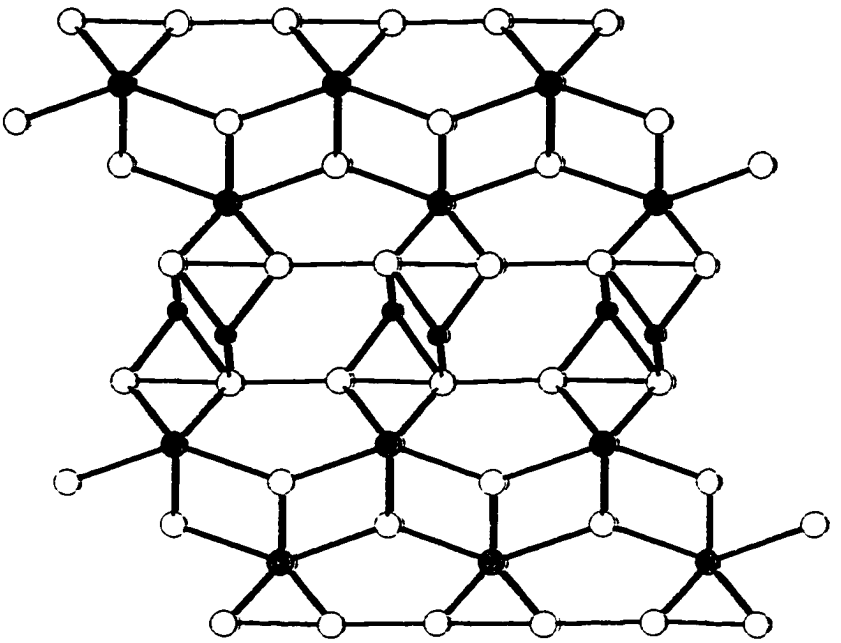

Figure 5.1. A view of the $CuTh_2Te_6$ structure down the [100] crystallographic direction. The shaded circles are the Th atoms, the filled circles are the Cu atoms, and the unfilled circles are the Te atoms

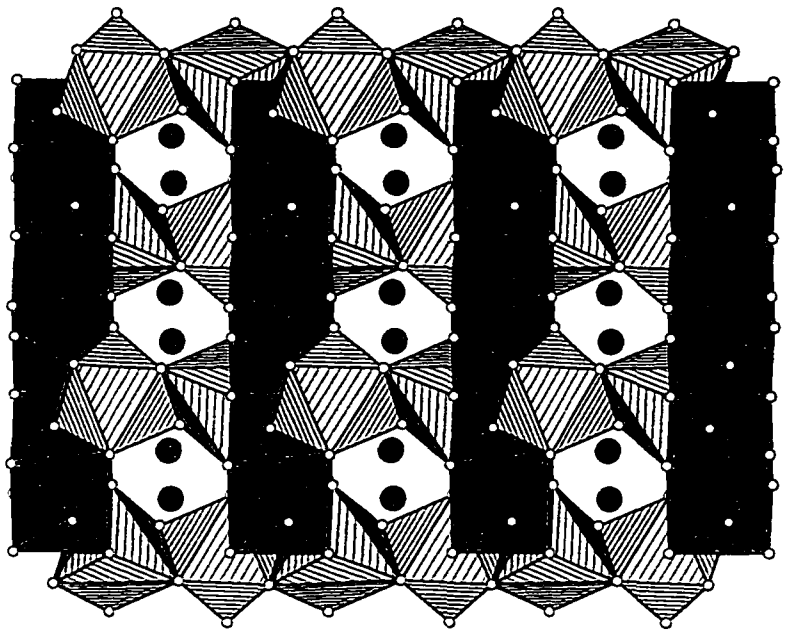

Figure 5.2. A view of the $SrTh_2Se_5$ structure down the [100] crystallographic direction. The shaded polyhedra are $Th(1)Se_8$, the striped polyhedra are $Th(2)Se_7$, the unfilled circles are the Se atoms, and the shaded circles are the Sr^{2+} cations.

channels running through them along the [100] direction. These channels are occupied by chains of Th(2) polyhedra. The Sr^{2+} cations reside in channels running along the [010] direction. A more detailed description of the U_3S_5 structure is found in Chapter 3.

The last three compounds in Table 5.1 have two-dimensional structures containing $[Th_2Q_6]^-$ layers. The $[Th_2Te_6]^-$ layers found the telluride compound are nearly identical to the $[Th_2Te_6]^{2-}$ layers found in $CuTh_2Te_6$. The tellurium atoms form infinite chains as they do in $CuTh_2Te_6$, and exhibit the same intermediate-range Te-Te interactions. Initial studies by Ibers and co-workers indicated, by comparison of unit cell dimensions, that the compound KTh_2Se_6 is isostructural with KTh_2Te_6. Further, more detailed, studies by Kanatzidis and co-workers concerning the KTh_2Se_6 structure determined that this is not the case.[78,79]

The key difference between the selenide and telluride phases is the positions of the chalcogenide atoms making up the top and bottom sheet of each $[Th_2Q_6]^-$ layer. The Se atoms form isolated $(Se_2)^{2-}$ anions with a Se-Se bond distance of 2.722 Å. The diselenide anions are separated from one another by a distance of 2.907 Å. The Se atoms do not form infinite chains as they do in the telluride compound, KTh_2Te_6. A view of KTh_2Te_6 down the [100] crystallographic direction is shown in Figure 5.3. One interesting feature of this structure is that the extra electrons injected into the compound from the intercalated K atoms causes the reductive elimination one fourth of the $(Se_2)^{2-}$ anions into two Se^{2-} anions. Kanatzidis and co-workers were able to resolve a superstructure, with dimensions $4a$ x $4b$ based on the subcell, that accounts for the ordering of the diselenide groups and the isolated selenium anions. They attributed the disorder of the Se layers to the presence of a charge density wave.[79]

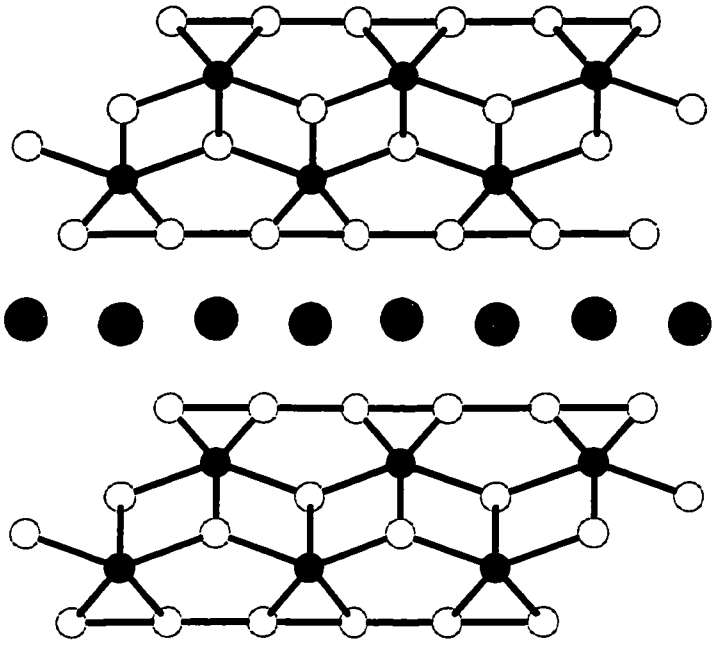

Figure 5.3. A view of the KTh_2Te_6 structure down the [100] crystallographic direction. The filled circles are the Th atoms, the shaded circles are the K^+ cations, and the unfilled circles are the Te atoms.

Charge density wave and site occupancy wave distortions are found in a number chalcogenide compounds.[80-82]Two examples of transitional metal chalcogenides that contain charge density waves are $TaSe_2$ and $NbSe_2$.[81] The binary rare earth compounds, $DySe_2$ and $DySe_{1.84}$, also exhibit charge density wave distortions.[82] Lee and co-workers published two papers describing the structural distortions found in the two binary dysprosium compounds along with the ternary compound $Rb_{0.33}DySe_{2.67}$.[81,82] The ternary compound is described in greater detail later in this chapter. Kanatzidis and co-workers published a similar paper concerning the site occupancy wave distortion found in the telluride compounds $CsCe_3Te_8$, $RbCe_3Te_8$, and KNd_3Te_8.[80]

The ternary thorium compounds synthesized by Ibers and Kanatzidis such as, KTh_2Q_6 and $CsTh_2Se_6$, are interesting because conventional electron counting does not yield a reasonable oxidation state for thorium. This difficulty is due to the presence of intermediate length Q-Q bonds. Based on its known chemistry, thorium is almost certainly in the 4+ oxidation state. Experiments were undertaken to determine if it was possible to synthesize a similar compound containing plutonium in place of thorium. A plutonium compound would be particularly interesting because both 3+ and 4+ would be reasonable plutonium oxidation states. The remainder of this chapter discusses the synthesis and characterization of a new ternary plutonium selenide compound with the formula KPu_3Se_8. Though the plutonium compound is not isostructural with the ATh_2Se_6 phases it is isostructural to $RbDy_3Se_8$ and exhibits the same site occupancy wave distortion. This new ternary compound is compared to both its parent structure, $PuSe_2$, and the related ternary compounds, $RbDy_3Se_8$, and KTh_2Se_6.[78,79]

Experimental

General Synthesis. Red phosphorous powder (99.9%) was obtained from Cerac. Selenium shot (99.999%) was purchased from Johnson Matthey. ^{239}Pu shot was obtained from Los Alamos National Laboratory. K_2Se_4 prepared from a stoichiometric ratio of the elements in liquid ammonia as described elsewhere. Ampoules for the reactions were all fused-silica tubes with 4 mm inner diameter and a 6 mm outer diameter. All reagents were stored and manipulated in an argon filled negative pressure glovebox. *Warning: ^{239}Pu is a radioactive element with a half-life of $2.41x10^4$ years.*

Synthesis of KPu_3Se_8 : KPu_3Se_8 was synthesized from a mixture of 0.0480g (0.20 mmol) Pu, 0.0320g (0.41 mmol) Se, and 0.3160g (0.80 mmol) K_2Se_4. The mixture was loaded into a fused silica ampoule and sealed under vacuum. The ampoule was then heated to 500 °C over 16 hours and held there for 200 hours. The ampoule was cooled to ambient temperature at a rate of 3 °C per hour. Excess flux was removed by washing with DMF. Black rectangular blocks with a metallic luster were then isolated by filtration and selected crystals were handpicked for analysis.

Physical Characterization. Single-crystal X-ray diffraction was performed on a modified Siemens P4 four-circle diffractometer equipped with a SMART CCD system detector or a Siemens SMART CCD system using graphite-monochromated Mo Kα radiation. X-ray absorption spectra were collected at the Stanford Synchrotron Radiation Laboratory (SSRL): unfocused beamline 4-2, Si (220), double-crystal monochromator, 3.0 GeV, 60-100 mA. Spectra are the average of four scans collected with 7 Ge detector elements. The Pu L_{III} edge spectra was normalized by setting the value of a polynomial fit through the pre-edge region to zero and that of a polynomial fit through the EXAFS

region to unity at 17700 eV. The spectrum was calibrated by setting the first inflection point in the spectrum for an external Zr foil to 17999.35 eV.

Structure Determination. Crystals were selected from the reaction mixtures and placed in a pool of epoxy. The crystals were then removed from the epoxy and placed inside a 0.5 mm capillary tubes. The capillary tubes were then removed from the glovebox, trimmed to the appropriate length and the ends sealed with epoxy. A coating of acrylic was applied to the surface of capillary tubes to provide the third and final layer of containment. The capillary tubes were then placed in the cold stream of the diffractometer.

Cell constants for all structures were initially calculated from reflections taken from approximately 30 frames of reflections. Final cell constants were calculated from all reflections observed in the actual data collection. Table 5.2 summarizes the crystal structure parameters for compounds **I.** The data were processed and corrected for absorption using SADABS.[48] The structure was solved by direct methods allowing the unambiguous space group assignments, and refined in full-matrix least-squares using the program SHELXTL[49] under the XSHELL package of programs.[50] The final cycle of refinement included all anisotropic displacement parameters. Secondary extinction coefficients were applied to the final refinements. Specific refinement issues related to the structure are explained in the Structure Refinement section. The supplementary information is listed in Appendix F in the form of a CIF file.

Table 5.2. Crystallographic Data for KPu_3Se_8,I .

	I
Empirical Formula	$K_{0.33}PuSe_{2.67}$
fw	462.68
a, Å	4.1257(5)
b, Å	25.642(3)
c, Å	3.9900(4)
V, $Å^3$	422.11(8)
Z	4
μ, (mm^{-1})	38.711
λ(Mo Kα), Å	0.71073
space group	Cmcm (No. 63)
temp., K	163(2)
$\rho_{calc.}$, g/cm^3	7.281
R1 % [a]	0.0561
wR2 % [a]	0.1571

[a] $R1 = \Sigma(|F_o| - |F_c|)/\Sigma|F_o|$ $\quad wR2 = [\Sigma[w(F_o^2 - F_c^2)^2] / \Sigma [w(F_o^2)^2]]^{1/2}$

Structure Refinement

The initial refinement of this structure was in the non-centrosymmetric space group $Cmc2_1$. Two atoms in the structure are disordered, K(1) and Se(3). K(1) sits on a symmetry element and Se(3) has one unusually large thermal parameter, U_{33}. Both K(1) and Se(3) appeared to be partially occupied. While the structure was refined to an R value of 0.07, significant electron density remained in the difference map with a highest peak of approximately 7.0 $eÅ^{-3}$. A search for missing symmetry elements was carried out using PLATON and an inversion center was located. The addition of the inversion center changed the space group to Cmcm. With this correction the R value dropped to 0.054 and the difference map flattened out (max = 2.880 $eÅ^{-3}$, min = -5.963 $eÅ^{-3}$). The best refinement was obtained by letting the occupancies of K(1) and Se(3) vary. This was first done isotropically. After the occupancies converged both atoms were allowed to vary anisotropically. After the final refinement, the site occupancy factors for K(1) and Se(3) were found to be 0.13889 and 0.16715 respectively. Each of the atoms in this structure resides on a special position with a site occupancy factor of 0.25000. Therefore the K(1) site is occupied 55% of the time while Se(3) is 66% of the time. In addition the Se(3) atoms are disorder over two positions approximately 0.6 Å apart. In effect, each of those two Se(3) sites is only occupied 1/3 of the time.

Based on the unit cell parameters KPu_3Se_8 is isostructural with $RbDy_3Se_8$. In the Dy compound the alkali metal position refined to an occupancy of 33% and the Se(3) site to an occupancy of 66%. Chemically, the refinement of the alkali metal position to 33% occupied in the Dy phase is more plausible than the K(1) site being 55% occupied in the Pu phase. There are numerous factors that can effect the final fractional occupancy of a

site. Given the fact that the occupancies of K(1) and Se(3) are related, and the large absorption caused by the heavy Pu and Se atoms, it is plausible to assume that the structures are truly identical and the K(1) site has an occupancy of 33% not 55%. The occupancy of the K(1) site was fixed at 33% for the final refinement. The R-value only increased slightly after fixing the K(1) occupancy. The final $R_1 = 0.0561$ was, it was 0.0541 before fixing K(1). The chemical formula for this structure is KPu_3Se_8.

Structure Description

KPu_3Se_8 , I. The compound crystallized as black plates in the orthorhombic space group Cmcm based on the systematic absences observed in the data. Refinement of the model's 25 independent parameters to the data (241 reflections) provided an excellent goodness-of-fit (GOF = 1.291). Table 5.2 contains the specific data collection and refinement information. Tables 5.3 and 5.4 contain the atomic coordinates and relevant bond distances respectively.

Compound **I** has a structure composed of $[Pu_3Se_8]^{1-}$ layers with K^+ cations residing in the interlayer space. Figure 5.4 contains a ball and stick representation of the structure viewed down the [100] direction. Each $[Pu_3Se_8]^{1-}$ layer contains one crystallographically unique Pu atom which is coordinated to nine Se atoms in a capped square anti-prismatic geometry as seen in Figure 5.5. The selenium atoms labeled Se(1) and Se(3) make up the top square face while Se(2) atoms make up the bottom square face and the capping atom. The plutonium-selenium bonds range from 2.976(1) Å to 3.171(8) Å with an average bond distance of 3.06(1) Å. This compound is isostructural with $RbDy_3Se_8$.

Table 5.3. Atomic coordinates (x 10^4) and equivalent isotropic displacement parameters ($Å^2$x 10^3) for KPu_3Se_8. U(eq) is defined as one third of the trace of the orthogonalized U^{ij} tensor.

	x	y	z	U(eq)
K(1)	0	-4847(9)	-7500	9(9)
Pu(1)	-5000	-3244(1)	-7500	13(1)
Se(1)	-5000	-4146(2)	-12500	32(2)
Se(2)	-5000	-2063(2)	-7500	12(2)
Se(3)	0	-4174(4)	-16650(80)	37(13)

Table 5.4. Bond Distances (Å) for KPu_3Se_8.

Pu(1)-Se(1)	3.054(4)	Pu(1)-Se(3)	3.171(8)
Pu(1)-Se(1A)	3.054(1)	Pu(1)-Se(3A)	3.171(8)
Pu(1)-Se(2)	3.028(4)	Pu(1)-Se(3B)	3.171(8)
Pu(1)-Se(2A)	2.976(1)	Pu(1)-Se(3C)	3.171(8)
Pu(1)-Se(2B)	2.976(1)	Se(2)-Se(3)	2.65(3)
Pu(1)-Se(2C)	2.976(1)		
Pu(1)-Se(2D)	2.976(1)		

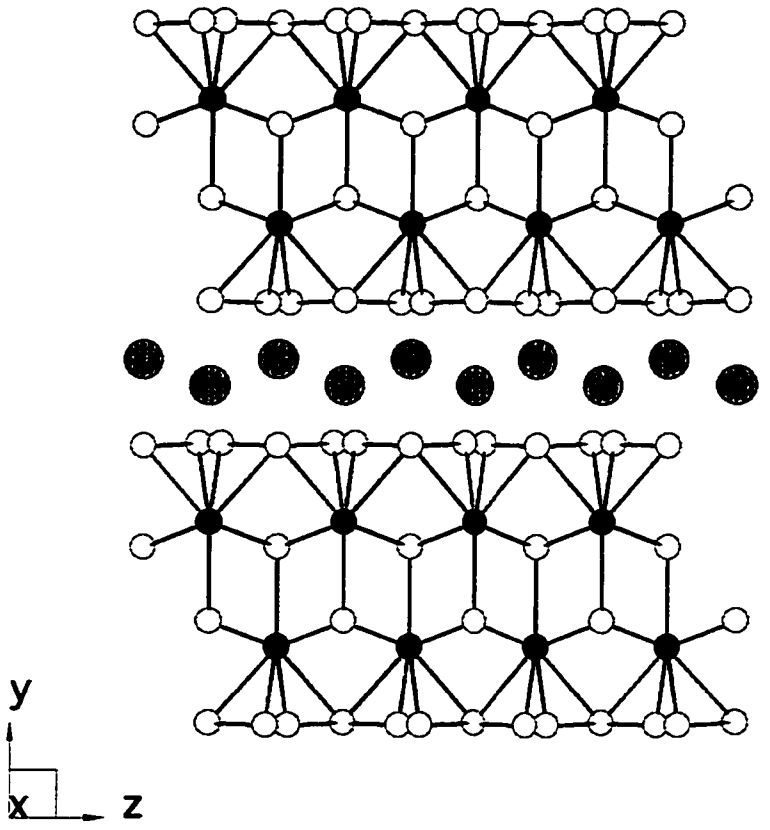

Figure 5.4. Edge-on view of KPu_3Se_8 down the [100] direction. The plutonium atoms are shown as black circles, the selenium atoms are the unfilled circles, and the K atoms are the shaded circles.

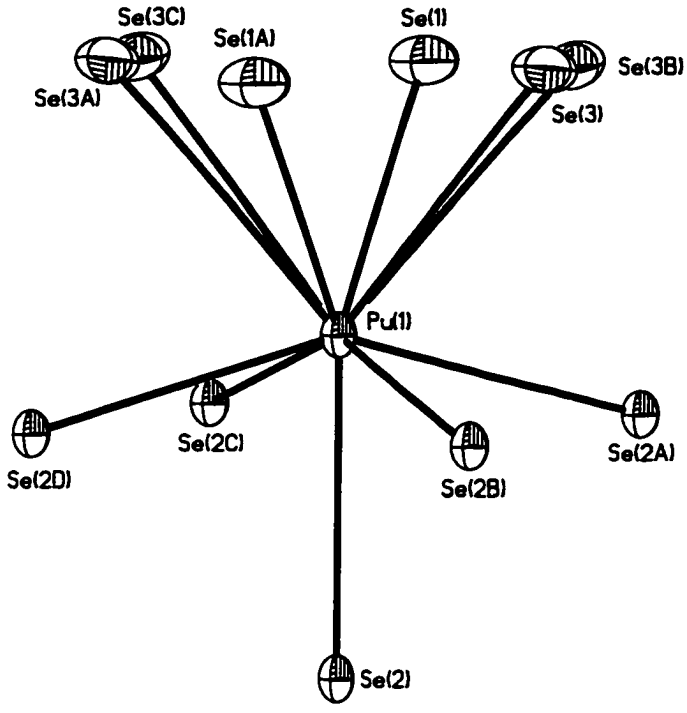

Figure 5.5. Thermal ellipsoid plot of the coordination environment around plutonium in KPu_3Se_8. Plutonium is coordinated by nine sulfur atoms in a capped square anti-prismatic geometry.

The fundamental layers in both structures closely resembles that of $NdTe_3$. Figure 5.6 contains two expanded views of a single $[Pu_3Se_8]^{1-}$ layer. Figure 5.6(a) identifies the three crystallographically unique selenium atoms in the structure. Each $[Pu_3Se_8]^{1-}$ layer can be thought of as containing three separate components: two square sheets of selenium atoms with a pseudo-tetragonal PuSe slab in between them. Figure 5.6(b) contains a view of these components with the Pu to square-sheet-Se bonds removed for clarity. Se(1) is coordinated to five plutonium atoms and is part of the pseudo-tetragonal PuSe(2) slab. Se(1) and Se(3) compose the square sheets of selenium atoms. Figure 5.7 contains a view of a single square sheet of Se atoms, and the underlying K^+ cations, down the [010] direction. While Se(1) and Se(2) are fully occupied and ordered, Se(3) is only 2/3 occupied. In addition, the Se(3) atom has moved off its ideal site of 4-fold symmetry and split into two positions 0.6 Å apart. These sites are labeled Se(3A) and Se(3B). It is clear that only one of the two sites can be occupied at any given time. Further complicating maters is the fact that the K(1) site is only 2.8 Å away from the Se(3) sites. This is too close for both sites to be occupied at any one time. Therefore, if K(1) is occupied then both Se(3A) and Se(3B) positions must be vacant. When K(1) is vacant then one of the two possible Se(3) positions can be occupied.

The partial occupancy of Se(3) plays an important role in the Se-Se bonding found in the square sheet layers. The Se(2)-Se(3) bond distance is longer than an average Se-Se single bond but still within bonding range, 2.65(3) Å versus 2.34 Å. With this type of intermediate range Se-Se interaction it is difficult to determine the oxidation state of selenium. The Se(2) and Se(3) atoms have fractional oxidation states that are less reduced than 2- but more oxidized than 1-.

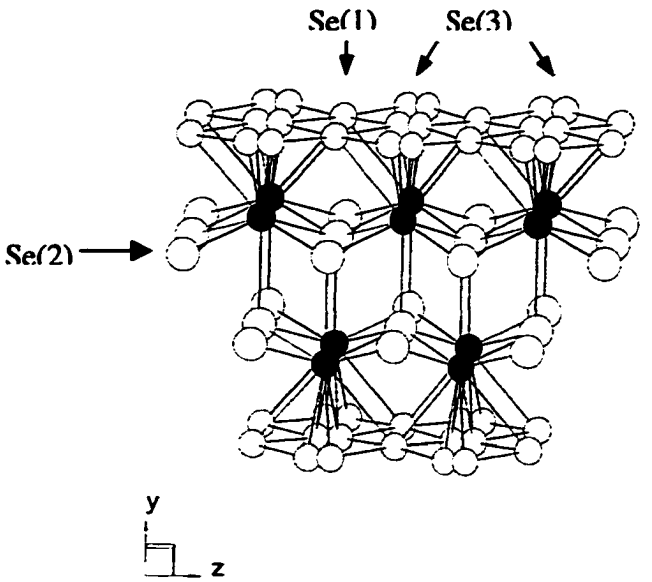

(a)

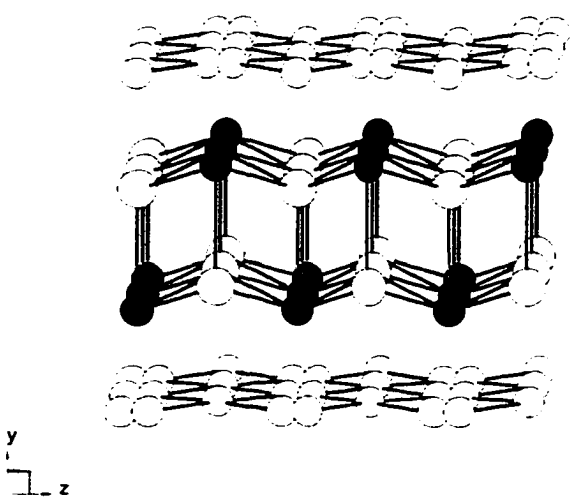

(b)

Figure 5.6. (a) Expanded view of a single $[Pu_3Se_8]^{1-}$ layer with the K atoms removed for clarity. (b) View of a single $[Pu_3Se_8]^{1-}$ layer emphasizing the pseudo-tetragonal PuSe(2) layer. The PuSe(2) layer is related to the $NdTe_3$ and Cu_2Sb structure types. The bonds from Pu to the Se atoms in the square sheets have been removed, along with the K atoms, for clarity. In both (a) and (b) the plutonium atoms are the black circles and the selenium atoms are the unfilled circles.

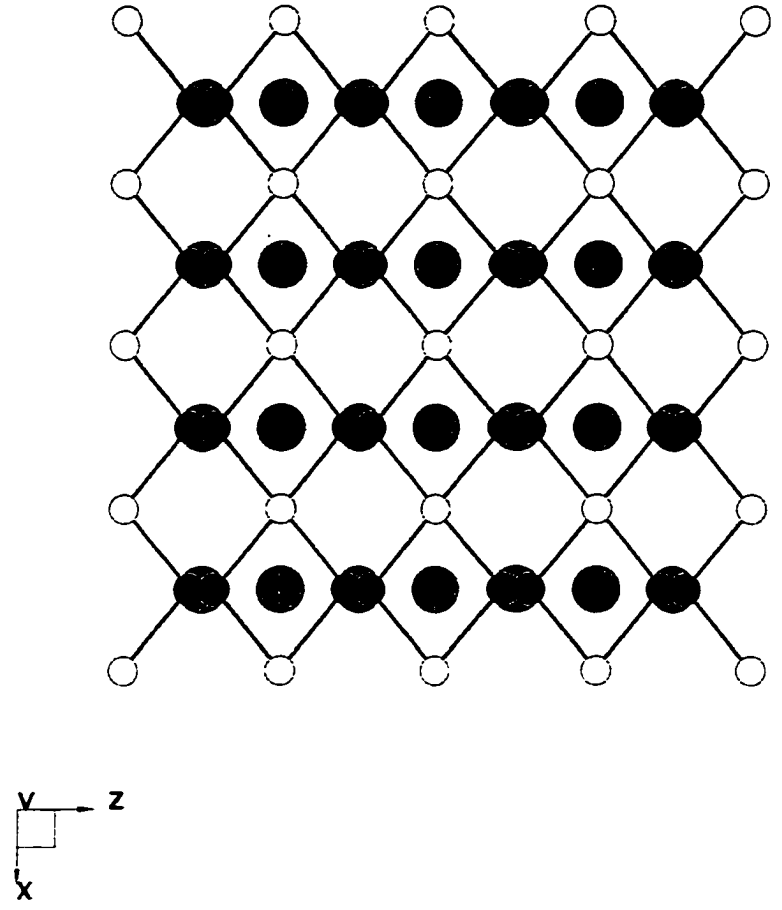

Figure 5.7. View of a single square selenium sheet and the underlying K^+ cations. The fully occupied selenium atoms, Se(1), are the unfilled circles; the partially occupied Se(3) atoms are the unfilled circles; the K^+ cations are the shaded circles.

If the Se(3) site was fully occupied and ordered then the Se atoms in the Se(2)Se(3) sheets would form a square network. Each Se(2) atom would be bound to four Se(3) atoms in a square planar geometry, likewise each Se(3) atom would be bound to four Se(2) atoms. Interestingly, this situation is found in the Fe_2As structure type and in the binary chalcogenide $PuSe_2$. The $PuSe_2$ structure will be discussed in greater detail later in this chapter.

As seen in Figure 5.7, each pair of Se(3) sites resides mid-way between two Se(2) columns. When either Se(3) site is occupied, that Se(3) atom is within bonding distance of two Se(2) atoms in the nearest column and is outside of bonding range to the two Se(2) atoms in the far column. Depending on pair vacancies and individual Se(3) site vacancies, the formation of a number of different polyselenide anions is possible. If, for example, all of the Se(A) sites are vacant and all of the Se(B) sites are occupied, infinite zig-zag chains are formed. The most probable scenario is that different lengths of Se chains, along with isolated Se^{2-} anions, are formed depending on the location of the defects. Two possible arrangements of the vacancies are seen in Figures 5.8a and 5.8b. One can envision the formation of a number of possible superstructures if a long-range ordering of the defects is present.

$RbDy_3Se_8$ Phase

Foran and Lee synthesized this dysprosium compound in 1993 and were able to examine the possible superstructures by utilizing electron diffraction and theoretical calculations.[81] They proposed that the distortion found in the square selenium sheets and Rb^+ ion layers is caused by the presence of a charge density wave. Their results indicate the formation of a superstructure, though they were not able to characterize it

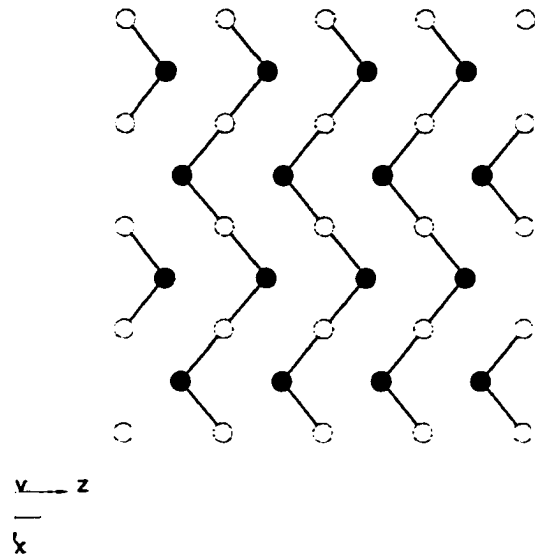

(a)

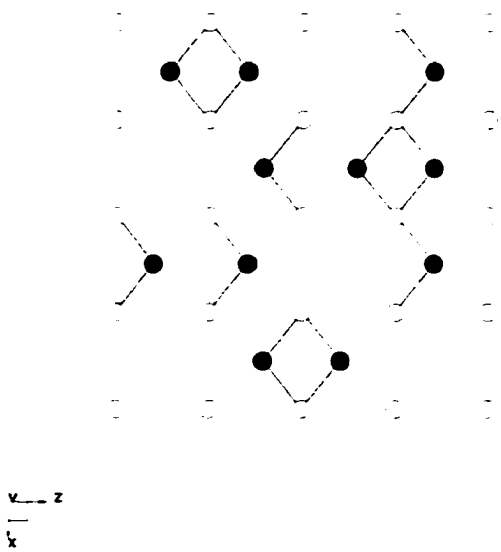

(b)

Figure 5.8(a and b). Two possible arrangements of Se(3) vacancies. The filled circles are Se(3) atoms while the unfilled circles are Se(1) atoms.

experimentally. They were, however, able to use Hückel theory to narrow down the possible superstructures to six lowest energy different arrangements of Se(3) defects. These possible arrangements are similar to the ones shown in Figure 5.8. Both the ternary plutonium and dysprosium compounds are related to another interesting actinide compound that contains a similar charge density wave distortion, KTh_2Se_6.

KTh_2Se_6 Phase

This compound was first synthesized by Ibers and co-workers, then further characterized by Kanatzidis and co-workers.[79] The overall structure is similar to the KPu_3Se_8 structure as shown in Figure 5.9(a). It contains $(Th_2Se_6)^{1-}$ layers separated by K^+ ions. The thorium atoms are coordinated to eight selenium atoms instead of nine, as in the KPu_3Se_8 structure. The Ibers-Kanatzidis phase does, however, contain square sheets of selenium atoms similar to the sheets found in KPu_3Se_8. Unlike the plutonium structure, the selenium atom positions in this sheet are fully occupied. However, even though the position is fully occupied, there is still disorder present.

In the thorium structure the selenium atoms in the square sheet are arranged such that Se-Se dimers are formed. What is unusual about the dimers is that the Se-Se distance is longer than a normal single bond (2.73 Å versus 2.35 Å). Kanatzidis was able to characterize, through electron diffraction and pair distribution function analysis, a superstructure that helps to explain this phenomenon. As discussed in the Introduction, the supercell has the dimensions $4a$ x $4b$ based on the subcell. Their results show that every fourth $(Se_2)^{2-}$ dimer in the square selenium sheet is broken forming two Se^{2-} anions. This arrangement of Se atoms is shown in Figure 5.9(b). This distortion is believed to be due to the formation of a charge density wave due to the presence of additional electrons

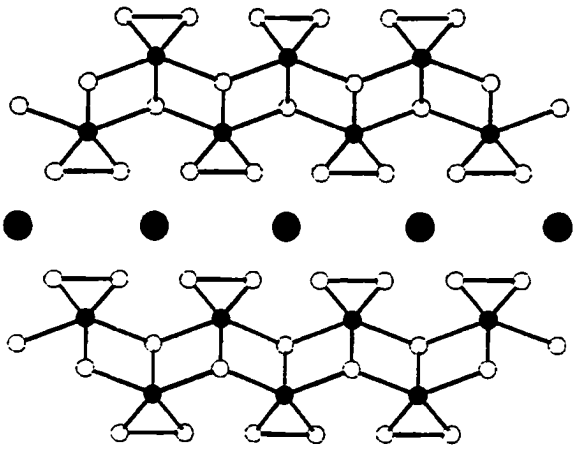

(a)

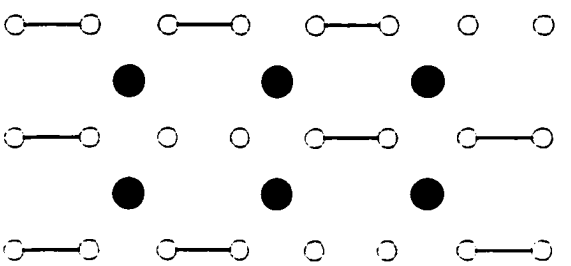

(b)

Figure 5.9(a) contains a view of KTh_2Se_6 structure down the [100] crystallographic direction. Figure 5.9(b) contains a view of the square Se sheet found in this structure. The small filled circles are the Th atoms, the unfilled circles are the Se atoms, and the large filled circles are the K^+ ions.

from the alkali metals. This distortion is very similar to the situation found in the plutonium phase.

One does not need to look far to find a third phase that is related to these interesting CDW modulated phases. From a structural standpoint, $PuSe_2$, could be considered the parent structure of KPu_3Se_8.

$PuSe_2$ Phase

Plutonium diselenide has a three-dimensional structure containing Pu coordination environments nearly identical to those found in the KPu_3Se_8 structure.[83] The major difference between the two structures is that KPu_3Se_8 contains an "intercalated" layer of K^+ ions. The square sheets of Se atoms in $PuSe_2$ are arranged in the same fashion as those in KPu_3Se_8, but the Se(3) site is fully occupied and ordered. Unlike KPu_3Se_8, plutonium diselenide does not exhibit a charge density wave distortion. As is the case for KTh_2Se_6, one possible cause for the charge density wave distortion found in the square selenium sheets in the KPu_3Se_8 structure is the presence of additional electrons from the intercalated K^+ ions. Figure 5.10(a) contains a view of the $PuSe_2$ structure while Figure 5.10(b) contains a view of the $PuSe_2$ square selenium sheet.

X-ray Absorption Near-Edge Spectroscopy (XANES)

XANES experiments were undertaken to gain information on the electron density around plutonium in KPu_3Se_8 and a number of binary plutonium chalcogenides. The energies of the L_{III} absorption edges for the compound examined in this study are listed in Table 5.5. At the time of this writing, final curve fits have yet to be carried out. For this reason, no errors are included in Table 5.5. Figure 5.11 contains a plot of the second

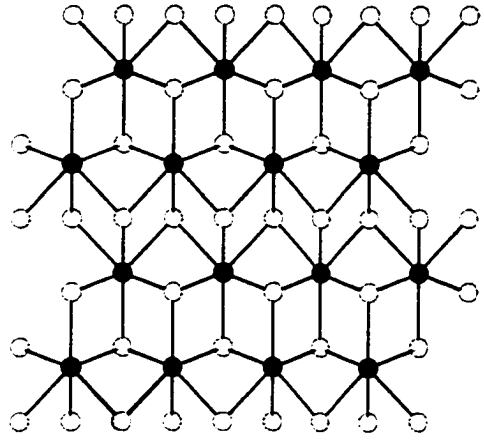

(a)

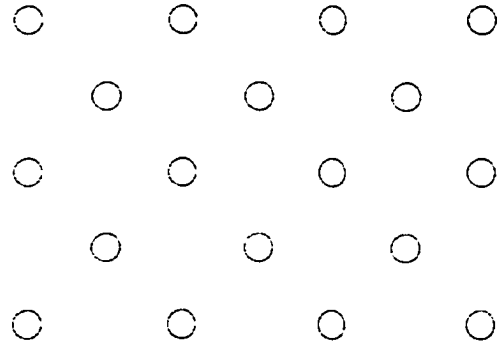

(b)

Figure 5.10(a) contains a view of $PuSe_2$, the parent structure of KPu_3Se_8 down the [100] crystallographic direction. Figure 5.10(b) contains a view of the undistorted square Se sheet found in this structure. In both figures, the plutonium atoms are the filled circles and the selenium atoms are the unfilled circles.

Table 5.5. The plutonium L_{III} absorption edges of the compounds examined in this study.

Sample	Edge Position (eV)
Pu Metal	18056
$PuSe_2$	18058
KPu_3Se_8	18058
Pu_2Se_3	18058
PuO_2	18062

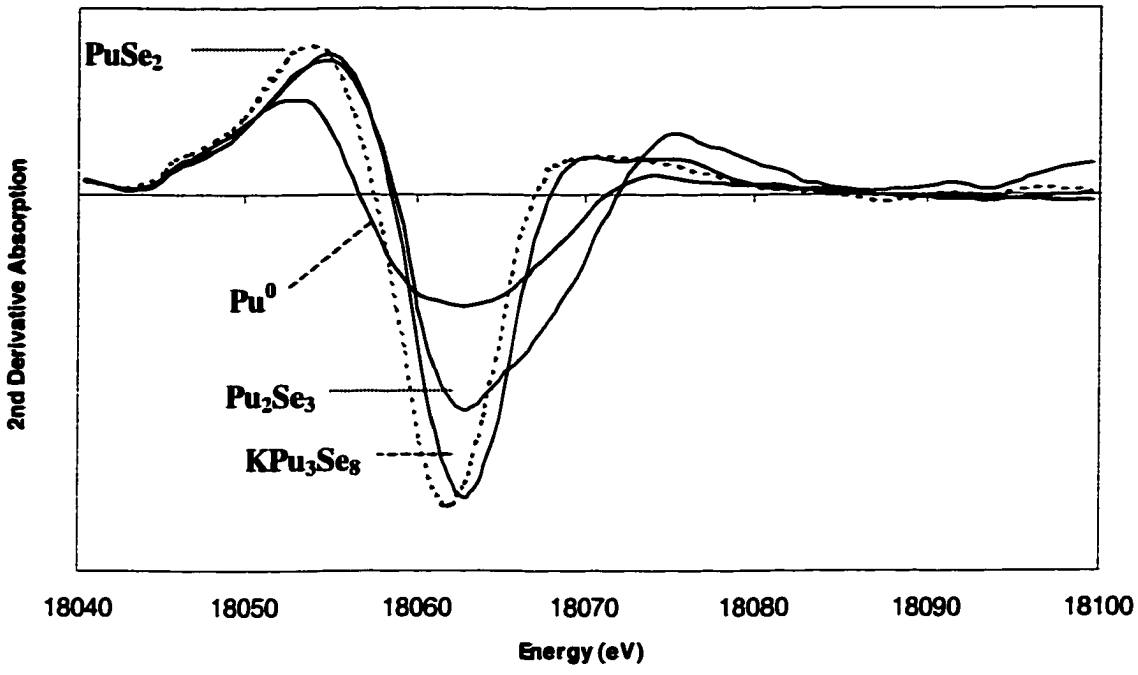

Figure 5.11. Plot of the second derivative of absorbance versus energy for the plutonium compounds examined in this study. The absorption edge is recorded where the second derivative first crosses the energy axis.

derivative of absorption versus energy for KPu_3Se_8. The absorption edge value is recorded where the second derivative first crosses the energy axis. In many systems, XANES is able to determine oxidation state information about the absorbing atom. The post-edge region is examined in EXAFS experiments. By analyzing the post-edge region it is possible to learn structural information about the environment around the target atom.

One key difference between X-ray diffraction and X-ray absorption experiments is that the former examines the long-range order of a system while the later is capable of examining the local region around a specific target atom. Due to the complexity of the theory needed to predict XANES spectra, the determination of oxidation states is largely empirical. That is, to successfully determine an atom's oxidation state it is important to have available a number of standards in which the target atom is in similar chemical environment compared to the sample being studied. Unfortunately, the number of plutonium compounds previously studied using XANES is exceedingly small. This adds some uncertainty in determining an absolute oxidation state number for the compounds examined in this study. What can be learned, however, is something about the relative amount of electron density around the plutonium atoms in these compounds. It is important to remember that in metallic systems the use of the oxidation state formalism becomes less valuable than in valence precise systems.

The key result from the XANES studies is that the absorption edges of these heavy chalcogenide systems appear close to the value found for plutonium metal (within 1-2 eV). This implies that the electronic environment around plutonium is very similar to that found in the metal.

These results are significantly different than what is found for PuO_2. The value for the oxide is much closer to what is found for Pu^{4+} in aqueous solutions. Though the overall trend is not unexpected due to the presence of the much softer S, Se, and Te atoms compared to O, the magnitude of the effect, and the similarity to plutonium metal, was unexpected.

The Extended X-ray Absorption Fine Structure (EXAFS) region of two binary plutonium selenides was also investigated. Figure 4.12 contains the Fourier Transform plots for $PuSe_2$ and Pu_2Se_3. Plots of the Radial Distribution Functions for $PuSe_2$ and Pu_2Se_3 are shown in Figure 4.13. While the final curve fits have yet to be completed valuable qualitative information can still be gained by looking at these plots. These two plots show that the plutonium atoms both compounds have similar chemical environments. For $PuSe_2$, preliminary curve fits indicate that the first shell of selenium atoms have Pu-Se bond distances of 3.012 Å with a sigma of 0.06. The next shell also appears to be composed of selenium atoms and has Pu-Se bond distances of 3.127 Å with a sigma of 0.08. The last shell that can be identified is composed of neighboring plutonium atoms found 4.093 Å (sigma of 0.06) away from the absorbing plutonium atom.

For Pu_2Se_3, preliminary curve fits indicate that the first shell is composed of selenium atoms with Pu-Se bond distances of 2.996 Å and sigma of 0.07. The next shell is also composed of selenium atoms with slightly longer Pu-Se bonds, 3.127 Å and a sigma of 0.09. The third and last identifiable shell is composed of plutonium atoms with Pu-Pu distances of 4.078 Å and a sigma of 0.09. These bond distances are all reasonable for Pu-Se single bonds based on the single crystal structure data of KPu_3Se_8.

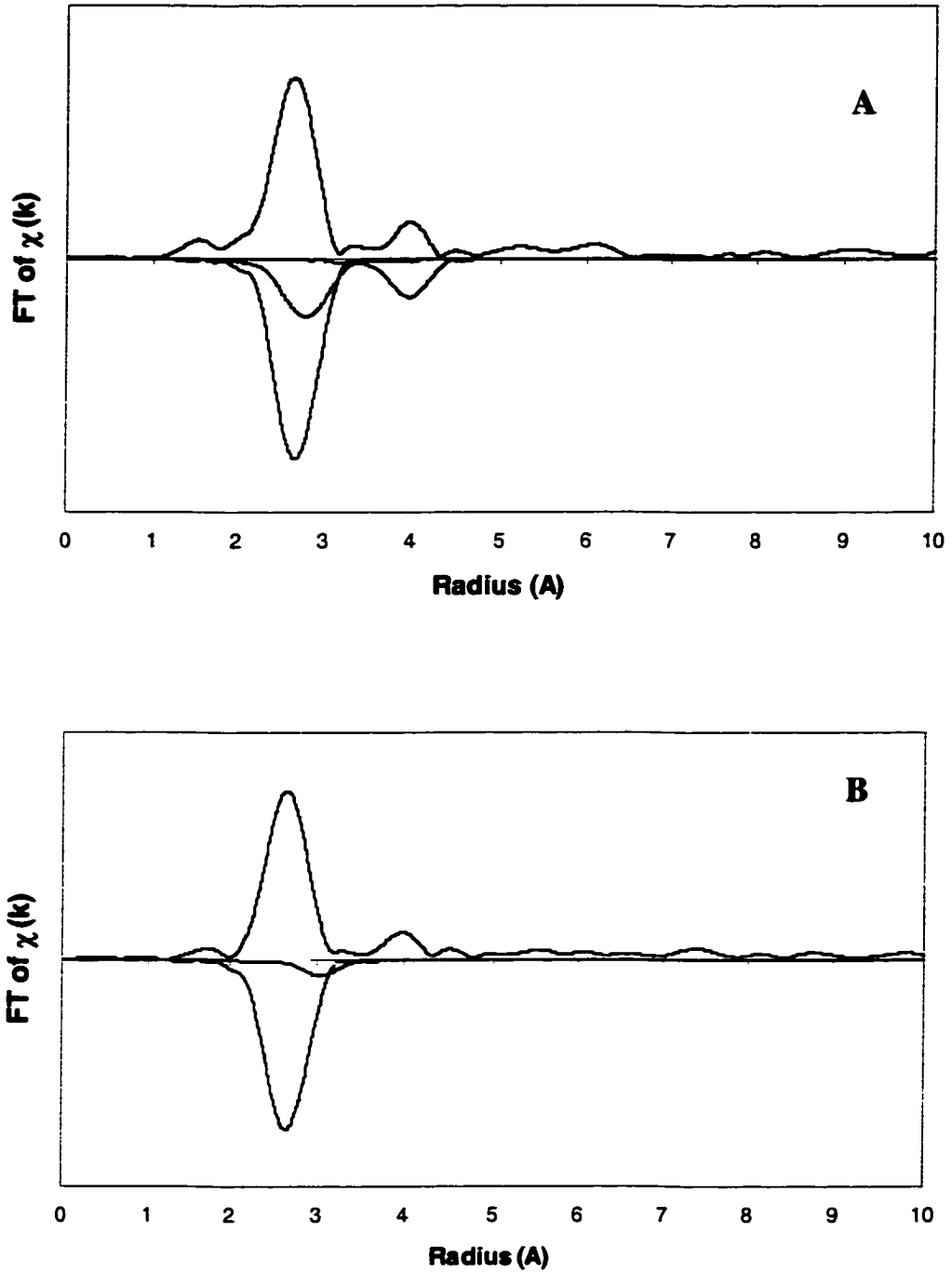

Figure 4.12. Fourier transform plots of $PuSe_2$ (A) and Pu_2Se_3 (B). $\chi(k)$ is the EXAFS function.

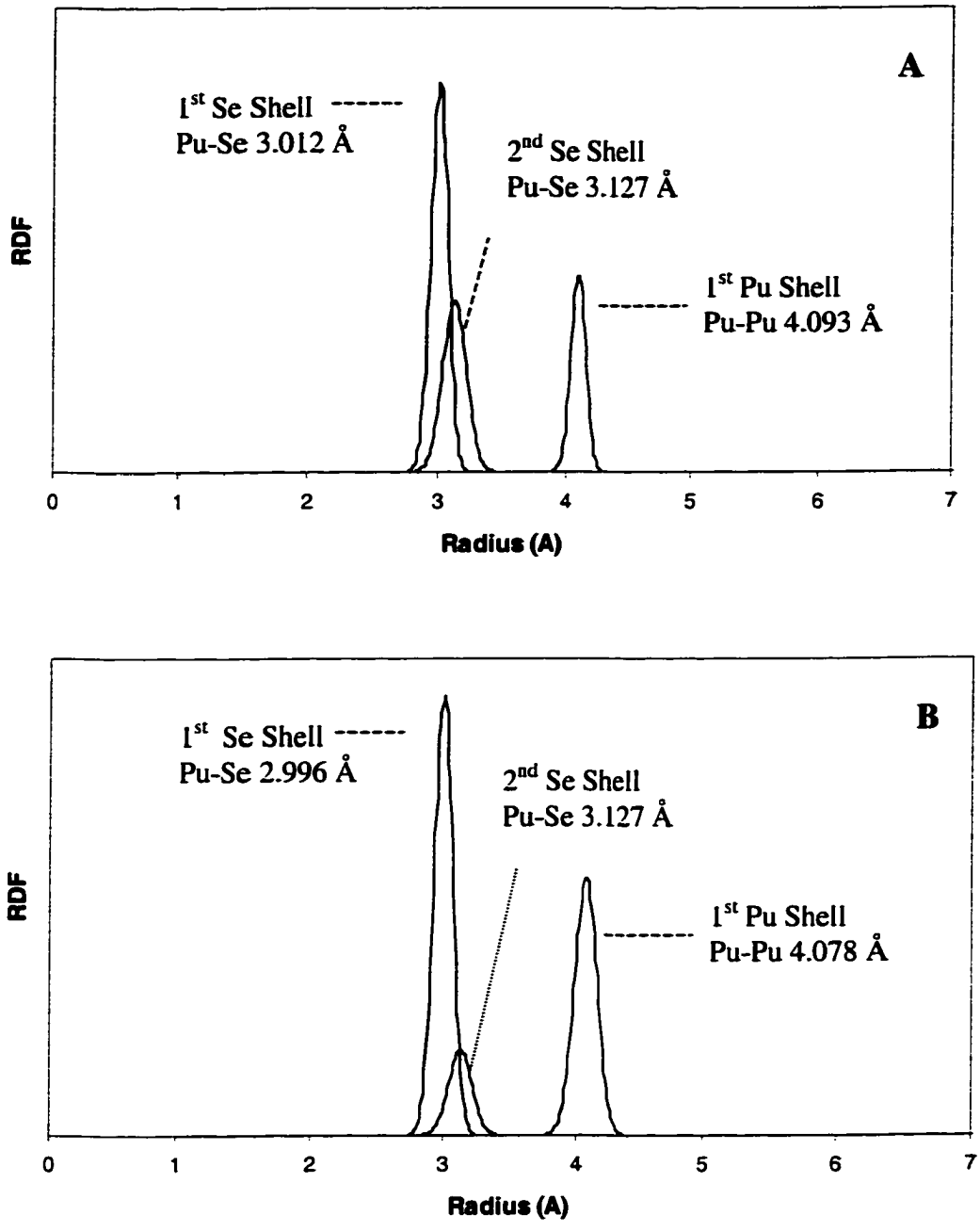

Figure 4.13. Plots of the radial distribution functions of $PuSe_2$ (A) and Pu_2Se_3 (B), from X-ray absorption experiments.

The average Pu-Se bond distance in the ternary compound is 3.042 Å. This EXAFS data represents the first detailed Pu-Se and Pu-Pu bond distances in the two binary selenides, $PuSe_2$ and Pu_2Se_3.

Conclusion

KPu_3Se_8 is the first ternary, non-oxide, plutonium chalcogenide compound to be characterized. It is also the first plutonium chalcogenide compound to show any lattice disorder. Based on the isostructural dysprosium phase, it is believed that the disorder is caused by a charge density wave.

As is the case in the ATh_2Q_6 compounds, the presence of intermediate range Se-Se bonds precludes the use of charge balancing to determine the oxidation state of plutonium. While XANES was utilized to help determine whether plutonium is in the 3+ or 4+ oxidation state, the results ultimately proved to be inconclusive. However, XANES studies on KPu_3Se_8, $PuSe_2$, and Pu_2Se_3 did yield one interesting fact, there is much more electron density on plutonium than previously thought. While it was expected that the absorption edge would shift to lower energy when a sulfur or selenium compound was compared to an oxide, the absolute value of the shift was quite large. These XANES studies are significant in terms of yielding new data for which to compare future plutonium compounds. Measurement of the magnetic moment on plutonium in KPu_3Se_8 will be carried in the future and should yield valuable information about the compound's electronic structure.

Chapter 6

Coordination Chemistry of Actinide Elements in Chalcogenide Environments

Introduction

Compared to transition metals, little is known about the coordination geometries adopted by actinide elements in various chemical environments. For many chemists the book Advanced Inorganic Chemistry, written by Cotton, Wilkinson, Murillo, and Bochmann, is a primary reference for finding information on the fundamental chemistry of a family of elements.[84] The chapter on actinide chemistry contains relatively little information on how these heavy elements interact with other elements in the periodic table. While the chapter does discuss the coordination environments of actinide atoms in simple binary oxides and halides, little is mentioned about coordination environments of these elements in complex ternary and quaternary systems.

In terms of the coordination chemistry of the actinide elements, uranium is probably the most thoroughly studied. Numerous aqueous and organometallic uranium compounds have been structurally characterized by single crystal X-ray diffraction. For the most part, the uranium atoms present in these compounds have coordination numbers of eight or nine. This is quite large compared to many transition metals. These high coordination numbers are expected based on the actinide's large size, high charge (oxidation state), and large number of valence orbitals available for bonding. In addition to complexes containing oxygen ligands, uranium complexes containing sulfur-based ligands are known to exist. Examples of these complexes are $[U(SBu^n)_6]^{2-}$ and [Li dme]$_4$[U(SCH_2CH_2S)].[84] Kanatzidis and co-workers characterized a molecular uranium selenide compound with the formula $K_4[U(Se_2)_4]$[31]. The uranium atom in this compound is coordinated to eight sulfur atoms in a distorted dodecahedral geometry.

Very little information is available concerning the coordination chemistry of plutonium. Advanced Inorganic Chemistry contains information only on plutonium oxide and halide binary compounds. The only other information on plutonium found in that reference concerns its complex aqueous chemistry. Recently, scientists at Los Alamos National Laboratory such as Clark, Neu, and Matonic have explored the coordination chemistry of plutonium in more complex systems[85,86]. They have found that plutonium can obtain many diverse coordination geometries in the solid-state. For example, they characterized a compound containing a 10-coordinate plutonium atom with the formula $[Pu(NO_3)_2\{2,6\text{-}[(C_6H_5)_2P(O)CH_2]_2C_5H_3NO\}_2](NO_3)_2$[86]. There are two organic ligands bound to plutonium in a tridentate fashion and two NO_3^- ligands bound in a bidentate fashion. These 10 oxygen atoms are arranged in a bicapped square anti-prismatic geometry. Two other compounds characterized by this group, $[Pu(H_2O)_9][CF_3SO_3]$ and $[Al(H_2O)_6][Pu(DFE)(H_2O)_3]_2[CF_3SO_3]_5$, contain plutonium coordinated to nine oxygen atoms in tricapped trigonal prismatic geometries[85].

Only four examples of plutonium coordinated to heavier chalcogen atoms are listed in the Inorganic Crystal Structure Database (ICSD).[1] These four compounds have the formulas PuS, Pu_2S_3, PuS_2, and Pu_2O_2S. These results were obtained in the late 1940's by Zacharisen, except for PuS_2, which was characterized by Marcon and Pascard in 1966.[36,83,87] In all cases the compounds were characterized by powder X-ray diffraction. The diffraction patterns of all four compounds were nearly identical to known cerium sulfide phases and were identified as such. No single crystal X-ray structures are known for plutonium chalcogenide compounds.

Before discussing the coordination environments of actinide elements in complex thiophosphate systems, it is prudent to review the possible idealized geometries that are often found in systems containing metals atoms having high coordination numbers. There are three commonly found idealized geometries for metals with a coordination number of seven: capped octahedral, capped trigonal prisms, and pentagonal bipyramids. For a coordination number of eight there are six idealized geometries: cubes, square anti-prisms, triangulated dodechedra, hexagonal bipyramids, bicapped trigonal prisms, and bicapped anti-trigonal prisms. Of these six, only the first three are prevalent for most elements. The bicapped trigonal prism is usually found only for rare earth and actinide elements.[84] Metals with a coordination number of nine typically adopt one of two geometries, either tricapped trigonal prisms or capped square anti-prisms. Finally, three idealized geometries exist for large metals that have a coordination number of ten: bicapped square anti-prisms, sphenocorona, and tetracapped trigonal prisms. Coordination numbers greater than ten are unusual even for the large actinide elements. However, the plutonium hexanitrate anion, $[Pu(NO_3)_6]^{2-}$, is one example of a metal in a 12-coordinate, distorted icosahedral geometry.[5]

The remainder of this chapter discusses the details of the local environments surrounding the actinide atoms in the ternary and quaternary structures described in the previous chapters of this dissertation. The results will be discussed in three separate sections based on the actinide element.

Thorium Chemistry

Chapter 3 discussed the synthesis and overall structural characterization of five new quaternary thorium thiophosphate compounds. Two of the compounds, $K_{10}Th_3(P_2S_7)_4(PS_4)_2$ and $Cs_4Th_2(P_2S_6)_3$, have two-dimensional layered structures. The other three compounds, $A_5Th(PS_4)_3$ (A = K, Rb, Cs), have structures consisting of one-dimensional dimers. The thorium atoms in these compounds are found in a diverse array of geometries, with coordination numbers ranging from eight to ten.

$K_{10}Th_3(P_2S_7)_4(PS_4)_2$

Two crystallographically unique thorium atoms are present in $K_{10}Th_3(P_2S_7)_4(PS_4)_2$, Th(1) and Th(2). Both Th(1) and Th(2) are coordinated to eight sulfur atoms in a distorted dodecahedral geometry. The coordination environments of both thorium atoms are shown in Figure 6.1. A dodecahedron can be described as two interpenetrating trapezoids. Using the environment around Th(1) as an example, one trapezoid is composed of S(2)-S(2A)-S(4)-S(4A) while the other is composed of S(1)-S(1A)-S(3)-S(3A). The torsion angles for the two trapezoids are 6.741° and 10.557° respectively. The Th-S bond distances are within the expected values for Th^{4+} and range from 2.844(2) Å to 2.924(2) Å with an average distance of 2.905(6) Å.

All of the sulfur atoms coordinated to thorium in this structure belong to thiophosphate ligands. Th(1) is coordinated to two $(P_2S_7)^{4-}$ ligands in an η^2-fashion and two $(PS_4)^{3-}$ ligands in an η^2-fashion as well. Th(2) is coordinated to three $(P_2S_7)^{4-}$ ligands and one $(PS_4)^{3-}$ ligands in an η^2-fashion. Figures 3.22 and 3.23 show the coordination modes of the two unique thiophosphate ligands.

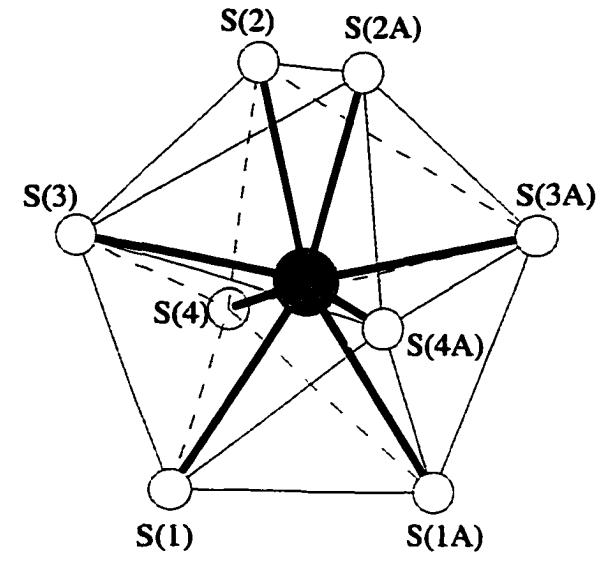

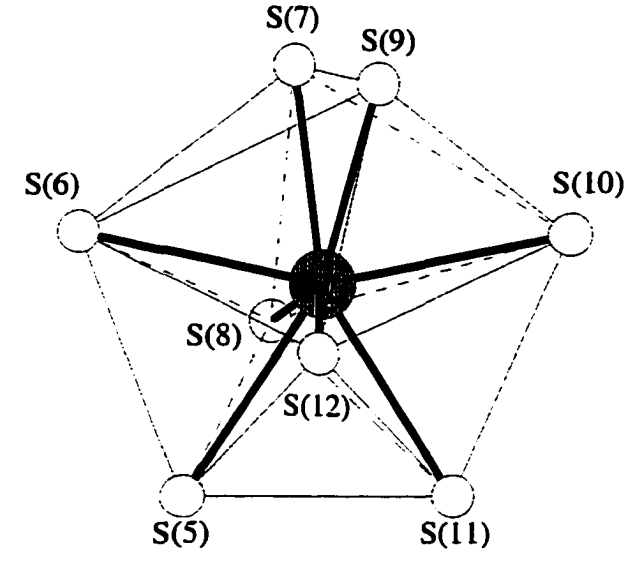

Figure 6.1. Coordination environments around Th(1) and Th(2) in $K_{10}Th_3(P_2S_7)_4(PS_4)_2$. Both atoms are coordinated to eight sulfur atoms in a distorted dodecahedral geometry.

$Cs_4Th_2(P_2S_6)_3$

This compound has a two-dimensional layered structure containing two crystallographically unique thorium atoms. The thorium atoms in $Cs_4Th_2(P_2S_6)_3$ have significantly different local coordination environments than those found in $K_{10}Th_3(P_2S_7)_4(PS_4)_2$. Figure 6.2 contains views of the coordination environments of both Th(1) and Th(2).

Th(1) is coordinated to ten sulfur atoms is a geometry that resembles a sphenocorona. In terms of calculated ligand repulsion energies, the sphenocorona has the second lowest energy of the three common 10-coordinate geometries. The 10-coordinate geometry with the lowest calculated repulsion energy is the bicapped square anti-prism. The sphenocorona has a geometry that is unfamiliar to many chemists. As seen in Figure 6.2, it contains one trapezoid consisting of S(6)-S(3)-S(5)-S(4) and lies perpendicular to the plane of the paper in the view shown. There are two square faces at the top of the polyhedron consisting of S(9)-S(9A)-S(3)-S(6), with a torsion angle of 2.268° and S(3)-S(6)-S(7)-S(8), with a torsion angle of 1.046°.

The Th(2) atom in $Cs_4Th_2(P_2S_6)_3$ is coordinated to nine sulfur atoms in a distorted tricapped trigonal prismatic geometry. This nine coordinate geometry is common in rare earth chalcophosphate compounds. The trigonal prism contains a top triangular face consisting of S(5)-S(11)-S(14) and a bottom triangular face consisting of S(6)-S(10)-S(12). The largest distortion from the idealized geometry is found in the rotation of the triangular faces. In an ideal trigonal prism the corners of the triangular faces would line up exactly. There are three sulfur atoms (S(13), S(15), S(7)) capping rectangular faces

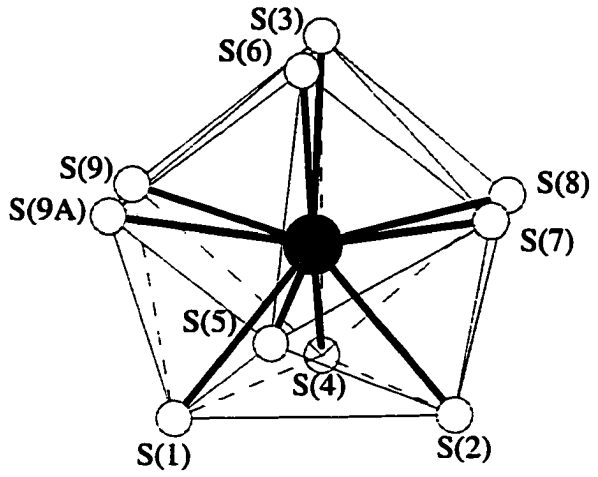

Th(1)

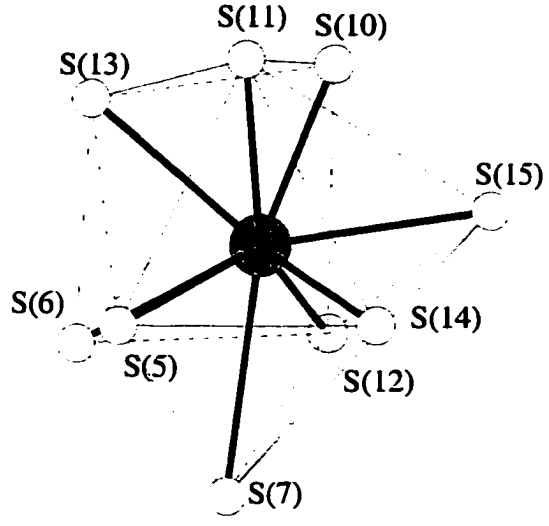

Th(2)

Figure 6.2. Coordination environments around Th(1) and Th(2) in $Cs_4Th_2(P_2S_6)_3$. Th(1) is coordinated to 10 sulfur atoms in a sphenocoronal geometry. Th(2) is coordinated to nine sulfur atoms in a tricapped trigonal prismatic geometry.

of the trigonal prism. The Th-S bond distances are within the expected values for Th^{4+} and range from 2.914(3) Å to 3.238(3) Å with an average distance of 2.99(1) Å.

All of the sulfur atoms in this structure belong to thiophosphate ligands. The ligand coordination environments of Th(1) and Th(2) are shown in Figures 3.29 and 3.30. Th(1) is coordinated by two $(P_2S_6)^{4-}$ ligands in an η^3-fashion and two $(P_2S_6)^{4-}$ ligands in an η^2-fashion. Th(2) is coordinated by four $(P_2S_6)^{4-}$, two in an η^3-fashion, one η^2-fashion, and one η^1-fashion.

$A_5Th(PS_4)_3$ (A = K, Rb, Cs)

These three thorium compounds, along with $K_5U(PS_4)_3$, form an interesting series of one-dimensional dimers. The details of how the four structures are related is described in Chapter 3. Briefly, while all four structures form dimers, the manner in which the two metal atoms are linked together varies. The thorium phases containing Rb and Cs form one structure type while the K containing phase has a different structure. The uranium compound has a structure different than any of the thorium phases. Only the coordination environments around thorium in $A_5Th(PS_4)_3$ will be discussed in this section.

The potassium phase contains one crystallographically unique thorium atom. Th(1) is coordinated to nine sulfur atoms in a capped square anti-prismatic geometry, as can be seen in Figure 6.3. One square face of the anti-prism is composed of S(2)-S(1)-S(7)-S(3), with a torsion angle of 9.053°. The other square face is composed of S(6)-S(5)-S(8)-S(4), with a torsion angle of 5.975°. The capping atom is S(2A) and has a Th-S bond distance of 3.168(2) Å. The S(2) atoms form an edge-sharing interaction with the neighboring Th atom to form the dimer. The Th-S bond distances are within the expected

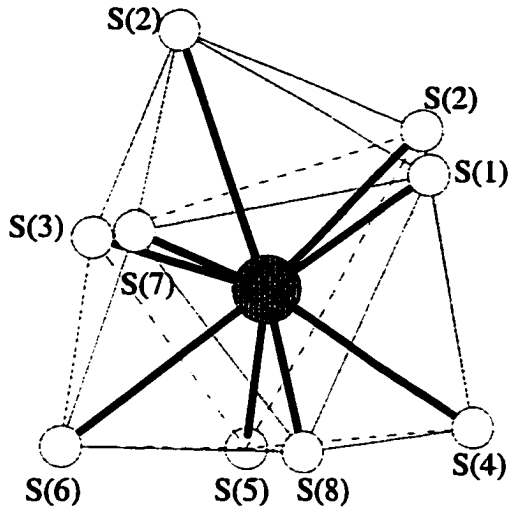

$K_5Th(PS_4)$

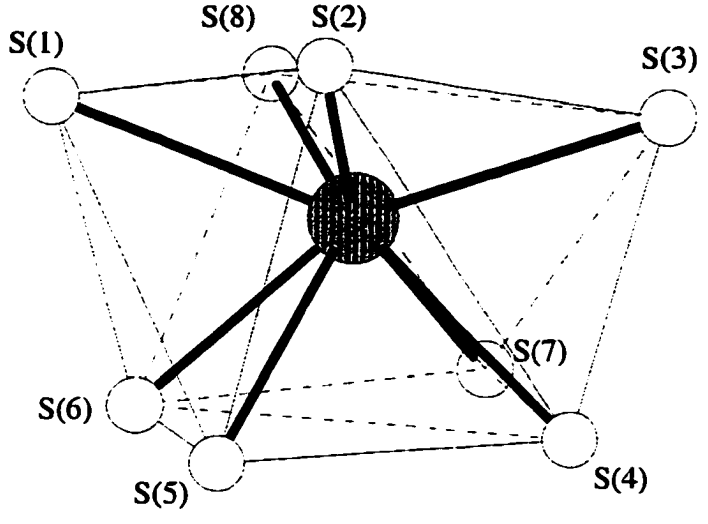

$(Rb, Cs)_5Th(PS_4)_3$

Figure 6.3. Coordination environments around the Th atoms in $K_5Th(PS_4)_3$, $Rb_5Th(PS_4)_3$, and $Cs_5Th(PS_4)_3$. The Th atom in $K_5Th(PS_4)_3$ is coordinated to nine sulfur atoms in a capped square anti-prismatic geometry. The Th atoms in the Rb and Cs phases are coordinated to eight sulfur atoms in a square anti-prismatic geometry.

values for Th^{4+} and range from 2.882(2) Å to 3.168(2) Å with an average distance of 2.993(6) Å.

All of the sulfur atoms coordinated to thorium in $K_5Th(PS_4)_3$ belong to thiophosphate ligands. Th(1) is coordinated to four $(PS_4)^{3-}$ ligands, one is coordinated in an η^3, face-capping, arrangement and three are coordinated in an η^2-fashion.

In the Rb and Cs phases, the thorium atoms are farther apart from one another, enough so that one of the S(2) atoms is to far away from Th(1) to be considered a Th-S single bond. This makes the coordination number of Th(1) eight, instead of nine as is the case in the K phase. Th(1) is coordinated to eight sulfur atoms in a square anti-prismatic geometry. In effect, the elongation of the Th· · · Th interaction has removed the capping sulfur atom from the Th(1) coordination sphere. The Th(1) atoms in the Rb and Cs phases are still coordinated to four $(PS_4)^{3-}$ ligands but their coordination modes are different. In the Rb and Cs phases thorium is coordinated by one η^3 ligand, two η^2 ligands, and one η^1 ligand. Figures 3.26 and 3.27 contain views of the thiophosphate coordination modes for the K phase and the Rb/Cs phase, respectively.

Uranium Chemistry

Three new quaternary uranium thiophosphates were characterized during the course of this research. Two of the compounds, $Cs_8U_5(P_3S_{10})_2(PS_4)_6$ and $U(P_2S_6)_2$, have complex three-dimensional structures while $K_5U(PS_4)_3$ has a structure consisting of one-dimensional dimers. The details of the extended structures of these compounds are discussed in Chapter 3. The following section will describe the local coordination environments found for uranium in a chalcogenide environment.

$Cs_8U_5(P_3S_{10})_2(PS_4)_6$

This compound contains three crystallographically unique uranium atoms in two different coordination environments. U(1) is coordinated to eight sulfur atoms in a distorted dodecahedral geometry, as seen in Figure 6.4. This coordination environment is similar to the coordination environments of the thorium atoms in $K_{10}Th_3(P_2S_7)_4(PS_4)_2$. Again, a dodecahedron can be thought of as containing two intersecting trapezoids. In this case the first trapezoid consists of S(3)-S(4)-S(1)-S(2). The second trapezoid consists of S(1)-S(2)-S(3)-S(4). The U(3) atom is also coordinated to eight sulfur atoms but in a bicapped trigonal prismatic geometry instead of dodecahedral. The top triangular face of the trigonal prism consists of S(16)-S(10)-S(11) while the bottom triangular face consists of S(13)-S(12)-S(15). The two capping atoms are S(14) and S(17). A view of the coordination environment of U(3) is seen in Figure 6.4. The U-S bond distances are within the expected values for U^{4+} and range from 2.74(4) Å to 2.94(4) Å with an average distance of 2.852(1) Å. The average value of 2.852(1) Å is 0.6 Å smaller than the average Th-S distance found in thorium thiophosphates. This corresponds to the smaller radius of U^{4+} compared to Th^{4+}.

All of the sulfur atoms coordinated to uranium in this compound belong to thiophosphate ligands. U(1) is coordinated by four $(PS_4)^{3-}$ ligands in an η^2-fashion. U(2) is coordinated by three $(PS_4)^{3-}$ ligands, all in an η^2-fashion, and one $(P_3S_{10})^{5-}$ ligand in an η^1-fashion. U(3) is coordinated by one η^1 $(P_3S_{10})^{5-}$ ligand, one η^3 $(P_3S_{10})^{5-}$ ligand and two η^2 $(PS_4)^{3-}$ ligands.

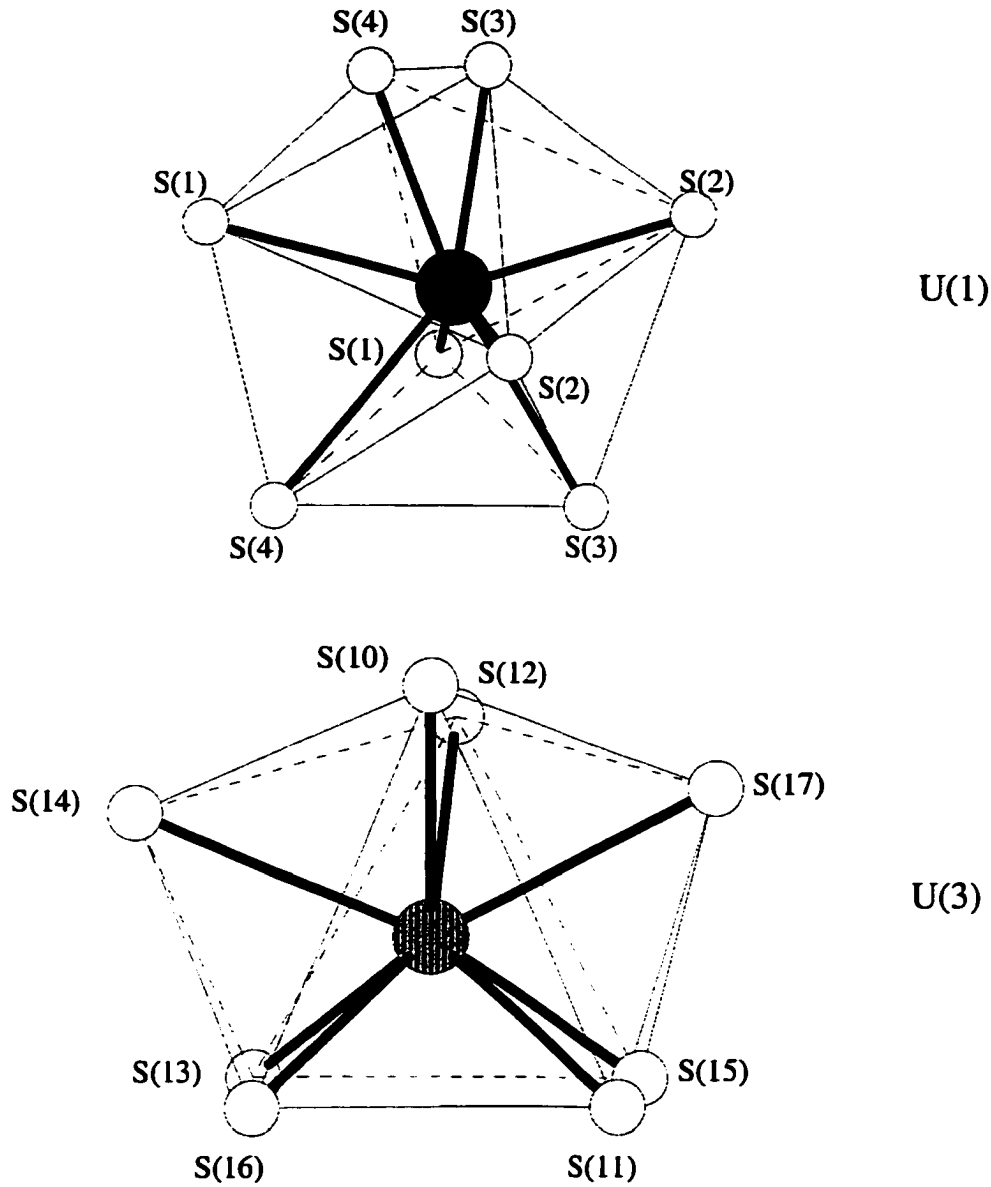

Figure 6.4 Coordination environments around the uranium atoms in $Cs_8U_5(P_3S_{10})_2(PS_4)_6$. U(1) is coordinated to eight sulfur atoms in dodecahedral geometry. U(2) and U(3) are coordinated to eight sulfur atoms as well, but in a bicapped trigonal prismatic geometry.

$U(P_2S_6)_2$

This compound contains one crystallographically unique uranium atom. U(1) is coordinated to eight sulfur atoms in a distorted dodecahedral geometry. Figure 6.5 contains a view of the local coordination environment around U(1). This coordination geometry is nearly identical to the uranium environment in $Cs_8U_5(P_3S_{10})_2(PS_4)_6$. There are two U-S bond distances in $U(P_2S_6)$, 2.804(6) Å and 2.861(6) Å. These values are similar to U-S bond distances found in the quaternary thiophosphates described above.

All of the sulfur atoms coordinated to uranium in this compound belong to thiophosphate ligands. U(1) is coordinated by four $(P_2S_6)^{2-}$ ligands in an η^2-fashion. The P_2S_6 ligands in this structure have a geometry similar to diborane and do not contain a P-P bond like the P_2S_6 ligands in the $Cs_4Th_2(P_2S_6)_3$ structure.

$K_5U(PS_4)_3$

As was the case for the thorium members of this series of actinide thiophosphate dimers, only one crystallographically distinct actinide atom is present in this structure. U(1) is coordinated to eight sulfur atoms in a distorted square anti-prismatic geometry. This environment closely resembles the thorium environments in the $(Rb, Cs)_5Th(PS_4)_3$ structures and will not be discussed in further detail here.

All of the sulfur ligands coordinated to uranium belong to thiophosphate ligands. Four $(PS_4)^{3-}$ ligands are coordinated to uranium in an η^2-fashion.

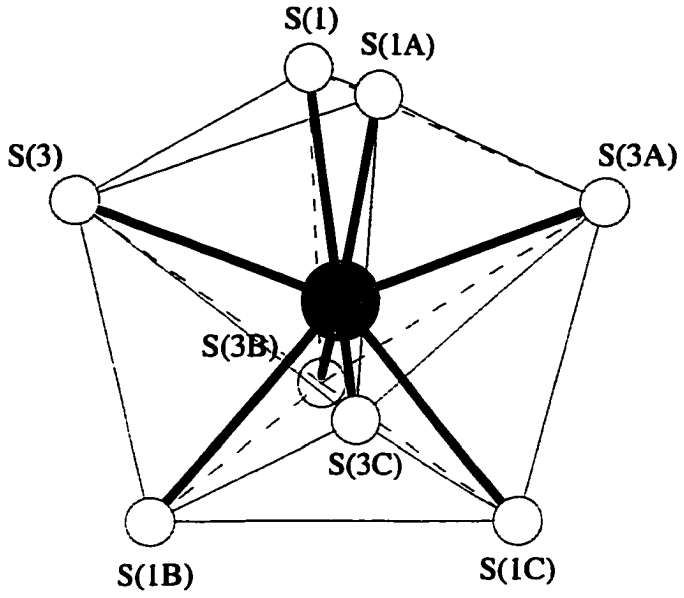

Figure 6.5. Coordination environment around the uranium atoms in $U(P_2S_6)_3$. U(1) is coordinated to eight sulfur atoms in a dodecahedral geometry.

Plutonium Chemistry

Studies of the reactivity of plutonium with chalcogen elements has yielded six new compounds characterized by single crystal X-ray diffraction. Five of the compounds are quaternary thiophosphates. The sixth compound is a ternary potassium plutonium selenide, KPu_3Se_8. The five thiophosphate compounds are $K_3Pu(PS_4)_2$, $APuP_2S_7$ (A = K, Rb, Cs), and $Rb_4Pu_2(P_2S_6)(PS_4)_2$. These compounds have extended structures ranging from one-dimensional chains in $K_3Pu(PS_4)_2$ to two dimensional layered networks in $Rb_4Pu_2(P_2S_6)(PS_4)_2$. The details of the extended structures of these compounds are discussed in Chapters 4 and 5. The remainder of this section will focus on the local coordination environments found for plutonium in a chalcogen environment.

$K_3Pu(PS_4)_2$

This compound contains one crystallographically unique plutonium atom. Pu(1) is coordinated to eight sulfur atoms in a bicapped trigonal prismatic geometry. A view of the local coordination environment around Pu(1) is shown in Figure 6.6. The top triangular face of the trigonal prism consists of S(9)-S(8)-S(5). The bottom triangular face is made up of S(9)-S(3)-S(2). Two of the rectangular faces are capped, one by S(6) and the other by S(3). The Pu-S bond distances range from 2.846(3) Å to 3.210(3) Å with an average bond distance of 2.979(8) Å. The capping sulfur atoms have the two longest metal-sulfur bond distances, 3.120(3) Å for Pu(1)-S(6) and 3.210(3) Å for Pu(1)-S(3). These Pu-S bond distances are similar to the Pu-S distances found in the Pu^{3+} binary compound, Pu_2S_3 (2.98 Å versus 2.93 Å).[36,87] The largest distortion from the idealized bicapped trigonal prismatic geometry is the relatively short distance between

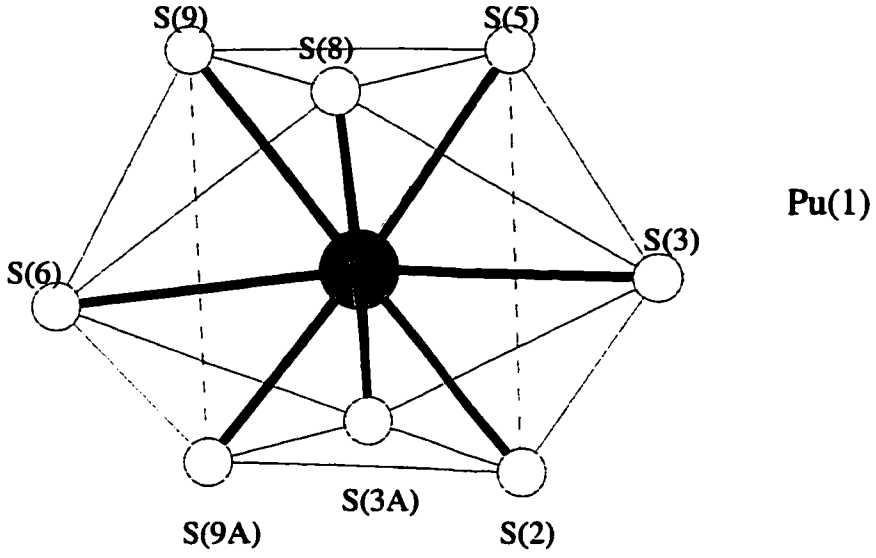

Figure 6.6. Coordination environment around the plutonium atoms in $K_3Pu(PS_4)_2$. Pu(1) is coordinated to eight sulfur atoms in a bicapped trigonal prismatic geometry.

the S(8) corner of the top triangular face and the corresponding corner of the bottom triangular face, S(3A).

All of the sulfur atoms coordinated to plutonium in this structure belong to thiophosphate ligands. Figure 4.5 contains a view of the ligand coordination environment around plutonium. Pu(1) is coordinated to four $(PS_4)^{3-}$ ligands in an η^2-fashion.

$APuP_2S_7$ (A = K, Rb, Cs)

These three compounds are isostructural with one another and contain one crystallographically unique plutonium atom. Pu(1) is coordinated in eight sulfur atoms in a highly distorted bicapped trigonal prismatic geometry. A view of the local coordination environment around Pu(1) is shown in Figure 6.7. The top triangular face consists of S(6)-S(3)-S(5) while the bottom face consists of S(5A)-S(7)-S(1). The largest distortion from an idealized bicapped trigonal prism is that the top and bottom triangular faces are not parallel to each other. The S(6)-Pu(1)-S(5A) angle, which makes up one side of the trigonal prism is much smaller than the angles which make up the other two sides, 74.36° compared to 91.70° for S(3)-Pu(1)-S(7) and 91.16° for S(5)-Pu(1)-S(1). The Pu-S bond distances in $KPuP_2S_7$ range from 2.861(3) Å to 3.056(3) Å with an average distance of 2.966(8) Å.

All of the sulfur atoms coordinated to plutonium in this structure belong to thiophosphate ligands. Figure 4.8 contains a view of the ligand coordination environment around plutonium. Pu(1) is coordinated by four $(P_2S_7)^{4-}$ ligands in an η^2-fashion.

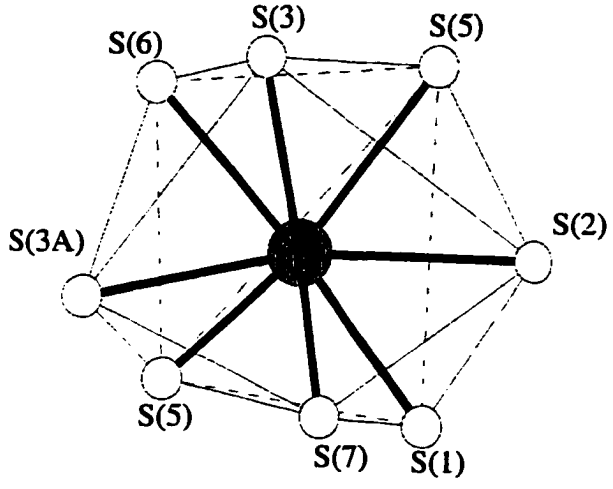

Figure 6.7. Coordination environment around the plutonium atoms in $KPuP_2S_7$. Pu(1) is coordinated to eight sulfur atoms in a highly distorted bicapped trigonal prismatic geometry.

$Rb_2Pu(P_2S_6)_{1/2}(PS_4)_2$

This two dimensional, layered compound contains one crystallographically distinct plutonium atom. Pu(1) is coordinated to eight sulfur atoms in a square anti-prismatic geometry. This geometry is in contrast to the bicapped trigonal prismatic arrangement of the eight coordinate plutonium atoms in $K_3Pu(PS_4)_2$ and $APuP_2S_7$. A view of the coordination environment around Pu(1) is shown in Figure 6.8. The top square face of the anti-prism is made up of S(1)-S(6)-S(4)-S(3) and has a torsion angle of 5.15°. The bottom square face is made up of S(1A)-S(5)-S(7)-S(2) and has a torsion angle of 6.75°. The Pu-S bond distances range from 2.865(3) Å to 3.240(3) Å with an average distance of 2.996(4) Å. This average Pu-S bond distance is similar to that found in $K_3Pu(PS_4)_2$, 2.996(4) Å versus 2.979(8) Å.

All of the sulfur atoms coordinated to plutonium in this structure belong to thiophosphate ligands. Figure 4.8 contains a view of the ligand coordination environment around plutonium. Pu(1) is coordinated by one $(P_2S_6)^{4-}$, ethane-like, ligand in an η^3-fashion, two $(PS_4)^{3-}$ ligands in an η^2-fashion, and one additional $(PS_4)^{3-}$ ligand in η^1-fashion.

KPu_3Se_8

This compound is the first ternary plutonium selenide characterized to date. It has a two-dimensional layered structure containing one crystallographically unique plutonium atom. Pu(1) is coordinated to nine selenium atoms in a capped square anti-prismatic geometry. A view of the coordination environment around Pu(1) is shown in Figure 6.9. The environment around plutonium is nearly undistorted from the idealized

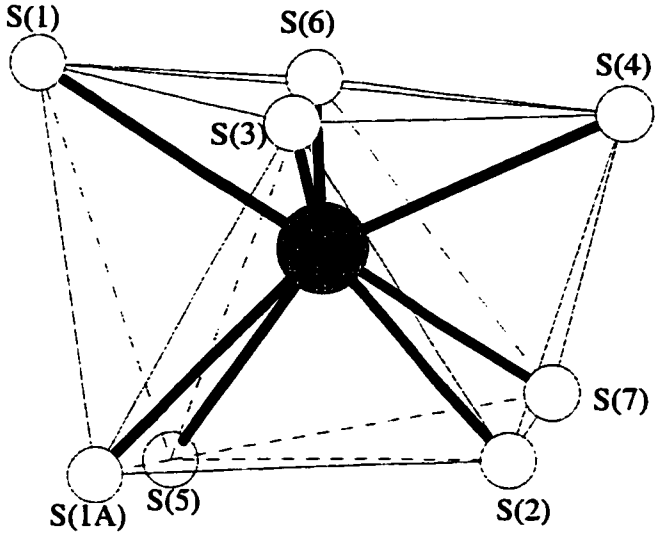

Figure 6.8. Coordination environment around the plutonium atoms in $Rb_2Pu(P_2S_6)_{1/2}(PS_4)$. Pu(1) is coordinated to eight sulfur atoms in square anti-prismatic geometry.

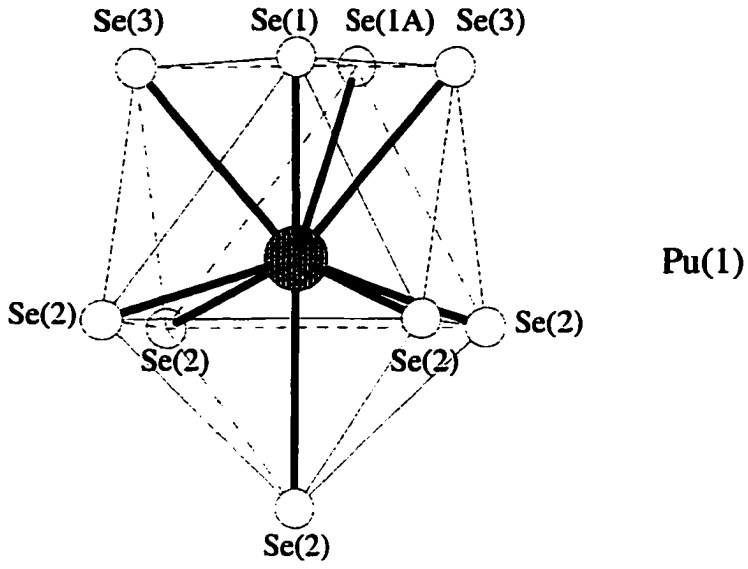

Figure 6.9. Coordination environment around the plutonium atoms in KPu_3Se_8. Pu(1) is coordinated to nine selenium atoms in a capped square anti-prismatic geometry.

geometry. One square face of the anti-prism is composed of four Se(2) atoms and has a torsion angle of 0.00°. The other square face is composed of S(3)-Se(1)-Se(3)-Se(1) and has a torsion angle of 3.21°. The capping atom, Se(2), is nearly perpendicular to the face composed of Se(2A)-Se(2B)-Se(2C)-Se(2D).

The plutonium-selenium bond distances in KPu_3Se_8 range from 2.976(1) Å to 3.171(8) Å with an average bond distance of 3.06(1) Å. This average Pu-Se bond distance is 0.078 Å longer than the average Pu-S bond distance found in the plutonium thiophosphates described above. Because selenium has a larger ionic radius than sulfur (1.98 Å versus 1.84 Å) it is expected that, on average, a Pu^{3+}-Se bond length would be 0.14 Å longer than a Pu^{3+}-S bond. The ionic radii of Pu^{3+} and Pu^{4+} are 1.00 Å and 0.86 Å, respectively. If plutonium was present in the 4+ oxidation state, the average Pu-Se bond length would be 0.14 Å shorter than if plutonium was in the 3+ oxidation state. Therefore, an average Pu^{4+}-Se bond length should be identical to a Pu^{3+}-S bond length, as the differences between S^{2-} and Se^{2-} radii is canceled out by the differences between Pu^{3+} and Pu^{4+} radii. The increase of only 0.078 Å of the average Pu-Se bond length in KPu_3Se_8 is not large enough to clearly indicate that all of the plutonium atoms are in the 3+ oxidation. Yet, it is possible that plutonium is present in a mixture of both 3+ and 4+ oxidation states. This would account for the slightly larger Pu-Se bond lengths found in the structure.

Conclusions

The investigation into the structural diversity of actinide chalcogenide compounds, described in Chapters 3-5, has yielded not only information on the

complicated extended structures of actinide compounds but also preferences in their coordination chemistry as well. While the coordination chemistry of many transition metals in chalcogen environments is well developed, little is known of the corresponding actinide chemistry.

The new quaternary thorium thiophosphate compounds described in this dissertation contain thorium atoms in five different coordination geometries with coordination numbers of 8, 9, and 10. Two different eight coordinate geometries were found, dodecahedra and square anti-prisms. Two different nine coordinate geometries were found, tricapped trigonal prisms and monocapped square anti-prisms. Finally, one 10-coordinate geometry was observed in the arrangement of a sphenocorona. In all cases, the thorium atoms were present in the 4+ oxidation state with Th-S bond distances ranging from 2.844(2) Å to 3.238(3) Å.

While the thorium was observed in many different coordination environments, the uranium atoms in all of the quaternary uranium thiophosphate compounds have coordination numbers of eight. Three different eight coordinate geometries were observed however, dodecahedra, bicapped trigonal prisms, and square anti-prisms. As was the case for thorium, the uranium atoms in all compounds were in the 4+ oxidation state. Uranium-sulfur bond distances were found ranging from 2.74(4) Å to 2.94(4) Å.

Five new quaternary plutonium thiophosphate, and one new ternary plutonium selenide, were structurally characterized in this work. In all of the thiophosphates, plutonium was found in one of two eight coordinate geometries, either bicapped trigonal prismatic or square anti-prismatic. Though the dodecahedral geometry was common in the uranium thiophosphates, it was not seen in any of the plutonium thiophosphates.

Plutonium is found in a dodecahedral geometry, however, in the defect sesqui-sulfide, Pu_2S_3. The preferred oxidation state of plutonium in a sulfur environment was found to be 3+. The plutonium-sulfur bond distances in these thiophosphates range from 2.846(3) Å to 3.24(3) Å. The plutonium atom in the ternary selenide compound, KPu_3Se_8, was observed to have a coordination number of nine with the selenium atoms arranged around plutonium in a capped square anti-prismatic geometry. This geometry is nearly identical to the plutonium environment in PuS_2. The oxidation state of plutonium in KPu_3Se_8 is not clear based on simple charge balancing. Based on the Pu-S bond distances its possible that the compound contains both plutonium(III) and plutonium(IV) atoms.

Interestingly, the Pu-S bond distances found in PuS_2 (2.89 Å and 2.92 Å) are similar to those found in the quaternary thiophosphates described above.[83] If the plutonium atoms in PuS_2 were in the 4+ oxidation state they should have Pu-S bond distances of 2.75 Å and 2.78 Å. It would appear that the plutonium atoms in PuS_2 are in the 3+ oxidation state. This is unexpected since all of the sulfur atoms in PuS_2 are in the 2- oxidation state. There are no intermediate range S-S interactions in the disulfide as there are in KPu_3Se_8.

In addition to learning valuable information on the diverse structural solid-state chemistry of actinide elements in chalcogen rich environments, this research has provided the scientific community with a better understanding of some of the fundamental coordination geometries these unique elements adopt.

References

(1) Inorganic Crystal Structure Database 1/2001 ed.; NIST; Vol. 2001.

(2) Hecker, S. S. "Los Alamos Science," Los Alamos National Laboratory, 2000.

(3) Smith, J. L.; Kmetko, E. A. *J Less Common Met.* **1983**, *90*, 83.

(4) Clark, D. "Chemical Complexities of Plutonium," Los Alamos National Laboratory, 2000.

(5) Katz, J. J.; Seaborg, G. T.; Morss, L. R. *The Chemistry of the Actinide Elements*; Chapman and Hall: New York, 1986; Vol. 1.

(6) Tatsumi, K.; Hoffmann, R. *Inorg. Chem.* **1980**, *19*, 2656-2658.

(7) In *Los Alamos Science*; 26 ed.; Cooper, N., Ed.; Los Alamos National Laboratory: Los Alamos, 2001; Vol. 1, pp 10-15.

(8) Sunshine, S. A.; Kang, D.; Ibers, J. A. *J. Am. Chem. Soc.* **1987**, *109*, 6202-6204.

(9) Kanatzidis, M. G.; Park, Y. *J. of the Am. Chem. Soc.* **1989**, *111*, 3767-3769.

(10) Kanatzidis, M. G. *Chem. Mater.* **1990**, *2*, 353-363.

(11) Kanatzidis, M. G.; Park, Y. *Chem. Mater.* **1990**, *2*, 99-101.

(12) Sunshine, S. A.; Ibers, J. A. *Inorg. Chem.* **1985**, *24*, 3611.

(13) McCarthy; Kanatzidis, M. G. *Chem. Mater.* **1993**, *5*, 1061-1063.

(14) Evenson, C. R.; Dorhout, P. K. *Inorg. Chem.* **2001**, *40*, 2875-2883.

(15) Briggs Piccoli, P. M.; Abney, K. D.; Schoonover, J. R.; Dorhout, P. K. *Inorg. Chem.* **2000**, *39*, 2970-2976.

(16) Evenson, C. R.; Dorhout, P. K. *Inorg. Chem.* **2001**, *40*, 2884-2891.

(17) Hess, R. F.; Abney, K. D.; Burris, J. L.; Hochheimer, H. D.; Dorhout, P. K. *Inorg. Chem.* **2000**, *40*, 2851-2859.

(18) Kanatzidis, M. G.; Chou, J. H. *J. Solid. State. Chem.* **1996**, *127*, 186-201.

(19) Kanatzidis, M. G.; McCarthy, T. J.; Tanzer, T. A.; Chen, L.-H.; Iordanidis, L. *Chem. Mater.* **1996**, *8*, 1465-1474.

(20) Narducci, A. A.; Ibers, J. A. *Inorg. Chem.* **1998**, *37*, 3798-3801.

(21) Narducci, A. A.; Ibers, J. A. *Chem. Mater.* **1998**, *10*, 2811-2823.

(22) Chondroudis, K.; Kanatzidis, M. G. *C. R. Acad. Sci. Paris* **1996**, *t. 322, Serie II b*, 887-894.

(23) Chondroudis, K.; Kanatzidis, M. G. *J. Am. Chem. Soc.* **1997**, *119*, 2574-2575.

(24) Briggs-Piccoli, P. M.; Abney, K. D.; Schoonover, J. R.; Dorhout, P. K. *Inorg. Chem.* **2001**, *40*, 4871-4875.

(25) Greenwood, N. N.; Earnshaw, A. *Chemistry of the Elements*; Pergamon Press: New York, 1984.

(26) Computer Program "RAD DECAY", calculates decay schemes for nuclides.

(27) Voelz, G. L. "Plutonium and Health," Los Alamos National Laboratory, 2000.

(28) Chondroudis, K.; Hanko, J. A.; Kanatzidis, M. G. *Inorg. Chem.* **1997**, *36*, 2623-2632.

(29) Chondroudis, K.; Kanatzidis, M. G.; Sayettat, J.; Jobic, S.; Brec, R. *Inorg. Chem.* **1997**, *36*, 5859-5868.

(30) Kanatzidis, M. G. *Current Opinion in Solid State & Materials Science* **1997**, *2*, 139-149.

(31) Sutorik, A. C.; Kanatzidis, M. G. *J. Am. Chem. Soc.* **1991**, *113*, 7754.

(32) Chondroudis, K.; Kanatzidis, M. G. *C R Acad Sci Ser II B* **1996**, *322*, 887-894.

(33) Sutorik, A. C.; Kanatzidis, M. G. *Chem. Mater.* **1997**, *9*, 387-398.

(34) Hund, F.; Duerrwaechter, W. *Z. anorg. allg. Chem.* **1951**, *265*, 67-72.

(35) Noel, H.; Potel, M. *Acta Crystallographica B* **1982**, *38*, 2444.

(36) Zachariasen, W. H. *Acta Cryst.* **1949**, *2*, 291.

(37) Kröniert, W.; Plieth, K. *Z. anorg. allg. Chem.* **1965**, *336*, 207.

(38) Potel, M.; Brochu, R.; Padiou, J.; Grandjean, D. *C. R. Acad. Sc. Paris, Série C* **1972**, *275*, 1419.

(39) Bronger, W.; Donike, A.; Schmitz, D. *Z. anorg. allg. Chem.* **1997**, *623*, 1715-1718.

(40) Ghouse, K. M. *Indian Journal for Pure and Applied Physics* **1968**, *6*, 265-268.

(41) Markarov, E. S.; Ivanov, V. I. *Dokl. Akad. Nauk SSSR* **1960**, *132*, 673-676.

(42) Ruzic, T.; Kojic-Prodic, B.; Liminga, R.; Popovic, S. *Inorg. Chim. Acta* **1974**, *8*, 273-278.

(43) Gorbunova, Y.; Linde, S.; Lavrov, A. V. *Zh. Fiz. Khim.* **1981**, *26*, 713-717.

(44) Chondroudis, K.; Kanatzidis, M. G. *J. Am. Chem. Soc.* **1997**, *119*, 2574-2575.

(45) Chondroudis, K.; Kanatzidis, M. G. *J. Am. Chem. Soc.* **1997**, *119*, 2574-2575.

(46) Liao, J.-H.; Kanatzidis, M. G. *Inorg. Chem.* **1992**, *31*, 431-439.

(47) Wilkinson, F.; Kelly, G. In *CRC Handbook of Organic Photochemistry*; Scaiano, J. C., Ed.; CRC Press: Boca Raton, FL, 1989; Vol. 1, pp 293-314.

(48) Sheldrick, G. M.; University of Göttingen: Göttingen, Germany, 1997.

(49) Sheldrick, G. M.; 5 ed.; Siemens Analytical X-Ray Instruments, Inc.: Madison, WI, 1997.

(50) Computer Program XSHELL Sheldrick; Siemens: Madison, WI, 1999.

(51) Fransisco, R. H. P.; Tepe, T.; Eckert, H. *J. Solid State Chem.* **1993**, *107*, 452-459.

(52) Chondroudis, K.; Kanatzidis, M. G. *Inorg. Chem.* **1998**, *37*, 2098-2099.

(53) Briggs-Piccoli, P. M.; Abney, K. D.; Schoonover, J. D.; Dorhout, P. K. *Inorg. Chem.* **2000**, in preparation.

(54) Bruker; 5 ed.; Siemens Analytical X-ray Systems, Inc.: Madison, WI, 1998.

(55) Do, J.; Kim, J.; Lah, S.; Yun, H. *Bull. Korean Chem. Soc.* **1993**, *14*, 678.

(56) Gieck, C.; Rocker, F.; Ksenofontov, V.; Gutlich, P.; Tremel, W. *Angew. Chem.* **2001**, *40*, 908-911.

(57) Carrillo-Cabrera, W.; Peters, K.; von Schnering, H. G. *Z. anorg. allg. Chem.* **1995**, *621*, 557-561.

(58) Patzmann, U.; Brockner, W.; Cyvin, B. N.; Cyvin, S. J. *J. Raman Spectrosc.* **1986**, *17*, 257-261.

(59) Mentzel, F.; Ohse, L.; Brockner, W. *Heteroat. Chem.* **1990**, *1*, 357-362.

(60) Blake, P. C.; Lappert, M. F.; Taylor, R. G.; Atwood, J. L.; Zhang, H. *Inorganica Chim. Acta* **1987**, *139*, 13-20.

(61) Menzel, F.; Brockner, W.; Carrillo-Cabrera, W. *Heteroat. Chem.* **1993**, *4*, 393-398.

(62) Evenson, C. R.; *Dissertation*; Colorado State University: Fort Collins, 2001.

(63) Weigel, R.; Katz, J. J.; Seaborg, G. T. In *The Chemistry of the Actinide Elements*; Katz, J. J., Seaborg, G. T., Morss, L. R., Eds.; Chapman and Hall: New York, 1986; Vol. 1, pp 499-886.

(64) *Plutonium Handbook*; American Nuclear Society: La Grange Park, IL, 1980.

(65) Cleveland, J. M. *The Chemistry of Plutonium*; American Nuclear Society: La Grange Park, IL, 1979.

(66) Allbutt, M.; Dell, R. M. *J. Nucl. Mat.* **1967**, *24*, 1-20.

(67) Gauthier, G.; Jobic, S.; Brec, R.; Rouxel, J. *Inorg. Chem.* **1998**, *37*, 2332-2333.

(68) Peterson, J. R.; Cunningham, B. B. *J. Inorg. Nucl. Chem.* **1968**, *30*, 1775-1783.

(69) Schewe-Miller, I.; Universität Stuttgart, 1990.

(70) Computer Program, SAINT, 4ed.; Siemens Analytical X-ray Systems, Inc.: Madison, WI, 1996.

(71) Bagnall, K. W. *The Actinide Elements (oxidation potentials)*; Elsevier: New York, 1972.

(72) Durand, E.; Evain, M.; Brec, R. *J. Solid State Chem.* **1993**, *102*, 146-155.

(73) Wells, A. F. *Three-dimensional Nets and Polyhedra*; John Wiley & Sons: New York, 1977.

(74) Whangbo, M.-W. *J. Chem. Phys.* **1980**, *73*, 3854.

(75) Whangbo, M.-H. *Inorg. Chem.* **1980**, *19*, 1728-1731.

(76) Goh *J. Solid. State. Chem.* **2001**, *160*, 195-204.

(77) Hess, R. F.; Abney, K. D.; Dorhout, P. K., in preparation.

(78) Wu, E. J.; Pell, M. A.; Ibers, J. A. *J. Alloys Comp.* **1997**, *255*, 106-109.

(79) Choi, K.-S.; Patschke, R.; Billinge, S. J. L.; Waner, M. J.; Dantus, M.; Kanatzidis, M. G. *J. Am Chem. Soc.* **1998**, *120*, 10706-10714.

(80) Patschke, R.; Heising, J.; Schindler, J.; Kannewurf, C. R.; Kanatzidis, M. *J. Solid. State. Chem.* **1998**, *135*, 111-115.

(81) Foran, B.; Lee, S.; Aronson, M. C. *Chem. Mater.* **1993**, *5*, 974-978.

(82) Lee, S.; Foran, B. *J. Am. Chem. Soc.* **1994**, *116*, 154-161.

(83) Marcon, J. P.; Pascard, R. *J. Inorg. Nucl. Chem.* **1966**, *28*, 2551-2560.

(84) Cotton, F. A.; Wilkinson; Murillo; Bochmann *Advanced Inorganic Chemistry*; 6th ed.

(85) Matonic, J. H.; Scott, B. L.; Neu, M. P. *Inorg. Chem.* **2001**, *40*, 2638-2639.

(86) Bond, E. M.; Duesler, E. N.; Paine, R. T.; Neu, M. P.; Matonic, J. H.; Scott, B. L. *Inorg. Chem.* **2000**, *39*, 4152-4155.

(87) Zachariasen, W. H. *Acta Cryst.* **1948**, *C1*, 265-268.

Appendix A

Procedures for Experiments Requiring the Use of Air Purifying Full-Face Respirators

Procedure for the Loading of TRU Reaction Ampoules

Necessary Equipment

1. Labeled quartz ampoules
   can be obtain from CSU Glass Shop
2. Parafilm
3. Vacuum line adapters (one per ampoule)
4. Three tanks of Ar gas

Preparation

1. Wrap ampoules in parafilm
   leave top ½" or so uncovered (will be inserted into adapter)
   leave an adequate "tab" for easy removal with tweezers
   be sure to wrap loosely or it will be difficult to remove
2. Adapters should already be in box from the last hot job, if not:
   wrap the bottom metal ring separately from the rest, it needs to be able to turn for tightening
   wrap the rest of the tube in one long piece, be sure the valve is closed
   be sure no parafilm is covering the metal fitting's opening
3. Place all needed equipment in glovebox
4. Remove any items that may contain large amounts of air and place in antechamber
5. Begin Ar purge, try to achieve 100-200 ppm O_2, may take from 4-6 hours

After Loading

1. Cover ampoule openings with Chemwipe and place in vacuum desiccator until hot job

Procedure for Sealing Ampoules Containing TRU Material

Necessary Personnel
One assistant
One Radiological Control Technician

Necessary Equipment
1. Full face air purifying respirators
2. Skull caps
3. Standard PPE
4. Tweezers
5. Numerous zip lock bags for waste and adapter transport
6. Plastic for covering work surfaces
7. Aluminum foil boat for freshly sealed hot tubes
8. Leather work gloves
9. Welder's goggles (3 pairs)

Preparation
1. Cover work areas with plastic
2. Line the "sealing" hood with Aluminum foil to protect vacuum hose and hood
3. Place foil boat in "sealing" hood
4. Be sure vacuum pump is on and torch is nearby
5. Remove waste glass from each adapter
6. When everyone is ready, remove ampoules from desiccator and attach to adapter
   this is best done under a stream of Ar gas using a desiccator lid as a nozzle
7. Place adapters in the antechamber
8. Everyone must be where their respirators at this point
   one person will be designated "hot" and the other "cold"
   the hot person should wear two pairs of gloves over their taped on pair

Decontamination
1. Working with one adapter at a time, hot person should begin unwrapping adapter
2. Working from vacuum end towards ampoule bottom remove parafilm until near the end
3. Care must be taken when removing last of the parafilm to NOT accidentally pull the ampoule from the adapter. Best avoided by having RCT check to see if upper portion of unwrapped ampoule is cold. Now the "cold" person can hold it in their hand while hot person remove the remainder of the parafilm.
4. Using "Fantastic" decontaminate any hot areas of unit.
5. The very bottom surface of the metal fitting usually contains fixed contamination. Address by using covering the metal ring with parafilm.
6. Place unit upright in a ziplock bag.
   Warning: the inside surfaces of the adapters are hot, be aware of the top opening

Sealing

1. Place adapters on vacuum line, allow a few minutes to pump down
2. The person sealing should be wearing: one taped pair of gloves
   one pair of leather gloves
   one pair of thick gloves on top
3. Light the torch, everyone should be wearing welder's goggles
4. Seal ampoule and place on aluminum boat to cool
5. Leave waste glass stub in place, do NOT remove because it is hot inside
6. When all tubes are sealed, and the RCT is ready, respirators can be removed
7. While adapters are on vacuum line, re-wrap them with parafilm so they are ready for the next job
8. Insert sealed ampoules into the air glovebox containing the tube furnace

If Ampoule Pops During Sealing

1. Stay calm you are wearing a repirator
2. Shut off the torch and have the RCT check for contamination
3. Wrap unit in parafilm while on vacuum line
4. Insert entire unit in "inert" glovebox for eventual reloading

Procedure for Loading and Sealing Capillaries Containing TRU Material for Use in Single Crystal X-ray Diffraction Experiments

Containment Requirements

Because the diffractometer is in an uncontrolled area each TRU crystal must have three layers of containment. The first layer of containment is provided by a coating of epoxy or grease on the crystal. The second layer of containment is provided by inserting the crystal in a glass or quartz capillary. Finally, the third layer of containment is provided by coating the sealed capillary with acrylic.

Necessary Personnel

one assistant
one Radiological Control Technician (RCT)

Necessary Equipment

1. 0.5 mm inner diameter capillary tubes (preferable quartz)
2. 0.2 mm inner diameter capillary tubes or similar size glass fibers
3. X mL glass vials
4. Parafilm
5. X gauge needle
6. Epoxy
7. Tweezers
8. Toe nail clippers
9. Video monitor
10. Three tanks of Ar gas

Capillary Preparation

1. Trim 0.5 mm capillary tubes so the will fit in the glass vial
2. Epoxy the trimmed end shut, allow to dry
3. Using two squares of parafilm, create a drum-like seal over the glass vial
4. Poke appropriate number of holes in the parafilm and insert capillaries.
   between 2 and 4 capillaries per vial works well
5. Place vial in the glovebox and purge with Ar gas

At this point you have made sure that the outside surface of you capillary tube will remain cold even inside the glove box. The only items that will get contaminated during this procedure are the outside of the vial and the opening of the capillary tubes. These will be thrown away during the sealing process leaving you with a cold capillary tube.

Loading the Capillary Tube

1. Select a single crystal and role it in epoxy or grease
2. Insert crystal into capillary tube using a smaller diameter capillary or a glass fiber.
   if possible try to remove fiber and leave behind just the crystal if not don't worry about it
3. When all capillaries are loaded place the vial in the antechamber
4. For increased protection from air, epoxy the loading end of the capillaries shut

Sealing the Capillary Tube

This procedure may be carried out as a hot job using respirators at the RCT's digression

1. One person will be designated "hot" and the other will be "cold"
   Be sure to have some epoxy mixed and ready in the hood
2. The hot person will remove the vial from the antechamber and both people will find the location of each crystal inside the capillary tubes
3. The hot person will pull one capillary tube out of the vial.
   At this point the opening of the tube is hot but the body of the tube is cold
4. The cold person will hold the bottom end of the tube and clip the capillary between the crystal and the hot person's fingers. The capillary tube should be no longer than ¾"
5. Immediately after clipping the open end of the capillary is dipped in epoxy and set in a petri dish to dry while the others are clipped.
6. The hot person can throw away each capillary top and finally the vial
7. After the epoxy dries trim any capillaries that are still to long.
8. When all are of appropriate length coat them with nail polish (acrylic)
9. When dry the RCT will check for contamination

A Broken Capillary Tube

The most common problem is having a capillary tube break during clipping. It is vital to stay calm and not move everything around. First try to locate the single crystal. Be sure that it is not on your hands. It will most likely be on a piece of the capillary or on the paper towels lining the floor of the hood. A typical crystal of X-ray quality size has an activity of around 50,000 counts per minute so the use of an alpha counter greatly increases your chance of finding the crystal. When the crystal is located you can either try to salvage it by placing it in a new, trimmed, capillary tube or by fixing it on the towel with epoxy and throwing it way in the TRU waste box.

Appendix B

Fourth Year Research Proposal

The Proposed Synthesis and Characterization of Superconducting Actinide Boride Intermetallics: Working Towards the Understanding of Electronic Properties in Actinide Systems

Abstract

The goal of this proposal is to synthesize and characterize new superconducting compounds containing an actinide element such as Th, U, Np, Pu, or Am. These compounds will be based on an existing system of binary boride, rare earth rhodium boride, and rare earth-transition metal compounds. These three classes of superconducting materials can contain a wide variety of rare earth elements. Many of these materials defy the once held belief that superconductivity and long range magnetic order cannot co-exist. This proposal addresses two areas of scientific interest. First is the search for new superconducting materials and a better understanding of why some materials superconduct while others do not. The second area of interest is elucidating the effect of the 5f electrons on structure formation and electronic properties. Three separate classes of actinide borides will be investigated. The first class will focus on the relatively simple binary and pseudo-ternary actinide borides based on the superconducting MgB_2 structure. These compounds should have formulas such as AnB_2 and $(An_xMg_{1-x})B_2$. The other two classes of materials that will be studied are actinide analogs of the $RERh_4B_4$ and RER_2B_2C (RE = rare earth element; R = Ni, Pd) superconducting and magnetic compounds.

Background

Since the discovery of superconductivity in mercury by Onnes in 1911,[1] numerous compounds have been found that exhibit this remarkable property. These compounds can be separated into different classes based on structure type and mechanism of superconductivity. Cuprates make up the most well known class of superconductors. These compounds have formulas such as $YBa_2Cu_3O_7$ (1-2-3 family) and are structurally related to perovskites. One member of the cuprate family has the highest superconducting transition temperature known, $Hg_{0.8}Tl_{0.2}Ba_2Ca_2Cu_3O_7$ with a T_c of 138 K.[2] Another class of materials that has already found industrial applications are transition metal-main group alloys. Nb_3Ge (T_c = 23.2 K) is the superconducting material that is used in medical magnetic resonance imaging (MRI) instruments.[2] Heavy fermion compounds such as UBe_{13} are yet another family of materials that are known to exhibit superconductivity.[3] These compounds typically contain a heavy element from the rare earth or actinide series. Due to relativistic effects, the conduction electrons of these materials have very large effective masses. The effect of these "heavy electrons" is to lower the fermi energy, which is counter productive for superconductivity [2]. While these materials do superconduct, they have very low transition temperatures (T_c) on the order of a few Kelvin.

Another interesting class of superconductors is based on boron containing materials. This class of compounds will be the focus of this proposal. Boride superconductors can be broken up into three families: binary borides such as MgB_2 and LaB_6, rare earth rhodium borides such as $LuRh_4B_4$, and rare earth-transition metal borocarbides such as $LuNi_2B_2C$.

Magnesium diboride, MgB_2, has been shown to have a surprisingly high T_c (39 K) and a relatively simple structure when compared to the complex quintary phases found in the cuprates.[4] The binary diboride structure consists of metal cations separated by graphite-like boron layers, as shown in Figure 1. The sample preparation of this intermetallic compound is accomplished by simply arc-melting the two elements together with the appropriate stoichiometry. Studies by Bud'ko and co-workers indicate that MgB_2 most likely superconducts via the same BCS (Bardeen, Cooper and Schrieffer) phonon-mediated mechanism that is found in the cuprates.[5] In addition to MgB_2, two other binary borides are known to exhibit superconductivity, YB_6 and LuB_{12}, with T_c values of 7.1 K and 0.44 K respectively. [6,7] Though actinide diborides, hexaborides, and dodecaborides have been structurally characterized, relatively little is known about their conductivity and magnetism.

The remaining families of superconducting borides, that are the focus of this proposal, are the ternary rare earth rhodium borides and the quaternary rare earth-transition metal borocarbides. Numerous compounds with the formulas $RERh_4B_4$ and REM_2B_2C (M = Ni and Pd) have been characterized. [8] [9-17] These two classes of compounds are interesting to the superconductor world since, depending upon the particular rare earth element, they can exhibit superconductivity and long-range magnetic order simultaneously. A fundamental characteristic of superconductivity is the perfect repulsion of a magnetic field. Because of this characteristic it was initially thought that superconductivity and magnetism could not co-exist. For example, in the class of cuprate superconductors the presence of even a minute amount of magnetic impurity will destroy superconductivity. Matthias and Hamaker and their co-workers reported the

characterization of a number of $RERh_4B_4$ compounds that exhibit both superconducting and ferromagnetic transitions when RE = Nd, Sm, Er, or Tm. [18,19,20] The Nd, Sm, and Tm compounds exhibit superconductivity and antiferromagnetic order simultaneously. The Er compound, however, exhibits what is called re-entrant superconductivity. A re-entrant superconductor will typically under go a normal to superconducting transition and then, at a lower temperature, undergo a second transition. This second transition is usually to a ferromagnetic or antiferromagnetic state and results in the destruction of superconductivity. $ErRh_4B_4$ undergoes a normal to superconducting transition at $T_{c1} = 8.7$ K but as the temperature decreases, a transition to a ferromagnetic state occurs. At this point, $T_{c2} = 0.9$ K, superconductivity is destroyed. When RE = Gd, Tb, or Dy only ferromagnetic behavior is observed.[8] $RERh_4B_4$ has a three dimensional tetragonal structure that contains Rh_4B_4 layers separated by layers of RE cations. Figure 2 show a picture of $LuRh_4B_4$ viewed down the [100] crystallographic direction.

Like the rare earth rhodium borides the borocarbides are another class of compounds in which superconductivity and magnetism can co-exist. These materials are known to have T_c values of up to 23 K, as found for YNi_2B_2C.[14] A number of other compounds are known with this same formula and structure. These REM_2B_2C compounds are tetragonal and can be considered a "stuffed" form of the $ThCr_2Si_2$ structure type. YNi_2B_2C has a 3D structure containing Ni_2B_2 layers separated by YC layers as seen in Figure 3. The Ni atoms are coordinated to four boron atoms in a tetrahedral geometry. The YC layer is a simple square sheet that is linked to the Ni_2B_2 layer via B-C bonds.[12] Other isostructural compounds are known for RE = Sc, Y, La, Ce, Sm, Tb, Dy, Ho, Er, Tm, and Lu.[12 14] A wide range of behaviors is encountered across this series. The Lu, Y, and Sc compounds are non-magnetic and have relatively high T_cs from 15-16.6 K. The Ho, Er, and Tm compounds exhibit superconductivity and magnetism with T_c ranging from 8-11 K. The Ho and Er compounds order antiferromagnetically while the Tm compound is ferromagnetic. This chemistry has been extended to the early actinides, Th and U, by both Lai and Hossain along with their co-workers. $ThNi_2B_2C$ was found to superconduct at 8.0 K while $ThPd_2B_2C$ has a T_c of 14.5 K.[14,13] One problem both researchers encountered is that all their samples, synthesized by arc-melting, were multi-phase. Both research groups synthesized a number of U phases but found that they did not superconduct.

Research goals

The primary objective of this proposal is to synthesize and characterize new actinide boride compounds that exhibit superconductivity. The formation of actinide phases will help to elucidate some of the fundamental differences between the actinide and the rare earth elements. One key difference in behavior is that while the majority of rare earth elements are found in the 3+ oxidation state many of the actinides can access multiple oxidation states, sometimes even in the same compound. Also, significant changes occur in the properties of the f-orbitals upon going from the 4f to 5f series. The 4f orbitals are typically very core-like and participate little in bonding. As a result, chemical behavior of the rare earth elements changes very little across the 4f series. In contrast, the 5f orbitals are far less contracted and have been shown to participate in bonding. They are also close in energy to the 6d and 7s orbitals which leads to unusual electron configurations. The nature of the 5f orbitals changes greatly across the actinide series

unlike the 4f orbitals of the rare earths. In the early actinide series (Ac → U) the 5f orbitals exhibit more transition metal-like behavior compared to the rare earth 4f orbitals. Upon progression across the 5f series to Pu, Am, and Cm the 5f orbitals contract and become more rare earth like. Therefore, significant differences in electronic properties may be found when replacing a rare earth element with an actinide in a known superconducting structure type. Because of the differences in orbital properties, it is difficult to know in advance whether or not isostructural rare earth/actinide phases will be formed. Systems where isostructural rare earth/actinide compounds have been synthesized are known. The uranium and lanthanum compounds, URu_2Si_2 and $LaIr_2Si_2$, are one example.[21] Another example is the yttrium and thorium compounds, YNi_2B_2C and $ThNi_2B_2C$.[21] The ionic radii of all four rare earth/actinide metals are similar with the largest being La^{3+} (1.16 Å) and the smallest U^{6+} (0.81 Å). Other systems have not lent themselves to the formation of isostructural rare earth/actinide compounds. For example, in the series of electron precise, alkali metal rare earth/actinide chalcophosphate compounds, no isostructural compounds have been characterized when the actinide metal is thorium or uranium. Isostructural rare earth/plutonium thiophosphate compounds have been characterized though.[22-25]

This research will be divided into two phases. Phase I will deal with the synthesis of new AnB_2 compounds and electronic property measurements of the known AnB_2 compounds, UB_2, NpB_2, and PuB_2. These binary borides have the simplest structure of the three classes of boride compounds to be investigated in this proposal and should be straightforward to synthesize. The goal of Phase II is the formation of actinide containing rhodium boride and borocarbide materials. Target compounds will have formulas such as $NpRh_4B_4$ and $PuNi_2B_2C$. It is expected that these materials will exhibit both superconductivity and magnetism as is seen in their rare earth analogs.

Materials preparation

Historically, all the materials discussed above have been prepared by arc melting. This technique involves melting the elements together in an arc under an inert atmosphere. Because this method reaches temperatures of 2000 °C to 3000 °C it is common in the preparation of refractory materials such as borides. While this technique is relatively simple to carry out, it has a significant draw back. Due to the high temperatures involved, the most thermodynamically stable phase usually forms. When looking for new materials this can be somewhat limiting. The initial experiments in each phase of this research will focus on the preparation of actinide materials that have the same stoichiometry and are isostructural with known boride phases. Examples of these compounds are NpB_2, URh_4B_4, and $PuNi_2B_2C$. Arc-melting is the most logical method of synthesis. While in an ideal system a starting ratio of elements identical to the target stoichiometry could be used, in many cases one of the elements will have a vastly different vapor pressure than the others. In this scenario, some of the element with a high vapor pressure will be lost and the final compound will be deficient in that element. As a result, many starting ratios will need to be examined before a single phase with the desired stoichiometry is found.

The formation of ternary and quaternary borides will also be carried out using metathesis reactions. These reactions can be carried out at much lower temperatures (650 °C to 850 °C) than is necessary when using elemental starting materials. One advantage

of a lower reaction temperature is that it is possible to synthesize materials that are not the most thermodynamically favored. When chemistry is only carried out at high temperatures interesting phases may often be overlooked.

Radiation Protection

It is important to note that all of the target compounds in this proposal are radioactive and as such certain precautions need to be taken. The actinide elements used in this research will be ^{232}Th, ^{238}U, ^{237}Np, ^{239}Pu, and ^{241}Am. All of these elements decay through alpha particle emission. The main hazard of working with alpha emitters is the potential for their inhalation or ingestion. It is important to note that some the daughter products of these isotopes may decay through other mechanisms such as beta particle , neutron, and gamma ray emission. The ^{232}Th and ^{238}U chemistry can be carried out in a standard, positive pressure, inert atmosphere glovebox due to the isotopes relatively low activity. The ^{237}Np, ^{239}Pu, and ^{241}Am chemistry, however, must be carried out in negative pressure inert atmosphere gloveboxes. These three isotopes have a much higher activity (i.e. shorter half-lives) than ^{232}Th and ^{238}U. The slightly negative pressure in transuranic gloveboxes helps reduce possible contamination when the atmosphere is compromised, such as in the event of a punctured glove. In addition to alpha decay, ^{241}Am also emits a high-energy gamma ray. For this reason, large quantities of ^{241}Am will be stored behind lead shielding.

Materials Characterization

Structure

The primary method of structural characterization will be through powder X-ray diffraction (pXRD). By comparing sample X-ray diffraction patterns to the patterns of known compounds it will be possible to determine what phases are present in each sample. In the cases where new structure types are formed Rietveld refinement will be used to elucidate the structure of the new compounds. It is important to note that for Rietveld refinement to be successful one must be able to identify which peaks in the powder pattern are due to the target compound. This is difficult when multiple phases are present in a single sample. Though the formation of X-ray quality single crystals is unlikely for such refractory materials, if any are present, single crystal X-ray diffraction will certainly be utilized.

Another method of structural characterization is X-ray absorption spectroscopy (XAS). Extended X-ray Absorption Fine Structure (EXAFS) will be used to aid in the elucidation of new structure types and in the examination of local structure in known phases. X-ray Absorption Spectroscopy is a valuable tool because it is able to probe the environment around a specific absorbing atom instead of looking at the entire extended structure as is the case in X-ray diffraction. The near-edge region of the XAS spectrum (XANES) will be examined in order to elucidate information on the electronic environment around a given atom. From this information it is possible to learn about the electronic structures of new compounds.

To further examine the electronic structure of the compounds in this proposal Ultraviolet Photoelectron Spectroscopy (UPS) will be utilized. This technique has proven to be useful in the experimental determination of the density of states at the fermi

level, $N(E_f)$. It has been found that a high $N(E_f)$ correlates with higher T_c values in superconducting system.

Physical Properties

The materials synthesized in this proposal will be examined in order to determine if they exhibit superconductivity. There are three properties of a material that can be used to find superconducting transitions: electrical resistivity (ρ), magnetic susceptibility (χ), and heat capacity (C). There are two vital characteristics of superconducting compounds. First is that at some temperature, T_c, the compound will undergo a transition to a state of zero resistance. This can be easily seen in a plot of ρ vs T. Electrical resistivity can be measured on pressed pellets using a Hall effect instrument. Second is that superconductors are also perfect diamagnets, which means they completely repel a magnetic field. This is known as the Meissner effect. A plot of AC magnetic susceptibility (χ_{ac}) versus temperature will show a drop in susceptibility to -1 at the superconducting transition. AC susceptibility can be measured on small powder samples using a Superconducting Quantum Interference Device (SQUID) magnetometer. Finally, the change in heat capacity (ΔC) of a material as a function of temperature is a good indicator of transitions. A plot of ΔC vs T will typically show a visible cusp at T_c. Heat capacity versus temperature can also be measured using the Physical Property Measurement System from Quantum Design.

Phase I Experiments

Initial experiments will focus on the synthesis and characterization of actinide solids based on the MgB_2 structure. Magnesium diboride is remarkable in that it has a relatively high T_c of 39K and even samples purchased in bulk will superconduct. An interesting set of compounds to explore would be $(An_xMg_{1-x})B_2$. By starting with small values of x one can learn something of the superconducting nature of MgB_2 and what effect actinide elements have on superconductivity. One important characteristic of superconductors is that they usually have a high density of states at the fermi level, $N(E_f)$. While studies have shown that the conduction band is of primarily boron character, the addition of f-orbital states should have a significant impact on the conduction properties.[26] For example, the substitution of Mg by Al causes a decrease in superconductivity,[26] whereas, the addition of f-electrons may not. Early reactions will be carried out via arc-melting the starting elements together. The known diboride phases UB_2, NpB_2, and PuB_2 will be synthesized as well and their conductivity and magnetism measured. It is hoped that arc-melting will yield single phases of the target materials. If arc-melting does not yield the desired compounds then synthesis using metathesis reactions will be investigated. For example, the reaction of $AnCl_4$ with excess $MgCl_2$ should yield an $An_xMg_yB_2$ phase and $MgCl_2$. It is the formation of the alkaline earth halide that is the driving force for the metathesis reaction. Other possible products include higher actinide borides that do not contain Mg such as AnB_4, AnB_6, and AnB_{12}. LuB_{12} is a superconductor with a very low transition temperature of 0.44 K.[7] Studies on other rare earth borides have shown that they too exhibit interesting physical properties such as valence fluctuation and magnetism.[7]

Phase II Experiments

The goal of this study is the synthesis and characterization of actinide rhodium borides ($AnRh_4B_4$) and actinide nickel borocarbides ($AnNi_2B_2C$). These materials are interesting in that they exhibit both superconductivity and long-range magnetic order. All of the materials in this proposal are best described as intermetallic compounds. Because these materials have metallic character, assigning oxidation states becomes somewhat irrelevant. What is more important to consider is the nature of the f-orbitals. Because conductivity, magnetism, and heat capacity are related to the electronic structure of a solid, the synthesis of $AnRh_4B_4$ and $AnNi_2B_2C$ analogues can yield information concerning the nature of the f-electrons in intermetallic compounds. A matter of interest to many actinide scientists is whether or not the 5f-electrons exhibit localized, rare earth like behavior, or delocalized, more transition metal like behavior.[27-31]

Early experiments will focus on using arc-melting to synthesize early actinide rhodium borides such as $ThRh_4B_4$ and URh_4B_4. The samples will first be characterized by powder X-ray diffraction to determine if they are isostructural to the known rare earth compounds and to be sure that they are single phase. In the case of multiple phase samples, Electron Microprobe Analysis (EMPA) will be used to reveal the number of phases and electron diffraction. High Resolution Electron Microscopy (HREM) will also be used to determine the structures of the new phases. These techniques were used with success in Zandbergen and co-workers studies on the Th-Pd-B-C system.[16] After structural characterization is complete, the samples' resistivity and magnetic susceptibility will be examined. Studies on the rare earth compounds indicate that while the formation of superconductivity lies in the Rh_4B_4 layers, any magnetic coupling between rare earth ions is significant.[8] The magnetic properties of actinide elements are complex and in many cases are vastly different than rare earth elements. Not only will these new compounds provide insight into synthetic actinide chemistry and superconductivity, they will also shed light on how and under what circumstances actinide compounds order magnetically. It is difficult to predict which actinide compounds will be magnetic. One general idea is that as the 5f band of an actinide element narrows there is a tendency towards establishing magnetic order. This band narrowing occurs with the sequential addition of 5f electrons. Unfortunately this idea is not universal, especially in the case of Pu compounds. For example, UIr_2, $NpIr_2$, and $PuIr_2$ form an isostructural series of compounds in which each member exhibits different magnetic properties. As expected UIr_2 is paramagnetic and $NpIr_2$ is antiferromagnetic but, $PuIr_2$ does not exhibit any magnetic order. Instead, it is a temperature independent paramagnet.[32] It is for this reason that the chemistry of transuranic elements must also be investigated. Even if future results indicate that $ThRh_4B_4$ and URh_4B_4 do not superconduct, there is a high probability that the corresponding Np, Pu, and Am compounds will exhibit entirely different behavior.

The last family of compounds that will be investigated are the borocarbides. Target compounds will be based on the known rare earth nickel borocarbides and will have formulas such as $AnNi_2B_2C$. Initial experiments will be conducted using arc-melting. Hopefully, these materials will exhibit the co-existence of superconductivity and magnetic order like their rare earth analogues. These early studies will focus briefly on Th and U but will quickly move on to the transuranic elements. It will be particularly

interesting to observe how the Np, Pu, and Am compounds differ from the Th and U phases already characterized.[13,14,16] Because several known Th and U borocarbides already exist, the synthesis of new borocarbides containing these elements will be carried out primarily using metathesis based reactions such as the one listed below:

$$NpCl_4 + CaNi_2B_2C \rightarrow NpNi_2B_2C + CaCl_2 + Cl_2(g)$$

These reactions will initially be run at intermediate temperatures ranging from 650 °C to 850 °C. Because of the relatively low temperatures used in these syntheses it is entirely possible that phases with new stoichiometries will be formed. The major by-product of this reaction will be $CaCl_2$ which can be easily separated from the target compound. As is the case in the rhodium boride system, it appears that the transition metal-boride layers are the source of the superconductivity in these compounds. Band structure calculations have shown that the density of states (DOS) at the fermi level is primarily made up of Ni 3d states.[12] Of particular interest is how the nickel:boride ratio and the presence of 5f states effects superconductivity and magnetic order. The target compounds will be characterized in the same manner as the AnB_2 and $AnRh_4B_4$ phases.

Significance of Proposed Research

The formation of new actinide borides will provide valuable insights into two areas of science. First, one can learn something about the effect of the 5f orbitals and the accessibility of multiple oxidation states of the actinides on phase formation. For rare earth elements, it is thought that the 4f orbitals play very little role in bonding, as they are highly core-like in nature. This is not true for the 5f orbitals of the early actinides, which are capable of covalent bonding in some cases. Second, the formation of any new superconducting phases is important to gather knowledge to help predict why one material superconducts while another does not. The materials proposed in this research will lead to a better understanding of both fundamental actinide chemistry and superconductivity.

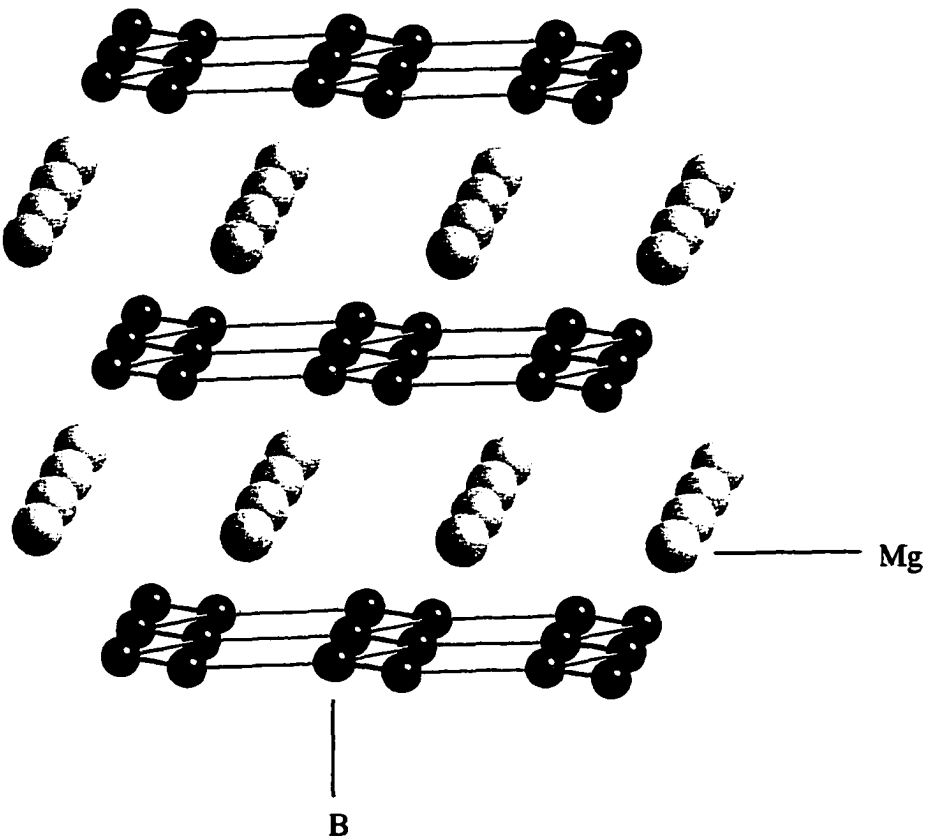

Figure 1. View of MgB_2 down the [100] crystallographic direction.

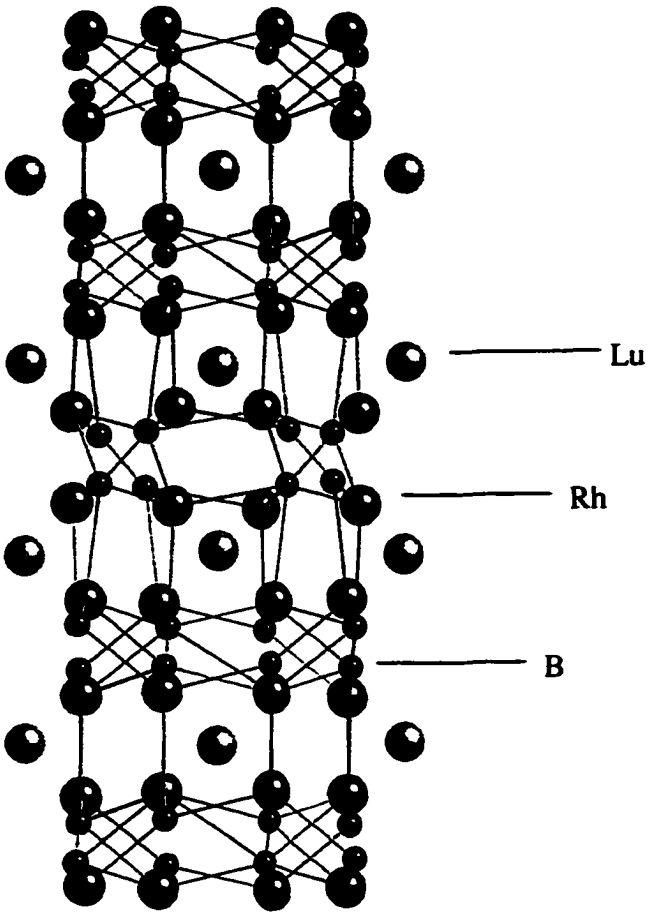

Figure 2. $LuRh_4B_4$ viewed down the [100] crystallographic direction.

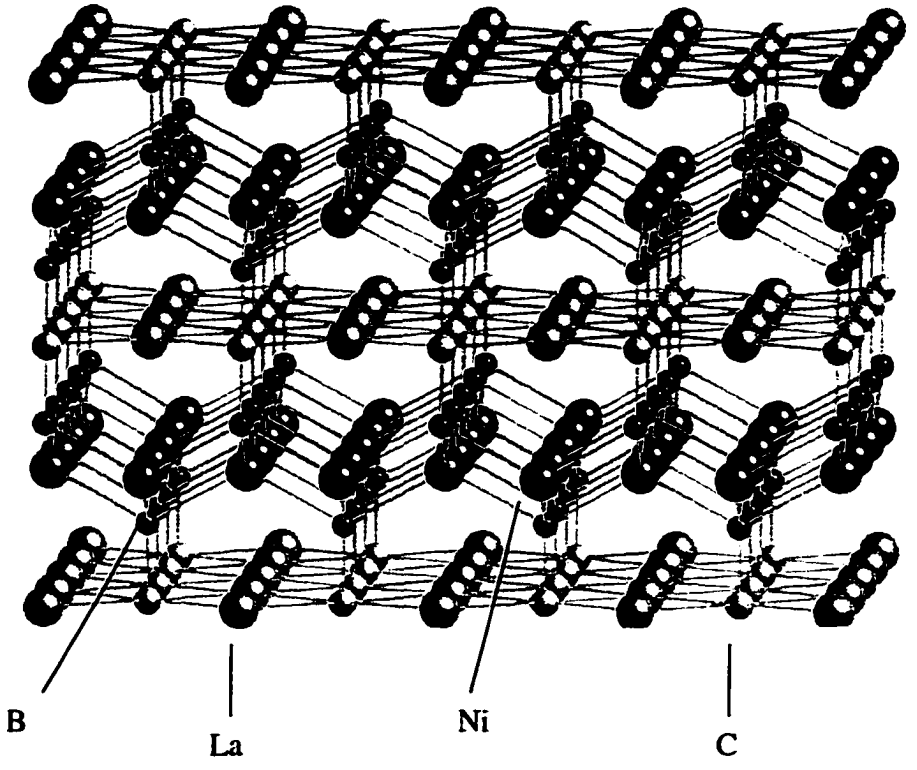

Figure 3. $LaNi_2B_2C$ viewed down the [100] crystallographic direction. From this view LaC and Ni_2B_2 layers are clearly visible. The carbon atoms are responsible for the interlayer connectivity.

References

(1) West, A. R. *Basic Solid State Chemistry*; second ed.; Wiley: Chichester, 1999.

(2) Eck, J; *Type II Superconductores* http://www.superconductors.org/Type2.htm.

(3) Kleiman, R. N.; Bishop, D. J.; Ott, H. R.; Fisk, Z.; Smith, J. L. *Physical Review Letters* **1990**, *64*, 1975-1978.

(4) Nagamatsu, J.; Nakagawa, N.; Muranaka, T.; Zenitani, Y.; Akimitsu, J. *Nature* **2001**, *410*, 63-64.

(5) Budko, S. L.; Lapertot, G.; Petrovic, C.; Cunningham, C. E.; Anderson, N.; Canfield, P. C. *Physical Review Letters* **2001**, *86*, 1877-1880.

(6) Matthias, B. T.; Geballe, T. H.; Andres, K.; Corenzwit, E.; Hull, G.; Maita, J. P. *Science* **1968**, *159*, 530.

(7) Batko, I.; Katkova, M.; Flachbart, K.; Filippov, V. B.; Paderno, Y. B.; Shicevalova, N. Y.; Wagner, T. *Journal of Alloys and Compounds* **1995**, *217*, L1-L3.

(8) Maple, M. B. In *Ternary Superconductors*; Shenoy, Dunlap, Fradin, Eds.; Elsevier North Holland Inc.: New York, 1981, pp 131-139.

(9) Felner, I.; Schmitt, D.; Barbara, B.; Godart, C.; Alleno, E. *Journal of Solid State Chemistry* **1997**, *133*, 5-10.

(10) Felser, C. *Journal of Solid State Chemistry* **2001**, *160*, 93-99.

(11) Goncalves, A.; Pereira, L.; Kuznietz, M.; Almeida, M.; Silva, A. S.; Godinho, M. *Physica B* **2000**, *281,282*, 1007-1009.

(12) Gupta, L. C. *Journal of Alloys and Compounds* **1997**, *262-263*, 22-27.

(13) Hossain, Z.; Gupta, L. C.; Nagarajan, R.; Raj, P.; Dhar, S. K.; Godart, C.; Suryanarayana, P.; Bagchi, S. N.; Date, V. G.; Purushotham, D. S. C.; Vijayaraghavan, R. *Europhysics Letters* **1994**, *28*, 55-59.

(14) Lai, C. C.; Lin, M. S.; You, Y. B.; Ku, H. C. *Physical Review B* **1995**, *51*, 420-423.

(15) Lynn, J. W. *Journal of Alloys and Compounds* **1997**, *250*, 552-558.

(16) Zandbergen, H. W.; Gortenmulder, T. J.; Sarrac, J. L.; Harrison, J. C.; de Andrade, M. C.; Hermann, J.; Han, S. H.; Fisk, Z.; Maple, M. B.; Cava, R. J. *Physica C* **1994**, *232*, 328-336.

(17) Ye, J.; Shishido, T.; Matsumoto, T.; Fukuda, T. *Journal of Alloys and Compounds* **1998**, *275-277*, 76-80.

(18) Matthias, B. T.; Corenzwit, E.; Vandenberg, J. M.; Barz, H. *Proc. Natl. Acad. Sci.* **1977**, 1334.

(19) Hamaker, H. C.; Woolf, L. D.; MacKay, H. B.; Fisk, Z.; Maple, M. B. *Solid State Commun.* **1979**, *31*, 139-144.

(20) Hamaker, H. C.; Woolf, L. D.; MacKay, H. B.; Fisk, Z.; Maple, M. B. *Solid State Commun.* **1979**, *32*, 289-294.

(21) King, R. B. *J. Solid State Chem.* **1997**, *131*, 394-398.

(22) Evenson, C. R.; Dorhout, P. K. *Inorg. Chem.* **2001**, *40*, 2875-2883.

(23) Evenson, C. R.; Dorhout, P. K. *Inorg. Chem.* **2001**, *40*, 2884-2891.

(24) Hess, R. F.; Abney, K. D.; Burris, J. L.; Hochheimer, H. D.; Dorhout, P. K. *Inorg. Chem.* **2000**, *40*, 2851-2859.

(25) Hess, R. F.; Abney, K. D.; Dorhout, P. K. *J. Am. Chem. Soc.* **2001**, in press.

(26) Slusky, J. S.; Rogado, N.; Regan, K. A.; Hayward, M. A.; Khalifah, P.; He, T.; Inumaru, K.; Loureiro, S. M.; Haas, M. K.; Zandbergen, H. W.; Cava, R. J. *Nature* **2001**, *410*, 343-345.

(27) Boring, A. M.; Smith, J. L. *Los Alamos Science* **2000**, 90-127.

(28) Johansson, B. *Physical Review B* **1975**, *11*, 2740.

(29) Johansson, B. *J. Phys. Chem. Solids* **1978**, *39*, 467.

(30) Johansson, B.; Eriksson, O. *Journal of less common metals* **1987**, *133*, 25-29.

(31) Rado, G. T.; Suhl, H. *Magnetism*; Academic Press: New York, 1966; Vol. IV.

(32) Eriksson, O.; Brooks, M. S. S.; Johansson, B.; Albers, R. C.; Boring, A. M. "Magnetism and Bonding in Actinide and Rare Earth Systems," Los Alamos National Laboratory, 1990.

Appendix C

List of Experiments

Plutonium Thiophosphate Reactions in
Potassium Sulfide/Phosphorus Fluxes

Reaction Number	Flux Composition K/Pu/P/S	Temperature/Time	Crystalline Products
RFH-II-135	8/2/6/27	500 °C / 200h	
RFH-II-137	3/1/2/15	500 °C / 200h	$K_3Pu(PS_4)_2$
RFH-II-185	3/1/2/8	500 °C / 200h	
RFH-II-189	3/1/6/15	500 °C / 200h	$KPuP_2S_7$ $K_3Pu(PS_4)_2$
RFH-II-233	3/1/4/15	500 °C / 200h	
RFH-II-237	3/1/6/20	500 °C / 200h	
RFH-II-279	2/1/6/15	500 °C / 200h	
RFH-II-283	6/1/6/15	500 °C / 200h	
RFH-II-307	3/2/1.5/15	500 °C / 200h	$K_3Pu(PS_4)_2$
RFH-II-355	2/1/7/11	500 °C / 200h	
RFH-II-359	4/1/4/8	500 °C / 200h	
RFH-II-363	2/1/2/11	500 °C / 200h	

Plutonium Thiophosphate Reactions in
Rubidium Sulfide/Phosphorus Fluxes

Reaction Number	Flux Composition Rb/Pu/P/S	Temperature/Time	Crystalline Products
RFH-II-139	3/1/2/15	500 °C / 200h	
RFH-II-193	8/2/6/27	500 °C / 200h	
RFH-II-197	8/2/3/27	500 °C / 200h	
RFH-II-225	3/1/6/15	500 °C / 200h	$Rb_2Pu(P_2S_6)_{1/2}(PS_4)$
RFH-II-287	2/1/6/15	500 °C / 200h	
RFH-II-291	3/1/4/15	500 °C / 200h	$RbPuP_2S_7$

Plutonium Thiophosphate Reactions in
Cesium Sulfide/Phosphorus Fluxes

Reaction Number	Flux Composition Cs/Pu/P/S	Temperature/Time	Crystalline Products
RFH-II-217	3/1/2/15	500 °C / 200h	
RFH-II-221	3/1/6/15	500 °C / 200h	
RFH-II-229	3/1/4/15	500 °C / 200h	$CsPuP_2S_7$
RFH-II-295	2/1/6/15	500 °C / 200h	$CsPuP_2S_7$
RFH-II-299	6/1/6/15	500 °C / 200h	
RFH-II-303	3/2/4/15	500 °C / 200h	

Plutonium Gallium Sulfide Reactions in
Alkali Metal Chalcogenide Fluxes

Reaction Number	Flux Composition A/Pu/Ga/S	Temperature/Time	Crystalline Products
RFH-II-365	3/1/4/15 A=K	500 °C / 200h	
RFH-II-367	3/1/4/15 A=Cs	500 °C / 200h	
RFH-II-369	3/1/1.5/12 A=Cs	500 °C / 200h	
RFH-II-371	3/1/2/15 A=K	500 °C / 200h	

Ternary Plutonium Selenide Reactions in
Alkali Metal Selenide Fluxes

Reaction Number	Flux Composition A/Pu/Se	Temperature/Time	Crystalline Products
RFH-II-025	6/1/12 A=K	500 °C / 200h	
RFH-II-027	8/1/18 A=K	500 °C / 200h	KPu_3Se_8
RFH-II-241	4/1/15 A=K	500 °C / 200h	
RFH-II-245	4/1/11 A=Cs	500 °C / 200h	
RFH-II-271	4/2/11 A=K	500 °C / 200h	
RFH-II-273	8/1/18 A=K	500 °C / 200h	KPu_3Se_8
RFH-II-275	8/1/18 A=K	500 °C / 200h	KPu_3Se_8
RFH-II-277	4/2/11 A=K	500 °C / 200h	
RFH-II-311	8/1/18 A=K	500 °C / 200h	KPu_3Se_8
RFH-II-317	8/1/18 A=K	500 °C / 200h	KPu_3Se_8
RFH-II-385	8/1/18 A=K	500 °C / 200h	KPu_3Se_8
RFH-II-387	8/1/18 A=K	500 °C / 200h	KPu_3Se_8

Ternary Plutonium Sulfide Reactions in
Alkali Metal Sulfide Fluxes

Reaction Number	Flux Composition A/Pu/Se	Temperature/Time	Crystalline Products
RFH-II-249	8/1/18	500 °C / 200h	
RFH-II-253	3/1/15	500 °C / 200h	

Binary Plutonium Chalcogenide Reactions

Reaction Number	Pu/Q Ratio	Temperature/Time	Products
RFH-II-313	1/2 Q=S	500 °C / 200h	PuS_2
RFH-II-315	2/3 Q=S	500 °C / 200h	Pu_2S_3
RFH-II-319	1/2 Q=Te	600 °C / 72h	$PuTe_2$
RFH-II-321	2/3 Q=Te	600 °C / 72h	Pu_2Te_3
RFH-II-323	2/3 Q=Se	500 °C / 200h	Pu_2Se_3

Uranium Thiophosphate Reactions in
Potassium Sulfide/Phosphorus Fluxes

Reaction Number	Flux Composition K/U/P/S	Temperature/Time	Crystalline Products
RFH-II-029	8/2/6/27	350 °C / 288h	
RFH-II-031	6/1/2/15	350 °C / 288h	
RFH-II-047	8/2/6/27	500 °C / 288h	
RFH-II-049	6/1/2/15	500 °C / 288h	
RFH-II-051	4/2/6/27	500 °C / 288h	
RFH-II-053	3/1/2/15	500 °C / 288h	$K_5U(PS_4)_3$
RFH-II-059	4/1/6/27	350 °C / 48h	
RFH-II-063	8/1/6/27	350 °C / 48h	
RFH-II-065	6/1/2/15	350 °C / 48h	
RFH-II-071	8/3/6/27	350 °C / 48h	
RFH-II-119	8/2/6/27	500 °C / 288h	
RFH-II-165	3/1/2/15	500 °C / 288h	$K_5U(PS_4)_3$
RFH-II-173	3/1/2/15	500 °C / 288h	$K_5U(PS_4)_3$
RFH-II-201	3/1/6/15	500 °C / 240h	
RFH-II-203	8/2/5/27	500 °C / 240h	
RFH-II-205	8/2/6/27	500 °C / 240h	
RFH-II-213	3/1/4/15	500 °C / 240h	

Uranium Thiophosphate Reactions in
Rubidium Sulfide/Phosphorous Fluxes

Reaction Number	Flux Composition Rb/U/P/S	Temperature/Time	Crystalline Products
RFH-II-033	8/2/6/27	350 °C / 288h	
RFH-II-035	6/1/2/15	350 °C / 288h	
RFH-II-067	8/2/6/27	350 °C / 48h	
RFH-II-069	6/1/2/15	350 °C / 48h	
RFH-II-073	8/3/6/27	350 °C / 48h	
RFH-II-123	3/1/2/15	750 °C / 100h	
RFH-II-125	3/1/4/15	750 °C / 100h	
RFH-II-127	2/1/2/15	750 °C / 100h	

Uranium Thiophosphate Reactions in
Cesium Sulfide/Phosphorous Fluxes

Reaction Number	Flux Composition Cs/U/P/S	Temperature/Time	Crystalline Products
RFH-II-105	3/1/2/15	350 °C / 288h	
RFH-II-121	8/2/6/27	500 °C / 288h	
RFH-II-129	3/1/2/15	750 °C / 100h	
RFH-II-131	3/1/4/15	750 °C / 100h	$Cs_8U_5(P_3S_{10})_2(PS_4)_6$
RFH-II-133	2/1/2/15	750 °C / 100h	
RFH-II-177	5/1/4/15	500 °C / 240h	
RFH-II-181	3/1/4/15	500 °C / 240h	$Cs_8U_5(P_3S_{10})_2(PS_4)_6$

Thorium Thiophosphate Reactions in
Potassium Sulfide/Phosphorous Fluxes

Reaction Number	Flux Composition K/Th/P/S	Temperature/Time	Crystalline Products
RFH-II-041	8/2/6/27	500 °C / 288h	$K_{10}Th_3(P_2S_7)_4(PS_4)_2$
RFH-II-055	4/1/6/27	500 °C / 288h	
RFH-II-057	6/1/6/27	500 °C / 288h	
RFH-II-075	8/2/6/27	500 °C / 288h	$K_{10}Th_3(P_2S_7)_4(PS_4)_2$
RFH-II-077	8/2/6/27	500 °C / 288h	$K_{10}Th_3(P_2S_7)_4(PS_4)_2$
RFH-II-079	8/2/6/27	500 °C / 288h	$K_{10}Th_3(P_2S_7)_4(PS_4)_2$
RFH-II-081	8/2/6/27	500 °C / 288h	$K_{10}Th_3(P_2S_7)_4(PS_4)_2$
RFH-II-083	6/1/2/15	500 °C / 288h	
RFH-II-085	6/2/2/15	500 °C / 288h	
RFH-II-089	8/2/2/27	500 °C / 288h	
RFH-II-091	8/2/3/27	500 °C / 288h	
RFH-II-093	8/2/8/27	500 °C / 288h	
RFH-II-095	8/2/5/27	500 °C / 288h	$K_5Th(PS_4)_3$
RFH-II-097	4/2/6/27	500 °C / 288h	
RFH-II-099	6/2/6/27	500 °C / 288h	
RFH-II-101	12/2/6/27	500 °C / 288h	
RFH-II-113	8/1/6/27	500 °C / 288h	
RFH-II-115	8/3/6/27	500 °C / 288h	
RFH-II-117	8/4/6/27	500 °C / 288h	
RFH-II-161	8/2/6/27	500 °C / 288h	$K_{10}Th_3(P_2S_7)_4(PS_4)_2$
RFH-II-207	3/1/2/15	500 °C / 288h	
RFH-II-209	3/16/15	500 °C / 288h	P_4S_9

Thorium Thiophosphate Reactions in
Rubidium Sulfide/Phosphorous Fluxes

Reaction Number	Flux Composition Rb/Th/P/S	Temperature/Time	Crystalline Products
RFH-II-043	6/1/2/15	500 °C / 288h	
RFH-II-045	8/2/6/27	500 °C / 288h	
RFH-II-087	6/2/2/15	500 °C / 288h	
RFH-II-147	8/2/6/27	500 °C / 288h	
RFH-II-151	8/2/6/27	500 °C / 288h	$Rb_5Th(PS_4)_3$
RFH-II-211	3/1/2/15	500 °C / 240h	

Thorium Thiophosphate Reactions in
Cesium Sulfide/Phosphorous Fluxes

Reaction Number	Flux Composition Cs/Th/P/S	Temperature/Time	Crystalline Products
RFH-II-103	8/2/6/27	500 °C / 288h	$Cs_5Th(PS_4)_3$
RFH-II-107	3/1/2/5	500 °C / 288h	
RFH-II-109	4/1/6/17	500 °C / 288h	$Cs_4Th_2(P_2S_6)_3$
RFH-II-153	8/2/6/27	500 °C / 288h	
RFH-II-157	8/2/6/27	500 °C / 288h	
RFH-II-215	8/2/5/27	500 °C / 240h	
RFH-II-383	4/1/6/19	500 °C / 200h	$Cs_4Th_2(P_2S_6)_3$

Ternary Uranium Chalcogenide Reactions in
Alkali Metal Chalcogenide Fluxes

Reaction Number	Flux Composition A/U/Q	Temperature/Time	Crystalline Products
RFH-II-009	1/1/3 A=K Q=Te	1190 °C / 48h	
RFH-II-011	1/1/3 A=Rb Q=Se	1190 °C / 48h	
RFH-II-023	8/1/18 A=K Q=Se	500 °C / 240h	
RFH-II-037	6/1/18 A=K Q=Se	350 °C / 288h	
RFH-II-039	8/1/18 A=K Q=Se	350 °C / 288h	
RFH-II-257	8/1/18 A=K Q=Se	500 °C / 200h	
RFH-II-261	4/1/11 A=K Q=Se	500 °C / 200h	
RFH-II-265	8/1/18 A=K Q=S	500 °C / 200h	
RFH-II-269	4/1/11 A=K Q=S	500 °C / 200h	
RFH-II-375	8/1/18 A=K Q=Se	500 °C / 200h	

Appendix D

Supplementary Information for Chapter 3

Table 1. Crystal data and structure refinement for $Cs_8U_5(P_3S_{10})_2(PS_4)_6$.

Identification code	$Cs_8U_5(P_3S_{10})_2(PS_4)_6$	
Empirical formula	$Cs_8U_5(P_3S_{10})_2(PS_4)_6$	
Formula weight	4035.71	
Temperature	163(2) K	
Wavelength	0.71073 Å	
Crystal system	Monoclinic	
Space group	P21/c	
Unit cell dimensions	a = 33.28970(10) Å	α= 90°.
	b = 14.92950(10) Å	β= 115.4780(10)°.
	c = 17.3528(2) Å	γ = 90°.
Volume	7785.60(11) $Å^3$	
Z	4	
Density (calculated)	3.443 Mg/m^3	
Absorption coefficient	15.499 mm^{-1}	
F(000)	7136	
Crystal size	0.28 x 0.12 x 0.08 mm^3	
Theta range for data collection	1.36 to 28.30°.	
Index ranges	-44<=h<=43, -19<=k<=19, -9<=l<=23	
Reflections collected	19869	
Independent reflections	9153 [R(int) = 0.0969]	
Absorption correction	SADABS	
Max. and min. transmission	0.942284 and 0.590480	
Refinement method	Full-matrix least-squares on F^2	
Data / restraints / parameters	9153 / 0 / 313	
Goodness-of-fit on F^2	0.970	
Final R indices [I>2sigma(I)]	R1 = 0.0590, wR2 = 0.0862	
R indices (all data)	R1 = 0.1342, wR2 = 0.1156	
Extinction coefficient	0.000020(4)	
Largest diff. peak and hole	2.728 and -1.960 $e.Å^{-3}$	

Table 2. Atomic coordinates (x 10^4) and equivalent isotropic displacement parameters ($Å^2$x 10^3) for $Cs_8U_5(P_3S_{10})_2(PS_4)_6$. U(eq) is defined as one third of the trace of the orthogonalized U^{ij} tensor.

	x	y	z	U(eq)
U(1)	0	4182(1)	2500	12(1)
U(2)	647(1)	1648(1)	3709(1)	11(1)
U(3)	-1585(1)	-2452(1)	1448(1)	12(1)
S(1)	777(1)	3107(3)	2744(2)	13(1)
S(2)	390(1)	5424(3)	1869(2)	18(1)
S(3)	723(1)	4886(3)	3891(2)	18(1)
S(4)	160(1)	3111(3)	4026(2)	13(1)
S(5)	944(1)	1103(3)	5404(2)	15(1)
S(6)	297(1)	1229(3)	1854(2)	15(1)
S(7)	1269(1)	2925(3)	4795(2)	16(1)
S(8)	1391(1)	840(3)	3756(2)	16(1)
S(9)	478(1)	-183(3)	3597(3)	16(1)
S(10)	-1291(1)	-2912(3)	3261(2)	15(1)
S(11)	-2425(1)	-3245(3)	1034(3)	18(1)
S(12)	-743(1)	-2966(3)	1668(3)	17(1)
S(13)	-1468(2)	-1206(3)	353(2)	19(1)
S(14)	-1058(1)	-1015(3)	2429(2)	13(1)
S(15)	-1786(1)	-3390(3)	-164(2)	19(1)
S(16)	-2159(1)	-1179(3)	1580(3)	17(1)
S(17)	-1475(1)	-4350(3)	1762(3)	17(1)
S(18)	800(1)	-2491(3)	5887(2)	18(1)
S(19)	2002(1)	-1562(3)	1281(3)	16(1)
S(20)	2719(2)	1201(3)	3225(3)	22(1)
S(21)	2050(1)	2909(3)	2059(2)	16(1)
S(22)	2901(2)	-2449(3)	1152(3)	23(1)
P(1)	1097(1)	-399(3)	3649(3)	12(1)
P(2)	-840(1)	-4267(3)	1907(2)	14(1)
P(3)	459(1)	2487(3)	1568(2)	12(1)
P(4)	2494(1)	2396(3)	3284(3)	17(1)
P(5)	1369(1)	2172(3)	5834(2)	12(1)

P(6)	-2330(1)	-2944(3)	-1169(2)	13(1)
Cs(1)	-126(1)	-2209(1)	3882(1)	23(1)
Cs(2)	1574(1)	680(1)	1819(1)	23(1)
Cs(3)	3743(1)	193(1)	-1162(1)	26(1)
Cs(4)	2574(1)	-446(1)	54(1)	25(1)

Table 3. Bond lengths [Å] and angles [°] for $Cs_8U_5(P_3S_{10})_2(PS_4)_6$.

S(1)-P(3)	2.069(5)	S(10)-Cs(1)	3.702(4)
S(1)-U(2)	2.891(4)	S(11)-P(6)#8	2.010(6)
S(1)-U(1)	2.915(4)	S(11)-U(3)	2.829(4)
S(2)-P(2)#1	2.058(6)	S(11)-Cs(4)#9	3.698(4)
S(2)-U(1)	2.747(4)	S(12)-P(2)	2.041(6)
S(2)-Cs(3)#2	3.705(5)	S(12)-U(3)	2.772(4)
S(2)-Cs(1)#1	3.737(4)	S(12)-Cs(1)#4	3.596(4)
S(3)-P(2)#1	2.033(6)	S(12)-Cs(1)	3.669(4)
S(3)-U(1)	2.780(4)	S(13)-P(1)#4	2.032(6)
S(3)-Cs(3)#3	3.586(4)	S(13)-U(3)	2.804(4)
S(4)-P(3)#4	2.084(6)	S(13)-Cs(2)#10	3.715(4)
S(4)-U(2)	2.910(4)	S(14)-P(1)#4	2.038(6)
S(4)-U(1)	2.939(4)	S(14)-U(3)	2.831(4)
S(4)-Cs(1)#5	3.918(4)	S(14)-Cs(1)	3.525(4)
S(5)-P(5)	2.048(6)	S(14)-Cs(2)#4	3.603(4)
S(5)-U(2)	2.792(4)	S(15)-P(6)	2.012(6)
S(5)-Cs(2)#6	3.617(4)	S(15)-U(3)	2.937(4)
S(5)-Cs(1)#5	3.818(4)	S(15)-Cs(3)#9	3.632(4)
S(6)-P(3)	2.073(6)	S(15)-Cs(4)#9	3.848(5)
S(6)-U(2)#4	2.928(4)	S(16)-P(6)#8	2.020(6)
S(6)-U(2)	2.980(4)	S(16)-U(3)	2.773(4)
S(7)-P(5)	2.026(6)	S(16)-Cs(4)#10	3.531(4)
S(7)-U(2)	2.849(4)	S(16)-Cs(2)#4	3.815(4)
S(7)-Cs(3)#3	4.143(4)	S(17)-P(2)	2.022(6)
S(8)-P(1)	2.063(6)	S(17)-U(3)	2.880(4)
S(8)-U(2)	2.725(4)	S(17)-Cs(3)#7	3.584(4)
S(8)-Cs(4)#6	3.646(4)	S(17)-Cs(4)#9	3.662(4)
S(8)-Cs(2)	3.672(4)	S(18)-P(3)#6	1.961(6)
S(9)-P(1)	2.048(6)	S(18)-Cs(1)	3.545(4)
S(9)-U(2)	2.781(4)	S(18)-Cs(2)#6	3.603(4)
S(9)-Cs(1)	3.782(4)	S(18)-Cs(3)#11	3.725(5)
S(10)-P(5)#5	2.026(6)	S(19)-P(5)#12	2.114(6)
S(10)-U(3)	2.946(4)	S(19)-P(4)#11	2.171(6)
S(10)-Cs(3)#7	3.538(4)	S(19)-Cs(4)	3.797(4)

S(19)-Cs(2)	3.905(4)	Cs(2)-S(14)#4	3.603(4)
S(20)-P(4)	1.954(6)	Cs(2)-S(5)#12	3.617(4)
S(20)-Cs(4)#6	3.592(5)	Cs(2)-S(13)#10	3.715(4)
S(20)-Cs(2)	3.617(4)	Cs(2)-S(16)#4	3.815(4)
S(20)-Cs(3)#6	3.738(5)	Cs(2)-Cs(4)#6	5.1611(14)
S(21)-P(6)#10	2.119(6)	Cs(2)-Cs(4)	5.661(2)
S(21)-P(4)	2.142(6)	Cs(3)-S(10)#15	3.538(4)
S(21)-Cs(2)	3.631(4)	Cs(3)-S(17)#15	3.584(4)
S(21)-Cs(3)#2	3.727(4)	Cs(3)-S(3)#11	3.586(4)
S(22)-P(4)#11	1.962(6)	Cs(3)-S(15)#16	3.632(4)
S(22)-Cs(4)	3.460(5)	Cs(3)-S(2)#2	3.705(5)
S(22)-Cs(4)#13	3.728(5)	Cs(3)-S(18)#3	3.725(5)
P(1)-S(13)#4	2.032(6)	Cs(3)-S(21)#2	3.727(4)
P(1)-S(14)#4	2.038(6)	Cs(3)-S(20)#12	3.738(5)
P(2)-S(3)#14	2.033(6)	Cs(3)-S(7)#11	4.143(4)
P(2)-S(2)#14	2.058(6)	Cs(3)-Cs(4)	5.252(2)
P(3)-S(18)#12	1.961(6)	Cs(4)-S(16)#10	3.531(4)
P(3)-S(4)#4	2.084(6)	Cs(4)-S(20)#12	3.592(5)
P(3)-Cs(1)#12	4.229(4)	Cs(4)-S(8)#12	3.646(4)
P(4)-S(22)#3	1.961(6)	Cs(4)-S(17)#16	3.662(4)
P(4)-S(19)#3	2.171(6)	Cs(4)-S(11)#16	3.699(4)
P(4)-Cs(2)	3.963(4)	Cs(4)-S(22)#13	3.728(5)
P(4)-Cs(4)#6	4.157(5)	Cs(4)-S(15)#16	3.848(5)
P(5)-S(10)#5	2.026(6)	Cs(4)-P(4)#12	4.157(5)
P(5)-S(19)#6	2.114(6)	Cs(4)-Cs(2)#12	5.1610(14)
P(6)-S(11)#8	2.010(6)	U(1)-S(2)#4	2.747(4)
P(6)-S(16)#8	2.020(6)	U(1)-S(3)#4	2.780(4)
P(6)-S(21)#10	2.119(6)	U(1)-S(1)#4	2.915(4)
Cs(1)-S(12)#4	3.596(4)	U(1)-S(4)#4	2.939(4)
Cs(1)-S(2)#14	3.737(4)	U(2)-S(6)#4	2.928(4)
Cs(1)-S(5)#5	3.818(4)	P(3)-S(1)-U(2)	95.3(2)
Cs(1)-S(4)#5	3.918(4)	P(3)-S(1)-U(1)	93.3(2)
Cs(1)-P(3)#6	4.229(4)	U(2)-S(1)-U(1)	98.89(12)
Cs(1)-U(3)	4.8901(12)	P(2)#1-S(2)-U(1)	89.9(2)
Cs(1)-Cs(1)#4	5.213(2)	P(2)#1-S(2)-Cs(3)#2	94.2(2)
Cs(2)-S(18)#12	3.603(4)	U(1)-S(2)-Cs(3)#2	122.23(14)

P(2)#1-S(2)-Cs(1)#1	96.0(2)	P(5)#5-S(10)-Cs(1)	95.0(2)
U(1)-S(2)-Cs(1)#1	134.18(15)	U(3)-S(10)-Cs(1)	94.02(11)
Cs(3)#2-S(2)-Cs(1)#1	102.64(10)	Cs(3)#7-S(10)-Cs(1)	106.73(11)
P(2)#1-S(3)-U(1)	89.5(2)	P(6)#8-S(11)-U(3)	90.4(2)
P(2)#1-S(3)-Cs(3)#3	121.3(2)	P(6)#8-S(11)-Cs(4)#9	156.7(2)
U(1)-S(3)-Cs(3)#3	146.8(2)	U(3)-S(11)-Cs(4)#9	107.12(12)
P(3)#4-S(4)-U(2)	94.8(2)	P(2)-S(12)-U(3)	93.0(2)
P(3)#4-S(4)-U(1)	92.3(2)	P(2)-S(12)-Cs(1)#4	124.7(2)
U(2)-S(4)-U(1)	97.91(12)	U(3)-S(12)-Cs(1)#4	139.34(15)
P(3)#4-S(4)-Cs(1)#5	83.6(2)	P(2)-S(12)-Cs(1)	98.4(2)
U(2)-S(4)-Cs(1)#5	99.09(11)	U(3)-S(12)-Cs(1)	97.84(12)
U(1)-S(4)-Cs(1)#5	162.79(14)	Cs(1)#4-S(12)-Cs(1)	91.71(10)
P(5)-S(5)-U(2)	91.9(2)	P(1)#4-S(13)-U(3)	91.5(2)
P(5)-S(5)-Cs(2)#6	102.6(2)	P(1)#4-S(13)-Cs(2)#10	119.8(2)
U(2)-S(5)-Cs(2)#6	140.28(15)	U(3)-S(13)-Cs(2)#10	147.92(14)
P(5)-S(5)-Cs(1)#5	91.2(2)	P(1)#4-S(14)-U(3)	90.6(2)
U(2)-S(5)-Cs(1)#5	103.71(12)	P(1)#4-S(14)-Cs(1)	125.0(2)
Cs(2)#6-S(5)-Cs(1)#5	112.59(10)	U(3)-S(14)-Cs(1)	100.02(12)
P(3)-S(6)-U(2)#4	94.5(2)	P(1)#4-S(14)-Cs(2)#4	99.4(2)
P(3)-S(6)-U(2)	92.7(2)	U(3)-S(14)-Cs(2)#4	118.75(13)
U(2)#4-S(6)-U(2)	100.38(12)	Cs(1)-S(14)-Cs(2)#4	120.41(11)
P(5)-S(7)-U(2)	90.7(2)	P(6)-S(15)-U(3)	114.8(2)
P(5)-S(7)-Cs(3)#3	89.0(2)	P(6)-S(15)-Cs(3)#9	102.7(2)
U(2)-S(7)-Cs(3)#3	137.92(14)	U(3)-S(15)-Cs(3)#9	140.67(14)
P(1)-S(8)-U(2)	90.3(2)	P(6)-S(15)-Cs(4)#9	91.1(2)
P(1)-S(8)-Cs(4)#6	104.8(2)	U(3)-S(15)-Cs(4)#9	101.24(12)
U(2)-S(8)-Cs(4)#6	144.70(14)	Cs(3)#9-S(15)-Cs(4)#9	89.14(10)
P(1)-S(8)-Cs(2)	96.8(2)	P(6)#8-S(16)-U(3)	91.8(2)
U(2)-S(8)-Cs(2)	120.53(13)	P(6)#8-S(16)-Cs(4)#10	100.5(2)
Cs(4)#6-S(8)-Cs(2)	89.69(10)	U(3)-S(16)-Cs(4)#10	116.72(13)
P(1)-S(9)-U(2)	89.0(2)	P(6)#8-S(16)-Cs(2)#4	144.8(2)
P(1)-S(9)-Cs(1)	116.7(2)	U(3)-S(16)-Cs(2)#4	113.90(13)
U(2)-S(9)-Cs(1)	151.64(15)	Cs(4)#10-S(16)-Cs(2)#4	89.18(10)
P(5)#5-S(10)-U(3)	127.4(2)	P(2)-S(17)-U(3)	90.3(2)
P(5)#5-S(10)-Cs(3)#7	107.7(2)	P(2)-S(17)-Cs(3)#7	98.5(2)
U(3)-S(10)-Cs(3)#7	118.83(13)	U(3)-S(17)-Cs(3)#7	119.32(13)

P(2)-S(17)-Cs(4)#9	128.5(2)	S(17)-P(2)-S(3)#14	111.9(3)
U(3)-S(17)-Cs(4)#9	106.92(12)	S(17)-P(2)-S(12)	106.4(3)
Cs(3)#7-S(17)-Cs(4)#9	112.80(11)	S(3)#14-P(2)-S(12)	111.1(3)
P(3)#6-S(18)-Cs(1)	96.1(2)	S(17)-P(2)-S(2)#14	111.9(3)
P(3)#6-S(18)-Cs(2)#6	102.4(2)	S(3)#14-P(2)-S(2)#14	107.2(3)
Cs(1)-S(18)-Cs(2)#6	120.26(13)	S(12)-P(2)-S(2)#14	108.3(2)
P(3)#6-S(18)-Cs(3)#11	103.7(2)	S(18)#12-P(3)-S(1)	114.2(3)
Cs(1)-S(18)-Cs(3)#11	111.75(11)	S(18)#12-P(3)-S(6)	115.1(3)
Cs(2)#6-S(18)-Cs(3)#11	117.75(11)	S(1)-P(3)-S(6)	104.2(2)
P(5)#12-S(19)-P(4)#11	108.6(2)	S(18)#12-P(3)-S(4)#4	114.0(2)
P(5)#12-S(19)-Cs(4)	130.1(2)	S(1)-P(3)-S(4)#4	105.4(2)
P(4)#11-S(19)-Cs(4)	90.6(2)	S(6)-P(3)-S(4)#4	102.7(2)
P(5)#12-S(19)-Cs(2)	92.8(2)	S(18)#12-P(3)-Cs(1)#12	56.45(15)
P(4)#11-S(19)-Cs(2)	146.9(2)	S(1)-P(3)-Cs(1)#12	158.2(2)
Cs(4)-S(19)-Cs(2)	94.60(10)	S(6)-P(3)-Cs(1)#12	97.5(2)
P(4)-S(20)-Cs(4)#6	92.3(2)	S(4)#4-P(3)-Cs(1)#12	67.04(15)
P(4)-S(20)-Cs(2)	85.1(2)	S(20)-P(4)-S(22)#3	119.2(3)
Cs(4)#6-S(20)-Cs(2)	91.44(11)	S(20)-P(4)-S(21)	113.0(3)
P(4)-S(20)-Cs(3)#6	144.8(2)	S(22)#3-P(4)-S(21)	97.4(2)
Cs(4)#6-S(20)-Cs(3)#6	91.52(10)	S(20)-P(4)-S(19)#3	114.6(3)
Cs(2)-S(20)-Cs(3)#6	129.77(13)	S(22)#3-P(4)-S(19)#3	109.0(3)
P(6)#10-S(21)-P(4)	113.5(2)	S(21)-P(4)-S(19)#3	100.9(2)
P(6)#10-S(21)-Cs(2)	104.2(2)	S(20)-P(4)-Cs(2)	65.4(2)
P(4)-S(21)-Cs(2)	82.4(2)	S(22)#3-P(4)-Cs(2)	84.1(2)
P(6)#10-S(21)-Cs(3)#2	97.5(2)	S(21)-P(4)-Cs(2)	65.2(2)
P(4)-S(21)-Cs(3)#2	138.5(2)	S(19)#3-P(4)-Cs(2)	162.6(2)
Cs(2)-S(21)-Cs(3)#2	116.99(11)	S(20)-P(4)-Cs(4)#6	59.7(2)
P(4)#11-S(22)-Cs(4)	104.9(2)	S(22)#3-P(4)-Cs(4)#6	63.7(2)
P(4)#11-S(22)-Cs(4)#13	88.2(2)	S(21)-P(4)-Cs(4)#6	141.3(2)
Cs(4)-S(22)-Cs(4)#13	117.54(12)	S(19)#3-P(4)-Cs(4)#6	116.8(2)
S(13)#4-P(1)-S(14)#4	106.9(2)	Cs(2)-P(4)-Cs(4)#6	78.89(9)
S(13)#4-P(1)-S(9)	111.2(3)	S(10)#5-P(5)-S(7)	111.1(3)
S(14)#4-P(1)-S(9)	111.4(2)	S(10)#5-P(5)-S(5)	114.1(3)
S(13)#4-P(1)-S(8)	111.4(2)	S(7)-P(5)-S(5)	106.6(2)
S(14)#4-P(1)-S(8)	109.1(3)	S(10)#5-P(5)-S(19)#6	112.9(2)
S(9)-P(1)-S(8)	106.9(2)	S(7)-P(5)-S(19)#6	108.8(3)

S(5)-P(5)-S(19)#6	102.8(3)	S(18)-Cs(1)-S(4)#5	53.79(9)
S(11)#8-P(6)-S(15)	116.8(3)	S(12)#4-Cs(1)-S(4)#5	119.01(9)
S(11)#8-P(6)-S(16)#8	106.9(3)	S(12)-Cs(1)-S(4)#5	129.68(9)
S(15)-P(6)-S(16)#8	113.5(3)	S(10)-Cs(1)-S(4)#5	74.25(8)
S(11)#8-P(6)-S(21)#10	113.1(3)	S(2)#14-Cs(1)-S(4)#5	84.39(9)
S(15)-P(6)-S(21)#10	97.2(2)	S(9)-Cs(1)-S(4)#5	128.66(9)
S(16)#8-P(6)-S(21)#10	109.1(2)	S(5)#5-Cs(1)-S(4)#5	62.57(9)
S(14)-Cs(1)-S(18)	152.66(10)	S(14)-Cs(1)-P(3)#6	133.17(9)
S(14)-Cs(1)-S(12)#4	121.99(10)	S(18)-Cs(1)-P(3)#6	27.46(9)
S(18)-Cs(1)-S(12)#4	76.32(9)	S(12)#4-Cs(1)-P(3)#6	102.72(9)
S(14)-Cs(1)-S(12)	58.89(9)	S(12)-Cs(1)-P(3)#6	155.35(10)
S(18)-Cs(1)-S(12)	148.20(10)	S(10)-Cs(1)-P(3)#6	102.77(9)
S(12)#4-Cs(1)-S(12)	77.11(11)	S(2)#14-Cs(1)-P(3)#6	102.66(9)
S(14)-Cs(1)-S(10)	56.36(9)	S(9)-Cs(1)-P(3)#6	101.77(9)
S(18)-Cs(1)-S(10)	127.76(9)	S(5)#5-Cs(1)-P(3)#6	74.88(8)
S(12)#4-Cs(1)-S(10)	134.07(10)	S(4)#5-Cs(1)-P(3)#6	29.32(8)
S(12)-Cs(1)-S(10)	64.16(9)	S(14)-Cs(1)-U(3)	34.76(7)
S(14)-Cs(1)-S(2)#14	103.11(9)	S(18)-Cs(1)-U(3)	163.88(8)
S(18)-Cs(1)-S(2)#14	101.80(10)	S(12)#4-Cs(1)-U(3)	111.17(7)
S(12)#4-Cs(1)-S(2)#14	72.88(10)	S(12)-Cs(1)-U(3)	34.16(7)
S(12)-Cs(1)-S(2)#14	53.31(9)	S(10)-Cs(1)-U(3)	36.94(6)
S(10)-Cs(1)-S(2)#14	64.62(9)	S(2)#14-Cs(1)-U(3)	68.41(6)
S(14)-Cs(1)-S(9)	81.71(9)	S(9)-Cs(1)-U(3)	109.45(6)
S(18)-Cs(1)-S(9)	86.32(10)	S(5)#5-Cs(1)-U(3)	74.36(6)
S(12)#4-Cs(1)-S(9)	71.47(10)	S(4)#5-Cs(1)-U(3)	111.18(6)
S(12)-Cs(1)-S(9)	101.46(9)	P(3)#6-Cs(1)-U(3)	139.48(6)
S(10)-Cs(1)-S(9)	137.59(9)	S(14)-Cs(1)-Cs(1)#4	77.45(7)
S(2)#14-Cs(1)-S(9)	140.26(10)	S(18)-Cs(1)-Cs(1)#4	119.10(7)
S(14)-Cs(1)-S(5)#5	58.84(9)	S(12)#4-Cs(1)-Cs(1)#4	44.70(7)
S(18)-Cs(1)-S(5)#5	99.99(9)	S(12)-Cs(1)-Cs(1)#4	43.59(7)
S(12)#4-Cs(1)-S(5)#5	171.63(10)	S(10)-Cs(1)-Cs(1)#4	107.20(7)
S(12)-Cs(1)-S(5)#5	108.50(9)	S(2)#14-Cs(1)-Cs(1)#4	77.65(7)
S(10)-Cs(1)-S(5)#5	54.06(9)	S(9)-Cs(1)-Cs(1)#4	64.79(6)
S(2)#14-Cs(1)-S(5)#5	115.40(10)	S(5)#5-Cs(1)-Cs(1)#4	135.92(6)
S(9)-Cs(1)-S(5)#5	100.97(9)	S(4)#5-Cs(1)-Cs(1)#4	158.84(6)
S(14)-Cs(1)-S(4)#5	117.99(9)	P(3)#6-Cs(1)-Cs(1)#4	146.51(7)

U(3)-Cs(1)-Cs(1)#4	72.47(2)	S(16)#4-Cs(2)-S(19)	54.98(9)
S(18)#12-Cs(2)-S(14)#4	109.21(10)	S(18)#12-Cs(2)-P(4)	90.50(10)
S(18)#12-Cs(2)-S(20)	118.93(10)	S(14)#4-Cs(2)-P(4)	125.38(9)
S(14)#4-Cs(2)-S(20)	115.80(10)	S(20)-Cs(2)-P(4)	29.43(10)
S(18)#12-Cs(2)-S(5)#12	98.84(10)	S(5)#12-Cs(2)-P(4)	166.80(10)
S(14)#4-Cs(2)-S(5)#12	60.10(9)	S(21)-Cs(2)-P(4)	32.39(9)
S(20)-Cs(2)-S(5)#12	138.70(10)	S(8)-Cs(2)-P(4)	75.98(9)
S(18)#12-Cs(2)-S(21)	63.64(10)	S(13)#10-Cs(2)-P(4)	102.96(9)
S(14)#4-Cs(2)-S(21)	148.67(10)	S(16)#4-Cs(2)-P(4)	89.54(9)
S(20)-Cs(2)-S(21)	56.26(9)	S(19)-Cs(2)-P(4)	116.54(9)
S(5)#12-Cs(2)-S(21)	148.11(9)	S(18)#12-Cs(2)-Cs(4)#6	122.75(7)
S(18)#12-Cs(2)-S(8)	89.64(9)	S(14)#4-Cs(2)-Cs(4)#6	75.14(6)
S(14)#4-Cs(2)-S(8)	54.65(9)	S(20)-Cs(2)-Cs(4)#6	44.09(7)
S(20)-Cs(2)-S(8)	84.87(10)	S(5)#12-Cs(2)-Cs(4)#6	127.08(7)
S(5)#12-Cs(2)-S(8)	113.14(10)	S(21)-Cs(2)-Cs(4)#6	83.80(7)
S(21)-Cs(2)-S(8)	94.09(10)	S(8)-Cs(2)-Cs(4)#6	44.95(6)
S(18)#12-Cs(2)-S(13)#10	69.40(10)	S(13)#10-Cs(2)-Cs(4)#6	148.59(7)
S(14)#4-Cs(2)-S(13)#10	131.57(9)	S(16)#4-Cs(2)-Cs(4)#6	43.16(6)
S(20)-Cs(2)-S(13)#10	104.59(10)	S(19)-Cs(2)-Cs(4)#6	94.09(6)
S(5)#12-Cs(2)-S(13)#10	72.08(9)	P(4)-Cs(2)-Cs(4)#6	52.22(7)
S(21)-Cs(2)-S(13)#10	76.66(9)	S(18)#12-Cs(2)-Cs(4)	116.96(7)
S(8)-Cs(2)-S(13)#10	159.04(10)	S(14)#4-Cs(2)-Cs(4)	118.05(7)
S(18)#12-Cs(2)-S(16)#4	156.23(10)	S(20)-Cs(2)-Cs(4)	74.62(8)
S(14)#4-Cs(2)-S(16)#4	53.06(9)	S(5)#12-Cs(2)-Cs(4)	73.64(7)
S(20)-Cs(2)-S(16)#4	66.80(10)	S(21)-Cs(2)-Cs(4)	90.32(7)
S(5)#12-Cs(2)-S(16)#4	85.65(9)	S(8)-Cs(2)-Cs(4)	151.90(7)
S(21)-Cs(2)-S(16)#4	121.50(9)	S(13)#10-Cs(2)-Cs(4)	48.37(7)
S(8)-Cs(2)-S(16)#4	67.33(9)	S(16)#4-Cs(2)-Cs(4)	86.75(7)
S(13)#10-Cs(2)-S(16)#4	133.52(10)	S(19)-Cs(2)-Cs(4)	41.96(6)
S(18)#12-Cs(2)-S(19)	143.13(9)	P(4)-Cs(2)-Cs(4)	93.85(7)
S(14)#4-Cs(2)-S(19)	76.38(9)	Cs(4)#6-Cs(2)-Cs(4)	108.32(3)
S(20)-Cs(2)-S(19)	87.64(10)	S(10)#15-Cs(3)-S(17)#15	53.82(9)
S(5)#12-Cs(2)-S(19)	51.06(9)	S(10)#15-Cs(3)-S(3)#11	97.40(10)
S(21)-Cs(2)-S(19)	128.84(10)	S(17)#15-Cs(3)-S(3)#11	148.23(10)
S(8)-Cs(2)-S(19)	119.72(9)	S(10)#15-Cs(3)-S(15)#16	137.08(11)
S(13)#10-Cs(2)-S(19)	79.87(9)	S(17)#15-Cs(3)-S(15)#16	138.87(9)

S(3)#11-Cs(3)-S(15)#16	70.35(9)	S(18)#3-Cs(3)-Cs(4)	116.71(7)
S(10)#15-Cs(3)-S(2)#2	66.55(10)	S(21)#2-Cs(3)-Cs(4)	77.99(7)
S(17)#15-Cs(3)-S(2)#2	55.23(9)	S(20)#12-Cs(3)-Cs(4)	43.13(7)
S(3)#11-Cs(3)-S(2)#2	104.10(10)	S(7)#11-Cs(3)-Cs(4)	55.27(6)
S(15)#16-Cs(3)-S(2)#2	155.34(10)	S(22)-Cs(4)-S(16)#10	163.28(11)
S(10)#15-Cs(3)-S(18)#3	153.09(10)	S(22)-Cs(4)-S(20)#12	94.88(10)
S(17)#15-Cs(3)-S(18)#3	110.45(10)	S(16)#10-Cs(4)-S(20)#12	70.16(10)
S(3)#11-Cs(3)-S(18)#3	89.76(9)	S(22)-Cs(4)-S(8)#12	101.61(10)
S(15)#16-Cs(3)-S(18)#3	69.70(10)	S(16)#10-Cs(4)-S(8)#12	70.67(10)
S(2)#2-Cs(3)-S(18)#3	86.55(9)	S(20)#12-Cs(4)-S(8)#12	85.61(10)
S(10)#15-Cs(3)-S(21)#2	133.07(9)	S(22)-Cs(4)-S(17)#16	89.02(10)
S(17)#15-Cs(3)-S(21)#2	92.63(9)	S(16)#10-Cs(4)-S(17)#16	104.26(10)
S(3)#11-Cs(3)-S(21)#2	118.89(10)	S(20)#12-Cs(4)-S(17)#16	117.19(10)
S(15)#16-Cs(3)-S(21)#2	49.81(9)	S(8)#12-Cs(4)-S(17)#16	154.17(10)
S(2)#2-Cs(3)-S(21)#2	124.27(9)	S(22)-Cs(4)-S(11)#16	125.24(10)
S(18)#3-Cs(3)-S(21)#2	61.57(9)	S(16)#10-Cs(4)-S(11)#16	71.43(10)
S(10)#15-Cs(3)-S(20)#12	57.91(10)	S(20)#12-Cs(4)-S(11)#16	135.32(10)
S(17)#15-Cs(3)-S(20)#12	75.68(10)	S(8)#12-Cs(4)-S(11)#16	102.39(10)
S(3)#11-Cs(3)-S(20)#12	101.67(10)	S(17)#16-Cs(4)-S(11)#16	53.25(9)
S(15)#16-Cs(3)-S(20)#12	83.70(10)	S(22)-Cs(4)-S(22)#13	62.46(12)
S(2)#2-Cs(3)-S(20)#12	120.83(10)	S(16)#10-Cs(4)-S(22)#13	101.73(10)
S(18)#3-Cs(3)-S(20)#12	145.65(10)	S(20)#12-Cs(4)-S(22)#13	54.90(10)
S(21)#2-Cs(3)-S(20)#12	84.79(10)	S(8)#12-Cs(4)-S(22)#13	55.47(10)
S(10)#15-Cs(3)-S(7)#11	50.83(9)	S(17)#16-Cs(4)-S(22)#13	147.21(10)
S(17)#15-Cs(3)-S(7)#11	103.95(9)	S(11)#16-Cs(4)-S(22)#13	157.37(10)
S(3)#11-Cs(3)-S(7)#11	52.38(9)	S(22)-Cs(4)-S(19)	55.04(10)
S(15)#16-Cs(3)-S(7)#11	94.43(9)	S(16)#10-Cs(4)-S(19)	129.40(10)
S(2)#2-Cs(3)-S(7)#11	100.79(9)	S(20)#12-Cs(4)-S(19)	130.42(10)
S(18)#3-Cs(3)-S(7)#11	142.13(8)	S(8)#12-Cs(4)-S(19)	66.87(9)
S(21)#2-Cs(3)-S(7)#11	132.93(9)	S(17)#16-Cs(4)-S(19)	102.12(9)
S(20)#12-Cs(3)-S(7)#11	58.38(9)	S(11)#16-Cs(4)-S(19)	91.94(10)
S(10)#15-Cs(3)-Cs(4)	89.97(7)	S(22)#13-Cs(4)-S(19)	75.61(9)
S(17)#15-Cs(3)-Cs(4)	118.39(7)	S(22)-Cs(4)-S(15)#16	133.41(10)
S(3)#11-Cs(3)-Cs(4)	68.80(7)	S(16)#10-Cs(4)-S(15)#16	54.17(9)
S(15)#16-Cs(3)-Cs(4)	47.11(8)	S(20)#12-Cs(4)-S(15)#16	82.67(10)
S(2)#2-Cs(3)-Cs(4)	154.89(7)	S(8)#12-Cs(4)-S(15)#16	124.37(9)

S(17)#16-Cs(4)-S(15)#16	53.16(9)	S(2)#4-U(1)-S(3)#4	73.15(12)
S(11)#16-Cs(4)-S(15)#16	56.32(9)	S(2)-U(1)-S(3)	73.15(12)
S(22)#13-Cs(4)-S(15)#16	137.38(9)	S(2)#4-U(1)-S(3)	77.24(12)
S(19)-Cs(4)-S(15)#16	146.92(9)	S(3)#4-U(1)-S(3)	135.5(2)
S(22)-Cs(4)-P(4)#12	72.93(10)	S(2)-U(1)-S(1)#4	148.79(11)
S(16)#10-Cs(4)-P(4)#12	90.51(9)	S(2)#4-U(1)-S(1)#4	83.55(12)
S(20)#12-Cs(4)-P(4)#12	28.01(9)	S(3)#4-U(1)-S(1)#4	72.52(12)
S(8)#12-Cs(4)-P(4)#12	73.85(9)	S(3)-U(1)-S(1)#4	135.79(11)
S(17)#16-Cs(4)-P(4)#12	131.98(9)	S(2)-U(1)-S(1)	83.55(12)
S(11)#16-Cs(4)-P(4)#12	161.59(9)	S(2)#4-U(1)-S(1)	148.79(11)
S(22)#13-Cs(4)-P(4)#12	28.14(9)	S(3)#4-U(1)-S(1)	135.78(11)
S(19)-Cs(4)-P(4)#12	102.66(9)	S(3)-U(1)-S(1)	72.52(12)
S(15)#16-Cs(4)-P(4)#12	110.35(9)	S(1)#4-U(1)-S(1)	113.2(2)
S(22)-Cs(4)-Cs(2)#12	116.31(8)	S(2)-U(1)-S(4)#4	86.65(12)
S(16)#10-Cs(4)-Cs(2)#12	47.65(7)	S(2)#4-U(1)-S(4)#4	142.47(11)
S(20)#12-Cs(4)-Cs(2)#12	44.47(7)	S(3)#4-U(1)-S(4)#4	70.71(11)
S(8)#12-Cs(4)-Cs(2)#12	45.36(7)	S(3)-U(1)-S(4)#4	137.90(12)
S(17)#16-Cs(4)-Cs(2)#12	147.01(7)	S(1)#4-U(1)-S(4)#4	76.35(11)
S(11)#16-Cs(4)-Cs(2)#12	115.64(7)	S(1)-U(1)-S(4)#4	68.72(11)
S(22)#13-Cs(4)-Cs(2)#12	54.08(7)	S(2)-U(1)-S(4)	142.47(11)
S(19)-Cs(4)-Cs(2)#12	109.64(6)	S(2)#4-U(1)-S(4)	86.65(12)
S(15)#16-Cs(4)-Cs(2)#12	94.13(6)	S(3)#4-U(1)-S(4)	137.90(12)
P(4)#12-Cs(4)-Cs(2)#12	48.89(6)	S(3)-U(1)-S(4)	70.72(11)
S(22)-Cs(4)-Cs(3)	105.43(8)	S(1)#4-U(1)-S(4)	68.72(11)
S(16)#10-Cs(4)-Cs(3)	69.76(7)	S(1)-U(1)-S(4)	76.35(11)
S(20)#12-Cs(4)-Cs(3)	45.35(7)	S(4)#4-U(1)-S(4)	114.1(2)
S(8)#12-Cs(4)-Cs(3)	124.83(7)	S(8)-U(2)-S(9)	73.75(12)
S(17)#16-Cs(4)-Cs(3)	73.23(7)	S(8)-U(2)-S(5)	86.19(12)
S(11)#16-Cs(4)-Cs(3)	99.71(7)	S(9)-U(2)-S(5)	75.90(12)
S(22)#13-Cs(4)-Cs(3)	97.81(7)	S(8)-U(2)-S(7)	83.35(12)
S(19)-Cs(4)-Cs(3)	160.37(7)	S(9)-U(2)-S(7)	140.48(12)
S(15)#16-Cs(4)-Cs(3)	43.75(7)	S(5)-U(2)-S(7)	70.75(12)
P(4)#12-Cs(4)-Cs(3)	69.70(6)	S(8)-U(2)-S(1)	89.48(12)
Cs(2)#12-Cs(4)-Cs(3)	79.51(2)	S(9)-U(2)-S(1)	140.93(12)
S(2)-U(1)-S(2)#4	95.1(2)	S(5)-U(2)-S(1)	139.15(11)
S(2)-U(1)-S(3)#4	77.24(12)	S(7)-U(2)-S(1)	68.41(11)

S(8)-U(2)-S(4)	154.16(12)	S(11)-U(3)-S(15)	76.34(12)
S(9)-U(2)-S(4)	129.70(12)	S(14)-U(3)-S(15)	139.67(12)
S(5)-U(2)-S(4)	89.60(12)	S(17)-U(3)-S(15)	70.67(12)
S(7)-U(2)-S(4)	71.22(12)	S(12)-U(3)-S(10)	86.35(12)
S(1)-U(2)-S(4)	77.20(12)	S(16)-U(3)-S(10)	89.73(12)
S(8)-U(2)-S(6)#4	138.26(12)	S(13)-U(3)-S(10)	143.02(12)
S(9)-U(2)-S(6)#4	67.11(12)	S(11)-U(3)-S(10)	90.67(12)
S(5)-U(2)-S(6)#4	97.58(11)	S(14)-U(3)-S(10)	72.48(11)
S(7)-U(2)-S(6)#4	137.20(12)	S(17)-U(3)-S(10)	67.16(11)
S(1)-U(2)-S(6)#4	111.99(11)	S(15)-U(3)-S(10)	137.82(12)
S(4)-U(2)-S(6)#4	67.58(11)	S(12)-U(3)-Cs(1)	48.01(9)
S(8)-U(2)-S(6)	82.39(12)	S(16)-U(3)-Cs(1)	109.94(9)
S(9)-U(2)-S(6)	75.19(12)	S(13)-U(3)-Cs(1)	99.18(9)
S(5)-U(2)-S(6)	150.87(12)	S(11)-U(3)-Cs(1)	139.11(9)
S(7)-U(2)-S(6)	133.69(12)	S(14)-U(3)-Cs(1)	45.23(8)
S(1)-U(2)-S(6)	67.64(11)	S(17)-U(3)-Cs(1)	84.89(8)
S(4)-U(2)-S(6)	111.79(11)	S(15)-U(3)-Cs(1)	126.31(8)
S(6)#4-U(2)-S(6)	74.32(13)	S(10)-U(3)-Cs(1)	49.04(8)
S(12)-U(3)-S(16)	150.51(13)		
S(12)-U(3)-S(13)	81.31(13)		
S(16)-U(3)-S(13)	84.46(13)		
S(12)-U(3)-S(11)	138.58(13)		
S(16)-U(3)-S(11)	70.60(12)		
S(13)-U(3)-S(11)	121.11(12)		
S(12)-U(3)-S(14)	78.33(12)		
S(16)-U(3)-S(14)	72.63(12)		
S(13)-U(3)-S(14)	70.93(11)		
S(11)-U(3)-S(14)	139.41(12)		
S(12)-U(3)-S(17)	70.26(12)		
S(16)-U(3)-S(17)	134.06(12)		
S(13)-U(3)-S(17)	137.52(13)		
S(11)-U(3)-S(17)	70.59(12)		
S(14)-U(3)-S(17)	129.53(11)		
S(12)-U(3)-S(15)	78.53(12)		
S(16)-U(3)-S(15)	121.58(12)		
S(13)-U(3)-S(15)	73.26(12)		

Symmetry transformations used to generate equivalent atoms:

#1 -x,y+1,-z+1/2 #2 -x+1/2,-y+1/2,-z #3 -x+1/2,y+1/2,-z+1/2

#4 -x,y,-z+1/2 #5 -x,-y,-z+1 #6 x,-y,z+1/2

#7 x-1/2,-y-1/2,z+1/2 #8 -x-1/2,-y-1/2,-z #9 x-1/2,y-1/2,z

#10 -x,-y,-z #11 -x+1/2,y-1/2,-z+1/2 #12 x,-y,z-1/2

#13 -x+1/2,-y-1/2,-z #14 -x,y-1,-z+1/2 #15 x+1/2,-y-1/2,z-1/2

#16 x+1/2,y+1/2,z

Table 4. Anisotropic displacement parameters ($Å^2 x\ 10^3$) for $Cs_8U_5(P_3S_{10})_2(PS_4)_6$. The anisotropic displacement factor exponent takes the form: $-2\pi^2[\ h^2\ a^{*2}U^{11} + ... + 2\ h\ k\ a^*\ b^*\ U^{12}\ ]$

	U^{11}	U^{22}	U^{33}	U^{23}	U^{13}	U^{12}
U(1)	14(1)	10(1)	11(1)	0	6(1)	0
U(2)	13(1)	10(1)	10(1)	1(1)	5(1)	1(1)
U(3)	14(1)	9(1)	13(1)	0(1)	6(1)	0(1)
S(1)	15(2)	13(2)	10(2)	0(2)	4(2)	2(2)
S(2)	20(2)	18(2)	15(2)	1(2)	6(2)	-6(2)
S(3)	22(2)	15(2)	15(2)	3(2)	7(2)	-3(2)
S(4)	13(2)	14(2)	13(2)	-2(2)	5(2)	-2(2)
S(5)	18(2)	14(2)	11(2)	0(2)	5(2)	-5(2)
S(6)	18(2)	13(2)	13(2)	-2(2)	6(2)	0(2)
S(7)	16(2)	11(2)	16(2)	1(2)	3(2)	-5(2)
S(8)	15(2)	14(2)	20(2)	-1(2)	8(2)	1(2)
S(9)	15(2)	11(2)	23(2)	0(2)	10(2)	-1(2)
S(10)	22(2)	13(2)	13(2)	-1(2)	9(2)	0(2)
S(11)	13(2)	17(2)	24(2)	-6(2)	9(2)	-1(2)
S(12)	18(2)	11(2)	25(2)	-2(2)	11(2)	2(2)
S(13)	29(3)	16(2)	12(2)	-1(2)	9(2)	-7(2)
S(14)	15(2)	10(2)	12(2)	-1(2)	3(2)	-1(2)
S(15)	22(2)	21(3)	13(2)	-4(2)	6(2)	5(2)
S(16)	20(2)	14(2)	20(2)	2(2)	11(2)	-3(2)
S(17)	12(2)	19(2)	19(2)	0(2)	6(2)	-3(2)
S(18)	17(2)	24(3)	19(2)	-1(2)	14(2)	-5(2)
S(19)	13(2)	13(2)	20(2)	-1(2)	5(2)	-1(2)
S(20)	24(2)	13(2)	25(2)	0(2)	7(2)	0(2)
S(21)	13(2)	20(2)	16(2)	1(2)	7(2)	-2(2)
S(22)	26(3)	23(3)	26(2)	3(2)	17(2)	3(2)
P(1)	16(2)	8(2)	14(2)	1(2)	7(2)	1(2)
P(2)	19(2)	11(2)	12(2)	-2(2)	8(2)	2(2)
P(3)	13(2)	13(2)	11(2)	-1(2)	5(2)	2(2)
P(4)	15(2)	19(3)	17(2)	-3(2)	7(2)	-1(2)
P(5)	17(2)	13(2)	9(2)	-1(2)	8(2)	-3(2)

P(6)	13(2)	14(2)	10(2)	0(2)	3(2)	-1(2)
Cs(1)	21(1)	28(1)	19(1)	-1(1)	7(1)	2(1)
Cs(2)	29(1)	17(1)	20(1)	-1(1)	9(1)	-4(1)
Cs(3)	34(1)	22(1)	25(1)	-6(1)	16(1)	2(1)
Cs(4)	37(1)	19(1)	18(1)	-1(1)	10(1)	-4(1)

Table 1. Crystal data and structure refinement for $K_{10}Th_3(P_2S_7)_4(PS_4)_2$.

Identification code	k10th3	
Empirical formula	$K_{10}Th_3(P_2S_7)_4(PS_4)_2$	
Formula weight	2550.98	
Temperature	163(2) K	
Wavelength	0.71073 Å	
Crystal system	Monoclinic	
Space group	C2/c	
Unit cell dimensions	a = 32.8085(6) Å	α= 90°.
	b = 9.0482(2) Å	β= 125.7200(10)°.
	c = 27.2972(3) Å	γ = 90°.
Volume	6579.0(2) $Å^3$	
Z	4	
Density (calculated)	2.575 Mg/m^3	
Absorption coefficient	8.801 mm^{-1}	
F(000)	4744	
Crystal size	0.28 x 0.10 x 0.08 mm^3	
Theta range for data collection	1.53 to 28.28°.	
Index ranges	-42<=h<=43, -9<=k<=12, -36<=l<=35	
Reflections collected	21318	
Independent reflections	7914 [R(int) = 0.0439]	
Absorption correction	SADABS	
Refinement method	Full-matrix least-squares on F^2	
Data / restraints / parameters	7914 / 0 / 268	
Goodness-of-fit on F^2	1.029	
Final R indices [I>2sigma(I)]	R1 = 0.0346, wR2 = 0.0648	
R indices (all data)	R1 = 0.0546, wR2 = 0.0714	
Extinction coefficient	0.000055(8)	
Largest diff. peak and hole	1.702 and -1.837 $e.Å^{-3}$	

Table 2. Atomic coordinates (x 10^4) and equivalent isotropic displacement parameters ($Å^2$x 10^3) for $K_{10}Th_3(P_2S_7)_4(PS_4)_2$. U(eq) is defined as one third of the trace of the orthogonalized U^{ij} tensor.

	x	y	z	U(eq)
Th(1)	0	9651(1)	2500	13(1)
Th(2)	1366(1)	6960(1)	5557(1)	13(1)
K(1)	1836(1)	460(2)	4265(1)	27(1)
K(2)	718(1)	2228(2)	6006(1)	64(1)
K(3)	281(1)	13851(2)	3734(1)	34(1)
K(4)	2733(1)	4315(2)	7363(1)	28(1)
K(5)	1478(1)	5546(2)	3369(1)	44(1)
S(1)	410(1)	6939(2)	3201(1)	21(1)
S(2)	496(1)	12435(2)	2608(1)	19(1)
S(3)	598(1)	10252(2)	3776(1)	20(1)
S(4)	909(1)	9172(2)	2559(1)	25(1)
S(5)	399(1)	7345(2)	4413(1)	19(1)
S(6)	1466(1)	7591(2)	4586(1)	18(1)
S(7)	2260(1)	5350(2)	5918(1)	19(1)
S(8)	1138(1)	3927(2)	5132(1)	22(1)
S(9)	2276(1)	8777(2)	6370(1)	19(1)
S(10)	1696(1)	6377(2)	6782(1)	21(1)
S(11)	526(1)	6136(2)	5603(1)	21(1)
S(12)	1113(1)	10003(2)	5463(1)	20(1)
S(13)	759(1)	8403(2)	6619(1)	21(1)
S(14)	838(1)	4690(2)	6918(1)	24(1)
S(15)	1876(1)	3800(2)	4602(1)	40(1)
S(16)	2129(1)	1602(2)	5638(1)	18(1)
S(17)	1899(1)	1946(2)	6714(1)	22(1)
S(18)	1697(1)	2172(2)	3116(1)	24(1)
P(1)	717(1)	8057(2)	3999(1)	15(1)
P(2)	977(1)	6242(2)	6522(1)	16(1)
P(3)	1838(1)	637(2)	6089(1)	15(1)
P(4)	1825(1)	3743(2)	5294(1)	18(1)
P(5)	1009(1)	1405(2)	2533(1)	16(1)

Table 3. Bond lengths [Å] and angles [°] for $K_{10}Th_3(P_2S_7)_4(PS_4)_2$.

Th(1)-S(3)	2.8798(13)	K(3)-S(2)#1	3.263(2)
Th(1)-S(3)#1	2.8798(13)	K(3)-S(14)#6	3.280(2)
Th(1)-S(1)#1	2.9125(15)	K(3)-S(1)#5	3.289(2)
Th(1)-S(1)	2.9126(15)	K(3)-S(3)	3.400(2)
Th(1)-S(2)	2.918(2)	K(3)-S(5)#5	3.570(2)
Th(1)-S(2)#1	2.9184(15)	K(3)-S(13)#6	3.592(2)
Th(1)-S(4)	2.9243(15)	K(3)-S(2)	3.757(2)
Th(1)-S(4)#1	2.9243(15)	K(3)-P(2)#6	3.765(2)
Th(2)-S(12)	2.8437(15)	K(3)-K(5)#5	4.831(2)
Th(2)-S(7)	2.8860(14)	K(4)-S(17)	3.093(2)
Th(2)-S(5)	2.8935(14)	K(4)-S(18)#3	3.143(2)
Th(2)-S(10)	2.8979(14)	K(4)-S(17)#7	3.150(2)
Th(2)-S(8)	2.9027(15)	K(4)-S(10)#8	3.304(2)
Th(2)-S(6)	2.9107(14)	K(4)-S(10)	3.357(2)
Th(2)-S(11)	2.9263(14)	K(4)-S(7)	3.418(2)
Th(2)-S(9)	2.9683(14)	K(4)-S(9)#8	3.510(2)
K(1)-S(15)	3.139(2)	K(4)-P(3)#7	3.784(2)
K(1)-S(6)#2	3.199(2)	K(4)-K(4)#7	4.9705(11)
K(1)-S(18)	3.280(2)	K(4)-K(4)#8	4.9705(11)
K(1)-S(7)#3	3.363(2)	K(5)-S(15)	3.226(2)
K(1)-S(16)	3.441(2)	K(5)-S(14)#9	3.229(2)
K(1)-S(3)#2	3.463(2)	K(5)-S(18)	3.299(2)
K(1)-S(15)#3	3.552(3)	K(5)-S(1)	3.494(2)
K(1)-K(5)#2	4.876(2)	K(5)-S(9)#10	3.767(2)
K(1)-K(5)	5.018(2)	K(5)-S(4)	3.784(2)
K(2)-S(5)#4	3.161(2)	K(5)-K(3)#2	4.831(2)
K(2)-S(17)	3.173(2)	K(5)-K(1)#5	4.876(2)
K(2)-S(12)#2	3.188(2)	S(1)-P(1)	2.055(2)
K(2)-S(14)	3.191(2)	S(1)-K(3)#2	3.289(2)
K(2)-S(11)	3.647(3)	S(2)-P(5)#5	2.037(2)
K(2)-S(8)	3.714(3)	S(2)-K(3)#1	3.263(2)
K(2)-P(2)	3.809(2)	S(3)-P(1)	2.047(2)
K(2)-P(3)	3.827(2)	S(3)-K(1)#5	3.463(2)
K(3)-S(8)#5	3.154(2)	S(4)-P(5)#5	2.055(2)

S(5)-P(1)	2.039(2)	P(5)-S(4)#2	2.055(2)
S(5)-K(2)#4	3.161(2)	P(5)-S(13)#9	2.131(2)
S(5)-K(3)#2	3.570(2)	S(3)-Th(1)-S(3)#1	158.24(6)
S(6)-P(1)	2.044(2)	S(3)-Th(1)-S(1)#1	132.88(4)
S(6)-K(1)#5	3.199(2)	S(3)#1-Th(1)-S(1)#1	68.75(4)
S(7)-P(4)	2.053(2)	S(3)-Th(1)-S(1)	68.75(4)
S(7)-K(1)#3	3.363(2)	S(3)#1-Th(1)-S(1)	132.88(4)
S(8)-P(4)	2.033(2)	S(1)#1-Th(1)-S(1)	65.21(6)
S(8)-K(3)#2	3.154(2)	S(3)-Th(1)-S(2)	76.66(4)
S(9)-P(3)#5	2.049(2)	S(3)#1-Th(1)-S(2)	84.54(4)
S(9)-K(4)#7	3.510(2)	S(1)#1-Th(1)-S(2)	144.06(4)
S(9)-K(5)#10	3.767(2)	S(1)-Th(1)-S(2)	130.14(4)
S(10)-P(2)	2.032(2)	S(3)-Th(1)-S(2)#1	84.54(4)
S(10)-K(4)#7	3.304(2)	S(3)#1-Th(1)-S(2)#1	76.66(4)
S(11)-P(2)	2.039(2)	S(1)#1-Th(1)-S(2)#1	130.14(4)
S(12)-P(3)#5	2.040(2)	S(1)-Th(1)-S(2)#1	144.05(4)
S(12)-K(2)#5	3.188(2)	S(2)-Th(1)-S(2)#1	60.65(6)
S(13)-P(5)#11	2.131(2)	S(3)-Th(1)-S(4)	90.52(4)
S(13)-P(2)	2.150(2)	S(3)#1-Th(1)-S(4)	92.69(4)
S(13)-K(3)#6	3.592(2)	S(1)#1-Th(1)-S(4)	88.62(4)
S(14)-P(2)	1.982(2)	S(1)-Th(1)-S(4)	76.95(4)
S(14)-K(5)#11	3.229(2)	S(2)-Th(1)-S(4)	68.41(4)
S(14)-K(3)#6	3.280(2)	S(2)#1-Th(1)-S(4)	128.60(4)
S(15)-P(4)	1.992(2)	S(3)-Th(1)-S(4)#1	92.69(4)
S(15)-K(1)#3	3.552(3)	S(3)#1-Th(1)-S(4)#1	90.52(4)
S(16)-P(4)	2.129(2)	S(1)#1-Th(1)-S(4)#1	76.95(4)
S(16)-P(3)	2.136(2)	S(1)-Th(1)-S(4)#1	88.62(4)
S(17)-P(3)	1.988(2)	S(2)-Th(1)-S(4)#1	128.60(4)
S(17)-K(4)#8	3.150(2)	S(2)#1-Th(1)-S(4)#1	68.41(4)
S(18)-P(5)	1.977(2)	S(4)-Th(1)-S(4)#1	162.94(6)
S(18)-K(4)#3	3.143(2)	S(12)-Th(2)-S(7)	134.80(4)
P(2)-K(3)#6	3.765(2)	S(12)-Th(2)-S(5)	73.00(4)
P(3)-S(12)#2	2.040(2)	S(7)-Th(2)-S(5)	133.21(4)
P(3)-S(9)#2	2.049(2)	S(12)-Th(2)-S(10)	99.98(4)
P(3)-K(4)#8	3.784(2)	S(7)-Th(2)-S(10)	83.85(4)
P(5)-S(2)#2	2.037(2)	S(5)-Th(2)-S(10)	134.72(4)

S(12)-Th(2)-S(8)	152.37(4)	S(16)-K(1)-S(3)#2	87.40(4)
S(7)-Th(2)-S(8)	68.41(4)	S(15)-K(1)-S(15)#3	74.84(6)
S(5)-Th(2)-S(8)	79.52(4)	S(6)#2-K(1)-S(15)#3	111.32(5)
S(10)-Th(2)-S(8)	97.19(4)	S(18)-K(1)-S(15)#3	100.04(5)
S(12)-Th(2)-S(6)	84.83(4)	S(7)#3-K(1)-S(15)#3	57.74(4)
S(7)-Th(2)-S(6)	77.14(4)	S(16)-K(1)-S(15)#3	63.98(4)
S(5)-Th(2)-S(6)	68.18(4)	S(3)#2-K(1)-S(15)#3	151.38(5)
S(10)-Th(2)-S(6)	157.06(4)	S(15)-K(1)-K(5)#2	168.95(6)
S(8)-Th(2)-S(6)	87.73(4)	S(6)#2-K(1)-K(5)#2	51.60(4)
S(12)-Th(2)-S(11)	91.04(4)	S(18)-K(1)-K(5)#2	95.34(4)
S(7)-Th(2)-S(11)	130.67(4)	S(7)#3-K(1)-K(5)#2	72.65(4)
S(5)-Th(2)-S(11)	67.10(4)	S(16)-K(1)-K(5)#2	130.73(5)
S(10)-Th(2)-S(11)	68.41(4)	S(3)#2-K(1)-K(5)#2	82.66(4)
S(8)-Th(2)-S(11)	75.38(4)	S(15)#3-K(1)-K(5)#2	115.11(5)
S(6)-Th(2)-S(11)	134.27(4)	S(15)-K(1)-K(5)	38.58(4)
S(12)-Th(2)-S(9)	69.18(4)	S(6)#2-K(1)-K(5)	149.28(5)
S(7)-Th(2)-S(9)	69.24(4)	S(18)-K(1)-K(5)	40.44(4)
S(5)-Th(2)-S(9)	136.97(4)	S(7)#3-K(1)-K(5)	95.93(4)
S(10)-Th(2)-S(9)	72.70(4)	S(16)-K(1)-K(5)	95.31(4)
S(8)-Th(2)-S(9)	137.25(4)	S(3)#2-K(1)-K(5)	88.52(4)
S(6)-Th(2)-S(9)	88.47(4)	S(15)#3-K(1)-K(5)	94.15(4)
S(11)-Th(2)-S(9)	132.12(4)	K(5)#2-K(1)-K(5)	132.27(4)
S(15)-K(1)-S(6)#2	131.13(6)	S(5)#4-K(2)-S(17)	167.26(9)
S(15)-K(1)-S(18)	77.57(5)	S(5)#4-K(2)-S(12)#2	127.52(7)
S(6)#2-K(1)-S(18)	141.46(6)	S(17)-K(2)-S(12)#2	63.23(5)
S(15)-K(1)-S(7)#3	111.36(6)	S(5)#4-K(2)-S(14)	77.61(5)
S(6)#2-K(1)-S(7)#3	111.90(5)	S(17)-K(2)-S(14)	91.73(6)
S(18)-K(1)-S(7)#3	66.68(4)	S(12)#2-K(2)-S(14)	154.85(7)
S(15)-K(1)-S(16)	56.89(4)	S(5)#4-K(2)-S(11)	79.22(5)
S(6)#2-K(1)-S(16)	81.59(5)	S(17)-K(2)-S(11)	101.31(6)
S(18)-K(1)-S(16)	133.94(6)	S(12)#2-K(2)-S(11)	121.18(8)
S(7)#3-K(1)-S(16)	121.19(5)	S(14)-K(2)-S(11)	58.60(5)
S(15)-K(1)-S(3)#2	90.22(6)	S(5)#4-K(2)-S(8)	120.28(8)
S(6)#2-K(1)-S(3)#2	60.88(4)	S(17)-K(2)-S(8)	69.24(5)
S(18)-K(1)-S(3)#2	100.35(5)	S(12)#2-K(2)-S(8)	63.84(5)
S(7)#3-K(1)-S(3)#2	150.31(6)	S(14)-K(2)-S(8)	106.82(7)

S(11)-K(2)-S(8)	57.90(5)	S(2)#1-K(3)-S(2)	49.03(5)
S(5)#4-K(2)-P(2)	88.78(5)	S(14)#6-K(3)-S(2)	112.22(5)
S(17)-K(2)-P(2)	85.50(5)	S(1)#5-K(3)-S(2)	78.12(5)
S(12)#2-K(2)-P(2)	135.27(7)	S(3)-K(3)-S(2)	60.08(4)
S(14)-K(2)-P(2)	31.34(4)	S(5)#5-K(3)-S(2)	135.37(5)
S(11)-K(2)-P(2)	31.65(3)	S(13)#6-K(3)-S(2)	100.92(5)
S(8)-K(2)-P(2)	75.89(5)	S(8)#5-K(3)-P(2)#6	109.36(5)
S(5)#4-K(2)-P(3)	159.64(7)	S(2)#1-K(3)-P(2)#6	74.32(4)
S(17)-K(2)-P(3)	31.26(4)	S(14)#6-K(3)-P(2)#6	31.74(4)
S(12)#2-K(2)-P(3)	32.20(4)	S(1)#5-K(3)-P(2)#6	110.30(5)
S(14)-K(2)-P(3)	122.65(6)	S(3)-K(3)-P(2)#6	105.37(5)
S(11)-K(2)-P(3)	111.93(6)	S(5)#5-K(3)-P(2)#6	83.73(5)
S(8)-K(2)-P(3)	59.37(4)	S(13)#6-K(3)-P(2)#6	33.89(4)
P(2)-K(2)-P(3)	109.71(5)	S(2)-K(3)-P(2)#6	123.33(5)
S(8)#5-K(3)-S(2)#1	157.96(6)	S(8)#5-K(3)-K(5)#5	89.13(5)
S(8)#5-K(3)-S(14)#6	124.94(6)	S(2)#1-K(3)-K(5)#5	95.13(5)
S(2)#1-K(3)-S(14)#6	69.86(5)	S(14)#6-K(3)-K(5)#5	123.20(5)
S(8)#5-K(3)-S(1)#5	105.24(5)	S(1)#5-K(3)-K(5)#5	46.33(4)
S(2)#1-K(3)-S(1)#5	93.15(5)	S(3)-K(3)-K(5)#5	92.40(5)
S(14)#6-K(3)-S(1)#5	79.06(5)	S(5)#5-K(3)-K(5)#5	88.36(4)
S(8)#5-K(3)-S(3)	86.63(5)	S(13)#6-K(3)-K(5)#5	152.21(5)
S(2)#1-K(3)-S(3)	71.61(5)	S(2)-K(3)-K(5)#5	51.42(3)
S(14)#6-K(3)-S(3)	128.81(6)	P(2)#6-K(3)-K(5)#5	154.74(5)
S(1)#5-K(3)-S(3)	135.48(6)	S(17)-K(4)-S(18)#3	90.45(5)
S(8)#5-K(3)-S(5)#5	66.59(4)	S(17)-K(4)-S(17)#7	141.24(5)
S(2)#1-K(3)-S(5)#5	135.01(6)	S(18)#3-K(4)-S(17)#7	127.80(6)
S(14)#6-K(3)-S(5)#5	70.91(5)	S(17)-K(4)-S(10)#8	78.10(5)
S(1)#5-K(3)-S(5)#5	58.29(4)	S(18)#3-K(4)-S(10)#8	73.75(5)
S(3)-K(3)-S(5)#5	153.20(5)	S(17)#7-K(4)-S(10)#8	104.37(5)
S(8)#5-K(3)-S(13)#6	111.93(6)	S(17)-K(4)-S(10)	78.51(5)
S(2)#1-K(3)-S(13)#6	58.58(4)	S(18)#3-K(4)-S(10)	136.62(6)
S(14)#6-K(3)-S(13)#6	59.69(4)	S(17)#7-K(4)-S(10)	76.55(5)
S(1)#5-K(3)-S(13)#6	135.30(6)	S(10)#8-K(4)-S(10)	141.33(5)
S(3)-K(3)-S(13)#6	71.88(4)	S(17)-K(4)-S(7)	82.84(5)
S(5)#5-K(3)-S(13)#6	116.10(5)	S(18)#3-K(4)-S(7)	67.49(4)
S(8)#5-K(3)-S(2)	122.48(6)	S(17)#7-K(4)-S(7)	114.82(6)

S(10)#8-K(4)-S(7)	136.36(5)	S(14)#9-K(5)-S(1)	88.76(5)
S(10)-K(4)-S(7)	69.55(4)	S(18)-K(5)-S(1)	129.05(7)
S(17)-K(4)-S(9)#8	87.37(5)	S(15)-K(5)-S(9)#10	98.60(6)
S(18)#3-K(4)-S(9)#8	134.44(6)	S(14)#9-K(5)-S(9)#10	95.73(5)
S(17)#7-K(4)-S(9)#8	62.38(4)	S(18)-K(5)-S(9)#10	81.13(5)
S(10)#8-K(4)-S(9)#8	61.28(4)	S(1)-K(5)-S(9)#10	149.41(6)
S(10)-K(4)-S(9)#8	87.31(5)	S(15)-K(5)-S(4)	142.71(6)
S(7)-K(4)-S(9)#8	156.23(6)	S(14)#9-K(5)-S(4)	66.11(5)
S(17)-K(4)-P(3)#7	119.10(5)	S(18)-K(5)-S(4)	140.66(6)
S(18)#3-K(4)-P(3)#7	132.53(5)	S(1)-K(5)-S(4)	59.71(4)
S(17)#7-K(4)-P(3)#7	31.67(4)	S(9)#10-K(5)-S(4)	94.60(5)
S(10)#8-K(4)-P(3)#7	77.13(4)	S(15)-K(5)-K(3)#2	60.74(5)
S(10)-K(4)-P(3)#7	88.02(4)	S(14)#9-K(5)-K(3)#2	101.93(5)
S(7)-K(4)-P(3)#7	145.47(5)	S(18)-K(5)-K(3)#2	92.94(5)
S(9)#8-K(4)-P(3)#7	32.36(3)	S(1)-K(5)-K(3)#2	42.91(4)
S(17)-K(4)-K(4)#7	118.02(6)	S(9)#10-K(5)-K(3)#2	159.34(5)
S(18)#3-K(4)-K(4)#7	139.71(5)	S(4)-K(5)-K(3)#2	102.28(5)
S(17)#7-K(4)-K(4)#7	36.84(3)	S(15)-K(5)-K(1)#5	95.22(5)
S(10)#8-K(4)-K(4)#7	136.30(6)	S(14)#9-K(5)-K(1)#5	117.98(5)
S(10)-K(4)-K(4)#7	41.34(4)	S(18)-K(5)-K(1)#5	158.51(6)
S(7)-K(4)-K(4)#7	87.26(4)	S(1)-K(5)-K(1)#5	70.50(4)
S(9)#8-K(4)-K(4)#7	78.31(5)	S(9)#10-K(5)-K(1)#5	80.79(4)
P(3)#7-K(4)-K(4)#7	59.38(4)	S(4)-K(5)-K(1)#5	52.74(4)
S(17)-K(4)-K(4)#8	37.63(4)	K(3)#2-K(5)-K(1)#5	99.95(4)
S(18)#3-K(4)-K(4)#8	89.04(4)	S(15)-K(5)-K(1)	37.37(4)
S(17)#7-K(4)-K(4)#8	125.11(6)	S(14)#9-K(5)-K(1)	109.66(5)
S(10)#8-K(4)-K(4)#8	42.14(3)	S(18)-K(5)-K(1)	40.16(3)
S(10)-K(4)-K(4)#8	105.13(5)	S(1)-K(5)-K(1)	109.04(5)
S(7)-K(4)-K(4)#8	116.79(5)	S(9)#10-K(5)-K(1)	97.91(4)
S(9)#8-K(4)-K(4)#8	62.92(4)	S(4)-K(5)-K(1)	167.18(6)
P(3)#7-K(4)-K(4)#8	93.78(5)	K(3)#2-K(5)-K(1)	66.14(3)
K(4)#7-K(4)-K(4)#8	131.06(6)	K(1)#5-K(5)-K(1)	132.27(4)
S(15)-K(5)-S(14)#9	145.55(7)	P(1)-S(1)-Th(1)	91.99(7)
S(15)-K(5)-S(18)	76.12(5)	P(1)-S(1)-K(3)#2	93.40(7)
S(14)#9-K(5)-S(18)	75.38(5)	Th(1)-S(1)-K(3)#2	151.28(6)
S(15)-K(5)-S(1)	94.42(6)	P(1)-S(1)-K(5)	101.78(7)

Th(1)-S(1)-K(5)	115.66(5)	Th(2)-S(8)-K(2)	103.86(5)
K(3)#2-S(1)-K(5)	90.76(5)	K(3)#2-S(8)-K(2)	111.40(6)
P(5)#5-S(2)-Th(1)	92.28(7)	P(3)#5-S(9)-Th(2)	89.70(6)
P(5)#5-S(2)-K(3)#1	102.56(7)	P(3)#5-S(9)-K(4)#7	81.22(6)
Th(1)-S(2)-K(3)#1	101.65(5)	Th(2)-S(9)-K(4)#7	103.29(5)
P(5)#5-S(2)-K(3)	142.99(7)	P(3)#5-S(9)-K(5)#10	112.59(7)
Th(1)-S(2)-K(3)	91.00(4)	Th(2)-S(9)-K(5)#10	137.60(5)
K(3)#1-S(2)-K(3)	112.82(5)	K(4)#7-S(9)-K(5)#10	115.08(5)
P(1)-S(3)-Th(1)	93.09(6)	P(2)-S(10)-Th(2)	91.82(6)
P(1)-S(3)-K(3)	160.22(8)	P(2)-S(10)-K(4)#7	111.01(7)
Th(1)-S(3)-K(3)	99.28(5)	Th(2)-S(10)-K(4)#7	110.17(5)
P(1)-S(3)-K(1)#5	87.71(7)	P(2)-S(10)-K(4)	141.37(8)
Th(1)-S(3)-K(1)#5	107.08(5)	Th(2)-S(10)-K(4)	103.86(5)
K(3)-S(3)-K(1)#5	103.14(5)	K(4)#7-S(10)-K(4)	96.52(4)
P(5)#5-S(4)-Th(1)	91.74(7)	P(2)-S(11)-Th(2)	90.85(6)
P(5)#5-S(4)-K(5)	146.96(8)	P(2)-S(11)-K(2)	78.54(7)
Th(1)-S(4)-K(5)	107.46(5)	Th(2)-S(11)-K(2)	105.00(5)
P(1)-S(5)-Th(2)	92.45(6)	P(3)#5-S(12)-Th(2)	93.45(7)
P(1)-S(5)-K(2)#4	128.46(9)	P(3)#5-S(12)-K(2)#5	91.42(7)
Th(2)-S(5)-K(2)#4	135.51(7)	Th(2)-S(12)-K(2)#5	138.22(7)
P(1)-S(5)-K(3)#2	85.83(7)	P(5)#11-S(13)-P(2)	106.87(8)
Th(2)-S(5)-K(3)#2	99.91(5)	P(5)#11-S(13)-K(3)#6	90.92(6)
K(2)#4-S(5)-K(3)#2	99.75(5)	P(2)-S(13)-K(3)#6	77.48(6)
P(1)-S(6)-Th(2)	91.86(6)	P(2)-S(14)-K(2)	91.80(8)
P(1)-S(6)-K(1)#5	95.29(7)	P(2)-S(14)-K(5)#11	121.59(8)
Th(2)-S(6)-K(1)#5	132.21(6)	K(2)-S(14)-K(5)#11	127.35(7)
P(4)-S(7)-Th(2)	89.89(6)	P(2)-S(14)-K(3)#6	87.76(7)
P(4)-S(7)-K(1)#3	88.22(7)	K(2)-S(14)-K(3)#6	105.57(6)
Th(2)-S(7)-K(1)#3	150.26(6)	K(5)#11-S(14)-K(3)#6	114.38(6)
P(4)-S(7)-K(4)	112.98(7)	P(4)-S(15)-K(1)	103.98(8)
Th(2)-S(7)-K(4)	102.62(5)	P(4)-S(15)-K(5)	142.73(9)
K(1)#3-S(7)-K(4)	105.41(5)	K(1)-S(15)-K(5)	104.06(6)
P(4)-S(8)-Th(2)	89.82(7)	P(4)-S(15)-K(1)#3	83.96(8)
P(4)-S(8)-K(3)#2	110.73(8)	K(1)-S(15)-K(1)#3	105.16(6)
Th(2)-S(8)-K(3)#2	110.13(5)	K(5)-S(15)-K(1)#3	111.53(7)
P(4)-S(8)-K(2)	127.27(8)	P(4)-S(16)-P(3)	111.97(8)

P(4)-S(16)-K(1)	91.85(6)	S(17)-P(3)-S(9)#2	118.09(9)
P(3)-S(16)-K(1)	124.83(7)	S(12)#2-P(3)-S(9)#2	107.65(9)
P(3)-S(17)-K(4)	121.07(8)	S(17)-P(3)-S(16)	113.34(9)
P(3)-S(17)-K(4)#8	92.04(7)	S(12)#2-P(3)-S(16)	109.07(8)
K(4)-S(17)-K(4)#8	105.53(4)	S(9)#2-P(3)-S(16)	95.71(8)
P(3)-S(17)-K(2)	92.86(7)	S(17)-P(3)-K(4)#8	56.29(6)
K(4)-S(17)-K(2)	130.61(7)	S(12)#2-P(3)-K(4)#8	109.78(7)
K(4)#8-S(17)-K(2)	108.05(7)	S(9)#2-P(3)-K(4)#8	66.43(6)
P(5)-S(18)-K(4)#3	101.02(8)	S(16)-P(3)-K(4)#8	140.62(7)
P(5)-S(18)-K(1)	93.47(7)	S(17)-P(3)-K(2)	55.89(6)
K(4)#3-S(18)-K(1)	114.24(6)	S(12)#2-P(3)-K(2)	56.37(6)
P(5)-S(18)-K(5)	102.03(8)	S(9)#2-P(3)-K(2)	140.41(8)
K(4)#3-S(18)-K(5)	137.54(7)	S(16)-P(3)-K(2)	123.25(8)
K(1)-S(18)-K(5)	99.40(5)	K(4)#8-P(3)-K(2)	84.48(5)
S(5)-P(1)-S(6)	105.65(8)	S(15)-P(4)-S(8)	119.11(10)
S(5)-P(1)-S(3)	113.58(9)	S(15)-P(4)-S(7)	111.47(10)
S(6)-P(1)-S(3)	111.55(9)	S(8)-P(4)-S(7)	105.57(9)
S(5)-P(1)-S(1)	109.79(9)	S(15)-P(4)-S(16)	99.46(9)
S(6)-P(1)-S(1)	110.60(9)	S(8)-P(4)-S(16)	110.17(9)
S(3)-P(1)-S(1)	105.74(8)	S(7)-P(4)-S(16)	111.04(9)
S(14)-P(2)-S(10)	116.29(10)	S(18)-P(5)-S(2)#2	112.36(9)
S(14)-P(2)-S(11)	113.87(9)	S(18)-P(5)-S(4)#2	116.61(9)
S(10)-P(2)-S(11)	107.08(8)	S(2)#2-P(5)-S(4)#2	106.77(9)
S(14)-P(2)-S(13)	112.17(9)	S(18)-P(5)-S(13)#9	113.09(9)
S(10)-P(2)-S(13)	107.71(9)	S(2)#2-P(5)-S(13)#9	107.71(9)
S(11)-P(2)-S(13)	98.02(8)	S(4)#2-P(5)-S(13)#9	99.21(9)
S(14)-P(2)-K(3)#6	60.51(6)		
S(10)-P(2)-K(3)#6	171.88(7)		
S(11)-P(2)-K(3)#6	80.83(6)		
S(13)-P(2)-K(3)#6	68.63(6)		
S(14)-P(2)-K(2)	56.86(7)		
S(10)-P(2)-K(2)	98.61(7)		
S(11)-P(2)-K(2)	69.81(7)		
S(13)-P(2)-K(2)	153.38(8)		
K(3)#6-P(2)-K(2)	85.75(4)		
S(17)-P(3)-S(12)#2	111.71(9)		

Symmetry transformations used to generate equivalent atoms:

#1 -x,y,-z+1/2 #2 x,y-1,z #3 -x+1/2,-y+1/2,-z+1

#4 -x,-y+1,-z+1 #5 x,y+1,z #6 -x,-y+2,-z+1

#7 -x+1/2,y+1/2,-z+3/2 #8 -x+1/2,y-1/2,-z+3/2

#9 x,-y+1,z-1/2 #10 -x+1/2,-y+3/2,-z+1 #11 x,-y+1,z+1/2

Table 4. Anisotropic displacement parameters ($Å^2 x\ 10^3$) for $K_{10}Th_3(P_2S_7)_4(PS_4)_2$. The anisotropic displacement factor exponent takes the form: $-2\pi^2[\ h^2\ a^{*2}U^{11} + ... + 2\ h\ k\ a^*\ b^*\ U^{12}\ ]$

	U^{11}	U^{22}	U^{33}	U^{23}	U^{13}	U^{12}
Th(1)	17(1)	13(1)	10(1)	0	8(1)	0
Th(2)	15(1)	14(1)	11(1)	0(1)	8(1)	0(1)
K(1)	37(1)	23(1)	33(1)	-1(1)	27(1)	-2(1)
K(2)	29(1)	68(1)	94(2)	-52(1)	35(1)	-8(1)
K(3)	39(1)	25(1)	23(1)	-1(1)	11(1)	-5(1)
K(4)	35(1)	28(1)	25(1)	-4(1)	19(1)	-2(1)
K(5)	61(1)	41(1)	28(1)	4(1)	25(1)	9(1)
S(1)	32(1)	14(1)	13(1)	1(1)	12(1)	0(1)
S(2)	23(1)	19(1)	20(1)	1(1)	16(1)	1(1)
S(3)	29(1)	14(1)	12(1)	0(1)	9(1)	3(1)
S(4)	31(1)	18(1)	40(1)	9(1)	28(1)	6(1)
S(5)	16(1)	27(1)	14(1)	4(1)	9(1)	0(1)
S(6)	18(1)	21(1)	17(1)	5(1)	12(1)	4(1)
S(7)	19(1)	16(1)	23(1)	-1(1)	13(1)	2(1)
S(8)	20(1)	16(1)	23(1)	-3(1)	9(1)	0(1)
S(9)	19(1)	16(1)	20(1)	1(1)	10(1)	0(1)
S(10)	20(1)	31(1)	14(1)	0(1)	11(1)	1(1)
S(11)	18(1)	35(1)	13(1)	-6(1)	10(1)	-6(1)
S(12)	20(1)	17(1)	22(1)	-4(1)	11(1)	0(1)
S(13)	32(1)	20(1)	19(1)	2(1)	20(1)	4(1)
S(14)	37(1)	20(1)	24(1)	-2(1)	22(1)	-7(1)
S(15)	87(1)	23(1)	37(1)	9(1)	51(1)	16(1)
S(16)	25(1)	15(1)	21(1)	2(1)	17(1)	3(1)
S(17)	29(1)	22(1)	19(1)	-7(1)	16(1)	-3(1)
S(18)	21(1)	30(1)	20(1)	2(1)	11(1)	1(1)
P(1)	19(1)	15(1)	12(1)	1(1)	10(1)	2(1)
P(2)	21(1)	17(1)	14(1)	-2(1)	12(1)	-2(1)
P(3)	18(1)	14(1)	15(1)	-1(1)	10(1)	-1(1)
P(4)	27(1)	15(1)	16(1)	1(1)	15(1)	3(1)
P(5)	20(1)	17(1)	16(1)	3(1)	13(1)	4(1)

Table 1. Crystal data and structure refinement for $K_5U(PS_4)_3$.

Identification code	final	
Empirical formula	$K_5U(PS_4)_3$	
Formula weight	911.16	
Temperature	163(2) K	
Wavelength	0.71073 Å	
Crystal system	Monoclinic	
Space group	P21/c	
Unit cell dimensions	a = 14.61320(10) Å	α= 90°.
	b = 17.0884(2) Å	β= 108.63°.
	c = 9.70820(10) Å	γ = 90°.
Volume	2297.31(4) $Å^3$	
Z	4	
Density (calculated)	2.634 Mg/m^3	
Absorption coefficient	9.257 mm^{-1}	
F(000)	1696	
Crystal size	0.20 x 0.19 x 0.09 mm^3	
Theta range for data collection	1.47 to 28.31°.	
Index ranges	-19<=h<=11, -22<=k<=21, -8<=l<=12	
Reflections collected	15123	
Independent reflections	5502 [R(int) = 0.0408]	
Absorption correction	SADABS	
Max. and min. transmission	0.942284 and 0.765009	
Refinement method	Full-matrix least-squares on F^2	
Data / restraints / parameters	5501 / 0 / 190	
Goodness-of-fit on F^2	1.187	
Final R indices [I>2sigma(I)]	R1 = 0.0376, wR2 = 0.0681	
R indices (all data)	R1 = 0.0618, wR2 = 0.0744	
Extinction coefficient	0.00033(5)	
Largest diff. peak and hole	2.863 and -1.793 $e.Å^{-3}$	

Table 2. Atomic coordinates (x 10^4) and equivalent isotropic displacement parameters ($Å^2$x 10^3) for $K_5U(PS_4)_3$. U(eq) is defined as one third of the trace of the orthogonalized U^{ij} tensor.

	x	y	z	U(eq)
U(1)	3337(1)	5008(1)	8902(1)	12(1)
K(1)	2083(3)	8052(2)	6065(4)	37(1)
K(1A)	2306(2)	8070(2)	6748(4)	26(1)
K(2)	143(1)	4704(1)	2153(2)	26(1)
K(3)	-765(1)	7037(1)	3429(2)	32(1)
K(4)	3140(1)	4948(1)	4432(2)	33(1)
K(5)	5531(1)	7008(1)	7185(2)	47(1)
S(1)	4058(1)	6461(1)	10349(2)	20(1)
S(2)	4783(1)	4759(1)	11717(2)	18(1)
S(3)	3738(1)	3792(1)	7182(2)	28(1)
S(4)	2790(1)	3512(1)	9537(2)	18(1)
S(5)	2137(1)	5131(1)	10655(2)	17(1)
S(6)	1585(1)	4860(1)	6577(2)	17(1)
S(7)	3089(1)	6273(1)	6982(2)	21(1)
S(8)	820(1)	6721(1)	6840(2)	28(1)
S(9)	1303(1)	6161(1)	3853(2)	28(1)
S(10)	4361(2)	6275(1)	13892(2)	46(1)
S(11)	2288(1)	3488(1)	12697(2)	27(1)
S(12)	509(1)	3663(1)	9574(2)	21(1)
P(1)	1628(1)	6029(1)	6009(2)	15(1)
P(2)	4835(1)	5943(1)	12274(2)	18(1)
P(3)	1900(1)	3921(1)	10660(2)	16(1)

Table 3. Bond lengths [Å] and angles [°] for $K_5U(PS_4)_3$.

U(1)-S(7)	2.802(2)	K(2)-S(6)#6	3.231(2)
U(1)-S(4)	2.8051(15)	K(2)-S(12)#6	3.238(2)
U(1)-S(5)	2.814(2)	K(2)-S(12)#7	3.251(2)
U(1)-S(6)	2.8325(15)	K(2)-S(5)#6	3.578(2)
U(1)-S(3)	2.842(2)	K(2)-P(3)#7	3.587(2)
U(1)-S(1)	2.8809(15)	K(2)-S(11)#7	3.655(2)
U(1)-S(2)	2.9030(15)	K(2)-S(5)#7	3.721(2)
U(1)-S(2)#1	3.021(2)	K(2)-P(1)#6	3.794(2)
U(1)-K(4)	4.258(2)	K(2)-K(2)#8	4.190(3)
K(1)-K(1A)	0.639(4)	K(2)-K(4)	4.251(2)
K(1)-S(5)#2	3.133(4)	K(3)-S(11)#4	3.278(2)
K(1)-S(8)	3.168(4)	K(3)-S(9)	3.278(2)
K(1)-S(1)#2	3.285(4)	K(3)-S(12)#6	3.282(2)
K(1)-S(7)	3.371(4)	K(3)-S(12)#4	3.341(2)
K(1)-P(1)	3.518(4)	K(3)-S(8)	3.423(2)
K(1)-S(9)#3	3.523(4)	K(3)-S(6)#6	3.455(2)
K(1)-S(10)#2	3.755(5)	K(3)-S(4)#6	3.533(2)
K(1)-S(12)#4	3.785(4)	K(3)-P(3)#4	3.851(2)
K(1)-K(3)	4.481(4)	K(3)-K(2)#5	4.717(2)
K(1)-K(4)#3	4.639(4)	K(4)-S(10)#7	3.033(3)
K(1)-K(2)#5	4.670(4)	K(4)-S(11)#7	3.045(2)
K(1A)-S(9)#3	3.158(4)	K(4)-S(3)	3.209(2)
K(1A)-S(8)	3.188(4)	K(4)-S(9)	3.295(2)
K(1A)-S(5)#2	3.235(3)	K(4)-S(7)	3.373(2)
K(1A)-S(10)#2	3.257(4)	K(4)-S(5)#7	3.502(2)
K(1A)-S(7)	3.260(3)	K(4)-S(6)	3.542(2)
K(1A)-S(1)#2	3.356(4)	K(4)-P(1)	3.578(2)
K(1A)-P(1)	3.634(3)	K(4)-K(1A)#2	4.209(4)
K(1A)-K(4)#3	4.209(4)	K(4)-K(5)#9	4.400(2)
K(1A)-K(1)#3	4.714(4)	K(5)-S(3)#10	3.225(2)
K(1A)-K(5)	4.940(4)	K(5)-S(11)#1	3.266(3)
K(1A)-K(3)	4.940(4)	K(5)-S(2)#1	3.282(2)
K(2)-S(8)#6	3.121(2)	K(5)-S(10)#7	3.350(3)
K(2)-S(9)	3.164(2)	K(5)-S(4)#1	3.457(2)

K(5)-S(1)#2	3.494(2)	S(11)-P(3)	2.015(2)
K(5)-P(2)#2	3.655(2)	S(11)-K(4)#12	3.045(2)
K(5)-S(7)	3.727(3)	S(11)-K(5)#1	3.266(3)
K(5)-K(4)#9	4.400(2)	S(11)-K(3)#13	3.278(2)
S(1)-P(2)	2.052(2)	S(11)-K(2)#12	3.655(2)
S(1)-K(1)#3	3.285(4)	S(12)-P(3)	2.017(2)
S(1)-K(1A)#3	3.356(4)	S(12)-K(2)#6	3.238(2)
S(1)-K(5)#3	3.494(2)	S(12)-K(2)#12	3.251(2)
S(2)-P(2)	2.089(2)	S(12)-K(3)#6	3.282(2)
S(2)-U(1)#1	3.021(2)	S(12)-K(3)#13	3.341(2)
S(2)-K(5)#1	3.283(2)	S(12)-K(1)#13	3.785(4)
S(3)-P(2)#1	2.032(2)	P(1)-K(2)#6	3.794(2)
S(3)-K(5)#11	3.225(2)	P(2)-S(3)#1	2.032(2)
S(4)-P(3)	2.068(2)	P(2)-K(5)#3	3.655(2)
S(4)-K(5)#1	3.457(2)	P(3)-K(2)#12	3.587(2)
S(4)-K(3)#6	3.533(2)	P(3)-K(3)#13	3.851(2)
S(5)-P(3)	2.098(2)	S(7)-U(1)-S(4)	149.79(5)
S(5)-K(1)#3	3.133(4)	S(7)-U(1)-S(5)	111.83(5)
S(5)-K(1A)#3	3.235(3)	S(4)-U(1)-S(5)	70.08(4)
S(5)-K(4)#12	3.502(2)	S(7)-U(1)-S(6)	69.31(4)
S(5)-K(2)#6	3.578(2)	S(4)-U(1)-S(6)	81.11(4)
S(5)-K(2)#12	3.721(2)	S(5)-U(1)-S(6)	84.80(5)
S(6)-P(1)	2.078(2)	S(7)-U(1)-S(3)	100.37(5)
S(6)-K(2)#6	3.231(2)	S(4)-U(1)-S(3)	65.75(5)
S(6)-K(3)#6	3.455(2)	S(5)-U(1)-S(3)	134.06(5)
S(7)-P(1)	2.083(2)	S(6)-U(1)-S(3)	76.70(5)
S(8)-P(1)	2.012(2)	S(7)-U(1)-S(1)	66.97(5)
S(8)-K(2)#6	3.121(2)	S(4)-U(1)-S(1)	139.81(5)
S(9)-P(1)	2.005(2)	S(5)-U(1)-S(1)	80.94(4)
S(9)-K(1A)#2	3.158(4)	S(6)-U(1)-S(1)	124.21(4)
S(9)-K(1)#2	3.523(4)	S(3)-U(1)-S(1)	143.55(5)
S(10)-P(2)	1.991(3)	S(7)-U(1)-S(2)	129.79(4)
S(10)-K(4)#12	3.033(3)	S(4)-U(1)-S(2)	80.35(4)
S(10)-K(1A)#3	3.257(4)	S(5)-U(1)-S(2)	81.30(5)
S(10)-K(5)#12	3.350(3)	S(6)-U(1)-S(2)	159.76(5)
S(10)-K(1)#3	3.755(5)	S(3)-U(1)-S(2)	102.78(5)

S(1)-U(1)-S(2)	67.94(4)	P(1)-K(1)-S(9)#3	106.33(11)
S(7)-U(1)-S(2)#1	72.43(4)	K(1A)-K(1)-S(10)#2	35.7(5)
S(4)-U(1)-S(2)#1	120.30(4)	S(5)#2-K(1)-S(10)#2	74.78(9)
S(5)-U(1)-S(2)#1	153.20(4)	S(8)-K(1)-S(10)#2	119.60(12)
S(6)-U(1)-S(2)#1	120.07(4)	S(1)#2-K(1)-S(10)#2	56.17(7)
S(3)-U(1)-S(2)#1	66.90(5)	S(7)-K(1)-S(10)#2	82.68(9)
S(1)-U(1)-S(2)#1	76.65(4)	P(1)-K(1)-S(10)#2	115.52(11)
S(2)-U(1)-S(2)#1	76.80(5)	S(9)#3-K(1)-S(10)#2	75.55(9)
S(7)-U(1)-K(4)	52.26(4)	K(1A)-K(1)-S(12)#4	108.0(5)
S(4)-U(1)-K(4)	105.70(4)	S(5)#2-K(1)-S(12)#4	76.72(9)
S(5)-U(1)-K(4)	139.98(4)	S(8)-K(1)-S(12)#4	66.97(8)
S(6)-U(1)-K(4)	55.67(4)	S(1)#2-K(1)-S(12)#4	142.82(12)
S(3)-U(1)-K(4)	48.91(4)	S(7)-K(1)-S(12)#4	128.43(11)
S(1)-U(1)-K(4)	114.37(4)	P(1)-K(1)-S(12)#4	95.41(10)
S(2)-U(1)-K(4)	138.39(4)	S(9)#3-K(1)-S(12)#4	57.86(7)
S(2)#1-U(1)-K(4)	64.52(4)	S(10)#2-K(1)-S(12)#4	130.01(11)
K(1A)-K(1)-S(5)#2	93.4(5)	K(1A)-K(1)-K(3)	133.1(5)
K(1A)-K(1)-S(8)	86.0(5)	S(5)#2-K(1)-K(3)	111.57(11)
S(5)#2-K(1)-S(8)	141.44(14)	S(8)-K(1)-K(3)	49.61(7)
K(1A)-K(1)-S(1)#2	90.9(5)	S(1)#2-K(1)-K(3)	134.10(12)
S(5)#2-K(1)-S(1)#2	70.30(8)	S(7)-K(1)-K(3)	92.79(9)
S(8)-K(1)-S(1)#2	148.21(13)	P(1)-K(1)-K(3)	58.27(6)
K(1A)-K(1)-S(7)	74.6(5)	S(9)#3-K(1)-K(3)	96.73(9)
S(5)#2-K(1)-S(7)	154.21(14)	S(10)#2-K(1)-K(3)	168.77(11)
S(8)-K(1)-S(7)	61.80(8)	S(12)#4-K(1)-K(3)	46.75(5)
S(1)#2-K(1)-S(7)	86.87(10)	K(1A)-K(1)-K(4)#3	44.7(5)
K(1A)-K(1)-P(1)	95.4(5)	S(5)#2-K(1)-K(4)#3	48.99(6)
S(5)#2-K(1)-P(1)	169.70(14)	S(8)-K(1)-K(4)#3	116.74(11)
S(8)-K(1)-P(1)	34.52(5)	S(1)#2-K(1)-K(4)#3	81.09(8)
S(1)#2-K(1)-P(1)	114.84(11)	S(7)-K(1)-K(4)#3	117.33(11)
S(7)-K(1)-P(1)	35.11(5)	P(1)-K(1)-K(4)#3	138.89(11)
K(1A)-K(1)-S(9)#3	50.8(5)	S(9)#3-K(1)-K(4)#3	45.09(6)
S(5)#2-K(1)-S(9)#3	75.34(9)	S(10)#2-K(1)-K(4)#3	40.68(5)
S(8)-K(1)-S(9)#3	74.68(9)	S(12)#4-K(1)-K(4)#3	90.18(8)
S(1)#2-K(1)-S(9)#3	126.01(12)	K(3)-K(1)-K(4)#3	136.66(9)
S(7)-K(1)-S(9)#3	111.25(11)	K(1A)-K(1)-K(2)#5	132.9(5)

S(5)#2-K(1)-K(2)#5	49.97(6)	S(7)-K(1A)-P(1)	34.63(5)
S(8)-K(1)-K(2)#5	105.01(10)	S(1)#2-K(1A)-P(1)	110.15(9)
S(1)#2-K(1)-K(2)#5	100.18(9)	K(1)-K(1A)-K(4)#3	129.1(5)
S(7)-K(1)-K(2)#5	150.88(12)	S(9)#3-K(1A)-K(4)#3	50.71(6)
P(1)-K(1)-K(2)#5	119.73(10)	S(8)-K(1A)-K(4)#3	129.04(10)
S(9)#3-K(1)-K(2)#5	87.49(8)	S(5)#2-K(1A)-K(4)#3	54.23(6)
S(10)#2-K(1)-K(2)#5	124.72(9)	S(10)#2-K(1A)-K(4)#3	45.77(6)
S(12)#4-K(1)-K(2)#5	43.69(5)	S(7)-K(1A)-K(4)#3	133.55(11)
K(3)-K(1)-K(2)#5	62.02(6)	S(1)#2-K(1A)-K(4)#3	87.18(8)
K(4)#3-K(1)-K(2)#5	91.74(7)	P(1)-K(1A)-K(4)#3	154.31(10)
K(1)-K(1A)-S(9)#3	120.2(5)	K(1)-K(1A)-K(1)#3	138.2(5)
K(1)-K(1A)-S(8)	82.4(5)	S(9)#3-K(1A)-K(1)#3	54.24(8)
S(9)#3-K(1A)-S(8)	79.74(9)	S(8)-K(1A)-K(1)#3	55.92(8)
K(1)-K(1A)-S(5)#2	75.2(5)	S(5)#2-K(1A)-K(1)#3	131.18(10)
S(9)#3-K(1A)-S(5)#2	79.28(8)	S(10)#2-K(1A)-K(1)#3	83.29(8)
S(8)-K(1A)-S(5)#2	135.64(12)	S(7)-K(1A)-K(1)#3	71.17(7)
K(1)-K(1A)-S(10)#2	137.7(6)	S(1)#2-K(1A)-K(1)#3	137.33(11)
S(9)#3-K(1A)-S(10)#2	88.13(10)	P(1)-K(1A)-K(1)#3	72.12(7)
S(8)-K(1A)-S(10)#2	136.70(12)	K(4)#3-K(1A)-K(1)#3	82.28(7)
S(5)#2-K(1A)-S(10)#2	80.89(9)	K(1)-K(1A)-K(5)	103.2(5)
K(1)-K(1A)-S(7)	94.5(5)	S(9)#3-K(1A)-K(5)	136.45(10)
S(9)#3-K(1A)-S(7)	124.92(11)	S(8)-K(1A)-K(5)	111.79(8)
S(8)-K(1A)-S(7)	62.86(7)	S(5)#2-K(1A)-K(5)	110.38(9)
S(5)#2-K(1A)-S(7)	154.99(12)	S(10)#2-K(1A)-K(5)	53.96(6)
S(10)#2-K(1A)-S(7)	92.71(10)	S(7)-K(1A)-K(5)	48.98(6)
K(1)-K(1A)-S(1)#2	78.1(5)	S(1)#2-K(1A)-K(5)	44.97(5)
S(9)#3-K(1A)-S(1)#2	137.27(11)	P(1)-K(1A)-K(5)	81.76(7)
S(8)-K(1A)-S(1)#2	142.98(12)	K(4)#3-K(1A)-K(5)	99.36(7)
S(5)#2-K(1A)-S(1)#2	68.21(7)	K(1)#3-K(1A)-K(5)	96.26(8)
S(10)#2-K(1A)-S(1)#2	60.64(7)	K(1)-K(1A)-K(3)	41.5(5)
S(7)-K(1A)-S(1)#2	87.53(9)	S(9)#3-K(1A)-K(3)	93.33(8)
K(1)-K(1A)-P(1)	74.5(5)	S(8)-K(1A)-K(3)	43.50(6)
S(9)#3-K(1A)-P(1)	111.94(10)	S(5)#2-K(1A)-K(3)	99.63(8)
S(8)-K(1A)-P(1)	33.50(5)	S(10)#2-K(1A)-K(3)	178.52(11)
S(5)#2-K(1A)-P(1)	149.27(12)	S(7)-K(1A)-K(3)	86.24(7)
S(10)#2-K(1A)-P(1)	126.38(11)	S(1)#2-K(1A)-K(3)	118.23(9)

P(1)-K(1A)-K(3)	52.74(5)	S(12)#7-K(2)-S(5)#7	57.60(4)
K(4)#3-K(1A)-K(3)	135.61(8)	S(5)#6-K(2)-S(5)#7	109.96(5)
K(1)#3-K(1A)-K(3)	97.35(8)	P(3)#7-K(2)-S(5)#7	33.30(3)
K(5)-K(1A)-K(3)	124.59(7)	S(11)#7-K(2)-S(5)#7	54.95(4)
S(8)#6-K(2)-S(9)	132.08(7)	S(8)#6-K(2)-P(1)#6	31.98(4)
S(8)#6-K(2)-S(6)#6	64.83(5)	S(9)-K(2)-P(1)#6	110.28(6)
S(9)-K(2)-S(6)#6	88.46(6)	S(6)#6-K(2)-P(1)#6	33.19(4)
S(8)#6-K(2)-S(12)#6	138.32(7)	S(12)#6-K(2)-P(1)#6	113.32(5)
S(9)-K(2)-S(12)#6	67.18(5)	S(12)#7-K(2)-P(1)#6	119.11(6)
S(6)#6-K(2)-S(12)#6	82.10(5)	S(5)#6-K(2)-P(1)#6	77.03(4)
S(8)#6-K(2)-S(12)#7	90.95(6)	P(3)#7-K(2)-P(1)#6	138.65(5)
S(9)-K(2)-S(12)#7	129.75(6)	S(11)#7-K(2)-P(1)#6	115.25(5)
S(6)#6-K(2)-S(12)#7	139.56(6)	S(5)#7-K(2)-P(1)#6	170.18(5)
S(12)#6-K(2)-S(12)#7	99.56(5)	S(8)#6-K(2)-K(2)#8	126.16(7)
S(8)#6-K(2)-S(5)#6	84.10(5)	S(9)-K(2)-K(2)#8	101.33(6)
S(9)-K(2)-S(5)#6	123.29(6)	S(6)#6-K(2)-K(2)#8	118.96(6)
S(6)#6-K(2)-S(5)#6	67.79(5)	S(12)#6-K(2)-K(2)#8	49.92(4)
S(12)#6-K(2)-S(5)#6	59.29(4)	S(12)#7-K(2)-K(2)#8	49.64(4)
S(12)#7-K(2)-S(5)#6	78.39(5)	S(5)#6-K(2)-K(2)#8	56.58(4)
S(8)#6-K(2)-P(3)#7	106.75(6)	P(3)#7-K(2)-K(2)#8	62.81(4)
S(9)-K(2)-P(3)#7	99.84(6)	S(11)#7-K(2)-K(2)#8	95.10(6)
S(6)#6-K(2)-P(3)#7	171.08(6)	S(5)#7-K(2)-K(2)#8	53.38(4)
S(12)#6-K(2)-P(3)#7	104.04(5)	P(1)#6-K(2)-K(2)#8	133.11(6)
S(12)#7-K(2)-P(3)#7	33.85(4)	S(8)#6-K(2)-K(4)	113.97(6)
S(5)#6-K(2)-P(3)#7	109.52(5)	S(9)-K(2)-K(4)	50.18(4)
S(8)#6-K(2)-S(11)#7	87.88(5)	S(6)#6-K(2)-K(4)	125.42(5)
S(9)-K(2)-S(11)#7	94.58(6)	S(12)#6-K(2)-K(4)	105.59(5)
S(6)#6-K(2)-S(11)#7	144.52(6)	S(12)#7-K(2)-K(4)	93.36(5)
S(12)#6-K(2)-S(11)#7	131.41(6)	S(5)#6-K(2)-K(4)	160.49(5)
S(12)#7-K(2)-S(11)#7	57.04(4)	P(3)#7-K(2)-K(4)	59.67(4)
S(5)#6-K(2)-S(11)#7	134.55(6)	S(11)#7-K(2)-K(4)	44.52(4)
P(3)#7-K(2)-S(11)#7	32.29(4)	S(5)#7-K(2)-K(4)	51.59(4)
S(8)#6-K(2)-S(5)#7	139.75(6)	P(1)#6-K(2)-K(4)	122.13(5)
S(9)-K(2)-S(5)#7	72.15(5)	K(2)#8-K(2)-K(4)	104.66(5)
S(6)#6-K(2)-S(5)#7	155.35(6)	S(11)#4-K(3)-S(9)	152.58(8)
S(12)#6-K(2)-S(5)#7	76.47(5)	S(11)#4-K(3)-S(12)#6	103.72(6)

S(9)-K(3)-S(12)#6	65.36(5)	S(12)#6-K(3)-K(2)	45.97(4)
S(11)#4-K(3)-S(12)#4	60.14(5)	S(12)#4-K(3)-K(2)	155.37(5)
S(9)-K(3)-S(12)#4	112.29(6)	S(8)-K(3)-K(2)	87.63(4)
S(12)#6-K(3)-S(12)#4	142.69(7)	S(6)#6-K(3)-K(2)	45.63(4)
S(11)#4-K(3)-S(8)	128.29(6)	S(4)#6-K(3)-K(2)	77.55(4)
S(9)-K(3)-S(8)	59.64(5)	P(3)#4-K(3)-K(2)	172.07(5)
S(12)#6-K(3)-S(8)	124.60(6)	K(1)-K(3)-K(2)	101.47(6)
S(12)#4-K(3)-S(8)	69.79(5)	S(11)#4-K(3)-K(2)#5	50.59(4)
S(11)#4-K(3)-S(6)#6	120.76(6)	S(9)-K(3)-K(2)#5	104.54(5)
S(9)-K(3)-S(6)#6	82.93(5)	S(12)#6-K(3)-K(2)#5	99.48(5)
S(12)#6-K(3)-S(6)#6	78.13(5)	S(12)#4-K(3)-K(2)#5	43.56(4)
S(12)#4-K(3)-S(6)#6	139.13(7)	S(8)-K(3)-K(2)#5	99.88(5)
S(8)-K(3)-S(6)#6	88.89(5)	S(6)#6-K(3)-K(2)#5	170.53(5)
S(11)#4-K(3)-S(4)#6	68.06(5)	S(4)#6-K(3)-K(2)#5	107.59(5)
S(9)-K(3)-S(4)#6	118.67(6)	P(3)#4-K(3)-K(2)#5	48.20(3)
S(12)#6-K(3)-S(4)#6	58.84(4)	K(1)-K(3)-K(2)#5	60.96(5)
S(12)#4-K(3)-S(4)#6	127.08(6)	K(2)-K(3)-K(2)#5	137.57(4)
S(8)-K(3)-S(4)#6	151.42(6)	S(11)#4-K(3)-K(1A)	108.99(6)
S(6)#6-K(3)-S(4)#6	63.26(4)	S(9)-K(3)-K(1A)	58.16(5)
S(11)#4-K(3)-P(3)#4	31.55(4)	S(12)#6-K(3)-K(1A)	111.85(6)
S(9)-K(3)-P(3)#4	143.15(6)	S(12)#4-K(3)-K(1A)	54.14(5)
S(12)#6-K(3)-P(3)#4	133.49(6)	S(8)-K(3)-K(1A)	39.87(5)
S(12)#4-K(3)-P(3)#4	31.56(4)	S(6)#6-K(3)-K(1A)	125.36(6)
S(8)-K(3)-P(3)#4	96.77(5)	S(4)#6-K(3)-K(1A)	167.50(7)
S(6)#6-K(3)-P(3)#4	127.60(6)	P(3)#4-K(3)-K(1A)	85.39(5)
S(4)#6-K(3)-P(3)#4	95.67(5)	K(1)-K(3)-K(1A)	5.42(6)
S(11)#4-K(3)-K(1)	107.76(7)	K(2)-K(3)-K(1A)	102.13(5)
S(9)-K(3)-K(1)	56.94(6)	K(2)#5-K(3)-K(1A)	64.08(5)
S(12)#6-K(3)-K(1)	107.46(7)	S(10)#7-K(4)-S(11)#7	132.56(7)
S(12)#4-K(3)-K(1)	55.60(6)	S(10)#7-K(4)-S(3)	125.82(7)
S(8)-K(3)-K(1)	44.83(6)	S(11)#7-K(4)-S(3)	84.85(6)
S(6)#6-K(3)-K(1)	128.51(7)	S(10)#7-K(4)-S(9)	89.58(7)
S(4)#6-K(3)-K(1)	162.09(7)	S(11)#7-K(4)-S(9)	104.69(6)
P(3)#4-K(3)-K(1)	86.26(6)	S(3)-K(4)-S(9)	121.28(7)
S(11)#4-K(3)-K(2)	143.82(5)	S(10)#7-K(4)-S(7)	77.12(6)
S(9)-K(3)-K(2)	44.67(4)	S(11)#7-K(4)-S(7)	148.74(7)

S(3)-K(4)-S(7)	82.34(5)	K(1A)#2-K(4)-K(2)	73.15(6)
S(9)-K(4)-S(7)	59.68(5)	S(10)#7-K(4)-U(1)	107.85(5)
S(10)#7-K(4)-S(5)#7	79.91(6)	S(11)#7-K(4)-U(1)	117.77(6)
S(11)#7-K(4)-S(5)#7	62.19(5)	S(3)-K(4)-U(1)	41.87(4)
S(3)-K(4)-S(5)#7	146.89(6)	S(9)-K(4)-U(1)	86.82(4)
S(9)-K(4)-S(5)#7	73.70(5)	S(7)-K(4)-U(1)	41.06(3)
S(7)-K(4)-S(5)#7	127.49(6)	S(5)#7-K(4)-U(1)	159.15(5)
S(10)#7-K(4)-S(6)	131.05(7)	S(6)-K(4)-U(1)	41.32(3)
S(11)#7-K(4)-S(6)	93.69(6)	P(1)-K(4)-U(1)	53.21(3)
S(3)-K(4)-S(6)	62.63(5)	K(1A)#2-K(4)-U(1)	121.57(6)
S(9)-K(4)-S(6)	59.05(5)	K(2)-K(4)-U(1)	104.81(4)
S(7)-K(4)-S(6)	55.14(4)	S(10)#7-K(4)-K(5)#9	98.93(6)
S(5)#7-K(4)-S(6)	119.11(6)	S(11)#7-K(4)-K(5)#9	47.89(5)
S(10)#7-K(4)-P(1)	99.54(6)	S(3)-K(4)-K(5)#9	78.19(5)
S(11)#7-K(4)-P(1)	117.39(7)	S(9)-K(4)-K(5)#9	147.72(6)
S(3)-K(4)-P(1)	90.17(5)	S(7)-K(4)-K(5)#9	152.57(6)
S(9)-K(4)-P(1)	33.61(4)	S(5)#7-K(4)-K(5)#9	77.24(4)
S(7)-K(4)-P(1)	34.71(4)	S(6)-K(4)-K(5)#9	128.09(6)
S(5)#7-K(4)-P(1)	107.02(5)	P(1)-K(4)-K(5)#9	161.50(6)
S(6)-K(4)-P(1)	33.93(4)	K(1A)#2-K(4)-K(5)#9	117.64(6)
S(10)#7-K(4)-K(1A)#2	50.31(7)	K(2)-K(4)-K(5)#9	103.80(4)
S(11)#7-K(4)-K(1A)#2	109.29(7)	U(1)-K(4)-K(5)#9	119.23(4)
S(3)-K(4)-K(1A)#2	163.37(7)	S(3)#10-K(5)-S(11)#1	88.76(6)
S(9)-K(4)-K(1A)#2	47.89(6)	S(3)#10-K(5)-S(2)#1	151.66(8)
S(7)-K(4)-K(1A)#2	81.05(6)	S(11)#1-K(5)-S(2)#1	89.19(6)
S(5)#7-K(4)-K(1A)#2	48.56(5)	S(3)#10-K(5)-S(10)#7	124.91(8)
S(6)-K(4)-K(1A)#2	106.54(6)	S(11)#1-K(5)-S(10)#7	97.53(7)
P(1)-K(4)-K(1A)#2	75.72(6)	S(2)#1-K(5)-S(10)#7	83.37(6)
S(10)#7-K(4)-K(2)	123.28(7)	S(3)#10-K(5)-S(4)#1	88.45(6)
S(11)#7-K(4)-K(2)	57.32(5)	S(11)#1-K(5)-S(4)#1	60.21(5)
S(3)-K(4)-K(2)	109.50(6)	S(2)#1-K(5)-S(4)#1	66.20(5)
S(9)-K(4)-K(2)	47.52(4)	S(10)#7-K(5)-S(4)#1	141.12(7)
S(7)-K(4)-K(2)	100.80(5)	S(3)#10-K(5)-S(1)#2	60.11(5)
S(5)#7-K(4)-K(2)	56.38(4)	S(11)#1-K(5)-S(1)#2	130.35(7)
S(6)-K(4)-K(2)	63.49(4)	S(2)#1-K(5)-S(1)#2	136.69(7)
P(1)-K(4)-K(2)	66.35(4)	S(10)#7-K(5)-S(1)#2	75.49(6)

S(4)#1-K(5)-S(1)#2	143.39(7)	K(1)#3-S(1)-K(1A)#3	10.98(7)
S(3)#10-K(5)-P(2)#2	33.62(4)	P(2)-S(1)-K(5)#3	77.68(7)
S(11)#1-K(5)-P(2)#2	121.58(7)	U(1)-S(1)-K(5)#3	164.58(7)
S(2)#1-K(5)-P(2)#2	143.60(8)	K(1)#3-S(1)-K(5)#3	98.16(8)
S(10)#7-K(5)-P(2)#2	108.64(7)	K(1A)#3-S(1)-K(5)#3	92.27(8)
S(4)#1-K(5)-P(2)#2	110.21(6)	P(2)-S(2)-U(1)	93.27(7)
S(1)#2-K(5)-P(2)#2	33.27(4)	P(2)-S(2)-U(1)#1	87.94(7)
S(3)#10-K(5)-S(7)	125.59(7)	U(1)-S(2)-U(1)#1	103.20(5)
S(11)#1-K(5)-S(7)	145.25(6)	P(2)-S(2)-K(5)#1	143.52(9)
S(2)#1-K(5)-S(7)	58.46(5)	U(1)-S(2)-K(5)#1	107.77(6)
S(10)#7-K(5)-S(7)	68.63(6)	U(1)#1-S(2)-K(5)#1	114.57(6)
S(4)#1-K(5)-S(7)	110.38(6)	P(2)#1-S(3)-U(1)	94.11(8)
S(1)#2-K(5)-S(7)	78.59(5)	P(2)#1-S(3)-K(4)	93.63(8)
P(2)#2-K(5)-S(7)	93.17(6)	U(1)-S(3)-K(4)	89.22(5)
S(3)#10-K(5)-K(4)#9	128.99(7)	P(2)#1-S(3)-K(5)#11	84.88(8)
S(11)#1-K(5)-K(4)#9	43.77(4)	U(1)-S(3)-K(5)#11	134.22(8)
S(2)#1-K(5)-K(4)#9	62.63(4)	K(4)-S(3)-K(5)#11	136.56(7)
S(10)#7-K(5)-K(4)#9	61.59(6)	P(3)-S(4)-U(1)	94.55(7)
S(4)#1-K(5)-K(4)#9	82.46(5)	P(3)-S(4)-K(5)#1	88.98(7)
S(1)#2-K(5)-K(4)#9	131.07(6)	U(1)-S(4)-K(5)#1	105.56(5)
P(2)#2-K(5)-K(4)#9	153.39(7)	P(3)-S(4)-K(3)#6	90.88(7)
S(7)-K(5)-K(4)#9	104.44(5)	U(1)-S(4)-K(3)#6	106.62(5)
S(3)#10-K(5)-K(1A)	85.29(6)	K(5)#1-S(4)-K(3)#6	147.73(6)
S(11)#1-K(5)-K(1A)	172.87(7)	P(3)-S(5)-U(1)	93.59(7)
S(2)#1-K(5)-K(1A)	97.91(6)	P(3)-S(5)-K(1)#3	164.96(11)
S(10)#7-K(5)-K(1A)	82.73(7)	U(1)-S(5)-K(1)#3	101.34(8)
S(4)#1-K(5)-K(1A)	123.42(7)	P(3)-S(5)-K(1A)#3	158.68(10)
S(1)#2-K(5)-K(1A)	42.76(5)	U(1)-S(5)-K(1A)#3	105.79(7)
P(2)#2-K(5)-K(1A)	52.06(5)	K(1)#3-S(5)-K(1A)#3	11.38(7)
S(7)-K(5)-K(1A)	41.29(5)	P(3)-S(5)-K(4)#12	85.61(7)
K(4)#9-K(5)-K(1A)	140.01(6)	U(1)-S(5)-K(4)#12	119.53(6)
P(2)-S(1)-U(1)	94.73(7)	K(1)#3-S(5)-K(4)#12	88.54(9)
P(2)-S(1)-K(1)#3	100.61(10)	K(1A)#3-S(5)-K(4)#12	77.22(7)
U(1)-S(1)-K(1)#3	96.42(8)	P(3)-S(5)-K(2)#6	88.04(7)
P(2)-S(1)-K(1A)#3	90.33(9)	U(1)-S(5)-K(2)#6	98.83(5)
U(1)-S(1)-K(1A)#3	101.27(7)	K(1)#3-S(5)-K(2)#6	87.92(8)

K(1A)#3-S(5)-K(2)#6	97.48(8)	P(1)-S(8)-K(1A)	85.49(9)
K(4)#12-S(5)-K(2)#6	141.40(6)	K(2)#6-S(8)-K(1A)	162.20(10)
P(3)-S(5)-K(2)#12	69.84(6)	K(1)-S(8)-K(1A)	11.54(7)
U(1)-S(5)-K(2)#12	159.81(6)	P(1)-S(8)-K(3)	90.44(8)
K(1)#3-S(5)-K(2)#12	95.18(8)	K(2)#6-S(8)-K(3)	101.11(6)
K(1A)#3-S(5)-K(2)#12	92.63(7)	K(1)-S(8)-K(3)	85.56(9)
K(4)#12-S(5)-K(2)#12	72.04(5)	K(1A)-S(8)-K(3)	96.63(8)
K(2)#6-S(5)-K(2)#12	70.04(5)	P(1)-S(9)-K(1A)#2	135.88(11)
P(1)-S(6)-U(1)	91.67(6)	P(1)-S(9)-K(2)	111.44(9)
P(1)-S(6)-K(2)#6	88.47(7)	K(1A)#2-S(9)-K(2)	105.78(8)
U(1)-S(6)-K(2)#6	107.02(6)	P(1)-S(9)-K(3)	94.82(8)
P(1)-S(6)-K(3)#6	160.25(8)	K(1A)#2-S(9)-K(3)	109.18(8)
U(1)-S(6)-K(3)#6	108.03(5)	K(2)-S(9)-K(3)	88.57(6)
K(2)#6-S(6)-K(3)#6	84.51(5)	P(1)-S(9)-K(4)	80.96(7)
P(1)-S(6)-K(4)	73.97(7)	K(1A)#2-S(9)-K(4)	81.40(8)
U(1)-S(6)-K(4)	83.01(5)	K(2)-S(9)-K(4)	82.30(6)
K(2)#6-S(6)-K(4)	160.22(6)	K(3)-S(9)-K(4)	167.68(7)
K(3)#6-S(6)-K(4)	109.02(5)	P(1)-S(9)-K(1)#2	144.86(11)
P(1)-S(7)-U(1)	92.45(7)	K(1A)#2-S(9)-K(1)#2	9.03(8)
P(1)-S(7)-K(1A)	82.57(9)	K(2)-S(9)-K(1)#2	98.65(8)
U(1)-S(7)-K(1A)	137.82(9)	K(3)-S(9)-K(1)#2	103.93(8)
P(1)-S(7)-K(1)	76.31(9)	K(4)-S(9)-K(1)#2	85.69(8)
U(1)-S(7)-K(1)	145.52(9)	P(2)-S(10)-K(4)#12	107.16(10)
K(1A)-S(7)-K(1)	10.90(7)	P(2)-S(10)-K(1A)#3	94.36(11)
P(1)-S(7)-K(4)	78.03(7)	K(4)#12-S(10)-K(1A)#3	83.92(8)
U(1)-S(7)-K(4)	86.67(5)	P(2)-S(10)-K(5)#12	131.27(11)
K(1A)-S(7)-K(4)	132.13(8)	K(4)#12-S(10)-K(5)#12	105.26(7)
K(1)-S(7)-K(4)	121.44(9)	K(1A)#3-S(10)-K(5)#12	124.53(9)
P(1)-S(7)-K(5)	156.48(9)	P(2)-S(10)-K(1)#3	87.79(10)
U(1)-S(7)-K(5)	107.87(5)	K(4)#12-S(10)-K(1)#3	85.53(8)
K(1A)-S(7)-K(5)	89.73(7)	K(1A)#3-S(10)-K(1)#3	6.58(8)
K(1)-S(7)-K(5)	92.28(8)	K(5)#12-S(10)-K(1)#3	130.27(9)
K(4)-S(7)-K(5)	91.14(6)	P(3)-S(11)-K(4)#12	100.34(8)
P(1)-S(8)-K(2)#6	92.79(8)	P(3)-S(11)-K(5)#1	95.42(9)
P(1)-S(8)-K(1)	82.29(10)	K(4)#12-S(11)-K(5)#1	88.33(6)
K(2)#6-S(8)-K(1)	171.79(10)	P(3)-S(11)-K(3)#13	90.12(7)

K(4)#12-S(11)-K(3)#13	156.74(8)	S(9)-P(1)-K(1A)	93.28(9)
K(5)#1-S(11)-K(3)#13	111.48(7)	S(8)-P(1)-K(1A)	61.01(8)
P(3)-S(11)-K(2)#12	71.98(7)	S(6)-P(1)-K(1A)	154.10(10)
K(4)#12-S(11)-K(2)#12	78.17(6)	S(7)-P(1)-K(1A)	62.80(8)
K(5)#1-S(11)-K(2)#12	159.25(7)	K(1)-P(1)-K(1A)	10.09(6)
K(3)#13-S(11)-K(2)#12	85.55(6)	K(4)-P(1)-K(1A)	114.41(7)
P(3)-S(12)-K(2)#6	99.42(7)	S(9)-P(1)-K(2)#6	123.90(8)
P(3)-S(12)-K(2)#12	82.24(7)	S(8)-P(1)-K(2)#6	55.23(7)
K(2)#6-S(12)-K(2)#12	80.44(5)	S(6)-P(1)-K(2)#6	58.33(6)
P(3)-S(12)-K(3)#6	99.33(8)	S(7)-P(1)-K(2)#6	127.40(8)
K(2)#6-S(12)-K(3)#6	87.26(5)	K(1)-P(1)-K(2)#6	118.10(8)
K(2)#12-S(12)-K(3)#6	167.68(7)	K(4)-P(1)-K(2)#6	129.65(5)
P(3)-S(12)-K(3)#13	88.32(7)	K(1A)-P(1)-K(2)#6	114.07(7)
K(2)#6-S(12)-K(3)#13	167.79(7)	S(10)-P(2)-S(3)#1	108.55(11)
K(2)#12-S(12)-K(3)#13	91.36(6)	S(10)-P(2)-S(1)	111.41(12)
K(3)#6-S(12)-K(3)#13	100.88(5)	S(3)#1-P(2)-S(1)	111.35(10)
P(3)-S(12)-K(1)#13	159.18(10)	S(10)-P(2)-S(2)	119.18(11)
K(2)#6-S(12)-K(1)#13	92.25(7)	S(3)#1-P(2)-S(2)	103.43(10)
K(2)#12-S(12)-K(1)#13	82.79(7)	S(1)-P(2)-S(2)	102.59(9)
K(3)#6-S(12)-K(1)#13	98.39(8)	S(10)-P(2)-K(5)#3	85.11(9)
K(3)#13-S(12)-K(1)#13	77.66(7)	S(3)#1-P(2)-K(5)#3	61.50(7)
S(9)-P(1)-S(8)	112.23(10)	S(1)-P(2)-K(5)#3	69.05(7)
S(9)-P(1)-S(6)	111.54(10)	S(2)-P(2)-K(5)#3	155.36(9)
S(8)-P(1)-S(6)	112.75(10)	S(11)-P(3)-S(12)	110.70(10)
S(9)-P(1)-S(7)	108.53(10)	S(11)-P(3)-S(4)	111.54(10)
S(8)-P(1)-S(7)	110.41(10)	S(12)-P(3)-S(4)	110.45(10)
S(6)-P(1)-S(7)	100.72(9)	S(11)-P(3)-S(5)	111.66(10)
S(9)-P(1)-K(1)	83.49(10)	S(12)-P(3)-S(5)	110.65(9)
S(8)-P(1)-K(1)	63.18(9)	S(4)-P(3)-S(5)	101.53(9)
S(6)-P(1)-K(1)	164.18(10)	S(11)-P(3)-K(2)#12	75.72(8)
S(7)-P(1)-K(1)	68.59(9)	S(12)-P(3)-K(2)#12	63.91(7)
S(9)-P(1)-K(4)	65.43(7)	S(4)-P(3)-K(2)#12	172.46(8)
S(8)-P(1)-K(4)	175.11(9)	S(5)-P(3)-K(2)#12	76.86(7)
S(6)-P(1)-K(4)	72.10(7)	S(11)-P(3)-K(3)#13	58.33(6)
S(7)-P(1)-K(4)	67.26(7)	S(12)-P(3)-K(3)#13	60.12(6)
K(1)-P(1)-K(4)	111.99(8)	S(4)-P(3)-K(3)#13	103.21(7)

S(5)-P(3)-K(3)#13	155.26(8)	K(2)#12-P(3)-K(3)#13	78.62(5)

Symmetry transformations used to generate equivalent atoms:

#1 -x+1,-y+1,-z+2 #2 x,-y+3/2,z-1/2 #3 x,-y+3/2,z+1/2

#4 -x,y+1/2,-z+3/2 #5 -x,y+1/2,-z+1/2 #6 -x,-y+1,-z+1

#7 x,y,z-1 #8 -x,-y+1,-z #9 -x+1,-y+1,-z+1

#10 -x+1,y+1/2,-z+3/2 #11 -x+1,y-1/2,-z+3/2

#12 x,y,z+1 #13 -x,y-1/2,-z+3/2

Table 4. Anisotropic displacement parameters ($Å^2 x\ 10^3$) for $K_5U(PS_4)_3$. The anisotropic displacement factor exponent takes the form: $-2\pi^2[\ h^2\ a^{*2}U^{11} + ... + 2\ h\ k\ a^*\ b^*\ U^{12}\ ]$

	U^{11}	U^{22}	U^{33}	U^{23}	U^{13}	U^{12}
U(1)	10(1)	10(1)	15(1)	0(1)	1(1)	0(1)
K(2)	25(1)	22(1)	33(1)	3(1)	15(1)	1(1)
K(3)	30(1)	24(1)	33(1)	-8(1)	-1(1)	9(1)
K(4)	33(1)	35(1)	29(1)	-9(1)	7(1)	0(1)
K(5)	39(1)	24(1)	62(1)	3(1)	-7(1)	7(1)
S(1)	19(1)	13(1)	22(1)	-2(1)	0(1)	-1(1)
S(2)	16(1)	16(1)	18(1)	2(1)	1(1)	2(1)
S(3)	17(1)	24(1)	40(1)	-7(1)	6(1)	0(1)
S(4)	18(1)	11(1)	25(1)	-1(1)	6(1)	1(1)
S(5)	19(1)	12(1)	22(1)	-1(1)	8(1)	-1(1)
S(6)	13(1)	11(1)	23(1)	1(1)	1(1)	0(1)
S(7)	13(1)	18(1)	26(1)	6(1)	-3(1)	-3(1)
S(8)	28(1)	15(1)	46(1)	-1(1)	19(1)	4(1)
S(9)	21(1)	40(1)	19(1)	7(1)	0(1)	1(1)
S(10)	56(1)	56(1)	35(1)	-25(1)	27(1)	-19(1)
S(11)	27(1)	27(1)	19(1)	8(1)	-2(1)	-7(1)
S(12)	14(1)	21(1)	23(1)	2(1)	0(1)	-4(1)
P(1)	11(1)	13(1)	18(1)	1(1)	2(1)	1(1)
P(2)	15(1)	19(1)	17(1)	-1(1)	2(1)	-4(1)
P(3)	15(1)	13(1)	16(1)	1(1)	1(1)	-3(1)

Table 1. Crystal data and structure refinement for $K_5Th(PS_4)_3$.

Identification code	k5th	
Empirical formula	$K_5Th(PS_4)_3$	
Formula weight	905.17	
Temperature	163(2) K	
Wavelength	0.71073 Å	
Crystal system	Monoclinic	
Space group	P21/n	
Unit cell dimensions	a = 9.74360(10) Å	α= 90°.
	b = 11.3894(2) Å	β= 90.0410(10)°.
	c = 20.0163(3) Å	γ = 90°.
Volume	2221.28(6) $Å^3$	
Z	4	
Density (calculated)	2.707 Mg/m^3	
Absorption coefficient	8.979 mm^{-1}	
F(000)	1688	
Crystal size	0.21 x 0.13 x 0.10 mm^3	
Theta range for data collection	1.02 to 28.30°.	
Index ranges	-12<=h<=10, -12<=k<=14, -25<=l<=26	
Reflections collected	14512	
Independent reflections	5322 [R(int) = 0.0495]	
Absorption correction	SADABS	
Max. and min. transmission	0.942284 and 0.682713	
Refinement method	Full-matrix least-squares on F^2	
Data / restraints / parameters	5322 / 0 / 192	
Goodness-of-fit on F^2	1.025	
Final R indices [I>2sigma(I)]	R1 = 0.0363, wR2 = 0.0745	
R indices (all data)	R1 = 0.0449, wR2 = 0.0780	
Extinction coefficient	0.00035(6)	
Largest diff. peak and hole	2.607 and -3.100 $e.Å^{-3}$	

Table 2. Atomic coordinates (x 10^4) and equivalent isotropic displacement parameters ($Å^2$x 10^3) for $K_5Th(PS_4)_3$. U(eq) is defined as one third of the trace of the orthogonalized U^{ij} tensor.

	x	y	z	U(eq)
Th(1)	1070(1)	6489(1)	806(1)	10(1)
K(1)	1131(4)	6558(1)	-2574(1)	20(1)
K(2)	1814(2)	9057(2)	-974(1)	29(1)
K(3)	-3595(2)	5902(2)	834(1)	39(1)
K(4)	6706(3)	6062(2)	-2498(1)	32(1)
K(5)	3802(2)	11412(1)	795(1)	20(1)
P(1)	3810(2)	8118(2)	793(1)	13(1)
P(2)	-930(3)	6718(1)	-812(1)	12(1)
P(3)	4023(3)	8312(2)	-2623(1)	13(1)
S(1)	2638(2)	4343(2)	801(2)	19(1)
S(2)	-772(2)	4367(2)	692(1)	14(1)
S(3)	-949(4)	7732(2)	26(1)	34(1)
S(4)	737(2)	5672(2)	2198(1)	16(1)
S(5)	-954(4)	7784(2)	1554(1)	27(1)
S(8)	3577(2)	7027(2)	1603(1)	19(1)
S(6)	2017(2)	9064(2)	784(2)	24(1)
S(7)	3589(2)	7025(2)	-18(1)	18(1)
S(9)	582(2)	6000(2)	-4194(2)	18(1)
S(10)	-942(3)	7732(2)	-1621(1)	19(1)
S(11)	2742(3)	4256(2)	-2383(1)	21(1)
S(12)	4167(3)	7358(2)	-1778(1)	19(1)

Table 3. Bond lengths [Å] and angles [°] for $K_5Th(PS_4)_3$.

Th(1)-S(5)	2.882(3)	K(2)-K(5)	4.845(3)
Th(1)-S(1)	2.882(2)	K(3)-S(11)#1	3.213(4)
Th(1)-S(3)	2.883(3)	K(3)-S(2)	3.271(3)
Th(1)-S(4)	2.954(2)	K(3)-S(8)#8	3.408(3)
Th(1)-S(8)	2.980(2)	K(3)-S(1)#1	3.415(4)
Th(1)-S(2)	3.020(2)	K(3)-S(7)#8	3.474(3)
Th(1)-S(7)	3.021(2)	K(3)-P(1)#8	3.575(3)
Th(1)-S(6)	3.074(2)	K(3)-S(9)#2	3.619(3)
Th(1)-S(2)#1	3.168(2)	K(3)-S(5)	3.645(4)
Th(1)-P(1)	3.251(2)	K(3)-S(3)	3.690(4)
Th(1)-K(4)#2	4.437(2)	K(3)-S(7)#1	3.712(3)
Th(1)-K(3)	4.594(2)	K(3)-K(1)#2	4.312(3)
K(1)-S(11)	3.080(3)	K(3)-K(5)#9	4.476(3)
K(1)-S(10)	3.083(4)	K(4)-S(12)	3.222(3)
K(1)-S(4)#1	3.214(3)	K(4)-S(4)#10	3.235(3)
K(1)-S(11)#3	3.264(3)	K(4)-S(8)#5	3.362(3)
K(1)-S(9)	3.346(4)	K(4)-S(10)#11	3.457(4)
K(1)-S(8)#4	3.390(4)	K(4)-S(6)#5	3.457(5)
K(1)-S(5)#5	3.419(5)	K(4)-S(5)#5	3.470(4)
K(1)-P(3)	3.456(4)	K(4)-S(1)#10	3.486(4)
K(1)-S(12)	3.481(4)	K(4)-P(3)	3.670(3)
K(1)-P(3)#6	3.721(2)	K(4)-K(1)#11	4.351(4)
K(1)-K(3)#5	4.312(3)	K(4)-Th(1)#5	4.437(2)
K(1)-K(2)	4.336(3)	K(4)-K(5)#7	4.488(4)
K(2)-S(11)#3	3.327(3)	K(4)-K(5)#5	4.878(3)
K(2)-S(10)	3.341(3)	K(5)-S(12)#7	3.121(3)
K(2)-S(9)#3	3.384(3)	K(5)-S(6)	3.190(3)
K(2)-S(12)	3.406(3)	K(5)-S(9)#12	3.249(2)
K(2)-S(7)	3.464(3)	K(5)-S(9)#3	3.295(4)
K(2)-S(6)	3.522(4)	K(5)-S(3)#9	3.372(4)
K(2)-S(3)	3.678(4)	K(5)-S(10)#9	3.385(3)
K(2)-P(2)	3.788(3)	K(5)-S(7)#7	3.472(3)
K(2)-K(5)#7	4.320(3)	K(5)-P(2)#9	3.517(3)
K(2)-K(1)#3	4.538(3)	K(5)-S(1)#13	3.526(3)

K(5)-P(1)	3.751(2)	S(7)-K(3)#11	3.474(3)
K(5)-K(2)#7	4.320(3)	S(7)-K(3)#1	3.712(3)
K(5)-K(3)#9	4.476(3)	S(9)-P(1)#4	1.998(2)
P(1)-S(9)#12	1.998(2)	S(9)-K(5)#4	3.249(2)
P(1)-S(6)	2.052(3)	S(9)-K(5)#6	3.295(4)
P(1)-S(8)	2.056(3)	S(9)-K(2)#6	3.384(3)
P(1)-S(7)	2.058(3)	S(9)-K(3)#5	3.619(3)
P(1)-K(3)#11	3.575(3)	S(10)-K(5)#9	3.385(3)
P(2)-S(10)	1.989(3)	S(10)-K(4)#8	3.457(4)
P(2)-S(3)	2.036(3)	S(11)-P(3)#6	2.027(4)
P(2)-S(1)#1	2.057(3)	S(11)-K(3)#1	3.213(4)
P(2)-S(2)#1	2.082(3)	S(11)-K(1)#6	3.264(3)
P(2)-K(5)#9	3.517(3)	S(11)-K(2)#6	3.327(3)
P(3)-S(12)	2.016(3)	S(12)-K(5)#7	3.121(3)
P(3)-S(11)#3	2.027(4)	S(5)-Th(1)-S(1)	143.03(7)
P(3)-S(4)#5	2.063(4)	S(5)-Th(1)-S(3)	64.10(6)
P(3)-S(5)#5	2.068(3)	S(1)-Th(1)-S(3)	140.87(7)
P(3)-K(1)#3	3.721(2)	S(5)-Th(1)-S(4)	66.20(6)
S(1)-P(2)#1	2.057(3)	S(1)-Th(1)-S(4)	78.17(7)
S(1)-K(3)#1	3.415(4)	S(3)-Th(1)-S(4)	126.18(8)
S(1)-K(4)#10	3.486(4)	S(5)-Th(1)-S(8)	100.25(8)
S(1)-K(5)#14	3.526(3)	S(1)-Th(1)-S(8)	75.05(7)
S(2)-P(2)#1	2.082(3)	S(3)-Th(1)-S(8)	138.42(7)
S(2)-Th(1)#1	3.168(2)	S(4)-Th(1)-S(8)	69.57(6)
S(3)-K(5)#9	3.372(4)	S(5)-Th(1)-S(2)	92.41(7)
S(4)-P(3)#2	2.063(4)	S(1)-Th(1)-S(2)	68.65(5)
S(4)-K(1)#1	3.214(3)	S(3)-Th(1)-S(2)	86.94(8)
S(4)-K(4)#10	3.235(3)	S(4)-Th(1)-S(2)	75.71(7)
S(5)-P(3)#2	2.068(3)	S(8)-Th(1)-S(2)	133.79(6)
S(5)-K(1)#2	3.419(5)	S(5)-Th(1)-S(7)	137.46(7)
S(5)-K(4)#2	3.470(4)	S(1)-Th(1)-S(7)	74.82(6)
S(8)-K(4)#2	3.362(3)	S(3)-Th(1)-S(7)	99.15(8)
S(8)-K(1)#12	3.390(4)	S(4)-Th(1)-S(7)	131.96(6)
S(8)-K(3)#11	3.408(3)	S(8)-Th(1)-S(7)	65.48(5)
S(6)-K(4)#2	3.457(5)	S(2)-Th(1)-S(7)	127.12(6)
S(7)-K(5)#7	3.472(3)	S(5)-Th(1)-S(6)	74.04(7)

S(1)-Th(1)-S(6)	130.52(5)	S(4)-Th(1)-K(3)	80.40(5)
S(3)-Th(1)-S(6)	74.23(8)	S(8)-Th(1)-K(3)	146.51(5)
S(4)-Th(1)-S(6)	110.36(8)	S(2)-Th(1)-K(3)	45.27(5)
S(8)-Th(1)-S(6)	64.29(6)	S(7)-Th(1)-K(3)	147.15(5)
S(2)-Th(1)-S(6)	160.19(6)	S(6)-Th(1)-K(3)	115.84(4)
S(7)-Th(1)-S(6)	63.61(6)	S(2)#1-Th(1)-K(3)	82.92(5)
S(5)-Th(1)-S(2)#1	125.94(7)	P(1)-Th(1)-K(3)	153.57(4)
S(1)-Th(1)-S(2)#1	77.49(7)	K(4)#2-Th(1)-K(3)	102.71(4)
S(3)-Th(1)-S(2)#1	64.90(6)	S(11)-K(1)-S(10)	128.77(10)
S(4)-Th(1)-S(2)#1	141.76(5)	S(11)-K(1)-S(4)#1	65.58(6)
S(8)-Th(1)-S(2)#1	130.14(6)	S(10)-K(1)-S(4)#1	80.01(9)
S(2)-Th(1)-S(2)#1	68.15(7)	S(11)-K(1)-S(11)#3	129.29(12)
S(7)-Th(1)-S(2)#1	67.58(6)	S(10)-K(1)-S(11)#3	80.16(7)
S(6)-Th(1)-S(2)#1	107.87(8)	S(4)#1-K(1)-S(11)#3	160.17(11)
S(5)-Th(1)-P(1)	105.92(7)	S(11)-K(1)-S(9)	92.27(8)
S(1)-Th(1)-P(1)	92.79(5)	S(10)-K(1)-S(9)	125.27(13)
S(3)-Th(1)-P(1)	105.97(8)	S(4)#1-K(1)-S(9)	89.25(8)
S(4)-Th(1)-P(1)	106.18(6)	S(11)#3-K(1)-S(9)	101.92(8)
S(8)-Th(1)-P(1)	38.22(5)	S(11)-K(1)-S(8)#4	147.01(10)
S(2)-Th(1)-P(1)	160.80(5)	S(10)-K(1)-S(8)#4	67.28(8)
S(7)-Th(1)-P(1)	38.08(5)	S(4)#1-K(1)-S(8)#4	94.25(11)
S(6)-Th(1)-P(1)	37.74(5)	S(11)#3-K(1)-S(8)#4	77.68(7)
S(2)#1-Th(1)-P(1)	104.04(6)	S(9)-K(1)-S(8)#4	60.19(7)
S(5)-Th(1)-K(4)#2	51.42(7)	S(11)-K(1)-S(5)#5	80.00(10)
S(1)-Th(1)-K(4)#2	117.54(7)	S(10)-K(1)-S(5)#5	139.98(8)
S(3)-Th(1)-K(4)#2	101.59(6)	S(4)#1-K(1)-S(5)#5	139.77(9)
S(4)-Th(1)-K(4)#2	59.50(5)	S(11)#3-K(1)-S(5)#5	60.03(8)
S(8)-Th(1)-K(4)#2	49.26(5)	S(9)-K(1)-S(5)#5	71.27(7)
S(2)-Th(1)-K(4)#2	130.08(5)	S(8)#4-K(1)-S(5)#5	104.93(8)
S(7)-Th(1)-K(4)#2	100.26(5)	S(11)-K(1)-P(3)	94.61(11)
S(6)-Th(1)-K(4)#2	50.95(8)	S(10)-K(1)-P(3)	107.54(8)
S(2)#1-Th(1)-K(4)#2	158.56(5)	S(4)#1-K(1)-P(3)	157.71(11)
P(1)-Th(1)-K(4)#2	62.18(5)	S(11)#3-K(1)-P(3)	34.97(7)
S(5)-Th(1)-K(3)	52.49(7)	S(9)-K(1)-P(3)	102.23(9)
S(1)-Th(1)-K(3)	113.63(5)	S(8)#4-K(1)-P(3)	108.03(7)
S(3)-Th(1)-K(3)	53.38(8)	S(5)#5-K(1)-P(3)	35.01(6)

S(11)-K(1)-S(12)	74.51(9)	P(3)#6-K(1)-K(2)	125.45(7)
S(10)-K(1)-S(12)	99.21(9)	K(3)#5-K(1)-K(2)	95.52(5)
S(4)#1-K(1)-S(12)	125.49(9)	S(11)#3-K(2)-S(10)	75.65(7)
S(11)#3-K(1)-S(12)	58.66(7)	S(11)#3-K(2)-S(9)#3	87.42(8)
S(9)-K(1)-S(12)	128.93(11)	S(10)-K(2)-S(9)#3	159.43(9)
S(8)#4-K(1)-S(12)	136.17(7)	S(11)#3-K(2)-S(12)	58.87(7)
S(5)#5-K(1)-S(12)	58.01(8)	S(10)-K(2)-S(12)	95.82(8)
P(3)-K(1)-S(12)	33.79(6)	S(9)#3-K(2)-S(12)	85.02(7)
S(11)-K(1)-P(3)#6	33.00(7)	S(11)#3-K(2)-S(7)	121.74(9)
S(10)-K(1)-P(3)#6	109.81(9)	S(10)-K(2)-S(7)	108.26(8)
S(4)#1-K(1)-P(3)#6	33.62(6)	S(9)#3-K(2)-S(7)	90.48(7)
S(11)#3-K(1)-P(3)#6	162.09(13)	S(12)-K(2)-S(7)	62.94(6)
S(9)-K(1)-P(3)#6	84.70(6)	S(11)#3-K(2)-S(6)	168.55(9)
S(8)#4-K(1)-P(3)#6	119.62(10)	S(10)-K(2)-S(6)	115.66(7)
S(5)#5-K(1)-P(3)#6	107.76(9)	S(9)#3-K(2)-S(6)	81.85(7)
P(3)-K(1)-P(3)#6	127.61(10)	S(12)-K(2)-S(6)	115.84(8)
S(12)-K(1)-P(3)#6	104.22(9)	S(7)-K(2)-S(6)	54.75(5)
S(11)-K(1)-K(3)#5	129.13(10)	S(11)#3-K(2)-S(3)	131.42(9)
S(10)-K(1)-K(3)#5	101.96(7)	S(10)-K(2)-S(3)	55.77(5)
S(4)#1-K(1)-K(3)#5	137.63(10)	S(9)#3-K(2)-S(3)	139.79(9)
S(11)#3-K(1)-K(3)#5	47.76(6)	S(12)-K(2)-S(3)	121.15(8)
S(9)-K(1)-K(3)#5	54.65(5)	S(7)-K(2)-S(3)	77.95(7)
S(8)#4-K(1)-K(3)#5	50.81(5)	S(6)-K(2)-S(3)	59.91(6)
S(5)#5-K(1)-K(3)#5	54.80(6)	S(11)#3-K(2)-P(2)	102.99(8)
P(3)-K(1)-K(3)#5	62.61(6)	S(10)-K(2)-P(2)	31.62(5)
S(12)-K(1)-K(3)#5	96.29(7)	S(9)#3-K(2)-P(2)	168.78(9)
P(3)#6-K(1)-K(3)#5	138.36(7)	S(12)-K(2)-P(2)	96.68(7)
S(11)-K(1)-K(2)	112.90(10)	S(7)-K(2)-P(2)	80.52(7)
S(10)-K(1)-K(2)	50.11(6)	S(6)-K(2)-P(2)	87.45(6)
S(4)#1-K(1)-K(2)	115.60(8)	S(3)-K(2)-P(2)	31.61(5)
S(11)#3-K(1)-K(2)	49.49(6)	S(11)#3-K(2)-K(5)#7	87.75(7)
S(9)-K(1)-K(2)	149.86(6)	S(10)-K(2)-K(5)#7	140.42(8)
S(8)#4-K(1)-K(2)	99.16(7)	S(9)#3-K(2)-K(5)#7	48.03(5)
S(5)#5-K(1)-K(2)	96.12(8)	S(12)-K(2)-K(5)#7	45.78(5)
P(3)-K(1)-K(2)	61.11(6)	S(7)-K(2)-K(5)#7	51.56(5)
S(12)-K(1)-K(2)	50.21(6)	S(6)-K(2)-K(5)#7	82.12(6)

S(3)-K(2)-K(5)#7	128.93(8)	S(2)-K(3)-S(1)#1	69.09(6)
P(2)-K(2)-K(5)#7	127.15(7)	S(8)#8-K(3)-S(1)#1	133.24(8)
S(11)#3-K(2)-K(1)	48.24(6)	S(11)#1-K(3)-S(7)#8	134.26(8)
S(10)-K(2)-K(1)	45.09(7)	S(2)-K(3)-S(7)#8	144.87(9)
S(9)#3-K(2)-K(1)	128.10(9)	S(8)#8-K(3)-S(7)#8	56.28(5)
S(12)-K(2)-K(1)	51.76(7)	S(1)#1-K(3)-S(7)#8	77.02(7)
S(7)-K(2)-K(1)	92.62(7)	S(11)#1-K(3)-P(1)#8	104.13(8)
S(6)-K(2)-K(1)	138.39(7)	S(2)-K(3)-P(1)#8	166.01(9)
S(3)-K(2)-K(1)	91.17(7)	S(8)#8-K(3)-P(1)#8	34.15(5)
P(2)-K(2)-K(1)	59.57(6)	S(1)#1-K(3)-P(1)#8	103.26(8)
K(5)#7-K(2)-K(1)	97.54(7)	S(7)#8-K(3)-P(1)#8	33.91(5)
S(11)#3-K(2)-K(1)#3	42.74(6)	S(11)#1-K(3)-S(9)#2	97.26(9)
S(10)-K(2)-K(1)#3	112.95(7)	S(2)-K(3)-S(9)#2	134.92(8)
S(9)#3-K(2)-K(1)#3	47.26(7)	S(8)#8-K(3)-S(9)#2	57.38(6)
S(12)-K(2)-K(1)#3	75.89(6)	S(1)#1-K(3)-S(9)#2	97.22(8)
S(7)-K(2)-K(1)#3	123.55(8)	S(7)#8-K(3)-S(9)#2	57.22(6)
S(6)-K(2)-K(1)#3	127.87(7)	P(1)#8-K(3)-S(9)#2	32.24(4)
S(3)-K(2)-K(1)#3	158.35(8)	S(11)#1-K(3)-S(5)	57.98(7)
P(2)-K(2)-K(1)#3	143.91(7)	S(2)-K(3)-S(5)	75.85(7)
K(5)#7-K(2)-K(1)#3	72.17(6)	S(8)#8-K(3)-S(5)	99.85(8)
K(1)-K(2)-K(1)#3	90.36(5)	S(1)#1-K(3)-S(5)	103.52(8)
S(11)#3-K(2)-K(5)	129.25(8)	S(7)#8-K(3)-S(5)	122.31(8)
S(10)-K(2)-K(5)	148.70(7)	P(1)#8-K(3)-S(5)	95.33(7)
S(9)#3-K(2)-K(5)	42.79(6)	S(9)#2-K(3)-S(5)	65.73(7)
S(12)-K(2)-K(5)	113.01(7)	S(11)#1-K(3)-S(3)	105.92(8)
S(7)-K(2)-K(5)	76.55(6)	S(2)-K(3)-S(3)	71.11(7)
S(6)-K(2)-K(5)	41.15(4)	S(8)#8-K(3)-S(3)	123.45(8)
S(3)-K(2)-K(5)	97.02(6)	S(1)#1-K(3)-S(3)	55.57(6)
P(2)-K(2)-K(5)	127.51(6)	S(7)#8-K(3)-S(3)	97.38(8)
K(5)#7-K(2)-K(5)	67.24(5)	P(1)#8-K(3)-S(3)	94.90(8)
K(1)-K(2)-K(5)	164.66(8)	S(9)#2-K(3)-S(3)	66.26(7)
K(1)#3-K(2)-K(5)	86.80(5)	S(5)-K(3)-S(3)	49.29(5)
S(11)#1-K(3)-S(2)	80.62(7)	S(11)#1-K(3)-S(7)#1	111.95(8)
S(11)#1-K(3)-S(8)#8	78.11(7)	S(2)-K(3)-S(7)#1	58.70(6)
S(2)-K(3)-S(8)#8	156.98(10)	S(8)#8-K(3)-S(7)#1	122.53(8)
S(11)#1-K(3)-S(1)#1	148.13(8)	S(1)#1-K(3)-S(7)#1	60.29(6)

S(7)#8-K(3)-S(7)#1	96.65(7)	S(12)-K(4)-S(5)#5	59.86(6)
P(1)#8-K(3)-S(7)#1	128.70(8)	S(4)#10-K(4)-S(5)#5	155.18(10)
S(9)#2-K(3)-S(7)#1	150.37(9)	S(8)#5-K(4)-S(5)#5	82.36(7)
S(5)-K(3)-S(7)#1	134.50(7)	S(10)#11-K(4)-S(5)#5	124.33(9)
S(3)-K(3)-S(7)#1	108.25(7)	S(6)#5-K(4)-S(5)#5	62.42(6)
S(11)#1-K(3)-K(1)#2	48.77(6)	S(12)-K(4)-S(1)#10	76.41(7)
S(2)-K(3)-K(1)#2	118.38(9)	S(4)#10-K(4)-S(1)#10	66.27(7)
S(8)#8-K(3)-K(1)#2	50.45(7)	S(8)#5-K(4)-S(1)#10	120.52(9)
S(1)#1-K(3)-K(1)#2	141.28(8)	S(10)#11-K(4)-S(1)#10	57.13(6)
S(7)#8-K(3)-K(1)#2	93.82(7)	S(6)#5-K(4)-S(1)#10	161.44(9)
P(1)#8-K(3)-K(1)#2	59.93(6)	S(5)#5-K(4)-S(1)#10	136.01(9)
S(9)#2-K(3)-K(1)#2	48.96(6)	S(12)-K(4)-P(3)	33.22(5)
S(5)-K(3)-K(1)#2	50.03(8)	S(4)#10-K(4)-P(3)	170.94(10)
S(3)-K(3)-K(1)#2	89.36(7)	S(8)#5-K(4)-P(3)	84.13(7)
S(7)#1-K(3)-K(1)#2	158.07(8)	S(10)#11-K(4)-P(3)	97.02(8)
S(11)#1-K(3)-K(5)#9	138.80(9)	S(6)#5-K(4)-P(3)	91.36(7)
S(2)-K(3)-K(5)#9	109.85(7)	S(5)#5-K(4)-P(3)	33.52(5)
S(8)#8-K(3)-K(5)#9	92.07(6)	S(1)#10-K(4)-P(3)	106.81(7)
S(1)#1-K(3)-K(5)#9	50.94(5)	S(12)-K(4)-K(1)#11	135.81(9)
S(7)#8-K(3)-K(5)#9	49.86(5)	S(4)#10-K(4)-K(1)#11	47.37(6)
P(1)#8-K(3)-K(5)#9	57.92(5)	S(8)#5-K(4)-K(1)#11	50.16(6)
S(9)#2-K(3)-K(5)#9	46.57(6)	S(10)#11-K(4)-K(1)#11	44.72(6)
S(5)-K(3)-K(5)#9	85.26(6)	S(6)#5-K(4)-K(1)#11	83.28(7)
S(3)-K(3)-K(5)#9	47.59(6)	S(5)#5-K(4)-K(1)#11	132.16(8)
S(7)#1-K(3)-K(5)#9	107.06(7)	S(1)#10-K(4)-K(1)#11	82.55(7)
K(1)#2-K(3)-K(5)#9	94.42(5)	P(3)-K(4)-K(1)#11	127.78(8)
S(12)-K(4)-S(4)#10	142.00(9)	S(12)-K(4)-Th(1)#5	86.98(6)
S(12)-K(4)-S(8)#5	111.06(8)	S(4)#10-K(4)-Th(1)#5	129.26(7)
S(4)#10-K(4)-S(8)#5	94.39(8)	S(8)#5-K(4)-Th(1)#5	42.18(4)
S(12)-K(4)-S(10)#11	91.70(9)	S(10)#11-K(4)-Th(1)#5	97.73(7)
S(4)#10-K(4)-S(10)#11	74.40(8)	S(6)#5-K(4)-Th(1)#5	43.69(4)
S(8)#5-K(4)-S(10)#11	63.62(7)	S(5)#5-K(4)-Th(1)#5	40.49(5)
S(12)-K(4)-S(6)#5	122.15(8)	S(1)#10-K(4)-Th(1)#5	148.65(8)
S(4)#10-K(4)-S(6)#5	95.25(7)	P(3)-K(4)-Th(1)#5	53.80(4)
S(8)#5-K(4)-S(6)#5	56.38(6)	K(1)#11-K(4)-Th(1)#5	91.68(5)
S(10)#11-K(4)-S(6)#5	118.00(8)	S(12)-K(4)-K(5)#7	44.06(5)

S(4)#10-K(4)-K(5)#7	109.60(8)	S(6)-K(5)-S(7)#7	145.68(9)
S(8)#5-K(4)-K(5)#7	92.95(7)	S(9)#12-K(5)-S(7)#7	92.62(7)
S(10)#11-K(4)-K(5)#7	48.32(6)	S(9)#3-K(5)-S(7)#7	60.23(6)
S(6)#5-K(4)-K(5)#7	142.39(8)	S(3)#9-K(5)-S(7)#7	103.73(9)
S(5)#5-K(4)-K(5)#7	95.16(7)	S(10)#9-K(5)-S(7)#7	132.41(7)
S(1)#10-K(4)-K(5)#7	50.59(5)	S(12)#7-K(5)-P(2)#9	103.08(7)
P(3)-K(4)-K(5)#7	61.65(5)	S(6)-K(5)-P(2)#9	94.24(6)
K(1)#11-K(4)-K(5)#7	93.04(7)	S(9)#12-K(5)-P(2)#9	159.51(7)
Th(1)#5-K(4)-K(5)#7	99.36(5)	S(9)#3-K(5)-P(2)#9	103.95(8)
S(12)-K(4)-K(5)#5	154.16(8)	S(3)#9-K(5)-P(2)#9	34.30(5)
S(4)#10-K(4)-K(5)#5	56.97(6)	S(10)#9-K(5)-P(2)#9	33.43(5)
S(8)#5-K(4)-K(5)#5	76.80(6)	S(7)#7-K(5)-P(2)#9	106.06(7)
S(10)#11-K(4)-K(5)#5	113.31(7)	S(12)#7-K(5)-S(1)#13	77.10(7)
S(6)#5-K(4)-K(5)#5	40.70(4)	S(6)-K(5)-S(1)#13	128.20(7)
S(5)#5-K(4)-K(5)#5	98.53(6)	S(9)#12-K(5)-S(1)#13	166.48(7)
S(1)#10-K(4)-K(5)#5	121.97(7)	S(9)#3-K(5)-S(1)#13	101.35(8)
P(3)-K(4)-K(5)#5	130.85(6)	S(3)#9-K(5)-S(1)#13	57.52(7)
K(1)#11-K(4)-K(5)#5	68.61(5)	S(10)#9-K(5)-S(1)#13	57.38(6)
Th(1)#5-K(4)-K(5)#5	83.42(4)	S(7)#7-K(5)-S(1)#13	75.61(6)
K(5)#7-K(4)-K(5)#5	161.57(6)	P(2)#9-K(5)-S(1)#13	33.97(5)
S(12)#7-K(5)-S(6)	136.57(10)	S(12)#7-K(5)-P(1)	116.63(7)
S(12)#7-K(5)-S(9)#12	92.11(8)	S(6)-K(5)-P(1)	33.16(5)
S(6)-K(5)-S(9)#12	65.31(5)	S(9)#12-K(5)-P(1)	32.15(4)
S(12)#7-K(5)-S(9)#3	124.13(8)	S(9)#3-K(5)-P(1)	81.73(6)
S(6)-K(5)-S(9)#3	88.47(9)	S(3)#9-K(5)-P(1)	106.86(7)
S(9)#12-K(5)-S(9)#3	77.81(8)	S(10)#9-K(5)-P(1)	106.86(6)
S(12)#7-K(5)-S(3)#9	134.39(8)	S(7)#7-K(5)-P(1)	120.72(7)
S(6)-K(5)-S(3)#9	77.84(8)	P(2)#9-K(5)-P(1)	127.38(6)
S(9)#12-K(5)-S(3)#9	133.45(8)	S(1)#13-K(5)-P(1)	161.35(7)
S(9)#3-K(5)-S(3)#9	73.62(7)	S(12)#7-K(5)-K(2)#7	51.45(6)
S(12)#7-K(5)-S(10)#9	94.87(9)	S(6)-K(5)-K(2)#7	115.85(6)
S(6)-K(5)-S(10)#9	78.21(7)	S(9)#12-K(5)-K(2)#7	50.73(5)
S(9)#12-K(5)-S(10)#9	132.82(8)	S(9)#3-K(5)-K(2)#7	83.22(6)
S(9)#3-K(5)-S(10)#9	131.82(8)	S(3)#9-K(5)-K(2)#7	153.00(9)
S(3)#9-K(5)-S(10)#9	58.39(6)	S(10)#9-K(5)-K(2)#7	144.07(8)
S(12)#7-K(5)-S(7)#7	65.67(7)	S(7)#7-K(5)-K(2)#7	51.40(5)

P(2)#9-K(5)-K(2)#7	149.43(6)	S(10)-P(2)-S(1)#1	110.2(2)
S(1)#13-K(5)-K(2)#7	115.78(6)	S(3)-P(2)-S(1)#1	108.5(2)
P(1)-K(5)-K(2)#7	82.79(5)	S(10)-P(2)-S(2)#1	116.3(2)
S(12)#7-K(5)-K(3)#9	100.41(6)	S(3)-P(2)-S(2)#1	104.5(2)
S(6)-K(5)-K(3)#9	122.91(9)	S(1)#1-P(2)-S(2)#1	107.13(10)
S(9)#12-K(5)-K(3)#9	127.36(8)	S(10)-P(2)-K(5)#9	69.64(11)
S(9)#3-K(5)-K(3)#9	52.89(5)	S(3)-P(2)-K(5)#9	68.95(12)
S(3)#9-K(5)-K(3)#9	53.90(7)	S(1)#1-P(2)-K(5)#9	73.25(9)
S(10)#9-K(5)-K(3)#9	97.03(6)	S(2)#1-P(2)-K(5)#9	172.81(12)
S(7)#7-K(5)-K(3)#9	49.90(5)	S(10)-P(2)-K(2)	61.69(10)
P(2)#9-K(5)-K(3)#9	63.75(5)	S(3)-P(2)-K(2)	71.21(13)
S(1)#13-K(5)-K(3)#9	48.77(6)	S(1)#1-P(2)-K(2)	170.13(12)
P(1)-K(5)-K(3)#9	133.06(7)	S(2)#1-P(2)-K(2)	82.24(10)
K(2)#7-K(5)-K(3)#9	100.89(5)	K(5)#9-P(2)-K(2)	97.85(6)
S(9)#12-P(1)-S(6)	118.18(12)	S(12)-P(3)-S(11)#3	109.9(2)
S(9)#12-P(1)-S(8)	112.88(14)	S(12)-P(3)-S(4)#5	113.1(2)
S(6)-P(1)-S(8)	103.32(13)	S(11)#3-P(3)-S(4)#5	112.97(12)
S(9)#12-P(1)-S(7)	113.85(13)	S(12)-P(3)-S(5)#5	110.01(12)
S(6)-P(1)-S(7)	102.84(14)	S(11)#3-P(3)-S(5)#5	109.5(2)
S(8)-P(1)-S(7)	104.19(11)	S(4)#5-P(3)-S(5)#5	101.00(14)
S(9)#12-P(1)-Th(1)	175.20(10)	S(12)-P(3)-K(1)	73.79(11)
S(6)-P(1)-Th(1)	66.47(7)	S(11)#3-P(3)-K(1)	67.34(12)
S(8)-P(1)-Th(1)	63.74(7)	S(4)#5-P(3)-K(1)	171.59(11)
S(7)-P(1)-Th(1)	64.91(7)	S(5)#5-P(3)-K(1)	71.51(12)
S(9)#12-P(1)-K(3)#11	75.10(8)	S(12)-P(3)-K(4)	61.09(10)
S(6)-P(1)-K(3)#11	166.69(10)	S(11)#3-P(3)-K(4)	166.87(13)
S(8)-P(1)-K(3)#11	68.48(9)	S(4)#5-P(3)-K(4)	80.04(11)
S(7)-P(1)-K(3)#11	70.36(9)	S(5)#5-P(3)-K(4)	67.92(12)
Th(1)-P(1)-K(3)#11	100.24(6)	K(1)-P(3)-K(4)	100.08(7)
S(9)#12-P(1)-K(5)	59.95(8)	S(12)-P(3)-K(1)#3	116.71(10)
S(6)-P(1)-K(5)	58.23(7)	S(11)#3-P(3)-K(1)#3	55.85(10)
S(8)-P(1)-K(5)	127.12(10)	S(4)#5-P(3)-K(1)#3	59.59(9)
S(7)-P(1)-K(5)	127.30(10)	S(5)#5-P(3)-K(1)#3	133.25(10)
Th(1)-P(1)-K(5)	124.69(6)	K(1)-P(3)-K(1)#3	122.59(8)
K(3)#11-P(1)-K(5)	135.04(7)	K(4)-P(3)-K(1)#3	135.68(11)
S(10)-P(2)-S(3)	109.92(11)	P(2)#1-S(1)-Th(1)	93.97(9)

P(2)#1-S(1)-K(3)#1	100.59(12)	K(1)#2-S(5)-K(4)#2	104.96(8)
Th(1)-S(1)-K(3)#1	102.60(8)	P(3)#2-S(5)-K(3)	87.20(12)
P(2)#1-S(1)-K(4)#10	93.41(12)	Th(1)-S(5)-K(3)	88.68(7)
Th(1)-S(1)-K(4)#10	101.84(9)	K(1)#2-S(5)-K(3)	75.17(9)
K(3)#1-S(1)-K(4)#10	150.80(8)	K(4)#2-S(5)-K(3)	164.94(9)
P(2)#1-S(1)-K(5)#14	72.78(9)	P(1)-S(8)-Th(1)	78.04(8)
Th(1)-S(1)-K(5)#14	166.75(8)	P(1)-S(8)-K(4)#2	95.21(10)
K(3)#1-S(1)-K(5)#14	80.30(7)	Th(1)-S(8)-K(4)#2	88.56(7)
K(4)#10-S(1)-K(5)#14	79.58(7)	P(1)-S(8)-K(1)#12	90.84(10)
P(2)#1-S(2)-Th(1)	89.59(9)	Th(1)-S(8)-K(1)#12	163.48(9)
P(2)#1-S(2)-Th(1)#1	89.92(9)	K(4)#2-S(8)-K(1)#12	80.23(7)
Th(1)-S(2)-Th(1)#1	111.85(7)	P(1)-S(8)-K(3)#11	77.37(9)
P(2)#1-S(2)-K(3)	167.66(12)	Th(1)-S(8)-K(3)#11	110.11(7)
Th(1)-S(2)-K(3)	93.75(7)	K(4)#2-S(8)-K(3)#11	157.55(9)
Th(1)#1-S(2)-K(3)	99.81(7)	K(1)#12-S(8)-K(3)#11	78.74(8)
P(2)-S(3)-Th(1)	99.28(12)	P(1)-S(6)-Th(1)	75.80(7)
P(2)-S(3)-K(5)#9	76.75(12)	P(1)-S(6)-K(5)	88.62(8)
Th(1)-S(3)-K(5)#9	165.45(13)	Th(1)-S(6)-K(5)	164.37(7)
P(2)-S(3)-K(2)	77.18(12)	P(1)-S(6)-K(4)#2	92.53(13)
Th(1)-S(3)-K(2)	89.82(11)	Th(1)-S(6)-K(4)#2	85.36(8)
K(5)#9-S(3)-K(2)	102.71(8)	K(5)-S(6)-K(4)#2	94.34(10)
P(2)-S(3)-K(3)	92.71(13)	P(1)-S(6)-K(2)	93.16(13)
Th(1)-S(3)-K(3)	87.79(7)	Th(1)-S(6)-K(2)	89.77(8)
K(5)#9-S(3)-K(3)	78.51(9)	K(5)-S(6)-K(2)	92.26(9)
K(2)-S(3)-K(3)	169.10(8)	K(4)#2-S(6)-K(2)	171.38(7)
P(3)#2-S(4)-Th(1)	94.40(9)	P(1)-S(7)-Th(1)	77.01(7)
P(3)#2-S(4)-K(1)#1	86.79(11)	P(1)-S(7)-K(2)	94.76(10)
Th(1)-S(4)-K(1)#1	122.19(9)	Th(1)-S(7)-K(2)	91.76(6)
P(3)#2-S(4)-K(4)#10	158.96(11)	P(1)-S(7)-K(5)#7	88.12(9)
Th(1)-S(4)-K(4)#10	106.39(7)	Th(1)-S(7)-K(5)#7	160.66(8)
K(1)#1-S(4)-K(4)#10	84.86(9)	K(2)-S(7)-K(5)#7	77.04(6)
P(3)#2-S(5)-Th(1)	96.44(11)	P(1)-S(7)-K(3)#11	75.73(9)
P(3)#2-S(5)-K(1)#2	73.48(12)	Th(1)-S(7)-K(3)#11	107.40(7)
Th(1)-S(5)-K(1)#2	161.14(11)	K(2)-S(7)-K(3)#11	155.65(9)
P(3)#2-S(5)-K(4)#2	78.56(12)	K(5)#7-S(7)-K(3)#11	80.24(7)
Th(1)-S(5)-K(4)#2	88.10(10)	P(1)-S(7)-K(3)#1	152.96(11)

Th(1)-S(7)-K(3)#1	93.47(7)
K(2)-S(7)-K(3)#1	110.97(7)
K(5)#7-S(7)-K(3)#1	105.20(7)
K(3)#11-S(7)-K(3)#1	83.35(7)
P(1)#4-S(9)-K(5)#4	87.90(9)
P(1)#4-S(9)-K(5)#6	94.21(12)
K(5)#4-S(9)-K(5)#6	102.19(8)
P(1)#4-S(9)-K(1)	93.16(13)
K(5)#4-S(9)-K(1)	104.62(9)
K(5)#6-S(9)-K(1)	152.41(8)
P(1)#4-S(9)-K(2)#6	168.03(12)
K(5)#4-S(9)-K(2)#6	81.24(6)
K(5)#6-S(9)-K(2)#6	92.99(7)
K(1)-S(9)-K(2)#6	84.80(9)
P(1)#4-S(9)-K(3)#5	72.66(8)
K(5)#4-S(9)-K(3)#5	160.54(7)
K(5)#6-S(9)-K(3)#5	80.53(7)
K(1)-S(9)-K(3)#5	76.39(7)
K(2)#6-S(9)-K(3)#5	118.04(7)
P(2)-S(10)-K(1)	104.38(12)
P(2)-S(10)-K(2)	86.69(11)
K(1)-S(10)-K(2)	84.80(10)
P(2)-S(10)-K(5)#9	76.93(11)
K(1)-S(10)-K(5)#9	165.18(11)
K(2)-S(10)-K(5)#9	110.01(7)
P(2)-S(10)-K(4)#8	95.57(11)
K(1)-S(10)-K(4)#8	83.20(8)
K(2)-S(10)-K(4)#8	167.98(10)
K(5)#9-S(10)-K(4)#8	81.98(8)
P(3)#6-S(11)-K(1)	91.14(12)
P(3)#6-S(11)-K(3)#1	100.58(12)
K(1)-S(11)-K(3)#1	107.39(9)
P(3)#6-S(11)-K(1)#6	77.69(12)
K(1)-S(11)-K(1)#6	165.85(9)
K(3)#1-S(11)-K(1)#6	83.47(8)
P(3)#6-S(11)-K(2)#6	94.62(11)
K(1)-S(11)-K(2)#6	90.11(9)
K(3)#1-S(11)-K(2)#6	156.40(10)
K(1)#6-S(11)-K(2)#6	82.26(9)
P(3)-S(12)-K(5)#7	109.33(12)
P(3)-S(12)-K(4)	85.69(11)
K(5)#7-S(12)-K(4)	90.06(9)
P(3)-S(12)-K(2)	92.51(11)
K(5)#7-S(12)-K(2)	82.77(7)
K(4)-S(12)-K(2)	171.58(10)
P(3)-S(12)-K(1)	72.41(11)
K(5)#7-S(12)-K(1)	160.79(10)
K(4)-S(12)-K(1)	109.13(8)
K(2)-S(12)-K(1)	78.03(8)

Symmetry transformations used to generate equivalent atoms:

#1 -x,-y+1,-z #2 x-1/2,-y+3/2,z+1/2 #3 -x+1/2,y+1/2,-z-1/2

#4 x-1/2,-y+3/2,z-1/2 #5 x+1/2,-y+3/2,z-1/2

#6 -x+1/2,y-1/2,-z-1/2 #7 -x+1,-y+2,-z #8 x-1,y,z

#9 -x,-y+2,-z #10 -x+1,-y+1,-z #11 x+1,y,z

#12 x+1/2,-y+3/2,z+1/2 #13 x,y+1,z #14 x,y-1,z

Table 4. Anisotropic displacement parameters ($Å^2 x\ 10^3$) for $K_5Th(PS_4)_3$. The anisotropic displacement factor exponent takes the form: $-2\pi^2[\ h^2\ a^{*2}U^{11} + ... + 2\ h\ k\ a^*\ b^*\ U^{12}\ ]$

	U^{11}	U^{22}	U^{33}	U^{23}	U^{13}	U^{12}
Th(1)	9(1)	11(1)	9(1)	0(1)	2(1)	1(1)
K(1)	18(1)	11(1)	31(1)	-2(1)	-2(1)	-1(1)
K(2)	26(1)	36(1)	24(1)	2(1)	1(1)	-9(1)
K(3)	28(1)	63(1)	27(1)	-12(1)	-3(1)	25(1)
K(4)	29(1)	44(1)	23(1)	8(1)	5(1)	16(1)
K(5)	16(1)	17(1)	26(1)	-1(1)	2(1)	1(1)
P(1)	11(1)	14(1)	14(1)	2(1)	1(1)	-2(1)
P(2)	14(1)	13(1)	9(1)	0(1)	4(1)	3(1)
P(3)	13(1)	16(1)	11(1)	-2(1)	1(1)	-1(1)
S(1)	12(1)	16(1)	28(1)	6(1)	4(1)	1(1)
S(2)	11(1)	15(1)	16(1)	-1(1)	2(1)	1(1)
S(3)	46(2)	38(2)	17(1)	-16(1)	-14(1)	28(2)
S(4)	12(1)	20(1)	15(1)	5(1)	5(1)	4(1)
S(5)	33(1)	32(1)	17(1)	13(1)	14(1)	22(1)
S(8)	21(1)	25(1)	11(1)	5(1)	0(1)	-9(1)
S(6)	11(1)	15(1)	46(1)	-2(1)	5(1)	1(1)
S(7)	18(1)	23(1)	13(1)	-2(1)	6(1)	-3(1)
S(9)	12(1)	20(1)	23(1)	-2(1)	0(1)	5(1)
S(10)	21(1)	20(1)	16(1)	6(1)	5(1)	2(1)
S(11)	14(1)	24(1)	26(1)	-2(1)	-2(1)	-2(1)
S(12)	22(1)	23(1)	12(1)	6(1)	3(1)	-2(1)

Table 1. Crystal data and structure refinement for $Rb_5Th(PS_4)_3$.

Identification code	rb5th	
Empirical formula	$Rb_5Th(PS_4)_3$	
Formula weight	1137.02	
Temperature	163(2) K	
Wavelength	0.71073 Å	
Crystal system	Monoclinic	
Space group	P21/c	
Unit cell dimensions	a = 13.197(4) Å	α= 90°.
	b = 9.997(4) Å	β= 100.773(11)°.
	c = 18.189(7) Å	γ = 90°.
Volume	2357.4(15) $Å^3$	
Z	4	
Density (calculated)	3.204 Mg/m^3	
Absorption coefficient	17.836 mm^{-1}	
F(000)	2048	
Crystal size	0.21 x 0.18 x 0.08 mm^3	
Theta range for data collection	1.57 to 28.26°.	
Index ranges	-17<=h<=17, -13<=k<=10, -24<=l<=12	
Reflections collected	11808	
Independent reflections	5407 [R(int) = 0.0895]	
Absorption correction	SADABS	
Max. and min. transmission	0.942284 and 0.355075	
Refinement method	Full-matrix least-squares on F^2	
Data / restraints / parameters	5407 / 0 / 191	
Goodness-of-fit on F^2	0.926	
Final R indices [I>2sigma(I)]	R1 = 0.0501, wR2 = 0.0969	
R indices (all data)	R1 = 0.0910, wR2 = 0.1111	
Extinction coefficient	0.00077(5)	
Largest diff. peak and hole	2.723 and -3.666 $e.Å^{-3}$	

Table 2. Atomic coordinates (x 10^4) and equivalent isotropic displacement parameters ($Å^2$x 10^3) for $Rb_5Th(PS_4)_3$. U(eq) is defined as one third of the trace of the orthogonalized U^{ij} tensor.

	x	y	z	U(eq)
Th(1)	1853(1)	1010(1)	351(1)	8(1)
P(1)	2871(2)	3717(3)	-193(2)	10(1)
P(2)	326(2)	9086(3)	-1346(2)	10(1)
P(3)	6428(2)	1040(3)	-1800(2)	11(1)
S(1)	422(2)	2557(3)	1020(2)	13(1)
S(2)	289(2)	-732(3)	893(2)	14(1)
S(3)	1840(2)	-956(3)	-823(2)	18(1)
S(5)	3436(2)	-1036(3)	645(2)	19(1)
S(4)	2758(2)	680(3)	1952(2)	15(1)
S(8)	2933(2)	3541(3)	943(1)	13(1)
S(6)	3573(2)	1989(3)	-449(2)	15(1)
S(7)	1351(2)	3395(3)	-666(2)	14(1)
S(9)	6574(2)	4525(3)	475(2)	14(1)
S(10)	238(2)	9044(3)	-2453(2)	17(1)
S(11)	7072(2)	2720(3)	-2128(2)	15(1)
S(12)	4932(2)	927(3)	-2299(2)	16(1)
Rb(1)	5151(1)	3877(1)	-1281(1)	16(1)
Rb(2)	1527(1)	6118(1)	-1910(1)	16(1)
Rb(3)	2044(1)	1570(1)	-2221(1)	31(1)
Rb(4)	5296(1)	1768(1)	1240(1)	25(1)
Rb(5)	1407(1)	-3608(1)	526(1)	23(1)

Table 3. Bond lengths [Å] and angles [°] for $Rb_5Th(PS_4)_3$.

Th(1)-S(1)	2.881(3)	S(1)-Rb(2)#4	3.542(3)
Th(1)-S(3)	2.899(3)	S(1)-Rb(3)#7	3.608(3)
Th(1)-S(5)	2.901(3)	S(2)-P(2)#4	2.073(4)
Th(1)-S(4)	2.953(3)	S(2)-Th(1)#1	3.285(3)
Th(1)-S(8)	3.003(3)	S(2)-Rb(5)	3.355(3)
Th(1)-S(2)	3.004(3)	S(3)-P(2)#8	2.047(4)
Th(1)-S(7)	3.015(3)	S(3)-Rb(2)#8	3.513(3)
Th(1)-S(6)	3.076(3)	S(3)-Rb(3)	3.630(4)
Th(1)-P(1)	3.256(3)	S(3)-Rb(5)	3.728(4)
Th(1)-S(2)#1	3.285(3)	S(5)-P(3)#5	2.075(4)
Th(1)-Rb(4)	4.592(2)	S(5)-Rb(1)#5	3.475(3)
Th(1)-Rb(5)	4.673(2)	S(5)-Rb(5)	3.689(4)
P(1)-S(9)#2	2.008(4)	S(5)-Rb(4)	3.750(4)
P(1)-S(6)	2.055(4)	S(4)-P(3)#5	2.073(4)
P(1)-S(7)	2.055(4)	S(4)-Rb(3)#7	3.352(3)
P(1)-S(8)	2.060(4)	S(4)-Rb(2)#7	3.377(3)
P(1)-Rb(5)#3	3.679(3)	S(4)-Rb(4)	3.963(3)
P(1)-Rb(1)	3.901(3)	S(8)-Rb(5)#3	3.491(3)
P(1)-Rb(2)	4.074(3)	S(8)-Rb(4)	3.539(3)
P(2)-S(10)	1.995(4)	S(8)-Rb(1)#2	3.585(3)
P(2)-S(3)#3	2.047(4)	S(8)-Rb(3)#7	3.742(3)
P(2)-S(1)#4	2.061(4)	S(6)-Rb(1)	3.371(3)
P(2)-S(2)#4	2.073(4)	S(6)-Rb(4)	3.470(3)
P(2)-Rb(2)	3.602(3)	S(6)-Rb(3)	3.493(3)
P(2)-Rb(3)#3	3.897(3)	S(7)-Rb(2)	3.575(3)
P(3)-S(12)	2.017(4)	S(7)-Rb(3)	3.623(3)
P(3)-S(11)	2.022(4)	S(7)-Rb(5)#3	3.691(3)
P(3)-S(4)#5	2.073(4)	S(7)-Rb(5)#1	3.702(3)
P(3)-S(5)#5	2.076(4)	S(9)-P(1)#2	2.008(4)
P(3)-Rb(1)	3.518(3)	S(9)-Rb(2)#2	3.327(3)
P(3)-Rb(4)#5	3.868(3)	S(9)-Rb(1)#2	3.336(3)
P(3)-Rb(2)#6	3.893(3)	S(9)-Rb(1)	3.449(3)
S(1)-P(2)#4	2.061(4)	S(9)-Rb(5)#5	3.615(3)
S(1)-Rb(5)#1	3.506(3)	S(9)-Rb(4)	3.640(3)

S(10)-Rb(2)#9	3.170(3)	Rb(4)-S(12)#7	3.617(3)
S(10)-Rb(2)	3.435(3)	Rb(4)-P(3)#5	3.868(3)
S(10)-Rb(3)#3	3.444(3)	Rb(4)-Rb(1)#2	4.396(2)
S(10)-Rb(3)#9	3.856(4)	Rb(4)-Rb(1)#7	4.596(2)
S(11)-Rb(2)#6	3.203(3)	Rb(5)-S(11)#5	3.335(3)
S(11)-Rb(5)#5	3.335(3)	Rb(5)-S(8)#8	3.491(3)
S(11)-Rb(1)	3.405(3)	Rb(5)-S(1)#1	3.506(3)
S(11)-Rb(4)#10	3.460(3)	Rb(5)-S(9)#5	3.615(3)
S(12)-Rb(1)#6	3.283(3)	Rb(5)-P(1)#8	3.679(3)
S(12)-Rb(4)#5	3.359(3)	Rb(5)-S(7)#8	3.691(3)
S(12)-Rb(1)	3.466(3)	Rb(5)-S(7)#1	3.702(3)
S(12)-Rb(4)#10	3.616(3)	Rb(5)-Rb(2)#8	4.472(2)
S(12)-Rb(3)	3.894(3)	Rb(5)-Rb(1)#5	4.501(2)
Rb(1)-S(12)#11	3.283(3)	S(1)-Th(1)-S(3)	139.55(8)
Rb(1)-S(9)#2	3.336(3)	S(1)-Th(1)-S(5)	143.81(8)
Rb(1)-S(5)#5	3.475(3)	S(3)-Th(1)-S(5)	64.06(8)
Rb(1)-S(8)#2	3.585(3)	S(1)-Th(1)-S(4)	79.60(8)
Rb(1)-Rb(4)#2	4.396(2)	S(3)-Th(1)-S(4)	126.59(8)
Rb(1)-Rb(5)#5	4.501(2)	S(5)-Th(1)-S(4)	66.10(8)
Rb(2)-S(10)#12	3.170(3)	S(1)-Th(1)-S(8)	72.59(8)
Rb(2)-S(11)#11	3.203(3)	S(3)-Th(1)-S(8)	140.55(8)
Rb(2)-S(9)#2	3.327(3)	S(5)-Th(1)-S(8)	104.52(9)
Rb(2)-S(4)#10	3.377(3)	S(4)-Th(1)-S(8)	70.30(8)
Rb(2)-S(3)#3	3.513(3)	S(1)-Th(1)-S(2)	68.15(8)
Rb(2)-S(1)#4	3.542(3)	S(3)-Th(1)-S(2)	86.49(8)
Rb(2)-P(3)#11	3.893(3)	S(5)-Th(1)-S(2)	92.63(9)
Rb(2)-Rb(5)#3	4.472(2)	S(4)-Th(1)-S(2)	77.73(8)
Rb(3)-S(4)#10	3.352(3)	S(8)-Th(1)-S(2)	132.82(7)
Rb(3)-S(10)#8	3.444(3)	S(1)-Th(1)-S(7)	75.42(8)
Rb(3)-S(1)#10	3.608(3)	S(3)-Th(1)-S(7)	96.55(9)
Rb(3)-S(8)#10	3.742(3)	S(5)-Th(1)-S(7)	137.64(8)
Rb(3)-S(10)#12	3.856(4)	S(4)-Th(1)-S(7)	134.09(8)
Rb(3)-P(2)#8	3.897(3)	S(8)-Th(1)-S(7)	65.74(8)
Rb(3)-Rb(2)#12	4.703(2)	S(2)-Th(1)-S(7)	125.04(8)
Rb(4)-S(12)#5	3.359(3)	S(1)-Th(1)-S(6)	128.98(8)
Rb(4)-S(11)#7	3.460(3)	S(3)-Th(1)-S(6)	76.74(8)

S(5)-Th(1)-S(6)	75.04(8)	S(8)-Th(1)-Rb(5)	149.92(6)
S(4)-Th(1)-S(6)	107.70(8)	S(2)-Th(1)-Rb(5)	45.72(5)
S(8)-Th(1)-S(6)	63.83(7)	S(7)-Th(1)-Rb(5)	143.82(6)
S(2)-Th(1)-S(6)	162.29(7)	S(6)-Th(1)-Rb(5)	117.39(5)
S(7)-Th(1)-S(6)	63.59(8)	P(1)-Th(1)-Rb(5)	154.99(5)
S(1)-Th(1)-P(1)	91.28(8)	S(2)#1-Th(1)-Rb(5)	81.96(5)
S(3)-Th(1)-P(1)	106.61(8)	Rb(4)-Th(1)-Rb(5)	105.55(2)
S(5)-Th(1)-P(1)	108.56(8)	S(9)#2-P(1)-S(6)	118.4(2)
S(4)-Th(1)-P(1)	106.18(8)	S(9)#2-P(1)-S(7)	113.8(2)
S(8)-Th(1)-P(1)	38.16(7)	S(6)-P(1)-S(7)	102.7(2)
S(2)-Th(1)-P(1)	158.31(7)	S(9)#2-P(1)-S(8)	112.5(2)
S(7)-Th(1)-P(1)	38.02(7)	S(6)-P(1)-S(8)	102.8(2)
S(6)-Th(1)-P(1)	37.74(7)	S(7)-P(1)-S(8)	105.1(2)
S(1)-Th(1)-S(2)#1	77.79(8)	S(9)#2-P(1)-Th(1)	175.08(15)
S(3)-Th(1)-S(2)#1	63.26(7)	S(6)-P(1)-Th(1)	66.39(11)
S(5)-Th(1)-S(2)#1	124.36(8)	S(7)-P(1)-Th(1)	64.62(10)
S(4)-Th(1)-S(2)#1	143.80(7)	S(8)-P(1)-Th(1)	64.27(11)
S(8)-Th(1)-S(2)#1	127.44(7)	S(9)#2-P(1)-Rb(5)#3	72.27(11)
S(2)-Th(1)-S(2)#1	67.76(9)	S(6)-P(1)-Rb(5)#3	168.76(14)
S(7)-Th(1)-S(2)#1	65.30(7)	S(7)-P(1)-Rb(5)#3	74.11(11)
S(6)-Th(1)-S(2)#1	108.50(8)	S(8)-P(1)-Rb(5)#3	68.35(11)
P(1)-Th(1)-S(2)#1	102.24(7)	Th(1)-P(1)-Rb(5)#3	102.85(8)
S(1)-Th(1)-Rb(4)	116.51(6)	S(9)#2-P(1)-Rb(1)	58.75(10)
S(3)-Th(1)-Rb(4)	103.90(6)	S(6)-P(1)-Rb(1)	59.74(10)
S(5)-Th(1)-Rb(4)	54.59(7)	S(7)-P(1)-Rb(1)	125.36(13)
S(4)-Th(1)-Rb(4)	58.67(6)	S(8)-P(1)-Rb(1)	128.49(14)
S(8)-Th(1)-Rb(4)	50.40(6)	Th(1)-P(1)-Rb(1)	126.11(8)
S(2)-Th(1)-Rb(4)	132.48(6)	Rb(5)#3-P(1)-Rb(1)	131.01(8)
S(7)-Th(1)-Rb(4)	100.08(6)	S(9)#2-P(1)-Rb(2)	54.23(11)
S(6)-Th(1)-Rb(4)	49.07(6)	S(6)-P(1)-Rb(2)	118.11(13)
P(1)-Th(1)-Rb(4)	62.12(5)	S(7)-P(1)-Rb(2)	61.29(10)
S(2)#1-Th(1)-Rb(4)	157.48(5)	S(8)-P(1)-Rb(2)	138.56(14)
S(1)-Th(1)-Rb(5)	113.63(6)	Th(1)-P(1)-Rb(2)	125.25(8)
S(3)-Th(1)-Rb(5)	52.91(7)	Rb(5)#3-P(1)-Rb(2)	70.23(6)
S(5)-Th(1)-Rb(5)	52.14(7)	Rb(1)-P(1)-Rb(2)	81.56(6)
S(4)-Th(1)-Rb(5)	81.68(6)	S(10)-P(2)-S(3)#3	109.7(2)

S(10)-P(2)-S(1)#4	109.5(2)	P(2)#4-S(1)-Rb(5)#1	100.08(13)
S(3)#3-P(2)-S(1)#4	109.2(2)	Th(1)-S(1)-Rb(5)#1	103.27(8)
S(10)-P(2)-S(2)#4	117.7(2)	P(2)#4-S(1)-Rb(2)#4	74.84(11)
S(3)#3-P(2)-S(2)#4	104.6(2)	Th(1)-S(1)-Rb(2)#4	169.48(10)
S(1)#4-P(2)-S(2)#4	105.9(2)	Rb(5)#1-S(1)-Rb(2)#4	78.76(7)
S(10)-P(2)-Rb(2)	68.99(12)	P(2)#4-S(1)-Rb(3)#7	100.01(13)
S(3)#3-P(2)-Rb(2)	70.90(11)	Th(1)-S(1)-Rb(3)#7	100.21(9)
S(1)#4-P(2)-Rb(2)	71.65(11)	Rb(5)#1-S(1)-Rb(3)#7	147.55(9)
S(2)#4-P(2)-Rb(2)	173.22(14)	Rb(2)#4-S(1)-Rb(3)#7	82.25(7)
S(10)-P(2)-Rb(3)#3	61.99(12)	P(2)#4-S(2)-Th(1)	90.84(12)
S(3)#3-P(2)-Rb(3)#3	67.13(12)	P(2)#4-S(2)-Th(1)#1	89.46(12)
S(1)#4-P(2)-Rb(3)#3	166.52(14)	Th(1)-S(2)-Th(1)#1	112.24(9)
S(2)#4-P(2)-Rb(3)#3	87.57(12)	P(2)#4-S(2)-Rb(5)	168.20(15)
Rb(2)-P(2)-Rb(3)#3	95.08(7)	Th(1)-S(2)-Rb(5)	94.41(8)
S(12)-P(3)-S(11)	110.1(2)	Th(1)#1-S(2)-Rb(5)	98.30(8)
S(12)-P(3)-S(4)#5	112.4(2)	P(2)#8-S(3)-Th(1)	101.52(13)
S(11)-P(3)-S(4)#5	113.1(2)	P(2)#8-S(3)-Rb(2)#8	75.69(12)
S(12)-P(3)-S(5)#5	110.4(2)	Th(1)-S(3)-Rb(2)#8	164.39(11)
S(11)-P(3)-S(5)#5	109.8(2)	P(2)#8-S(3)-Rb(3)	81.56(12)
S(4)#5-P(3)-S(5)#5	100.6(2)	Th(1)-S(3)-Rb(3)	93.05(9)
S(12)-P(3)-Rb(1)	71.83(12)	Rb(2)#8-S(3)-Rb(3)	101.60(8)
S(11)-P(3)-Rb(1)	70.00(12)	P(2)#8-S(3)-Rb(5)	93.68(13)
S(4)#5-P(3)-Rb(1)	172.24(14)	Th(1)-S(3)-Rb(5)	88.76(8)
S(5)#5-P(3)-Rb(1)	71.62(11)	Rb(2)#8-S(3)-Rb(5)	76.21(7)
S(12)-P(3)-Rb(4)#5	60.23(11)	Rb(3)-S(3)-Rb(5)	175.16(9)
S(11)-P(3)-Rb(4)#5	168.77(15)	P(3)#5-S(5)-Th(1)	96.37(13)
S(4)#5-P(3)-Rb(4)#5	77.19(12)	P(3)#5-S(5)-Rb(1)#5	73.85(12)
S(5)#5-P(3)-Rb(4)#5	71.08(12)	Th(1)-S(5)-Rb(1)#5	163.90(11)
Rb(1)-P(3)-Rb(4)#5	100.34(7)	P(3)#5-S(5)-Rb(5)	89.01(13)
S(12)-P(3)-Rb(2)#6	117.42(13)	Th(1)-S(5)-Rb(5)	89.49(8)
S(11)-P(3)-Rb(2)#6	55.19(10)	Rb(1)#5-S(5)-Rb(5)	77.78(8)
S(4)#5-P(3)-Rb(2)#6	60.08(10)	P(3)#5-S(5)-Rb(4)	77.35(12)
S(5)#5-P(3)-Rb(2)#6	132.17(14)	Th(1)-S(5)-Rb(4)	86.33(9)
Rb(1)-P(3)-Rb(2)#6	124.51(8)	Rb(1)#5-S(5)-Rb(4)	103.49(8)
Rb(4)#5-P(3)-Rb(2)#6	132.95(8)	Rb(5)-S(5)-Rb(4)	165.18(8)
P(2)#4-S(1)-Th(1)	94.64(13)	P(3)#5-S(4)-Th(1)	94.89(12)

P(3)#5-S(4)-Rb(3)#7	159.42(15)	Th(1)-S(7)-Rb(2)	163.29(10)
Th(1)-S(4)-Rb(3)#7	104.77(8)	P(1)-S(7)-Rb(3)	92.12(12)
P(3)#5-S(4)-Rb(2)#7	87.78(12)	Th(1)-S(7)-Rb(3)	91.26(8)
Th(1)-S(4)-Rb(2)#7	120.77(10)	Rb(2)-S(7)-Rb(3)	80.42(7)
Rb(3)#7-S(4)-Rb(2)#7	87.35(7)	P(1)-S(7)-Rb(5)#3	73.50(11)
P(3)#5-S(4)-Rb(4)	72.14(11)	Th(1)-S(7)-Rb(5)#3	107.68(8)
Th(1)-S(4)-Rb(4)	81.80(6)	Rb(2)-S(7)-Rb(5)#3	75.95(7)
Rb(3)#7-S(4)-Rb(4)	104.31(8)	Rb(3)-S(7)-Rb(5)#3	152.49(9)
Rb(2)#7-S(4)-Rb(4)	151.56(9)	P(1)-S(7)-Rb(5)#1	149.01(14)
P(1)-S(8)-Th(1)	77.58(11)	Th(1)-S(7)-Rb(5)#1	96.28(7)
P(1)-S(8)-Rb(5)#3	78.39(12)	Rb(2)-S(7)-Rb(5)#1	100.42(7)
Th(1)-S(8)-Rb(5)#3	113.19(9)	Rb(3)-S(7)-Rb(5)#1	118.54(8)
P(1)-S(8)-Rb(4)	93.69(12)	Rb(5)#3-S(7)-Rb(5)#1	79.90(7)
Th(1)-S(8)-Rb(4)	88.76(8)	P(1)#2-S(9)-Rb(2)#2	96.45(13)
Rb(5)#3-S(8)-Rb(4)	153.91(9)	P(1)#2-S(9)-Rb(1)#2	90.28(13)
P(1)-S(8)-Rb(1)#2	90.27(12)	Rb(2)#2-S(9)-Rb(1)#2	102.92(8)
Th(1)-S(8)-Rb(1)#2	160.09(9)	P(1)#2-S(9)-Rb(1)	95.11(13)
Rb(5)#3-S(8)-Rb(1)#2	79.00(7)	Rb(2)#2-S(9)-Rb(1)	152.89(10)
Rb(4)-S(8)-Rb(1)#2	76.20(7)	Rb(1)#2-S(9)-Rb(1)	101.46(8)
P(1)-S(8)-Rb(3)#7	159.58(15)	P(1)#2-S(9)-Rb(5)#5	75.79(11)
Th(1)-S(8)-Rb(3)#7	95.06(7)	Rb(2)#2-S(9)-Rb(5)#5	80.09(7)
Rb(5)#3-S(8)-Rb(3)#7	87.36(7)	Rb(1)#2-S(9)-Rb(5)#5	166.03(9)
Rb(4)-S(8)-Rb(3)#7	105.29(7)	Rb(1)-S(9)-Rb(5)#5	79.12(7)
Rb(1)#2-S(8)-Rb(3)#7	101.38(7)	P(1)#2-S(9)-Rb(4)	167.93(15)
P(1)-S(6)-Th(1)	75.87(11)	Rb(2)#2-S(9)-Rb(4)	83.61(7)
P(1)-S(6)-Rb(1)	88.49(12)	Rb(1)#2-S(9)-Rb(4)	77.99(7)
Th(1)-S(6)-Rb(1)	164.29(10)	Rb(1)-S(9)-Rb(4)	90.05(7)
P(1)-S(6)-Rb(4)	95.80(13)	Rb(5)#5-S(9)-Rb(4)	115.98(8)
Th(1)-S(6)-Rb(4)	88.87(8)	P(2)-S(10)-Rb(2)#9	104.80(14)
Rb(1)-S(6)-Rb(4)	94.33(8)	P(2)-S(10)-Rb(2)	78.19(12)
P(1)-S(6)-Rb(3)	95.91(13)	Rb(2)#9-S(10)-Rb(2)	162.23(11)
Th(1)-S(6)-Rb(3)	92.75(8)	P(2)-S(10)-Rb(3)#3	87.26(13)
Rb(1)-S(6)-Rb(3)	87.25(7)	Rb(2)#9-S(10)-Rb(3)#3	90.55(9)
Rb(4)-S(6)-Rb(3)	168.22(10)	Rb(2)-S(10)-Rb(3)#3	107.16(9)
P(1)-S(7)-Th(1)	77.36(11)	P(2)-S(10)-Rb(3)#9	93.75(13)
P(1)-S(7)-Rb(2)	88.42(12)	Rb(2)#9-S(10)-Rb(3)#9	82.20(8)

Rb(2)-S(10)-Rb(3)#9	80.11(7)	S(11)-Rb(1)-S(9)	99.22(8)
Rb(3)#3-S(10)-Rb(3)#9	172.70(10)	S(12)#11-Rb(1)-S(12)	97.09(4)
P(3)-S(11)-Rb(2)#6	93.59(13)	S(9)#2-Rb(1)-S(12)	130.29(8)
P(3)-S(11)-Rb(5)#5	100.44(13)	S(6)-Rb(1)-S(12)	76.49(7)
Rb(2)#6-S(11)-Rb(5)#5	107.19(9)	S(11)-Rb(1)-S(12)	57.59(7)
P(3)-S(11)-Rb(1)	76.09(12)	S(9)-Rb(1)-S(12)	129.14(8)
Rb(2)#6-S(11)-Rb(1)	166.34(10)	S(12)#11-Rb(1)-S(5)#5	135.15(7)
Rb(5)#5-S(11)-Rb(1)	83.79(7)	S(9)#2-Rb(1)-S(5)#5	127.80(7)
P(3)-S(11)-Rb(4)#10	96.97(13)	S(6)-Rb(1)-S(5)#5	74.39(8)
Rb(2)#6-S(11)-Rb(4)#10	88.43(8)	S(11)-Rb(1)-S(5)#5	58.29(7)
Rb(5)#5-S(11)-Rb(4)#10	155.66(10)	S(9)-Rb(1)-S(5)#5	71.33(7)
Rb(1)-S(11)-Rb(4)#10	84.03(7)	S(12)-Rb(1)-S(5)#5	57.90(7)
P(3)-S(12)-Rb(1)#6	105.96(13)	S(12)#11-Rb(1)-P(3)	103.84(8)
P(3)-S(12)-Rb(4)#5	88.36(13)	S(9)#2-Rb(1)-P(3)	154.77(7)
Rb(1)#6-S(12)-Rb(4)#5	87.56(8)	S(6)-Rb(1)-P(3)	92.06(7)
P(3)-S(12)-Rb(1)	74.62(12)	S(11)-Rb(1)-P(3)	33.91(7)
Rb(1)#6-S(12)-Rb(1)	159.87(10)	S(9)-Rb(1)-P(3)	101.23(7)
Rb(4)#5-S(12)-Rb(1)	112.53(9)	S(12)-Rb(1)-P(3)	33.56(7)
P(3)-S(12)-Rb(4)#10	92.40(13)	S(5)#5-Rb(1)-P(3)	34.53(7)
Rb(1)#6-S(12)-Rb(4)#10	79.00(7)	S(12)#11-Rb(1)-S(8)#2	66.66(7)
Rb(4)#5-S(12)-Rb(4)#10	166.21(10)	S(9)#2-Rb(1)-S(8)#2	95.58(7)
Rb(1)-S(12)-Rb(4)#10	80.88(8)	S(6)-Rb(1)-S(8)#2	143.27(7)
P(3)-S(12)-Rb(3)	148.98(14)	S(11)-Rb(1)-S(8)#2	76.19(7)
Rb(1)#6-S(12)-Rb(3)	104.07(8)	S(9)-Rb(1)-S(8)#2	57.45(6)
Rb(4)#5-S(12)-Rb(3)	85.31(7)	S(12)-Rb(1)-S(8)#2	133.63(7)
Rb(1)-S(12)-Rb(3)	79.89(6)	S(5)#5-Rb(1)-S(8)#2	102.36(8)
Rb(4)#10-S(12)-Rb(3)	100.79(7)	P(3)-Rb(1)-S(8)#2	105.59(7)
S(12)#11-Rb(1)-S(9)#2	96.99(8)	S(12)#11-Rb(1)-P(1)	120.62(7)
S(12)#11-Rb(1)-S(6)	140.36(8)	S(9)#2-Rb(1)-P(1)	30.97(6)
S(9)#2-Rb(1)-S(6)	62.72(7)	S(6)-Rb(1)-P(1)	31.77(6)
S(12)#11-Rb(1)-S(11)	76.96(7)	S(11)-Rb(1)-P(1)	157.72(7)
S(9)#2-Rb(1)-S(11)	171.18(8)	S(9)-Rb(1)-P(1)	82.88(7)
S(6)-Rb(1)-S(11)	125.95(8)	S(12)-Rb(1)-P(1)	103.94(7)
S(12)#11-Rb(1)-S(9)	122.92(8)	S(5)#5-Rb(1)-P(1)	102.37(7)
S(9)#2-Rb(1)-S(9)	78.54(8)	P(3)-Rb(1)-P(1)	123.82(7)
S(6)-Rb(1)-S(9)	87.98(7)	S(8)#2-Rb(1)-P(1)	121.93(7)

S(12)#11-Rb(1)-Rb(4)#2	53.86(6)	S(10)#12-Rb(2)-S(1)#4	82.25(8)
S(9)#2-Rb(1)-Rb(4)#2	54.10(5)	S(11)#11-Rb(2)-S(1)#4	127.26(8)
S(6)-Rb(1)-Rb(4)#2	116.81(6)	S(9)#2-Rb(2)-S(1)#4	102.60(8)
S(11)-Rb(1)-Rb(4)#2	117.24(6)	S(4)#10-Rb(2)-S(1)#4	162.29(8)
S(9)-Rb(1)-Rb(4)#2	81.37(5)	S(10)-Rb(2)-S(1)#4	56.64(7)
S(12)-Rb(1)-Rb(4)#2	148.61(6)	S(3)#3-Rb(2)-S(1)#4	56.64(7)
S(5)#5-Rb(1)-Rb(4)#2	150.36(6)	S(10)#12-Rb(2)-S(7)	66.62(7)
P(3)-Rb(1)-Rb(4)#2	151.13(6)	S(11)#11-Rb(2)-S(7)	147.04(8)
S(8)#2-Rb(1)-Rb(4)#2	51.43(5)	S(9)#2-Rb(2)-S(7)	58.98(7)
P(1)-Rb(1)-Rb(4)#2	85.04(5)	S(4)#10-Rb(2)-S(7)	94.49(8)
S(12)#11-Rb(1)-Rb(5)#5	99.24(6)	S(10)-Rb(2)-S(7)	137.99(7)
S(9)#2-Rb(1)-Rb(5)#5	128.84(6)	S(3)#3-Rb(2)-S(7)	106.99(8)
S(6)-Rb(1)-Rb(5)#5	120.15(6)	S(1)#4-Rb(2)-S(7)	81.76(7)
S(11)-Rb(1)-Rb(5)#5	47.44(6)	S(10)#12-Rb(2)-P(2)	108.10(8)
S(9)-Rb(1)-Rb(5)#5	52.06(5)	S(11)#11-Rb(2)-P(2)	94.19(8)
S(12)-Rb(1)-Rb(5)#5	95.22(5)	S(9)#2-Rb(2)-P(2)	104.03(7)
S(5)#5-Rb(1)-Rb(5)#5	53.23(6)	S(4)#10-Rb(2)-P(2)	154.20(7)
P(3)-Rb(1)-Rb(5)#5	61.77(5)	S(10)-Rb(2)-P(2)	32.83(7)
S(8)#2-Rb(1)-Rb(5)#5	49.58(5)	S(3)#3-Rb(2)-P(2)	33.41(6)
P(1)-Rb(1)-Rb(5)#5	132.28(6)	S(1)#4-Rb(2)-P(2)	33.51(6)
Rb(4)#2-Rb(1)-Rb(5)#5	100.66(3)	S(7)-Rb(2)-P(2)	111.28(7)
S(10)#12-Rb(2)-S(11)#11	125.97(8)	S(10)#12-Rb(2)-P(3)#11	108.16(7)
S(10)#12-Rb(2)-S(9)#2	123.68(8)	S(11)#11-Rb(2)-P(3)#11	31.21(7)
S(11)#11-Rb(2)-S(9)#2	95.62(8)	S(9)#2-Rb(2)-P(3)#11	87.90(7)
S(10)#12-Rb(2)-S(4)#10	80.40(8)	S(4)#10-Rb(2)-P(3)#11	32.14(6)
S(11)#11-Rb(2)-S(4)#10	62.51(7)	S(10)-Rb(2)-P(3)#11	101.87(7)
S(9)#2-Rb(2)-S(4)#10	89.98(8)	S(3)#3-Rb(2)-P(3)#11	109.51(7)
S(10)#12-Rb(2)-S(10)	99.30(4)	S(1)#4-Rb(2)-P(3)#11	158.00(7)
S(11)#11-Rb(2)-S(10)	73.89(7)	S(7)-Rb(2)-P(3)#11	120.03(7)
S(9)#2-Rb(2)-S(10)	130.54(8)	P(2)-Rb(2)-P(3)#11	125.40(7)
S(4)#10-Rb(2)-S(10)	123.11(7)	S(10)#12-Rb(2)-P(1)	94.57(8)
S(10)#12-Rb(2)-S(3)#3	138.71(8)	S(11)#11-Rb(2)-P(1)	120.03(7)
S(11)#11-Rb(2)-S(3)#3	82.64(8)	S(9)#2-Rb(2)-P(1)	29.32(6)
S(9)#2-Rb(2)-S(3)#3	74.13(7)	S(4)#10-Rb(2)-P(1)	88.05(7)
S(4)#10-Rb(2)-S(3)#3	140.23(7)	S(10)-Rb(2)-P(1)	147.50(7)
S(10)-Rb(2)-S(3)#3	56.80(7)	S(3)#3-Rb(2)-P(1)	94.02(7)

S(1)#4-Rb(2)-P(1)	96.82(7)	S(4)#10-Rb(3)-S(10)#12	71.45(7)
S(7)-Rb(2)-P(1)	30.28(6)	S(10)#8-Rb(3)-S(10)#12	87.07(4)
P(2)-Rb(2)-P(1)	114.74(7)	S(6)-Rb(3)-S(10)#12	111.40(7)
P(3)#11-Rb(2)-P(1)	101.46(6)	S(1)#10-Rb(3)-S(10)#12	52.55(6)
S(10)#12-Rb(2)-Rb(5)#3	104.02(6)	S(7)-Rb(3)-S(10)#12	59.55(6)
S(11)#11-Rb(2)-Rb(5)#3	129.91(6)	S(3)-Rb(3)-S(10)#12	113.33(7)
S(9)#2-Rb(2)-Rb(5)#3	52.78(5)	S(8)#10-Rb(3)-S(10)#12	104.36(7)
S(4)#10-Rb(2)-Rb(5)#3	138.57(6)	S(4)#10-Rb(3)-S(12)	76.10(7)
S(10)-Rb(2)-Rb(5)#3	97.19(5)	S(10)#8-Rb(3)-S(12)	122.29(8)
S(3)#3-Rb(2)-Rb(5)#3	54.06(6)	S(6)-Rb(3)-S(12)	69.69(7)
S(1)#4-Rb(2)-Rb(5)#3	50.27(5)	S(1)#10-Rb(3)-S(12)	115.46(7)
S(7)-Rb(2)-Rb(5)#3	53.19(5)	S(7)-Rb(3)-S(12)	120.22(7)
P(2)-Rb(2)-Rb(5)#3	64.43(5)	S(3)-Rb(3)-S(12)	96.43(7)
P(3)#11-Rb(2)-Rb(5)#3	139.03(5)	S(8)#10-Rb(3)-S(12)	59.34(6)
P(1)-Rb(2)-Rb(5)#3	50.74(5)	S(10)#12-Rb(3)-S(12)	147.33(7)
S(4)#10-Rb(3)-S(10)#8	142.42(8)	S(4)#10-Rb(3)-P(2)#8	159.98(8)
S(4)#10-Rb(3)-S(6)	98.81(8)	S(10)#8-Rb(3)-P(2)#8	30.76(6)
S(10)#8-Rb(3)-S(6)	117.92(7)	S(6)-Rb(3)-P(2)#8	88.83(7)
S(4)#10-Rb(3)-S(1)#10	64.78(7)	S(1)#10-Rb(3)-P(2)#8	102.83(7)
S(10)#8-Rb(3)-S(1)#10	77.65(7)	S(7)-Rb(3)-P(2)#8	75.60(7)
S(6)-Rb(3)-S(1)#10	159.04(8)	S(3)-Rb(3)-P(2)#8	31.31(6)
S(4)#10-Rb(3)-S(7)	94.03(8)	S(8)#10-Rb(3)-P(2)#8	130.45(7)
S(10)#8-Rb(3)-S(7)	101.24(7)	S(10)#12-Rb(3)-P(2)#8	88.54(7)
S(6)-Rb(3)-S(7)	53.58(7)	S(12)-Rb(3)-P(2)#8	123.90(7)
S(1)#10-Rb(3)-S(7)	112.08(8)	S(4)#10-Rb(3)-Rb(2)	46.54(5)
S(4)#10-Rb(3)-S(3)	161.58(8)	S(10)#8-Rb(3)-Rb(2)	128.18(7)
S(10)#8-Rb(3)-S(3)	55.64(7)	S(6)-Rb(3)-Rb(2)	80.99(5)
S(6)-Rb(3)-S(3)	62.78(7)	S(1)#10-Rb(3)-Rb(2)	78.17(5)
S(1)#10-Rb(3)-S(3)	132.86(7)	S(7)-Rb(3)-Rb(2)	49.34(5)
S(7)-Rb(3)-S(3)	74.98(7)	S(3)-Rb(3)-Rb(2)	124.31(6)
S(4)#10-Rb(3)-S(8)#10	57.50(7)	S(8)#10-Rb(3)-Rb(2)	102.42(5)
S(10)#8-Rb(3)-S(8)#10	101.20(7)	S(10)#12-Rb(3)-Rb(2)	42.52(5)
S(6)-Rb(3)-S(8)#10	127.09(8)	S(12)-Rb(3)-Rb(2)	109.45(5)
S(1)#10-Rb(3)-S(8)#10	56.57(7)	P(2)#8-Rb(3)-Rb(2)	117.65(6)
S(7)-Rb(3)-S(8)#10	151.44(7)	S(4)#10-Rb(3)-Rb(2)#12	106.04(6)
S(3)-Rb(3)-S(8)#10	132.94(8)	S(10)#8-Rb(3)-Rb(2)#12	42.38(5)

S(6)-Rb(3)-Rb(2)#12	133.73(6)
S(1)#10-Rb(3)-Rb(2)#12	48.27(5)
S(7)-Rb(3)-Rb(2)#12	85.84(6)
S(3)-Rb(3)-Rb(2)#12	88.15(5)
S(8)#10-Rb(3)-Rb(2)#12	99.16(6)
S(10)#12-Rb(3)-Rb(2)#12	46.02(5)
S(12)-Rb(3)-Rb(2)#12	153.87(6)
P(2)#8-Rb(3)-Rb(2)#12	56.85(5)
Rb(2)-Rb(3)-Rb(2)#12	88.52(3)
S(12)#5-Rb(4)-S(11)#7	75.22(7)
S(12)#5-Rb(4)-S(6)	116.43(8)
S(11)#7-Rb(4)-S(6)	167.66(8)
S(12)#5-Rb(4)-S(8)	108.56(7)
S(11)#7-Rb(4)-S(8)	119.52(7)
S(6)-Rb(4)-S(8)	54.59(7)
S(12)#5-Rb(4)-S(12)#7	92.92(4)
S(11)#7-Rb(4)-S(12)#7	55.72(7)
S(6)-Rb(4)-S(12)#7	117.05(8)
S(8)-Rb(4)-S(12)#7	63.80(7)
S(12)#5-Rb(4)-S(9)	157.54(8)
S(11)#7-Rb(4)-S(9)	85.89(7)
S(6)-Rb(4)-S(9)	83.52(7)
S(8)-Rb(4)-S(9)	91.17(7)
S(12)#7-Rb(4)-S(9)	86.16(7)
S(12)#5-Rb(4)-S(5)	56.08(7)
S(11)#7-Rb(4)-S(5)	131.30(7)
S(6)-Rb(4)-S(5)	60.46(7)
S(8)-Rb(4)-S(5)	79.62(7)
S(12)#7-Rb(4)-S(5)	121.23(7)
S(9)-Rb(4)-S(5)	141.33(7)
S(12)#5-Rb(4)-P(3)#5	31.41(6)
S(11)#7-Rb(4)-P(3)#5	102.62(7)
S(6)-Rb(4)-P(3)#5	87.67(7)
S(8)-Rb(4)-P(3)#5	81.88(7)
S(12)#7-Rb(4)-P(3)#5	95.92(7)
S(9)-Rb(4)-P(3)#5	170.91(7)
S(5)-Rb(4)-P(3)#5	31.57(6)
S(12)#5-Rb(4)-S(4)	54.57(6)
S(11)#7-Rb(4)-S(4)	103.77(7)
S(6)-Rb(4)-S(4)	81.56(7)
S(8)-Rb(4)-S(4)	54.05(6)
S(12)#7-Rb(4)-S(4)	72.42(7)
S(9)-Rb(4)-S(4)	144.39(7)
S(5)-Rb(4)-S(4)	48.81(6)
P(3)#5-Rb(4)-S(4)	30.67(6)
S(12)#5-Rb(4)-Rb(1)#2	139.29(6)
S(11)#7-Rb(4)-Rb(1)#2	84.86(6)
S(6)-Rb(4)-Rb(1)#2	83.35(5)
S(8)-Rb(4)-Rb(1)#2	52.37(5)
S(12)#7-Rb(4)-Rb(1)#2	47.14(5)
S(9)-Rb(4)-Rb(1)#2	47.92(5)
S(5)-Rb(4)-Rb(1)#2	131.50(6)
P(3)#5-Rb(4)-Rb(1)#2	128.82(6)
S(4)-Rb(4)-Rb(1)#2	98.16(5)
S(12)#5-Rb(4)-Th(1)	83.16(5)
S(11)#7-Rb(4)-Th(1)	142.50(6)
S(6)-Rb(4)-Th(1)	42.05(5)
S(8)-Rb(4)-Th(1)	40.84(5)
S(12)#7-Rb(4)-Th(1)	96.03(5)
S(9)-Rb(4)-Th(1)	119.27(5)
S(5)-Rb(4)-Th(1)	39.08(5)
P(3)#5-Rb(4)-Th(1)	51.76(5)
S(4)-Rb(4)-Th(1)	39.53(4)
Rb(1)#2-Rb(4)-Th(1)	92.42(3)
S(12)#5-Rb(4)-Rb(1)#7	45.53(5)
S(11)#7-Rb(4)-Rb(1)#7	47.47(5)
S(6)-Rb(4)-Rb(1)#7	137.49(6)
S(8)-Rb(4)-Rb(1)#7	91.30(5)
S(12)#7-Rb(4)-Rb(1)#7	48.13(5)
S(9)-Rb(4)-Rb(1)#7	126.05(6)
S(5)-Rb(4)-Rb(1)#7	91.90(5)
P(3)#5-Rb(4)-Rb(1)#7	60.33(5)

S(4)-Rb(4)-Rb(1)#7	56.47(5)
Rb(1)#2-Rb(4)-Rb(1)#7	95.28(3)
Th(1)-Rb(4)-Rb(1)#7	95.88(3)
S(11)#5-Rb(5)-S(2)	79.24(7)
S(11)#5-Rb(5)-S(8)#8	78.38(7)
S(2)-Rb(5)-S(8)#8	156.01(8)
S(11)#5-Rb(5)-S(1)#1	146.35(8)
S(2)-Rb(5)-S(1)#1	68.93(7)
S(8)#8-Rb(5)-S(1)#1	134.57(7)
S(11)#5-Rb(5)-S(9)#5	97.31(8)
S(2)-Rb(5)-S(9)#5	135.27(7)
S(8)#8-Rb(5)-S(9)#5	56.83(6)
S(1)#1-Rb(5)-S(9)#5	97.70(7)
S(11)#5-Rb(5)-P(1)#8	103.49(7)
S(2)-Rb(5)-P(1)#8	166.71(7)
S(8)#8-Rb(5)-P(1)#8	33.26(6)
S(1)#1-Rb(5)-P(1)#8	105.16(7)
S(9)#5-Rb(5)-P(1)#8	31.94(6)
S(11)#5-Rb(5)-S(5)	56.73(7)
S(2)-Rb(5)-S(5)	74.48(7)
S(8)#8-Rb(5)-S(5)	99.98(7)
S(1)#1-Rb(5)-S(5)	102.79(7)
S(9)#5-Rb(5)-S(5)	67.11(7)
P(1)#8-Rb(5)-S(5)	95.96(7)
S(11)#5-Rb(5)-S(7)#8	132.22(7)
S(2)-Rb(5)-S(7)#8	148.35(8)
S(8)#8-Rb(5)-S(7)#8	54.02(7)
S(1)#1-Rb(5)-S(7)#8	80.62(7)
S(9)#5-Rb(5)-S(7)#8	55.54(6)
P(1)#8-Rb(5)-S(7)#8	32.39(6)
S(5)-Rb(5)-S(7)#8	122.34(7)
S(11)#5-Rb(5)-S(7)#1	111.31(7)
S(2)-Rb(5)-S(7)#1	57.48(7)
S(8)#8-Rb(5)-S(7)#1	124.52(7)
S(1)#1-Rb(5)-S(7)#1	60.00(6)
S(9)#5-Rb(5)-S(7)#1	151.19(7)
P(1)#8-Rb(5)-S(7)#1	130.90(7)
S(5)-Rb(5)-S(7)#1	131.91(7)
S(7)#8-Rb(5)-S(7)#1	100.10(7)
S(11)#5-Rb(5)-S(3)	104.13(8)
S(2)-Rb(5)-S(3)	69.43(7)
S(8)#8-Rb(5)-S(3)	124.80(7)
S(1)#1-Rb(5)-S(3)	55.02(7)
S(9)#5-Rb(5)-S(3)	68.34(7)
P(1)#8-Rb(5)-S(3)	97.36(7)
S(5)-Rb(5)-S(3)	49.00(6)
S(7)#8-Rb(5)-S(3)	100.35(7)
S(7)#1-Rb(5)-S(3)	106.16(7)
S(11)#5-Rb(5)-Rb(2)#8	139.03(6)
S(2)-Rb(5)-Rb(2)#8	110.37(6)
S(8)#8-Rb(5)-Rb(2)#8	92.28(5)
S(1)#1-Rb(5)-Rb(2)#8	50.98(5)
S(9)#5-Rb(5)-Rb(2)#8	47.13(5)
P(1)#8-Rb(5)-Rb(2)#8	59.03(5)
S(5)-Rb(5)-Rb(2)#8	86.63(5)
S(7)#8-Rb(5)-Rb(2)#8	50.86(5)
S(7)#1-Rb(5)-Rb(2)#8	106.82(5)
S(3)-Rb(5)-Rb(2)#8	49.72(5)
S(11)#5-Rb(5)-Rb(1)#5	48.77(5)
S(2)-Rb(5)-Rb(1)#5	116.53(6)
S(8)#8-Rb(5)-Rb(1)#5	51.42(5)
S(1)#1-Rb(5)-Rb(1)#5	140.05(6)
S(9)#5-Rb(5)-Rb(1)#5	48.82(5)
P(1)#8-Rb(5)-Rb(1)#5	59.85(5)
S(5)-Rb(5)-Rb(1)#5	48.99(5)
S(7)#8-Rb(5)-Rb(1)#5	92.23(5)
S(7)#1-Rb(5)-Rb(1)#5	158.66(5)
S(3)-Rb(5)-Rb(1)#5	88.46(5)
Rb(2)#8-Rb(5)-Rb(1)#5	94.48(3)

Symmetry transformations used to generate equivalent atoms:

#1 -x,-y,-z #2 -x+1,-y+1,-z #3 x,y+1,z #4 -x,-y+1,-z

#5 -x+1,-y,-z #6 -x+1,y-1/2,-z-1/2 #7 x,-y+1/2,z+1/2

#8 x,y-1,z #9 -x,y+1/2,-z-1/2 #10 x,-y+1/2,z-1/2

#11 -x+1,y+1/2,-z-1/2 #12 -x,y-1/2,-z-1/2

Table 4. Anisotropic displacement parameters ($Å^2 x\ 10^3$) for $Rb_5Th(PS_4)_3$. The anisotropic displacement factor exponent takes the form: $-2\pi^2[\ h^2\ a^{*2}U^{11} + ... + 2\ h\ k\ a^*\ b^*\ U^{12}\ ]$

	U^{11}	U^{22}	U^{33}	U^{23}	U^{13}	U^{12}
Th(1)	9(1)	5(1)	10(1)	0(1)	3(1)	1(1)
P(1)	12(1)	6(1)	11(1)	1(1)	3(1)	-2(1)
P(2)	10(1)	11(1)	9(1)	1(1)	1(1)	1(1)
P(3)	14(1)	7(1)	12(1)	-1(1)	2(1)	1(1)
S(1)	17(2)	5(1)	19(2)	-1(1)	9(1)	0(1)
S(2)	16(1)	6(1)	21(2)	-1(1)	8(1)	1(1)
S(3)	14(1)	19(2)	21(2)	-13(1)	-1(1)	4(1)
S(5)	26(2)	19(2)	11(1)	0(1)	2(1)	15(1)
S(4)	23(2)	10(1)	11(1)	1(1)	4(1)	6(1)
S(8)	19(2)	12(1)	9(1)	0(1)	5(1)	-5(1)
S(6)	16(1)	7(1)	23(2)	-1(1)	9(1)	-1(1)
S(7)	11(1)	16(2)	14(1)	7(1)	-2(1)	-2(1)
S(9)	16(1)	7(1)	21(2)	5(1)	5(1)	-2(1)
S(10)	23(2)	17(2)	12(1)	2(1)	5(1)	7(1)
S(11)	16(2)	9(1)	20(2)	-1(1)	3(1)	-1(1)
S(12)	14(1)	15(2)	19(1)	-1(1)	-3(1)	0(1)
Rb(1)	19(1)	11(1)	20(1)	0(1)	8(1)	1(1)
Rb(2)	17(1)	11(1)	20(1)	-1(1)	6(1)	1(1)
Rb(3)	45(1)	26(1)	19(1)	6(1)	1(1)	-17(1)
Rb(4)	25(1)	21(1)	24(1)	6(1)	-5(1)	-5(1)
Rb(5)	24(1)	17(1)	26(1)	-6(1)	-2(1)	8(1)

Table 1. Crystal data and structure refinement for $Cs_5Th(PS_4)_3$.

Identification code	80	
Empirical formula	$Cs_5Th(PS_4)_3$	
Formula weight	1374.22	
Temperature	163(2) K	
Wavelength	0.71073 Å	
Crystal system	Monoclinic	
Space group	P21/c	
Unit cell dimensions	a = 13.5624(1) Å	α= 90°.
	b = 10.3007(1) Å	β= 100.6700(10)°.
	c = 18.6738(1) Å	γ = 90°.
Volume	2563.66(3) $Å^3$	
Z	4	
Density (calculated)	3.560 Mg/m^3	
Absorption coefficient	13.967 mm^{-1}	
F(000)	2408	
Crystal size	0.33 x 0.24 x 0.10 mm^3	
Theta range for data collection	1.53 to 28.29°.	
Index ranges	-17<=h<=17, -12<=k<=13, -24<=l<=18	
Reflections collected	16368	
Independent reflections	6099 [R(int) = 0.0724]	
Absorption correction	SADABS	
Max. and min. transmission	0.942284 and 0.582425	
Refinement method	Full-matrix least-squares on F^2	
Data / restraints / parameters	6099 / 0 / 190	
Goodness-of-fit on F^2	1.041	
Final R indices [I>2sigma(I)]	R1 = 0.0452, wR2 = 0.1092	
R indices (all data)	R1 = 0.0611, wR2 = 0.1182	
Largest diff. peak and hole	4.876 and -3.227 $e.Å^{-3}$	

Table 2. Atomic coordinates (x 10^4) and equivalent isotropic displacement parameters ($Å^2$x 10^3) for $Cs_5Th(PS_4)_3$. U(eq) is defined as one third of the trace of the orthogonalized U^{ij} tensor.

	x	y	z	U(eq)
Th(1)	1861(1)	938(1)	376(1)	12(1)
P(1)	2848(2)	3589(2)	-162(1)	13(1)
P(2)	306(2)	9083(2)	-1309(1)	14(1)
P(3)	6454(2)	1077(2)	-1769(1)	16(1)
S(1)	461(2)	2488(2)	1001(1)	16(1)
S(2)	309(2)	-692(2)	894(2)	23(1)
S(3)	1774(2)	-974(3)	-776(1)	22(1)
S(5)	3364(2)	-1098(3)	641(1)	25(1)
S(4)	2789(2)	628(2)	1922(1)	22(1)
S(8)	2918(2)	3393(2)	941(1)	18(1)
S(6)	3531(2)	1915(2)	-430(1)	20(1)
S(7)	1368(2)	3243(2)	-629(1)	18(1)
S(9)	6630(2)	4686(2)	418(1)	19(1)
S(10)	269(2)	9007(3)	-2387(1)	22(1)
S(11)	7082(2)	2672(2)	-2125(1)	20(1)
S(12)	4986(2)	977(3)	-2238(2)	26(1)
Cs(1)	5136(1)	3954(1)	-1298(1)	22(1)
Cs(2)	1506(1)	6050(1)	-1880(1)	19(1)
Cs(3)	2088(1)	1549(1)	-2230(1)	31(1)
Cs(4)	5396(1)	1725(1)	1176(1)	32(1)
Cs(5)	1330(1)	-3693(1)	554(1)	25(1)

Table 3. Bond lengths [Å] and angles [°] for $Cs_5Th(PS_4)_3$.

Th(1)-S(1)	2.887(2)	S(1)-Cs(2)#3	3.702(2)
Th(1)-S(5)	2.903(2)	S(1)-Cs(3)#7	3.751(2)
Th(1)-S(3)	2.903(2)	S(2)-P(2)#3	2.070(3)
Th(1)-S(4)	2.945(2)	S(2)-Cs(5)	3.493(2)
Th(1)-S(2)	2.990(2)	S(3)-P(2)#8	2.055(3)
Th(1)-S(8)	3.000(2)	S(3)-Cs(2)#8	3.674(3)
Th(1)-S(7)	3.023(2)	S(3)-Cs(3)	3.837(3)
Th(1)-S(6)	3.109(2)	S(3)-Cs(5)	3.864(3)
Th(1)-P(1)	3.280(2)	S(3)-Cs(4)#4	4.116(2)
Th(1)-Cs(4)	4.8192(7)	S(5)-P(3)#4	2.075(3)
Th(1)-Cs(5)	4.8453(8)	S(5)-Cs(1)#4	3.658(3)
Th(1)-Cs(3)	4.9708(7)	S(5)-Cs(5)	3.823(3)
P(1)-S(9)#1	2.003(3)	S(5)-Cs(4)	4.004(3)
P(1)-S(8)	2.054(3)	S(5)-Cs(4)#4	4.107(2)
P(1)-S(6)	2.062(3)	S(4)-P(3)#4	2.080(3)
P(1)-S(7)	2.066(3)	S(4)-Cs(3)#7	3.526(2)
P(1)-Cs(5)#2	3.858(2)	S(4)-Cs(2)#7	3.531(2)
P(1)-Cs(1)	4.087(2)	S(4)-Cs(1)#7	4.177(3)
P(1)-Cs(2)	4.226(2)	S(8)-Cs(5)#2	3.687(3)
P(2)-S(10)	2.006(3)	S(8)-Cs(4)	3.728(2)
P(2)-S(3)#2	2.055(3)	S(8)-Cs(1)#1	3.772(2)
P(2)-S(1)#3	2.063(3)	S(8)-Cs(3)#7	3.791(2)
P(2)-S(2)#3	2.070(3)	S(6)-Cs(4)	3.552(3)
P(2)-Cs(2)	3.767(2)	S(6)-Cs(3)	3.582(3)
P(2)-Cs(3)#2	4.097(2)	S(6)-Cs(1)	3.617(2)
P(3)-S(11)	2.019(3)	S(7)-Cs(5)#6	3.718(2)
P(3)-S(12)	2.024(3)	S(7)-Cs(2)	3.743(2)
P(3)-S(5)#4	2.075(3)	S(7)-Cs(3)	3.743(2)
P(3)-S(4)#4	2.080(3)	S(7)-Cs(5)#2	3.857(3)
P(3)-Cs(1)	3.652(2)	S(9)-P(1)#1	2.003(3)
P(3)-Cs(2)#5	4.075(2)	S(9)-Cs(2)#1	3.443(2)
P(3)-Cs(4)#4	4.108(2)	S(9)-Cs(1)#1	3.444(2)
S(1)-P(2)#3	2.063(3)	S(9)-Cs(1)	3.542(2)
S(1)-Cs(5)#6	3.642(2)	S(9)-Cs(5)#4	3.721(2)

S(9)-Cs(4)	3.871(2)	Cs(4)-S(12)#7	3.912(3)
S(10)-Cs(2)#9	3.299(3)	Cs(4)-S(5)#4	4.107(2)
S(10)-Cs(2)	3.522(3)	Cs(4)-P(3)#4	4.108(2)
S(10)-Cs(3)#2	3.571(3)	Cs(4)-S(3)#4	4.116(2)
S(10)-Cs(3)#9	4.037(3)	Cs(4)-Cs(1)#1	4.5217(10)
S(11)-Cs(2)#5	3.351(2)	Cs(4)-Cs(2)#1	4.7523(9)
S(11)-Cs(5)#4	3.466(3)	Cs(5)-S(11)#4	3.466(3)
S(11)-Cs(1)	3.550(2)	Cs(5)-S(1)#6	3.642(2)
S(11)-Cs(4)#10	3.605(3)	Cs(5)-S(8)#8	3.687(3)
S(12)-Cs(1)#5	3.417(3)	Cs(5)-S(7)#6	3.717(2)
S(12)-Cs(4)#4	3.511(3)	Cs(5)-S(9)#4	3.721(2)
S(12)-Cs(1)	3.520(3)	Cs(5)-S(7)#8	3.857(3)
S(12)-Cs(4)#10	3.912(3)	Cs(5)-P(1)#8	3.858(2)
S(12)-Cs(3)	3.977(3)	Cs(5)-Cs(2)#8	4.6021(9)
Cs(1)-S(12)#11	3.417(3)	Cs(5)-Cs(5)#13	4.6672(13)
Cs(1)-S(9)#1	3.444(2)	S(1)-Th(1)-S(5)	145.49(7)
Cs(1)-S(5)#4	3.658(3)	S(1)-Th(1)-S(3)	137.35(6)
Cs(1)-S(8)#1	3.772(2)	S(5)-Th(1)-S(3)	64.33(7)
Cs(1)-S(4)#10	4.177(3)	S(1)-Th(1)-S(4)	81.79(7)
Cs(1)-Cs(4)#1	4.5216(10)	S(5)-Th(1)-S(4)	66.12(7)
Cs(2)-S(10)#12	3.299(3)	S(3)-Th(1)-S(4)	127.15(7)
Cs(2)-S(11)#11	3.351(2)	S(1)-Th(1)-S(2)	67.97(6)
Cs(2)-S(9)#1	3.443(2)	S(5)-Th(1)-S(2)	93.04(7)
Cs(2)-S(4)#10	3.531(2)	S(3)-Th(1)-S(2)	85.66(7)
Cs(2)-S(3)#2	3.674(3)	S(4)-Th(1)-S(2)	79.66(7)
Cs(2)-S(1)#3	3.702(2)	S(1)-Th(1)-S(8)	72.48(6)
Cs(2)-P(3)#11	4.075(2)	S(5)-Th(1)-S(8)	105.91(7)
Cs(2)-Cs(5)#2	4.6020(9)	S(3)-Th(1)-S(8)	141.59(6)
Cs(3)-S(4)#10	3.526(2)	S(4)-Th(1)-S(8)	69.95(7)
Cs(3)-S(10)#8	3.571(3)	S(2)-Th(1)-S(8)	132.74(6)
Cs(3)-S(1)#10	3.751(2)	S(1)-Th(1)-S(7)	74.35(6)
Cs(3)-S(8)#10	3.791(2)	S(5)-Th(1)-S(7)	137.81(6)
Cs(3)-S(10)#12	4.036(3)	S(3)-Th(1)-S(7)	95.70(7)
Cs(3)-P(2)#8	4.097(2)	S(4)-Th(1)-S(7)	134.31(7)
Cs(4)-S(12)#4	3.511(3)	S(2)-Th(1)-S(7)	123.65(6)
Cs(4)-S(11)#7	3.605(3)	S(8)-Th(1)-S(7)	65.95(6)

S(1)-Th(1)-S(6)	127.53(6)	S(3)-Th(1)-Cs(3)	50.36(5)
S(5)-Th(1)-S(6)	76.40(7)	S(4)-Th(1)-Cs(3)	151.68(5)
S(3)-Th(1)-S(6)	78.12(7)	S(2)-Th(1)-Cs(3)	124.23(5)
S(4)-Th(1)-S(6)	106.97(7)	S(8)-Th(1)-Cs(3)	97.21(4)
S(2)-Th(1)-S(6)	163.30(7)	S(7)-Th(1)-Cs(3)	48.70(5)
S(8)-Th(1)-S(6)	63.51(6)	S(6)-Th(1)-Cs(3)	45.82(5)
S(7)-Th(1)-S(6)	62.79(6)	P(1)-Th(1)-Cs(3)	59.48(4)
S(1)-Th(1)-P(1)	89.99(6)	Cs(4)-Th(1)-Cs(3)	92.515(12)
S(5)-Th(1)-P(1)	109.89(7)	Cs(5)-Th(1)-Cs(3)	103.225(13)
S(3)-Th(1)-P(1)	107.51(7)	S(9)#1-P(1)-S(8)	111.95(15)
S(4)-Th(1)-P(1)	105.42(7)	S(9)#1-P(1)-S(6)	119.35(14)
S(2)-Th(1)-P(1)	156.71(6)	S(8)-P(1)-S(6)	102.79(14)
S(8)-Th(1)-P(1)	37.86(6)	S(9)#1-P(1)-S(7)	114.25(15)
S(7)-Th(1)-P(1)	37.99(6)	S(8)-P(1)-S(7)	105.45(13)
S(6)-Th(1)-P(1)	37.54(6)	S(6)-P(1)-S(7)	101.45(14)
S(1)-Th(1)-Cs(4)	118.20(5)	S(9)#1-P(1)-Th(1)	173.71(12)
S(5)-Th(1)-Cs(4)	56.06(6)	S(8)-P(1)-Th(1)	63.67(9)
S(3)-Th(1)-Cs(4)	104.19(4)	S(6)-P(1)-Th(1)	66.74(9)
S(4)-Th(1)-Cs(4)	59.62(5)	S(7)-P(1)-Th(1)	64.25(9)
S(2)-Th(1)-Cs(4)	135.53(5)	S(9)#1-P(1)-Cs(5)#2	70.94(9)
S(8)-Th(1)-Cs(4)	50.66(5)	S(8)-P(1)-Cs(5)#2	69.65(9)
S(7)-Th(1)-Cs(4)	98.81(4)	S(6)-P(1)-Cs(5)#2	169.49(11)
S(6)-Th(1)-Cs(4)	47.43(5)	S(7)-P(1)-Cs(5)#2	74.45(9)
P(1)-Th(1)-Cs(4)	61.03(4)	Th(1)-P(1)-Cs(5)#2	102.92(5)
S(1)-Th(1)-Cs(5)	113.55(5)	S(9)#1-P(1)-Cs(1)	57.26(8)
S(5)-Th(1)-Cs(5)	52.07(6)	S(8)-P(1)-Cs(1)	129.14(10)
S(3)-Th(1)-Cs(5)	52.89(5)	S(6)-P(1)-Cs(1)	62.17(8)
S(4)-Th(1)-Cs(5)	82.40(5)	S(7)-P(1)-Cs(1)	124.66(11)
S(2)-Th(1)-Cs(5)	45.76(5)	Th(1)-P(1)-Cs(1)	128.89(7)
S(8)-Th(1)-Cs(5)	150.80(5)	Cs(5)#2-P(1)-Cs(1)	128.19(6)
S(7)-Th(1)-Cs(5)	142.89(5)	S(9)#1-P(1)-Cs(2)	53.72(9)
S(6)-Th(1)-Cs(5)	118.86(5)	S(8)-P(1)-Cs(2)	138.87(11)
P(1)-Th(1)-Cs(5)	156.22(4)	S(6)-P(1)-Cs(2)	117.86(11)
Cs(4)-Th(1)-Cs(5)	107.227(13)	S(7)-P(1)-Cs(2)	62.29(9)
S(1)-Th(1)-Cs(3)	119.35(5)	Th(1)-P(1)-Cs(2)	126.07(6)
S(5)-Th(1)-Cs(3)	95.15(5)	Cs(5)#2-P(1)-Cs(2)	69.22(4)

Cs(1)-P(1)-Cs(2)	79.20(4)	Cs(2)#5-P(3)-Cs(4)#4	132.90(6)
S(10)-P(2)-S(3)#2	109.05(14)	P(2)#3-S(1)-Th(1)	94.73(10)
S(10)-P(2)-S(1)#3	109.19(15)	P(2)#3-S(1)-Cs(5)#6	101.11(10)
S(3)#2-P(2)-S(1)#3	109.68(15)	Th(1)-S(1)-Cs(5)#6	104.93(7)
S(10)-P(2)-S(2)#3	118.0(2)	P(2)#3-S(1)-Cs(2)#3	75.71(8)
S(3)#2-P(2)-S(2)#3	105.30(15)	Th(1)-S(1)-Cs(2)#3	170.44(8)
S(1)#3-P(2)-S(2)#3	105.35(13)	Cs(5)#6-S(1)-Cs(2)#3	77.60(4)
S(10)-P(2)-Cs(2)	67.40(10)	P(2)#3-S(1)-Cs(3)#7	101.94(10)
S(3)#2-P(2)-Cs(2)	71.48(9)	Th(1)-S(1)-Cs(3)#7	100.33(6)
S(1)#3-P(2)-Cs(2)	72.24(9)	Cs(5)#6-S(1)-Cs(3)#7	143.98(7)
S(2)#3-P(2)-Cs(2)	174.57(13)	Cs(2)#3-S(1)-Cs(3)#7	81.74(5)
S(10)-P(2)-Cs(3)#2	60.66(9)	P(2)#3-S(2)-Th(1)	91.61(10)
S(3)#2-P(2)-Cs(3)#2	68.10(9)	P(2)#3-S(2)-Cs(5)	167.87(13)
S(1)#3-P(2)-Cs(3)#2	166.09(11)	Th(1)-S(2)-Cs(5)	96.41(6)
S(2)#3-P(2)-Cs(3)#2	88.31(10)	P(2)#8-S(3)-Th(1)	103.97(11)
Cs(2)-P(2)-Cs(3)#2	94.37(5)	P(2)#8-S(3)-Cs(2)#8	76.49(10)
S(11)-P(3)-S(12)	109.9(2)	Th(1)-S(3)-Cs(2)#8	165.45(9)
S(11)-P(3)-S(5)#4	110.3(2)	P(2)#8-S(3)-Cs(3)	82.11(10)
S(12)-P(3)-S(5)#4	111.25(15)	Th(1)-S(3)-Cs(3)	94.00(7)
S(11)-P(3)-S(4)#4	113.11(14)	Cs(2)#8-S(3)-Cs(3)	100.43(6)
S(12)-P(3)-S(4)#4	111.7(2)	P(2)#8-S(3)-Cs(5)	94.55(10)
S(5)#4-P(3)-S(4)#4	100.32(14)	Th(1)-S(3)-Cs(5)	90.30(6)
S(11)-P(3)-Cs(1)	70.97(9)	Cs(2)#8-S(3)-Cs(5)	75.21(5)
S(12)-P(3)-Cs(1)	70.05(10)	Cs(3)-S(3)-Cs(5)	175.08(7)
S(5)#4-P(3)-Cs(1)	73.66(9)	P(2)#8-S(3)-Cs(4)#4	140.37(11)
S(4)#4-P(3)-Cs(1)	173.82(12)	Th(1)-S(3)-Cs(4)#4	110.53(6)
S(11)-P(3)-Cs(2)#5	54.92(9)	Cs(2)#8-S(3)-Cs(4)#4	74.96(4)
S(12)-P(3)-Cs(2)#5	117.26(11)	Cs(3)-S(3)-Cs(4)#4	76.71(5)
S(5)#4-P(3)-Cs(2)#5	131.44(11)	Cs(5)-S(3)-Cs(4)#4	104.00(6)
S(4)#4-P(3)-Cs(2)#5	60.03(8)	P(3)#4-S(5)-Th(1)	96.51(10)
Cs(1)-P(3)-Cs(2)#5	124.97(7)	P(3)#4-S(5)-Cs(1)#4	73.35(10)
S(11)-P(3)-Cs(4)#4	167.49(12)	Th(1)-S(5)-Cs(1)#4	165.45(9)
S(12)-P(3)-Cs(4)#4	58.68(10)	P(3)#4-S(5)-Cs(5)	89.99(11)
S(5)#4-P(3)-Cs(4)#4	72.40(10)	Th(1)-S(5)-Cs(5)	91.13(7)
S(4)#4-P(3)-Cs(4)#4	77.63(10)	Cs(1)#4-S(5)-Cs(5)	78.69(6)
Cs(1)-P(3)-Cs(4)#4	98.90(5)	P(3)#4-S(5)-Cs(4)	77.99(11)

Th(1)-S(5)-Cs(4)	86.96(7)	P(1)-S(6)-Cs(3)	97.09(11)
Cs(1)#4-S(5)-Cs(4)	100.71(6)	Th(1)-S(6)-Cs(3)	95.69(6)
Cs(5)-S(5)-Cs(4)	167.53(7)	Cs(4)-S(6)-Cs(3)	165.05(8)
P(3)#4-S(5)-Cs(4)#4	148.23(12)	P(1)-S(6)-Cs(1)	87.56(10)
Th(1)-S(5)-Cs(4)#4	110.77(7)	Th(1)-S(6)-Cs(1)	163.22(8)
Cs(1)#4-S(5)-Cs(4)#4	82.14(5)	Cs(4)-S(6)-Cs(1)	90.97(6)
Cs(5)-S(5)-Cs(4)#4	104.93(6)	Cs(3)-S(6)-Cs(1)	84.86(5)
Cs(4)-S(5)-Cs(4)#4	87.24(5)	P(1)-S(7)-Th(1)	77.76(9)
P(3)#4-S(4)-Th(1)	95.13(10)	P(1)-S(7)-Cs(5)#6	148.13(12)
P(3)#4-S(4)-Cs(3)#7	159.87(13)	Th(1)-S(7)-Cs(5)#6	100.40(6)
Th(1)-S(4)-Cs(3)#7	104.43(7)	P(1)-S(7)-Cs(2)	88.46(9)
P(3)#4-S(4)-Cs(2)#7	89.28(10)	Th(1)-S(7)-Cs(2)	164.37(7)
Th(1)-S(4)-Cs(2)#7	120.22(8)	Cs(5)#6-S(7)-Cs(2)	95.19(5)
Cs(3)#7-S(4)-Cs(2)#7	85.01(5)	P(1)-S(7)-Cs(3)	92.33(9)
P(3)#4-S(4)-Cs(1)#7	82.72(10)	Th(1)-S(7)-Cs(3)	93.95(6)
Th(1)-S(4)-Cs(1)#7	153.28(8)	Cs(5)#6-S(7)-Cs(3)	119.47(6)
Cs(3)#7-S(4)-Cs(1)#7	77.67(5)	Cs(2)-S(7)-Cs(3)	79.13(5)
Cs(2)#7-S(4)-Cs(1)#7	86.45(5)	P(1)-S(7)-Cs(5)#2	74.49(9)
P(1)-S(8)-Th(1)	78.47(10)	Th(1)-S(7)-Cs(5)#2	108.19(6)
P(1)-S(8)-Cs(5)#2	78.86(10)	Cs(5)#6-S(7)-Cs(5)#2	76.04(5)
Th(1)-S(8)-Cs(5)#2	113.17(7)	Cs(2)-S(7)-Cs(5)#2	74.51(5)
P(1)-S(8)-Cs(4)	92.09(9)	Cs(3)-S(7)-Cs(5)#2	150.66(7)
Th(1)-S(8)-Cs(4)	90.84(6)	P(1)#1-S(9)-Cs(2)#1	98.32(11)
Cs(5)#2-S(8)-Cs(4)	151.58(7)	P(1)#1-S(9)-Cs(1)#1	93.45(10)
P(1)-S(8)-Cs(1)#1	90.39(10)	Cs(2)#1-S(9)-Cs(1)#1	100.63(6)
Th(1)-S(8)-Cs(1)#1	161.08(7)	P(1)#1-S(9)-Cs(1)	98.11(11)
Cs(5)#2-S(8)-Cs(1)#1	78.99(5)	Cs(2)#1-S(9)-Cs(1)	152.08(8)
Cs(4)-S(8)-Cs(1)#1	74.15(4)	Cs(1)#1-S(9)-Cs(1)	100.74(6)
P(1)-S(8)-Cs(3)#7	159.38(11)	P(1)#1-S(9)-Cs(5)#4	78.49(9)
Th(1)-S(8)-Cs(3)#7	97.36(6)	Cs(2)#1-S(9)-Cs(5)#4	79.83(5)
Cs(5)#2-S(8)-Cs(3)#7	84.45(5)	Cs(1)#1-S(9)-Cs(5)#4	171.89(8)
Cs(4)-S(8)-Cs(3)#7	108.25(6)	Cs(1)-S(9)-Cs(5)#4	81.53(5)
Cs(1)#1-S(8)-Cs(3)#7	98.27(6)	P(1)#1-S(9)-Cs(4)	169.10(12)
P(1)-S(6)-Th(1)	75.72(9)	Cs(2)#1-S(9)-Cs(4)	80.82(5)
P(1)-S(6)-Cs(4)	97.07(11)	Cs(1)#1-S(9)-Cs(4)	76.12(4)
Th(1)-S(6)-Cs(4)	92.44(6)	Cs(1)-S(9)-Cs(4)	87.09(5)

Cs(5)#4-S(9)-Cs(4)	111.88(6)	S(12)#11-Cs(1)-S(9)#1	101.47(6)
P(2)-S(10)-Cs(2)#9	105.85(11)	S(12)#11-Cs(1)-S(12)	98.21(2)
P(2)-S(10)-Cs(2)	80.89(10)	S(9)#1-Cs(1)-S(12)	127.67(6)
Cs(2)#9-S(10)-Cs(2)	159.75(9)	S(12)#11-Cs(1)-S(9)	121.94(6)
P(2)-S(10)-Cs(3)#2	90.02(11)	S(9)#1-Cs(1)-S(9)	79.26(6)
Cs(2)#9-S(10)-Cs(3)#2	90.37(6)	S(12)-Cs(1)-S(9)	127.37(6)
Cs(2)-S(10)-Cs(3)#2	108.94(7)	S(12)#11-Cs(1)-S(11)	78.97(6)
P(2)-S(10)-Cs(3)#9	94.29(10)	S(9)#1-Cs(1)-S(11)	176.14(6)
Cs(2)#9-S(10)-Cs(3)#9	80.40(5)	S(12)-Cs(1)-S(11)	55.81(6)
Cs(2)-S(10)-Cs(3)#9	80.05(5)	S(9)-Cs(1)-S(11)	97.23(6)
Cs(3)#2-S(10)-Cs(3)#9	170.58(8)	S(12)#11-Cs(1)-S(6)	140.25(6)
P(3)-S(11)-Cs(2)#5	95.53(11)	S(9)#1-Cs(1)-S(6)	59.53(5)
P(3)-S(11)-Cs(5)#4	101.65(11)	S(12)-Cs(1)-S(6)	74.54(6)
Cs(2)#5-S(11)-Cs(5)#4	106.95(7)	S(9)-Cs(1)-S(6)	90.51(6)
P(3)-S(11)-Cs(1)	76.50(9)	S(11)-Cs(1)-S(6)	122.43(6)
Cs(2)#5-S(11)-Cs(1)	166.88(8)	S(12)#11-Cs(1)-P(3)	104.82(6)
Cs(5)#4-S(11)-Cs(1)	85.08(5)	S(9)#1-Cs(1)-P(3)	149.29(6)
P(3)-S(11)-Cs(4)#10	101.13(11)	S(12)-Cs(1)-P(3)	32.72(5)
Cs(2)#5-S(11)-Cs(4)#10	86.11(6)	S(9)-Cs(1)-P(3)	99.60(6)
Cs(5)#4-S(11)-Cs(4)#10	152.39(8)	S(11)-Cs(1)-P(3)	32.52(5)
Cs(1)-S(11)-Cs(4)#10	85.26(5)	S(6)-Cs(1)-P(3)	89.91(5)
P(3)-S(12)-Cs(1)#5	105.94(12)	S(12)#11-Cs(1)-S(5)#4	134.47(6)
P(3)-S(12)-Cs(4)#4	91.83(11)	S(9)#1-Cs(1)-S(5)#4	124.05(6)
Cs(1)#5-S(12)-Cs(4)#4	88.74(7)	S(12)-Cs(1)-S(5)#4	56.21(6)
P(3)-S(12)-Cs(1)	77.23(11)	S(9)-Cs(1)-S(5)#4	71.20(6)
Cs(1)#5-S(12)-Cs(1)	156.90(9)	S(11)-Cs(1)-S(5)#4	55.56(5)
Cs(4)#4-S(12)-Cs(1)	114.21(7)	S(6)-Cs(1)-S(5)#4	74.09(6)
P(3)-S(12)-Cs(4)#10	91.75(11)	P(3)-Cs(1)-S(5)#4	32.99(5)
Cs(1)#5-S(12)-Cs(4)#10	75.85(5)	S(12)#11-Cs(1)-S(8)#1	68.18(6)
Cs(4)#4-S(12)-Cs(4)#10	164.58(8)	S(9)#1-Cs(1)-S(8)#1	98.43(5)
Cs(1)-S(12)-Cs(4)#10	81.21(6)	S(12)-Cs(1)-S(8)#1	133.90(5)
P(3)-S(12)-Cs(3)	152.22(13)	S(9)-Cs(1)-S(8)#1	54.63(5)
Cs(1)#5-S(12)-Cs(3)	101.07(6)	S(11)-Cs(1)-S(8)#1	78.14(5)
Cs(4)#4-S(12)-Cs(3)	82.30(5)	S(6)-Cs(1)-S(8)#1	143.20(6)
Cs(1)-S(12)-Cs(3)	80.51(5)	P(3)-Cs(1)-S(8)#1	105.84(5)
Cs(4)#10-S(12)-Cs(3)	101.11(6)	S(5)#4-Cs(1)-S(8)#1	101.29(6)

S(12)#11-Cs(1)-P(1)	122.86(5)	S(10)#12-Cs(2)-S(4)#10	80.31(6)
S(9)#1-Cs(1)-P(1)	29.29(5)	S(11)#11-Cs(2)-S(4)#10	59.54(6)
S(12)-Cs(1)-P(1)	101.48(5)	S(9)#1-Cs(2)-S(4)#10	91.11(6)
S(9)-Cs(1)-P(1)	84.96(5)	S(10)-Cs(2)-S(4)#10	121.27(6)
S(11)-Cs(1)-P(1)	152.67(6)	S(10)#12-Cs(2)-S(3)#2	138.95(6)
S(6)-Cs(1)-P(1)	30.27(5)	S(11)#11-Cs(2)-S(3)#2	83.55(6)
P(3)-Cs(1)-P(1)	120.18(5)	S(9)#1-Cs(2)-S(3)#2	75.95(6)
S(5)#4-Cs(1)-P(1)	100.39(5)	S(10)-Cs(2)-S(3)#2	54.67(6)
S(8)#1-Cs(1)-P(1)	123.25(5)	S(4)#10-Cs(2)-S(3)#2	139.00(6)
S(12)#11-Cs(1)-S(4)#10	51.95(5)	S(10)#12-Cs(2)-S(1)#3	85.01(6)
S(9)#1-Cs(1)-S(4)#10	80.97(5)	S(11)#11-Cs(2)-S(1)#3	125.16(5)
S(12)-Cs(1)-S(4)#10	74.21(6)	S(9)#1-Cs(2)-S(1)#3	102.81(6)
S(9)-Cs(1)-S(4)#10	157.27(6)	S(10)-Cs(2)-S(1)#3	54.58(5)
S(11)-Cs(1)-S(4)#10	102.15(5)	S(4)#10-Cs(2)-S(1)#3	163.82(6)
S(6)-Cs(1)-S(4)#10	89.06(5)	S(3)#2-Cs(2)-S(1)#3	54.31(5)
P(3)-Cs(1)-S(4)#10	103.12(5)	S(10)#12-Cs(2)-S(7)	69.50(6)
S(5)#4-Cs(1)-S(4)#10	130.14(6)	S(11)#11-Cs(2)-S(7)	146.19(6)
S(8)#1-Cs(1)-S(4)#10	118.12(5)	S(9)#1-Cs(2)-S(7)	56.60(5)
P(1)-Cs(1)-S(4)#10	83.27(5)	S(10)-Cs(2)-S(7)	139.41(5)
S(12)#11-Cs(1)-Cs(4)#1	57.02(5)	S(4)#10-Cs(2)-S(7)	96.03(6)
S(9)#1-Cs(1)-Cs(4)#1	56.20(4)	S(3)#2-Cs(2)-S(7)	107.80(6)
S(12)-Cs(1)-Cs(4)#1	152.59(5)	S(1)#3-Cs(2)-S(7)	85.08(5)
S(9)-Cs(1)-Cs(4)#1	79.32(4)	S(10)#12-Cs(2)-P(2)	109.04(6)
S(11)-Cs(1)-Cs(4)#1	121.79(4)	S(11)#11-Cs(2)-P(2)	93.71(5)
S(6)-Cs(1)-Cs(4)#1	115.72(4)	S(9)#1-Cs(2)-P(2)	104.50(6)
P(3)-Cs(1)-Cs(4)#1	154.29(4)	S(10)-Cs(2)-P(2)	31.72(5)
S(5)#4-Cs(1)-Cs(4)#1	149.19(5)	S(4)#10-Cs(2)-P(2)	151.02(6)
S(8)#1-Cs(1)-Cs(4)#1	52.47(4)	S(3)#2-Cs(2)-P(2)	32.03(5)
P(1)-Cs(1)-Cs(4)#1	85.45(4)	S(1)#3-Cs(2)-P(2)	32.05(5)
S(4)#10-Cs(1)-Cs(4)#1	80.42(4)	S(7)-Cs(2)-P(2)	112.94(5)
S(10)#12-Cs(2)-S(11)#11	122.38(6)	S(10)#12-Cs(2)-P(3)#11	105.89(5)
S(10)#12-Cs(2)-S(9)#1	124.14(6)	S(11)#11-Cs(2)-P(3)#11	29.55(5)
S(11)#11-Cs(2)-S(9)#1	97.96(6)	S(9)#1-Cs(2)-P(3)#11	90.55(5)
S(10)#12-Cs(2)-S(10)	99.51(2)	S(10)-Cs(2)-P(3)#11	99.90(5)
S(11)#11-Cs(2)-S(10)	73.29(6)	S(4)#10-Cs(2)-P(3)#11	30.68(5)
S(9)#1-Cs(2)-S(10)	130.29(6)	S(3)#2-Cs(2)-P(3)#11	109.49(5)

S(1)#3-Cs(2)-P(3)#11	154.09(5)	S(6)-Cs(3)-S(8)#10	129.93(5)
S(7)-Cs(2)-P(3)#11	120.65(5)	S(7)-Cs(3)-S(8)#10	151.29(6)
P(2)-Cs(2)-P(3)#11	123.24(5)	S(1)#10-Cs(3)-S(8)#10	54.98(5)
S(10)#12-Cs(2)-P(1)	96.40(6)	S(4)#10-Cs(3)-S(3)	161.97(6)
S(11)#11-Cs(2)-P(1)	120.65(5)	S(10)#8-Cs(3)-S(3)	52.87(5)
S(9)#1-Cs(2)-P(1)	27.96(5)	S(6)-Cs(3)-S(3)	61.36(5)
S(10)-Cs(2)-P(1)	147.10(5)	S(7)-Cs(3)-S(3)	70.84(5)
S(4)#10-Cs(2)-P(1)	89.66(5)	S(1)#10-Cs(3)-S(3)	132.70(5)
S(3)#2-Cs(2)-P(1)	95.22(5)	S(8)#10-Cs(3)-S(3)	137.59(6)
S(1)#3-Cs(2)-P(1)	98.76(5)	S(4)#10-Cs(3)-S(12)	76.78(6)
S(7)-Cs(2)-P(1)	29.25(4)	S(10)#8-Cs(3)-S(12)	124.00(6)
P(2)-Cs(2)-P(1)	115.51(5)	S(6)-Cs(3)-S(12)	69.53(5)
P(3)#11-Cs(2)-P(1)	103.16(5)	S(7)-Cs(3)-S(12)	118.41(5)
S(10)#12-Cs(2)-Cs(5)#2	106.24(4)	S(1)#10-Cs(3)-S(12)	117.13(5)
S(11)#11-Cs(2)-Cs(5)#2	131.19(5)	S(8)#10-Cs(3)-S(12)	62.62(5)
S(9)#1-Cs(2)-Cs(5)#2	52.75(4)	S(3)-Cs(3)-S(12)	98.12(5)
S(10)-Cs(2)-Cs(5)#2	96.11(4)	S(4)#10-Cs(3)-S(10)#12	70.93(6)
S(4)#10-Cs(2)-Cs(5)#2	140.90(5)	S(10)#8-Cs(3)-S(10)#12	86.18(2)
S(3)#2-Cs(2)-Cs(5)#2	54.28(4)	S(6)-Cs(3)-S(10)#12	112.20(5)
S(1)#3-Cs(2)-Cs(5)#2	50.62(4)	S(7)-Cs(3)-S(10)#12	62.26(5)
S(7)-Cs(2)-Cs(5)#2	53.88(4)	S(1)#10-Cs(3)-S(10)#12	50.24(5)
P(2)-Cs(2)-Cs(5)#2	64.45(4)	S(8)#10-Cs(3)-S(10)#12	100.81(5)
P(3)#11-Cs(2)-Cs(5)#2	140.94(4)	S(3)-Cs(3)-S(10)#12	111.28(5)
P(1)-Cs(2)-Cs(5)#2	51.61(3)	S(12)-Cs(3)-S(10)#12	147.42(6)
S(4)#10-Cs(3)-S(10)#8	143.84(6)	S(4)#10-Cs(3)-P(2)#8	158.31(6)
S(4)#10-Cs(3)-S(6)	100.88(6)	S(10)#8-Cs(3)-P(2)#8	29.31(5)
S(10)#8-Cs(3)-S(6)	113.79(6)	S(6)-Cs(3)-P(2)#8	86.20(5)
S(4)#10-Cs(3)-S(7)	96.10(6)	S(7)-Cs(3)-P(2)#8	72.11(5)
S(10)#8-Cs(3)-S(7)	97.43(5)	S(1)#10-Cs(3)-P(2)#8	103.75(5)
S(6)-Cs(3)-S(7)	51.67(5)	S(8)#10-Cs(3)-P(2)#8	133.23(5)
S(4)#10-Cs(3)-S(1)#10	63.21(5)	S(3)-Cs(3)-P(2)#8	29.79(5)
S(10)#8-Cs(3)-S(1)#10	80.63(5)	S(12)-Cs(3)-P(2)#8	124.74(5)
S(6)-Cs(3)-S(1)#10	158.23(6)	S(10)#12-Cs(3)-P(2)#8	87.40(5)
S(7)-Cs(3)-S(1)#10	112.49(5)	S(4)#10-Cs(3)-Cs(2)	47.53(4)
S(4)#10-Cs(3)-S(8)#10	55.38(5)	S(10)#8-Cs(3)-Cs(2)	126.50(4)
S(10)#8-Cs(3)-S(8)#10	104.69(6)	S(6)-Cs(3)-Cs(2)	81.06(4)

S(7)-Cs(3)-Cs(2)	50.43(4)	S(8)-Cs(4)-S(5)	75.01(5)
S(1)#10-Cs(3)-Cs(2)	77.20(4)	S(9)-Cs(4)-S(5)	143.65(5)
S(8)#10-Cs(3)-Cs(2)	101.09(4)	S(12)#7-Cs(4)-S(5)	116.13(5)
S(3)-Cs(3)-Cs(2)	121.26(4)	S(12)#4-Cs(4)-S(5)#4	117.89(6)
S(12)-Cs(3)-Cs(2)	109.45(4)	S(6)-Cs(4)-S(5)#4	69.39(5)
S(10)#12-Cs(3)-Cs(2)	43.01(4)	S(11)#7-Cs(4)-S(5)#4	117.66(5)
P(2)#8-Cs(3)-Cs(2)	114.84(4)	S(8)-Cs(4)-S(5)#4	118.26(5)
S(4)#10-Cs(3)-Cs(1)	57.16(4)	S(9)-Cs(4)-S(5)#4	63.32(5)
S(10)#8-Cs(3)-Cs(1)	158.81(4)	S(12)#7-Cs(4)-S(5)#4	149.12(6)
S(6)-Cs(3)-Cs(1)	47.88(4)	S(5)-Cs(4)-S(5)#4	92.76(5)
S(7)-Cs(3)-Cs(1)	78.85(4)	S(12)#4-Cs(4)-P(3)#4	29.50(5)
S(1)#10-Cs(3)-Cs(1)	120.20(4)	S(6)-Cs(4)-P(3)#4	83.76(5)
S(8)#10-Cs(3)-Cs(1)	86.52(4)	S(11)#7-Cs(4)-P(3)#4	101.73(5)
S(3)-Cs(3)-Cs(1)	106.89(4)	S(8)-Cs(4)-P(3)#4	76.88(5)
S(12)-Cs(3)-Cs(1)	45.62(4)	S(9)-Cs(4)-P(3)#4	168.24(5)
S(10)#12-Cs(3)-Cs(1)	109.69(4)	S(12)#7-Cs(4)-P(3)#4	92.36(5)
P(2)#8-Cs(3)-Cs(1)	134.02(4)	S(5)-Cs(4)-P(3)#4	29.60(5)
Cs(2)-Cs(3)-Cs(1)	66.812(13)	S(5)#4-Cs(4)-P(3)#4	118.44(6)
S(12)#4-Cs(4)-S(6)	111.35(6)	S(12)#4-Cs(4)-S(3)#4	101.15(6)
S(12)#4-Cs(4)-S(11)#7	77.02(6)	S(6)-Cs(4)-S(3)#4	113.55(5)
S(6)-Cs(4)-S(11)#7	165.90(6)	S(11)#7-Cs(4)-S(3)#4	74.41(5)
S(12)#4-Cs(4)-S(8)	101.99(6)	S(8)-Cs(4)-S(3)#4	156.33(6)
S(6)-Cs(4)-S(8)	52.38(5)	S(9)-Cs(4)-S(3)#4	66.48(5)
S(11)#7-Cs(4)-S(8)	115.80(6)	S(12)#7-Cs(4)-S(3)#4	121.27(5)
S(12)#4-Cs(4)-S(9)	161.81(6)	S(5)-Cs(4)-S(3)#4	116.12(5)
S(6)-Cs(4)-S(9)	86.37(6)	S(5)#4-Cs(4)-S(3)#4	44.16(5)
S(11)#7-Cs(4)-S(9)	86.51(5)	P(3)#4-Cs(4)-S(3)#4	123.60(5)
S(8)-Cs(4)-S(9)	92.03(5)	S(12)#4-Cs(4)-Cs(1)#1	135.24(5)
S(12)#4-Cs(4)-S(12)#7	89.73(2)	S(6)-Cs(4)-Cs(1)#1	83.86(4)
S(6)-Cs(4)-S(12)#7	115.28(6)	S(11)#7-Cs(4)-Cs(1)#1	82.34(4)
S(11)#7-Cs(4)-S(12)#7	52.04(5)	S(8)-Cs(4)-Cs(1)#1	53.37(4)
S(8)-Cs(4)-S(12)#7	63.81(5)	S(9)-Cs(4)-Cs(1)#1	47.68(4)
S(9)-Cs(4)-S(12)#7	86.09(5)	S(12)#7-Cs(4)-Cs(1)#1	47.13(4)
S(12)#4-Cs(4)-S(5)	53.02(5)	S(5)-Cs(4)-Cs(1)#1	128.21(4)
S(6)-Cs(4)-S(5)	58.65(5)	S(5)#4-Cs(4)-Cs(1)#1	106.87(4)
S(11)#7-Cs(4)-S(5)	129.79(5)	P(3)#4-Cs(4)-Cs(1)#1	124.51(4)

S(3)#4-Cs(4)-Cs(1)#1	110.91(4)	S(8)#8-Cs(5)-S(7)#8	51.45(5)
S(12)#4-Cs(4)-Cs(2)#1	116.19(4)	S(7)#6-Cs(5)-S(7)#8	103.96(5)
S(6)-Cs(4)-Cs(2)#1	131.43(4)	S(9)#4-Cs(5)-S(7)#8	53.56(5)
S(11)#7-Cs(4)-Cs(2)#1	44.71(4)	S(5)-Cs(5)-S(7)#8	120.68(5)
S(8)-Cs(4)-Cs(2)#1	122.81(4)	S(11)#4-Cs(5)-P(1)#8	103.06(5)
S(9)-Cs(4)-Cs(2)#1	45.66(4)	S(2)-Cs(5)-P(1)#8	163.76(5)
S(12)#7-Cs(4)-Cs(2)#1	75.00(4)	S(1)#6-Cs(5)-P(1)#8	106.93(5)
S(5)-Cs(4)-Cs(2)#1	162.13(4)	S(8)#8-Cs(5)-P(1)#8	31.49(5)
S(5)#4-Cs(4)-Cs(2)#1	80.10(4)	S(7)#6-Cs(5)-P(1)#8	134.09(5)
P(3)#4-Cs(4)-Cs(2)#1	144.78(4)	S(9)#4-Cs(5)-P(1)#8	30.57(5)
S(3)#4-Cs(4)-Cs(2)#1	48.29(4)	S(5)-Cs(5)-P(1)#8	95.45(5)
Cs(1)#1-Cs(4)-Cs(2)#1	69.657(15)	S(7)#8-Cs(5)-P(1)#8	31.06(5)
S(11)#4-Cs(5)-S(2)	77.45(6)	S(11)#4-Cs(5)-S(3)	100.24(5)
S(11)#4-Cs(5)-S(1)#6	142.15(6)	S(2)-Cs(5)-S(3)	65.77(5)
S(2)-Cs(5)-S(1)#6	67.33(6)	S(1)#6-Cs(5)-S(3)	53.19(5)
S(11)#4-Cs(5)-S(8)#8	80.36(6)	S(8)#8-Cs(5)-S(3)	124.13(5)
S(2)-Cs(5)-S(8)#8	157.18(6)	S(7)#6-Cs(5)-S(3)	101.86(5)
S(1)#6-Cs(5)-S(8)#8	135.48(5)	S(9)#4-Cs(5)-S(3)	70.56(5)
S(11)#4-Cs(5)-S(7)#6	113.09(5)	S(5)-Cs(5)-S(3)	47.41(5)
S(2)-Cs(5)-S(7)#6	57.08(6)	S(7)#8-Cs(5)-S(3)	101.81(5)
S(1)#6-Cs(5)-S(7)#6	58.08(5)	P(1)#8-Cs(5)-S(3)	98.41(5)
S(8)#8-Cs(5)-S(7)#6	129.61(5)	S(11)#4-Cs(5)-Cs(2)#8	135.69(4)
S(11)#4-Cs(5)-S(9)#4	95.44(5)	S(2)-Cs(5)-Cs(2)#8	108.97(5)
S(2)-Cs(5)-S(9)#4	133.41(6)	S(1)#6-Cs(5)-Cs(2)#8	51.78(3)
S(1)#6-Cs(5)-S(9)#4	98.70(5)	S(8)#8-Cs(5)-Cs(2)#8	90.65(4)
S(8)#8-Cs(5)-S(9)#4	53.98(5)	S(7)#6-Cs(5)-Cs(2)#8	106.00(4)
S(7)#6-Cs(5)-S(9)#4	151.45(5)	S(9)#4-Cs(5)-Cs(2)#8	47.42(4)
S(11)#4-Cs(5)-S(5)	54.65(5)	S(5)-Cs(5)-Cs(2)#8	85.02(4)
S(2)-Cs(5)-S(5)	71.38(5)	S(7)#8-Cs(5)-Cs(2)#8	51.61(4)
S(1)#6-Cs(5)-S(5)	99.50(5)	P(1)#8-Cs(5)-Cs(2)#8	59.16(4)
S(8)#8-Cs(5)-S(5)	99.81(5)	S(3)-Cs(5)-Cs(2)#8	50.51(4)
S(7)#6-Cs(5)-S(5)	128.23(5)	S(11)#4-Cs(5)-Cs(5)#13	149.15(5)
S(9)#4-Cs(5)-S(5)	67.50(5)	S(2)-Cs(5)-Cs(5)#13	106.91(5)
S(11)#4-Cs(5)-S(7)#8	131.37(5)	S(1)#6-Cs(5)-Cs(5)#13	59.75(4)
S(2)-Cs(5)-S(7)#8	151.13(6)	S(8)#8-Cs(5)-Cs(5)#13	89.59(4)
S(1)#6-Cs(5)-S(7)#8	84.27(5)	S(7)#6-Cs(5)-Cs(5)#13	53.33(4)

S(9)#4-Cs(5)-Cs(5)#13	102.05(4)
S(5)-Cs(5)-Cs(5)#13	156.16(4)
S(7)#8-Cs(5)-Cs(5)#13	50.63(3)
P(1)#8-Cs(5)-Cs(5)#13	81.16(4)
S(3)-Cs(5)-Cs(5)#13	109.44(4)
Cs(2)#8-Cs(5)-Cs(5)#13	72.92(2)

Symmetry transformations used to generate equivalent atoms:

#1 -x+1,-y+1,-z #2 x,y+1,z #3 -x,-y+1,-z

#4 -x+1,-y,-z #5 -x+1,y-1/2,-z-1/2 #6 -x,-y,-z

#7 x,-y+1/2,z+1/2 #8 x,y-1,z #9 -x,y+1/2,-z-1/2

#10 x,-y+1/2,z-1/2 #11 -x+1,y+1/2,-z-1/2 #12 -x,y-1/2,-z-1/2

#13 -x,-y-1,-z

Table 4. Anisotropic displacement parameters ($Å^2 x\ 10^3$) for $Cs_5Th(PS_4)_3$. The anisotropic displacement factor exponent takes the form: $-2\pi^2[\ h^2\ a^{*2}U^{11} + ... + 2\ h\ k\ a^*\ b^*\ U^{12}\ ]$

	U^{11}	U^{22}	U^{33}	U^{23}	U^{13}	U^{12}
Th(1)	12(1)	15(1)	10(1)	0(1)	4(1)	2(1)
P(1)	13(1)	14(1)	10(1)	1(1)	3(1)	-1(1)
P(2)	12(1)	19(1)	11(1)	1(1)	3(1)	0(1)
P(3)	18(1)	19(1)	9(1)	1(1)	-1(1)	3(1)
S(1)	17(1)	16(1)	17(1)	1(1)	7(1)	1(1)
S(2)	27(1)	16(1)	28(1)	-1(1)	15(1)	0(1)
S(3)	13(1)	31(1)	20(1)	-10(1)	-3(1)	2(1)
S(5)	33(1)	32(1)	8(1)	0(1)	2(1)	17(1)
S(4)	37(1)	18(1)	10(1)	2(1)	5(1)	8(1)
S(8)	20(1)	25(1)	10(1)	1(1)	2(1)	-5(1)
S(6)	20(1)	22(1)	19(1)	-1(1)	4(1)	2(1)
S(7)	14(1)	25(1)	14(1)	6(1)	-1(1)	-2(1)
S(9)	19(1)	19(1)	18(1)	1(1)	4(1)	-5(1)
S(10)	29(1)	29(1)	10(1)	3(1)	6(1)	2(1)
S(11)	23(1)	18(1)	19(1)	1(1)	5(1)	0(1)
S(12)	19(1)	32(1)	23(1)	-2(1)	-6(1)	-1(1)
Cs(1)	20(1)	27(1)	21(1)	-2(1)	7(1)	3(1)
Cs(2)	19(1)	22(1)	19(1)	1(1)	5(1)	1(1)
Cs(3)	41(1)	36(1)	14(1)	4(1)	1(1)	-15(1)
Cs(4)	26(1)	39(1)	26(1)	9(1)	-9(1)	-5(1)
Cs(5)	20(1)	27(1)	26(1)	-7(1)	-3(1)	6(1)

Table 1. Crystal data and structure refinement for $Cs_4Th_2(P_2S_6)_3$.

Identification code	cs4th2p6s18	
Empirical formula	$Cs_4Th_2(P_2S_6)_3$	
Formula weight	879.31	
Temperature	293(2) K	
Wavelength	0.71073 Å	
Crystal system	Triclinic	
Space group	P-1	
Unit cell dimensions	a = 12.303(4) Å	α= 114.607(8)°.
	b = 12.471(4) Å	β= 102.547(6)°.
	c = 12.541(4) Å	γ = 99.889(7)°.
Volume	1631.5(9) $Å^3$	
Z	4	
Density (calculated)	3.580 Mg/m^3	
Absorption coefficient	14.951 mm^{-1}	
F(000)	1556	
Crystal size	0.22 x 0.20 x 0.19 mm^3	
Theta range for data collection	1.77 to 28.27°.	
Index ranges	-14<=h<=16, -16<=k<=9, -16<=l<=16	
Reflections collected	10977	
Independent reflections	7605 [R(int) = 0.0363]	
Completeness to theta = 28.27°	93.7 %	
Absorption correction	SADABS	
Refinement method	Full-matrix least-squares on F^2	
Data / restraints / parameters	7605 / 0 / 272	
Goodness-of-fit on F^2	0.871	
Final R indices [I>2sigma(I)]	R1 = 0.0421, wR2 = 0.0916	
R indices (all data)	R1 = 0.0680, wR2 = 0.0952	
Extinction coefficient	0.00001(4)	
Largest diff. peak and hole	5.200 and -3.500 $e.Å^{-3}$	

Table 2. Atomic coordinates (x 10^4) and equivalent isotropic displacement parameters ($Å^2$x 10^3) for $Cs_4Th_2(P_2S_6)_3$. U(eq) is defined as one third of the trace of the orthogonalized U^{ij} tensor.

	x	y	z	U(eq)
Th(1)	6466(1)	6783(1)	-41(1)	8(1)
Th(2)	13900(1)	7148(1)	-3203(1)	8(1)
Cs(1)	9004(1)	4317(1)	-2606(1)	15(1)
Cs(2)	11242(1)	8535(1)	-1024(1)	17(1)
Cs(3)	11692(1)	2283(1)	-4459(1)	22(1)
Cs(4)	16495(1)	10745(1)	-2719(1)	21(1)
P(1)	7844(3)	4532(3)	119(3)	10(1)
P(2)	13167(3)	5831(3)	-1261(3)	10(1)
P(3)	12352(3)	12007(3)	1883(3)	10(1)
P(4)	13552(3)	3649(3)	-6412(3)	8(1)
P(5)	13007(3)	10301(3)	-2537(3)	10(1)
P(6)	7749(3)	1302(3)	-5556(3)	10(1)
S(1)	6630(3)	4282(3)	-1398(3)	11(1)
S(2)	8442(3)	7261(3)	-876(3)	12(1)
S(3)	5999(3)	8180(3)	2452(3)	14(1)
S(4)	8544(3)	6391(3)	1254(3)	11(1)
S(5)	5357(2)	5587(3)	-2886(3)	10(1)
S(6)	4261(3)	7567(3)	-510(3)	11(1)
S(7)	6438(3)	8651(3)	-1110(3)	11(1)
S(8)	8261(3)	9182(3)	1854(3)	13(1)
S(9)	5816(3)	5312(3)	1366(3)	11(1)
S(10)	11532(3)	7317(3)	-4099(3)	12(1)
S(11)	12639(3)	4695(3)	-5540(3)	12(1)
S(12)	13989(3)	9598(3)	-1593(3)	14(1)
S(13)	12052(3)	5530(3)	-2873(3)	12(1)
S(14)	15553(3)	7108(3)	-4492(3)	12(1)
S(15)	13698(3)	8295(3)	-4835(3)	14(1)
S(16)	8780(3)	980(3)	-4360(3)	16(1)
S(17)	11342(3)	10857(3)	2221(3)	16(1)
S(18)	11117(3)	6518(3)	210(3)	13(1)

Table 3. Bond lengths [Å] and angles [°] for $Cs_4Th_2(P_2S_6)_3$.

Th(1)-S(2)	2.914(3)	Cs(2)-S(18)	3.458(3)
Th(1)-S(1)	2.934(3)	Cs(2)-S(17)#5	3.555(3)
Th(1)-S(4)	2.949(3)	Cs(2)-S(7)#5	3.612(3)
Th(1)-S(8)	3.001(3)	Cs(2)-S(2)	3.615(3)
Th(1)-S(9)#1	3.051(3)	Cs(2)-S(10)	3.635(3)
Th(1)-S(6)	3.059(3)	Cs(2)-S(12)	3.740(3)
Th(1)-S(5)	3.094(3)	Cs(2)-S(17)	3.848(3)
Th(1)-S(3)	3.119(3)	Cs(2)-S(13)	3.933(3)
Th(1)-S(7)	3.136(3)	Cs(2)-P(3)	4.070(3)
Th(1)-S(9)	3.150(3)	Cs(2)-P(5)	4.098(3)
Th(2)-S(12)	2.842(3)	Cs(2)-S(6)#2	4.101(3)
Th(2)-S(14)	2.854(3)	Cs(3)-S(13)	3.584(3)
Th(2)-S(15)	2.939(3)	Cs(3)-S(16)#6	3.589(3)
Th(2)-S(5)#2	2.949(3)	Cs(3)-S(3)#4	3.661(3)
Th(2)-S(10)	2.964(3)	Cs(3)-S(17)#7	3.672(3)
Th(2)-S(13)	2.991(3)	Cs(3)-S(16)	3.721(3)
Th(2)-S(11)	3.047(3)	Cs(3)-S(4)#4	3.756(3)
Th(2)-S(6)#2	3.110(3)	Cs(3)-S(11)	3.890(3)
Th(2)-S(7)#2	3.238(3)	Cs(3)-S(9)#4	3.928(3)
Th(2)-Cs(4)	4.7596(16)	Cs(3)-S(14)#8	3.961(3)
Th(2)-Cs(2)	4.8007(14)	Cs(3)-Cs(4)#8	5.1917(15)
Cs(1)-S(11)#3	3.495(3)	Cs(3)-Cs(2)#3	5.5860(19)
Cs(1)-S(18)	3.501(3)	Cs(4)-S(3)#5	3.580(3)
Cs(1)-S(4)#4	3.563(3)	Cs(4)-S(17)#9	3.688(3)
Cs(1)-S(1)	3.573(3)	Cs(4)-S(15)#10	3.707(3)
Cs(1)-S(18)#4	3.589(3)	Cs(4)-S(18)#9	3.712(3)
Cs(1)-S(10)#3	3.606(3)	Cs(4)-S(15)	3.727(3)
Cs(1)-S(2)	3.682(3)	Cs(4)-S(16)#11	3.867(3)
Cs(1)-S(16)	3.735(3)	Cs(4)-S(7)#2	3.909(3)
Cs(1)-P(6)	3.761(3)	Cs(4)-S(14)	3.941(3)
Cs(1)-S(15)#3	3.860(3)	Cs(4)-S(12)	3.951(3)
Cs(1)-P(1)	3.909(3)	Cs(4)-S(1)#11	3.972(3)
Cs(1)-S(13)	3.934(3)	Cs(4)-S(6)#5	4.112(3)
Cs(2)-S(8)#5	3.423(3)	Cs(4)-Cs(2)#9	4.5326(17)

P(1)-S(18)#4	1.967(4)	S(6)-Th(2)#14	3.110(3)
P(1)-S(1)	2.016(4)	S(6)-Cs(2)#14	4.101(3)
P(1)-S(4)	2.044(4)	S(6)-Cs(4)#5	4.112(3)
P(1)-P(2)#4	2.219(4)	S(7)-P(3)#5	2.053(4)
P(1)-Cs(1)#4	3.991(3)	S(7)-Th(2)#14	3.238(3)
P(2)-S(13)	2.024(4)	S(7)-Cs(2)#5	3.612(3)
P(2)-S(6)#2	2.034(4)	S(7)-Cs(4)#14	3.909(3)
P(2)-S(9)#4	2.035(4)	S(8)-P(5)#5	2.012(4)
P(2)-P(1)#4	2.219(4)	S(8)-Cs(2)#5	3.423(3)
P(3)-S(17)	1.975(4)	S(9)-P(2)#4	2.035(4)
P(3)-S(2)#5	2.029(4)	S(9)-Th(1)#1	3.051(3)
P(3)-S(7)#5	2.053(4)	S(9)-Cs(3)#4	3.928(3)
P(3)-P(4)#12	2.211(4)	S(10)-P(6)#3	2.049(4)
P(3)-Cs(2)#5	4.179(3)	S(10)-Cs(1)#3	3.606(3)
P(4)-S(11)	2.002(4)	S(11)-Cs(1)#3	3.495(3)
P(4)-S(14)#8	2.024(4)	S(14)-P(4)#8	2.024(4)
P(4)-S(5)#3	2.063(4)	S(14)-Cs(3)#8	3.961(3)
P(4)-P(3)#7	2.211(4)	S(15)-P(6)#3	2.035(4)
P(5)-S(8)#5	2.012(4)	S(15)-Cs(4)#10	3.707(3)
P(5)-S(3)#5	2.019(4)	S(15)-Cs(1)#3	3.860(3)
P(5)-S(12)	2.058(4)	S(16)-Cs(3)#6	3.589(3)
P(5)-P(6)#3	2.235(4)	S(16)-Cs(4)#13	3.867(3)
P(6)-S(16)	1.967(4)	S(17)-Cs(2)#5	3.555(3)
P(6)-S(15)#3	2.035(4)	S(17)-Cs(3)#12	3.672(3)
P(6)-S(10)#3	2.049(4)	S(17)-Cs(4)#9	3.688(3)
P(6)-P(5)#3	2.235(4)	S(18)-P(1)#4	1.967(4)
S(1)-Cs(4)#13	3.972(3)	S(18)-Cs(1)#4	3.589(3)
S(2)-P(3)#5	2.029(4)	S(18)-Cs(4)#9	3.712(3)
S(3)-P(5)#5	2.019(4)	S(2)-Th(1)-S(1)	78.52(8)
S(3)-Cs(4)#5	3.580(3)	S(2)-Th(1)-S(4)	67.60(8)
S(3)-Cs(3)#4	3.661(3)	S(1)-Th(1)-S(4)	67.60(8)
S(4)-Cs(1)#4	3.563(3)	S(2)-Th(1)-S(8)	68.87(8)
S(4)-Cs(3)#4	3.756(3)	S(1)-Th(1)-S(8)	132.36(8)
S(5)-P(4)#3	2.063(4)	S(4)-Th(1)-S(8)	68.26(8)
S(5)-Th(2)#14	2.949(3)	S(2)-Th(1)-S(9)#1	130.34(8)
S(6)-P(2)#14	2.034(4)	S(1)-Th(1)-S(9)#1	63.30(8)

S(4)-Th(1)-S(9)#1	118.89(8)	S(7)-Th(1)-S(9)	159.57(7)
S(8)-Th(1)-S(9)#1	160.50(8)	S(12)-Th(2)-S(14)	111.82(9)
S(2)-Th(1)-S(6)	126.18(8)	S(12)-Th(2)-S(15)	77.03(9)
S(1)-Th(1)-S(6)	124.86(8)	S(14)-Th(2)-S(15)	61.77(8)
S(4)-Th(1)-S(6)	160.84(8)	S(12)-Th(2)-S(5)#2	131.22(9)
S(8)-Th(1)-S(6)	102.53(8)	S(14)-Th(2)-S(5)#2	69.50(8)
S(9)#1-Th(1)-S(6)	64.68(8)	S(15)-Th(2)-S(5)#2	130.65(8)
S(2)-Th(1)-S(5)	76.52(8)	S(12)-Th(2)-S(10)	75.27(9)
S(1)-Th(1)-S(5)	65.72(8)	S(14)-Th(2)-S(10)	123.15(8)
S(4)-Th(1)-S(5)	125.27(8)	S(15)-Th(2)-S(10)	65.98(8)
S(8)-Th(1)-S(5)	133.17(8)	S(5)#2-Th(2)-S(10)	147.57(8)
S(9)#1-Th(1)-S(5)	59.84(8)	S(12)-Th(2)-S(13)	104.93(9)
S(6)-Th(1)-S(5)	73.52(8)	S(14)-Th(2)-S(13)	143.24(8)
S(2)-Th(1)-S(3)	132.14(8)	S(15)-Th(2)-S(13)	130.00(9)
S(1)-Th(1)-S(3)	133.45(8)	S(5)#2-Th(2)-S(13)	86.22(8)
S(4)-Th(1)-S(3)	90.82(8)	S(10)-Th(2)-S(13)	66.49(8)
S(8)-Th(1)-S(3)	63.44(8)	S(12)-Th(2)-S(11)	150.15(9)
S(9)#1-Th(1)-S(3)	97.52(8)	S(14)-Th(2)-S(11)	80.61(8)
S(6)-Th(1)-S(3)	70.05(8)	S(15)-Th(2)-S(11)	86.47(9)
S(5)-Th(1)-S(3)	142.91(8)	S(5)#2-Th(2)-S(11)	78.19(8)
S(2)-Th(1)-S(7)	65.52(8)	S(10)-Th(2)-S(11)	75.33(8)
S(1)-Th(1)-S(7)	123.92(8)	S(13)-Th(2)-S(11)	67.31(8)
S(4)-Th(1)-S(7)	126.65(8)	S(12)-Th(2)-S(6)#2	68.72(8)
S(8)-Th(1)-S(7)	72.26(8)	S(14)-Th(2)-S(6)#2	129.74(8)
S(9)#1-Th(1)-S(7)	110.37(8)	S(15)-Th(2)-S(6)#2	145.67(8)
S(6)-Th(1)-S(7)	61.52(8)	S(5)#2-Th(2)-S(6)#2	74.80(8)
S(5)-Th(1)-S(7)	65.02(8)	S(10)-Th(2)-S(6)#2	105.99(8)
S(3)-Th(1)-S(7)	102.25(8)	S(13)-Th(2)-S(6)#2	64.08(8)
S(2)-Th(1)-S(9)	134.11(8)	S(11)-Th(2)-S(6)#2	125.12(8)
S(1)-Th(1)-S(9)	72.30(8)	S(12)-Th(2)-S(7)#2	68.68(8)
S(4)-Th(1)-S(9)	68.82(8)	S(14)-Th(2)-S(7)#2	73.42(8)
S(8)-Th(1)-S(9)	107.05(8)	S(15)-Th(2)-S(7)#2	105.81(8)
S(9)#1-Th(1)-S(9)	63.41(10)	S(5)#2-Th(2)-S(7)#2	65.35(8)
S(6)-Th(1)-S(9)	99.63(8)	S(10)-Th(2)-S(7)#2	143.93(8)
S(5)-Th(1)-S(9)	119.71(8)	S(13)-Th(2)-S(7)#2	121.68(8)
S(3)-Th(1)-S(9)	61.36(8)	S(11)-Th(2)-S(7)#2	140.66(8)

S(6)#2-Th(2)-S(7)#2	59.86(7)	S(18)-Cs(1)-S(2)	61.96(7)
S(12)-Th(2)-Cs(4)	56.01(7)	S(4)#4-Cs(1)-S(2)	120.29(7)
S(14)-Th(2)-Cs(4)	55.81(6)	S(1)-Cs(1)-S(2)	61.32(7)
S(15)-Th(2)-Cs(4)	51.54(7)	S(18)#4-Cs(1)-S(2)	91.55(7)
S(5)#2-Th(2)-Cs(4)	105.90(6)	S(10)#3-Cs(1)-S(2)	126.89(7)
S(10)-Th(2)-Cs(4)	105.20(6)	S(11)#3-Cs(1)-S(16)	111.80(7)
S(13)-Th(2)-Cs(4)	160.94(6)	S(18)-Cs(1)-S(16)	126.82(7)
S(11)-Th(2)-Cs(4)	128.86(6)	S(4)#4-Cs(1)-S(16)	68.41(7)
S(6)#2-Th(2)-Cs(4)	104.31(5)	S(1)-Cs(1)-S(16)	103.67(7)
S(7)#2-Th(2)-Cs(4)	54.60(5)	S(18)#4-Cs(1)-S(16)	81.56(7)
S(12)-Th(2)-Cs(2)	51.10(7)	S(10)#3-Cs(1)-S(16)	55.68(7)
S(14)-Th(2)-Cs(2)	160.56(6)	S(2)-Cs(1)-S(16)	164.60(7)
S(15)-Th(2)-Cs(2)	101.81(6)	S(11)#3-Cs(1)-P(6)	81.40(7)
S(5)#2-Th(2)-Cs(2)	127.53(6)	S(18)-Cs(1)-P(6)	155.33(7)
S(10)-Th(2)-Cs(2)	49.13(6)	S(4)#4-Cs(1)-P(6)	96.92(7)
S(13)-Th(2)-Cs(2)	54.86(6)	S(1)-Cs(1)-P(6)	100.10(7)
S(11)-Th(2)-Cs(2)	110.20(6)	S(18)#4-Cs(1)-P(6)	104.39(7)
S(6)#2-Th(2)-Cs(2)	57.83(6)	S(10)#3-Cs(1)-P(6)	32.22(6)
S(7)#2-Th(2)-Cs(2)	103.71(6)	S(2)-Cs(1)-P(6)	142.66(7)
Cs(4)-Th(2)-Cs(2)	106.42(3)	S(16)-Cs(1)-P(6)	30.42(7)
S(11)#3-Cs(1)-S(18)	119.22(7)	S(11)#3-Cs(1)-S(15)#3	67.57(7)
S(11)#3-Cs(1)-S(4)#4	157.85(7)	S(18)-Cs(1)-S(15)#3	165.39(7)
S(18)-Cs(1)-S(4)#4	58.77(7)	S(4)#4-Cs(1)-S(15)#3	120.43(7)
S(11)#3-Cs(1)-S(1)	84.00(7)	S(1)-Cs(1)-S(15)#3	71.44(7)
S(18)-Cs(1)-S(1)	95.73(7)	S(18)#4-Cs(1)-S(15)#3	96.97(7)
S(4)#4-Cs(1)-S(1)	117.89(7)	S(10)#3-Cs(1)-S(15)#3	50.86(7)
S(11)#3-Cs(1)-S(18)#4	139.95(7)	S(2)-Cs(1)-S(15)#3	114.87(7)
S(18)-Cs(1)-S(18)#4	69.43(8)	S(16)-Cs(1)-S(15)#3	53.01(7)
S(4)#4-Cs(1)-S(18)#4	61.99(7)	P(6)-Cs(1)-S(15)#3	30.94(7)
S(1)-Cs(1)-S(18)#4	55.96(7)	S(11)#3-Cs(1)-P(1)	111.69(7)
S(11)#3-Cs(1)-S(10)#3	62.28(7)	S(18)-Cs(1)-P(1)	70.74(7)
S(18)-Cs(1)-S(10)#3	143.31(7)	S(4)#4-Cs(1)-P(1)	88.96(7)
S(4)#4-Cs(1)-S(10)#3	105.21(7)	S(1)-Cs(1)-P(1)	30.84(6)
S(1)-Cs(1)-S(10)#3	120.12(7)	S(18)#4-Cs(1)-P(1)	30.03(6)
S(18)#4-Cs(1)-S(10)#3	136.01(7)	S(10)#3-Cs(1)-P(1)	145.58(7)
S(11)#3-Cs(1)-S(2)	65.46(7)	S(2)-Cs(1)-P(1)	65.19(6)

S(16)-Cs(1)-P(1)	104.10(7)	S(18)-Cs(2)-S(17)	83.03(7)
P(6)-Cs(1)-P(1)	116.38(7)	S(17)#5-Cs(2)-S(17)	87.32(8)
S(15)#3-Cs(1)-P(1)	94.84(7)	S(7)#5-Cs(2)-S(17)	54.14(7)
S(11)#3-Cs(1)-S(13)	97.62(7)	S(2)-Cs(2)-S(17)	77.60(7)
S(18)-Cs(1)-S(13)	65.35(7)	S(10)-Cs(2)-S(17)	160.45(7)
S(4)#4-Cs(1)-S(13)	60.80(7)	S(12)-Cs(2)-S(17)	109.12(7)
S(1)-Cs(1)-S(13)	159.27(7)	S(8)#5-Cs(2)-S(13)	116.88(7)
S(18)#4-Cs(1)-S(13)	119.39(7)	S(18)-Cs(2)-S(13)	65.72(7)
S(10)#3-Cs(1)-S(13)	78.01(7)	S(17)#5-Cs(2)-S(13)	122.90(7)
S(2)-Cs(1)-S(13)	100.43(7)	S(7)#5-Cs(2)-S(13)	118.85(7)
S(16)-Cs(1)-S(13)	94.94(7)	S(2)-Cs(2)-S(13)	101.66(7)
P(6)-Cs(1)-S(13)	100.57(7)	S(10)-Cs(2)-S(13)	50.94(6)
S(15)#3-Cs(1)-S(13)	128.33(7)	S(12)-Cs(2)-S(13)	74.12(7)
P(1)-Cs(1)-S(13)	135.12(7)	S(17)-Cs(2)-S(13)	144.09(7)
S(8)#5-Cs(2)-S(18)	171.13(8)	S(8)#5-Cs(2)-P(3)	66.17(7)
S(8)#5-Cs(2)-S(17)#5	66.54(7)	S(18)-Cs(2)-P(3)	106.78(7)
S(18)-Cs(2)-S(17)#5	119.97(7)	S(17)#5-Cs(2)-P(3)	89.29(7)
S(8)#5-Cs(2)-S(7)#5	61.87(7)	S(7)#5-Cs(2)-P(3)	30.26(6)
S(18)-Cs(2)-S(7)#5	109.30(7)	S(2)-Cs(2)-P(3)	102.64(7)
S(17)#5-Cs(2)-S(7)#5	111.74(7)	S(10)-Cs(2)-P(3)	132.20(6)
S(8)#5-Cs(2)-S(2)	122.71(7)	S(12)-Cs(2)-P(3)	83.45(7)
S(18)-Cs(2)-S(2)	63.06(7)	S(17)-Cs(2)-P(3)	28.71(6)
S(17)#5-Cs(2)-S(2)	57.00(7)	S(13)-Cs(2)-P(3)	146.95(7)
S(7)#5-Cs(2)-S(2)	131.61(7)	S(8)#5-Cs(2)-P(5)	29.32(7)
S(8)#5-Cs(2)-S(10)	69.29(7)	S(18)-Cs(2)-P(5)	147.97(7)
S(18)-Cs(2)-S(10)	115.44(7)	S(17)#5-Cs(2)-P(5)	90.35(7)
S(17)#5-Cs(2)-S(10)	88.45(7)	S(7)#5-Cs(2)-P(5)	63.10(7)
S(7)#5-Cs(2)-S(10)	110.46(7)	S(2)-Cs(2)-P(5)	146.61(7)
S(2)-Cs(2)-S(10)	115.55(7)	S(10)-Cs(2)-P(5)	50.47(6)
S(8)#5-Cs(2)-S(12)	56.45(7)	S(12)-Cs(2)-P(5)	30.00(6)
S(18)-Cs(2)-S(12)	118.77(7)	S(17)-Cs(2)-P(5)	110.47(7)
S(17)#5-Cs(2)-S(12)	120.35(7)	S(13)-Cs(2)-P(5)	90.00(6)
S(7)#5-Cs(2)-S(12)	55.01(7)	P(3)-Cs(2)-P(5)	81.82(6)
S(2)-Cs(2)-S(12)	173.02(7)	S(8)#5-Cs(2)-S(6)#2	106.81(7)
S(10)-Cs(2)-S(12)	57.47(7)	S(18)-Cs(2)-S(6)#2	68.22(6)
S(8)#5-Cs(2)-S(17)	91.56(7)	S(17)#5-Cs(2)-S(6)#2	165.85(7)

S(7)#5-Cs(2)-S(6)#2	73.17(7)	S(13)-Cs(3)-S(14)#8	90.81(7)
S(2)-Cs(2)-S(6)#2	130.39(6)	S(16)#6-Cs(3)-S(14)#8	96.06(7)
S(10)-Cs(2)-S(6)#2	77.43(6)	S(3)#4-Cs(3)-S(14)#8	75.24(7)
S(12)-Cs(2)-S(6)#2	50.59(6)	S(17)#7-Cs(3)-S(14)#8	61.01(7)
S(17)-Cs(2)-S(6)#2	105.70(7)	S(16)-Cs(3)-S(14)#8	164.05(7)
S(13)-Cs(2)-S(6)#2	47.49(6)	S(4)#4-Cs(3)-S(14)#8	128.92(7)
P(3)-Cs(2)-S(6)#2	99.47(6)	S(11)-Cs(3)-S(14)#8	51.80(6)
P(5)-Cs(2)-S(6)#2	80.02(6)	S(9)#4-Cs(3)-S(14)#8	75.63(7)
S(13)-Cs(3)-S(16)#6	171.05(7)	S(13)-Cs(3)-Cs(1)	52.43(5)
S(13)-Cs(3)-S(3)#4	104.31(7)	S(16)#6-Cs(3)-Cs(1)	121.40(6)
S(16)#6-Cs(3)-S(3)#4	72.10(7)	S(3)#4-Cs(3)-Cs(1)	117.54(6)
S(13)-Cs(3)-S(17)#7	117.89(7)	S(17)#7-Cs(3)-Cs(1)	124.64(6)
S(16)#6-Cs(3)-S(17)#7	70.68(7)	S(16)-Cs(3)-Cs(1)	48.97(5)
S(3)#4-Cs(3)-S(17)#7	117.37(7)	S(4)#4-Cs(3)-Cs(1)	46.26(5)
S(13)-Cs(3)-S(16)	101.39(7)	S(11)-Cs(3)-Cs(1)	93.63(5)
S(16)#6-Cs(3)-S(16)	72.98(8)	S(9)#4-Cs(3)-Cs(1)	86.76(5)
S(3)#4-Cs(3)-S(16)	111.00(7)	S(14)#8-Cs(3)-Cs(1)	142.33(5)
S(17)#7-Cs(3)-S(16)	103.77(7)	S(13)-Cs(3)-Cs(4)#8	139.42(5)
S(13)-Cs(3)-S(4)#4	62.44(6)	S(16)#6-Cs(3)-Cs(4)#8	48.12(5)
S(16)#6-Cs(3)-S(4)#4	108.64(7)	S(3)#4-Cs(3)-Cs(4)#8	72.40(5)
S(3)#4-Cs(3)-S(4)#4	71.29(7)	S(17)#7-Cs(3)-Cs(4)#8	45.27(5)
S(17)#7-Cs(3)-S(4)#4	169.57(7)	S(16)-Cs(3)-Cs(4)#8	117.80(6)
S(16)-Cs(3)-S(4)#4	66.60(7)	S(4)#4-Cs(3)-Cs(4)#8	141.93(5)
S(13)-Cs(3)-S(11)	53.01(7)	S(11)-Cs(3)-Cs(4)#8	91.42(5)
S(16)#6-Cs(3)-S(11)	135.94(7)	S(9)#4-Cs(3)-Cs(4)#8	108.22(5)
S(3)#4-Cs(3)-S(11)	117.01(7)	S(14)#8-Cs(3)-Cs(4)#8	48.77(5)
S(17)#7-Cs(3)-S(11)	67.29(7)	Cs(1)-Cs(3)-Cs(4)#8	164.69(2)
S(16)-Cs(3)-S(11)	129.52(7)	S(13)-Cs(3)-Cs(2)#3	95.45(5)
S(4)#4-Cs(3)-S(11)	115.10(7)	S(16)#6-Cs(3)-Cs(2)#3	90.27(5)
S(13)-Cs(3)-S(9)#4	54.69(6)	S(3)#4-Cs(3)-Cs(2)#3	155.47(5)
S(16)#6-Cs(3)-S(9)#4	121.62(7)	S(17)#7-Cs(3)-Cs(2)#3	38.63(5)
S(3)#4-Cs(3)-S(9)#4	49.71(6)	S(16)-Cs(3)-Cs(2)#3	78.45(5)
S(17)#7-Cs(3)-S(9)#4	136.35(7)	S(4)#4-Cs(3)-Cs(2)#3	131.99(5)
S(16)-Cs(3)-S(9)#4	119.85(7)	S(11)-Cs(3)-Cs(2)#3	64.45(5)
S(4)#4-Cs(3)-S(9)#4	53.31(6)	S(9)#4-Cs(3)-Cs(2)#3	145.87(5)
S(11)-Cs(3)-S(9)#4	82.81(7)	S(14)#8-Cs(3)-Cs(2)#3	90.30(5)

Cs(1)-Cs(3)-Cs(2)#3	86.02(3)	S(7)#2-Cs(4)-S(12)	51.99(6)
Cs(4)#8-Cs(3)-Cs(2)#3	83.15(3)	S(14)-Cs(4)-S(12)	73.41(6)
S(3)#5-Cs(4)-S(17)#9	156.95(7)	S(3)#5-Cs(4)-S(1)#11	56.72(7)
S(3)#5-Cs(4)-S(15)#10	83.45(7)	S(17)#9-Cs(4)-S(1)#11	133.28(7)
S(17)#9-Cs(4)-S(15)#10	119.00(7)	S(15)#10-Cs(4)-S(1)#11	68.84(7)
S(3)#5-Cs(4)-S(18)#9	101.32(7)	S(18)#9-Cs(4)-S(1)#11	51.73(6)
S(17)#9-Cs(4)-S(18)#9	81.92(7)	S(15)-Cs(4)-S(1)#11	120.15(7)
S(15)#10-Cs(4)-S(18)#9	97.57(7)	S(16)#11-Cs(4)-S(1)#11	94.28(6)
S(3)#5-Cs(4)-S(15)	67.31(7)	S(7)#2-Cs(4)-S(1)#11	130.16(7)
S(17)#9-Cs(4)-S(15)	106.52(7)	S(14)-Cs(4)-S(1)#11	165.64(7)
S(15)#10-Cs(4)-S(15)	86.39(7)	S(12)-Cs(4)-S(1)#11	99.73(6)
S(18)#9-Cs(4)-S(15)	167.57(7)	S(3)#5-Cs(4)-S(6)#5	54.38(7)
S(3)#5-Cs(4)-S(16)#11	135.55(7)	S(17)#9-Cs(4)-S(6)#5	108.56(7)
S(17)#9-Cs(4)-S(16)#11	67.51(7)	S(15)#10-Cs(4)-S(6)#5	126.85(7)
S(15)#10-Cs(4)-S(16)#11	53.14(7)	S(18)#9-Cs(4)-S(6)#5	65.96(6)
S(18)#9-Cs(4)-S(16)#11	78.26(7)	S(15)-Cs(4)-S(6)#5	102.24(7)
S(15)-Cs(4)-S(16)#11	113.18(7)	S(16)#11-Cs(4)-S(6)#5	144.10(7)
S(3)#5-Cs(4)-S(7)#2	103.99(7)	S(7)#2-Cs(4)-S(6)#5	70.18(6)
S(17)#9-Cs(4)-S(7)#2	53.09(6)	S(14)-Cs(4)-S(6)#5	118.01(6)
S(15)#10-Cs(4)-S(7)#2	160.71(7)	S(12)-Cs(4)-S(6)#5	49.11(6)
S(18)#9-Cs(4)-S(7)#2	98.32(7)	S(1)#11-Cs(4)-S(6)#5	61.53(6)
S(15)-Cs(4)-S(7)#2	80.37(7)	S(3)#5-Cs(4)-Cs(2)#9	110.77(6)
S(16)#11-Cs(4)-S(7)#2	120.19(7)	S(17)#9-Cs(4)-Cs(2)#9	54.65(5)
S(3)#5-Cs(4)-S(14)	110.39(7)	S(15)#10-Cs(4)-Cs(2)#9	144.13(6)
S(17)#9-Cs(4)-S(14)	61.07(7)	S(18)#9-Cs(4)-Cs(2)#9	48.34(5)
S(15)#10-Cs(4)-S(14)	105.31(7)	S(15)-Cs(4)-Cs(2)#9	129.36(5)
S(18)#9-Cs(4)-S(14)	142.48(7)	S(16)#11-Cs(4)-Cs(2)#9	101.75(6)
S(15)-Cs(4)-S(14)	45.54(6)	S(7)#2-Cs(4)-Cs(2)#9	50.00(5)
S(16)#11-Cs(4)-S(14)	92.04(7)	S(14)-Cs(4)-Cs(2)#9	100.22(5)
S(7)#2-Cs(4)-S(14)	55.48(6)	S(12)-Cs(4)-Cs(2)#9	82.06(5)
S(3)#5-Cs(4)-S(12)	52.80(6)	S(1)#11-Cs(4)-Cs(2)#9	91.10(5)
S(17)#9-Cs(4)-S(12)	104.80(7)	S(6)#5-Cs(4)-Cs(2)#9	56.39(5)
S(15)#10-Cs(4)-S(12)	129.16(7)	S(18)#4-P(1)-S(1)	115.05(19)
S(18)#9-Cs(4)-S(12)	113.70(7)	S(18)#4-P(1)-S(4)	119.55(19)
S(15)-Cs(4)-S(12)	55.84(7)	S(1)-P(1)-S(4)	107.44(18)
S(16)#11-Cs(4)-S(12)	165.43(7)	S(18)#4-P(1)-P(2)#4	111.17(17)

S(1)-P(1)-P(2)#4	104.64(18)	S(14)#8-P(4)-P(3)#7	102.47(17)
S(4)-P(1)-P(2)#4	96.55(17)	S(5)#3-P(4)-P(3)#7	101.41(17)
S(18)#4-P(1)-Cs(1)	65.95(12)	S(8)#5-P(5)-S(3)#5	105.98(18)
S(1)-P(1)-Cs(1)	65.33(12)	S(8)#5-P(5)-S(12)	113.26(19)
S(4)-P(1)-Cs(1)	98.11(13)	S(3)#5-P(5)-S(12)	111.21(19)
P(2)#4-P(1)-Cs(1)	164.25(15)	S(8)#5-P(5)-P(6)#3	110.90(18)
S(18)#4-P(1)-Cs(1)#4	61.29(12)	S(3)#5-P(5)-P(6)#3	113.82(18)
S(1)-P(1)-Cs(1)#4	157.70(15)	S(12)-P(5)-P(6)#3	101.88(16)
S(4)-P(1)-Cs(1)#4	62.99(11)	S(8)#5-P(5)-Cs(2)	56.40(11)
P(2)#4-P(1)-Cs(1)#4	96.69(13)	S(3)#5-P(5)-Cs(2)	152.10(15)
Cs(1)-P(1)-Cs(1)#4	95.08(7)	S(12)-P(5)-Cs(2)	65.33(12)
S(13)-P(2)-S(6)#2	105.88(17)	P(6)#3-P(5)-Cs(2)	93.59(12)
S(13)-P(2)-S(9)#4	117.18(19)	S(16)-P(6)-S(15)#3	115.85(19)
S(6)#2-P(2)-S(9)#4	106.87(18)	S(16)-P(6)-S(10)#3	117.3(2)
S(13)-P(2)-P(1)#4	109.24(18)	S(15)#3-P(6)-S(10)#3	103.81(17)
S(6)#2-P(2)-P(1)#4	116.52(18)	S(16)-P(6)-P(5)#3	113.89(18)
S(9)#4-P(2)-P(1)#4	101.59(16)	S(15)#3-P(6)-P(5)#3	102.33(18)
S(17)-P(3)-S(2)#5	117.4(2)	S(10)#3-P(6)-P(5)#3	101.62(17)
S(17)-P(3)-S(7)#5	115.17(19)	S(16)-P(6)-Cs(1)	74.06(13)
S(2)#5-P(3)-S(7)#5	106.87(18)	S(15)#3-P(6)-Cs(1)	77.23(13)
S(17)-P(3)-P(4)#12	113.07(18)	S(10)#3-P(6)-Cs(1)	69.74(12)
S(2)#5-P(3)-P(4)#12	103.36(17)	P(5)#3-P(6)-Cs(1)	170.72(14)
S(7)#5-P(3)-P(4)#12	98.78(17)	P(1)-S(1)-Th(1)	90.39(13)
S(17)-P(3)-Cs(2)	69.37(13)	P(1)-S(1)-Cs(1)	83.83(13)
S(2)#5-P(3)-Cs(2)	93.93(13)	Th(1)-S(1)-Cs(1)	111.28(9)
S(7)#5-P(3)-Cs(2)	62.43(11)	P(1)-S(1)-Cs(4)#13	85.11(12)
P(4)#12-P(3)-Cs(2)	157.82(14)	Th(1)-S(1)-Cs(4)#13	166.72(10)
S(17)-P(3)-Cs(2)#5	58.09(12)	Cs(1)-S(1)-Cs(4)#13	80.71(6)
S(2)#5-P(3)-Cs(2)#5	59.87(11)	P(3)#5-S(2)-Th(1)	93.57(14)
S(7)#5-P(3)-Cs(2)#5	140.90(15)	P(3)#5-S(2)-Cs(2)	91.09(13)
P(4)#12-P(3)-Cs(2)#5	119.65(13)	Th(1)-S(2)-Cs(2)	163.91(11)
Cs(2)-P(3)-Cs(2)#5	81.02(6)	P(3)#5-S(2)-Cs(1)	116.97(14)
S(11)-P(4)-S(14)#8	116.80(19)	Th(1)-S(2)-Cs(1)	108.86(8)
S(11)-P(4)-S(5)#3	116.37(18)	Cs(2)-S(2)-Cs(1)	82.49(7)
S(14)#8-P(4)-S(5)#3	108.10(18)	P(5)#5-S(3)-Th(1)	84.44(13)
S(11)-P(4)-P(3)#7	109.70(18)	P(5)#5-S(3)-Cs(4)#5	96.38(13)

Th(1)-S(3)-Cs(4)#5	124.57(10)	P(2)#4-S(9)-Th(1)#1	94.20(13)
P(5)#5-S(3)-Cs(3)#4	96.58(14)	P(2)#4-S(9)-Th(1)	108.41(14)
Th(1)-S(3)-Cs(3)#4	98.21(8)	Th(1)#1-S(9)-Th(1)	116.59(10)
Cs(4)#5-S(3)-Cs(3)#4	136.23(9)	P(2)#4-S(9)-Cs(3)#4	85.28(13)
P(1)-S(4)-Th(1)	89.44(13)	Th(1)#1-S(9)-Cs(3)#4	149.28(9)
P(1)-S(4)-Cs(1)#4	86.27(12)	Th(1)-S(9)-Cs(3)#4	92.42(7)
Th(1)-S(4)-Cs(1)#4	175.41(10)	P(6)#3-S(10)-Th(2)	88.91(13)
P(1)-S(4)-Cs(3)#4	118.41(13)	P(6)#3-S(10)-Cs(1)#3	78.05(12)
Th(1)-S(4)-Cs(3)#4	99.34(8)	Th(2)-S(10)-Cs(1)#3	99.54(8)
Cs(1)#4-S(4)-Cs(3)#4	84.14(7)	P(6)#3-S(10)-Cs(2)	111.78(14)
P(4)#3-S(5)-Th(2)#14	87.30(12)	Th(2)-S(10)-Cs(2)	92.79(8)
P(4)#3-S(5)-Th(1)	109.22(14)	Cs(1)#3-S(10)-Cs(2)	164.49(10)
Th(2)#14-S(5)-Th(1)	103.27(9)	P(4)-S(11)-Th(2)	120.07(15)
P(2)#14-S(6)-Th(1)	93.98(13)	P(4)-S(11)-Cs(1)#3	112.16(14)
P(2)#14-S(6)-Th(2)#14	87.31(13)	Th(2)-S(11)-Cs(1)#3	100.39(8)
Th(1)-S(6)-Th(2)#14	100.36(8)	P(4)-S(11)-Cs(3)	88.47(12)
P(2)#14-S(6)-Cs(2)#14	84.24(13)	Th(2)-S(11)-Cs(3)	106.65(8)
Th(1)-S(6)-Cs(2)#14	176.81(9)	Cs(1)#3-S(11)-Cs(3)	130.92(9)
Th(2)#14-S(6)-Cs(2)#14	82.23(6)	P(5)-S(12)-Th(2)	111.08(15)
P(2)#14-S(6)-Cs(4)#5	100.40(13)	P(5)-S(12)-Cs(2)	84.67(13)
Th(1)-S(6)-Cs(4)#5	110.84(8)	Th(2)-S(12)-Cs(2)	92.65(8)
Th(2)#14-S(6)-Cs(4)#5	147.08(9)	P(5)-S(12)-Cs(4)	85.25(13)
Cs(2)#14-S(6)-Cs(4)#5	66.99(5)	Th(2)-S(12)-Cs(4)	87.38(8)
P(3)#5-S(7)-Th(1)	86.85(12)	Cs(2)-S(12)-Cs(4)	169.21(9)
P(3)#5-S(7)-Th(2)#14	107.41(14)	P(2)-S(13)-Th(2)	90.83(13)
Th(1)-S(7)-Th(2)#14	96.04(8)	P(2)-S(13)-Cs(3)	95.21(13)
P(3)#5-S(7)-Cs(2)#5	87.31(13)	Th(2)-S(13)-Cs(3)	116.05(9)
Th(1)-S(7)-Cs(2)#5	108.45(9)	P(2)-S(13)-Cs(2)	89.01(13)
Th(2)#14-S(7)-Cs(2)#5	152.22(9)	Th(2)-S(13)-Cs(2)	86.68(7)
P(3)#5-S(7)-Cs(4)#14	87.89(12)	Cs(3)-S(13)-Cs(2)	156.74(9)
Th(1)-S(7)-Cs(4)#14	174.08(9)	P(2)-S(13)-Cs(1)	102.12(13)
Th(2)#14-S(7)-Cs(4)#14	82.94(7)	Th(2)-S(13)-Cs(1)	157.54(10)
Cs(2)#5-S(7)-Cs(4)#14	74.00(6)	Cs(3)-S(13)-Cs(1)	81.34(6)
P(5)#5-S(8)-Th(1)	87.79(13)	Cs(2)-S(13)-Cs(1)	75.41(6)
P(5)#5-S(8)-Cs(2)#5	94.28(13)	P(4)#8-S(14)-Th(2)	90.66(13)
Th(1)-S(8)-Cs(2)#5	117.02(10)	P(4)#8-S(14)-Cs(4)	113.96(14)

Th(2)-S(14)-Cs(4)	87.39(7)
P(4)#8-S(14)-Cs(3)#8	86.18(13)
Th(2)-S(14)-Cs(3)#8	166.71(10)
Cs(4)-S(14)-Cs(3)#8	82.14(6)
P(6)#3-S(15)-Th(2)	89.90(13)
P(6)#3-S(15)-Cs(4)#10	96.50(13)
Th(2)-S(15)-Cs(4)#10	170.27(11)
P(6)#3-S(15)-Cs(4)	114.72(15)
Th(2)-S(15)-Cs(4)	90.34(8)
Cs(4)#10-S(15)-Cs(4)	93.61(7)
P(6)#3-S(15)-Cs(1)#3	71.83(12)
Th(2)-S(15)-Cs(1)#3	94.55(8)
Cs(4)#10-S(15)-Cs(1)#3	80.58(7)
Cs(4)-S(15)-Cs(1)#3	171.89(9)
P(6)-S(16)-Cs(3)#6	110.00(15)
P(6)-S(16)-Cs(3)	101.29(14)
Cs(3)#6-S(16)-Cs(3)	107.02(8)
P(6)-S(16)-Cs(1)	75.51(13)
Cs(3)#6-S(16)-Cs(1)	167.41(10)
Cs(3)-S(16)-Cs(1)	82.30(7)
P(6)-S(16)-Cs(4)#13	92.88(14)
Cs(3)#6-S(16)-Cs(4)#13	88.17(7)
Cs(3)-S(16)-Cs(4)#13	153.86(9)
Cs(1)-S(16)-Cs(4)#13	80.14(7)
P(3)-S(17)-Cs(2)#5	93.77(14)
P(3)-S(17)-Cs(3)#12	109.49(15)
Cs(2)#5-S(17)-Cs(3)#12	101.22(8)
P(3)-S(17)-Cs(4)#9	95.53(14)
Cs(2)#5-S(17)-Cs(4)#9	162.39(10)
Cs(3)#12-S(17)-Cs(4)#9	89.72(7)
P(3)-S(17)-Cs(2)	81.92(13)
Cs(2)#5-S(17)-Cs(2)	92.68(8)
Cs(3)#12-S(17)-Cs(2)	161.15(9)
Cs(4)#9-S(17)-Cs(2)	73.92(6)
P(1)#4-S(18)-Cs(2)	115.63(14)
P(1)#4-S(18)-Cs(1)	89.17(14)
Cs(2)-S(18)-Cs(1)	87.48(7)
P(1)#4-S(18)-Cs(1)#4	84.02(13)
Cs(2)-S(18)-Cs(1)#4	154.14(9)
Cs(1)-S(18)-Cs(1)#4	110.57(8)
P(1)#4-S(18)-Cs(4)#9	93.23(14)
Cs(2)-S(18)-Cs(4)#9	78.34(7)
Cs(1)-S(18)-Cs(4)#9	165.23(9)
Cs(1)#4-S(18)-Cs(4)#9	84.18(7)

Symmetry transformations used to generate equivalent atoms:

#1 -x+1,-y+1,-z #2 x+1,y,z #3 -x+2,-y+1,-z-1

#4 -x+2,-y+1,-z #5 -x+2,-y+2,-z #6 -x+2,-y,-z-1

#7 x,y-1,z-1 #8 -x+3,-y+1,-z-1 #9 -x+3,-y+2,-z

#10 -x+3,-y+2,-z-1 #11 x+1,y+1,z #12 x,y+1,z+1

#13 x-1,y-1,z #14 x-1,y,z

Table 4. Anisotropic displacement parameters ($Å^2 x\ 10^3$) for $Cs_4Th_2(P_2S_6)_3$. The anisotropic displacement factor exponent takes the form: $-2\pi^2[\ h^2\ a^{*2}U^{11} + ... + 2\ h\ k\ a^*\ b^*\ U^{12}\ ]$

	U^{11}	U^{22}	U^{33}	U^{23}	U^{13}	U^{12}
Th(1)	8(1)	7(1)	9(1)	3(1)	2(1)	3(1)
Th(2)	9(1)	6(1)	8(1)	3(1)	2(1)	4(1)
Cs(1)	15(1)	15(1)	12(1)	5(1)	2(1)	6(1)
Cs(2)	18(1)	15(1)	20(1)	10(1)	6(1)	5(1)
Cs(3)	32(1)	16(1)	20(1)	7(1)	9(1)	10(1)
Cs(4)	18(1)	19(1)	24(1)	9(1)	2(1)	5(1)
P(1)	9(2)	10(2)	11(2)	5(1)	4(1)	6(1)
P(2)	10(2)	11(2)	10(2)	6(1)	3(1)	4(1)
P(3)	11(2)	7(2)	10(2)	3(1)	3(1)	4(1)
P(4)	10(2)	5(1)	9(2)	2(1)	3(1)	4(1)
P(5)	12(2)	5(1)	10(2)	1(1)	1(1)	4(1)
P(6)	12(2)	7(1)	10(2)	3(1)	3(1)	6(1)
S(1)	10(2)	11(1)	10(2)	4(1)	-1(1)	6(1)
S(2)	12(2)	13(2)	14(2)	9(1)	4(1)	6(1)
S(3)	18(2)	10(2)	15(2)	6(1)	5(1)	4(1)
S(4)	11(2)	9(1)	12(2)	5(1)	2(1)	4(1)
S(5)	8(2)	8(1)	12(2)	4(1)	2(1)	4(1)
S(6)	9(2)	9(1)	11(2)	4(1)	0(1)	2(1)
S(7)	13(2)	9(1)	11(2)	3(1)	4(1)	4(1)
S(8)	13(2)	8(1)	16(2)	4(1)	4(1)	4(1)
S(9)	12(2)	10(1)	16(2)	8(1)	5(1)	8(1)
S(10)	12(2)	9(1)	14(2)	4(1)	3(1)	4(1)
S(11)	11(2)	10(1)	10(2)	1(1)	3(1)	4(1)
S(12)	18(2)	8(1)	12(2)	2(1)	0(1)	7(1)
S(13)	12(2)	12(2)	11(2)	5(1)	3(1)	4(1)
S(14)	15(2)	13(2)	9(2)	6(1)	3(1)	7(1)
S(15)	18(2)	18(2)	15(2)	11(1)	10(1)	11(1)
S(16)	17(2)	15(2)	15(2)	8(1)	-1(1)	7(1)
S(17)	16(2)	14(2)	19(2)	9(1)	6(2)	3(1)
S(18)	12(2)	14(2)	17(2)	8(1)	6(1)	9(1)

Appendix E

Supplementary Information for Chapter 4

Table 1. Crystal data and structure refinement for $K_3Pu(PS_4)_2$.

Identification code	$K_3Pu(PS_4)_2$	
Empirical formula	K3 P2 Pu S8	
Formula weight	677.72	
Temperature	293(2) K	
Wavelength	0.71073 Å	
Crystal system	Monoclinic	
Space group	P21/c	
Unit cell dimensions	a = 9.1575(10) Å	a= 90°.
	b = 16.8660(19) Å	b= 90.610(3)°.
	c = 9.5377(10) Å	g = 90°.
Volume	1473.0(3) $Å^3$	
Z	4	
Density (calculated)	3.056 Mg/m^3	
Absorption coefficient	6.633 mm^{-1}	
F(000)	1236	
Crystal size	0.2 x 0.18 x 0.09 mm^3	
Theta range for data collection	2.22 to 23.24°.	
Index ranges	-8<=h<=8, -18<=k<=6, -10<=l<=8	
Reflections collected	2340	
Independent reflections	1726 [R(int) = 0.0182]	
Completeness to theta = 23.24°	81.5 %	
Refinement method	Full-matrix least-squares on F^2	
Data / restraints / parameters	1726 / 0 / 127	
Goodness-of-fit on F^2	1.065	
Final R indices [I>2sigma(I)]	R1 = 0.0371, wR2 = 0.0880	
R indices (all data)	R1 = 0.0453, wR2 = 0.0918	
Largest diff. peak and hole	1.916 and -1.744 $e.Å^{-3}$	

Table 2. Atomic coordinates (x 10^4) and equivalent isotropic displacement parameters ($Å^2$x 10^3) for $K_3Pu(PS_4)_2$. U(eq) is defined as one third of the trace of the orthogonalized U^{ij} tensor.

	x	y	z	U(eq)
Pu(1)	7286(1)	-142(1)	5243(1)	21(1)
P(1)	10250(3)	979(2)	7208(2)	22(1)
P(2)	4956(3)	-999(2)	7447(3)	22(1)
K(1)	7686(3)	4679(2)	4861(2)	38(1)
K(2)	3787(4)	2936(2)	3745(3)	54(1)
K(3)	8841(5)	2125(2)	3665(3)	68(1)
S(1)	10671(4)	1255(2)	9215(3)	31(1)
S(2)	8137(4)	1274(2)	6718(3)	31(1)
S(3)	10418(4)	-220(2)	6781(3)	27(1)
S(5)	7153(3)	-1123(2)	7743(3)	31(1)
S(6)	4422(4)	174(2)	7604(3)	33(1)
S(7)	3827(4)	-1770(2)	8604(3)	35(1)
S(8)	8366(4)	-1580(2)	4085(3)	30(1)
S(9)	4648(3)	-1207(2)	5335(3)	26(1)

Table 3. Bond lengths [Å] and angles [°] for $K_3Pu(PS_4)_2$

Pu(1)-S(8)	2.846(3)	K(1)-K(2)#9	4.451(4)
Pu(1)-S(2)	2.875(3)	K(2)-S(1)#10	3.199(5)
Pu(1)-S(5)	2.905(3)	K(2)-S(9)#1	3.361(4)
Pu(1)-S(9)#1	2.933(3)	K(2)-S(7)#6	3.361(5)
Pu(1)-S(3)#2	2.934(3)	K(2)-S(6)#7	3.421(4)
Pu(1)-S(9)	3.012(3)	K(2)-S(8)#11	3.424(4)
Pu(1)-S(6)#1	3.120(3)	K(2)-S(5)#1	3.475(4)
Pu(1)-S(3)	3.210(3)	K(2)-P(2)#1	3.648(4)
Pu(1)-P(2)	3.340(3)	K(2)-S(8)#1	3.672(4)
Pu(1)-K(3)	4.354(3)	K(2)-S(7)#1	3.709(5)
Pu(1)-K(1)#3	4.484(3)	K(2)-K(1)#9	4.451(4)
P(1)-S(1)	2.003(3)	K(2)-K(3)#12	4.731(5)
P(1)-S(8)#2	2.046(4)	K(3)-S(1)#7	3.246(4)
P(1)-S(2)	2.048(4)	K(3)-S(7)#1	3.301(5)
P(1)-S(3)	2.068(4)	K(3)-S(3)#2	3.312(4)
P(1)-K(1)#3	3.643(4)	K(3)-S(2)	3.316(4)
P(1)-K(3)#3	3.723(4)	K(3)-S(2)#7	3.338(4)
P(2)-S(7)	2.000(4)	K(3)-S(8)#2	3.446(5)
P(2)-S(5)	2.039(4)	K(3)-S(9)#1	3.685(5)
P(2)-S(6)	2.043(4)	K(3)-P(1)#7	3.723(4)
P(2)-S(9)	2.061(3)	K(3)-K(2)#13	4.731(5)
P(2)-K(2)#1	3.648(4)	S(1)-K(1)#14	3.174(4)
P(2)-K(1)#4	3.727(4)	S(1)-K(2)#15	3.199(5)
K(1)-S(1)#5	3.174(4)	S(1)-K(1)#3	3.220(4)
K(1)-S(7)#6	3.175(4)	S(1)-K(3)#3	3.246(4)
K(1)-S(5)#7	3.198(4)	S(2)-K(3)#3	3.338(4)
K(1)-S(1)#7	3.220(4)	S(2)-K(1)#3	3.430(4)
K(1)-S(6)#6	3.220(4)	S(3)-Pu(1)#2	2.934(3)
K(1)-S(2)#7	3.430(4)	S(3)-K(3)#2	3.312(4)
K(1)-S(3)#5	3.631(4)	S(3)-K(1)#14	3.631(4)
K(1)-P(1)#7	3.643(4)	S(5)-K(1)#3	3.198(4)
K(1)-S(6)#7	3.673(5)	S(5)-K(2)#1	3.475(4)
K(1)-P(2)#6	3.727(4)	S(6)-Pu(1)#1	3.120(3)
K(1)-K(1)#8	4.379(6)	S(6)-K(1)#4	3.220(4)

S(6)-K(2)#3	3.421(4)	S(5)-Pu(1)-S(3)	69.34(8)
S(6)-K(1)#3	3.673(5)	S(9)#1-Pu(1)-S(3)	130.72(7)
S(7)-K(1)#4	3.175(4)	S(3)#2-Pu(1)-S(3)	70.50(8)
S(7)-K(3)#1	3.301(5)	S(9)-Pu(1)-S(3)	132.49(7)
S(7)-K(2)#4	3.361(5)	S(6)#1-Pu(1)-S(3)	146.54(8)
S(7)-K(2)#1	3.709(5)	S(8)-Pu(1)-P(2)	95.89(7)
S(8)-P(1)#2	2.046(4)	S(2)-Pu(1)-P(2)	102.90(8)
S(8)-K(2)#16	3.424(4)	S(5)-Pu(1)-P(2)	37.30(8)
S(8)-K(3)#2	3.446(5)	S(9)#1-Pu(1)-P(2)	93.76(8)
S(8)-K(2)#1	3.672(4)	S(3)#2-Pu(1)-P(2)	166.25(8)
S(9)-Pu(1)#1	2.933(3)	S(9)-Pu(1)-P(2)	37.42(6)
S(9)-K(2)#1	3.361(4)	S(6)#1-Pu(1)-P(2)	102.87(8)
S(9)-K(3)#1	3.685(5)	S(3)-Pu(1)-P(2)	105.58(7)
S(8)-Pu(1)-S(2)	143.52(9)	S(8)-Pu(1)-K(3)	119.83(8)
S(8)-Pu(1)-S(5)	81.46(8)	S(2)-Pu(1)-K(3)	49.59(7)
S(2)-Pu(1)-S(5)	94.87(8)	S(5)-Pu(1)-K(3)	143.16(7)
S(8)-Pu(1)-S(9)#1	143.11(8)	S(9)#1-Pu(1)-K(3)	56.81(8)
S(2)-Pu(1)-S(9)#1	66.88(8)	S(3)#2-Pu(1)-K(3)	49.49(8)
S(5)-Pu(1)-S(9)#1	124.44(8)	S(9)-Pu(1)-K(3)	143.03(7)
S(8)-Pu(1)-S(3)#2	70.57(7)	S(6)#1-Pu(1)-K(3)	82.91(7)
S(2)-Pu(1)-S(3)#2	87.52(8)	S(3)-Pu(1)-K(3)	84.24(7)
S(5)-Pu(1)-S(3)#2	134.05(9)	P(2)-Pu(1)-K(3)	144.20(8)
S(9)#1-Pu(1)-S(3)#2	98.64(8)	S(8)-Pu(1)-K(1)#3	120.30(7)
S(8)-Pu(1)-S(9)	77.62(8)	S(2)-Pu(1)-K(1)#3	49.91(7)
S(2)-Pu(1)-S(9)	133.97(8)	S(5)-Pu(1)-K(1)#3	45.31(7)
S(5)-Pu(1)-S(9)	66.18(8)	S(9)#1-Pu(1)-K(1)#3	95.31(6)
S(9)#1-Pu(1)-S(9)	89.15(8)	S(3)#2-Pu(1)-K(1)#3	123.96(7)
S(3)#2-Pu(1)-S(9)	136.36(7)	S(9)-Pu(1)-K(1)#3	97.61(6)
S(8)-Pu(1)-S(6)#1	79.68(8)	S(6)#1-Pu(1)-K(1)#3	153.23(7)
S(2)-Pu(1)-S(6)#1	124.78(8)	S(3)-Pu(1)-K(1)#3	59.67(6)
S(5)-Pu(1)-S(6)#1	132.82(8)	P(2)-Pu(1)-K(1)#3	60.22(6)
S(9)#1-Pu(1)-S(6)#1	63.45(7)	K(3)-Pu(1)-K(1)#3	99.39(6)
S(3)#2-Pu(1)-S(6)#1	77.69(9)	S(1)-P(1)-S(8)#2	110.30(18)
S(9)-Pu(1)-S(6)#1	67.69(8)	S(1)-P(1)-S(2)	109.49(17)
S(8)-Pu(1)-S(3)	80.23(8)	S(8)#2-P(1)-S(2)	109.39(17)
S(2)-Pu(1)-S(3)	64.79(8)	S(1)-P(1)-S(3)	113.66(16)

S(8)#2-P(1)-S(3)	108.53(16)	S(7)#6-K(1)-S(1)#7	95.00(11)
S(2)-P(1)-S(3)	105.31(17)	S(5)#7-K(1)-S(1)#7	112.08(11)
S(1)-P(1)-K(1)#3	61.71(12)	S(1)#5-K(1)-S(6)#6	82.01(10)
S(8)#2-P(1)-K(1)#3	167.77(14)	S(7)#6-K(1)-S(6)#6	65.47(9)
S(2)-P(1)-K(1)#3	67.54(12)	S(5)#7-K(1)-S(6)#6	100.86(11)
S(3)-P(1)-K(1)#3	83.60(12)	S(1)#7-K(1)-S(6)#6	141.95(11)
S(1)-P(1)-K(3)#3	60.52(12)	S(1)#5-K(1)-S(2)#7	125.03(11)
S(8)#2-P(1)-K(3)#3	91.07(13)	S(7)#6-K(1)-S(2)#7	95.71(10)
S(2)-P(1)-K(3)#3	63.02(12)	S(5)#7-K(1)-S(2)#7	79.84(9)
S(3)-P(1)-K(3)#3	160.03(17)	S(1)#7-K(1)-S(2)#7	59.55(8)
K(1)#3-P(1)-K(3)#3	76.95(10)	S(6)#6-K(1)-S(2)#7	148.89(13)
S(7)-P(2)-S(5)	111.85(18)	S(1)#5-K(1)-S(3)#5	59.66(8)
S(7)-P(2)-S(6)	117.58(19)	S(7)#6-K(1)-S(3)#5	80.58(9)
S(5)-P(2)-S(6)	108.98(18)	S(5)#7-K(1)-S(3)#5	126.15(11)
S(7)-P(2)-S(9)	111.25(18)	S(1)#7-K(1)-S(3)#5	78.05(9)
S(5)-P(2)-S(9)	104.03(17)	S(6)#6-K(1)-S(3)#5	67.07(9)
S(6)-P(2)-S(9)	101.89(15)	S(2)#7-K(1)-S(3)#5	137.06(11)
S(7)-P(2)-Pu(1)	164.99(16)	S(1)#5-K(1)-P(1)#7	98.11(10)
S(5)-P(2)-Pu(1)	59.69(10)	S(7)#6-K(1)-P(1)#7	111.92(10)
S(6)-P(2)-Pu(1)	77.43(12)	S(5)#7-K(1)-P(1)#7	83.60(9)
S(9)-P(2)-Pu(1)	62.63(11)	S(1)#7-K(1)-P(1)#7	33.21(7)
S(7)-P(2)-K(2)#1	75.92(14)	S(6)#6-K(1)-P(1)#7	175.12(12)
S(5)-P(2)-K(2)#1	68.75(12)	S(2)#7-K(1)-P(1)#7	33.48(7)
S(6)-P(2)-K(2)#1	164.99(15)	S(3)#5-K(1)-P(1)#7	108.74(10)
S(9)-P(2)-K(2)#1	65.39(11)	S(1)#5-K(1)-S(6)#7	119.12(11)
Pu(1)-P(2)-K(2)#1	89.17(9)	S(7)#6-K(1)-S(6)#7	88.04(10)
S(7)-P(2)-K(1)#4	58.42(12)	S(5)#7-K(1)-S(6)#7	57.35(9)
S(5)-P(2)-K(1)#4	125.65(13)	S(1)#7-K(1)-S(6)#7	127.44(10)
S(6)-P(2)-K(1)#4	59.64(12)	S(6)#6-K(1)-S(6)#7	86.09(10)
S(9)-P(2)-K(1)#4	129.98(16)	S(2)#7-K(1)-S(6)#7	67.93(8)
Pu(1)-P(2)-K(1)#4	136.43(9)	S(3)#5-K(1)-S(6)#7	153.15(11)
K(2)#1-P(2)-K(1)#4	134.33(11)	P(1)#7-K(1)-S(6)#7	98.05(9)
S(1)#5-K(1)-S(7)#6	136.41(10)	S(1)#5-K(1)-P(2)#6	112.02(9)
S(1)#5-K(1)-S(5)#7	66.85(9)	S(7)#6-K(1)-P(2)#6	32.45(7)
S(7)#6-K(1)-S(5)#7	144.38(13)	S(5)#7-K(1)-P(2)#6	124.97(11)
S(1)#5-K(1)-S(1)#7	93.56(11)	S(1)#7-K(1)-P(2)#6	122.70(10)

S(6)#6-K(1)-P(2)#6	33.20(7)	S(1)#10-K(2)-S(5)#1	102.44(12)
S(2)#7-K(1)-P(2)#6	122.90(11)	S(9)#1-K(2)-S(5)#1	56.39(8)
S(3)#5-K(1)-P(2)#6	73.41(8)	S(7)#6-K(2)-S(5)#1	126.40(11)
P(1)#7-K(1)-P(2)#6	144.37(10)	S(6)#7-K(2)-S(5)#1	137.10(12)
S(6)#7-K(1)-P(2)#6	83.92(9)	S(8)#11-K(2)-S(5)#1	75.54(9)
S(1)#5-K(1)-K(1)#8	47.22(8)	S(1)#10-K(2)-P(2)#1	135.28(13)
S(7)#6-K(1)-K(1)#8	126.09(12)	S(9)#1-K(2)-P(2)#1	33.89(6)
S(5)#7-K(1)-K(1)#8	89.51(10)	S(7)#6-K(2)-P(2)#1	99.33(10)
S(1)#7-K(1)-K(1)#8	46.34(8)	S(6)#7-K(2)-P(2)#1	132.85(13)
S(6)#6-K(1)-K(1)#8	118.57(11)	S(8)#11-K(2)-P(2)#1	98.57(10)
S(2)#7-K(1)-K(1)#8	92.49(10)	S(5)#1-K(2)-P(2)#1	33.15(8)
S(3)#5-K(1)-K(1)#8	58.77(8)	S(1)#10-K(2)-S(8)#1	72.65(11)
P(1)#7-K(1)-K(1)#8	59.13(8)	S(9)#1-K(2)-S(8)#1	62.79(9)
S(6)#7-K(1)-K(1)#8	143.11(11)	S(7)#6-K(2)-S(8)#1	90.95(11)
P(2)#6-K(1)-K(1)#8	132.00(11)	S(6)#7-K(2)-S(8)#1	148.61(13)
S(1)#5-K(1)-K(2)#9	45.94(9)	S(8)#11-K(2)-S(8)#1	106.54(13)
S(7)#6-K(1)-K(2)#9	115.01(10)	S(5)#1-K(2)-S(8)#1	63.28(8)
S(5)#7-K(1)-K(2)#9	57.04(8)	P(2)#1-K(2)-S(8)#1	77.96(9)
S(1)#7-K(1)-K(2)#9	139.47(11)	S(1)#10-K(2)-S(7)#1	147.44(13)
S(6)#6-K(1)-K(2)#9	49.88(8)	S(9)#1-K(2)-S(7)#1	56.34(8)
S(2)#7-K(1)-K(2)#9	136.41(10)	S(7)#6-K(2)-S(7)#1	98.65(13)
S(3)#5-K(1)-K(2)#9	80.65(8)	S(6)#7-K(2)-S(7)#1	101.47(12)
P(1)#7-K(1)-K(2)#9	133.05(10)	S(8)#11-K(2)-S(7)#1	89.34(10)
S(6)#7-K(1)-K(2)#9	82.34(8)	S(5)#1-K(2)-S(7)#1	55.39(8)
P(2)#6-K(1)-K(2)#9	82.57(8)	P(2)#1-K(2)-S(7)#1	31.53(6)
K(1)#8-K(1)-K(2)#9	93.14(10)	S(8)#1-K(2)-S(7)#1	109.49(9)
S(1)#10-K(2)-S(9)#1	135.41(14)	S(1)#10-K(2)-K(1)#9	45.47(8)
S(1)#10-K(2)-S(7)#6	113.89(12)	S(9)#1-K(2)-K(1)#9	146.68(10)
S(9)#1-K(2)-S(7)#6	70.11(9)	S(7)#6-K(2)-K(1)#9	80.68(8)
S(1)#10-K(2)-S(6)#7	78.56(10)	S(6)#7-K(2)-K(1)#9	46.02(7)
S(9)#1-K(2)-S(6)#7	144.89(14)	S(8)#11-K(2)-K(1)#9	81.14(8)
S(7)#6-K(2)-S(6)#7	89.42(10)	S(5)#1-K(2)-K(1)#9	147.43(12)
S(1)#10-K(2)-S(8)#11	60.11(8)	P(2)#1-K(2)-K(1)#9	178.86(12)
S(9)#1-K(2)-S(8)#11	130.78(11)	S(8)#1-K(2)-K(1)#9	103.18(10)
S(7)#6-K(2)-S(8)#11	157.20(12)	S(7)#1-K(2)-K(1)#9	147.33(11)
S(6)#7-K(2)-S(8)#11	68.01(9)	S(1)#10-K(2)-K(3)#12	43.16(8)

S(9)#1-K(2)-K(3)#12	99.14(10)	S(7)#1-K(3)-S(9)#1	57.02(9)
S(7)#6-K(2)-K(3)#12	132.02(12)	S(3)#2-K(3)-S(9)#1	78.77(10)
S(6)#7-K(2)-K(3)#12	115.50(10)	S(2)-K(3)-S(9)#1	54.10(9)
S(8)#11-K(2)-K(3)#12	60.87(8)	S(2)#7-K(3)-S(9)#1	108.72(13)
S(5)#1-K(2)-K(3)#12	60.41(9)	S(8)#2-K(3)-S(9)#1	111.51(10)
P(2)#1-K(2)-K(3)#12	92.37(10)	S(1)#7-K(3)-P(1)#7	32.49(6)
S(8)#1-K(2)-K(3)#12	46.33(8)	S(7)#1-K(3)-P(1)#7	99.68(10)
S(7)#1-K(2)-K(3)#12	114.01(10)	S(3)#2-K(3)-P(1)#7	135.49(15)
K(1)#9-K(2)-K(3)#12	88.45(8)	S(2)-K(3)-P(1)#7	140.44(11)
S(1)#10-K(2)-K(1)	112.00(10)	S(2)#7-K(3)-P(1)#7	33.14(8)
S(9)#1-K(2)-K(1)	99.29(10)	S(8)#2-K(3)-P(1)#7	101.75(11)
S(7)#6-K(2)-K(1)	42.01(7)	S(9)#1-K(3)-P(1)#7	139.65(13)
S(6)#7-K(2)-K(1)	50.40(8)	S(1)#7-K(3)-Pu(1)	148.63(10)
S(8)#11-K(2)-K(1)	117.07(10)	S(7)#1-K(3)-Pu(1)	79.92(8)
S(5)#1-K(2)-K(1)	145.14(11)	S(3)#2-K(3)-Pu(1)	42.34(6)
P(2)#1-K(2)-K(1)	112.71(11)	S(2)-K(3)-Pu(1)	41.31(6)
S(8)#1-K(2)-K(1)	131.88(10)	S(2)#7-K(3)-Pu(1)	147.27(12)
S(7)#1-K(2)-K(1)	90.99(10)	S(8)#2-K(3)-Pu(1)	78.10(7)
K(1)#9-K(2)-K(1)	66.54(7)	S(9)#1-K(3)-Pu(1)	41.76(5)
K(3)#12-K(2)-K(1)	154.43(9)	P(1)#7-K(3)-Pu(1)	177.78(13)
S(1)#7-K(3)-S(7)#1	129.47(11)	S(1)#7-K(3)-K(1)	44.62(8)
S(1)#7-K(3)-S(3)#2	137.02(16)	S(7)#1-K(3)-K(1)	99.34(11)
S(7)#1-K(3)-S(3)#2	83.75(10)	S(3)#2-K(3)-K(1)	172.71(12)
S(1)#7-K(3)-S(2)	109.12(11)	S(2)-K(3)-K(1)	98.09(10)
S(7)#1-K(3)-S(2)	110.33(13)	S(2)#7-K(3)-K(1)	48.22(7)
S(3)#2-K(3)-S(2)	74.63(9)	S(8)#2-K(3)-K(1)	105.50(9)
S(1)#7-K(3)-S(2)#7	60.30(8)	S(9)#1-K(3)-K(1)	97.31(11)
S(7)#1-K(3)-S(2)#7	69.19(9)	P(1)#7-K(3)-K(1)	50.74(7)
S(3)#2-K(3)-S(2)#7	138.81(13)	Pu(1)-K(3)-K(1)	131.46(11)
S(2)-K(3)-S(2)#7	143.20(16)	S(1)#7-K(3)-K(2)#13	42.40(8)
S(1)#7-K(3)-S(8)#2	75.25(10)	S(7)#1-K(3)-K(2)#13	139.89(12)
S(7)#1-K(3)-S(8)#2	154.05(12)	S(3)#2-K(3)-K(2)#13	94.89(12)
S(3)#2-K(3)-S(8)#2	70.72(10)	S(2)-K(3)-K(2)#13	107.83(10)
S(2)-K(3)-S(8)#2	59.18(9)	S(2)#7-K(3)-K(2)#13	87.38(10)
S(2)#7-K(3)-S(8)#2	134.44(13)	S(8)#2-K(3)-K(2)#13	50.43(8)
S(1)#7-K(3)-S(9)#1	139.40(14)	S(9)#1-K(3)-K(2)#13	161.78(9)

P(1)#7-K(3)-K(2)#13	54.70(8)	Pu(1)#2-S(3)-Pu(1)	109.50(8)
Pu(1)-K(3)-K(2)#13	124.39(8)	P(1)-S(3)-K(3)#2	171.57(18)
K(1)-K(3)-K(2)#13	87.00(8)	Pu(1)#2-S(3)-K(3)#2	88.18(10)
S(1)#7-K(3)-K(2)	104.61(11)	Pu(1)-S(3)-K(3)#2	99.43(10)
S(7)#1-K(3)-K(2)	50.10(9)	P(1)-S(3)-K(1)#14	84.72(12)
S(3)#2-K(3)-K(2)	118.33(11)	Pu(1)#2-S(3)-K(1)#14	104.54(10)
S(2)-K(3)-K(2)	85.02(11)	Pu(1)-S(3)-K(1)#14	145.23(10)
S(2)#7-K(3)-K(2)	66.40(10)	K(3)#2-S(3)-K(1)#14	88.34(10)
S(8)#2-K(3)-K(2)	140.44(12)	P(2)-S(5)-Pu(1)	83.01(11)
S(9)#1-K(3)-K(2)	44.00(7)	P(2)-S(5)-K(1)#3	98.83(14)
P(1)#7-K(3)-K(2)	95.66(9)	Pu(1)-S(5)-K(1)#3	94.45(9)
Pu(1)-K(3)-K(2)	85.76(8)	P(2)-S(5)-K(2)#1	78.10(13)
K(1)-K(3)-K(2)	60.39(7)	Pu(1)-S(5)-K(2)#1	100.26(9)
K(2)#13-K(3)-K(2)	146.69(9)	K(1)#3-S(5)-K(2)#1	164.42(12)
P(1)-S(1)-K(1)#14	99.02(14)	P(2)-S(6)-Pu(1)#1	92.17(12)
P(1)-S(1)-K(2)#15	97.36(15)	P(2)-S(6)-K(1)#4	87.16(14)
K(1)#14-S(1)-K(2)#15	88.59(11)	Pu(1)#1-S(6)-K(1)#4	110.49(12)
P(1)-S(1)-K(1)#3	85.08(14)	P(2)-S(6)-K(2)#3	165.30(15)
K(1)#14-S(1)-K(1)#3	86.44(11)	Pu(1)#1-S(6)-K(2)#3	101.94(10)
K(2)#15-S(1)-K(1)#3	174.77(13)	K(1)#4-S(6)-K(2)#3	84.10(10)
P(1)-S(1)-K(3)#3	86.99(13)	P(2)-S(6)-K(1)#3	85.10(14)
K(1)#14-S(1)-K(3)#3	172.88(12)	Pu(1)#1-S(6)-K(1)#3	155.30(12)
K(2)#15-S(1)-K(3)#3	94.44(12)	K(1)#4-S(6)-K(1)#3	93.91(10)
K(1)#3-S(1)-K(3)#3	90.30(12)	K(2)#3-S(6)-K(1)#3	83.74(10)
P(1)-S(2)-Pu(1)	99.25(13)	P(2)-S(7)-K(1)#4	89.14(13)
P(1)-S(2)-K(3)	96.50(15)	P(2)-S(7)-K(3)#1	98.02(14)
Pu(1)-S(2)-K(3)	89.10(9)	K(1)#4-S(7)-K(3)#1	96.78(13)
P(1)-S(2)-K(3)#3	83.83(13)	P(2)-S(7)-K(2)#4	100.11(16)
Pu(1)-S(2)-K(3)#3	173.96(14)	K(1)#4-S(7)-K(2)#4	92.88(11)
K(3)-S(2)-K(3)#3	95.73(9)	K(3)#1-S(7)-K(2)#4	159.55(12)
P(1)-S(2)-K(1)#3	78.98(12)	P(2)-S(7)-K(2)#1	72.55(13)
Pu(1)-S(2)-K(1)#3	90.22(9)	K(1)#4-S(7)-K(2)#1	161.66(12)
K(3)-S(2)-K(1)#3	175.27(14)	K(3)#1-S(7)-K(2)#1	86.84(11)
K(3)#3-S(2)-K(1)#3	85.26(10)	K(2)#4-S(7)-K(2)#1	89.63(12)
P(1)-S(3)-Pu(1)#2	88.93(13)	P(1)#2-S(8)-Pu(1)	91.83(12)
P(1)-S(3)-Pu(1)	89.00(13)	P(1)#2-S(8)-K(2)#16	89.89(13)

Pu(1)-S(8)-K(2)#16	108.04(11)
P(1)#2-S(8)-K(3)#2	92.71(15)
Pu(1)-S(8)-K(3)#2	104.12(10)
K(2)#16-S(8)-K(3)#2	147.63(12)
P(1)#2-S(8)-K(2)#1	171.02(15)
Pu(1)-S(8)-K(2)#1	96.93(9)
K(2)#16-S(8)-K(2)#1	89.29(10)
K(3)#2-S(8)-K(2)#1	83.24(9)
P(2)-S(9)-Pu(1)#1	97.35(12)
P(2)-S(9)-Pu(1)	79.95(12)
Pu(1)#1-S(9)-Pu(1)	90.85(8)
P(2)-S(9)-K(2)#1	80.72(12)
Pu(1)#1-S(9)-K(2)#1	167.76(13)
Pu(1)-S(9)-K(2)#1	100.65(10)
P(2)-S(9)-K(3)#1	85.90(13)
Pu(1)#1-S(9)-K(3)#1	81.42(9)
Pu(1)-S(9)-K(3)#1	162.90(10)
K(2)#1-S(9)-K(3)#1	86.37(10)

Symmetry transformations used to generate equivalent atoms:

#1 -x+1,-y,-z+1 #2 -x+2,-y,-z+1 #3 x,-y+1/2,z+1/2

#4 -x+1,y-1/2,-z+3/2 #5 -x+2,y+1/2,-z+3/2 #6 -x+1,y+1/2,-z+3/2

#7 x,-y+1/2,z-1/2 #8 -x+2,-y+1,-z+1 #9 -x+1,-y+1,-z+1

#10 x-1,-y+1/2,z-1/2 #11 -x+1,y+1/2,-z+1/2 #12 x-1,y,z

#13 x+1,y,z #14 -x+2,y-1/2,-z+3/2 #15 x+1,-y+1/2,z+1/2

#16 -x+1,y-1/2,-z+1/2

Table 4. Anisotropic displacement parameters ($Å^2 x\ 10^3$) for $K_3Pu(PS_4)_2$. The anisotropic displacement factor exponent takes the form: $-2p^2[\ h^2\ a^{*2}U^{11} + ... + 2\ h\ k\ a^*\ b^*\ U^{12}\ ]$

	U^{11}	U^{22}	U^{33}	U^{23}	U^{13}	U^{12}
Pu(1)	25(1)	21(1)	18(1)	1(1)	-4(1)	0(1)
P(1)	25(2)	24(2)	16(1)	-1(1)	-4(1)	1(1)
P(2)	25(2)	26(2)	16(1)	2(1)	-3(1)	-1(1)
K(1)	46(2)	41(2)	28(1)	1(1)	9(1)	-1(1)
K(2)	53(3)	37(2)	71(2)	-4(1)	-25(2)	11(2)
K(3)	97(3)	39(2)	69(2)	19(2)	-44(2)	-19(2)
S(1)	37(2)	39(2)	18(1)	-7(1)	-7(1)	1(1)
S(2)	28(2)	31(2)	35(2)	-8(1)	-13(1)	6(1)
S(3)	32(2)	21(2)	27(1)	1(1)	-1(1)	0(1)
S(5)	27(2)	45(2)	20(1)	3(1)	-7(1)	2(1)
S(6)	48(3)	25(2)	26(1)	0(1)	-3(1)	1(1)
S(7)	40(2)	33(2)	32(2)	11(1)	2(1)	-7(1)
S(8)	37(2)	23(2)	29(1)	2(1)	3(1)	-4(1)
S(9)	28(2)	33(2)	18(1)	-3(1)	-6(1)	7(1)

Table 1. Crystal data and structure refinement for $KPuP_2S_7$.

Identification code	$KPuP_2S_7$	
Empirical formula	K P2 Pu S7	
Formula weight	567.46	
Temperature	293(2) K	
Wavelength	0.71073 Å	
Crystal system	Monoclinic	
Space group	P21/c	
Unit cell dimensions	a = 9.6405(10) Å	a= 90°.
	b = 12.2551(12) Å	b= 90.218(2)°.
	c = 9.0152(8) Å	g = 90°.
Volume	1065.10(18) $Å^3$	
Z	4	
Density (calculated)	3.539 Mg/m^3	
Absorption coefficient	8.185 mm^{-1}	
F(000)	1020	
Crystal size	0.5 x 0.1 x 0.1 mm^3	
Theta range for data collection	2.11 to 22.50°.	
Index ranges	-10<=h<=10, -13<=k<=13, -9<=l<=9	
Reflections collected	3458	
Independent reflections	1376 [R(int) = 0.0423]	
Completeness to theta = 22.50°	98.4 %	
Absorption correction	SADABS	
Refinement method	Full-matrix least-squares on F^2	
Data / restraints / parameters	1376 / 0 / 100	
Goodness-of-fit on F^2	1.061	
Final R indices [I>2sigma(I)]	R1 = 0.0324, wR2 = 0.0662	
R indices (all data)	R1 = 0.0444, wR2 = 0.0689	
Largest diff. peak and hole	2.248 and -0.897 $e.Å^{-3}$	

Table 2. Atomic coordinates (x 10^4) and equivalent isotropic displacement parameters ($Å^2$x 10^3) for $KPuP_2S_7$. U(eq) is defined as one third of the trace of the orthogonalized U^{ij} tensor.

	x	y	z	U(eq)
Pu(1)	8563(1)	6429(1)	1082(1)	11(1)
K(1)	13929(3)	6936(2)	-1314(3)	25(1)
S(1)	10163(3)	4404(2)	1804(3)	14(1)
S(2)	6621(3)	5244(2)	-704(3)	16(1)
S(3)	11492(3)	6949(2)	1452(3)	14(1)
S(4)	6270(3)	5550(2)	2898(3)	17(1)
S(5)	9095(3)	8331(2)	-725(3)	14(1)
S(6)	6254(3)	7938(2)	1119(3)	16(1)
S(7)	7502(3)	10555(2)	785(3)	14(1)
P(1)	11867(3)	5371(2)	1981(3)	12(1)
P(2)	7226(3)	8999(2)	-226(3)	11(1)

Table 3. Bond lengths [Å] and angles [°] for $KPuP_2S_7$.

Pu(1)-S(2)	2.861(3)	S(7)-K(1)#6	3.405(4)
Pu(1)-S(5)	2.890(3)	P(1)-S(2)#2	2.007(4)
Pu(1)-S(6)	2.894(3)	P(1)-S(7)#10	2.115(4)
Pu(1)-S(3)	2.912(3)	P(2)-S(4)#5	2.001(4)
Pu(1)-S(5)#1	2.937(3)	S(2)-Pu(1)-S(5)	102.10(8)
Pu(1)-S(4)	2.960(3)	S(2)-Pu(1)-S(6)	80.17(8)
Pu(1)-S(1)	2.993(3)	S(5)-Pu(1)-S(6)	68.24(8)
Pu(1)-S(1)#2	3.056(3)	S(2)-Pu(1)-S(3)	143.88(8)
K(1)-S(6)#3	3.232(4)	S(5)-Pu(1)-S(3)	73.39(8)
K(1)-S(2)#2	3.276(4)	S(6)-Pu(1)-S(3)	127.17(8)
K(1)-S(6)#4	3.363(4)	S(2)-Pu(1)-S(5)#1	135.55(8)
K(1)-S(2)#4	3.366(4)	S(5)-Pu(1)-S(5)#1	116.16(6)
K(1)-S(4)#2	3.369(4)	S(6)-Pu(1)-S(5)#1	93.21(8)
K(1)-S(3)#5	3.377(4)	S(3)-Pu(1)-S(5)#1	72.55(8)
K(1)-S(7)#6	3.405(4)	S(2)-Pu(1)-S(4)	68.76(8)
K(1)-S(3)	3.433(4)	S(5)-Pu(1)-S(4)	137.73(8)
K(1)-K(1)#5	4.7150(16)	S(6)-Pu(1)-S(4)	69.52(8)
K(1)-K(1)#1	4.7150(16)	S(3)-Pu(1)-S(4)	137.91(8)
S(1)-P(1)	2.032(4)	S(5)#1-Pu(1)-S(4)	67.80(8)
S(1)-Pu(1)#2	3.056(3)	S(2)-Pu(1)-S(1)	92.11(8)
S(2)-P(1)#2	2.007(4)	S(5)-Pu(1)-S(1)	134.35(8)
S(2)-K(1)#2	3.276(4)	S(6)-Pu(1)-S(1)	157.40(8)
S(2)-K(1)#7	3.366(4)	S(3)-Pu(1)-S(1)	70.00(8)
S(3)-P(1)	2.024(4)	S(5)#1-Pu(1)-S(1)	77.41(7)
S(3)-K(1)#1	3.377(4)	S(4)-Pu(1)-S(1)	87.88(8)
S(4)-P(2)#1	2.001(4)	S(2)-Pu(1)-S(1)#2	67.41(8)
S(4)-K(1)#2	3.369(4)	S(5)-Pu(1)-S(1)#2	73.56(7)
S(5)-P(2)	2.031(4)	S(6)-Pu(1)-S(1)#2	122.34(8)
S(5)-Pu(1)#5	2.937(3)	S(3)-Pu(1)-S(1)#2	77.18(8)
S(6)-P(2)	2.011(4)	S(5)#1-Pu(1)-S(1)#2	142.98(8)
S(6)-K(1)#8	3.232(4)	S(4)-Pu(1)-S(1)#2	130.75(7)
S(6)-K(1)#7	3.363(4)	S(1)-Pu(1)-S(1)#2	72.52(8)
S(7)-P(1)#9	2.115(4)	S(6)#3-K(1)-S(2)#2	123.41(11)
S(7)-P(2)	2.130(4)	S(6)#3-K(1)-S(6)#4	89.25(10)

S(2)#2-K(1)-S(6)#4	92.55(10)	S(6)#4-K(1)-K(1)#1	43.26(7)
S(6)#3-K(1)-S(2)#4	67.03(9)	S(2)#4-K(1)-K(1)#1	91.56(7)
S(2)#2-K(1)-S(2)#4	62.17(9)	S(4)#2-K(1)-K(1)#1	132.08(10)
S(6)#4-K(1)-S(2)#4	66.84(9)	S(3)#5-K(1)-K(1)#1	116.67(9)
S(6)#3-K(1)-S(4)#2	77.18(9)	S(7)#6-K(1)-K(1)#1	66.39(8)
S(2)#2-K(1)-S(4)#2	59.29(8)	S(3)-K(1)-K(1)#1	45.70(7)
S(6)#4-K(1)-S(4)#2	130.04(11)	K(1)#5-K(1)-K(1)#1	145.88(12)
S(2)#4-K(1)-S(4)#2	63.56(8)	P(1)-S(1)-Pu(1)	87.07(12)
S(6)#3-K(1)-S(3)#5	92.10(10)	P(1)-S(1)-Pu(1)#2	86.22(12)
S(2)#2-K(1)-S(3)#5	123.20(11)	Pu(1)-S(1)-Pu(1)#2	107.48(8)
S(6)#4-K(1)-S(3)#5	134.55(10)	P(1)#2-S(2)-Pu(1)	92.18(13)
S(2)#4-K(1)-S(3)#5	151.76(11)	P(1)#2-S(2)-K(1)#2	97.56(13)
S(4)#2-K(1)-S(3)#5	94.30(10)	Pu(1)-S(2)-K(1)#2	102.03(10)
S(6)#3-K(1)-S(7)#6	109.86(10)	P(1)#2-S(2)-K(1)#7	134.33(15)
S(2)#2-K(1)-S(7)#6	126.31(10)	Pu(1)-S(2)-K(1)#7	106.37(10)
S(6)#4-K(1)-S(7)#6	81.25(9)	K(1)#2-S(2)-K(1)#7	117.83(9)
S(2)#4-K(1)-S(7)#6	147.78(12)	P(1)-S(3)-Pu(1)	89.45(13)
S(4)#2-K(1)-S(7)#6	148.62(11)	P(1)-S(3)-K(1)#1	97.06(13)
S(3)#5-K(1)-S(7)#6	55.73(8)	Pu(1)-S(3)-K(1)#1	145.97(11)
S(6)#3-K(1)-S(3)	176.88(11)	P(1)-S(3)-K(1)	92.54(13)
S(2)#2-K(1)-S(3)	59.19(8)	Pu(1)-S(3)-K(1)	125.56(11)
S(6)#4-K(1)-S(3)	88.91(9)	K(1)#1-S(3)-K(1)	87.63(9)
S(2)#4-K(1)-S(3)	114.44(10)	P(2)#1-S(4)-Pu(1)	91.37(13)
S(4)#2-K(1)-S(3)	105.92(10)	P(2)#1-S(4)-K(1)#2	129.31(15)
S(3)#5-K(1)-S(3)	87.41(9)	Pu(1)-S(4)-K(1)#2	97.82(9)
S(7)#6-K(1)-S(3)	67.37(8)	P(2)-S(5)-Pu(1)	92.34(12)
S(6)#3-K(1)-K(1)#5	45.49(7)	P(2)-S(5)-Pu(1)#5	91.42(13)
S(2)#2-K(1)-K(1)#5	140.42(10)	Pu(1)-S(5)-Pu(1)#5	127.04(10)
S(6)#4-K(1)-K(1)#5	120.92(9)	P(2)-S(6)-Pu(1)	92.63(13)
S(2)#4-K(1)-K(1)#5	109.52(7)	P(2)-S(6)-K(1)#8	136.62(15)
S(4)#2-K(1)-K(1)#5	81.96(8)	Pu(1)-S(6)-K(1)#8	125.06(11)
S(3)#5-K(1)-K(1)#5	46.67(7)	P(2)-S(6)-K(1)#7	98.85(14)
S(7)#6-K(1)-K(1)#5	82.56(9)	Pu(1)-S(6)-K(1)#7	105.65(9)
S(3)-K(1)-K(1)#5	134.08(7)	K(1)#8-S(6)-K(1)#7	91.25(10)
S(6)#3-K(1)-K(1)#1	132.30(8)	P(1)#9-S(7)-P(2)	110.32(15)
S(2)#2-K(1)-K(1)#1	73.00(7)	P(1)#9-S(7)-K(1)#6	94.46(12)

P(2)-S(7)-K(1)#6	144.98(15)
S(2)#2-P(1)-S(3)	110.69(17)
S(2)#2-P(1)-S(1)	108.95(17)
S(3)-P(1)-S(1)	113.28(18)
S(2)#2-P(1)-S(7)#10	112.28(18)
S(3)-P(1)-S(7)#10	99.97(16)
S(1)-P(1)-S(7)#10	111.51(16)
S(4)#5-P(2)-S(6)	118.29(19)
S(4)#5-P(2)-S(5)	109.33(18)
S(6)-P(2)-S(5)	106.78(16)
S(4)#5-P(2)-S(7)	99.79(16)
S(6)-P(2)-S(7)	112.22(17)
S(5)-P(2)-S(7)	110.26(17)

Symmetry transformations used to generate equivalent atoms:

#1 x,-y+3/2,z+1/2 #2 -x+2,-y+1,-z #3 x+1,-y+3/2,z-1/2

#4 x+1,y,z #5 x,-y+3/2,z-1/2 #6 -x+2,-y+2,-z

#7 x-1,y,z #8 x-1,-y+3/2,z+1/2 #9 -x+2,y+1/2,-z+1/2

#10 -x+2,y-1/2,-z+1/2

Table 4. Anisotropic displacement parameters ($Å^2 x\ 10^3$) for $KPuP_2S_7$. The anisotropic displacement factor exponent takes the form: $-2p^2[\ h^2\ a^{*2}U^{11} + ... + 2\ h\ k\ a^*\ b^*\ U^{12}\ ]$

	U^{11}	U^{22}	U^{33}	U^{23}	U^{13}	U^{12}
Pu(1)	16(1)	9(1)	8(1)	1(1)	1(1)	1(1)
K(1)	33(2)	21(1)	21(2)	3(1)	1(1)	3(1)
S(1)	19(2)	10(1)	12(2)	0(1)	0(1)	-1(1)
S(2)	17(2)	18(2)	12(2)	-3(1)	0(1)	2(1)
S(3)	19(2)	10(1)	14(2)	1(1)	-1(1)	0(1)
S(4)	26(2)	16(2)	7(2)	0(1)	-3(1)	-6(1)
S(5)	16(2)	14(2)	12(2)	3(1)	2(1)	3(1)
S(6)	19(2)	11(1)	17(2)	2(1)	6(1)	1(1)
S(7)	23(2)	10(1)	10(2)	-1(1)	-3(1)	0(1)
P(1)	20(2)	8(1)	9(2)	2(1)	0(1)	2(1)
P(2)	20(2)	7(1)	6(2)	1(1)	0(1)	2(1)

Table 1. Crystal data and structure refinement for $RbPuP_2S_7$.

Identification code	$RbPuP_2S_7$	
Empirical formula	P2 Pu Rb S7	
Formula weight	613.83	
Temperature	293(2) K	
Wavelength	0.71073 Å	
Crystal system	Monoclinic	
Space group	P21/c	
Unit cell dimensions	a = 9.8011(6) Å	a= 90°.
	b = 12.3977(7) Å	b= 90.5640(10)°.
	c = 9.0263(5) Å	g = 90°.
Volume	1096.74(11) $Å^3$	
Z	4	
Density (calculated)	3.718 Mg/m^3	
Absorption coefficient	11.979 mm^{-1}	
F(000)	1092	
Crystal size	0.22 x 0.11 x 0.10 mm^3	
Theta range for data collection	2.08 to 28.31°.	
Index ranges	-12<=h<=12, -16<=k<=13, -11<=l<=10	
Reflections collected	7470	
Independent reflections	2460 [R(int) = 0.0537]	
Completeness to theta = 28.31°	90.3 %	
Absorption correction	SADABS	
Refinement method	Full-matrix least-squares on F^2	
Data / restraints / parameters	2460 / 0 / 101	
Goodness-of-fit on F^2	0.777	
Final R indices [I>2sigma(I)]	R1 = 0.0510, wR2 = 0.1317	
R indices (all data)	R1 = 0.0663, wR2 = 0.1455	
Extinction coefficient	0.0020(4)	
Largest diff. peak and hole	6.840 and -4.151 $e.Å^{-3}$	

Table 2. Atomic coordinates (x 10^4) and equivalent isotropic displacement parameters ($Å^2$x 10^3) for $RbPuP_2S_7$. U(eq) is defined as one third of the trace of the orthogonalized U^{ij} tensor.

	x	y	z	U(eq)
Pu(1)	3591(1)	6428(1)	1068(1)	11(1)
Rb(1)	-1061(1)	6953(1)	-1327(1)	21(1)
P(1)	-3173(3)	9652(3)	-3011(3)	11(1)
P(2)	-2284(3)	11020(3)	227(3)	10(1)
S(1)	5142(3)	4405(3)	1800(3)	14(1)
S(2)	1680(3)	5262(3)	-738(3)	16(1)
S(3)	6456(3)	6910(3)	1461(3)	14(1)
S(4)	1324(3)	5579(3)	2900(3)	17(1)
S(5)	4120(3)	8318(3)	-736(3)	13(1)
S(6)	1350(3)	7940(3)	1122(3)	15(1)
S(7)	-2544(3)	9478(3)	-761(3)	14(1)

Table 3. Bond lengths [Å] and angles [°] for $RbPuP_2S_7$.

Pu(1)-S(2)	2.862(3)	S(4)-P(2)#13	2.003(4)
Pu(1)-S(6)	2.889(3)	S(4)-Rb(1)#4	3.454(4)
Pu(1)-S(3)	2.890(3)	S(4)-Rb(1)#1	3.917(4)
Pu(1)-S(5)	2.904(3)	S(5)-P(2)#8	2.035(4)
Pu(1)-S(5)#1	2.943(3)	S(5)-Pu(1)#3	2.943(3)
Pu(1)-S(4)	2.975(3)	S(6)-P(2)#8	2.001(4)
Pu(1)-S(1)	3.003(3)	S(6)-Rb(1)#1	3.318(3)
Pu(1)-S(1)#2	3.061(3)	S(2)-Pu(1)-S(6)	81.03(9)
Rb(1)-S(6)#3	3.318(3)	S(2)-Pu(1)-S(3)	143.53(9)
Rb(1)-S(2)#4	3.378(4)	S(6)-Pu(1)-S(3)	126.97(9)
Rb(1)-S(3)#5	3.434(3)	S(2)-Pu(1)-S(5)	101.99(9)
Rb(1)-S(2)	3.445(3)	S(6)-Pu(1)-S(5)	68.00(9)
Rb(1)-S(6)	3.446(3)	S(3)-Pu(1)-S(5)	73.92(9)
Rb(1)-S(4)#4	3.454(4)	S(2)-Pu(1)-S(5)#1	136.07(9)
Rb(1)-S(7)	3.491(3)	S(6)-Pu(1)-S(5)#1	92.31(9)
Rb(1)-S(3)#6	3.518(3)	S(3)-Pu(1)-S(5)#1	72.29(8)
Rb(1)-S(4)#3	3.917(4)	S(5)-Pu(1)-S(5)#1	115.63(6)
Rb(1)-Rb(1)#1	4.7124(8)	S(2)-Pu(1)-S(4)	69.50(8)
Rb(1)-Rb(1)#3	4.7124(8)	S(6)-Pu(1)-S(4)	69.39(9)
P(1)-S(2)#7	2.006(4)	S(3)-Pu(1)-S(4)	137.33(8)
P(1)-S(3)#5	2.026(4)	S(5)-Pu(1)-S(4)	137.35(9)
P(1)-S(1)#5	2.030(4)	S(5)#1-Pu(1)-S(4)	67.56(8)
P(1)-S(7)	2.127(4)	S(2)-Pu(1)-S(1)	91.77(9)
P(2)-S(6)#8	2.001(4)	S(6)-Pu(1)-S(1)	157.18(9)
P(2)-S(4)#9	2.003(4)	S(3)-Pu(1)-S(1)	69.92(8)
P(2)-S(5)#8	2.035(4)	S(5)-Pu(1)-S(1)	134.82(8)
P(2)-S(7)	2.123(4)	S(5)#1-Pu(1)-S(1)	77.86(8)
S(1)-P(1)#10	2.030(4)	S(4)-Pu(1)-S(1)	87.80(9)
S(1)-Pu(1)#2	3.061(3)	S(2)-Pu(1)-S(1)#2	67.49(8)
S(2)-P(1)#11	2.006(4)	S(6)-Pu(1)-S(1)#2	123.24(8)
S(2)-Rb(1)#4	3.378(4)	S(3)-Pu(1)-S(1)#2	76.80(8)
S(3)-P(1)#10	2.026(4)	S(5)-Pu(1)-S(1)#2	73.85(9)
S(3)-Rb(1)#10	3.434(3)	S(5)#1-Pu(1)-S(1)#2	142.74(8)
S(3)-Rb(1)#12	3.518(3)	S(4)-Pu(1)-S(1)#2	131.48(9)

S(1)-Pu(1)-S(1)#2	72.30(9)	S(3)#6-Rb(1)-S(4)#3	123.88(8)
S(6)#3-Rb(1)-S(2)#4	123.24(9)	S(6)#3-Rb(1)-Rb(1)#1	131.27(6)
S(6)#3-Rb(1)-S(3)#5	94.92(8)	S(2)#4-Rb(1)-Rb(1)#1	72.77(6)
S(2)#4-Rb(1)-S(3)#5	121.64(8)	S(3)#5-Rb(1)-Rb(1)#1	115.60(6)
S(6)#3-Rb(1)-S(2)	64.63(8)	S(2)-Rb(1)-Rb(1)#1	91.98(6)
S(2)#4-Rb(1)-S(2)	64.14(9)	S(6)-Rb(1)-Rb(1)#1	44.74(5)
S(3)#5-Rb(1)-S(2)	152.42(8)	S(4)#4-Rb(1)-Rb(1)#1	130.87(7)
S(6)#3-Rb(1)-S(6)	86.69(8)	S(7)-Rb(1)-Rb(1)#1	66.29(6)
S(2)#4-Rb(1)-S(6)	93.46(8)	S(3)#6-Rb(1)-Rb(1)#1	46.58(5)
S(3)#5-Rb(1)-S(6)	134.82(9)	S(4)#3-Rb(1)-Rb(1)#1	87.22(6)
S(2)-Rb(1)-S(6)	65.67(8)	S(6)#3-Rb(1)-Rb(1)#3	46.96(6)
S(6)#3-Rb(1)-S(4)#4	78.57(8)	S(2)#4-Rb(1)-Rb(1)#3	139.84(7)
S(2)#4-Rb(1)-S(4)#4	58.30(8)	S(3)#5-Rb(1)-Rb(1)#3	48.08(6)
S(3)#5-Rb(1)-S(4)#4	94.85(8)	S(2)-Rb(1)-Rb(1)#3	108.40(6)
S(2)-Rb(1)-S(4)#4	64.22(8)	S(6)-Rb(1)-Rb(1)#3	120.39(6)
S(6)-Rb(1)-S(4)#4	129.38(9)	S(4)#4-Rb(1)-Rb(1)#3	82.46(6)
S(6)#3-Rb(1)-S(7)	111.48(8)	S(7)-Rb(1)-Rb(1)#3	83.46(6)
S(2)#4-Rb(1)-S(7)	124.83(8)	S(3)#6-Rb(1)-Rb(1)#3	134.11(6)
S(3)#5-Rb(1)-S(7)	54.81(7)	S(4)#3-Rb(1)-Rb(1)#3	66.36(5)
S(2)-Rb(1)-S(7)	148.01(8)	Rb(1)#1-Rb(1)-Rb(1)#3	146.56(6)
S(6)-Rb(1)-S(7)	82.61(8)	S(2)#7-P(1)-S(3)#5	110.97(19)
S(4)#4-Rb(1)-S(7)	147.76(8)	S(2)#7-P(1)-S(1)#5	109.43(19)
S(6)#3-Rb(1)-S(3)#6	177.78(9)	S(3)#5-P(1)-S(1)#5	112.79(19)
S(2)#4-Rb(1)-S(3)#6	57.57(7)	S(2)#7-P(1)-S(7)	111.67(19)
S(3)#5-Rb(1)-S(3)#6	86.05(8)	S(3)#5-P(1)-S(7)	100.25(17)
S(2)-Rb(1)-S(3)#6	115.09(8)	S(1)#5-P(1)-S(7)	111.51(18)
S(6)-Rb(1)-S(3)#6	91.21(8)	S(6)#8-P(2)-S(4)#9	118.4(2)
S(4)#4-Rb(1)-S(3)#6	103.35(8)	S(6)#8-P(2)-S(5)#8	106.74(19)
S(7)-Rb(1)-S(3)#6	67.48(8)	S(4)#9-P(2)-S(5)#8	109.17(18)
S(6)#3-Rb(1)-S(4)#3	54.19(7)	S(6)#8-P(2)-S(7)	112.20(18)
S(2)#4-Rb(1)-S(4)#3	147.57(8)	S(4)#9-P(2)-S(7)	99.38(18)
S(3)#5-Rb(1)-S(4)#3	89.81(8)	S(5)#8-P(2)-S(7)	110.80(19)
S(2)-Rb(1)-S(4)#3	92.11(8)	P(1)#10-S(1)-Pu(1)	86.95(14)
S(6)-Rb(1)-S(4)#3	55.25(7)	P(1)#10-S(1)-Pu(1)#2	85.92(13)
S(4)#4-Rb(1)-S(4)#3	132.76(4)	Pu(1)-S(1)-Pu(1)#2	107.70(9)
S(7)-Rb(1)-S(4)#3	64.89(7)	P(1)#11-S(2)-Pu(1)	91.95(14)

P(1)#11-S(2)-Rb(1)#4	98.04(15)
Pu(1)-S(2)-Rb(1)#4	102.49(9)
P(1)#11-S(2)-Rb(1)	135.63(16)
Pu(1)-S(2)-Rb(1)	106.61(10)
Rb(1)#4-S(2)-Rb(1)	115.86(9)
P(1)#10-S(3)-Pu(1)	90.15(14)
P(1)#10-S(3)-Rb(1)#10	97.53(13)
Pu(1)-S(3)-Rb(1)#10	146.97(11)
P(1)#10-S(3)-Rb(1)#12	93.41(14)
Pu(1)-S(3)-Rb(1)#12	126.40(10)
Rb(1)#10-S(3)-Rb(1)#12	85.34(7)
P(2)#13-S(4)-Pu(1)	91.48(14)
P(2)#13-S(4)-Rb(1)#4	128.84(17)
Pu(1)-S(4)-Rb(1)#4	98.40(9)
P(2)#13-S(4)-Rb(1)#1	85.00(14)
Pu(1)-S(4)-Rb(1)#1	105.86(9)
Rb(1)#4-S(4)-Rb(1)#1	137.81(9)
P(2)#8-S(5)-Pu(1)	92.05(14)
P(2)#8-S(5)-Pu(1)#3	91.75(13)
Pu(1)-S(5)-Pu(1)#3	127.26(11)
P(2)#8-S(6)-Pu(1)	93.20(14)
P(2)#8-S(6)-Rb(1)#1	136.85(16)
Pu(1)-S(6)-Rb(1)#1	125.77(11)
P(2)#8-S(6)-Rb(1)	98.80(14)
Pu(1)-S(6)-Rb(1)	105.97(10)
Rb(1)#1-S(6)-Rb(1)	88.31(8)
P(2)-S(7)-P(1)	110.04(18)
P(2)-S(7)-Rb(1)	145.10(15)
P(1)-S(7)-Rb(1)	93.90(13)

Symmetry transformations used to generate equivalent atoms:

#1 x,-y+3/2,z+1/2 #2 -x+1,-y+1,-z #3 x,-y+3/2,z-1/2

#4 -x,-y+1,-z #5 x-1,-y+3/2,z-1/2 #6 x-1,y,z

#7 -x,y+1/2,-z-1/2 #8 -x,-y+2,-z #9 -x,y+1/2,-z+1/2

#10 x+1,-y+3/2,z+1/2 #11 -x,y-1/2,-z-1/2 #12 x+1,y,z

#13 -x,y-1/2,-z+1/2

Table 4. Anisotropic displacement parameters ($Å^2 x\ 10^3$) for $RbPuP_2S_7$. The anisotropic displacement factor exponent takes the form: $-2p^2[\ h^2\ a^{*2}U^{11} + ... + 2\ h\ k\ a^*\ b^*\ U^{12}\ ]$

	U^{11}	U^{22}	U^{33}	U^{23}	U^{13}	U^{12}
Pu(1)	11(1)	13(1)	8(1)	1(1)	-1(1)	1(1)
Rb(1)	22(1)	23(1)	19(1)	2(1)	2(1)	4(1)
P(1)	14(1)	13(2)	7(1)	-1(1)	-2(1)	0(1)
P(2)	12(1)	11(2)	8(1)	0(1)	0(1)	2(1)
S(1)	14(1)	15(2)	12(1)	-2(1)	0(1)	-1(1)
S(2)	13(1)	23(2)	11(1)	-1(1)	-1(1)	2(1)
S(3)	16(2)	13(2)	14(1)	3(1)	-2(1)	-1(1)
S(4)	22(2)	20(2)	11(1)	1(1)	-4(1)	-6(1)
S(5)	13(1)	16(2)	11(1)	1(1)	0(1)	3(1)
S(6)	15(1)	16(2)	15(1)	0(1)	5(1)	1(1)
S(7)	20(2)	14(2)	7(1)	0(1)	-5(1)	0(1)

Table 1. Crystal data and structure refinement for $CsPuP_2S_7$.

Identification code	$CsPuP_2S_7$	
Empirical formula	Cs P2 Pu S7	
Formula weight	661.27	
Temperature	293(2) K	
Wavelength	0.71073 Å	
Crystal system	Monoclinic	
Space group	P21/c	
Unit cell dimensions	a = 10.1034(7) Å	a= 90°.
	b = 12.5412(9) Å	b= 91.0070(10)°.
	c = 9.0306(6) Å	g = 90°.
Volume	1144.08(14) $Å^3$	
Z	4	
Density (calculated)	3.839 Mg/m^3	
Absorption coefficient	10.392 mm^{-1}	
F(000)	1164	
Crystal size	0.20 x 0.17 x 0.17 mm^3	
Theta range for data collection	2.02 to 28.26°.	
Index ranges	-13<=h<=13, 0<=k<=16, 0<=l<=9	
Reflections collected	2275	
Independent reflections	2275 [R(int) = 0.0000]	
Completeness to theta = 28.26°	80.2 %	
Absorption correction	SADABS,	
Refinement method	Full-matrix least-squares on F^2	
Data / restraints / parameters	2275 / 0 / 100	
Goodness-of-fit on F^2	0.920	
Final R indices [I>2sigma(I)]	R1 = 0.0486, wR2 = 0.1125	
R indices (all data)	R1 = 0.0693, wR2 = 0.1221	
Largest diff. peak and hole	2.186 and -2.086 $e.Å^{-3}$	

Table 2. Atomic coordinates (x 10^4) and equivalent isotropic displacement parameters ($Å^2$x 10^3) for $CsPuP_2S_7$. U(eq) is defined as one third of the trace of the orthogonalized U^{ij} tensor.

	x	y	z	U(eq)
Pu(1)	3642(1)	6427(1)	1048(1)	13(1)
Cs(1)	-1022(1)	6977(1)	-1339(1)	22(1)
P(1)	-2387(3)	11043(3)	243(4)	14(1)
P(2)	-3235(3)	9675(3)	-2989(4)	13(1)
S(1)	1502(3)	7941(3)	1132(4)	16(1)
S(2)	1427(3)	5624(3)	2886(4)	18(1)
S(3)	5124(3)	4404(3)	1801(4)	16(1)
S(4)	-2629(3)	9509(2)	-735(4)	15(1)
S(5)	4164(3)	8307(3)	-750(4)	16(1)
S(6)	6422(3)	6873(3)	1467(4)	17(1)
S(7)	1783(3)	5291(3)	-779(4)	17(1)

Table 3. Bond lengths [Å] and angles [°] for $CsPuP_2S_7$.

Pu(1)-S(7)	2.858(3)	S(5)-P(1)#7	2.032(5)
Pu(1)-S(1)	2.879(3)	S(5)-Pu(1)#3	2.949(4)
Pu(1)-S(6)	2.883(3)	S(6)-P(2)#11	2.030(5)
Pu(1)-S(5)	2.917(3)	S(6)-Cs(1)#11	3.535(3)
Pu(1)-S(5)#1	2.949(4)	S(6)-Cs(1)#12	3.652(4)
Pu(1)-S(2)	2.984(4)	S(7)-P(2)#13	2.011(5)
Pu(1)-S(3)	3.017(3)	S(7)-Cs(1)#4	3.520(4)
Pu(1)-S(3)#2	3.062(4)	S(7)-Pu(1)-S(1)	81.86(10)
Cs(1)-S(1)#3	3.454(4)	S(7)-Pu(1)-S(6)	143.24(10)
Cs(1)-S(7)#4	3.520(4)	S(1)-Pu(1)-S(6)	126.79(10)
Cs(1)-S(6)#5	3.535(3)	S(7)-Pu(1)-S(5)	101.84(10)
Cs(1)-S(7)	3.565(3)	S(1)-Pu(1)-S(5)	67.96(10)
Cs(1)-S(2)#4	3.569(4)	S(6)-Pu(1)-S(5)	74.38(9)
Cs(1)-S(1)	3.570(4)	S(7)-Pu(1)-S(5)#1	136.63(10)
Cs(1)-S(4)	3.612(3)	S(1)-Pu(1)-S(5)#1	91.21(10)
Cs(1)-S(6)#6	3.652(4)	S(6)-Pu(1)-S(5)#1	72.07(10)
Cs(1)-S(2)#3	3.965(4)	S(5)-Pu(1)-S(5)#1	115.05(6)
Cs(1)-Cs(1)#1	4.7018(6)	S(7)-Pu(1)-S(2)	70.21(10)
Cs(1)-Cs(1)#3	4.7018(6)	S(1)-Pu(1)-S(2)	68.74(10)
P(1)-S(1)#7	2.001(5)	S(6)-Pu(1)-S(2)	136.97(10)
P(1)-S(2)#8	2.004(5)	S(5)-Pu(1)-S(2)	136.66(9)
P(1)-S(5)#7	2.032(5)	S(5)#1-Pu(1)-S(2)	67.42(9)
P(1)-S(4)	2.128(5)	S(7)-Pu(1)-S(3)	91.68(9)
P(2)-S(7)#9	2.011(5)	S(1)-Pu(1)-S(3)	156.70(10)
P(2)-S(3)#5	2.027(4)	S(6)-Pu(1)-S(3)	69.81(9)
P(2)-S(6)#5	2.030(5)	S(5)-Pu(1)-S(3)	135.33(9)
P(2)-S(4)	2.126(5)	S(5)#1-Pu(1)-S(3)	78.14(9)
S(1)-P(1)#7	2.001(5)	S(2)-Pu(1)-S(3)	88.00(10)
S(1)-Cs(1)#1	3.454(4)	S(7)-Pu(1)-S(3)#2	67.56(9)
S(2)-P(1)#10	2.004(5)	S(1)-Pu(1)-S(3)#2	124.33(10)
S(2)-Cs(1)#4	3.569(4)	S(6)-Pu(1)-S(3)#2	76.46(9)
S(2)-Cs(1)#1	3.965(4)	S(5)-Pu(1)-S(3)#2	74.16(9)
S(3)-P(2)#11	2.027(4)	S(5)#1-Pu(1)-S(3)#2	142.54(9)
S(3)-Pu(1)#2	3.062(4)	S(2)-Pu(1)-S(3)#2	132.29(9)

S(3)-Pu(1)-S(3)#2	72.25(11)	S(6)#6-Cs(1)-S(2)#3	126.92(8)
S(1)#3-Cs(1)-S(7)#4	123.65(8)	S(1)#3-Cs(1)-Cs(1)#1	129.72(6)
S(1)#3-Cs(1)-S(6)#5	99.09(9)	S(7)#4-Cs(1)-Cs(1)#1	72.53(6)
S(7)#4-Cs(1)-S(6)#5	118.02(8)	S(6)#5-Cs(1)-Cs(1)#1	114.34(6)
S(1)#3-Cs(1)-S(7)	61.12(8)	S(7)-Cs(1)-Cs(1)#1	92.45(6)
S(7)#4-Cs(1)-S(7)	67.94(9)	S(2)#4-Cs(1)-Cs(1)#1	128.95(6)
S(6)#5-Cs(1)-S(7)	153.21(9)	S(1)-Cs(1)-Cs(1)#1	46.94(6)
S(1)#3-Cs(1)-S(2)#4	81.33(8)	S(4)-Cs(1)-Cs(1)#1	66.56(6)
S(7)#4-Cs(1)-S(2)#4	56.61(8)	S(6)#6-Cs(1)-Cs(1)#1	48.07(5)
S(6)#5-Cs(1)-S(2)#4	94.36(8)	S(2)#3-Cs(1)-Cs(1)#1	88.19(6)
S(7)-Cs(1)-S(2)#4	66.34(8)	S(1)#3-Cs(1)-Cs(1)#3	49.04(6)
S(1)#3-Cs(1)-S(1)	82.86(7)	S(7)#4-Cs(1)-Cs(1)#3	138.67(6)
S(7)#4-Cs(1)-S(1)	95.42(8)	S(6)#5-Cs(1)-Cs(1)#3	50.23(6)
S(6)#5-Cs(1)-S(1)	135.97(8)	S(7)-Cs(1)-Cs(1)#3	106.75(6)
S(7)-Cs(1)-S(1)	63.57(8)	S(2)#4-Cs(1)-Cs(1)#3	83.17(6)
S(2)#4-Cs(1)-S(1)	129.04(8)	S(1)-Cs(1)-Cs(1)#3	119.59(6)
S(1)#3-Cs(1)-S(4)	114.38(8)	S(4)-Cs(1)-Cs(1)#3	84.69(6)
S(7)#4-Cs(1)-S(4)	121.67(8)	S(6)#6-Cs(1)-Cs(1)#3	133.49(5)
S(6)#5-Cs(1)-S(4)	53.14(8)	S(2)#3-Cs(1)-Cs(1)#3	66.94(5)
S(7)-Cs(1)-S(4)	149.13(8)	Cs(1)#1-Cs(1)-Cs(1)#3	147.61(4)
S(2)#4-Cs(1)-S(4)	144.47(8)	S(1)#7-P(1)-S(2)#8	118.4(2)
S(1)-Cs(1)-S(4)	85.75(7)	S(1)#7-P(1)-S(5)#7	106.9(2)
S(1)#3-Cs(1)-S(6)#6	177.40(8)	S(2)#8-P(1)-S(5)#7	109.4(2)
S(7)#4-Cs(1)-S(6)#6	55.25(8)	S(1)#7-P(1)-S(4)	111.5(2)
S(6)#5-Cs(1)-S(6)#6	83.40(8)	S(2)#8-P(1)-S(4)	99.40(19)
S(7)-Cs(1)-S(6)#6	116.77(8)	S(5)#7-P(1)-S(4)	111.2(2)
S(2)#4-Cs(1)-S(6)#6	99.27(8)	S(7)#9-P(2)-S(3)#5	109.4(2)
S(1)-Cs(1)-S(6)#6	94.84(8)	S(7)#9-P(2)-S(6)#5	110.9(2)
S(4)-Cs(1)-S(6)#6	66.52(8)	S(3)#5-P(2)-S(6)#5	112.7(2)
S(1)#3-Cs(1)-S(2)#3	52.46(8)	S(7)#9-P(2)-S(4)	111.49(19)
S(7)#4-Cs(1)-S(2)#3	148.42(8)	S(3)#5-P(2)-S(4)	111.5(2)
S(6)#5-Cs(1)-S(2)#3	92.49(7)	S(6)#5-P(2)-S(4)	100.58(19)
S(7)-Cs(1)-S(2)#3	88.76(7)	P(1)#7-S(1)-Pu(1)	93.44(16)
S(2)#4-Cs(1)-S(2)#3	133.79(4)	P(1)#7-S(1)-Cs(1)#1	137.26(17)
S(1)-Cs(1)-S(2)#3	54.01(7)	Pu(1)-S(1)-Cs(1)#1	126.89(11)
S(4)-Cs(1)-S(2)#3	69.09(7)	P(1)#7-S(1)-Cs(1)	98.61(16)

Pu(1)-S(1)-Cs(1)	106.76(10)
Cs(1)#1-S(1)-Cs(1)	84.01(8)
P(1)#10-S(2)-Pu(1)	91.37(15)
P(1)#10-S(2)-Cs(1)#4	128.32(17)
Pu(1)-S(2)-Cs(1)#4	99.95(10)
P(1)#10-S(2)-Cs(1)#1	86.94(15)
Pu(1)-S(2)-Cs(1)#1	108.56(10)
Cs(1)#4-S(2)-Cs(1)#1	134.02(9)
P(2)#11-S(3)-Pu(1)	86.79(14)
P(2)#11-S(3)-Pu(1)#2	85.87(15)
Pu(1)-S(3)-Pu(1)#2	107.75(11)
P(2)-S(4)-P(1)	109.77(19)
P(2)-S(4)-Cs(1)	93.66(14)
P(1)-S(4)-Cs(1)	143.94(16)
P(1)#7-S(5)-Pu(1)	91.69(15)
P(1)#7-S(5)-Pu(1)#3	91.84(15)
Pu(1)-S(5)-Pu(1)#3	127.32(12)
P(2)#11-S(6)-Pu(1)	90.46(15)
P(2)#11-S(6)-Cs(1)#11	97.73(14)
Pu(1)-S(6)-Cs(1)#11	148.57(13)
P(2)#11-S(6)-Cs(1)#12	94.74(15)
Pu(1)-S(6)-Cs(1)#12	127.98(11)
Cs(1)#11-S(6)-Cs(1)#12	81.70(7)
P(2)#13-S(7)-Pu(1)	91.87(15)
P(2)#13-S(7)-Cs(1)#4	99.13(15)
Pu(1)-S(7)-Cs(1)#4	103.69(10)
P(2)#13-S(7)-Cs(1)	137.33(17)
Pu(1)-S(7)-Cs(1)	107.37(10)
Cs(1)#4-S(7)-Cs(1)	112.06(9)

Symmetry transformations used to generate equivalent atoms:

#1 x,-y+3/2,z+1/2 #2 -x+1,-y+1,-z #3 x,-y+3/2,z-1/2

#4 -x,-y+1,-z #5 x-1,-y+3/2,z-1/2 #6 x-1,y,z

#7 -x,-y+2,-z #8 -x,y+1/2,-z+1/2 #9 -x,y+1/2,-z-1/2

#10 -x,y-1/2,-z+1/2 #11 x+1,-y+3/2,z+1/2 #12 x+1,y,z

#13 -x,y-1/2,-z-1/2

Table 4. Anisotropic displacement parameters ($Å^2 x\ 10^3$) for $CsPuP_2S_7$. The anisotropic displacement factor exponent takes the form: $-2p^2[\ h^2\ a^{*2}U^{11} + ...\ + 2\ h\ k\ a^*\ b^*\ U^{12}\ ]$

	U^{11}	U^{22}	U^{33}	U^{23}	U^{13}	U^{12}
Pu(1)	13(1)	13(1)	12(1)	0(1)	0(1)	1(1)
Cs(1)	21(1)	22(1)	23(1)	2(1)	2(1)	3(1)
P(1)	18(2)	9(2)	14(2)	0(1)	-1(1)	1(1)
P(2)	14(2)	13(2)	11(2)	-1(1)	0(1)	2(1)
S(1)	19(2)	16(2)	15(2)	3(1)	4(1)	4(1)
S(2)	19(2)	21(2)	14(2)	0(1)	-3(1)	-4(1)
S(3)	16(2)	14(2)	18(2)	-2(1)	-2(1)	-3(1)
S(4)	23(2)	11(1)	11(2)	0(1)	-3(1)	1(1)
S(5)	16(2)	18(2)	15(2)	1(1)	1(1)	2(1)
S(6)	17(2)	14(2)	19(2)	2(1)	0(1)	2(1)
S(7)	16(2)	19(2)	16(2)	0(1)	0(1)	0(1)

Table 1. Crystal data and structure refinement for $Rb_4Pu_2P_4S_{14}$.

Identification code	$Rb_4Pu_2P_4S_{14}$	
Empirical formula	P4 Pu2 Rb4 S14	
Formula weight	1398.60	
Temperature	293(2) K	
Wavelength	0.71073 Å	
Crystal system	Monoclinic	
Space group	C2/c	
Unit cell dimensions	a = 22.9433(15) Å	a= 90°.
	b = 6.8198(3) Å	b= 122.0050(10)°.
	c = 18.8266(10) Å	g = 90°.
Volume	2498.0(2) $Å^3$	
Z	4	
Density (calculated)	3.719 Mg/m^3	
Absorption coefficient	14.393 mm^{-1}	
F(000)	2480	
Crystal size	0.25 x 0.12 x 0.10 mm^3	
Theta range for data collection	2.09 to 28.35°.	
Index ranges	-30<=h<=30, -7<=k<=7, -24<=l<=24	
Reflections collected	7747	
Independent reflections	2567 [R(int) = 0.0254]	
Completeness to theta = 28.35°	82.4 %	
Absorption correction	SADABS	
Refinement method	Full-matrix least-squares on F^2	
Data / restraints / parameters	2567 / 0 / 110	
Goodness-of-fit on F^2	1.146	
Final R indices [I>2sigma(I)]	R1 = 0.0453, wR2 = 0.1164	
R indices (all data)	R1 = 0.0501, wR2 = 0.1198	
Extinction coefficient	0.00055(6)	
Largest diff. peak and hole	7.068 and -4.757 $e.Å^{-3}$	

Table 2. Atomic coordinates (x 10^4) and equivalent isotropic displacement parameters ($Å^2$x 10^3) for $Rb_4Pu_2P_4S_{14}$. U(eq) is defined as one third of the trace of the orthogonalized U^{ij} tensor.

	x	y	z	U(eq)
Pu(1)	1511(1)	5308(1)	2313(1)	11(1)
Rb(1)	1976(1)	4971(2)	275(1)	24(1)
Rb(2)	-158(1)	10141(2)	1132(1)	21(1)
S(1)	2209(1)	9352(4)	2630(1)	15(1)
S(2)	1004(1)	7607(4)	3157(1)	16(1)
S(3)	2651(1)	5039(4)	4008(2)	17(1)
S(4)	1007(1)	2779(4)	3137(1)	15(1)
S(5)	1013(1)	7597(4)	817(1)	15(1)
S(6)	1081(1)	2378(4)	1020(1)	16(1)
S(7)	-146(1)	5176(4)	1082(2)	16(1)
P(1)	1659(1)	-92(3)	1366(1)	11(1)
P(2)	474(1)	4828(3)	-1878(2)	12(1)

Table 3. Bond lengths [Å] and angles [°] for $Rb_4Pu_2P_4S_{14}$.

Pu(1)-S(3)	2.865(3)	S(1)-Pu(1)#4	2.955(2)
Pu(1)-S(5)	2.875(2)	S(1)-Rb(2)#4	3.379(2)
Pu(1)-S(2)	2.881(2)	S(2)-P(2)#10	2.038(3)
Pu(1)-S(6)	2.889(2)	S(2)-Rb(3)#7	3.360(2)
Pu(1)-S(4)	2.936(2)	S(2)-Rb(2)#10	3.812(3)
Pu(1)-S(1)#1	2.955(2)	S(3)-P(1)#4	2.048(3)
Pu(1)-S(1)	3.085(2)	S(3)-Rb(2)#10	3.463(2)
Pu(1)-S(7)	3.240(3)	S(3)-Rb(2)#4	3.556(3)
Pu(1)-Rb(2)	4.5018(10)	S(3)-Rb(2)#1	3.644(3)
Pu(1)-Rb(3)	4.6316(10)	S(4)-P(2)#10	2.031(3)
Rb(2)-S(1)#1	3.379(2)	S(4)-Rb(3)#11	3.430(2)
Rb(2)-S(5)	3.395(2)	S(4)-Rb(3)#12	3.734(3)
Rb(2)-S(3)#2	3.463(2)	S(4)-Rb(2)#10	3.743(3)
Rb(2)-S(6)	3.519(2)	S(5)-P(1)#6	2.031(3)
Rb(2)-S(3)#1	3.556(3)	S(5)-Rb(3)#9	3.473(2)
Rb(2)-S(7)#3	3.577(3)	S(6)-P(1)	2.026(3)
Rb(2)-S(3)#4	3.644(3)	S(6)-Rb(3)#12	3.329(2)
Rb(2)-P(2)	3.676(3)	S(6)-Rb(3)#3	3.842(3)
Rb(2)-S(4)#2	3.743(3)	S(7)-P(2)#3	2.002(3)
Rb(2)-S(2)#2	3.812(3)	S(7)-Rb(3)#12	3.435(3)
Rb(2)-Rb(2)#5	4.564(2)	S(7)-Rb(2)#3	3.577(3)
Rb(3)-S(6)#6	3.329(2)	P(1)-S(5)#12	2.031(3)
Rb(3)-S(2)#7	3.360(2)	P(1)-S(3)#1	2.048(3)
Rb(3)-S(7)	3.388(3)	P(1)-S(1)#12	2.053(3)
Rb(3)-S(4)#8	3.430(2)	P(1)-Rb(3)#12	3.957(2)
Rb(3)-S(7)#6	3.435(3)	P(2)-S(7)#3	2.002(3)
Rb(3)-S(5)#9	3.473(2)	P(2)-S(4)#2	2.031(3)
Rb(3)-S(5)	3.503(2)	P(2)-S(2)#2	2.038(3)
Rb(3)-S(2)	3.723(3)	P(2)-P(2)#13	2.194(5)
Rb(3)-S(4)#6	3.734(3)	P(2)-Rb(3)#3	3.881(3)
Rb(3)-S(6)#3	3.842(3)	P(2)-Rb(3)#9	3.918(3)
Rb(3)-P(2)#3	3.881(3)	S(3)-Pu(1)-S(5)	141.26(7)
Rb(3)-P(2)#9	3.918(3)	S(3)-Pu(1)-S(2)	79.49(6)
S(1)-P(1)#6	2.053(3)	S(5)-Pu(1)-S(2)	100.25(7)

S(3)-Pu(1)-S(6)	126.64(7)	S(6)-Pu(1)-Rb(3)	105.14(5)
S(5)-Pu(1)-S(6)	76.66(7)	S(4)-Pu(1)-Rb(3)	102.41(4)
S(2)-Pu(1)-S(6)	141.59(6)	S(1)#1-Pu(1)-Rb(3)	136.67(5)
S(3)-Pu(1)-S(4)	75.91(6)	S(1)-Pu(1)-Rb(3)	70.65(4)
S(5)-Pu(1)-S(4)	140.67(6)	S(7)-Pu(1)-Rb(3)	46.99(5)
S(2)-Pu(1)-S(4)	68.96(7)	Rb(2)-Pu(1)-Rb(3)	97.835(19)
S(6)-Pu(1)-S(4)	89.11(6)	S(1)#1-Rb(2)-S(5)	76.13(6)
S(3)-Pu(1)-S(1)#1	69.05(6)	S(1)#1-Rb(2)-S(3)#2	129.13(6)
S(5)-Pu(1)-S(1)#1	91.51(6)	S(5)-Rb(2)-S(3)#2	143.87(7)
S(2)-Pu(1)-S(1)#1	141.68(6)	S(1)#1-Rb(2)-S(6)	63.28(6)
S(6)-Pu(1)-S(1)#1	76.55(6)	S(5)-Rb(2)-S(6)	62.23(6)
S(4)-Pu(1)-S(1)#1	120.91(6)	S(3)#2-Rb(2)-S(6)	147.40(7)
S(3)-Pu(1)-S(1)	76.60(7)	S(1)#1-Rb(2)-S(3)#1	64.26(6)
S(5)-Pu(1)-S(1)	66.40(6)	S(5)-Rb(2)-S(3)#1	116.67(6)
S(2)-Pu(1)-S(1)	74.13(6)	S(3)#2-Rb(2)-S(3)#1	98.88(6)
S(6)-Pu(1)-S(1)	133.79(6)	S(6)-Rb(2)-S(3)#1	56.43(5)
S(4)-Pu(1)-S(1)	137.10(6)	S(1)#1-Rb(2)-S(7)#3	122.95(6)
S(1)#1-Pu(1)-S(1)	77.65(4)	S(5)-Rb(2)-S(7)#3	61.61(5)
S(3)-Pu(1)-S(7)	145.85(6)	S(3)#2-Rb(2)-S(7)#3	106.98(6)
S(5)-Pu(1)-S(7)	66.90(6)	S(6)-Rb(2)-S(7)#3	63.76(5)
S(2)-Pu(1)-S(7)	75.28(6)	S(3)#1-Rb(2)-S(7)#3	101.53(6)
S(6)-Pu(1)-S(7)	68.30(6)	S(1)#1-Rb(2)-S(3)#4	79.03(6)
S(4)-Pu(1)-S(7)	73.77(6)	S(5)-Rb(2)-S(3)#4	56.67(5)
S(1)#1-Pu(1)-S(7)	141.89(6)	S(3)#2-Rb(2)-S(3)#4	98.86(6)
S(1)-Pu(1)-S(7)	117.07(6)	S(6)-Rb(2)-S(3)#4	113.64(6)
S(3)-Pu(1)-Rb(2)	117.21(5)	S(3)#1-Rb(2)-S(3)#4	142.61(8)
S(5)-Pu(1)-Rb(2)	48.94(5)	S(7)#3-Rb(2)-S(3)#4	104.32(6)
S(2)-Pu(1)-Rb(2)	147.75(5)	S(1)#1-Rb(2)-P(2)	154.07(6)
S(6)-Pu(1)-Rb(2)	51.39(5)	S(5)-Rb(2)-P(2)	88.06(6)
S(4)-Pu(1)-Rb(2)	139.31(5)	S(3)#2-Rb(2)-P(2)	74.97(6)
S(1)#1-Pu(1)-Rb(2)	48.64(4)	S(6)-Rb(2)-P(2)	91.25(6)
S(1)-Pu(1)-Rb(2)	82.94(4)	S(3)#1-Rb(2)-P(2)	106.86(6)
S(7)-Pu(1)-Rb(2)	96.15(4)	S(7)#3-Rb(2)-P(2)	32.01(5)
S(3)-Pu(1)-Rb(3)	127.93(5)	S(3)#4-Rb(2)-P(2)	109.43(6)
S(5)-Pu(1)-Rb(3)	49.08(5)	S(1)#1-Rb(2)-S(4)#2	162.21(7)
S(2)-Pu(1)-Rb(3)	53.45(5)	S(5)-Rb(2)-S(4)#2	89.80(6)

S(3)#2-Rb(2)-S(4)#2	59.20(5)	S(6)#6-Rb(3)-S(2)#7	162.38(7)
S(6)-Rb(2)-S(4)#2	119.68(6)	S(6)#6-Rb(3)-S(7)	115.87(6)
S(3)#1-Rb(2)-S(4)#2	133.04(6)	S(2)#7-Rb(3)-S(7)	60.80(6)
S(7)#3-Rb(2)-S(4)#2	55.96(5)	S(6)#6-Rb(3)-S(4)#8	118.05(6)
S(3)#4-Rb(2)-S(4)#2	84.17(6)	S(2)#7-Rb(3)-S(4)#8	62.59(6)
P(2)-Rb(2)-S(4)#2	31.76(5)	S(7)-Rb(3)-S(4)#8	123.38(6)
S(1)#1-Rb(2)-S(2)#2	144.92(6)	S(6)#6-Rb(3)-S(7)#6	61.36(6)
S(5)-Rb(2)-S(2)#2	116.37(6)	S(2)#7-Rb(3)-S(7)#6	122.66(6)
S(3)#2-Rb(2)-S(2)#2	60.44(5)	S(7)-Rb(3)-S(7)#6	176.25(8)
S(6)-Rb(2)-S(2)#2	92.49(6)	S(4)#8-Rb(3)-S(7)#6	60.09(6)
S(3)#1-Rb(2)-S(2)#2	81.41(6)	S(6)#6-Rb(3)-S(5)#9	75.69(6)
S(7)#3-Rb(2)-S(2)#2	54.93(5)	S(2)#7-Rb(3)-S(5)#9	121.82(6)
S(3)#4-Rb(2)-S(2)#2	135.83(6)	S(7)-Rb(3)-S(5)#9	115.01(6)
P(2)-Rb(2)-S(2)#2	31.52(5)	S(4)#8-Rb(3)-S(5)#9	93.91(6)
S(4)#2-Rb(2)-S(2)#2	51.68(6)	S(7)#6-Rb(3)-S(5)#9	62.31(6)
S(1)#1-Rb(2)-Pu(1)	41.03(4)	S(6)#6-Rb(3)-S(5)	57.25(6)
S(5)-Rb(2)-Pu(1)	39.68(4)	S(2)#7-Rb(3)-S(5)	117.98(6)
S(3)#2-Rb(2)-Pu(1)	169.00(5)	S(7)-Rb(3)-S(5)	58.80(6)
S(6)-Rb(2)-Pu(1)	39.90(4)	S(4)#8-Rb(3)-S(5)	167.76(6)
S(3)#1-Rb(2)-Pu(1)	80.95(4)	S(7)#6-Rb(3)-S(5)	118.18(6)
S(7)#3-Rb(2)-Pu(1)	83.74(4)	S(5)#9-Rb(3)-S(5)	95.49(6)
S(3)#4-Rb(2)-Pu(1)	75.57(4)	S(6)#6-Rb(3)-S(2)	96.05(6)
P(2)-Rb(2)-Pu(1)	115.71(4)	S(2)#7-Rb(3)-S(2)	66.70(6)
S(4)#2-Rb(2)-Pu(1)	128.42(4)	S(7)-Rb(3)-S(2)	63.43(6)
S(2)#2-Rb(2)-Pu(1)	130.02(4)	S(4)#8-Rb(3)-S(2)	94.76(6)
S(1)#1-Rb(2)-Rb(2)#5	98.08(5)	S(7)#6-Rb(3)-S(2)	118.70(6)
S(5)-Rb(2)-Rb(2)#5	164.24(6)	S(5)#9-Rb(3)-S(2)	170.15(5)
S(3)#2-Rb(2)-Rb(2)#5	50.32(5)	S(5)-Rb(3)-S(2)	75.30(5)
S(6)-Rb(2)-Rb(2)#5	102.03(5)	S(6)#6-Rb(3)-S(4)#6	70.44(5)
S(3)#1-Rb(2)-Rb(2)#5	48.55(4)	S(2)#7-Rb(3)-S(4)#6	95.75(6)
S(7)#3-Rb(2)-Rb(2)#5	112.17(5)	S(7)-Rb(3)-S(4)#6	119.85(6)
S(3)#4-Rb(2)-Rb(2)#5	137.38(5)	S(4)#8-Rb(3)-S(4)#6	66.18(6)
P(2)-Rb(2)-Rb(2)#5	91.67(5)	S(7)#6-Rb(3)-S(4)#6	62.25(6)
S(4)#2-Rb(2)-Rb(2)#5	98.24(5)	S(5)#9-Rb(3)-S(4)#6	123.72(6)
S(2)#2-Rb(2)-Rb(2)#5	60.61(4)	S(5)-Rb(3)-S(4)#6	101.95(5)
Pu(1)-Rb(2)-Rb(2)#5	128.47(4)	S(2)-Rb(3)-S(4)#6	56.46(6)

S(6)#6-Rb(3)-S(6)#3	98.62(5)	P(2)#10-S(2)-Pu(1)	86.94(10)
S(2)#7-Rb(3)-S(6)#3	94.51(6)	P(2)#10-S(2)-Rb(3)#7	88.40(9)
S(7)-Rb(3)-S(6)#3	62.08(6)	Pu(1)-S(2)-Rb(3)#7	170.71(8)
S(4)#8-Rb(3)-S(6)#3	123.05(6)	P(2)#10-S(2)-Rb(3)	104.71(11)
S(7)#6-Rb(3)-S(6)#3	115.21(6)	Pu(1)-S(2)-Rb(3)	88.11(6)
S(5)#9-Rb(3)-S(6)#3	52.94(6)	Rb(3)#7-S(2)-Rb(3)	85.31(6)
S(5)-Rb(3)-S(6)#3	69.10(5)	P(2)#10-S(2)-Rb(2)#10	70.54(10)
S(2)-Rb(3)-S(6)#3	124.61(6)	Pu(1)-S(2)-Rb(2)#10	98.16(7)
S(4)#6-Rb(3)-S(6)#3	168.80(5)	Rb(3)#7-S(2)-Rb(2)#10	87.84(5)
S(6)#6-Rb(3)-P(2)#3	138.79(6)	Rb(3)-S(2)-Rb(2)#10	171.79(6)
S(2)#7-Rb(3)-P(2)#3	31.67(5)	P(1)#4-S(3)-Pu(1)	92.04(11)
S(7)-Rb(3)-P(2)#3	31.04(5)	P(1)#4-S(3)-Rb(2)#10	161.05(13)
S(4)#8-Rb(3)-P(2)#3	93.34(5)	Pu(1)-S(3)-Rb(2)#10	106.86(7)
S(7)#6-Rb(3)-P(2)#3	152.68(6)	P(1)#4-S(3)-Rb(2)#4	95.58(11)
S(5)#9-Rb(3)-P(2)#3	131.38(6)	Pu(1)-S(3)-Rb(2)#4	104.85(7)
S(5)-Rb(3)-P(2)#3	86.32(5)	Rb(2)#10-S(3)-Rb(2)#4	81.12(6)
S(2)-Rb(3)-P(2)#3	52.67(5)	P(1)#4-S(3)-Rb(2)#1	90.78(10)
S(4)#6-Rb(3)-P(2)#3	103.04(6)	Pu(1)-S(3)-Rb(2)#1	111.71(8)
S(6)#3-Rb(3)-P(2)#3	83.53(6)	Rb(2)#10-S(3)-Rb(2)#1	81.14(6)
S(6)#6-Rb(3)-P(2)#9	86.99(6)	Rb(2)#4-S(3)-Rb(2)#1	142.61(8)
S(2)#7-Rb(3)-P(2)#9	92.99(5)	P(2)#10-S(4)-Pu(1)	85.60(10)
S(7)-Rb(3)-P(2)#9	153.01(6)	P(2)#10-S(4)-Rb(3)#11	87.79(9)
S(4)#8-Rb(3)-P(2)#9	31.20(5)	Pu(1)-S(4)-Rb(3)#11	170.58(8)
S(7)#6-Rb(3)-P(2)#9	30.71(5)	P(2)#10-S(4)-Rb(3)#12	105.65(10)
S(5)#9-Rb(3)-P(2)#9	83.21(6)	Pu(1)-S(4)-Rb(3)#12	91.16(6)
S(5)-Rb(3)-P(2)#9	142.99(6)	Rb(3)#11-S(4)-Rb(3)#12	84.17(6)
S(2)-Rb(3)-P(2)#9	101.96(6)	P(2)#10-S(4)-Rb(2)#10	72.29(10)
S(4)#6-Rb(3)-P(2)#9	52.03(5)	Pu(1)-S(4)-Rb(2)#10	98.70(7)
S(6)#3-Rb(3)-P(2)#9	131.82(6)	Rb(3)#11-S(4)-Rb(2)#10	85.63(5)
P(2)#3-Rb(3)-P(2)#9	121.97(6)	Rb(3)#12-S(4)-Rb(2)#10	169.68(7)
P(1)#6-S(1)-Pu(1)#4	89.38(9)	P(1)#6-S(5)-Pu(1)	96.85(10)
P(1)#6-S(1)-Pu(1)	90.24(10)	P(1)#6-S(5)-Rb(2)	98.43(10)
Pu(1)#4-S(1)-Pu(1)	127.46(8)	Pu(1)-S(5)-Rb(2)	91.39(7)
P(1)#6-S(1)-Rb(2)#4	161.80(13)	P(1)#6-S(5)-Rb(3)#9	92.52(10)
Pu(1)#4-S(1)-Rb(2)#4	90.33(6)	Pu(1)-S(5)-Rb(3)#9	170.04(8)
Pu(1)-S(1)-Rb(2)#4	104.27(6)	Rb(2)-S(5)-Rb(3)#9	90.55(5)

P(1)#6-S(5)-Rb(3)	87.03(10)
Pu(1)-S(5)-Rb(3)	92.60(6)
Rb(2)-S(5)-Rb(3)	172.82(8)
Rb(3)#9-S(5)-Rb(3)	84.51(6)
P(1)-S(6)-Pu(1)	115.54(11)
P(1)-S(6)-Rb(3)#12	92.01(11)
Pu(1)-S(6)-Rb(3)#12	100.72(6)
P(1)-S(6)-Rb(2)	97.11(10)
Pu(1)-S(6)-Rb(2)	88.71(6)
Rb(3)#12-S(6)-Rb(2)	162.60(8)
P(1)-S(6)-Rb(3)#3	82.40(10)
Pu(1)-S(6)-Rb(3)#3	161.67(8)
Rb(3)#12-S(6)-Rb(3)#3	81.38(5)
Rb(2)-S(6)-Rb(3)#3	85.16(5)
P(2)#3-S(7)-Pu(1)	103.18(11)
P(2)#3-S(7)-Rb(3)	88.19(11)
Pu(1)-S(7)-Rb(3)	88.63(6)
P(2)#3-S(7)-Rb(3)#12	88.08(11)
Pu(1)-S(7)-Rb(3)#12	91.81(6)
Rb(3)-S(7)-Rb(3)#12	176.25(8)
P(2)#3-S(7)-Rb(2)#3	76.71(10)
Pu(1)-S(7)-Rb(2)#3	179.88(8)
Rb(3)-S(7)-Rb(2)#3	91.37(6)
Rb(3)#12-S(7)-Rb(2)#3	88.18(6)
S(6)-P(1)-S(5)#12	107.72(14)
S(6)-P(1)-S(3)#1	110.37(14)
S(5)#12-P(1)-S(3)#1	110.35(14)
S(6)-P(1)-S(1)#12	114.89(14)
S(5)#12-P(1)-S(1)#12	106.28(14)
S(3)#1-P(1)-S(1)#12	107.15(14)
S(6)-P(1)-Rb(3)#12	57.21(8)
S(5)#12-P(1)-Rb(3)#12	62.14(8)
S(3)#1-P(1)-Rb(3)#12	157.11(12)
S(1)#12-P(1)-Rb(3)#12	95.74(9)
S(7)#3-P(2)-S(4)#2	116.92(15)
S(7)#3-P(2)-S(2)#2	115.38(15)
S(4)#2-P(2)-S(2)#2	108.07(14)
S(7)#3-P(2)-P(2)#13	104.26(16)
S(4)#2-P(2)-P(2)#13	105.30(12)
S(2)#2-P(2)-P(2)#13	105.74(12)
S(7)#3-P(2)-Rb(2)	71.28(10)
S(4)#2-P(2)-Rb(2)	75.95(10)
S(2)#2-P(2)-Rb(2)	77.94(10)
P(2)#13-P(2)-Rb(2)	175.28(14)
S(7)#3-P(2)-Rb(3)#3	60.77(9)
S(4)#2-P(2)-Rb(3)#3	157.41(12)
S(2)#2-P(2)-Rb(3)#3	59.94(8)
P(2)#13-P(2)-Rb(3)#3	96.71(7)
Rb(2)-P(2)-Rb(3)#3	82.52(5)
S(7)#3-P(2)-Rb(3)#9	61.21(9)
S(4)#2-P(2)-Rb(3)#9	61.01(9)
S(2)#2-P(2)-Rb(3)#9	157.26(12)
P(2)#13-P(2)-Rb(3)#9	96.65(7)
Rb(2)-P(2)-Rb(3)#9	79.92(5)
Rb(3)#3-P(2)-Rb(3)#9	121.97(6)

Symmetry transformations used to generate equivalent atoms:

#1 -x+1/2,y-1/2,-z+1/2 #2 x,-y+1,z-1/2 #3 -x,-y+1,-z

#4 -x+1/2,y+1/2,-z+1/2 #5 -x+1/2,-y+1/2,-z #6 x,y+1,z

#7 -x,y,-z+1/2 #8 -x,y+1,-z+1/2 #9 -x,-y+2,-z

#10 x,-y+1,z+1/2 #11 -x,y-1,-z+1/2 #12 x,y-1,z

#13 -x,y,-z-1/2

Table 4. Anisotropic displacement parameters ($Å^2 x\ 10^3$) for $Rb_4Pu_2P_4S_{14}$. The anisotropic displacement factor exponent takes the form: $-2p^2[\ h^2\ a^{*2}U^{11} + ... + 2\ h\ k\ a^*\ b^*\ U^{12}\ ]$

	U^{11}	U^{22}	U^{33}	U^{23}	U^{13}	U^{12}
Pu(1)	12(1)	12(1)	14(1)	0(1)	11(1)	0(1)
Rb(2)	31(1)	27(1)	23(1)	2(1)	20(1)	3(1)
Rb(3)	26(1)	16(1)	32(1)	3(1)	23(1)	2(1)
S(1)	16(1)	17(1)	15(1)	0(1)	11(1)	-3(1)
S(2)	19(1)	11(1)	24(1)	-3(1)	17(1)	-3(1)
S(3)	17(1)	23(1)	19(1)	0(1)	15(1)	1(1)
S(4)	17(1)	12(1)	24(1)	3(1)	15(1)	2(1)
S(5)	16(1)	14(1)	16(1)	0(1)	9(1)	-3(1)
S(6)	17(1)	14(1)	21(1)	0(1)	11(1)	2(1)
S(7)	21(1)	19(1)	18(1)	0(1)	16(1)	0(1)
P(1)	12(1)	11(1)	13(1)	1(1)	9(1)	1(1)
P(2)	14(1)	12(1)	16(1)	0(1)	12(1)	1(1)

Appendix F

Supplementary Information for Chapter 5

Table 1. Crystal data and structure refinement for KPu_3Se_8.

Identification code	KPu_3Se_8	
Empirical formula	K0.33 Pu Se2.67	
Formula weight	462.68	
Temperature	293(2) K	
Wavelength	0.71073 Å	
Crystal system	Orthorhombic	
Space group	Cmcm	
Unit cell dimensions	a = 4.1257(5) Å	□= 90°.
	b = 25.642(3) Å	□= 90°.
	c = 3.9900(4) Å	□ = 90°.
Volume	422.11(8) $Å^3$	
Z	4	
Density (calculated)	7.281 Mg/m^3	
Absorption coefficient	38.711 mm^{-1}	
F(000)	764	
Crystal size	0.2 x 0.1 x 0.08 mm^3	
Theta range for data collection	1.59 to 28.28°.	
Index ranges	0<=h<=5, 0<=k<=33, 0<=l<=3	
Reflections collected	241	
Independent reflections	241 [R(int) = 0.0000]	
Completeness to theta = 28.28°	70.7 %	
Refinement method	Full-matrix least-squares on F^2	
Data / restraints / parameters	241 / 0 / 25	
Goodness-of-fit on F^2	1.291	
Final R indices [I>2sigma(I)]	R1 = 0.0561, wR2 = 0.1543	
R indices (all data)	R1 = 0.0604, wR2 = 0.1571	
Largest diff. peak and hole	3.122 and -6.016 $e.Å^{-3}$	

Table 2. Atomic coordinates (x 10^4) and equivalent isotropic displacement parameters ($Å^2$x 10^3) for KPu_3Se_8. U(eq) is defined as one third of the trace of the orthogonalized U^{ij} tensor.

	x	y	z	U(eq)
K(1)	0	-4847(9)	-7500	9(9)
Pu(1)	-5000	-3244(1)	-7500	13(1)
Se(1)	-5000	-4146(2)	-12500	32(2)
Se(2)	-5000	-2063(2)	-7500	12(2)
Se(3)	0	-4174(4)	-16650(80)	37(13)

Table 3. Bond lengths [Å] and angles [°] for KPu_3Se_8.

K(1)-Se(3)#1	1.76(3)	Se(3)#2-K(1)-K(1)#3	122.6(17)
K(1)-Se(3)#2	1.76(3)	Se(3)#1-K(1)-K(1)#4	122.6(17)
K(1)-K(1)#3	2.144(18)	Se(3)#2-K(1)-K(1)#4	100.3(14)
K(1)-K(1)#4	2.144(18)	K(1)#3-K(1)-K(1)#4	137(2)
K(1)-Se(3)#5	3.01(3)	Se(3)#1-K(1)-Se(3)#5	157.8(16)
K(1)-Se(3)#4	3.01(3)	Se(3)#2-K(1)-Se(3)#5	135.5(5)
Pu(1)-Se(2)#6	2.9756(11)	K(1)#3-K(1)-Se(3)#5	101.9(15)
Pu(1)-Se(2)#7	2.9756(11)	K(1)#4-K(1)-Se(3)#5	35.1(11)
Pu(1)-Se(2)#8	2.9756(11)	Se(3)#1-K(1)-Se(3)#4	135.5(5)
Pu(1)-Se(2)#9	2.9756(11)	Se(3)#2-K(1)-Se(3)#4	157.8(16)
Pu(1)-Se(2)	3.028(4)	K(1)#3-K(1)-Se(3)#4	35.1(11)
Pu(1)-Se(1)#1	3.054(4)	K(1)#4-K(1)-Se(3)#4	101.9(15)
Pu(1)-Se(1)	3.054(4)	Se(3)#5-K(1)-Se(3)#4	66.8(11)
Pu(1)-Se(3)#10	3.171(8)	Se(2)#6-Pu(1)-Se(2)#7	87.78(4)
Pu(1)-Se(3)#11	3.171(8)	Se(2)#6-Pu(1)-Se(2)#8	149.34(15)
Pu(1)-Se(3)#1	3.171(8)	Se(2)#7-Pu(1)-Se(2)#8	84.20(4)
Pu(1)-Se(3)#2	3.171(8)	Se(2)#6-Pu(1)-Se(2)#9	84.20(4)
Se(1)-Se(3)#2	2.65(2)	Se(2)#7-Pu(1)-Se(2)#9	149.34(15)
Se(1)-Se(3)#12	2.65(2)	Se(2)#8-Pu(1)-Se(2)#9	87.78(4)
Se(1)-Se(3)#10	2.65(2)	Se(2)#6-Pu(1)-Se(2)	74.67(8)
Se(1)-Se(3)	2.65(2)	Se(2)#7-Pu(1)-Se(2)	74.67(8)
Se(1)-Pu(1)#13	3.054(4)	Se(2)#8-Pu(1)-Se(2)	74.67(8)
Se(2)-Pu(1)#6	2.9756(11)	Se(2)#9-Pu(1)-Se(2)	74.67(8)
Se(2)-Pu(1)#7	2.9756(11)	Se(2)#6-Pu(1)-Se(1)#1	76.24(7)
Se(2)-Pu(1)#8	2.9756(11)	Se(2)#7-Pu(1)-Se(1)#1	76.24(7)
Se(2)-Pu(1)#9	2.9756(11)	Se(2)#8-Pu(1)-Se(1)#1	129.65(7)
Se(3)-Se(3)#14	0.68(6)	Se(2)#9-Pu(1)-Se(1)#1	129.65(7)
Se(3)-K(1)#13	1.76(3)	Se(2)-Pu(1)-Se(1)#1	139.21(6)
Se(3)-Se(1)#15	2.65(2)	Se(2)#6-Pu(1)-Se(1)	129.65(7)
Se(3)-K(1)#4	3.01(3)	Se(2)#7-Pu(1)-Se(1)	129.65(7)
Se(3)-Pu(1)#16	3.171(8)	Se(2)#8-Pu(1)-Se(1)	76.24(7)
Se(3)-Pu(1)#13	3.171(8)	Se(2)#9-Pu(1)-Se(1)	76.24(7)
Se(3)#1-K(1)-Se(3)#2	22(2)	Se(2)-Pu(1)-Se(1)	139.21(6)
Se(3)#1-K(1)-K(1)#3	100.3(14)	Se(1)#1-Pu(1)-Se(1)	81.57(12)

Se(2)#6-Pu(1)-Se(3)#10	136.2(5)	Se(3)#12-Se(1)-Se(3)#10	77.4(11)
Se(2)#7-Pu(1)-Se(3)#10	79.6(4)	Se(3)#2-Se(1)-Se(3)	77.4(11)
Se(2)#8-Pu(1)-Se(3)#10	71.1(4)	Se(3)#12-Se(1)-Se(3)	102.5(11)
Se(2)#9-Pu(1)-Se(3)#10	125.3(5)	Se(3)#10-Se(1)-Se(3)	176.9(5)
Se(2)-Pu(1)-Se(3)#10	138.75(14)	Se(3)#2-Se(1)-Pu(1)	67.2(4)
Se(1)#1-Pu(1)-Se(3)#10	60.1(5)	Se(3)#12-Se(1)-Pu(1)	115.4(4)
Se(1)-Pu(1)-Se(3)#10	50.3(4)	Se(3)#10-Se(1)-Pu(1)	67.2(4)
Se(2)#6-Pu(1)-Se(3)#11	125.3(5)	Se(3)-Se(1)-Pu(1)	115.4(4)
Se(2)#7-Pu(1)-Se(3)#11	71.1(4)	Se(3)#2-Se(1)-Pu(1)#13	115.4(4)
Se(2)#8-Pu(1)-Se(3)#11	79.6(4)	Se(3)#12-Se(1)-Pu(1)#13	67.2(4)
Se(2)#9-Pu(1)-Se(3)#11	136.2(5)	Se(3)#10-Se(1)-Pu(1)#13	115.4(4)
Se(2)-Pu(1)-Se(3)#11	138.75(14)	Se(3)-Se(1)-Pu(1)#13	67.2(4)
Se(1)#1-Pu(1)-Se(3)#11	50.3(4)	Pu(1)-Se(1)-Pu(1)#13	81.57(12)
Se(1)-Pu(1)-Se(3)#11	60.1(5)	Pu(1)#6-Se(2)-Pu(1)#7	87.78(4)
Se(3)#10-Pu(1)-Se(3)#11	12.3(11)	Pu(1)#6-Se(2)-Pu(1)#8	149.34(15)
Se(2)#6-Pu(1)-Se(3)#1	71.1(4)	Pu(1)#7-Se(2)-Pu(1)#8	84.20(4)
Se(2)#7-Pu(1)-Se(3)#1	125.3(5)	Pu(1)#6-Se(2)-Pu(1)#9	84.20(4)
Se(2)#8-Pu(1)-Se(3)#1	136.2(5)	Pu(1)#7-Se(2)-Pu(1)#9	149.34(15)
Se(2)#9-Pu(1)-Se(3)#1	79.6(4)	Pu(1)#8-Se(2)-Pu(1)#9	87.78(4)
Se(2)-Pu(1)-Se(3)#1	138.75(14)	Pu(1)#6-Se(2)-Pu(1)	105.33(8)
Se(1)#1-Pu(1)-Se(3)#1	50.3(4)	Pu(1)#7-Se(2)-Pu(1)	105.33(8)
Se(1)-Pu(1)-Se(3)#1	60.1(5)	Pu(1)#8-Se(2)-Pu(1)	105.33(8)
Se(3)#10-Pu(1)-Se(3)#1	82.5(3)	Pu(1)#9-Se(2)-Pu(1)	105.33(8)
Se(3)#11-Pu(1)-Se(3)#1	81.2(2)	Se(3)#14-Se(3)-K(1)#13	78.9(10)
Se(2)#6-Pu(1)-Se(3)#2	79.6(4)	Se(3)#14-Se(3)-Se(1)#15	128.7(6)
Se(2)#7-Pu(1)-Se(3)#2	136.2(5)	K(1)#13-Se(3)-Se(1)#15	98.5(6)
Se(2)#8-Pu(1)-Se(3)#2	125.3(5)	Se(3)#14-Se(3)-Se(1)	128.7(5)
Se(2)#9-Pu(1)-Se(3)#2	71.1(4)	K(1)#13-Se(3)-Se(1)	98.5(6)
Se(2)-Pu(1)-Se(3)#2	138.75(14)	Se(1)#15-Se(3)-Se(1)	102.5(11)
Se(1)#1-Pu(1)-Se(3)#2	60.1(5)	Se(3)#14-Se(3)-K(1)#4	123.4(6)
Se(1)-Pu(1)-Se(3)#2	50.3(4)	K(1)#13-Se(3)-K(1)#4	44.5(5)
Se(3)#10-Pu(1)-Se(3)#2	81.2(2)	Se(1)#15-Se(3)-K(1)#4	71.2(6)
Se(3)#11-Pu(1)-Se(3)#2	82.5(3)	Se(1)-Se(3)-K(1)#4	71.2(6)
Se(3)#1-Pu(1)-Se(3)#2	12.3(11)	Se(3)#14-Se(3)-Pu(1)#16	83.8(6)
Se(3)#2-Se(1)-Se(3)#12	176.9(5)	K(1)#13-Se(3)-Pu(1)#16	135.8(6)
Se(3)#2-Se(1)-Se(3)#10	102.5(11)	Se(1)#15-Se(3)-Pu(1)#16	62.6(2)

Se(1)-Se(3)-Pu(1)#16	123.6(7)	Se(1)#15-Se(3)-Pu(1)#13	123.6(7)
K(1)#4-Se(3)-Pu(1)#16	133.4(6)	Se(1)-Se(3)-Pu(1)#13	62.6(2)
Se(3)#14-Se(3)-Pu(1)#13	83.8(6)	K(1)#4-Se(3)-Pu(1)#13	133.4(6)
K(1)#13-Se(3)-Pu(1)#13	135.8(6)	Pu(1)#16-Se(3)-Pu(1)#13	81.2(2)

Symmetry transformations used to generate equivalent atoms:

#1 x,y,z+1 #2 x,y,-z-5/2 #3 -x,-y-1,-z-1

#4 -x,-y-1,-z-2 #5 -x,-y-1,z+1/2 #6 -x-1/2,-y-1/2,-z-1

#7 -x-3/2,-y-1/2,-z-1 #8 -x-3/2,-y-1/2,-z-2

#9 -x-1/2,-y-1/2,-z-2 #10 x-1,y,-z-5/2 #11 x-1,y,z+1

#12 x-1,y,z #13 x,y,z-1 #14 x,y,-z-7/2 #15 x+1,y,z

#16 x+1,y,z-1

Table 4. Anisotropic displacement parameters ($Å^2 x\ 10^3$) for KPu_3Se_8. The anisotropic displacement factor exponent takes the form: $-2\pi^2[h^2 a^{*2} U^{11} + ... + 2 h k a^* b^* U^{12}]$

	U^{11}	U^{22}	U^{33}	U^{23}	U^{13}	U^{12}
K(1)	15(9)	13(10)	0(30)	0	0	0
Pu(1)	11(1)	16(1)	12(2)	0	0	0
Se(1)	39(2)	19(2)	37(5)	0	0	0
Se(2)	11(2)	17(2)	9(5)	0	0	0
Se(3)	24(3)	18(3)	70(40)	-9(7)	0	0